The double-humped fission barrier

S. Bjørnholm

The Niels Bohr Institute, University of Copenhagen, Denmark

J. E. Lynn

Atomic Energy Research Establishment, Harwell, England and Los Alamos Scientific Laboratory, New Mexico

The concept of the double-humped fission barrier of actinide nuclei has made possible an understanding of a vast amount of data on nuclear fission during the past decade. In this article the analysis of most available relevant data is reviewed, and a synthesis of the fission barrier parameters and their trends over the actinide region is built up. The sequence of the work begins with an outline (but not a critical discussion) of the theoretical foundation of the double-humped barrier, and this is followed by a full account of the nuclear reaction theory required to describe fission reactions within the concept of such a barrier. This reaction theory provides the theoretical tools for a quantitative understanding of a range of phenomena of such kinds as spontaneously fissioning isomers, their half-live and yields, vibrational resonances and narrower intermediate structure in fission cross sections, and the general trends and magnitudes of fission cross sections at excitation energies near the top of the fission barrier. The magnitudes and trends of fission barrier parameters and the level structure of highly deformed nuclei that are extracted from the data on these phenomena are discussed in the light of current concepts of nuclear structure. Also, the possibility of a three-humped and more complex barriers is reviewed.

CONTENTS

I. INTRODUCTION

A. Classical picture of the fission process

This review is intended to cover the fascinating developments of low-energy nuclear fission over the past decade. By the term "low-energy" we imply energies of the fissioning nucleus that are comparable to the potential energy barrier in the deformation path toward fission. The phenomena discussed in this review are those that are governed by the properties of the fission barrier as such, rather than those that seem to be determined at the later stages of fission, i.e., just prior to, or even after, scission, at which point the two incipient fission products just separate.

The concept of the fission barrier has been based on the classical theory of the electrically charged liquid drop ever since the work of Bohr and Wheeler (1939); this itself was based on the original suggestion of Meitner and Frisch (1939). The analogy of nuclear behavior to that of a charged liquid drop is suggested

by the standard semiempirical formula for nuclear ground-state energies:

$$E = E_{\text{vol}} + E_{\text{surf}} + E_{\text{coul}} + E_{\text{pair}} = -c_1 A + c_2 A^{2/3} + c_3 (Z^2/A^{1/3}) \pm \delta \,. \tag{1.1}$$

Since the nuclear radius is proportional to $A^{1/3}$ the first three terms in this equation are proportional to nuclear volume, surface area, and Coulomb repulsion energy, respectively. The remaining "odd-even" term is essentially quantal in origin. It is a small correction of the form $\delta = 11\, A^{-1/2}$ MeV to be added or subtracted for doubly odd or doubly even nuclei, respectively. Of the same origin are isospin-dependent terms, depending on the difference in proton and neutron numbers, Z and N, respectively. Myers and Swiatecki (1966) suggest that this be assumed to reduce the magnitude of the surface as well as the volume energy:

$$c_1 = a_1[1 - \gamma(N - Z/A)^2] \,, \tag{1.2}$$

$$c_2 = a_2[1 - \kappa(N - Z/A)^2] \,. \tag{1.3}$$

If the nuclear "fluid" is assumed to be incompressible, an estimate of the energy necessary to deform the nucleus is made by identifying the second and third terms as the surface and Coulomb energies of a classical liquid drop. It was easily shown by Bohr and Wheeler that a spherical liquid drop nucleus is unstable if

$$\frac{E_{\text{coul}}}{2E_{\text{surf}}} = \frac{c_3}{2c_2}\frac{Z^2}{A} > 1 \,. \tag{1.4}$$

The above ratio, which is called the fissility parameter denoted by X, also reads

$$\frac{E_{\text{coul}}}{2E_{\text{surf}}} = \frac{c_3}{2a_2[1 - \kappa(N - Z/A)^2]}\frac{Z^2}{A} = X \,. \tag{1.5}$$

A large number of papers spread over a period of more than 20 years have been devoted to the computation of the energy of deformation of the nucleus in terms of the liquid drop model. Most studies have concentrated on drops with $X \approx 0.7$–0.8, which are the values appropriate to the actinide nuclei. A typical set of energy contours in the plane defined by two of the most important deformation parameters (the quadrupole and hexadecapole coefficients in a Legendre polynomial of the liquid drop surface) is shown in Fig. 1(a). The energetically most favorable path towards fission is indicated by the broken line and the potential energy barrier presented along this path is shown in Fig. 1(b); the barrier peak in Fig. 1(b) corresponds to the point denoted "col", or saddle, shown in Fig. 1(a).

The droplet model of Myers and Swiatecki (1969) and Myers (1977) is presently the most refined description of average nuclear properties based on the liquid drop concept.

Nuclear reactions leading to fission have been interpreted on the basis of this kind of fission barrier, especially its height. Such data are particularly concerned with reaction rates. By contrast the spontaneous fission half-lives of nuclear ground states are sensitive not only to the effective height of the barrier but also to the width and the inertial parameter associated with the nuclear collective motion along the fission

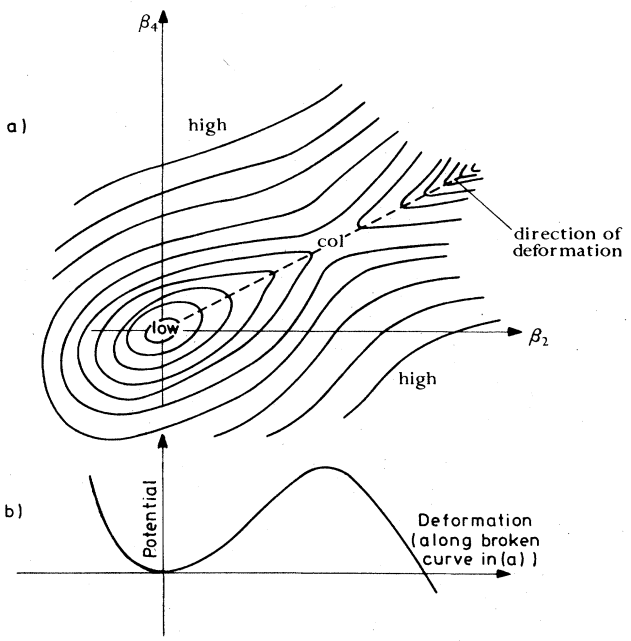

FIG. 1. (a) Schematic diagram of potential energy contours of a fissionable nucleus as a function of the quadrupole and hexadecapole deformation parameters. (b) The potential energy along the minimum energy trajectory for increasing elongation.

path. This inertial parameter is usually incorporated with the curvature of the barrier to obtain a parameter that leads to the transmission coefficient. Thus, if the barrier is assumed to have an inverted harmonic oscillator form, the curvature (which is proportional to the restoring force constant C of the oscillator) and inertial parameter B give the frequency of an oscillator, $\omega = (C/B)^{1/2}$, and it can be deduced (Hill and Wheeler, 1953) that the transmission coefficient of the barrier is

$$T = \{1 + \exp[2\pi(E_F - E)/\hbar\omega]\}^{-1} \,, \tag{1.6}$$

where E_F is the peak barrier energy, and E the nuclear excitation energy. Analysis of spontaneous fission half-lives using peak barrier energies known from induced fission reactions reveals that the tunneling parameter $\hbar\omega$ usually lies in the range 0.35–0.40 MeV (Swiatecki, 1955). Such a low value implies that the effective inertia of the tunneling motion exceeds the minimum possible (irrotational) value by a considerable amount.

Estimates of the half-life of a particular mode of decay of a nuclear state can be obtained from statistical considerations. The arguments of Blatt and Weisskopf (1952) in particular are simple and appealing. Consider a system with uniformly spaced levels with eigenvalues $E_n = E_0 + nD$. The classical behavior of the system at time t is obtained by superposing a large number of eigenfunctions and is represented by the wave function

$$\Psi(t) = \sum_{n=1}^{N} a_n \phi_n \exp\left(\frac{-iE_n t}{\hbar}\right) = \exp\left(\frac{-iE_0 t}{\hbar}\right)\sum_{n=1}^{N} a_n \phi_n \exp\left(\frac{-inDt}{\hbar}\right), \tag{1.7}$$

where the ϕ_n's contain the spatial dependence. Clearly, the period of motion of this wave function is

$$P = 2\pi\hbar/D\,. \tag{1.8}$$

Thus the classical configuration corresponding to the formation of the nucleus in a particular mode (or channel) μ will be repeated after a period of time of the order of P. The nucleus will now be in a position to decay through the original mode (channel) of formation, and will only be inhibited from doing so by the existence of an external barrier, the transmission coefficient of which is T_μ. Thus the lifetime τ_μ for this particular mode alone will be of the order of P/T_μ and the partial width of the state is

$$\Gamma_{(\mu)} \approx \hbar/\tau_\mu \approx \frac{D}{2\pi} T_\mu\,. \tag{1.9}$$

The different modes μ correspond to states of excitation of the internal degrees of freedom of the system. Thus the total fission width of the nucleus will be given by Eq. (1.9) summed over all states of internal excitation at the saddle point. For energies well above the barrier this leads to the statistical formula (Bohr and Wheeler, 1939) for the fission width,

$$\Gamma_{(f)} = (D/2\pi)N\,, \tag{1.10}$$

where N is the number of levels of internal excitation available to the reaction,

$$N = \int_{E_F}^{E} dE' \rho^*(E' - E_F)\,, \tag{1.11}$$

ρ^* being the density of such levels at the saddle point and E_F the fission threshold energy.

When coupled with the wave function corresponding to distortion through the saddle point, the various states of internal excitation comprised in the quantity N together make up the overall "transition state" of the fissioning nucleus. A. Bohr (1956) first considered the influence of the properties of the individual components of the transition state on the fission process. The actinide nuclei have values of the fissility parameter X in the region of 0.75 considerably less than unity, and this implies, according to the liquid drop model, that such nuclei are appreciably elongated at their saddle points (the major to minor axis ratio being of the order of 2). Thus the lowest states of internal excitation at the saddle point ought to be well described by the unified model (Bohr and Mottelson, 1975) of nuclear structure. In particular, if the saddle-point nucleus has cylindrical symmetry about its direction of elongation, the quantity K describing the projection of the total angular momentum of the state on the cylindrical symmetry axis should be a good quantum number. An excited nucleus formed with specified angular momentum projection along a specified direction in space will therefore have its axis of elongation at the saddle point related to this space direction, this relation being governed by the distribution of K values among the components of the transition state (see Fig. 2). The preservation of this relationship between the saddle and scission points implies that the angular distribution of fission products will bear this same relationship to the original specified space direction. As an example of this theory,

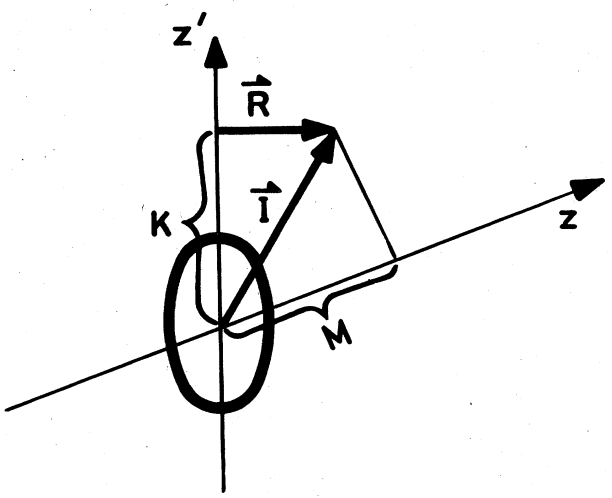

FIG. 2. The relationship between total angular momentum **I** and rotation **R** of a spheroidal nucleus, and the projection of **I** on the z axis of the laboratory reference frame (M) and the symmetry axis z' of the nucleus (K).

Bohr cited the case of low-energy photofission of an even nucleus (spin parity = 0^+). Electric dipole absorption of the gamma ray leads to an excited nucleus with total angular momentum and parity 1^-, the projection of angular momentum along the gamma-ray direction being ± 1. The lowest 1^- state of the distorted saddle point nucleus is expected, from the unified model and in agreement with observation of low-lying ground-state excitations, to have $K = 0$. This implies that the nuclear elongation direction must be, on average, perpendicular to the gamma-ray direction of incidence, and hence the threshold photofission will result in a "sideways" angular distribution of fission products (see Fig. 3), in agreement with observation. At higher energies, a second 1^- component, or "channel," will become energetically available in the transition state; this is expected to have $K = 1$, and the photofission angular distribution is therefore expected to be more nearly (though not completely) isotropic, and this behavior is also observed.

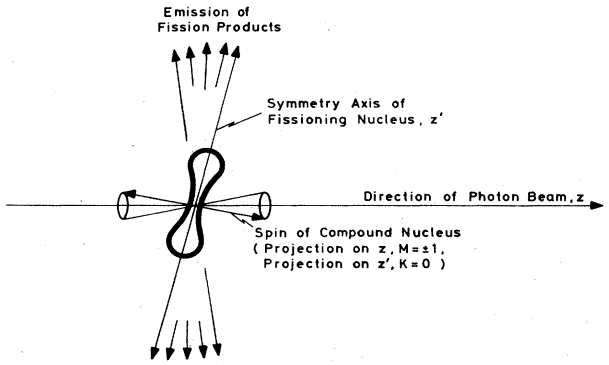

FIG. 3. The relations of Fig. 2 explain the angular distribution of fission products from an even nucleus in a photofission reaction dominated by dipole absorption and fission through a transition state with $K = 0$.

Bohr's "channel theory of fission" was applied to the analysis of most low-energy fission phenomena during the next decade. It seemed that this combination of the charged liquid drop picture of the fission barrier with the unified nuclear structure description of the excitation of internal degrees of freedom was basically capable of explaining fission phenomena that would result from features "frozen" into the system at an early stage of its development. An important example of phenomena that were thus qualitatively, or even semiquantitatively, explained by this theory is the behavior of the neutron-induced fission cross section of even actinide nuclei. The fission barriers of the odd-neutron compound nuclei are higher than their neutron separation energies, so the cross sections as a function of energy show a marked exponentially rising tunnel effect, as in Fig. 4. In addition to this overall increase and eventual saturation, there is rising and falling structure of a minor kind. The explanation that was advanced for this rising and falling [originally, it appears, by Mottelson (unpublished) but expounded principally by Wheeler (1956, 1963)] assumes competition in the decay of the compound nucleus between fission and neutron inelastic scattering. In a rising part of the fission cross-section curve it is assumed that the energy of the compound nucleus is approaching the threshold E of a Bohr "fission channel." The rate of rise falls off as this threshold is exceeded and the tunneling factor, Eq. (1.6), asymptotically approaches unity. If a neutron inelastic scattering threshold is now crossed by increasing the excitation energy further the share that fission takes in the decay of the compound nucleus is reduced and the fission cross section falls somewhat until the threshold of the next Bohr channel approaches. (For details see the discussion in connection with Fig. 78.)

B. New observations implying shell structure at the fission barrier

The first apparent weakness in this whole picture of the fission barrier lay in the quantitative estimates of barrier heights from the liquid drop theory. The liquid drop force constants deduced from analysis of nuclear masses according to Eq. (1.1) can be adjusted to lead to barrier heights for the actinides of the order of 5–6 MeV (above the ground state), but it is by no means possible to explain how the barriers can remain constant in the range from ^{230}Th ($X = 0.76$) to ^{253}Cf ($X = 0.82$) as observed; the liquid drop predictions change from 7.5 to 2.8 MeV in this range. It had long been known, however, that substantial deviations from Eq. (1.1) occurred for nuclei near-shell closures. Equation (1.1), with fitted constants might overestimate the ground-state energy of magic nuclei such as ^{208}Pb by 10–15 MeV. Attempts were therefore made to incorporate the nucleon shell effects into the semiempirical formula. Myers and Swiatecki (1966) first attempted to do this in a way that would give a semiempirical energy formula explaining all the stability features of the known nuclei; these features were, principally, the ground-state energies, the ground-state quadrupole moments, and the fission barriers. They made the assumption that shell effects would be largest for a nucleus when in its spherical configuration. Thus, starting from an equation that is the generalization (by liquid drop theory) of Eq. (1.1) to a body with variable deformation,

$$E = E_v(A, Z) + E_s(A, Z) f(\text{shape}) + E_c(A, Z) g(\text{shape}) \qquad (1.12)$$

[here, g(shape) is the dimensionless ratio of the electrostatic energy of a distorted drop to that of the sphere, while f(shape) is the similarly defined ratio of surface energies], they add a shell term which depends on N and Z and falls off as a Gaussian with deformation.

In work carried out a little later along related lines, Strutinsky (1967a, b) concentrated on deriving the shell-correction term from actual shell model energy levels in a binding field of varying shape, rather than in a semiempirical way. In this approach the shell correction was calculated essentially by summing the energies of occupied single-particle Nilsson orbitals in a potential well of given deformation and subtracting from this the energy calculated by integrating over a suitably

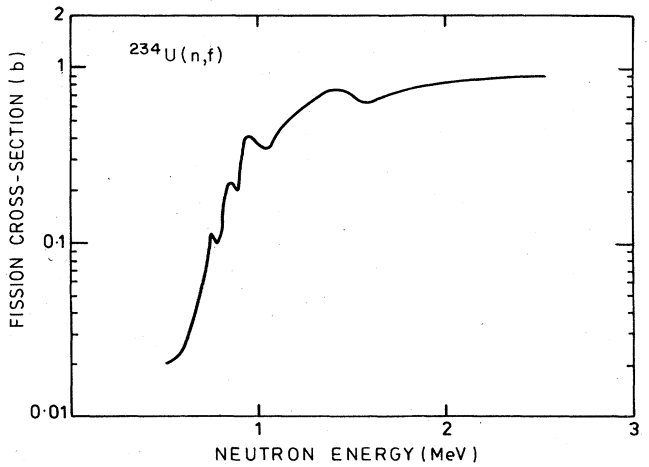

FIG. 4. Neutron fission cross section of ^{234}U. This shows the general feature of a very sharp rise in cross section from subbarrier energies, which is characteristic of quantal barrier tunneling.

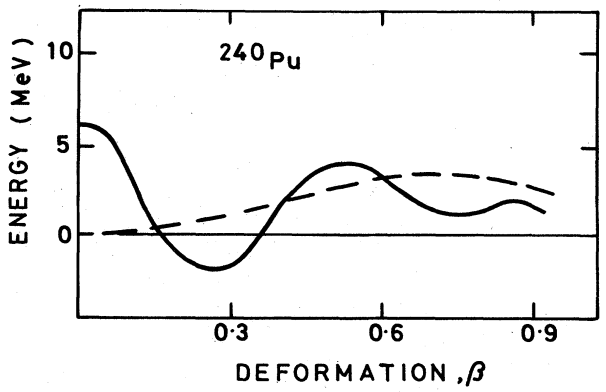

FIG. 5. Potential energy curve towards fission as calculated by Strutinsky (1967ab) from his theory of shell correction energy superposed on the liquid drop energy.

averaged single-particle level density. The addition of such a correction to the normal liquid drop term not only led to the reproduction of observed ground-state quadrupole moments, the deviations of magic nuclei energies from the smoothed liquid drop behavior, and fission barriers of the right order of magnitude, but also indicated an oscillation of the energy curve of actinide nuclei with increasing deformation (see Fig. 5). This oscillation is of course due to a superposition of an oscillatory behavior of the shell-correction term onto the liquid drop energy term. In other words, Strutinsky found that "shell" effects could exist for deformed as well as spherical potential wells. It is the existence of this oscillatory feature, often known as the double-humped barrier, that has been of central importance in understanding the new and striking experimental discoveries in low-energy fission. The theory of the Strutinsky potential energy function is described in greater detail in Sec. II. Here we mention that the quantitative calculations indicate that for the actinides the first maximum in the barrier is some 6 or 7 MeV high, the secondary minimum, at a prolate deformation corresponding to a ratio of axes of 2:1, is some 2 or 3 MeV shallower than the main well, while the second maximum has about the same height as the first for uranium, and decreases for the heavier actinides.

The first experimental observation for which the theory of a double-humped barrier provided an explanation was the occurrence of spontaneously fissioning isomers. The first such isomer had been discovered by Polikanov *et al.* (1962); this proved to be a 14 msec isomeric state of ^{242}Am with spontaneous fission as its principal mode of decay (Flerov and Polikanov, 1964). The spontaneous fission half-life was appropriate to a state with an excitation energy of several MeV, so its peculiar property was apparently its extraordinary stability against gamma decay. A few more such isomers with similar half-lives were discovered in the following years, all in doubly odd Am nuclei, and it was confirmed by direct measurement by Bjørnholm *et al.* (1967) that the excitation energy (for ^{240}Am) was indeed close to 3 MeV. The hypothesis that the spontaneously fissioning isomer might be a state lodged in a second minimum of the deformation energy curve was first advanced by Polikanov *et al.* (1962), referring to the discussion by Hill and Wheeler (1953) of prolate-oblate isomerism, and later by Flerov and Druin (1966). These suggestions received support from subsequent theoretical work in which the aforementioned approach due to Strutinsky (1967) played a pivotal role.

It was also suspected at about this time that structure apparent in fast neutron-induced fission cross sections could not be explained quantitatively by the theory of competition between successively opening fission and inelastic neutron scattering channels (Lynn, 1966a). In the cross sections for ^{230}Th (see Fig. 6) and ^{232}Th, for example, there are strong resonancelike peaks. The angular distributions of fission products released in fast neutron- and deuteron-stripping-induced reactions also show sharp changes as a function of excitation energy. The scale of such structure is in the range 10–100 keV, which rules out any association with

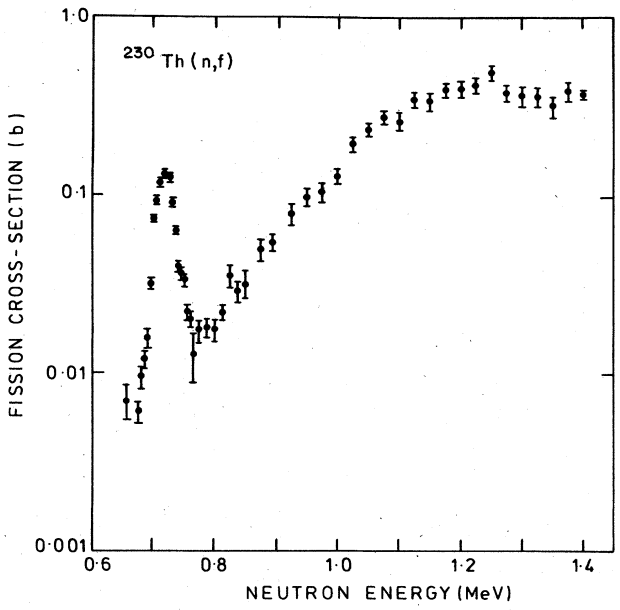

FIG. 6. Neutron fission cross section of ^{230}Th [data of James *et al.* (1972)].

single-particle modes of the entrance channel (generally believed to have widths on the scale of MeV) as an alternative explanation to the competition theory.

The explanation that now became available for these phenomena was essentially that higher vibrational states in the secondary well (carrying most of the fission strength) are only weakly damped into the normal compound nucleus motion (Lynn, 1968a, b, c; Bjørnholm and Strutinsky, 1969).

The discovery of a third phenomenon now seemed to confirm the central assumption of a doubled-humped fission barrier hypothesis. The new phenomenon is narrow intermediate structure in slow neutron fission cross sections in measurements where the neutron resolution is comparable with the fine-structure resonance widths. The target nuclei for which this effect has been discovered in its most dramatic form are the even-even and odd-Z actinides. These normally have fission cross sections for thermal neutron bombardment that are extremely small compared with radiative capture, and this property naturally holds for the lowest few resonances of the cross section. However, if the cross sections are studied over a much more extended energy range, it is found that narrow bands of resonances in which fission is comparable to capture occur at intervals 1 or 2 orders of magnitude greater than the normal resonance spacing. The first, and most striking, examples discovered of this phenomenon are in the cross sections of the target nuclei ^{237}Np (Paya *et al.*, 1968) and ^{240}Pu (Migneco and Theobald, 1968) (see Fig. 7).

We can now summarize our understanding of these phenomena as follows. The spontaneously fissioning isomer of a nucleus is explained as being the "ground-state" zero-point vibration in the secondary well. It is, in fact, the lowest state of a whole set of levels of increasing complexity as the energy increases, associated with the highly deformed shape at the secondary

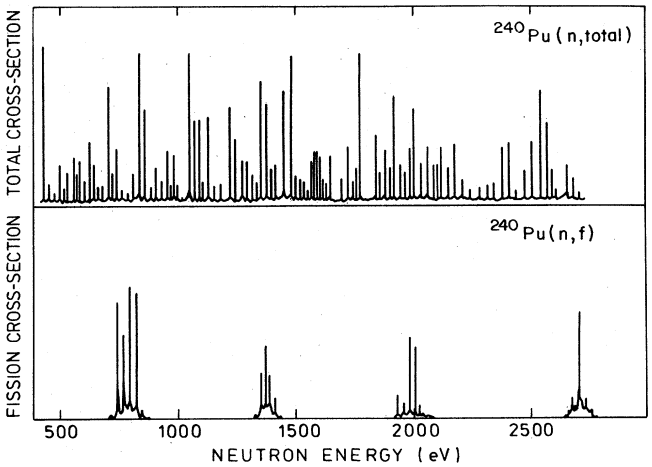

FIG. 7. Above: the total neutron cross section of ^{240}Pu (Kolar and Böckhoff, 1968), showing the large number of fine-structure resonances. Below: the neutron fission cross section of ^{240}Pu (Migneco and Theobald, 1968) showing a very few fine-structure resonances of appreciable strength and those clustered into a few groups that constitute intermediate resonances in the fission channel.

minimum. These levels fission readily compared with states of normal deformation at the same energy. They are also much less dense because more of their energy is tied up in potential energy of deformation and is not available for excitation of the internal degrees of freedom. Obviously these are the levels that are responsible for the narrow intermediate structure phenomenon in fission, each such level corresponding to a single group of fission resonances in the cross section, and the width of each group being a measure either of the strength of coupling between the "highly deformed state" and the "normal states," or of the fission width of the highly deformed state, whichever is greater. The high intermediate barrier between the two wells is responsible for the very weak coupling between the two sets of states that makes the structure so readily apparent. The "gross" structure that is apparent in the cross sections of other fission reactions measured with "poor" resolution (i.e., resolution that envelopes very many fine-structure resonances) follows from an assumption of weak damping of certain simple modes of the highly deformed nucleus into its complex level structure. These simple modes correspond to little or no excitation of the single-particle degrees of freedom of the nucleus, the available energy being carried by a stretching vibration of the secondary well, the mode thus having a correspondingly high fission strength. The weak damping, at nominal excitation energies of some 5 or 6 MeV, can be explained by the much reduced energy available for internal excitation of the nucleus in its highly deformed shape.

C. About this review

A number of reviews on the barrier aspects of fission have appeared during the last decade (for example, Strutinski and Pauli, 1969; Lynn, 1969; Brack *et al.*, 1972; Nix, 1972; Michaudon, 1973, 1976; Grant, 1976). Our aim in this review is to give a critical and comprehensive account of the information about the double-humped fission barrier that can be deduced from experimental work. We hope thereby to provide a body of reliable data on deformation properties of the actinide nuclei that can be compared with the results of theoretical calculations. Such a testing ground is obviously of great importance for nuclear theory. To provide a first orientation for the analysis of the experimental data and a basis for subsequent comparison, we begin Sec. II by giving a *summary* of the results of theoretical work at the present time. A critical review of the theory is not attempted here; it has been covered elsewhere by authorities on the subject. This chapter is followed by a full account of the theory for reactions proceeding through a double-humped barrier. Both the statistical theories, from which simple, yet useful, limiting expressions may be established, and more formal theories are described. This chapter provides the foundation for analyzing the experimental data.

Experimental work in this field has been extremely active over the past years. Shape isomers are being formed and investigated from a wide range of reactions employing both low- and high-energy particles. Their energies are being found by measurement of the excitation curves for their formation, while their half-lives give information about the penetrability of the outer barrier of the double-humped potential, and their formation yields can give relative barrier heights. This work is mainly discussed in Sec. IV.

Prompt fission is also being examined with a variety of reactions. Fast neutrons with high-energy resolution are used to measure fission cross section and fission product angular distributions in order to elucidate properties of the vibrational states in the second minimum. To reach even lower energies, below the neutron threshold of the compound nucleus, two-stage reactions following bombardment with high-energy projectiles are extremely useful. Reactions such as $(p,p'f)$, (t,pf), and, in particular, (d,pf) are all being used. Since the only competing process in the decay of the compound nuclear states at this energy is gamma-ray emission, fission can be measured sensitively far below the barrier energy. The chief requirement in these measurements is good energy resolution in defining the fissioning compound nucleus states. Photofission, with its comparative simplicity in spin and parity of the fissioning compound nucleus plays a special role in this field. All these experimental topics are covered in Sec. V. One of the most sensitive tools is decay after slow neutron absorption; this displays intermediate structure from which deductions are made about both the inner and outer barrier penetrabilities. The topic is treated in Sec. VI. But much information on barrier heights comes from the study of cross sections with energy resolution that is insufficient to resolve intermediate structure, but covers a range of excitation from deep sub-barrier energies to well above the barrier. Understanding the influence shell effects exert in defining the shape and the total energy of the nucleus as it proceeds towards fission has also led to the recognition that the saddle points of the two-humped barrier may have a lower symmetry and consequently a higher density of transition states

than expected from liquid drop theory. This affects the magnitude as well as the shape of the fission cross-section curves. These aspects are explored in Sec. VII. The barrier data from all these different methods are collected and summarized, nucleus by nucleus, in Sec. VIII, where a comparison with theoretical calculations of the double-humped barrier is made. The level structure of rotational and intrinsic excitations built on the isomeric shape is reviewed in Sec. IX. The question of more highly complex barriers than the two-humped one is reviewed in Sec. X in the light of recent experimental advances; and Sec. XI finally summarizes the main points. In the appendix the most commonly used parametrizations of deformed shapes are reviewed.

II. SUMMARY OF BARRIER THEORY

A. Potential energy surfaces

The primary preoccupation of fission theory is the determination of the potential energy surface in the space of the various collective coordinates defining the shape of a deforming nucleus. Efforts to do this still use the liquid drop model as the starting point. Myers and Swiatecki's (1966) first attempts to improve the liquid drop theory were followed by Strutinsky's (1967ab) which represented a breakthrough by developing a more fundamental way of calculating the shell effects, thus enabling the theory to be extrapolated to large deformations.

The basis of Strutinsky's method of calculating nuclear energies, either as a function of nuclear mass or as a function of deformation, is now well known. Very briefly outlined it is this: in a pure independent-particle shell model, neutrons and protons fill the levels of a deformed potential well up to a certain level, the Fermi energy, corresponding to the particular nucleus of interest. The energies of the filled levels are then summed to give the nuclear ground-state energy at the chosen deformation of the well. It is well known, of course, that because of the residual interactions, and hence the correlated motions, among the nucleons, which cannot be described in the framework of a simple potential well model, this is a quite inaccurate procedure for extracting the absolute energy of a real nucleus. For this the liquid drop model with semi-empirically adjusted parameters gives much more realistic estimates of the nuclear binding energies, within 15 MeV or so at worst relative to binding energies of hundreds of MeV over the whole periodic table; but it does not give any of the correlations with nuclear shell closures that appear in the observed binding energies.

Strutinsky's way of obtaining accurate estimates of absolute nuclear energies is to hypothesize that summing the single-particle state energies as shown in the left half of Fig. 8 will reproduce the relative change in energy from nucleus to nucleus due to the shell structure at a given deformation. To obtain this change, denoted by E_{shell}, it is only necessary to subtract from the independent-particle energy a similar sum calculated from the independent particle levels smeared out in some way to remove the shell structure, as illustrated schematically in the right half of Fig. 8. The gross

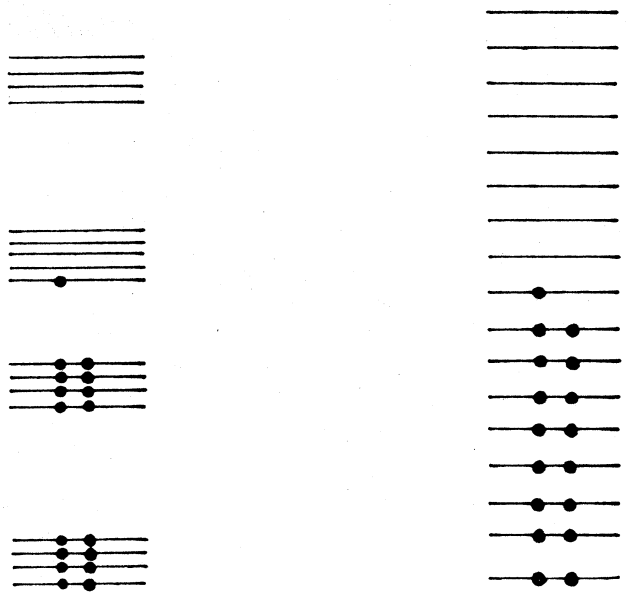

FIG. 8. Schematic diagram of Strutinsky shell-correction method illustrating the difference between bunched energy levels and a smooth level ordering. In practical calculations actual energy levels are used.

energy that is thus removed is then replaced by a realistic energy term calculated from the liquid drop model E_{LDM}. Thus,

$$E = E_{\text{LDM}} + E_{\text{shell}} . \tag{2.1}$$

Strutinsky's method when applied to the broad mass of nuclei with the energy minimized as a function of deformation for every nucleus, was immediately successful in reproducing accurately the nuclear binding energies. Furthermore, when the energy was calculated as a function of extended deformation for the actinide nuclei, in order to calculate fission barrier heights to compare with observation, he discovered a secondary dip (Fig. 9 and Figs. 5 and 46) in the energy at deformations corresponding roughly to the traditional liquid drop saddle shape. It is now recognized that this deformation corresponds to a spheroidal shape with a ratio of major to minor axes of 2:1. This symmetry gives rise to considerable shell structure and hence great stability for particular nuclei with the appropriate neutron and proton numbers, in analogy with spherical potential wells (see Fig. 10). The dip, or secondary well, offered an explanation for the spontaneously fissioning isomers that had been known for a few years, and for the phenomena of intermediate structure in fission cross sections that were being discovered about that time. Strutinsky's theory therefore immediately became spectacularly successful.

Since then great efforts have been put into the calculation of potential energy surfaces as a function of deformation. Some of these have been devoted to studying the possibility of new metastable shapes among the lighter nuclei, and to the estimation of the stability of superheavy nuclei with respect to alpha, beta, and fission decay.

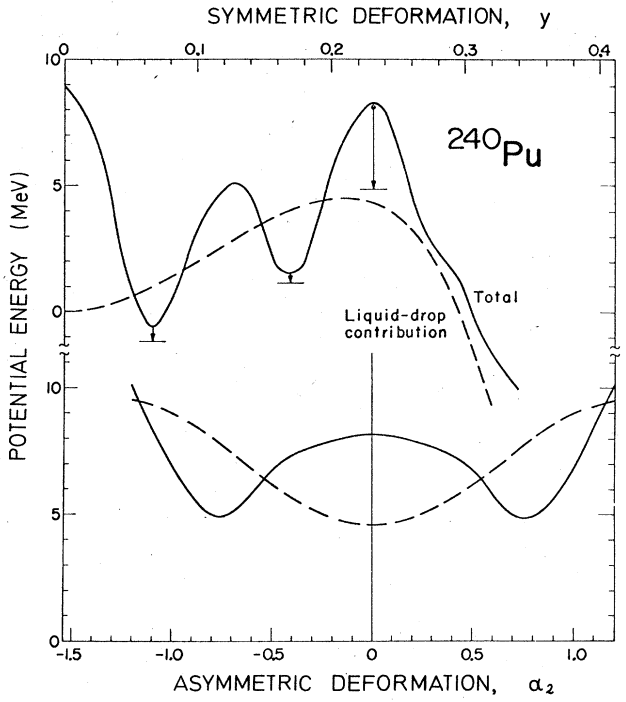

FIG. 9. Above: Nuclear energy calculated as a function of deformation for axial and reflection symmetric shapes for ^{240}Pu using Strutinsky's prescription. Arrow on outer barrier B at elongation $y = 0.23$ gives lowering of barrier calculated from reflection asymmetric deformations. This is illustrated below where the energy as a function of the mass asymmetry parameter α_z for a fixed elongation $y = 0.23$ is given. Dashed line indicates the liquid drop deformation energy. Calculation from Nix (1972).

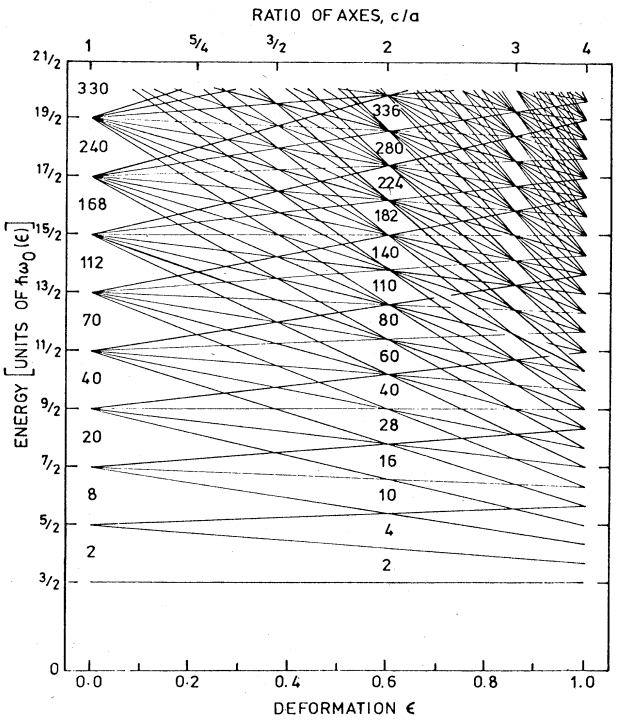

FIG. 10. Energy levels of a harmonic oscillator potential for prolate spheroidal deformations. Numbers in diagram are numbers of particles filling the shell. From Nix (1972).

1. The barrier region

a. Basis and technical treatment of Strutinsky theory

The justification of the Strutinsky method for determining nuclear energies, the technical method for carrying it out, and the physical nature of the results have been reviewed in detail by Brack *et al.* (1972). Another comprehensive review containing less detail but also with a complete bibliography has been written by Nix (1972).

Basic justifications of the Strutinsky method start from the Hartree–Fock theory. Brack *et al.* (1972) show how the expression for the energy of a nucleus in Hartree–Fock theory, in which the single-particle potential is self-consistent with the single-particle density matrix generated by that potential, can be written in terms of shell-model single-particle energies and densities to second order in the difference between the shell-model and the self-consistent densities. The significant feature of the new expression for the Hartree–Fock energy is that apart from the simple sum over occupied shell-model levels, the remaining principal term is expressed in terms of *averaged* single-particle densities, and is therefore smooth in its dependence on nucleon numbers and nuclear shape. It is this smooth term plus a smooth component extracted from the sum over occupied single-particle levels that is replaced by a liquid drop expression for the energy E_{LDM}. The most recent review of the Hartree–Fock method is due to Brack (1980).

Most of the methods for extracting the smooth component from the sum of occupied energy levels are based on Strutinsky's own technical procedures for averaging over the shell-model energy levels with a suitable weighting function. This weighting function can be expressed as sums of products of Gaussians and Hermite polynomials, the width of the Gaussian being governed mainly by the energy spacing between major shells just below the Fermi energy. Such averaging procedures can run into conceptual if not practical difficulties if the shell-model potential is a realistic one permitting a continuum of unbound eigenstates, like the Woods–Saxon potential for instance. Bengtsson (1974) has therefore initiated a method in which each individual shell-model level as a function of deformation is smoothed by fitting it with the cube root of a fourth-order polynomial in the deformation parameter; this particular form of the fitting function is suggested by the Thomas–Fermi statistical model. The smooth component of the sum of occupied energy levels is then simply given by the sum of the occupied smoothed energy levels resulting from this fitting procedure, and the unbound levels thus require no consideration. The shell correction energy E_{shell} thus defined for neutrons in ^{238}Pu is shown in Fig. 11 in comparison with the result from the same set of shell-model levels using the Strutinsky procedure. The overall agreement, especially for prolate deformations in which we are most interested in fission theory, is seen to be remarkably good, although local differences of up to 1 MeV can occur.

b. Comparison with Hartree-Fock calculations

Apart from work on the justification of the Strutinsky theory in a basic way, there have been attempts to calculate nuclear deformation energies directly from Hartree–Fock theory. These employ the Skyrme effective nucleon-nucleon interaction (Skyrme, 1956) with parameters adjusted to reproduce gross nuclear properties, as given by Vautherin and Brink (1972). The result of the work of Flocard *et al.* (1974) showing the binding energy for ^{240}Pu as a function of the quadrupole moment of the nucleon density is presented in Fig. 12. No allowance is made for axial asymmetry or reflection asymmetry in the nuclear shape in this calculation. It looks qualitatively very similar to the deformation energy curves that result from calculations using the Strutinsky method, but the energy differences between the extrema are greater. For example, the first barrier height (v_A) is at about 9 MeV relative to the primary well depth (v_I), whereas Strutinsky calculations with a similar restriction on the range of nuclear shapes explored would give about 6 MeV for this quantity. There are recognized sources of error in the present Hartree–Fock calculation, however, that approach the order of 1 MeV; they arise from the necessity to project out the O^+ ground state from the calculated state with no constraint on angular momentum, and from the truncation of the harmonic oscillator basis states used in the numerical work. At large deformations, all calculations based on the assumption of axial and reflection symmetry give too high barriers. This difficulty is not restricted to the Hartree–Fock approach.

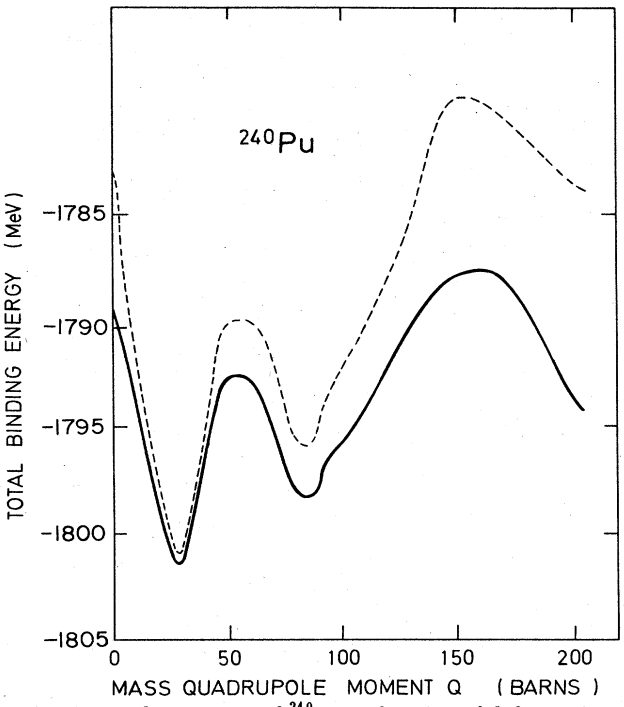

FIG. 12. Binding energy of ^{240}Pu as function of deformation (the parameter Q is the quadrupole moment of the matter density; see Appendix) calculated with a Hartree–Fock method due to Vautherin and Brink (1972). Dashed and solid curves correspond to pairing-interaction strength independent of nuclear surface area and proportional to surface area respectively. From Flocard *et al.* (1974).

c. Nuclear models employed in Strutinsky calculations

Apart from the possible source of error arising from the actual principle of the Strutinsky theory and possible errors from the technical treatment of smoothing procedures, the basic parametrizations of the models used in the theory contain uncertainties that will give rise to errors in calculations based on the theory. The main source of this kind of error is likely to come from the liquid drop model, which provides the basic (or macroscopic) energy term in the Strutinsky theory, but there are also likely to be significant uncertainties from the shell model adopted, and smaller errors from the treatment of the pairing interaction, which is shell dependent and is also incorporated into the Strutinsky theory. This last term depends not only on the choice of shell model but also on the hypothesis assumed for the dependence of the interaction strength on surface area. Note, in this connection, that virtually all calculations with the Strutinsky method have been made for even nuclei.

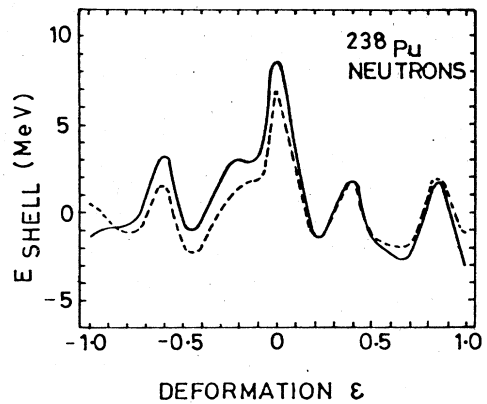

FIG. 11. Comparison of two different technical procedures for calculating the Strutinsky shell-correction energy from the same set of shell-model levels. The solid curve is calculated using the normal energy-averaging procedure for every specific deformation. The dashed curve is from the summing of smoothed energy levels fitted to the actual shell model levels over a large range of deformation. From Bengtsson (1974).

(i) Liquid drop and droplet models. The nuclear energy in the basic liquid drop model of the nucleus is characterized by a volume term proportional to the mass number A, a surface energy term proportional to the surface area, and hence to $A^{2/3}$ for a spherical nucleus, and a Coulomb energy term, proportional to $A^{-1/3}$ for a spherical nucleus:

$$E_{\rm LD} = -c_1 A + c_2 A^{2/3} f(\text{shape}) + \frac{3}{5}\frac{e^2 Z^2}{r_0 A^{1/3}} g(\text{shape}) \quad (2.2)$$

[cf. Eqs. (1.1)–(1.3 and 1.12)]. So far as the fission barrier is concerned, the important terms in Eq. (2.2) are the surface energy and Coulomb energy terms, and the sum of their contributions to the liquid drop energy relative to the energy of a spherical liquid drop can be written as

$$E_{\rm LD}(\text{shape}) - E_{\rm LD}(0) = \{[f(\text{shape}) - 1] + 2X[g(\text{shape}) - 1]\} E_s(0), \quad (2.3)$$

where $E_s(0)$, the surface energy of a spherical liquid drop, is $c_2 A^{2/3}$ and X, the fissility parameter, is defined as the ratio of the Coulomb energy of a spherical drop to $2E_s(0)$:

$$X = \left(\frac{3}{5}\right)\left(\frac{e^2}{r_0}\right) \cdot \frac{(Z^2/A)}{2a_2\left[1 - \kappa\left(\frac{N-Z}{A}\right)^2\right]} . \quad (2.4)$$

The fissility parameter and hence the values of the coefficients a_2 and κ, are crucial in determining the shape dependence of the liquid drop energy and therefore of fission barriers. These coefficients have to be determined empirically from an overall fit to nuclear binding energies and, where possible, to experimental fission barriers. For reliable determination of the coefficients, Eq. (2.2) is too crude as it stands, and it is recognized that in that formula the volume and surface terms are only the leading terms of a systematic expansion of the binding energy of a finite body with a relatively thin surface region in which the matter density falls to zero. The ratio of surface diffuseness to nuclear radius is of order $A^{-1/3}$, so a refinement of Eq. (2.2) takes the expansion to higher powers in $A^{-1/3}$. This is the droplet model of Myers and Swiatecki (1969). In this model, terms in $A^{1/3}$ are associated with energy of curvature of the surface and redistribution of Coulomb energy in the surface, and other terms are associated with the compressibility of nuclear matter. The many parameters involved are determined partly from fitting to experimental data and partly from statistical calculations based on Thomas–Fermi theory; fitting to experimental data has to take account of shell effects both in ground-state masses and in fission barriers, and this is generally done in the empirical way outlined by Myers and Swiatecki (1966, 1967). Values of the liquid drop (or droplet) coefficients actually used for calculations of fission barriers by the Strutinsky method vary. One common set is that due to Myers and Swiatecki (1967) (liquid drop model):

$$r_0 = 1.2249 \text{ fm},$$

giving

$$\tfrac{3}{5}(e^2/r_0) = 0.7053 \text{ MeV},$$

$$a_2 = 17.9439 \text{ MeV}, \quad \kappa = 1.7826 . \quad (2.5)$$

Another set coming into vogue is derived from a redetermination of droplet model coefficients by Myers (1977); from these an equivalent set of liquid drop coefficients can be determined, among which an effective neutron-proton asymmetry coefficient $\kappa_{\rm eff}$ turns out to have a value of about 3.4. These changes imply a general lowering of the fission barriers. At the same time the large effective κ value causes barrier heights to decrease with increasing neutron number (and fixed Z value) for nuclei situated in a broad interval near beta stability, as opposed to barriers calculated from a κ value of 1.78 [Eq. (2.5)], which increase when neutrons are added. The precise value of the surface neutron-proton asymmetry coefficient is probably the main uncertainty arising from the liquid drop or the droplet model in calculating fission barrier heights. Of course, all parameters are highly correlated.

(ii) Shell models. There is wide variety in the choice of shell model for calculating the shell-correction energy entering fission barrier calculations. Strutinsky's own calculations (1967) employed a deformed Woods–Saxon potential which has the advantage of physical realism for nuclear shapes that are not too strongly deformed. The potential is defined so as to have a constant skin thickness about an effective surface defining the shape. Figure 13 shows the landscapes of independent proton and neutron shell corrections as functions of nucleon number (Z or N, respectively) and elongation c. The diagram is based on the Woods–Saxon potential (Brack *et al.*, 1972). Such a potential encounters difficulties for strongly necked-in shapes, and here a variation suggested by physical notions of the effect of finite range nucleon forces has advantages; this is the diffuse-surface potential obtained by folding a Yukawa function with a square-well potential of the nuclear shape required (Bolsterli *et al.*, 1972):

$$V(\mathbf{r}) = -\frac{V_0}{4\pi a^3}\int_\tau d^3r' \frac{\exp[-|\mathbf{r}-\mathbf{r}'|/a]}{|\mathbf{r}-\mathbf{r}'|/a} , \quad (2.6)$$

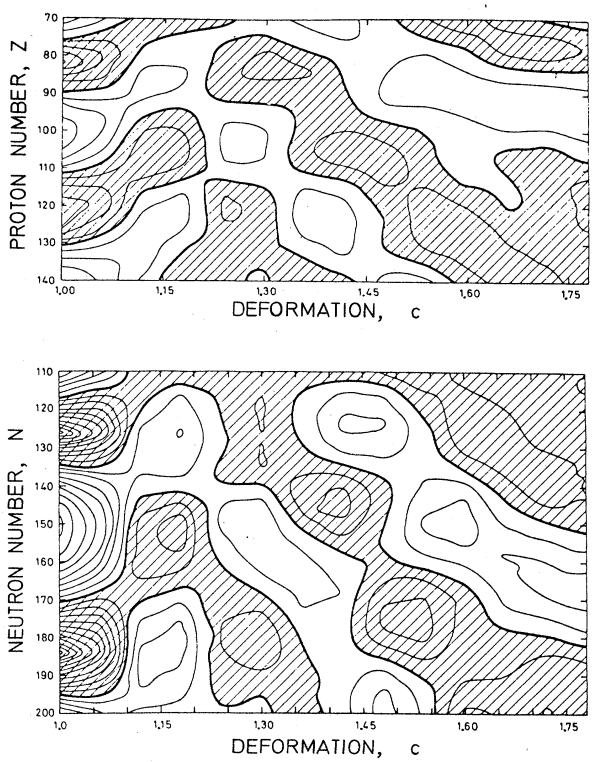

FIG. 13. Contour maps of the shell energy correction for protons and neutrons, respectively. The Woods–Saxon potential parameters used are those appropriate for ^{240}Pu. The thick curves are zero energy lines and the increment per line is 1 MeV. The shaded areas have negative values. The deformation parameter (see Appendix), $c = 1$, corresponds to a sphere; the isomeric minimum occurs for $c = 1.42$ and neutron number $N = 144$. From Brack *et al.* (1972).

where V_0 is the square well depth. The range a of the Yukawa function can be chosen to give the desired surface diffuseness. Parameters of such potentials are generally chosen to reproduce a given set of experimental data on single particle levels. Nix and his collaborators chose to fit their potential to the levels of ^{208}Pb in their earlier calculations (Bolsterli *et al.*, 1972), but in a later set Möller and Nix (1974) have adjusted their parameters to fit the levels of heavy deformed actinide nuclei. The difference in the two sets of potential well parameters amounts to about 11% in the surface diffuseness parameter (smaller in the 1974 version) and 12% and 6% in the neutron and proton spin-orbit interaction (greater in the 1974 version).

The other class of shell-model potentials in common use is based on the harmonic oscillator. In general these have distinct computational advantages and permit the exploration of a greater variety of nuclear shapes. Calculations of the potential energy landscape in the region of the barrier are generally performed within the framework of the one-center modified oscillator model (Nilsson model) with the shell-model potential having, typically, the following form:

$$V = V_{\rm osc} + V_{\rm corr} , \tag{2.7}$$

$$V_{\rm osc} = \frac{1}{2}\hbar\omega_0\rho^2\left[1 - \frac{2}{3}\epsilon\left(\frac{4\pi}{5}\right)^{1/2} Y_{20}\cdot\cos\gamma + 2\epsilon_4 P_4 + \frac{2}{3}\epsilon\left(\frac{4\pi}{5}\right)^{1/2}\frac{\sin\gamma}{(2)^{1/2}}(Y_{22}+Y_{2-2})\right], \tag{2.7a}$$

$$V_{\rm corr} = -k\cdot\hbar\mathring{\omega}_0[2\mathbf{l}_t\cdot\mathbf{s} + \mu(\mathbf{l}_t^2 - \langle\mathbf{l}_t^2\rangle)] . \tag{2.7b}$$

The correction term, depending principally on the square of the orbital angular momentum $\mathbf{l}_t$, has the effect of flattening the potential towards its outer edges and also contains a spin-orbit interaction. The parameters k and μ are adjustable for optimal reproduction of experimental single-particle level schemes. The variable ρ is the radius vector length in "stretched" coordinates and is defined by

$$\rho^2 = \frac{M}{\hbar}(\omega_x x^2 + \omega_y y^2 + \omega_z z^2) . \tag{2.8}$$

The oscillator frequencies for the principal ellipsoidal axes are related to the parameter ω_0 (itself governed by the shape parameters ϵ, ϵ_4, and γ) through the relations

$$\omega_x = \omega_0[1 - \tfrac{2}{3}\epsilon\cdot\cos(\gamma + 2\pi/3)] ,$$
$$\omega_y = \omega_0[1 - \tfrac{2}{3}\epsilon\cdot\cos(\gamma - 2\pi/3)] ,$$
$$\omega_z = \omega_0[1 - \tfrac{2}{3}\epsilon\cdot\cos\gamma] ,$$

and ω_0 is related to the spherical oscillator frequency $\mathring{\omega}_0$ through a volume conservation condition. A typical numerical value adopted by Nilsson *et al.* (1969) for the last parameter is

$$\hbar\mathring{\omega}_0 = \frac{41.0}{A^{1/3}}\left(1 \pm \frac{1}{3}\frac{N-Z}{A}\right), \tag{2.9}$$

the plus and minus signs referring to proton and neutron potentials, respectively.

The deformation parameters ϵ, ϵ_4, and γ refer to quadrupole deformation (nuclear elongation), hexadecapole deformation (waistline "necking-in" or broadening) and degree of axial asymmetry, respectively. The parameter γ is generally treated through its range of values 0 to 60°, 0° representing axial symmetry of a prolate body, and 60° the opposite extreme of axial symmetry of an oblate body. Other degrees of freedom in the shape can be introduced within this framework, still allowing practical computation, and two such important parameters are the deformations associated with the third and fifth Legendre polynomials; these parameters allow the description of a pearlike asymmetry in the nuclear shape, often referred to as mass or volume asymmetry. Apart from these parameters to describe deformed nuclear shapes many other parameters have been employed by other authors. The relationships amongst the commoner of these is described in the Appendix.

More sophisticated shell-model effects can be incorporated within the Strutinsky theory. One of these is a shell-correction term to the Coulomb energy due to Larsson *et al.* (1974), which is normally computed simply as a liquid drop term with uniform charge density over the nucleus. For this, the Coulomb repulsion energy is calculated directly from the single-particle wave functions; the proton densities arising from these can change sharply with changing deformation giving rise to changes in the occupation of single-particle levels near the Fermi energy with very different radial and angular distributions.

The treatment of pairing correlation energies also gives room for elaborations. One of these is the dependence of the pairing interaction strength on surface area, as already mentioned. Another is the introduction of the quadrupole pairing force (Larsson *et al.*, 1974). This arises from the well-known expansion of a delta force in terms of spherical harmonics,

$$\delta(\mathbf{r}_1 - \mathbf{r}_2) = \frac{\delta(r_1 - r_2)}{r_1 r_2}\sum_{\lambda\mu} Y_{\lambda\mu}(1)Y_{\lambda\mu}(2) , \tag{2.10}$$

with only terms in $\lambda = 0,2$, $\mu = 0$ being retained.

d. Results of calculations

(i) Inner barrier. The shell correction as a function of deformation is obviously correlated with the local density of single-particle levels in the shell model around the highest occupied level, the Fermi energy. High single-particle densities give rise to a positive shell correction (less stability) and vice versa. An oscillating shell correction superimposed on the liquid drop saddle region gives rise to the double-humped barrier. Variation of the shell-correction amplitude or phase with changing proton and neutron number, together with the variation of the liquid drop potential barrier with changing fissility parameter, gives rise to variation of the double-humped barrier from nucleus to nucleus. The contribution to the shell correction from the pairing correlation effect is opposite in sign, being negative at high single-particle densities, but is much smaller in magnitude than the main shell effect.

The phrase "double-humped barrier" expresses the main feature of the potential energy of deformation of heavy nuclei as a function of elongation of the nucleus

towards fission. Early calculations assumed a maximum degree of symmetry in the shape in the course of this elongation. Pashkevich (1969) first investigated the potential energy as a function of axial asymmetry along this path and noted that the secondary well in the barrier was stable with respect to this asymmetry. This work and later work by Larsson *et al.* (1972), Schultheiss and Schultheiss (1971), and Larsson and Leander (1974) all concentrated on investigating the potential energy surface in the plane of elongation and the γ degree of freedom, and has established in general that the nucleus may have axial asymmetry at the first saddle point (A) but regains axial symmetry at the secondary well (II). Typical results of Larsson and Leander (1974) are shown in Fig. 14. For ^{236}Th the inner barrier occurs at a value of $\gamma \approx 10^\circ$ but the potential energy on the axially symmetric path is only ~0.4 MeV higher than the saddle; whereas for ^{250}Cm the barrier energy drop at an axial asymmetry $\gamma \approx 17^\circ$ is a substantial 1.8 MeV. There is a trend for increasing stability of axially asymmetric shape at the inner barrier both with increasing neutron number and increasing mass number as shown in Fig. 15. As far as the actual magnitudes of the barrier heights are concerned, the axially asymmetric values of Fig. 15 tend to be a little lower in general (on average ~0.5 MeV) than experimental data (see Secs. VII and VIII), after making allowance for zero-point β-vibration energy of the ground state. For the Th nuclei they are considerably lower, but there may be special reasons in theory and interpretation of experimental data for this [see (*ii*) below]. For each element the trend of the calculated value with neutron number is gently peaked at $N \approx 150$.

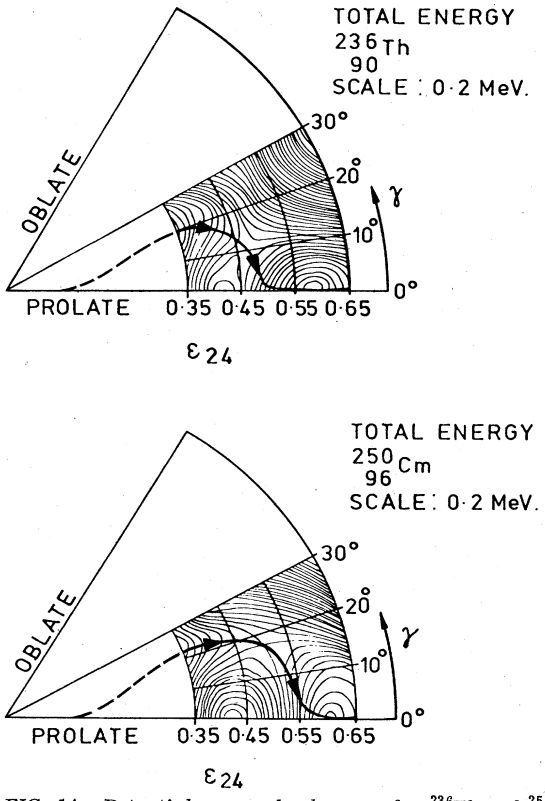

FIG. 14. Potential energy landscapes for ^{236}Th and ^{250}Cm. The plane is one of nuclear elongation (ϵ) versus axial asymmetry (γ); see Appendix. The nuclear shape is chosen so that the energy is minimized as a function of the hexadecapole deformation parameter ϵ_4. Energy contours are at intervals of 0.2 MeV. The heavy solid line with arrows follows roughly the track of minimum potential energy with increasing elongation through barrier *A* and secondary well II. From Larsson and Leander (1974).

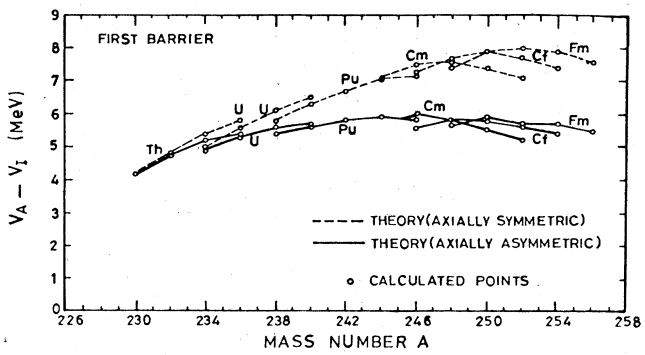

FIG. 15. Inner barrier height as calculated from Strutinsky theory with a modified harmonic oscillator shell model with and without the axial asymmetry degree of freedom. Pairing interaction strength was assumed proportional to surface area, and the liquid drop neutron-proton asymmetry constant $\kappa = 1.78$. From Larsson and Leander (1974).

The agreement of this kind of calculation with data seems to be improved if the quadrupole pairing interaction is included (Larsson *et al.*, 1974), particularly for Th nuclei, for which the inner barrier is raised by about 1 MeV. For Pu nuclei quadrupole pairing raises the inner barrier by about 0.5 MeV. It should be noted that in these calculations the liquid drop energy has been refitted so that the calculation reproduces experimental data on the secondary well.

(ii) Secondary well. Calculations on the energy of the second minimum relative to that of the first minimum, this time due to Möller and Nix (1974) (using still the modified harmonic oscillator shell-model potential), are shown in Fig. 16. In general these energies are in the range 2–3 MeV and agree with available experimental data on spontaneously fissioning isomers to this extent (see Secs. IV and VIII for experimental data). However, interpretation of experimental fission cross-section data on Th isotopes [see, for example, James *et al.* (1972) and discussion in Sec. V] indicates that the secondary well is higher than 4 MeV for these light nuclei and so disagrees with the trends of the calculation.

The overall trend of the curves in Fig. 16 (with a minimum about $N \approx 144$ and a peak about $N \approx 152$) is also given by calculations using the folded Yukawa model of Möller and Nix (1974). However, there are discrepancies in absolute value of up to ~0.5 MeV between the two sets of calculations, changing in sign between Th and Fm. More recent calculations based on single-particle diagrams of the type shown on Fig. 23 tend to locate the second shell minimum at neutron number $N = 148$.

(iii) Outer barrier. Early calculations in which the nuclear shape was assumed axially and reflection symmetric indicated that the outer barrier was higher than

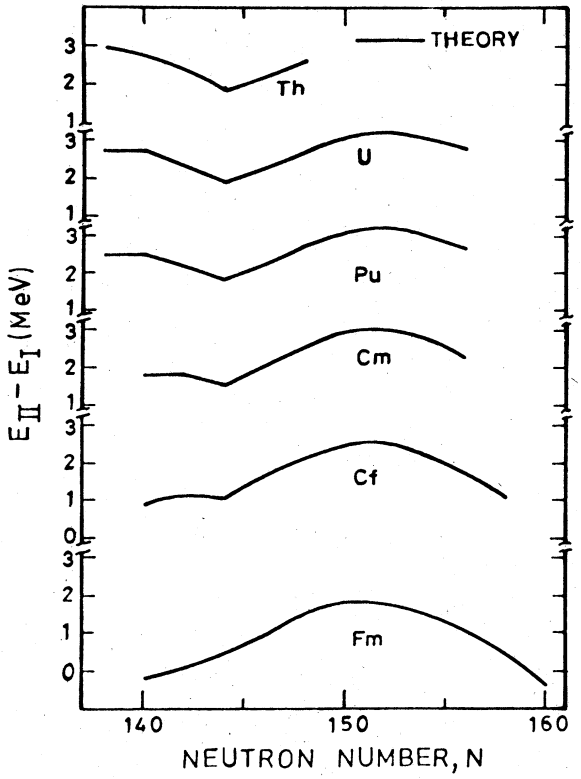

FIG. 16. Calculated energy of second minimum using Strutinsky theory with modified harmonic oscillator shell-model potential. The liquid drop neutron-proton asymmetry constant $\kappa = 2.8$. From Möller and Nix (1974).

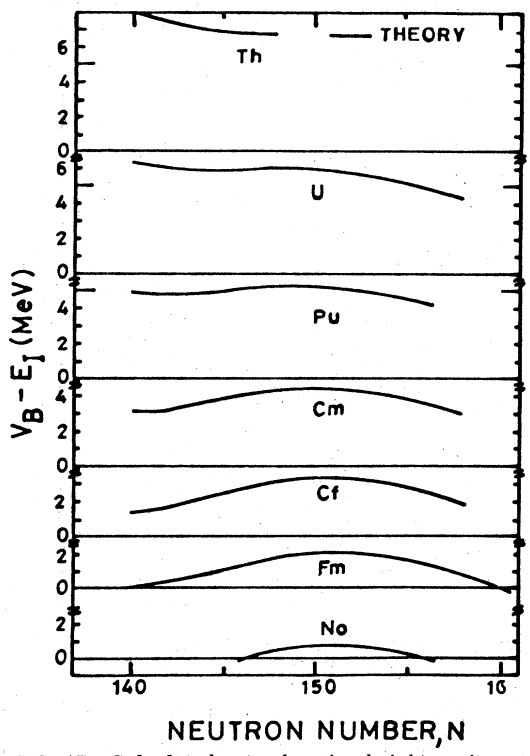

FIG. 17. Calculated outer barrier heights using modified harmonic oscillator shell-model potential. From Möller and Nix (1974).

the inner one in the actinides by some 3–4 MeV (see Fig. 9). Experimental data on spontaneous fission isomer half-lives and excitation cross sections (discussed in Sec. IV) and intermediate structure in fission cross sections (see Sec. VI) refuted this; indeed, analysis of data on plutonium and heavier nuclei suggested that experimentally the outer barrier is the lower. The discrepancy was removed at least qualitatively by the calculations of Möller and Nilsson (1970) and by Möller (1972) demonstrating that reflection asymmetry in the nuclear shape (included in the shell-model potential as third- and fifth-order Legendre polynomials) gave potential energy minima at the elongations corresponding to the outer barrier. There is no calculational evidence for axial asymmetry also existing at the outer barrier. Indeed, the existence of pronounced changes with energy of the angular distributions of fission products is held to be evidence against axial asymmetry.

More recent calculated values of the outer barrier height due to Möller and Nix (1974) are shown in Fig. 17. The curves for individual elements do not show marked structure or trends except for the highest elements, but there is a strongly falling tendency with increasing nuclear charge, which is borne out by experimental data on fission isomer excitation yields. These calculations employ a modified harmonic-oscillator shell-model potential, and they show discrepancies of up to ~1 MeV (changing sign in going from Th to Fm) with calculations based on a folded Yukawa potential [Eq. (2.6)].

The calculations based on the folded Yukawa shell-model potential show a new feature in the potential energy curve in the second barrier region; this is a tendency in the low Z, moderate N nuclei for the outer barrier to be further split into two subsidiary peaks with a shallow minimum between them (see Fig. 18). If this is a real physical effect it will explain experimental fission data on Th isotopes which demand an interpretation involving a double barrier with a very shallow well between them (further discussion is found in Secs. V, IX, and X).

(iv) Probable accuracy of quantitative calculations on fission barrier parameters. In Table I the theoretical results on fission barriers for three specific nuclei are compared. These nuclei are quite central to the nuclear stability line and to the actinide group of elements and therefore ought to provide reasonable tests for theoretical calculation. Some of the differences in the numbers are due to very significant differences in the physics assumed, e.g., degree of asymmetry in shape allowed. Even where sets of numbers should be comparable, because differences are confined to the choice of shell model, as in rows 1 and 3 (columns 3–5) or rows 1 and 2 (column 6) differences of the order of 1 MeV in the estimated quantity occur. This can probably be taken as a measure of the accuracy of the theory at the present time. This statement is supported by a comparison of the measured nuclear ground-state masses of the actinides and lower nuclei with the values calculated by Möller and Nix (1974) using the folded Yukawa shell model within the Strutinsky theory; the

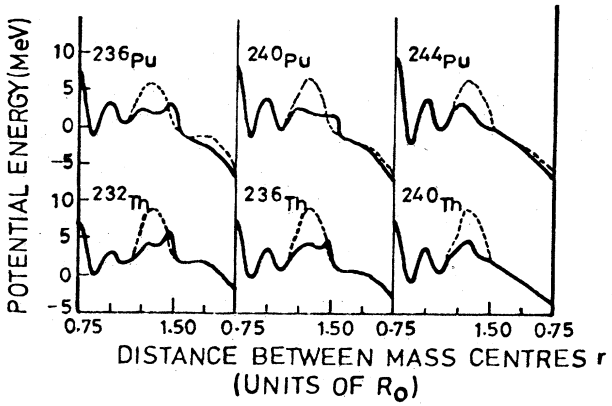

FIG. 18. Calculated fission barrier potential energy curves, using folded Yukawa shell-model potential. From Möller and Nix (1974). The dashed curves assume reflection symmetry in the nuclear shape, but the solid curves allow for minimization of the potential with respect to reflection asymmetry.

average discrepancy is about zero, but there are systematic trends of the discrepancy curves as a function of neutron number, the trends having a slope of ~0.25 MeV per neutron pair (compare Fig. 138). The accuracy of the theory is extremely good when set against the nuclear binding energies of nearly 2000 MeV, but they are not accurate enough to supply on their own the relevant barrier parameters for calculation of nuclear cross sections required by technology, for instance.

2. Potential energy between saddle and scission

The point to emerge from the theoretical calculations of the kind described above in Sec. II.A.1.d.iii, that the saddle point at the outer barrier of actinide nuclei occurs for reflection asymmetric nuclear shapes, invites the speculation that this is the reason for mass asymmetry in the final mass division of these nuclei. Much work has been done on this point, and forms one of the most interesting further developments based on the shell-correction method, leading towards an apparent solution of the formerly intractable problem of mass asymmetry in fission. In broad terms, the theoretical work has concentrated on mapping out the energy surface well beyond the outer saddle point and well down the slope towards the scission point where the two incipient fission fragments finally part company. By contrast with the region of deformation up to the outer saddle point, this region is a hazy, ill understood area from the overall point of view including the dynamical effects. The whole question of nuclear viscosity arises here in a very important way. There is a general feeling that viscosity must act selectively. Some quantities seem to be frozen in at the saddle point, e.g., the pro-

TABLE I. Comparative results on fission barrier heights from a range of calculations. The barrier heights are quoted in MeV relative to the primary minimum of the potential energy curve. For comparison with experimental data (normally quoted relative to the nuclear ground state) a zero-point beta-vibration energy should be subtracted from these numbers.

Reference	Remarks on calculation	U_A (^{240}Pu)	U_A (^{244}Pu)	U_A (^{232}Th)	U_B (^{232}Th)
Möller and Nix (1974)	Folded Yukawa shell model. No axial asymmetry in deformation but reflection asymmetry allowed	5.45	6.3	2.9	5.7
Möller and Nix (1974)	Modified harmonic oscillator shell model. No axial asymmetry but reflection asymmetry allowed	6.3	7.1	4.9	8.0
Larsson and Leander (1974)	Modified harmonic oscillator shell model. No axial asymmetry	6.3	7.1	4.7	
Larsson and Leander (1974)	Modified harmonic oscillator shell model. Axial asymmetry allowed	5.6	5.9	4.7	
Flocard *et al.* (1974)	Hartree–Fock calculation. No axial asymmetry or reflection asymmetry. Pairing interaction strength proportional to surface area	9.0			
Flocard *et al.* (1974)	Ditto, but pairing interaction strength constant	11.0			

jection of the nuclear spin on the major axis of deformation, thus determining the angular distributions of the fission fragments relative to some laboratory-based axis that is significant in the original formation of the excited fissioning nucleus. The finding of mass asymmetry in the energy surface at the outer barrier at first sight indicates that the broad trends of mass division in the final fission products may also be largely frozen in here. More detailed studies of the way in which mass yields in fission are determined indicate that the potential energy surface plays a crucial role in mass division. The important feature is not just the potential energy at the outer barrier but rather the potential energy landscape several MeV below the outer saddle point. This alone points to the fact that the dynamics of the problem must be of vital importance in controlling the mass division, as it is also for determining the spontaneous fission half-lives.

B. Dynamical considerations

The potential energy landscapes for deformation of the nucleus discussed in Sec. II.A.2 above provide the essential foundation for discussing the fission process and already suggest many of the most striking phenomena to be observed, but, with such complicated potential energy surfaces, and with the consideration that the nucleus is a microscopic body, strongly influenced by the motion of a single or a few nucleons, it is apparent that the dynamics of fission is still a major problem. For large deformations a description of the deformation in normal modes based on a Legendre polynomial expansion of the surface is not practicable; the alternative choices of suitable deformation parameters are arbitrary, guided by physical intuition, and as a result the inertial tensor can take a complicated nondiagonal form. The inertial tensor is strongly affected by single-particle and pairing effects as well as being a measure of "collective motion." In addition, the effects of "viscosity" in the nuclear motion play an important role. Many of the quantities observable in fission (e.g., cross sections at low energies, properties of spontaneously fissioning isomers) do not require a theory of viscosity for their explanations; these can be based on extensions of normal quantal ideas, including calculations of the inertial tensor.

The dynamical requirement of an expression for the kinetic energy in terms of generalized collective coordinates q_i

$$T=\tfrac{1}{2}\sum_{i,j} B_{ij}(q)\dot{q}_i\dot{q}_j \tag{2.11}$$

demands the knowledge of the inertial tensor as a function of the collective coordinates. This is the essential complement to the potential energy and can be either modeled according to hydrodynamic concepts (Nix, 1967) or can be computed microscopically from the same shell-model level schemes used to construct the shell correction to the potential energy in the Strutinsky method (compare Fig. 44). The classical liquid drop model is already sufficiently complex that straightforward analytical expressions for the inertia have not been derived except for very small deviations from a sphere, in which case the inertial parameter associated with the lowest normal mode (the quadrupole term in the spherical harmonic expansion of the surface) for irrotational flow is

$$B_\beta = 3MR_0^2/8\pi\,, \tag{2.12}$$

β being the coefficient for the second spherical harmonic Y_{20} in the expansion of the surface, M the nuclear mass, and R_0 the nuclear radius. For his studies of the later stages of fission towards the scission point Nix (1969) used the Werner–Wheeler numerical method, in which the internal hydrodynamic flow is approximated by the flow of circular layers of fluid perpendicular to the symmetry axis.

Phenomenological expressions for the inertia have also been employed; for example, if the fragment separation r is employed as the fission variable the asymptotic inertial parameter at large separations is the reduced mass of the fragments μ, while at the other extreme of small deformation it tends toward Eq. (2.12) for irrotational flow. A typical expression for B_{rr}, due to Randrup *et al.* (1973), is

$$B_{rr}=\{1+\tfrac{17}{15}k\exp[-(r-0.75R_0)/d]\}\mu\,, \tag{2.13}$$

where R_0 is the spherical nuclear radius, and k and d are parameters that describe deviations from the irrotational value (for irrotational flow $k=1, d=R_0/2.542$).

Microscopic calculations of the inertial tensor are normally based on the cranking model, originally developed by Inglis (1954) for calculation of nuclear moments of inertia, in which the independent particle or quasiparticle system is assumed to be driven in a specific form of collective motion by an external force, and the inertial parameter is determined from the generated kinetic energy and the collective velocity. Its application to fission was first developed by Sobiczewski *et al.* (1969b) and Damgaard *et al.* (1969). The cranking model expression involves virtual excitations from the ground state $|0\rangle$ of the deforming system to excited states $|m\rangle$:

$$B_{ij}=2\hbar^2\sum_{m\neq 0}\frac{\langle 0|\partial/\partial q_i|m\rangle\langle m|\partial/\partial q_j|0\rangle}{E_m-E_0}\,. \tag{2.14}$$

For a pure independent-particle system this expression, literally evaluated, contains singularities at single-particle level crossings. Within the shell-correction framework of the Strutinsky theory, however, pairing forces are included in the shell-model treatment; the resulting energy gap separating the ground state from other states removes these singularities and leads to an inertial tensor of reasonable physical magnitude. A simple statistical expression for the dependence of the inertia on the energy gap Δ and the density of single-particle states $g_{\rm eff}$ at the Fermi energy is developed by Damgaard *et al.* (1969):

$$B\sim\frac{\hbar^2}{2}\left|\frac{\partial H}{\partial q}\right|^2\frac{g_{\rm eff}}{\Delta^2}\,. \tag{2.15}$$

A typical detailed calculation of the inertia from the cranking model is shown in Fig. 19; this is due to Pauli and Ledergeber (1974). As to be expected from Eq. (2.15) it is correlated with the shell correction to the potential energy of deformation of the nucleus. The

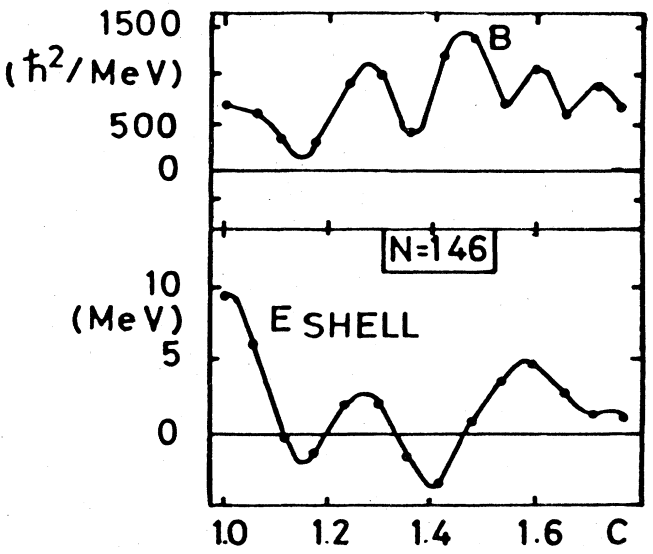

FIG. 19. Intertial parameter B_{cc} corresponding to the collective parameter for nuclear elongation c compared to the shell correction energy E_{shell}. From Pauli and Ledergerber (1974).

structure in the inertial parameter implies that the potential energy alone does not provide a simple guide to the dynamical motion of the system through deformation space. This is demonstrated by Pauli and Ledergeber's treatment of spontaneous fission half-lives. The half-life is proportional to the Gamow barrier tunneling factor

$$\tau \sim (1/\omega)\exp[2K/\hbar]$$

$$K = \int_{q_1}^{q_2} dq[2B_q|E - V(q)|]^{1/2}. \tag{2.16}$$

The integral K, the action integral, is calculated along a trajectory q through deformation space, defined to give the least value of K. The inertial parameter B_q for this trajectory is determined from the inertial tensor by

$$B_q = \sum_{i,j} B_{ij}(\partial q_i/\partial q)(\partial q_j/\partial q). \tag{2.17}$$

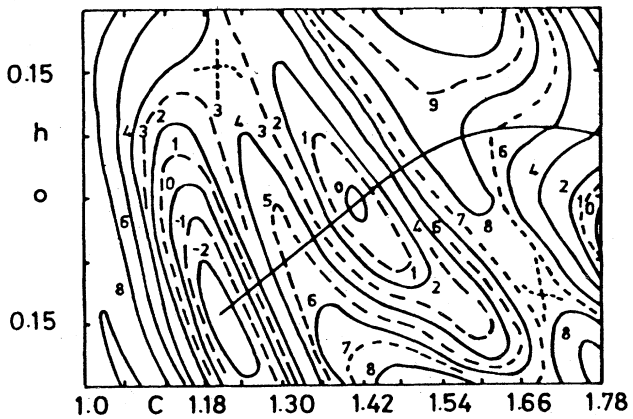

FIG. 20. Least action trajectory for ground-state spontaneous fission of ^{240}Pu through potential energy landscape in plane of elongation parameter c and neck constriction h. From Pauli Ledergerber (1974).

The trajectory calculated from this prescription for symmetric deformations in ^{240}Pu is shown in Fig. 20. It is apparent that the "dynamic" barrier for this trajectory is higher than the static barrier. Calculations of spontaneous fission half-lives of ground states using these calculations of the inertia and the least action principle give remarkably close agreement with data provided that the surface energy constant of the liquid drop model is suitably adjusted (see Fig. 21). This, as shown in the diagram, differs for different elements. Agreement is poorer (discrepancy up to 4 orders of magnitudes) if it is attempted to use a universal surface energy constant (see also Fig. 45). Half-lives of spontaneously fissioning isomers are shown in Fig. 22.

Pauli and Ledergeber suggest as a hypothesis that the least action trajectory determined for spontaneous fission should also be the path for near-barrier fission. This would have the attraction of explaining the high intermediate barriers observed for Th isotopes where the dynamic barriers are particularly high compared to the static barriers of Pauli (1974). It is nevertheless a very controversial idea and needs to be properly tested by a calculation of the development of the wave function over the barrier in a two- or few-dimensional deformation space.

C. Structure of shape isomers and related states

1. Single-particle states

The properties of the spontaneously fissioning isomers associated with the secondary well of the double-humped

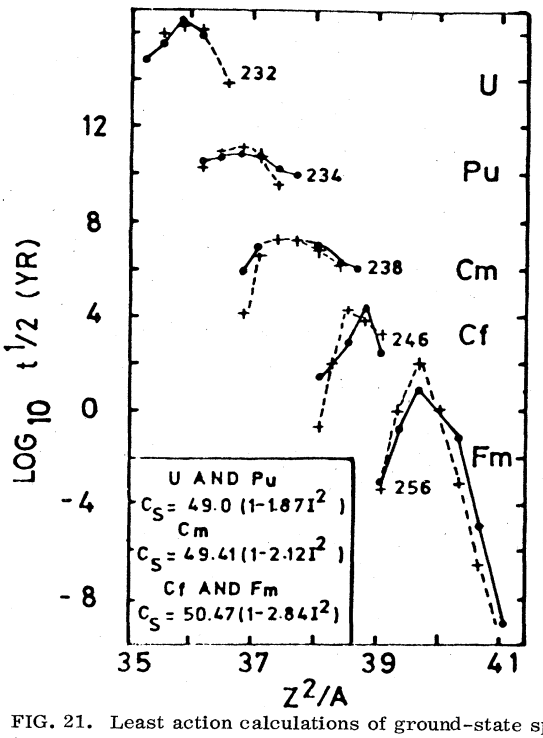

FIG. 21. Least action calculations of ground-state spontaneous fission half-lives with optimized adjustments of surface energy constants for different groups of elements. From Pauli and Ledergerber (1974). Points are from theory, crosses from experiment.

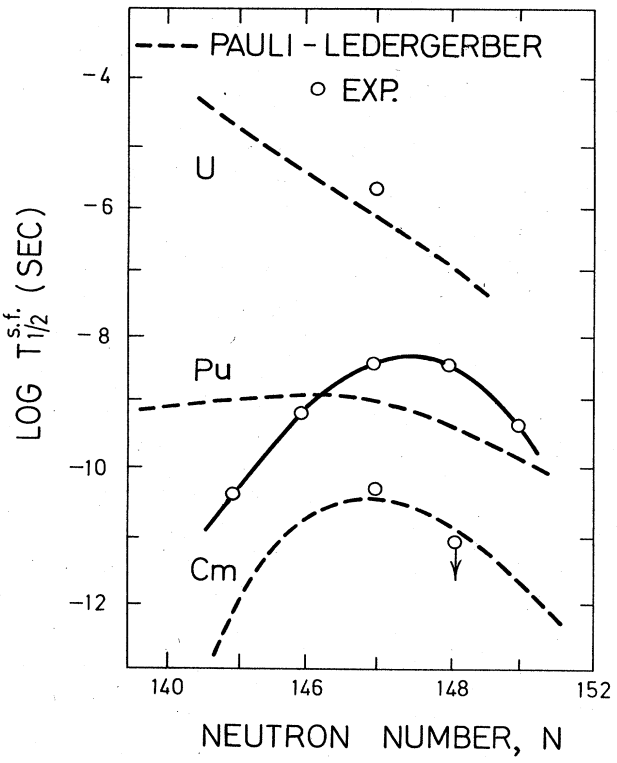

FIG. 22. Least action calculation spontaneously fissioning isomer half-lives. From Pauli and Ledergerber (1974).

barrier can be discussed by means of fairly standard nuclear models. The single-particle character of low-lying states associated with the secondary well can be obtained by extensions of Nilsson diagrams to the greater deformations, as already calculated for the purpose of forming the nuclear potential deformation energy in the Strutinsky theory. A set of single-particle diagrams for the extended deformation at the second minimum is shown in Fig. 23; this has been compiled by Metag (1979) from computations of various authors. Data on highly deformed single-particle levels in odd-A isomers that can be tested against the predictions of such diagrams are already available; see Sec. IX.

2. Rotational bands

The deformed shell-model level schemes can also be used to determine the moment of inertia of the rotational bands associated with the spontaneously fissioning isomers. Generally, the cranking model of Inglis (1954) is used for these calculations, and the pairing force is included. A typical calculation on ^{240}Pu, due to Pauli and Ledergerber (1974) is shown in Fig. 24. It is very similar to a calculation by Sobiczewski *et al.* (1973); see also Sec. IX.

3. Vibrational states

In addition to particle excitations and the associated rotational bands the level spectrum of the second well, particularly of even nuclei, will contain collective states of distinctly vibrational nature. Among these

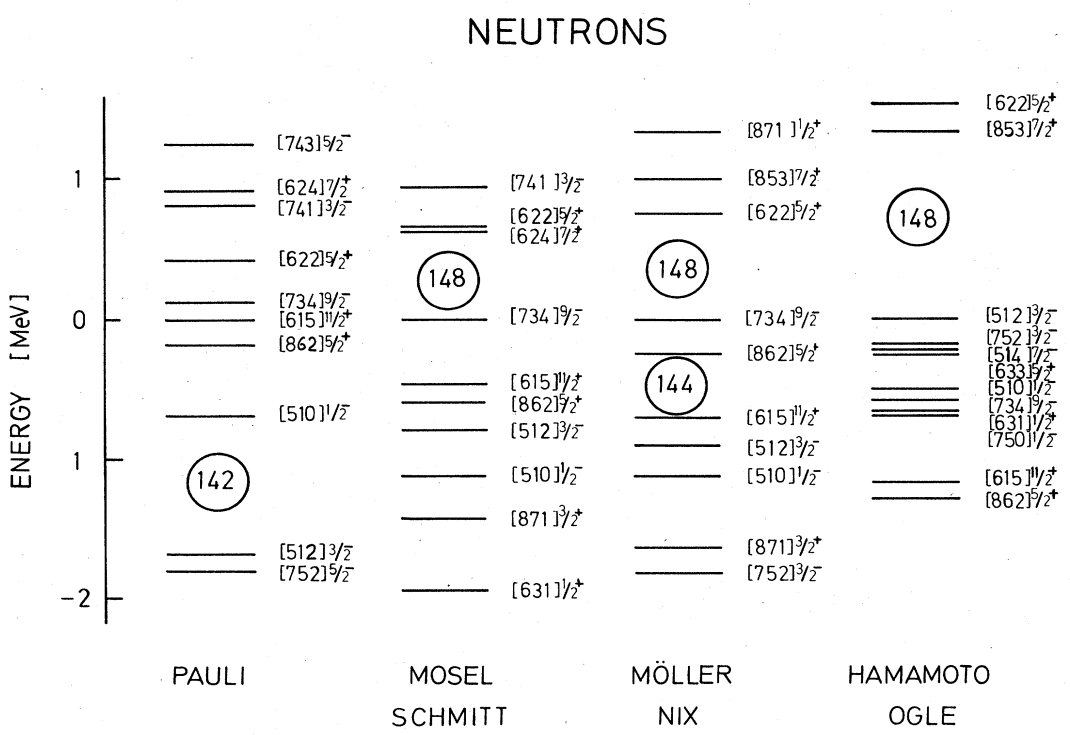

FIG. 23. Calculated single-particle neutron level schemes at the deformation of the second minimum, calculated for different shell models by different authors. From Metag (1980).

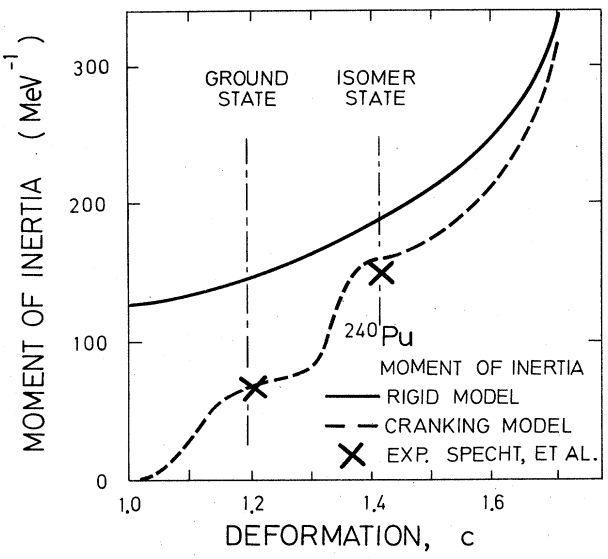

FIG. 24. Calculated moment of inertia of the lowest rotational band for ^{240}Pu as function of elongation c. From Pauli and Ledergerber (1974).

the stretching, or β, vibration plays a special role, as the one that is directly coupled to the fission motion. At the energies where one, two, and higher vibrational modes occur one observes resonance fission, as described in more detail in Sec. V. Two-phonon and higher vibrational states have so far not been observed in the excitation spectrum of the ordinary ground state of deformed nuclei. The specific coupling to the fission mode makes such higher states observable for the shape isomeric nuclei. Also the increasing spreading of the vibrational strength to the neighboring states within a broad energy interval can in principle be studied (Sec. V).

The position of the β-vibrational states can be calculated microscopically from the single-particle wave functions of the states surrounding the Fermi level and the strength of the residual interaction, by the random phase method (Zielinska-Pfabe and Gabrakov, 1973). Although calculations of the energies of such states in the first well have appeared to be very sensitive to details of the ordering of the single-particle states involved, making it perhaps premature to expect reliable theoretical predictions for β vibrations in the second well, such calculations for the second well would be of considerable interest.

III. REACTION THEORIES FOR THE FISSION PROCESS

A. One-dimensional barrier penetration theories

Phenomenological models that deal with the fission channel on a one-dimensional basis, either ignoring the existence of the other degrees of freedom of the system, or treating them simply as a gross absorption out of the fission mode, are very commonly used in the analysis of fission data.

Models of the first class are based on the estimate of the fission width obtained from simple statistical theory [Wigner, 1938; Blatt and Weisskopf, 1952; see Eq. (1.9)] for the decay of a system over a classical barrier; this is now modified for near-barrier fission by multiplication by a transmission coefficient T that incorporates the quantal barrier tunneling effect (the Gamow factor). The transmission coefficient is normally calculated by solving the Schrödinger equation in one dimension, with boundary condition defined by restraining the wave function on the right of the barrier to a progressive wave, i.e., one traveling from left to right in this convention.

1. Single-barrier peak

a. Rectangular barrier

The transmission coefficient is most easily derived in the case of a barrier with sharp edges (Fig. 25). The deformation variable is denoted by η (for this has no associations with any of the specialized definitions of deformation that occur in the literature; see Appendix) and the inertial parameter associated with this degree of freedom is denoted by B and assumed to be independent of deformation. The potential energy $\mathcal{U}$ is assumed to be zero for $\eta<0$, $\mathcal{U}_F$ for $0\leq\eta\leq\eta_2$, and $\mathcal{U}_\infty$ for $\eta>\eta_2$. If an incident wave with total energy E is progressing from small values of η to increasing η, in the stationary wave representation the wave function solution of the Schrödinger wave equation $-(\hbar^2/2B)(\partial^2\phi/\partial\eta^2)+(\mathcal{U}-E)\phi=0$ has the form

$$\phi = e^{ik\eta} + ae^{-ik_0\eta}, \quad \eta<0 \text{ (incident wave and reflected wave)} \tag{3.1a}$$

$$\phi = be^{ik_F\eta} + ce^{-ik_F\eta}, \quad 0\leq\eta\leq\eta_2 \tag{3.1b}$$

$$\phi = de^{ik_\infty\eta}, \quad \eta_2<\eta \text{ (transmitted wave only)} \tag{3.1c}$$

The wave numbers are related to the "velocity," giving the rate of change of deformation of the system, through the usual de Broglie relationships,

$$k_0 = Bv_0/\hbar = (2EB/\hbar^2)^{1/2}, \tag{3.2a}$$

$$k_F = [2(E-\mathcal{U}_F)B/\hbar^2]^{1/2} \quad (=i\kappa_F, \text{ if } E<\mathcal{U}_F), \tag{3.2b}$$

$$k_\infty = Bv_\infty/\hbar = [2(E-\mathcal{U}_\infty)B/\hbar^2]^{1/2}. \tag{3.2c}$$

The incident flux is just the velocity v_0, while the flux of the transmitted wave is $|d|^2v_\infty$, giving for the transmission coefficient $T=|d|^2v_\infty/v_0$. The coefficients a, b, c, d are found by matching the wave function at $\eta=0$ and η_2, giving finally

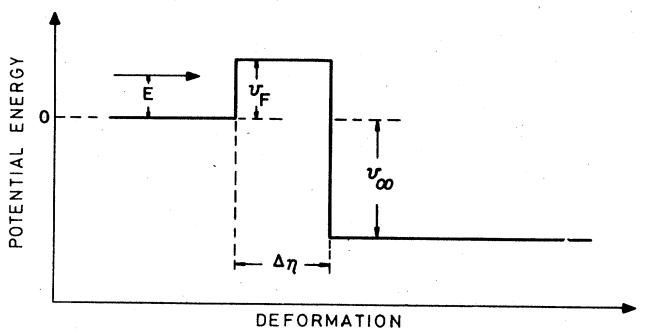

FIG. 25. Rectangular barrier in the potential energy $\mathcal{U}$ vs deformation η.

$$T = \frac{4k_F^2 k_0 k_\infty}{[k_F^4 - k_F^2(k_0^2+k_\infty^2) + k_0^2 k_\infty^2]\sin^2 k_F\eta_2 + k_F^2(k_0+k_\infty)^2}, \quad E > \mathcal{U}_F \tag{3.3a}$$

$$T = \frac{4\kappa_F^2 k_0 k_\infty}{[\kappa_F^4 + \kappa_F^2(k_0^2+k_\infty^2) + k_0^2 k_\infty^2]\sinh^2 \kappa_F\eta_2 + \kappa_F^2(k_0+k_\infty)^2}, \quad E < \mathcal{U}_F \tag{3.3b}$$

Some examples of this function are given in Fig. 26 for parameters that would be typical, in order of magnitude, for actinide fission barriers.

b. Other barrier forms

The oscillating character at above-barrier energies of the transmission coefficients shown in Fig. 26 are peculiar, among single-barrier peaks, to the rectangular barrier with its sharp edges. Transmission coefficients of more realistic barriers must therefore be sought. Since it is apparent from Eq. (3.3) and Fig. 26 that the most important parameters affecting the transmission coefficient are the barrier width and height, relative to the kinetic energy, while the potentials on either side are comparatively unimportant, the mathematical details may be simplified by considering only symmetric barriers.

(i) Triangular barrier. The triangular barrier is the most obvious case to consider next (Fig. 27). The wave functions within the barrier region can be expressed as Airy functions:

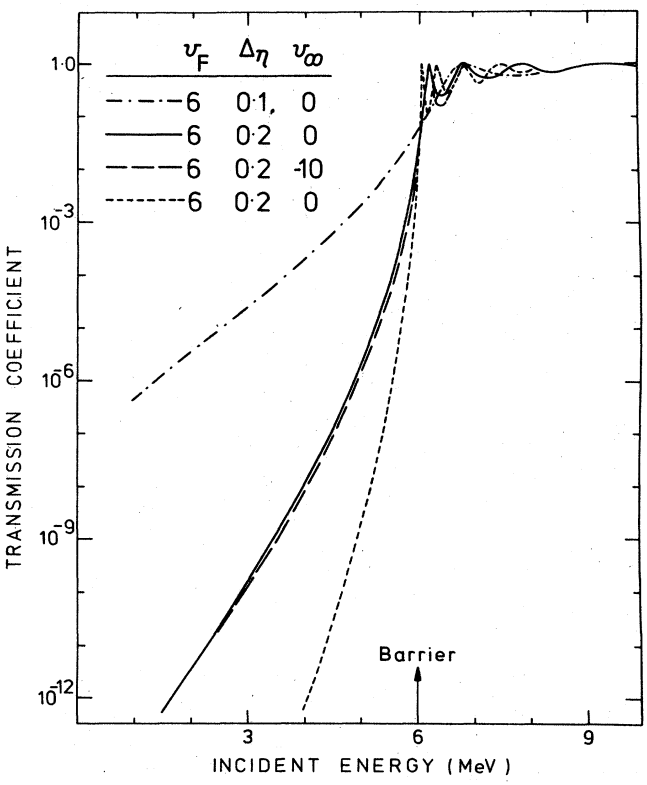

FIG. 26. Transmission coefficient calculated for the passage of a wave through a rectangular barrier (Fig. 25). The inertial parameter is chosen so that $2B/\hbar^2 = 1200$ MeV^{-1} (the deformation parameter η is dimensionless).

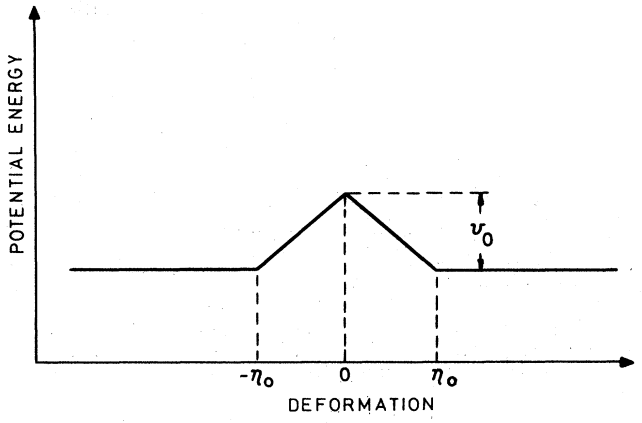

FIG. 27. Symmetric triangular barrier in the potential energy $\mathcal{U}$ vs deformation η.

$$\phi = aAi(\xi) + bBi(\xi), \tag{3.4}$$

where ξ is related to the slope of the potential hill ($\mathcal{U} = \mathcal{U}_0 - c|\eta - \eta_0|$) and the energy by $\xi = (2Bc/\hbar^2)^{1/3}[|\eta - \eta_0| + (\mathcal{U}_0 - E)/c]$, while the Airy functions have the asymptotic forms

$$Ai(\xi) = \frac{1}{\pi}\int_0^\infty dz\cos(\xi z + \tfrac{1}{3}z^3) \sim \frac{1}{2\sqrt{\pi}}\xi^{-1/4}\exp(-\tfrac{2}{3}\xi^{3/2})$$

$$Bi(\xi) = \frac{1}{\pi}\int_0^\infty dz\,[e^{z\xi - 1/3z^3} + \sin(z\xi + \tfrac{1}{3}z^3)]$$

$$\sim \frac{1}{\sqrt{\pi}}\xi^{1/4}\exp(\tfrac{2}{3}\xi^{3/2}) \tag{3.5}$$

valid if $2(2B/\hbar^2)^{1/2}E^{3/2}/c \gg 1$ and $2(2B/\hbar^2)^{1/2}(\mathcal{U}_0 - E)^{3/2}/c \gg 1$. Matching of the wave functions (3.1a), (3.1c) to (3.4) at the discontinuities and use of the asymptotic forms for the Airy functions leads to

$$T = \exp\left[-\frac{8}{3}\left(\frac{2B}{\hbar^2}\right)^{1/2}\frac{(\mathcal{U}_0 - E)^{3/2}}{c}\right]. \tag{3.6}$$

(ii) Hyperbolic cosine barrier. All discontinuities in potential gradients are avoided in the hyperbolic cosine barrier (Fig. 28), expressed by

$$\mathcal{U}(\eta) = \mathcal{U}_0/\cosh^2(\alpha\eta). \tag{3.7}$$

The wave functions in this case take the form of hypergeometric functions,

$$\phi = \frac{1}{\cosh^s\alpha\eta}\Big\{aF(-\tfrac{1}{2}s + \tfrac{1}{2}ik/\alpha, -\tfrac{1}{2}s - \tfrac{1}{2}ik/\alpha, \tfrac{1}{2}, -\sinh^2\alpha\eta) + b\sinh\alpha\eta F(-\tfrac{1}{2}s + \tfrac{1}{2}ik/\alpha + \tfrac{1}{2}, -\tfrac{1}{2}s - \tfrac{1}{2}ik/\alpha + \tfrac{1}{2}, \tfrac{3}{2}, -\sinh^2\alpha\eta)\Big\}, \tag{3.8}$$

where $k = (2BE/\hbar^2)^{1/2}$, $s = \frac{1}{2}[-1 + (1 - 8B\mathcal{U}_0/\alpha^2\hbar^2)^{1/2}]$ and the resulting barrier transmission coefficient is [e.g., see Landau and Lifshitz (1958)]

$$T = \frac{\sinh^2(\pi k/\alpha)}{\sinh^2(\pi k/\alpha) + \cos^2[\frac{1}{2}\pi(1 - 8B\mathcal{U}_0/\hbar^2\alpha^2)^{1/2}]}$$

if $8B\mathcal{U}_0/\hbar^2\alpha^2 < 1$ (3.9a)

or

$$T = \frac{\sinh^2(\pi k/\alpha)}{\sinh^2(\pi k/\alpha) + \cosh^2[\frac{1}{2}\pi(8B\mathcal{U}_0/\hbar^2\alpha^2 - 1)^{1/2}]}$$

if $8B\mathcal{U}_0/\hbar^2\alpha^2 > 1$. (3.9b)

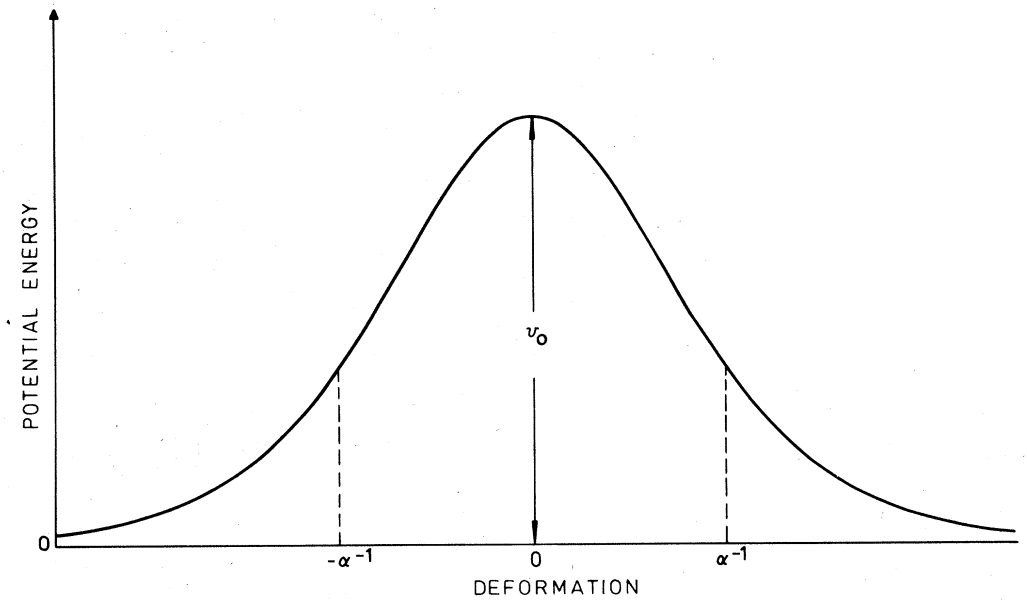

FIG. 28. Hyperbolic cosine barrier in the potential energy $\mathcal{U}$ vs deformation η.

(iii) Inverted parabolic barrier. The barrier that is almost universally employed in nuclear fission studies is the inverted parabolic one, generally known as the "inverted harmonic oscillator," the "oscillator" having circular frequency denoted by ω:

$$\mathcal{U} = \mathcal{U}_F - \tfrac{1}{2}C_F(\eta - \eta_F)^2 \tag{3.10}$$

$$\omega = (C_F/B)^{1/2}. \tag{3.11}$$

The general solution of the Schrödinger equation for such a potential is the parabolic cylinder function, the standard form of which can be written [see, e.g., Abramowitz and Stegun (1965)]

$$W(a,\pm x) = \frac{(\cosh\pi a)^{1/4}}{2\sqrt{\pi}} \times \{|\Gamma(\tfrac{1}{4}+\tfrac{1}{2}ia)\,y_1(x) \mp \sqrt{2}\,|\Gamma(\tfrac{3}{4}+\tfrac{1}{2}ia)\,|y_2(x)\}, \tag{3.12a}$$

where y_1 and y_2 are related to the confluent hypergeometric functions

$$y_1 = e^{-(1/4)x^2}{}_1F_1(\tfrac{1}{2}a+\tfrac{1}{4};\tfrac{1}{2};\tfrac{1}{2}x^2) = e^{-(1/4)x^2}\{1+(a+\tfrac{1}{2})(x^2/2!)+(a+\tfrac{1}{2})(a+\tfrac{5}{2})(x^4/4!)+\cdots\}, \tag{3.12b}$$

$$y_2 = e^{-(1/4)x^2}\{1+(a-\tfrac{1}{2})(x^2/2!)+(a-\tfrac{1}{2})(a-\tfrac{5}{2})(x^4/4!)+\cdots\}, \tag{3.12c}$$

and

$$x = (4C_F B/\hbar^2)^{1/4}(\eta - \eta_F) \tag{3.13}$$

$$a = (\mathcal{U}_F - E)/\hbar\omega. \tag{3.14}$$

From the standard form complex solutions of the Schrödinger equation can be built with the asymptotic forms (for large $|x|$) of waves progressing to either the left or right. Thus the solution

$$E(a,x) = c^{-1/2}W(a,x) + ic^{1/2}W(a,-x) \tag{3.15}$$

[with $c = [1+\exp(2\pi a)]^{1/2} - \exp(\pi a)$] has, as the leading term in its asymptotic expansion for $x \gg |a|$,

$$E(a,x) \sim \sqrt{2}\,x^{ia-1/2}\exp[\tfrac{1}{4}ix^2 + \arg\Gamma(\tfrac{1}{2}+ia) + \tfrac{1}{2}\pi],$$

and corresponds to a transmitted wave to the right of the barrier. The same solution with argument $-x$ corresponds to a reflected wave to the left of the barrier, while the solution

$$E^*(a,-x) = c^{-1/2}W(a,-x) - ic^{1/2}W(a,+x) \tag{3.16}$$

corresponds to an incident wave to the left of the barrier. Thus, to the right of the barrier

$$\phi = BE(a,x), \quad x \text{ positive}$$

and to the left

$$\phi = E^*(a,-x) + AE(a,-x), \quad x \text{ negative}.$$

Since the asymptotic forms of E and E^* hold for their analytic extension into the complex η plane, this enables a connection to be made between these forms, giving

$$A = B(e^{i\pi})^{-ia-1/2}.$$

The result for the transmission coefficient is therefore

$$T = 1/\{1+\exp[2\pi(\mathcal{U}_F - E)/\hbar\omega\}, \tag{3.17}$$

a well-known result due to Hill and Wheeler (1953). This result is one that is very commonly used in the analysis and presentation of fission reaction data. It is to be noted that the transmission function increases monotonically with energy; for energies far below the barrier it increases purely exponentially and above the barrier it reaches asymptotically to unity.

c. General approximate form for a single-humped barrier

The last formula is a special case of the general formula for a barrier with only a single extremum; this was given by Fröman and Fröman (1965, 1970) in the JWKB approximation. As in the exact treatment of the parabolic barrier the asymptotic wave forms to left and right of the barrier are connected by following

a path on the wave-number sheet, k (with phase corresponding to positive value of $k=[2B(E-\upsilon)/\hbar^2]^{1/2}$, when the argument is real and η lies to the left of the barrier[1]) in the complex η plane. The transmission coefficient is given by

$$T\approx[1+\exp(2K)]^{-1}, \tag{3.18}$$

where, in first order,

$$K=-\mathrm{Im}\int_{\eta_{a'}}^{\eta_{b'}}d\eta\left[\frac{2B(E-\upsilon)}{\hbar^2}\right]^{1/2}. \tag{3.19}$$

Here, $\eta_{a'},\eta_{b'}$ are just the points η_a,η_b at which $\upsilon(\eta)=E$, in the sub-barrier case when the barrier peak exceeds the available energy E; K is then real and positive. However, in the superbarrier case, the path of integration for K proceeds in the upper half-plane of the above-mentioned Riemann sheet and connects arbitrary points (on the real η axis) to the left and right of the cut joining the zeros of k in the upper and lower half-planes of η. In this case K is real and negative. Fröman and Fröman (1970) also treat higher-order phase integral approximations to K.

2. Double-peaked barrier

a. General JWKB treatment

Whereas the single-peaked barrier exhibits a transmission function that rises almost monotonically with energy in an exponential manner, the characteristic features of the transmission of the double-peaked barrier are dominated by the virtual states of the potential well that lies between the two peaks; these states give rise to resonances in the transmission function, and the effect of the potential maxima on either side of the well is felt mainly in the widths of these resonances and in the minima between the resonances.

These features are revealed by the JWKB treatment of the problem. Within the secondary well of the barrier, where the kinetic energy is positive, the quasiclassical approximation to the wave function is

$$\phi(\eta)\sim\frac{1}{\{2B[E-\upsilon(\eta)]\}^{1/2}}\left[C_1\exp\left(\frac{i}{\hbar}\int d\eta[2B(E-\upsilon)]^{1/2}\right)\right.$$
$$\left.+C_2\exp\left(-\frac{i}{\hbar}\int d\eta[2B(E-\upsilon)]^{1/2}\right)\right]. \tag{3.20}$$

Between the two turning points η_b and η_c where $E=\upsilon$, this wave function reduces to the form of either

$$\frac{C}{\{2B[E-\upsilon(\eta)]\}^{1/2}}\sin\left(\frac{i}{\hbar}\int_{\eta_b}^{\eta}d\eta[2B(E-\upsilon)]^{1/2}+\frac{\pi}{4}\right),$$

or

$$\frac{C}{\{2B[E-\upsilon(\eta)]\}^{1/2}}\sin\left(\frac{1}{\hbar}\int_{\eta}^{\eta_c}d\eta[2B(E-\upsilon)]^{1/2}+\frac{\pi}{4}\right),$$

if the condition is imposed that the solution of the exact Schrödinger equation vanishes as $\eta\to\pm\infty$. For these two expressions to be identical at η, the sum ϕ of their phases must equal an odd-integral multiple of $\frac{1}{2}\pi$:

$$\phi=\frac{1}{\hbar}\int_{\eta_b}^{\eta_c}d\eta[2B(E-\upsilon)]^{1/2}=(n+\tfrac{1}{2})\pi, \tag{3.21}$$

which is Bohr's quantization condition. When the barriers on either side of the secondary well are finite, so that the wave function does not vanish for $\eta\to\pm\infty$, the condition (3.21) on ϕ for discrete solutions is no longer required for the general solution, but the amplitude of the wave function between the wells is maximized at an energy close to the above quantization condition, i.e., resonance occurs. This is reflected in the expression for the transmission function, for which, in the JWKB approximation, Ignatyuk *et al.* (1969) deduced that

$$T\approx\tfrac{1}{4}(T_AT_B)[[\tfrac{1}{4}(T_A+T_B)]^2\sin^2\phi(E)+\cos^2\phi(E)]^{-1}, \tag{3.22}$$

where T_A and T_B are the transmission coefficients of the barriers A and B treated separately (as in Sec. III.A.1).

This formula has been criticized on the grounds of arbitrary use of the JWKB connection formulas (for which see, e.g., Kemble, 1958) at the classical turning points η_a and η_b. Leboeuf and Sharma (1973a) give Eq. (3.22) without the term in $\sin^2\phi$ in the denominator as the correct first-order JWKB approximation, but this formula is actually less satisfactory than Eq. (3.22) in that it diverges at the resonance condition of Eq. (3.21). Fröman and Dammert (1970) give the general approximate form

$$T\approx\frac{\exp\{-2(K_A+K_B)\}}{(S-1)^2+4S\cos^2\alpha}, \tag{3.23a}$$

$$S=[1+\exp(-2K_A)]^{1/2}[1+\exp(-2K_B)]^{1/2}, \tag{3.23b}$$

with expressions for K_A and K_B in higher-order phase integral approximations, which reduce in first order to the expression (3.19) introduced in Sec. II.A.1. c (for barrier B, of course, the turning points η_c,η_d must replace η_a and η_b in that expression), while the phase angle α has correction terms on ϕ, resulting in

$$\alpha\approx\int_{\eta_b}^{\eta_c}d\eta\left[\frac{2B(E-\upsilon)}{\hbar^2}\right]^{1/2}-\sigma_A-\sigma_B, \tag{3.23c}$$

with

$$\sigma_A\approx\frac{1}{2}\left[\frac{K_A}{\pi}\ln\left|\frac{K_A}{\pi}\right|-\frac{K_A}{\pi}+\arg\Gamma\left(\frac{1}{2}-\frac{iK_A}{\pi}\right)\right], \tag{3.23d}$$

and a similar formula for σ_B in terms of K_B. The final term in the formula for the correction phases σ has been given approximately by Ford *et al.* (1959) as

$$\frac{1}{2}\arg\Gamma\left(\frac{1}{2}-\frac{iK}{\pi}\right)\approx-\frac{K}{2\pi}\ln\left[\left(\frac{K}{\pi e}\right)^2+\left(\frac{1}{4\gamma}\right)^2\right]^{1/2},$$

where γ is Euler's constant with value 0.577 2157. The function σ_A and the approximation Eq. (3.23d) for it are shown in Fig. 29. Leboeuf and Sharma (1973b) also give expressions for various near-barrier situations; these are encompassed by Fröman and Dammert's expression, Eq. (3.23), so they need not be restated here.

The resonance condition for Eq. (3.23a) is discussed in some detail by Fröman and Dammert. They note that for a symmetric double barrier the resonance condition is exactly

[1] In the sub-barrier case this corresponds to the phase $k^{1/2}=e^{-i\pi/4}\,|k^{1/2}|$ when $E<\upsilon$ on the real η axis.

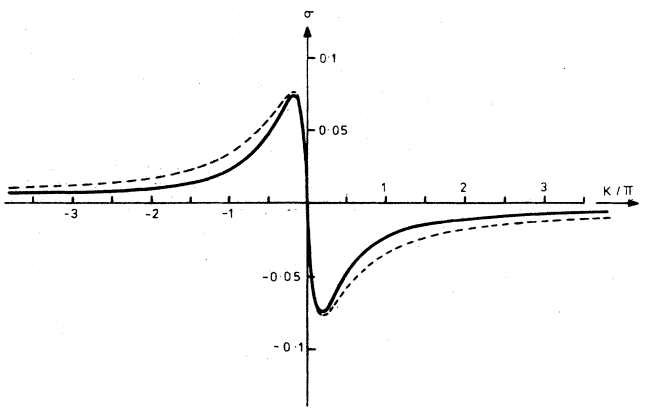

FIG. 29. The phase correction σ to the phase angle α that gives rise to resonant effects in tunneling through a double-humped barrier. It is shown here as a function of the wave-number integral K. After Fröman and Dammert (1970). The dashed curve is an approximation due to Ford *et al.* (1959).

$$\alpha = (n+\tfrac{1}{2})\pi\,, \tag{3.24}$$

where n is an integer, and at this energy the transmission is exactly unity. For energies far below the peaks of both barriers this same condition for resonance is approximately true; in fact the quantity $4S\cos^2\alpha$ is the dominant term in the denominator of Eq. (3.23a) except when $\cos\alpha$ is very close to zero, and hence, in this strongly sub-barrier situation, the transmission function has the appearance of high, very narrow peaks on a low but exponentially increasing base. In the case of a symmetric double barrier these peaks rise to a transmission value of unity. Equation (3.23a) can be written approximately

$$T \approx \frac{\cosh^{-2}(K_A - K_B)}{1+\{\cos\alpha/[\tfrac{1}{4}\exp(-2K_A)+\tfrac{1}{4}\exp(-2K_B)]\}^2}\,, \tag{3.25}$$

giving $T_{\max}\approx\cosh^{-2}(K_A-K_B)$ at resonance. Close to the resonance condition $\cos\alpha$ can be written $\alpha-(n+\frac{1}{2})\pi$, thus demonstrating that the half-width of the resonance is $\Delta\alpha\approx\frac{1}{2}[\exp(-2K_A)+\exp(-2K_B)]$ which, in terms of energy, is

$$\Gamma\approx\hbar\,[\exp(-2K_A)+\exp(-2K_B)]\Big/\int_{\eta_b}^{\eta_c} d\eta[(E-\mathcal{U})/2B]^{-1/2}\,. \tag{3.26}$$

The denominator in this expression is the reciprocal of the classical oscillation frequency between the two barriers. The resonance width therefore is simply interpreted through the Heisenberg uncertainty principle, i.e., it is Planck's constant (divided by 2π) multiplied into the escape probability (oscillation frequency times probability of tunneling the barriers) from the intermediate well.

Other points to be noted about the JWKB formula are, firstly, that well below the peaks replacement of α [Eq. (3.23c)] by ϕ [Eq. (3.21)] gives rise to very small error in α, but this nevertheless implies a large shift in the resonance in comparison with its width. Secondly, between resonances, the transmission has minima close to the value

$$T\approx\tfrac{1}{4}\exp\{-2(K_A+K_B)\}\approx\tfrac{1}{4}(T_AT_B)\,. \tag{3.27}$$

b. Special treatments

(i) Double-peaked rectangular barrier. In the barrier formed of rectangular sections shown in Fig. 30 the wave function has the form

$$\begin{aligned}
\phi &= e^{ik_4\eta}+c_4e^{-ik_4\eta}\,, && \eta<\eta_3\\
\phi &= b_3e^{ik_3\eta}+c_3e^{-ik_3\eta}\,, && \eta_3\le\eta\le\eta_2\\
\phi &= b_2e^{ik_2\eta}+c_2e^{-ik_2\eta}\,, && \eta_2\le\eta\le\eta_1\\
\phi &= b_1e^{ik_1\eta}+c_1e^{-ik_1\eta}\,, && \eta_1\le\eta\le\eta_0\\
\phi &= b_0e^{ik_0\eta}\,, && \eta_0\le\eta\,,
\end{aligned} \tag{3.28}$$

with

$$k_4=(2EB/\hbar^2)^{1/2}\,,\quad k_3=[2(E-\mathcal{U}_A)B/\hbar^2]^{1/2}\,,$$

$$k_2=[2(E-\mathcal{U}_{II})B/\hbar^2]^{1/2}\,,\quad k_1=[2(E-\mathcal{U}_B)B/\hbar^2]^{1/2}\,,$$

and $k_0=[2(E-\mathcal{U}_0)B/\hbar^2]^{1/2}$. The transmission coefficient $T=|b_0|^2v_0/v_4$ is found by matching ϕ across the boundaries $\eta_3,\eta_2,\eta_1,\eta_0$. The final expression is somewhat unwieldy to write down, and in practice it is simpler to start with the form of the asymptotic outgoing wave in the final region ($\eta_0<\eta$), calculate numerically the coefficients b_1,c_1 relative to b_0 from the matching at η_0 and hence calculate the "parent" coefficients b_n,c_n at each preceding boundary until the value of b_0 relative to unity is obtained from the matching at η_3. The matching conditions at η_0 are

$$\frac{b_1}{c_1}=\frac{k_1+k_0}{k_1-k_0}\,e^{-2ik_1\eta_0}\,, \tag{3.29a}$$

while those at η_1 are

$$\frac{b_2}{c_2}=\frac{(b_1/c_1)(k_1+k_2)e^{i(k_1-k_2)\eta_1}+(k_2-k_1)e^{-i(k_1+k_2)\eta_1}}{(b_1/c_1)(k_2-k_1)e^{i(k_1+k_2)\eta_1}+(k_1+k_2)e^{i(k_2-k_1)\eta_1}}\,, \tag{3.29b}$$

and generally at η_n are

$$\frac{b_{n+1}}{c_{n+1}}=\frac{(b_n/c_n)(k_n+k_{n+1})e^{i(k_n-k_{n+1})\eta_n}+(k_{n+1}-k_n)e^{-i(k_n+k_{n+1})\eta_n}}{(b_n/c_n)(k_{n+1}-k_n)e^{i(k_n+k_{n+1})\eta_n}+(k_n+k_{n+1})e^{i(k_{n+1}-k_n)\eta_n}}\,. \tag{3.29c}$$

Since the transmitted flux is equal to unity minus the reflected flux, the transmission coefficient is just

$$T=1-\left|\frac{c_1}{b_1}\right|^2 \tag{3.30}$$

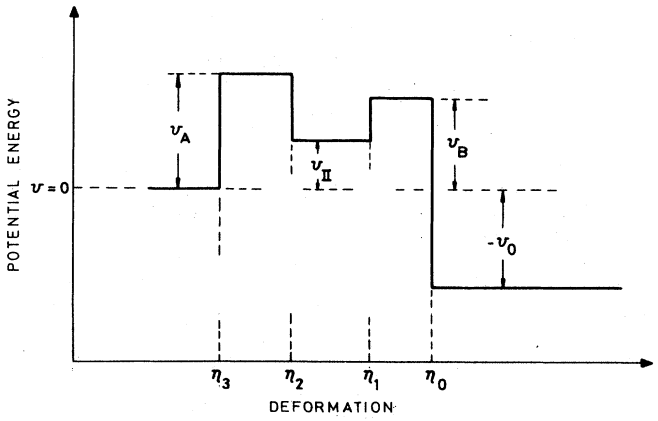

FIG. 30. Double-humped rectangular barrier in the potential energy $\mathcal{U}$ vs deformation η.

(b_4 being unity).

This numerical procedure can be applied to any arbitrarily shaped barrier, by approximating the barrier with a sufficiently large number of constant potential steps. The transmission coefficient corresponding to barrier penetration from the ground state through a realistic double-humped barrier can be calculated within a factor of 2 by breaking the barrier into the order of 1000 equal steps. Many of the numerical calculations given, by way of example, below, have been calculated by this method.

(ii) Smoothly joined harmonic segments. Another barrier form for which an exact numerical solution can be obtained is that in which the double-humped barrier is composed of harmonic segments of the form

$$\begin{aligned} \upsilon &= \upsilon_A - \tfrac{1}{2}C_A(\eta-\eta_A)^2, \quad \eta<\eta_y \\ \upsilon &= \upsilon_{II} + \tfrac{1}{2}C_{II}(\eta-\eta_{II})^2, \quad \eta_y \le \eta \le \eta_z \\ \upsilon &= \upsilon_B - \tfrac{1}{2}C_B(\eta-\eta_B)^2, \quad \eta>\eta_z . \end{aligned} \tag{3.31}$$

Such a barrier has been considered particularly by Cramer and Nix (1970) and Wong and Bang (1969). For smooth joining the points η_y, η_z are given by

$$\eta_y = \eta_{II} - \left[\frac{2(\upsilon_A-\upsilon_{II})C_A}{C_{II}(C_A+C_{II})}\right]^{1/2}, \tag{3.32a}$$

$$\eta_z = \eta_B - \left[\frac{2(\upsilon_B-\upsilon_{II})C_{II}}{C_B(C_{II}+C_B)}\right]^{1/2}, \tag{3.32b}$$

and also lead to the conditions that

$$\eta_{II} = \eta_z + \frac{C_B}{C_{II}}(\eta_z-\eta_B), \tag{3.32c}$$

$$\eta_A = \eta_y + \frac{C_{II}}{C_A}(\eta_y-\eta_{II}). \tag{3.32d}$$

The solutions of the Schrödinger equation for these potentials are the parabolic cylinder functions, with forms (3.15) and (3.16), for the regions $\eta<\eta_y$ and $\eta>\eta_z$, the quantities a and x being calculated for the appropriate values of υ_A, C_A, η_A and υ_B, C_B, η_B. In the intermediate region ($\eta_y \le \eta < \eta_z$) the Schrödinger equation has general solutions of the form

$$U(a_{II},x_{II}) = \frac{1}{\sqrt{\pi}}\left[\frac{\Gamma(\frac{1}{4}-a_{II}/2)}{2^{a_{II}/2+1/4}}\cos\left(\frac{\pi}{4}+\frac{\pi a_{II}}{2}\right)y_1(x_{II}) - \frac{\Gamma(\frac{3}{4}-a_{II}/2)}{2^{a_{II}/2-1/4}}\sin\left(\frac{\pi}{4}+\frac{\pi a_{II}}{2}\right)y_2(x_{II})\right], \tag{3.33a}$$

$$V(a_{II},x_{II}) = \frac{1}{\sqrt{\pi}\Gamma(\frac{1}{2}-a_{II})}\left[\frac{\Gamma(\frac{1}{4}-a_{II}/2)}{2^{a_{II}/2+1/4}}\sin\left(\frac{\pi}{4}+\frac{\pi a_{II}}{2}\right)y_1(x_{II}) + \frac{\Gamma(\frac{3}{4}-a_{II}/2)}{2^{a_{II}/2-1/4}}\cos\left(\frac{\pi}{4}+\frac{\pi a_{II}}{2}\right)y_2(x_{II})\right], \tag{3.33b}$$

the functions y_1, y_2 being those of Eq. (3.12) while $a_{II} = (\upsilon_{II}-E)/\hbar\omega_{II}$, $x_{II} = (4C_{II}B/\hbar^2)^{1/4}(\eta-\eta_{II})$. The required wave function in this region is formed from a superposition of U and V. All the appropriate solutions in the three regions and their derivatives can be calculated from the series expansions (3.12b), (3.12c), matched at the points η_y, η_z, and hence the transmission factor deduced. An example of the computed coefficient for a barrier with $\upsilon_A = 6$ MeV, $\upsilon_{II} = 2$ MeV, $\upsilon_B = 5$ MeV, $\hbar\omega_A = 1.3$ MeV, $\hbar\omega_{II} = 2.0$ MeV, and $\hbar\omega_B = 0.48$ MeV is shown in Fig. 31 (Cramer and Nix, 1970), and is compared with calculations from the JWKB formula of Ignatyuk *et al.* (1969). The shape of the barrier is also shown in this figure, together with the parabola joining points, and the virtual vibrational energy levels in the secondary well are also indicated. At the 4.76-MeV level the energy calculated by the simple JWKB formula [Eq. (3.22)] differs from the exact energy by 18 keV.

3. Effects of variable inertia

In the single barrier peak case it appeared that rather broad superbarrier resonances, or oscillations, appear in the transmission coefficient through the square potential. These disappear as the potential edges become softer until, in the limit of the inverted parabola, not even a trace of an inflection remains in the monotonically rising transmission function. These conclusions, however, are only rigorously valid if the inertia associated with the deformation variable η is in-

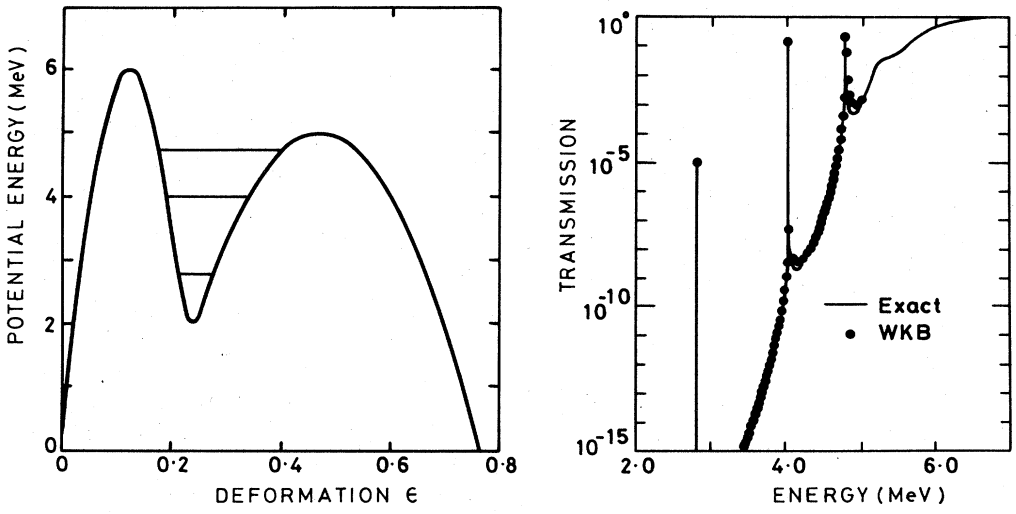

FIG. 31. Examples of transmission coefficient for a double-humped barrier composed of parabolic segments [from Cramer and Nix (1970)], and comparison with a JWKB calculation of Ignatyuk *et al.* (1969).

dependent of η. It is possible, if the inertial parameter varies sufficiently with deformation, that superbarrier resonances might appear in the transmission through a rather rounded barrier (Hofmann, 1972). This can be demonstrated by transforming from the deformation variable η to a new variable x for which the inertia is a constant B_0, the transformation being defined by

$$x = \int^{\eta} [B(\eta')/B_0]^{1/2} d\eta' , \tag{3.34}$$

and writing the Schrödinger equation in this new variable, in terms of which the potential energy $\tilde{\upsilon}(x)$ will have a different form. In particular, if the inertial parameter $B(\eta)$ follows qualitatively the rise and fall near the top of the barrier and is nearly constant elsewhere, as expected in some cranking model calculations (see Sec. II.B.1), $\tilde{\upsilon}(x)$ will have a much squarer form than $\upsilon(\eta)$.

Hofmann (1972a) has investigated the degree of softness of the edges of the barrier $\tilde{\upsilon}(x)$ required to give a reasonable degree of superbarrier oscillation. If $\tilde{\upsilon}(x)$ has the form of an inverted Eckart potential

$$\tilde{\upsilon}(x) = \upsilon_0\{1 + \exp[-(x_F - x)/d]\}^{-1} , \quad (x_F \gg d) , \tag{3.35}$$

the ratio of edge diffuseness parameter d to width (at half maximum) $2x_F$ is found to be ≈ 0.14 for resonances to disappear. This is a rather small ratio and leads to the feeling that superbarrier structure is likely to occur for a realistically shaped fission barrier only if the inertial parameter of the fission motion varies quite strongly. The degree of dependence of oscillation on the ratio of diffuseness to barrier width is illustrated in Fig. 32.

More complicated superbarrier oscillation effects can occur for the double-humped barrier.

4. Barrier transmission with absorption

As stated above, the one-dimensional treatment of the fission process can be extended to take some account of other degrees of freedom by treating excitation of the latter as a simple absorption out of the fission mode. This method is very familiar in the treatment of nucleon scattering by complex nuclei, being just the optical model of nuclear reactions. In the application of the optical model to the fission process it is necessary to include the well(s) in addition to the barrier in the potential energy function for the deformation mode.

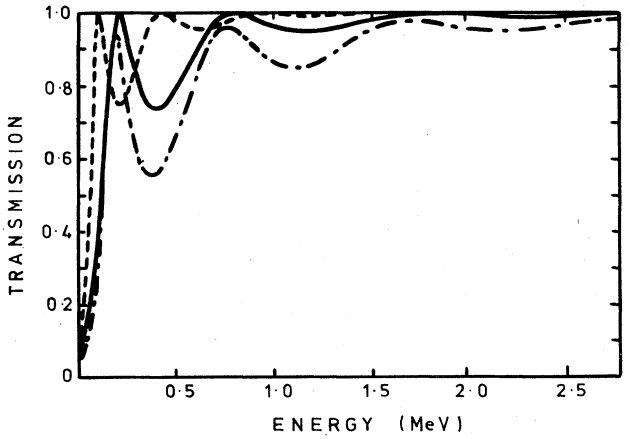

FIG. 32. Oscillations in the barrier transmission coefficient for different values of the ratio of edge diffuseness to barrier width (Hofmann, 1972a). The energy scale is relative to the barrier peak, which is 5.49 MeV. For the continuous curve $B_0 = 483$ MeV/$\hbar^2$, $x_F = 0.1212$, $d = 0.01$; dashed curve, $B_0 = 966$ MeV/$\hbar^2$; dash-dot curve, $B_0 = 483$ MeV/$\hbar^2$, $d = 0.005$.

In the original application of this method to fission through a single-peaked barrier (Lynn, 1966a) there is no difficulty in principle in obtaining the transmission function, and hence the fission strength function. An imaginary component is introduced into the potential well representing the internal compound nucleus region. This can be either a constant component between certain adopted limits of deformation, or have some functional form attenuating to zero in the region of the potential barrier. An incident wave of form $\exp(-ik_0\eta)$ in the deformation mode is now considered to fall on this potential, and the result of the interaction gives an outgoing wave with amplitude S_{ff}; beyond a deformation value η_0 expressing the range of the potential barrier beyond the internal region, the wave function has the form

$$\phi = \exp(-ik_0\eta) + S_{ff}\exp(ik_0\eta) , \quad \eta > \eta_0 . \tag{3.36}$$

The amplitude S_{ff} is calculated by solving the Schrödinger equation (usually by numerical integration), the governing boundary condition to give the correct solution being that the wave function is real and regular at some value of the deformation $\eta_{\min}$ sufficiently far on the low deformation side of the potential well. A resulting value of S_{ff} with modulus unity implies pure scattering of the fission wave. The difference between unity and $|S_{ff}|^2$ gives the absorption into the internal region, i.e., compound nucleus formation; the cross section for compound nucleus formation from an "inverse-fission" channel is proportional to $1 - |S_{ff}|^2$, and this expression is normally defined as the transmission coefficient T_f corresponding exactly to the simple barrier transmission already considered in Sec. III.A.1;

$$T_f = 1 - |S_{ff}|^2 . \tag{3.37}$$

A typical transmission coefficient thus calculated is shown in Fig. 33. It is seen that resonance effects can be found, but these are due to weakly damped vibrations in the deep potential well. Such small imaginary components are not normally expected at the excitation energies considered here.

Such a treatment has also been applied to the double-humped potential barrier (Bondorf, 1970; Holmberg *et al.*, 1969). If the imaginary component of the potential is confined to the primary well, transmission coefficients that display the vibrational resonance peaks described above in Sec. III.A.2 can be expected. These are undamped vibrational resonances (zero damping in the secondary well), and spreading the imaginary potential across both the primary and secondary well is not a strictly correct way of treating the damping in the secondary well. In the calculations of Holmberg *et al.* (1969) small imaginary components are assigned to both potential wells, and double resonances are found; one of these is a vibrational resonance in the secondary

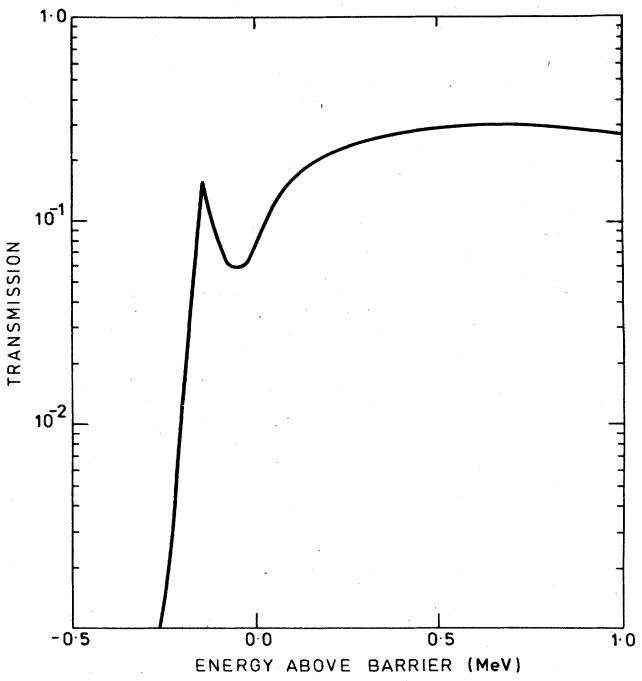

FIG. 33. Transmission coefficient calculated by the scattering method for a potential barrier bounding a complex potential well [from Lynn (1968a)]. The real well depth is about 6 MeV and the imaginary depth only 30 keV.

well and the other a vibrational resonance in the primary well. The latter is not expected, as stated above in our remarks about the single-peaked barrier.

The difficulty in this model is that absorption into the secondary well has to be considered separately from that in the primary well; use of an imaginary potential in both wells simply lumps together the absorption in the two wells. The picture here is that an incident inverse-fission wave penetrates the secondary well with attenuation, and this attenuated direct component is absorbed in the primary well, while the component absorbed in the secondary well can be reemitted into the fission channel, or suffer a transition irrevocably into some other degree of freedom, or be emitted into the primary well. The total flux reaching, and being absorbed, into the primary well is the quantity of interest here. Bondorf (1970) and Back *et al.* (1971) have modified the model to obtain the transmission coefficient correctly by making the simplifying assumption that all the flux reaching the primary well is absorbed completely. The wave function at some deformation η_1 close to the entry (at barrier A) into the primary well therefore has no returning wave and is given by

$$\phi = a \exp(-ik_1\eta), \quad \eta \leq \eta_1 \tag{3.38}$$

{or, more exactly, to take the attenuation distance $1/K$ in the primary well into account, $\phi = a \exp[-K(\eta_1 - \eta) - ik_1\eta]$; the factor $\exp[-K(\eta_1 - \eta)]$ is required if the imaginary potential starts at η_1 with a nonzero value}. The flux that is absorbed directly into the primary well is thus $k_1|a|^2/k_\infty$, while that absorbed in the secondary well is $1 - |S_{ff}|^2$. Of the secondary well absorption a fraction

$$p_A = \frac{T_A}{T_A + T_B + T_\gamma} \tag{3.39}$$

is emitted into the primary well, T_A and T_B being transmission coefficients from the secondary well across barriers A and B, and T_γ the transmission probability for deexciting radiation across compound levels (class-II states) associated with the secondary well deformation. Thus

$$T_f = \frac{k_1|a|^2}{k_\infty} + p_A(1 - |S_{ff}|^2). \tag{3.40}$$

Of the two terms on the right-hand side of this equation the first can be interpreted as a "direct" one, being the fraction of the wave that is transmitted right across the secondary well without absorption. The second term corresponds to reemission after absorption into the compound motion of the secondary well and hence is expected to have a microscopic structure corresponding to the class-II compound states associated with this motion. The detailed structure of the first term is expected to be just the much broader one of the vibrational resonances in the secondary well.

A schematic example of the transmission coefficient of Eq. (3.40) is shown in Fig. 34 in comparison with the result for zero damping in the secondary well.

B. Statistical models

When absorption out of the fission mode is very strong a limit has been reached that is just the opposite of the simple undamped barrier transmission models of the double-humped barrier. This limit can be treated by assuming statistical equilibrium among all the degrees of freedom of the nucleus. Such a model is therefore appropriate to moderately high excitation energies ("hot" nuclei), in distinction to the barrier transmission model which can only be expected to describe low excitations in the secondary well.

In a hot nucleus with very many degrees of freedom only a relatively small amount of excitation energy will be concentrated on motion in the deformation mode; this amount will be of the order of the nuclear temperature θ. If this temperature is much less than the barrier between the wells in the potential energy of deformation the nuclear system will survive for a relatively long time in one or other equilibrium shape before changing shape, or decaying by particle emission, radiation, or breakup by fission. Thus, in first approximation, two sets of states, associated with each equilibrium shape, and denoted by class I for the first well and class II for the second, exist in the nucleus. The probability of decay of these states can be represented by transmission coefficients that take account of barriers (deformation, centrifugal, or Coulomb) as well as the internal nature of the states in the energy region under consideration. These transmission coefficients can be defined through the reciprocity theorem in terms of the probability of the formation of such states of the compound nucleus in the inverse process to the given decay mode. Thus, for a formation process α, the maximum possible average cross section is $\pi\lambda_\alpha^2 g_J$, where λ_α is the de Broglie wavelength (divided by 2π) of the relative motion of pro-

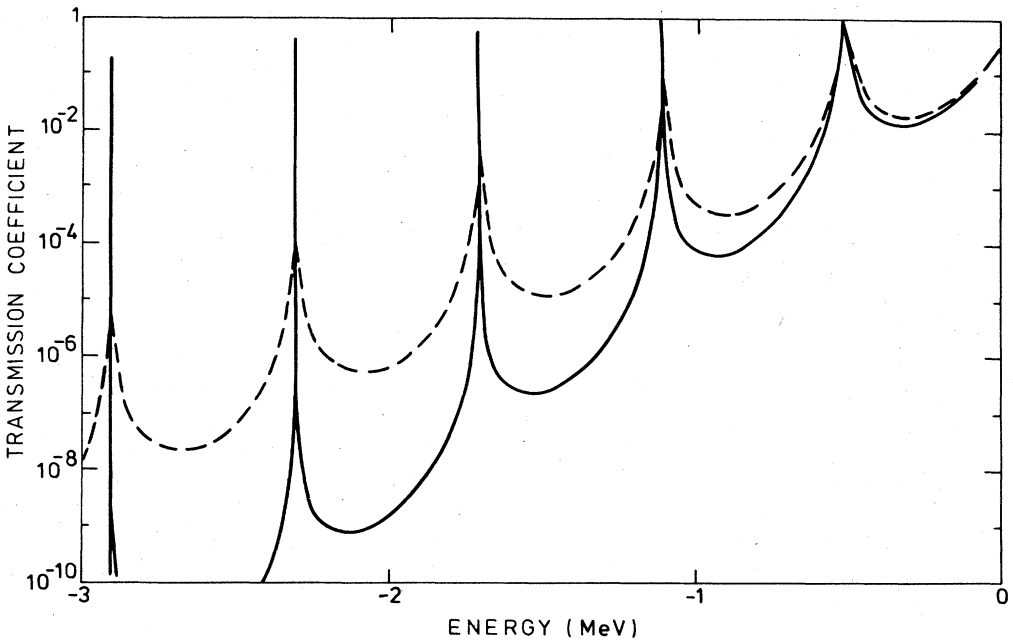

FIG. 34. Schematic picture of the transmission coefficient through a double-humped barrier with damping (represented by an imaginary component in the potential energy) in the secondary well (broken curve) compared with the case of zero damping (full curve). In the first case the imaginary component is 50 keV.

jectile and target, and g_J is the statistical weighting factor for formation of the compound nucleus with total angular momentum J. The actual cross section for compound nucleus formation is denoted by

$$\sigma_{\alpha(\mathrm{CN})} = \pi \lambda_\alpha^2 g_J T_\alpha , \tag{3.41}$$

where T_α is the transmission coefficient for this mode of formation. When the ratio of partial width to level spacing Γ_α/D is small, $T_\alpha = 2\pi\Gamma_\alpha/D$; and it has been established fairly conclusively (Moldauer, 1967) that, in general,

$$T_\alpha = 1 - \exp[-2\pi\Gamma_\alpha/D] . \tag{3.42}$$

Transmission coefficients for making transitions from shape I to shape II, denoted by $T_{\mathrm{I}(A)}$, and vice versa, denoted by $T_{\mathrm{II}(A)}$, can be defined in analogy with the decay coefficients.

1. Probability treatment

From the transmission coefficients the probability of decay of a class-I state by process α is

$$P_{\mathrm{I}(\alpha)} = \frac{T_{\mathrm{I}(\alpha)}}{\sum_\beta T_{\mathrm{I}(\beta)} + T_{\mathrm{I}(A)}} , \tag{3.43}$$

and the probability of a transition from a class-I state to a class-II state is

$$P_{\mathrm{I}\to\mathrm{II}} = \frac{T_{\mathrm{I}(A)}}{\sum_\beta T_{\mathrm{I}(\beta)} + T_{\mathrm{I}(A)}} . \tag{3.44}$$

Similarly, probabilities for decay or shape transition of a class-II state are

$$P_{\mathrm{II}(\alpha')} = \frac{T_{\mathrm{II}(\alpha')}}{\sum_{\beta'} T_{\mathrm{II}(\beta')} + T_{\mathrm{II}(A)}} , \tag{3.45}$$

$$P_{\mathrm{II}\to\mathrm{I}} = \frac{T_{\mathrm{II}(A)}}{\sum_{\beta'} T_{\mathrm{II}(\beta')} + T_{\mathrm{II}(A)}} . \tag{3.46}$$

Given these probabilities the overall decay of the nucleus can be calculated. Let us assume that the nucleus is initially populated entirely in class-I states. The initial stage of decay consists of a fraction $P_{\mathrm{I}(d)} = \sum_\beta P_{\mathrm{I}(\beta)}$ decaying to all residual systems allowed to class-I decay (these will principally be, according to the Franck–Condon principle, class-I states of lower excitation in the same nucleus, reached by gamma transitions, and residual nuclei of class-I shape reached by neutron emission) and a fraction $P_{\mathrm{I}\to\mathrm{II}}$ changing to shape II. The second stage of decay therefore consists of a fraction $P_{\mathrm{I}\to\mathrm{II}} \cdot P_{\mathrm{II}(d')}$ (where $P_{\mathrm{II}(d')} = \sum_{\beta'} P_{\mathrm{II}(\beta')}$) decaying by processes allowed by the Franck–Condon principle for class-II state decay (this is either fission, over barrier B, or formation of residual nuclei in shape II) and a fraction $P_{\mathrm{I}\to\mathrm{II}} \cdot P_{\mathrm{II}\to\mathrm{I}}$ changing back to shape I. The third stage consists of this new fraction $P_{\mathrm{I}\to\mathrm{II}} \cdot P_{\mathrm{II}\to\mathrm{I}}$ dividing as in the first stage, and if the process is followed through and the infinite series thus generated are summed we have for the final fraction of decay to shapes I or II (II here includes fission), respectively,

$$F_{(d_{\mathrm{I}})} = \sum_{n=0}^{\infty} (P_{\mathrm{I}\to\mathrm{II}} \cdot P_{\mathrm{II}\to\mathrm{I}})^n P_{\mathrm{I}(d_{\mathrm{I}})} = \frac{P_{\mathrm{I}(d_{\mathrm{I}})}}{1 - P_{\mathrm{I}\to\mathrm{II}} P_{\mathrm{II}\to\mathrm{I}}}$$
$$= T_{\mathrm{I}(d)} \frac{T_{\mathrm{II}(A)} + T_{\mathrm{II}(d')}}{\{(T_{\mathrm{I}(d)} + T_{\mathrm{I}(A)})(T_{\mathrm{II}(A)} + T_{\mathrm{II}(d')}) - T_{\mathrm{I}(A)} T_{\mathrm{II}(A)}\}} , \tag{3.47}$$

$$F_{(d_{II})} = \sum_{n=0}^{\infty} (P_{I\to II}P_{II\to I})^n P_{I\to II}P_{II(d')}$$
$$= \frac{P_{I\to II}P_{II(d')}}{1-P_{I\to II}P_{II\to I}}$$
$$= \frac{T_{I(A)}T_{II(d')}}{(T_{I(d)}+T_{I(A)})(T_{II(d')}+T_{II(A)})-T_{I(A)}T_{II(A)}} . \quad (3.48)$$

The fractions for individual decay processes are contained within these expressions. Thus the fraction of decay by prompt fission, for example, is given by

$$F_{(F)} = \frac{T_{I(A)}T_{II(B)}}{(T_{I(d)}+T_{I(A)})(T_{II(d')}+T_{II(A)})-T_{I(A)}T_{II(A)}} . \quad (3.49)$$

For decay of the compound nucleus excited initially in a class-I shape the ratio of decay either by fission or to residual nuclei of shape II, relative to decay to shape I states, is therefore

$$\frac{F_{(d_{II})}}{F_{(d_I)}} = \frac{T_{I(A)}T_{II(d')}}{(T_{II(A)}+T_{II(d')})T_{I(d)}} . \quad (3.50)$$

This expression is remarkable for the factor $T_{I(A)}/(T_{II(A)}+T_{II(d')})$ by which the ratio is reduced below that expected for completely mixed compound nucleus motion, $T_{II(d')}/T_{I(d)}$. For the kind of fission barrier exhibited by the actinide nuclei, fission decay ($T_{II(B)}$) completely dominates particle or radiative decay. If the barrier A is much lower than B then it is expected that $T_{II(A)} \gg T_{II(B)}$, and since, according to the theory of reaction rates over a single barrier (Wigner, 1938) $T_{I(A)} = T_{II(A)}$, Eq. (3.50) reduces consequently to the complete mixing expression. If, on the other hand, B is much lower than A, the factor $T_{I(A)}/(T_{II(A)}+T_{II(B)})$ is much less than unity; and this implies a partial decoupling persisting between the class-I and class-II states.

2. Time-dependent treatment

Such decoupling can be demonstrated more explicitly (Bjørnholm and Strutinsky, 1969) by studying the time development of the system, with a population normalized to unity at time, $\tau = 0$ in the first well, and set to zero in the second well,

$$n_1(0) = 1, \quad n_2(0) = 0 .$$

The rate of change of these populations in time is given by

$$\frac{\partial n_1}{\partial \tau} = -\Gamma_{I(t)}n_1 + \Gamma_{II(\to I)}n_2 \quad (3.51a)$$

$$\frac{\partial n_2}{\partial \tau} = \Gamma_{I(\to II)}n_1 - \Gamma_{II(t)}n_2 , \quad (3.51b)$$

where $\Gamma_{I(t)}$, $\Gamma_{II(t)}$ are the total width of class-I and class-II states, being the sum of a decay width ($\Gamma_{I(d)}$ or $\Gamma_{II(d)}$, respectively) and a width for shape transition ($\Gamma_{I(\to II)}$ or $\Gamma_{II(\to I)}$). The solution to the coupled differential equation (3.51) is

$$n_1 = \frac{1}{2\Delta}[(\Delta - \Gamma_{I(t)} + \Gamma_{II(t)})e^{-S_e\tau} + (\Delta + \Gamma_{I(t)} - \Gamma_{II(t)})e^{-S_g\tau}], \quad (3.52a)$$

$$n_2 = \frac{\Gamma_{I(\to II)}}{\Delta}(e^{-S_e\tau} - e^{-S_g\tau}), \quad (3.52b)$$

where

$$S_e = \tfrac{1}{2}(\Gamma_{I(t)} + \Gamma_{II(t)} - \Delta) \quad (3.52c)$$

$$S_g = \tfrac{1}{2}(\Gamma_{I(t)} + \Gamma_{II(t)} + \Delta) \quad (3.52d)$$

$$\Delta = [R^2 + 4\Gamma_{I(\to II)}(\Gamma_{I(d)} - \Gamma_{II(d)})]^{1/2} \quad (3.52e)$$

$$R = \Gamma_{I(d)} - \Gamma_{I(\to II)} - \Gamma_{II(t)} . \quad (3.52f)$$

From Eqs. (3.52) any specific decay rate may be computed. Thus the fission rate is determined from n_2 by

$$\frac{\partial n_f}{\partial \tau} = \Gamma_{II(f)}n_2(\tau) , \quad (3.53)$$

and by integrating this over all time we find the branching ratio for fission $\bar{\Gamma}_{(f)}/\bar{\Gamma}_{(t)}$

$$\frac{\bar{\Gamma}_{(f)}}{\bar{\Gamma}_{(t)}} = n_f(\infty) = \frac{\Gamma_{I(\to II)}\Gamma_{II(f)}}{\Gamma_{I(t)}\Gamma_{II(t)} - \Gamma_{I(\to II)}\Gamma_{II(\to I)}} . \quad (3.54)$$

Our immediate interest, however, is in the number of nuclei remaining undecayed after time τ

$$N(\tau) = n_1(\tau) + n_2(\tau)$$
$$= \frac{1}{2\Delta}[(\Delta - R)e^{-S_e\tau} + (\Delta + R)e^{-S_g\tau}] . \quad (3.55)$$

This formula indicates the existence of two decay modes of the coupled system.

To determine the partial decay widths of the coupled system from the branching ratios, such as Eq. (3.54), it is necessary to compute the average total width. The prescription of Bjørnholm and Strutinsky (1969) is to compute the time τ_e for decay of the total population of the system N to the value $1/e$. This can be done numerically, or approximations can be considered that lead to an analytical expression for Γ_t.

For weak coupling of the primary well to the secondary well, $\Gamma_{I\to II}$ can be neglected in comparison with other widths, giving

$$R \approx \Gamma_{I(d)} - \Gamma_{II(t)} , \quad (3.56)$$

$$\Delta \approx R + 2\Gamma_{I\to II}(\Gamma_{I(d)} - \Gamma_{II(d)})/|R| . \quad (3.57)$$

This leads to a principal component in $N(\tau)$ with half-life $1/S_g$ corresponding to a total width Γ_t

$$\Gamma_t \approx \Gamma_{I(d)} + \Gamma_{I\to II}\frac{(\Gamma_{I(d)} - \Gamma_{II(d)})}{(\Gamma_{I(d)} - \Gamma_{II(d)})} , \quad (3.58)$$

and hence

$$\Gamma_f \approx \frac{\Gamma_{I\to II}\Gamma_{II(f)}}{\Gamma_{II(t)}} . \quad (3.59)$$

Strong coupling between the two wells operates when either $\Gamma_{I\to II}$ or $\Gamma_{II\to I}$ is larger than both the decay widths $\Gamma_{I(d)}$, $\Gamma_{II(d)}$, and in this case

$$\Gamma_t \approx S_e \approx \frac{\Gamma_{I\to II}\Gamma_{II(d)} + \Gamma_{II\to I}\Gamma_{I(d)}}{\Gamma_{I\to II} + \Gamma_{II\to I}} . \quad (3.60)$$

Hence,

$$\Gamma_f \approx \frac{\Gamma_{I\to II}\Gamma_{II(f)}}{\Gamma_{I\to II} + \Gamma_{II\to I}} . \quad (3.61)$$

The time development of a two-well system has been generalized (Sperber and Aframe, 1972) to the case where changing populations at different energies are considered and the transition widths are energy dependent. For this purpose a set of integrodifferential equations must be solved.

C. Formal treatment of fission reaction theory

The treatment of most details of fission reactions at low energies requires the consideration of the role of degrees of freedom other than the fission mode in more detail than the simple damping incorporated in phenomenological theories. Theories that treat these other degrees of freedom explicitly from the start can be regarded as formal reaction theories incorporating the fission process.

A few formal reaction theories incorporating fission have been proposed. The principal phenomenon to be explained by such formal theories is the appearance of intermediate structure in fission cross sections (see the examples in Figs. 6 and 7). This can be accounted for by quite general approaches. For example, Weigmann (1968) postulates the existence of an intermediate state, which may be of complicated character, that couples to the fission channel; this state is assumed to be localized to the deformation of the secondary well. The normal states of the system are coupled to the open-particle channel and to the intermediate state by the methods of Weidenmüller and Dietrich (1966) and Mahaux and Weidenmüller (1967). Nörenberg (1970) showed how the intermediate state can be defined by the generator coordinate method of Hill and Wheeler (1953) and Griffin and Wheeler (1957).

More precise definitions of the complicated interacting states can be made within the R-matrix theory of nuclear reactions (Lynn, 1968a, b; 1973), and this allows quantitative calculations of intermediate structure and related phenomena for various assumptions about the fission barrier. In the original R-matrix theory for reactions involving absorption and emission of relatively simple particles (Wigner and Eisenbud, 1947; Lane and Thomas, 1958) discrete solutions (the internal R-matrix states) of the Schrödinger equation are set up in a nuclear internal region with boundary conditions imposed at the entrances to the reaction channels; internal wave functions are written as expansions of these basis solutions and enable the matching conditions between the internal and channel wave functions to be expressed; this leads in turn to the collision matrix (the elements of which are defined as the amplitudes of outgoing waves in the channel for incoming wave of unit flux in any given entrance channel) and cross sections for the reactions. One of the special features of this approach for fission through a double-humped barrier is the introduction of two sets of auxiliary internal R-matrix states, the wave functions of the states of each set being largely confined to deformation regions corresponding to the primary and secondary wells, respectively, of the deformation potential. Just as the R-matrix states of the conventional R-matrix theory can be made by judicious choice of boundary conditions to correspond closely to the resonances ("compound nucleus states") observed in reaction cross sections, so these two sets of auxiliary states correspond approximately to the normal fine-structure resonances observed in simple particle or capture reactions (class-I auxiliary states) and to the intermediate structure groups observed in fission cross sections (class-II auxiliary states). It is to be emphasized that these latter states can be very complicated ones depending on the many intrinsic degrees of freedom of the nucleus as well as the prolate deformation mode; they are thus to be described as "compound states" with the nuclear shape essentially confined to the highly deformed values associated with the secondary minimum.

The other special feature is the introduction of the concept of the deformation channel. The channel entrance can be set at a fixed elongation of the incipient fissioning nucleus, and this will normally be close to a barrier peak in the deformation energy. In this region of deformation the nucleus can be expected to be in a state of intrinsic excitation (Bohr 1956) analogous to the states of excitation of the product nuclei in a particle reaction channel. In this review, the R-matrix theory as thus extended to the fission process is employed as the principal framework for analysis and discussion of the detailed phenomena in near-barrier fission. This theory is therefore described more fully below.

1. The Hamiltonian operator and explicit reference to the deformation mode

In order to write the nuclear Hamiltonian in a form suitable for describing the fission reaction in formal R-matrix theory, it is necessary to choose a deformation parameter that will describe the separation of the parts of the divided nucleus as well as small deformations of the original compound nucleus. A discussion of deformation parameters that have been employed in various aspects of fission theory is given in the Appendix. The deformation parameters described there can be classified into those that are dependent on a description of the surface shape of the nucleus and those of a statistical character, related to the individual nucleon coordinates. The shortcomings of a surface shape parameter in a formal reaction theory, namely, the necessity of assuming a specific form for the shape that will, moreover, be useful for all stages of the fission process, can be avoided by using one of the statistical parameters. At this stage we shall not choose a specific deformation parameter, but shall merely refer to it with the generalized symbol η. The remaining $3A$-4 degrees of freedom (it being assumed that the three degrees of freedom associated with the center of mass have already been separated out) are known collectively as the "intrinsic" degrees of freedom and are denoted collectively by the symbol ξ.

It is now assumed that the kinetic energy operator of the nuclear Hamiltonian can be separated into components referring explicitly to the deformation parameter η and the intrinsic coordinates ξ, respectively. While it is possible to choose a deformation parameter η that allows its kinetic energy operator to be independent of the intrinsic degrees of freedom, it is not in general possible at the same time to free the remaining component of the kinetic energy from all dependence on deformation. Thus

$$T = T_\eta + T_\xi(\eta) . \tag{3.62}$$

Likewise the potential energy $V(\eta, \xi)$ will not, in general, be a separable function of η and ξ, and it is necessary to find a prescription that will give an approxima-

tion to the overall dependence of the potential energy on η. The prescription that we choose is in the spirit of Strutinsky's theory of the deformation energy, and consists of representing the potential energy for the deformation by the minimum total intrinsic energy surface. More precisely, of the eigenvalues $\varepsilon_\mu(\eta)$ of the operator

$$H_\xi(\eta) = T_\xi(\eta) + V(\eta, \xi), \tag{3.63}$$

for a fixed value of η, the lowest eigenvalue $\varepsilon_0(\eta)$ is taken as the deformation potential energy $\upsilon(\eta)$. An intrinsic Hamiltonian term $H_{\rm int}$ can now be defined for some chosen value of deformation η_0, and also a "coupling" term H_c depending on both deformation and intrinsic variables. Thus

$$H = H_\eta + H_{\rm int}(\xi, \eta_0) + H_c(\eta, \xi, \eta_0), \tag{3.64}$$

where

$$H_\eta = T_\eta + \upsilon(\eta), \tag{3.65}$$

$$H_{\rm int}(\xi, \eta_0) = T_\xi(\eta_0) - \varepsilon_0(\eta_0) + V(\eta_0, \xi), \tag{3.66}$$

$$H_c = T_\xi(\eta) - \varepsilon_0(\eta) + V(\eta, \xi) - H_{\rm int}(\eta_0). \tag{3.67}$$

It is useful to be able to generalize the intrinsic Hamiltonian to any other value of deformation η. Therefore we shall denote the eigenvalues and eigenfunctions of $H_{\rm int}(\eta)$ by $\mathcal{E}_\mu(\eta)$ and $\chi_\mu(\eta)$, and from the definition of $H_{\rm int}$, the eigenvalues $\mathcal{E}_\mu(\eta)$ are just $\varepsilon_\mu(\eta) - \varepsilon_0(\eta)$, the intrinsic excitation energies with respect to "ground" at the fixed deformation η. The eigenfunctions and eigenvalues of H_η are denoted by $\Phi_\nu(\eta)$ and ϵ_ν.

2. Form of the kinetic energy operator for the deformation variable

In phenomenological models of the liquid drop type, the usual procedure in setting up the Hamiltonian is to write the kinetic and potential energy terms for irrotational flow in terms of the shape parameters (denoted here by α_λ). The quantal operator for the kinetic energy term is then written according to the Schrödinger prescription:

$$T = -\frac{\hbar^2}{2} \sum_{\lambda,\mu} \frac{1}{\sqrt{B}} \frac{\partial}{\partial \alpha_\lambda} \left(\sqrt{B}\, B^{\lambda\mu} \frac{\partial}{\partial \alpha_\mu} \right), \tag{3.68}$$

where $B_{\lambda\mu}$ is the relevant element of the covariant inertial tensor, B is the determinant of this tensor, and $B^{\lambda\mu}$ is the element of the related contravariant tensor

$$\sum_\nu B^{\lambda\nu} B_{\nu\mu} = \delta^\lambda_\mu. \tag{3.69}$$

Discussions of the ambiguities of this procedure, particularly when the shape variables constitute only a part of the total degrees of freedom of the system, have been given by Jensen and Koppe (1971), Dietrich (1972), Hofmann (1972b), and Nörenberg (1973). Briefly, it turns out that the ambiguity in the kinetic energy term for any single variable is equivalent to a curvature term to be added to the potential energy.

As an example of the phenomenological procedure we can take the simple quadrupole deformation parameter β of Eq. (A7). For small values of β the kinetic energy operator is

$$T_\beta = -\frac{\hbar^2}{2B_\beta} \frac{\partial^2}{\partial \beta^2}. \tag{3.70}$$

The inertial parameter B_β for the irrotational liquid drop is

$$B_\beta = 3AmR_0^2/8\pi, \tag{3.71}$$

where m is the nucleon mass, so that Am is the liquid drop mass, and R_0 is the radius of the drop. If the potential energy has the quadratic form

$$V_\beta = \tfrac{1}{2} C_\beta \beta^2, \tag{3.72}$$

with stiffness parameter C_β, as expected in the liquid drop model, the solutions of the Schrödinger equation in the β variable are the well-known Hermite functions with eigenvalues

$$E_n = (n + \tfrac{1}{2})\hbar\omega_\beta = (n + \tfrac{1}{2})\hbar (C_\beta/B_\beta)^{1/2}. \tag{3.73}$$

The form of the kinetic energy operator for statistical deformation parameters can be derived without ambiguity from the Schrödinger form for the Cartesian coordinates of a system of particles (here assumed to have equal mass, m):

$$T = -\frac{\hbar^2}{2m} \sum_i \left(\frac{\partial^2}{\partial x_i^2} + \frac{\partial^2}{\partial y_i^2} + \frac{\partial^2}{\partial z_i^2} \right). \tag{3.74}$$

The general equation for transforming the second derivative in a particular coordinate, say x_i, into the second derivatives of a new set of coordinates ξ_j is

$$\frac{\partial^2 \psi}{\partial x_i^2} = \sum_j \left\{ \frac{\partial^2 \psi}{\partial \xi_j^2} \left(\frac{\partial \xi_j}{\partial x_i} \right)^2 + \frac{\partial \psi}{\partial \xi_j} \frac{\partial^2 \xi_j}{\partial x_i^2} \right\} + \sum_{j \neq k} \frac{\partial^2 \psi}{\partial \xi_j \partial \xi_k} \left(\frac{\partial \xi_j}{\partial x_i} \right) \left(\frac{\partial \xi_k}{\partial x_i} \right). \tag{3.75}$$

Hence, the generalized Laplacian term of Eq. (3.74) is

$$\sum_i \left(\frac{\partial^2 \psi}{\partial x_i^2} + \frac{\partial^2 \psi}{\partial y_i^2} + \frac{\partial^2 \psi}{\partial z_i^2} \right) = \sum_j \left\{ \frac{\partial^2 \psi}{\partial \xi_j^2} \sum_i \left[\left(\frac{\partial \xi_j}{\partial x_i} \right)^2 + \left(\frac{\partial \xi_j}{\partial y_i} \right)^2 + \left(\frac{\partial \xi_j}{\partial z_i} \right)^2 \right] + \frac{\partial \psi}{\partial \xi_j} \sum_i \left(\frac{\partial^2 \xi_j}{\partial x_i^2} + \frac{\partial^2 \xi_j}{\partial y_i^2} + \frac{\partial^2 \xi_j}{\partial z_i^2} \right) \right\}$$
$$+ \sum_{j \neq k} \frac{\partial^2 \psi}{\partial \xi_j \partial \xi_k} \sum_i \left(\frac{\partial \xi_j}{\partial x_i} \frac{\partial \xi_k}{\partial x_i} + \frac{\partial \xi_j}{\partial y_i} \frac{\partial \xi_k}{\partial y_i} + \frac{\partial \xi_j}{\partial z_i} \frac{\partial \xi_k}{\partial z_i} \right). \tag{3.76}$$

The condition of orthogonality for the new coordinates ξ_j is

$$\sum_i \left(\frac{\partial \xi_j}{\partial x_i} \frac{\partial \xi_k}{\partial x_i} + \frac{\partial \xi_j}{\partial y_i} \frac{\partial \xi_k}{\partial y_i} + \frac{\partial \xi_j}{\partial z_i} \frac{\partial \xi_k}{\partial z_i} \right) = \delta_{jk}. \tag{3.77}$$

Hence, the summation over $j \neq k$ on the right-hand side of Eq. (3.76) vanishes for an orthogonal coordinate system.

Equation (3.76) can be formally expressed in terms of the scale factors h_j

$$h_j^2=\left[\sum_i\left\{\left(\frac{\partial\xi_j}{\partial x_i}\right)^2+\left(\frac{\partial\xi_j}{\partial y_i}\right)^2+\left(\frac{\partial\xi_j}{\partial z_i}\right)^2\right\}\right]^{-1} \tag{3.78}$$

as

$$\sum_i\left(\frac{\partial^2\psi}{\partial x_i^2}+\frac{\partial^2\psi}{\partial y_i^2}+\frac{\partial^2\psi}{\partial z_i^2}\right)=\frac{1}{\Pi_k h_k}\sum_j\frac{\partial}{\partial\xi_j}\left[\frac{\Pi_k h_k}{h_j^2}\frac{\partial\psi}{\partial\xi_j}\right] \tag{3.79}$$

for an orthogonal system.

As an example of the application of Eq. (3.79), if the deformation parameter η of a new coordinate set is taken to be the quadrupole moment Q defined by Eq. (A21), the kinetic energy operator is

$$T_Q=-\frac{\hbar^2(4Q+8A\overline{r^2})}{2m}\frac{\partial^2}{\partial Q^2}, \tag{3.80}$$

where $\overline{r^2}$ is the mean square of the radial positions of the nucleons (with respect to the center of mass). The inertial parameter appropriate to the quadrupole moment appears in this operator as

$$B_Q=\frac{m}{4Q+8A\overline{r^2}}. \tag{3.81}$$

For asymptotically large separation l of the two fission products the quadrupole moment is

$$Q=\frac{2A_1A_2}{A_1+A_2}l^2=\frac{2M}{m}l^2, \tag{3.82a}$$

where A_1 and A_2 are the mass numbers of the product and M is their reduced mass. In this asymptotic situation the kinetic energy operator of Eq. (3.80) becomes

$$T_Q=-\frac{\hbar^2}{2M}\frac{\partial^2}{\partial l^2}. \tag{3.82b}$$

For near-spherical spheroidal deformation on the other hand, the quadrupole moment can be related to the spheroidal deformation parameter β [see Eq. (A22)]

$$Q\approx\frac{3AR_0^2}{(5\pi)^{1/2}}\cdot\beta, \tag{3.82c}$$

and the inertial parameter $B_Q\sim(5m/24AR_0^2)\{1-(\frac{5}{4\pi})^{1/2}\beta\}$ The kinetic energy operator transformed into its form for β in this limit is just

$$T_\beta=-\frac{\hbar^2}{2B_\beta}\frac{\partial^2}{\partial\beta^2}, \tag{3.82d}$$

with the inertial parameter of Eq. (3.71) appropriate to irrotational flow.

The most easily handled of parameters of the statistical class is the mean square radius parameter

$$\mathfrak{R}=\left\{\sum_i(x_i^2+y_i^2+z_i^2)\right\}^{1/2}, \tag{3.83}$$

to which corresponds a kinetic energy operator

$$T_{\mathfrak{R}}=-\frac{\hbar^2}{2m\mathfrak{R}^{3A-4}}\frac{\partial}{\partial\mathfrak{R}}\left(\mathfrak{R}^{3A-4}\frac{\partial}{\partial\mathfrak{R}}\right). \tag{3.84}$$

3. General R-matrix theory

a. Green's theorem for the nuclear internal region

The central relationship of R-matrix theory connects the values and derivatives of the wave function of the compound nucleus at the channel entrances. For this purpose the compound nucleus is defined as an internal region of the configuration space of all the nucleons in the interacting system. The internal region itself is delineated by setting boundaries in the energetically open reaction channels. At this surface the relation between values and derivatives is deduced by means of Green's theorem. The wave functions of the Schrödinger equation for the nuclear Hamiltonian in the internal region are denoted by Ψ_1 and Ψ_2 for two energies E_1 and E_2. The left- and right-hand sides of the Schrödinger equation for one of these solutions is multiplied by the complex conjugate of the other solution; this is subtracted from the transpose equation and then integrated over the internal region, thus:

$$\int_\tau d\tau[\Psi_1 H\Psi_2^*-\Psi_2^* H\Psi_1]=(E_2-E_1)\int_\tau d\tau\,\Psi_2^*\Psi_1, \tag{3.85}$$

where τ denotes the internal volume. This can be reduced to an integral over the internal surface by Green's theorem. To do this the potential energy terms of the Hamiltonian are assumed to have the usual self-adjoint property, which allows them to vanish from the integrand on the left-hand side of Eq. (3.85), leaving only the terms which involve the kinetic energy operator of H. Thus Eq. (3.85) becomes

$$(E_2-E_1)\int_\tau d\tau\,\Psi_2^*\Psi_1=\int_{\mathcal{S}}d\mathcal{S}\left(\frac{\hbar^2}{2B_c}\right)\left(\Psi_2^*\nabla_n\Psi_1-\Psi_1\nabla_n\Psi_2^*\right), \tag{3.86}$$

where $\mathcal{S}$ denotes the surface of the internal region, B_c signifies the inertial parameter of each channel c in which a boundary of the internal region is placed, and ∇_n is the gradient operator normal to the surface $\mathcal{S}$. This integral can be expressed as a product of value and derivative quantities at the channel entrances:

$$(E_2-E_1)\int_\tau d\tau\Psi_2^*\Psi_1=\sum_c(V_{2c}^*D_{1c}-V_{1c}D_{2c}^*). \tag{3.87}$$

The values V_c and derivatives D_c are defined as the projections of the wave function Ψ and its gradient against a channel surface function describing the state of the system in the channel for all degrees of freedom other than the channel variable. The total set of channels in the sum on the rhs of Eq. (3.87) comprises deformation as well as particle channels.

It should be noted that if the ratio of value to derivative for each channel has a fixed value (boundary condition) independent of the labeling of the state, then the states Ψ_1, Ψ_2 are orthogonal; this is the basis of the definition of the R-matrix eigenstates (see Sec. III.C. 3.b.).

Equation (3.87) is a compact formal way of writing a result which can probably be most easily demonstrated by making expansions of the wave functions Ψ in a way that is appropriate to a physical description of the channels. First, consider a set of channels that are characterized by the residual system (in configuration space outside of the internal system) having a particular grouping of nucleons (e.g., an alpha particle plus residual nucleus or a neutron plus residual nucleus); this is the channel type α and for it a specific inertial parameter B_α and a channel separation parameter ρ_α can be assigned. For the simple particle channels given as examples above, the inertial parameter is just the reduced mass of the separated residual nuclei, and the channel separation parameter is their radial separation (measured between their individual centers of mass).

The particular grouping of nucleons designated as a single-channel type can occur in various states of internal excitation and in different modes of relative angular momentum. Each combination of state of excitation and angular momentum constitutes a separate channel, denoted by c, and the complete wave function describing the state of excitation and relative angular momentum is denoted by ϕ_c. The wave function describing the relative motion in the channel is denoted by $u_c(\rho_\alpha)$. The appropriate expansion of Ψ_n for the set of channels of type α (denoted by $c\{\alpha\}$) is, therefore,

$$\Psi_n=\sum_{c\{\alpha\}} C_c^{(n)}\phi_c u_c^{(n)}(\rho_\alpha), \tag{3.88}$$

with expansion coefficients $C_c^{(n)}$. Such an expansion is not limited to the external region, defined by a channel boundary $\rho_\alpha \geq R_\alpha$, but can also be continued into the internal region. However, if the channel functions ϕ_c are limited to internal states of excitation that are all bound and the wave function of relative motion u_c describes unbound relative motion, then the expansion (3.88) is incomplete in the internal region; completeness is to be achieved by adding similar expansions over other types of channels.

However, with the limitation at present to the expansion (3.88) and the appropriate rearrangement of the kinetic energy operator for explicit dependence on the channel separation parameter ρ_α and other degrees of freedom (including the internal ones of the residual system) $\xi_1^{(\alpha)},\ldots,\xi_k^{(\alpha)}$, say, Eq. (3.85) becomes

$$\begin{aligned}(E_2-E_1)\int_\tau d\tau\,\Psi_2^*\Psi_1=(E_2-E_1)\int\cdots\int_0^{R_\alpha} h_{\rho_\alpha}d\rho_\alpha\, h_{\xi_1}^{(\alpha)}\,d\xi_1^{(\alpha)}\cdots \\ \times h_{\xi_k}^{(\alpha)}\;\; d\xi_k^{(\alpha)}\sum_{c\{\alpha\}}C_c^{(2)}\phi_c^*u_c^{(2)*}(\rho_\alpha)\sum_{c'\{\alpha\}}C_{c'}^{(1)}\phi_{c'}u_{c'}^{(1)}(\rho_\alpha) \\ =\int\cdots\int_0^{P_\alpha} h_{\rho_\alpha}d\rho_\alpha\cdots h_{\xi_k}^{(\alpha)}\,d\xi_k^{(\alpha)}\sum_{c\{\alpha\},c'\{\alpha\}}C_c^{(2)}C_{c'}^{(1)}\left\{\phi_c^*\phi_{c'}\left(\frac{\hbar^2}{2m}\right)\left[\frac{u_c^{(2)*}}{\Pi h}\frac{\partial}{\partial\rho_\alpha}\left(\frac{\Pi h}{h^2\rho_\alpha}\frac{\partial u_{c'}^{(1)}}{\partial\rho_\alpha}\right)\right.\right. \\ \left.-\frac{u_{c'}^{(1)}}{\Pi h}\frac{\partial}{\partial\rho_\alpha}\left(\frac{\Pi h}{h_{\rho\alpha}^2}\frac{\partial u_c^{(2)*}}{\partial\rho_\alpha}\right)\right]-u_c^{(2)*}u_{c'}^{(1)} \\ \times\left[\phi_c^*\sum_j T_{\xi_j}^{(\alpha)}\,\phi_{c'}\right. \\ \left.\left.-\phi_{c'}\sum_j T_{\xi_j}^{(\alpha)}\,\phi_c^*\right]\right\}. \end{aligned}\tag{3.89}$$

The terms in $T_{\xi_j}^{(\alpha)}$ vanish so long as they involve bound states $\phi_{c\alpha}$, i.e., do not involve channels that are not of type α. In this case the term involving the kinetic energy of the channel pair reduces to

$$\begin{aligned}&\int\cdots\int h_{\rho_\alpha}\frac{h_{\xi_1}^{(\alpha)}}{f_\alpha^2(\rho_\alpha)}d\xi_1^{(\alpha)}\cdots h_{\xi_k}^{(\alpha)}\;d\xi_k^{(\alpha)}\sum_{c\{\alpha\}c'\{\alpha\}}C_c^{(2)}C_{c'}^{(1)}\phi_c^*\phi_{c'} \\ &\left(\frac{\hbar^2}{2m}\right)\left[\frac{f_\alpha(\rho_\alpha)u_{c'}^{(2)*}}{h_{\rho_\alpha}^2}\frac{\partial(fu_{c'}^{(1)})}{\partial\rho_\alpha}-\frac{f_\alpha(\rho_\alpha)u_{c'}^{(1)}}{h_{\rho\alpha}^2}\frac{\partial(fu_{c'}^{(2)*})}{\partial\rho_\alpha}\right]_0^{R_\alpha}=\left(+\frac{\hbar^2}{2m}\right)\sum_{c\{\alpha\}}C_c^{(2)}C_c^{(1)}\left[\frac{f_\alpha u_c^{(2)*}}{h_{\rho\alpha}^2}\frac{\partial(f_\alpha u_c^{(1)})}{\partial\rho_\alpha}-\frac{f_\alpha u_c^{(1)}}{h_{\rho\alpha}^2}\frac{\partial(f_\alpha u_c^{(2)*})}{\partial\rho_\alpha}\right]_0^{R_\alpha},\end{aligned}\tag{3.90}$$

where $f_\alpha^2(\rho_\alpha)$ is a factor giving the dependence of the product $h_{\xi_1}^{(\alpha)}\ldots h_{\xi_k}^{(\alpha)}$ upon ρ_α. If the nuclei of channels of type α are divided into A_1 and $A-A_1$ nucleons, respectively, the separation parameter is

$$\rho_\alpha=\left[\left(\frac{1}{A_1}\sum_{i=1}^{A_1}x_i-\frac{1}{A-A_1}\sum_{j=A_1+1}^{A}x_j\right)^2+\left(\frac{1}{A_1}\sum_{i=1}^{A_1}y_i-\frac{1}{A-A_1}\sum_{j=A_1+1}^{A}y_j\right)^2+\left(\frac{1}{A_1}\sum_{i=1}^{A_1}z_i-\frac{1}{A-A_1}\sum_{j=A_1+1}^{A}z_j\right)^2\right]^{1/2}. \tag{3.91}$$

From this it is straightforward to derive

$$\frac{1}{h_{\rho_\alpha}^2}=\frac{A}{A_1(A-A_1)}, \tag{3.92}$$

and

$$\prod_{j=1}^{k}h_{\xi_j}^{(\alpha)}\propto\rho_\alpha^2=f_\alpha^2(\rho_\alpha). \tag{3.93}$$

For channels of this type, the value and derivative quantities of the general Eq. (3.87) can be written

$$V_{nc}=\left(\frac{\hbar^2}{2M_\alpha R_\alpha}\right)^{1/2}C_c^{(n)}R_\alpha u_c^{(n)}(R_\alpha), \tag{3.94}$$

and

$$D_{nc}=\left(\frac{\hbar^2R_\alpha}{2M_\alpha}\right)^{1/2}C_c^{(n)}\left[\frac{\partial}{\partial\rho_\alpha}(\rho_\alpha u_c^{(n)})\right]_{\rho_\alpha=R_\alpha}, \tag{3.95}$$

respectively; here, $M_\alpha=B_\alpha$ is the reduced mass of the two particles in the channel. Note that the normalization of the channel function is

$$\int\cdots\int\frac{\Pi h}{f_\alpha^2}d\xi_1^{(\alpha)}\ldots d\xi_k^{(\alpha)}\quad\phi_{c_\alpha}^*\phi_{c'_\alpha}=\delta_{c_\alpha c'_\alpha},$$

which implies that the normalization of basis radial eigenfunctions (for the description of the internal region) appropriate to the channel is

$$\int_0^{R_\alpha}d\rho_\alpha f_\alpha^2(\rho_\alpha)u_\lambda^*u_{\lambda'}=\delta_{\lambda\lambda'}.$$

The same kind of analysis can be applied to channels characterized by a deformation parameter η, such as the quadrupole moment Q or the root-mean-squared radius $\mathcal{R}$. The appropriate expansion in this case is

$$\Psi_n=\sum_{c_\mu}C_{c_\mu}^{(n)}\chi_{c_\mu}\Phi_{(\mu)}^{(n)}(\eta) \tag{3.96}$$

(the deformation channel being labeled by the intrinsic state of excitation μ), and the expansion of the volume integral is

$$(E_2-E_1)\int_\tau d\tau\,\Psi_2^*\Psi_1=\int\cdots\int_{\eta_{\min}}^{\eta_0} h_\eta d_\eta\cdots h_{\xi_k}d\xi_k \times\sum_{c_\mu,c'_\mu} C_{c_\mu}^{(2)}C_{c'_\mu}^{(1)}\left\{\chi_{c_\mu}^*\chi_{c'_\mu}\left(\frac{\hbar^2}{2m}\right)\left[\frac{\Phi_{(\mu)}^{(2)*}}{\Pi h}\frac{\partial}{\partial\eta}\frac{\Pi h}{h_\eta^2}\frac{\partial\Phi_{(\mu')}^{(1)}}{\partial\eta}-\frac{\Phi_{(\mu')}^{(1)}}{\Pi h}\frac{\partial}{\partial\eta}\left(\frac{\Pi h}{h_\eta^2}\frac{\partial\Phi_{(\mu)}^{(2)*}}{\partial\eta}\right)\right]\right. \left.+\Phi^{(2)*}\Phi^{(1)}\left[\chi_{c_\mu}^*\sum_j T_{\xi_j}\chi_{c'_\mu}-\chi_{c'_\mu}\sum_j T_{\xi_j}\chi_{c_\mu}^*\right]\right\}, \tag{3.97}$$

where η_0 defines the entrance to the fission channels. As in the separated-particle case, if the expansion (3.96) is limited to bound intrinsic wave functions χ_μ that are appropriate to a description of the fission process, the term on the right-hand side involving the kinetic energy operators T_{ξ_j} vanishes. On the other hand, if the expansion (3.96) is defined to be formally complete, this term corresponds to the contributions to the surface integral from the other (separated-particle) channels of the kind already dealt with in Eq. (3.90). The contribution to the surface integral can now be written as before

$$\int\cdots\int h_\eta\frac{h_{\xi_1}}{f^2(\eta)}d\xi_1\cdots h_{\xi_k}d\xi_k\sum_{c_\mu,c'_\mu}C_{c_\mu}^{(2)}C_{c'_\mu}^{(1)}\chi_{c_\mu}^*\chi_{c'_\mu} \times\left(\frac{\hbar^2}{2m}\right)\left[\frac{f(\eta)\Phi_{(\mu)}^{(2)*}}{h_\eta^2}\frac{\partial(f\Phi_{(\mu')}^{(1)})}{\partial\eta}-\frac{f(\eta)\Phi_{(\mu')}^{(1)}}{h_\eta^2}\frac{\partial(f\Phi_{(\mu)}^{(2)*})}{\partial\eta}\right]_{\eta_{\min}}^{\eta_0}=\left(\frac{\hbar^2}{2m}\right)\sum_{c_\mu}C_{c_\mu}^{(1)}C_{c_\mu}^{(2)}\left[\frac{f\Phi_{(\mu)}^{(2)}}{h_\eta^2}\frac{\partial(f\Phi_{(\mu)}^{(1)})}{\partial\eta}-\frac{f\Phi_{(\mu)}^{(1)}}{h_\eta^2}\frac{\partial(f\Phi_{(\mu)}^{(2)*})}{\partial\eta}\right]_{\eta_{\min}}^{\eta_0}. \tag{3.98}$$

Here the factor f is just $\mathfrak{R}^{(3A-4)/2}$ when η is chosen to be $\mathfrak{R}$. The right-hand side of Eq. (3.98) becomes a term in the general equation for the volume integral (3.87) with the value and derivative quantities now written

$$V_{c_\mu}=\left(\frac{\hbar^2}{2B_\eta f_0}\right)^{1/2}C_{c_\mu}f_0\Phi_{(\mu)}(\eta_0), \tag{3.99}$$

$$D_{c_\mu}=\left(\frac{\hbar^2 f_0}{2B_\eta}\right)^{1/2}C_{c_\mu}\left[\frac{\partial(f\Phi_{(\mu)})}{\partial\eta}\right]_{\eta=\eta_c}, \tag{3.100}$$

where the inertial parameter B_η is equal to mh_η^2 and f_0 denotes $f(\eta_0)$.

b. R-matrix eigenstates

In standard R-matrix theory a special set of eigenfunctions X_λ with eigenvalues E_λ is defined; the members of this set are solutions of the complete Schrödinger equation within the internal region, but with specific real and energy-independent boundary conditions applied at the channel entrance. The value and derivative quantities of these specific eigenfunctions are denoted by $\gamma_{\lambda(c)}$ and $\delta_{\lambda(c)}$, rather than by the notation V_c, D_c already employed [see Eqs. (3.94) (3.95) and (3.99), (3.100)] for these quantities for general wave functions of the internal region without specified boundary conditions. The boundary conditions of the eigenfunctions X_λ are denoted by

$$\frac{\delta_{\lambda(c)}}{\gamma_{\lambda(c)}}=\mathfrak{B}_c. \tag{3.101}$$

The substitution of this boundary condition in the Green's theorem relation of Equation (3.87) establishes the orthogonality of the eigenfunctions X_λ, which we shall refer to from this point as the R-matrix eigenstates.

c. The central R-matrix relationship

The fundamental R-matrix relationship, which states the relation between the value and derivative quantities of *any* internal wave function Ψ, is given in terms of the values $\gamma_{\lambda(c)}$ (which are commonly known as the reduced width amplitudes) and the eigenvalues E_λ of the R-matrix eigenstates X_λ. The general wave function Ψ at energy E is expanded in terms of the R-matrix states

$$\Psi=\sum_\lambda A_\lambda X_\lambda \tag{3.102}$$

(note that this is not a uniform expansion), and the expansion coefficients

$$A_\lambda=\int_\tau d\tau X_\lambda^*\Psi \tag{3.103}$$

are obtained from the Green's theorem relationship, giving finally the required equation

$$V_{c'}=\sum_c R_{c'c}(D_c-\mathfrak{B}_c V_c), \tag{3.104}$$

where

$$R_{c'c}=\sum_\lambda\frac{\gamma_{\lambda(c')}\gamma_{\lambda(c)}}{E_\lambda-E}. \tag{3.105}$$

d. Outgoing and incoming wave functions

The collision matrix of the nuclear system is obtained by matching the sum of incoming and outgoing waves in every channel to the internal wavefunction through Eq. (3.104) and the logarithmic derivatives of the outgoing waves in the channels. The outgoing wave O_c in any channel is defined as the solution, with asymptotic character of increasing separation or extension, of the component of the Schrödinger equation referring only to the channel variable. The character of increasing (or decreasing) separation is established by calculating the flux in the channel from the asymptotic wave function. As examples, the outgoing wave O_c in an s-wave neutron channel has the form

$$O_c=\exp(ik_c\rho_c), \tag{3.106a}$$

while an incoming wave I_c is

$$I_c=\exp(-ik_c\rho_c), \tag{3.106b}$$

where the wave number k_c is $\sqrt{(2M_cE/\hbar^2)}$. For particle channels, generally both these functions are solutions of the radial Schrödinger equation in the channel, written as

$$\left[\frac{\partial^2}{\partial\rho_c^2}-\frac{2M_c}{\hbar^2}\mathcal{V}_c\right]O_c=-\frac{2M_c}{\hbar^2}(E-\varepsilon_c)O_c, \tag{3.107}$$

(for the outgoing wave, and similarly for the incoming wave) where ε_c is the total excitation energy of the residual particles, M_c is the reduced mass of the residual particles in the channel, and v_c is the potential energy between the two residual particles in the channel, including the centrifugal potential term $\hbar^2 l_c(l_c+1)/2M_c\rho_c^2$. Further details of these wave functions are given by Lane and Thomas (1958).

The logarithmic derivative of an outgoing wave in an energetically open channel is complex, and its real and imaginary parts are known as the shift S_c and penetration P_c factors, respectively:

$$L_c \equiv S_c + iP_c = \left[\frac{\rho_c}{O_c}\frac{\partial O_c}{\partial \rho_c}\right]_{\rho_c=R_c} . \tag{3.108}$$

For fission channels defined at some point of deformation η_0 before the scission point, some reservations have to be made in defining similar wave functions and related qualities. This is due to the presence of a region of mixing forces between the channel deformation and scission point. This already implies that a unique excitation energy equivalent to the ε_c of Eq. (3.107) cannot be defined for the full extent of the channel. Therefore an equation of the type (3.107), namely

$$-\frac{\hbar^2}{2B}\left[\frac{\partial^2(f\Phi)}{\partial\eta^2} - \Phi\frac{\partial^2 f}{\partial\eta^2}\right] + [v(\eta) - E + \mathcal{E}_\mu] f\Phi = 0 , \tag{3.109}$$

would have to be understood in the sense of being valid for a specific internal state energy $\mathcal{E}_\mu$ as defined by the eigenvalues of the Hamiltonian (3.66), in the immediate neighborhood of the channel deformation, while beyond this point the potential energy term would require generalization to describe the deformation channel mixing terms, and after the scission point a complete superposition of true fission product outgoing waves must result from the original wave O_μ, with their fluxes (integrated over the full solid angle) totalling unity. From this description, however, some incoming waves for different channels μ' must occur in principle and will affect the normal R-matrix formulation. This is further discussed in Sec. III.C.3.*f*. For the present we assume that such ingoing wave components are negligibly small, as indeed can reasonably be expected if the channel deformation parameter is close to an outer saddle point before a long, monotonic potential energy descent towards the scission point. With this assumption we can define the penetration and shift factors for a deformation channel in direct analogy with Eq. (3.108):

$$L_\mu = S_\mu + iP_\mu = \left[\frac{f}{O_\mu}\frac{\partial O_\mu}{\partial\eta}\right]_{\eta_\mu=\eta_0} . \tag{3.110}$$

e. Deduction of the collision matrix and cross sections

The collision matrix for any set of reactions passing through a common compound system is defined in terms of the amplitudes of outgoing waves generated in the exit channels of the reaction by unit amplitude wave in an entrance channel. For the purpose of this definition the radial wave functions of Eqs. (3.106) and (3.107) are multiplied by the internal wave function ψ_c describing the state of excitation of the channel particles and their state of relative angular momentum, and are divided by the channel radius variable and the square root of the relative velocity v_c of the channel particles at infinite radius; this last factor ensures that unit amplitude of the incoming or outgoing wave corresponds to unit flux spread over the full unit sphere. These extended definitions of the incoming and outgoing wave functions are denoted by $\mathcal{I}_c$ and $\mathcal{O}_c$:

$$\mathcal{I}_c = \rho_c^{-1}\psi_c(i^l Y_{lm})I_c/v_c^{1/2} , \tag{3.111a}$$

$$\mathcal{O}_c = \rho_c^{-1}\psi_c(i^l Y_{lm})O_c/v_c^{1/2} . \tag{3.111b}$$

Similar functions for the deformation channels are defined by

$$\mathcal{I}_\mu = f^{-1}\chi_\mu I_\mu/v_\mu^{1/2} , \tag{3.112a}$$

$$\mathcal{O}_\mu = f^{-1}\chi_\mu O_\mu/v_\mu^{1/2} , \tag{3.112b}$$

v_μ being the rate of change with time of the deformation variable in the channel μ.

With these definitions the general solution of the wave function in the external region can be written

$$\Psi = \sum_{cc'}(\delta_{c'c}\mathcal{I}_c - U_{c'c}\mathcal{O}_{c'})y_c , \tag{3.113}$$

where the $U_{c'c}$ are the elements of the collision matrix and the y_c are the amplitudes of the incoming waves in the various channels c. The scattered wave into any channel c' may be defined as the difference between the actual wavefunction Ψ in the channel and the incident wave:

$$\Psi_{\text{scat, in } c'} = \sum_c y_c(e^{2i\omega_c}\delta_{c'c} - U_{c'c})\mathcal{O}_{c'} . \tag{3.114}$$

Thus if the y_c correspond to bombardment of a target nucleus by a unit flux plane wave of projectile particles, the cross section for producing a scattered wave is given by the squared modulus of this expression after integrating over the channel wave function and solid angle elements. Full details of such cross-section expressions are given by Lane and Thomas (1958); here we simply quote the well-known expression for the cross section integrated over the full solid angle:

$$\sigma_{cc'} = \frac{\pi}{k_c^2} g_J |\delta_{cc'} - U_{c'c}|^2 . \tag{3.115}$$

Here g_J is a spin statistical factor depending on the total angular momentum J of the system and the spins of target and projectile nuclei.

The values and derivatives of the wave function of Eq. (3.113) at the channel entrances must equal those of the wave function of the internal region. Therefore they must satisfy Eq. (3.104). The value and derivative quantities obtained from Eq. (3.113) are

$$V_c = \left(\frac{\hbar^2}{2M_cR_c}\right)^{1/2}\frac{1}{v_c^{1/2}}\left(y_c I_c - \sum_{c'} y_{c'}U_{cc'}O_c\right), \tag{3.116a}$$

$$D_c = \left(\frac{\hbar^2 R_c}{2M_c}\right)^{1/2}\frac{1}{v_c^{1/2}}\left(y_c\frac{\partial I_c}{\partial\rho_c} - \sum_{c'} y_{c'}U_{cc'}\frac{\partial O_c}{\partial\rho_c}\right) \tag{3.116b}$$

(with precisely similar quantities for the deformation channels μ), and the matching to the internal value and

derivative quantities by means of the R-matrix relation Eq. (3.104) and rearrangement leads to the expression for the collision matrix

$$\mathbf{U}=\boldsymbol{\Omega}\mathbf{P}^{1/2}\{1-\mathbf{R}(\mathbf{L}-\boldsymbol{\mathfrak{B}})\}^{-1}\{1-\mathbf{R}(\mathbf{L}^{*}-\boldsymbol{\mathfrak{B}})\}\mathbf{P}^{-1/2}\boldsymbol{\Omega}\,. \tag{3.117}$$

Here, $\boldsymbol{\Omega}$, $\mathbf{P}$, $\mathbf{L}$, and $\boldsymbol{\mathfrak{B}}$ are all diagonal matrices representing a hard-sphere phase shift ($\Omega_c^2=I_c/O_c$ at $\rho_c=R_c$), penetration factors, outgoing-wave logarithmic derivatives, and boundary conditions at the edges of the internal region, respectively.

f. Modifications to the R-matrix formalism for interactions in the deformation channels

The theory developed so far has introduced the concept of deformation channels, and by implication such a channel does not necessarily have to be defined as opening at a deformation corresponding to the separation of the nuclear system into two distinct (fission product) nuclei. Indeed, there are great advantages, for the discussion of "total fission" cross sections or of cross sections for phenomena obviously governed by features of the barrier, in considering deformation channel entrances as being close to the barrier; for one thing there will be only a limited number of deformation channels then entering the discussion, rather than the very large number that would correspond to the fission products in all their various states of excitations and angular momentum relationships.

However, the obvious difficulty arises when it comes to making detailed calculations using the theory that the form of the logarithmic derivative, hence the shift and penetration factors, of the outgoing wave functions in the deformation channels is not easily established. This is unlike the particle channels for which very precisely defined and calculable shift and penetration factors can be established at channel radii sufficiently far outside the nuclear interaction region. There are two distinct problems here. One is that the form of the potential energy function between saddle and scission point, and hence of the outgoing wave function is not precisely known. For any *assumed* potential form, however, the outgoing wave function and its logarithmic derivative [Eq. (3.110)] can be calculated numerically by starting with a simple form for f_0 [such as $\exp(ik\eta)$] at a very large deformation and using the step technique described in Sec. III.A.2.*b*.(*i*). Typical numerical results achieved by this procedure that also demonstrate the dependence of shift and penetration factors on the form of barrier assumed are shown in Fig. 35.

The second and more fundamental problem is that the region between saddle and scission in the deformation channel cannot be described as a simple potential energy function in the deformation degree of freedom alone. Interaction with other degrees of freedom exists in this zone. This interaction may be comparatively weak for the lowest spin-parity 0^+ deformation channel of even compound nuclei (another manifestation of the superfluidity phenomenon) but is certainly strong for most other deformation channels. The consequence is that channel mixing will occur, and an outgoing wave entering the interaction zone at low deformation will

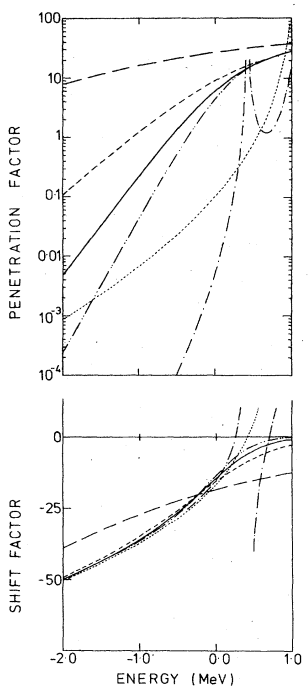

FIG. 35. Typical shift and penetration factors for a single barrier peak with channel entrance at the deformation corresponding to the peak. The barrier falls to −180 MeV below the peak. The inertial parameter is 4.015×10^{-46} g cm^2. Three inverted harmonic oscillator barriers are shown, denoted by ·····$\hbar\omega$ = 0.6 MeV, —$\hbar\omega$ = 0.8 MeV, ---$\hbar\omega$ = 1.2 MeV. The curve —— denotes a linear ramp falling through 90 MeV over a deformation interval of 1. —·— denotes constant potential for an interval 0.194 from the channel deformation, followed by a linear ramp, ··· similar, but the constant potential is limited to a deformation interval of 0.1.

reappear in very many different channels. Normally, the waves in the new channels will be outgoing waves or incoming waves with much reduced kinetic energy in the deformation mode (thus having very weak amplitudes at the channel entrance), and the probability that an incoming wave will appear in the original or in a channel with comparable kinetic energy should be negligible. The actual numerical treatment to obtain shift and penetration factors can be accomplished phenomenologically using a numerical method similar to that described above, but with a complex potential energy function in the channel.

Finally, it is desirable to be able to treat formally the case in which incoming waves returned from the interaction zone in the channel are not negligible. This is particularly likely to occur when the most significant feature of the interaction zone is a potential trap of some kind. The formal treatment that can be used is the "extended penetration factor method" (Lynn, 1973). In deformation space an intermediate region encompassing the interaction zone is introduced, bounded by η_c (the deformation channel entrance) and η_d, a value of deformation beyond the interaction. The Green's theorem relation [see Sec. III.C.3*a* and Eq. (3.85)] for this intermediate region, the volume of which is denoted by τ(int), is

$$(E_2 - E_1)\int_{\tau(\text{int})} d\tau\, \Psi_2^\dagger \Psi_1 = \sum_\mu \left\{ \frac{\hbar^2}{2B(\eta)} \left[f(\eta)\Phi_{(\mu)}^{(2)}(\eta)\left(\frac{\partial f \Phi_{(\mu)}^{(1)}}{\partial \eta}\right) - f(\eta)\Phi_{(\mu)}^{(1)}(\eta)\left(\frac{\partial f \Phi_{(\mu)}^{(2)}}{\partial \eta}\right)\right]\right\}_{\eta_c}^{\eta_d} . \tag{3.118}$$

(The sign † refers to taking complex conjugate of the intrinsic components alone of the wave function.) In this expression the labeling of the channels according to intrinsic states χ_μ can refer to different sets of intrinsic states, one set for evaluation of the terms at η_c and the other for η_d. Value $V_{(\mu)}$ and derivative $D_{(\mu)}$ quantities for the deformation channels can be defined at values of η_c and η_d in analogy with Eqs. (3.99) and (3.100). Eigenstates for the intermediate region are denoted by Z_λ with complex eigenvalues F_λ; they are orthonormal complex solutions of the nuclear Hamiltonian in the intermediate region with boundary conditions

$$\frac{D_{\lambda(\mu)}(\eta_c)}{V_{\lambda(\mu)}(\eta_c)} = \mathfrak{B}_\mu , \tag{3.119}$$

$$\frac{D_{\lambda(\mu)}(\eta_d)}{V_{\lambda(\mu)}(\eta_d)} = \frac{1}{\Phi_{\varepsilon^{(\mu)}}(\eta_d)}\left(\frac{\partial f \Phi_{\varepsilon(\mu)}}{\partial \eta}\right)_{\eta_d} \equiv S_\mu(\eta_d) + iP_\mu(\eta_d) , \tag{3.120}$$

in which $\Phi_{\varepsilon(\mu)}$ is a solution of the outgoing-wave type of the Schrödinger equation,

$$[T_\eta + \mathcal{U}(\eta)]\Phi_{\varepsilon(\mu)} = \varepsilon^{(\mu)}\Phi_{\varepsilon(\mu)} , \tag{3.121}$$

the energy being that available to the deformation mode,

$$\varepsilon^{(\mu)} = E - \mathcal{E}_\mu(\eta_\alpha) . \tag{3.122}$$

A general solution of the Schrödinger equation at energy E in the intermediate region can now be expanded in terms of the eigenstates Z_λ (in analogy with the development of Sec. III.C.3.*c*), and the logarithmic derivative of this solution at η_c in the channel μ can be shown to be

$$\frac{D_\mu(\eta_c)}{V_\mu(\eta_c)} \equiv S_\mu(\eta_c) + iP_\mu(\eta_c) = \mathfrak{B}_\mu - \sum_{\lambda'} (R_{\text{int}}^{-1})_{\mu\mu'} \frac{V_{(\mu')}(\eta_c)}{V_{(\mu)}(\eta_c)} , \tag{3.123}$$

the (complex) intermediate R-matrix element being

$$R_{\text{int},\mu\mu'} = \sum_\lambda \frac{V_{\lambda(\mu)}(\eta_c)V_{\lambda(\mu')}(\eta_c)}{F_\lambda - E} . \tag{3.124}$$

g. Alternative expressions and approximations for the collision matrix

Equation (3.117) is in general much too complicated for practical use. In the usual case of nuclear reactions there are very many channels available as well as an infinite number of eigenstates. Usually, many of the channels will be closed, but this fact is not expressed in the R matrix and the problem has to be faced, at least formally, of inverting the non-diagonal matrix of very large order $\{1 - \mathbf{R}(\mathbf{L} - \mathfrak{B})\}$. The methods for doing this are reviewed in detail by Lane and Thomas (1958). Here a brief synopsis is presented.

(*i*) *Single-level formula.* The commonest and most drastic simplification is to truncate the sum over levels in the R matrix [Eq. (3.105)] to a single term; the remaining terms can be either ignored or represented by a diagonal constant. With this simplification in the physics the matrix inversion can be carried out exactly. The result for the reaction cross section ($c' \neq c$) is the well-known single-level Breit–Wigner formula

$$\sigma_{cc'} = \frac{\pi}{k_c^2} g_J \frac{\Gamma_{\lambda(c)}\Gamma_{\lambda(c')}}{(E_\lambda - \Delta_\lambda - E)^2 + \frac{1}{4}\Gamma_\lambda^2} , \tag{3.125}$$

where $\Gamma_{\lambda(c)}$, $\Gamma_{\lambda(c')}$ are the partial widths for channels c and c', Γ_λ is the total width, and Δ_λ the level shift. These are defined in terms of the R matrix reduced widths and the penetration and shift factors by

$$\Gamma_{\lambda(c)} = 2P_c\gamma_{\lambda(c)}^2 , \tag{3.126}$$

$$\Gamma_\lambda = \sum_{c''} \Gamma_{\lambda(c'')} , \tag{3.127}$$

$$\Delta_\lambda = \sum_{c''} (S_{c''} - \mathfrak{B}_{c''})\gamma_{\lambda(c'')}^2 , \tag{3.128}$$

where the reduced width amplitudes $\gamma_{\lambda(c)}$ are defined in Eq. (3.101a).

(*ii*) *Level-matrix formulation.* A formal method of inverting the matrix $\{1 - R(L - \mathfrak{B})\}$, which, in practice, allows the truncation of the level sums in the final cross-section expressions to any required degree, is to transform from the form (3.117) to a form involving the inversion of a level matrix **C** (Thomas, 1955; Lane and Thomas, 1958);

$$U_{c'c} = \Omega_{c'}\Omega_c\left(\delta_{c'c} + 2iP_{c'}^{1/2}\sum_{\lambda\lambda'}\gamma_{\lambda(c')}\gamma_{\lambda'(c)}A_{\lambda\lambda'}P_c^{1/2}\right) , \tag{3.129a}$$

$$\mathbf{A} = \mathbf{C}^{-1} , \tag{3.129b}$$

$$C_{\lambda\lambda'} = (E_\lambda - E)\delta_{\lambda\lambda'} - \Delta_{\lambda\lambda'} - \tfrac{1}{2}i\Gamma_{\lambda\lambda'} . \tag{3.129c}$$

The generalized level shift and width quantities here are defined by

$$\Delta_{\lambda\lambda'} = \sum_{c''} (S_{c''} - \mathfrak{B}_{c''})\gamma_{\lambda(c'')}\gamma_{\lambda'(c'')} , \tag{3.130a}$$

$$\Gamma_{\lambda\lambda'} = 2\sum_{c''} P_{c''}\gamma_{\lambda(c'')}\gamma_{\lambda'(c'')} . \tag{3.130b}$$

It is numerically feasible to carry out the inversion of Eq. (3.129b) with the explicit retention of several levels. Thus Eqs. (3.129) form a very useful many-level formalism for practical situations, and were introduced into the analysis of fission cross-section data in the neutron resonance region by Vogt (1958, 1960).

Even the narrow level approximation of this formulation contains first-order level-level interference terms in the cross section. In this case the level matrix **C** and its inverse **A** are diagonal. In addition to single-level Breit-Wigner terms of the type (3.125) (summed over levels λ) in the cross section, interference terms occur having the form

$$\sigma_{cc',\text{int}} = \frac{\pi}{k_c^2} g_J \sum_{\lambda\neq\lambda'} \Gamma_{\lambda(c)}^{1/2}\Gamma_{\lambda(c')}^{1/2}\Gamma_{\lambda'(c)}^{1/2}\Gamma_{\lambda'(c')}^{1/2} \times \frac{(E_\lambda - E)(E_{\lambda'} - E) + \frac{1}{4}\Gamma_\lambda\Gamma_{\lambda'}}{[(E_\lambda - E)^2 + \frac{1}{4}\Gamma_\lambda^2][(E_{\lambda'} - E)^2 + \frac{1}{4}\Gamma_{\lambda'}^2]} . \tag{3.131}$$

(iii) Reduced R-matrix formulation. An alternative way of restricting the R-matrix so that inversion of $\mathbf{1} - \mathbf{R}(\mathbf{L} - \mathfrak{B})$ becomes a numerical possibility is the reduced R-matrix method (Teichmann and Wigner, 1952;

Thomas, 1955). In the most restricted and useful form of this all the closed channels and most of those only slightly open [expressed by their partial widths, as defined in Eq. (1.126), being very much smaller than the spacing between levels] are eliminated in explicit reference in the expression for the collision matrix. The collision submatrix $\mathbf{U}_{rr}$ referring only to the explicitly retained channels has a form analogous to Eq. (3.117):

$$\mathbf{U}_{rr}=\Omega_r\mathbf{P}_r^{1/2}[1-\mathbf{R}_{rr}(\mathbf{L}_r-\mathcal{B}_r)]^{-1}[1-\mathbf{R}_{rr}(\mathbf{L}_r-\mathcal{B}_r)]\mathbf{P}_r^{-1/2}\Omega_r\,. \tag{3.132}$$

The reduced R-matrix $\mathbf{R}_{rr}$ now has a complex form

$$(R_{rr})_{cc'}\approx\sum_\lambda\frac{\gamma_{\lambda(c)}\gamma_{\lambda(c')}}{E_\lambda-\Delta_\lambda^e-E-\frac{1}{2}i\Gamma_\lambda^e}\,, \tag{3.133a}$$

where the level shifts and width quantities are sums only over eliminated channels, denoted as a subset by e:

$$\Delta_\lambda^e=\sum_{c''\text{ in }e}(S_{c''}-\mathcal{B}_{c''})\gamma_{\lambda(c'')}^2 \tag{3.133b}$$

$$\Gamma_\lambda^e=2\sum_{c''\text{ in }e}P_{c''}\gamma_{\lambda(c'')}^2\,. \tag{3.133c}$$

The application of this formalism to fission in particular was introduced by Reich and Moore (1958).

(*iv*) *S-matrix formulation.* An alternative formulation of the collision matrix stems from its analytic extension into the complex energy plane (Humblet and Rosenfeld, 1961). This formulation, the S-matrix theory, is obtained from the expansion in the complex energy plane about its poles at the complex energies $E_l^{(H)}-\frac{1}{2}i\Gamma_l^{(H)}$:

$$U_{c'c}=\delta_{c'c}-\mathcal{P}_{c'}\mathcal{P}_c\left\{Q_{c'c}-i\sum_l\frac{G_{l(c')}G_{l(c)}\exp[i(\xi_{l(c')}+\xi_{l(c)})]}{|\mathcal{P}_{c'}(E_l)\mathcal{P}_c(E_l)|\,(E-E_l^{(H)}+\frac{1}{2}i\Gamma_l^{(H)})}\right\}. \tag{3.134}$$

Here the $\mathcal{P}_c$ are threshold factors, containing the explicit energy dependence on centrifugal and coulomb potential barriers, $Q_{c'c}$ is a background function, regular and slowly varying, the $G_{l(c)}$ are partial width amplitudes associated with the pole l, and the $\xi_{l(c)}$ are associated phase factors. The numerator of each term in the sum of Eq. (3.134) is the residue of the pole at $E_l^{(H)}-\frac{1}{2}i\Gamma_l^{(H)}$.

In the narrow-level approximation there is an obvious relation between these poles and the R-matrix parameters, that is, $E_l^{(H)}\sim E_\lambda-\Delta_\lambda$, $\Gamma_l^{(H)}\sim\Gamma_\lambda$, $G_{l(c)}^2\sim\Gamma_{\lambda(c)}\sim n\pi$, where n is an integer.

When the narrow level approximation is not valid there is no such simple correspondence between the poles and the R-matrix parameters. Resonancelike features in the cross section are obviously much more closely related in width and position to the S-matrix parameters than to the R-matrix parameters. It is often useful therefore to be able to deduce the S-matrix poles from the R-matrix parameters, and this is done by diagonalization of the level matrix $\mathbf{C}$ appearing in Eq. (3.129c). Special cases of such diagonalization (mostly for two R-matrix levels) are discussed by Lynn (1968a, 1966b). For example, when two R-matrix levels overlap [the sum of their widths as defined by Eq. (3.127) is less than half their separation] and the bulk of their widths is confined to one or few channels, there is a strong repulsion of the corresponding S-matrix poles in the *imaginary* direction in the complex energy plane (and also attraction in the real direction). This implies that the imaginary components of the poles, and hence the widths of the corresponding resonance features in the cross section, are, respectively, much larger and much smaller than the larger and smaller of the two R-matrix level widths. The usually dominant narrow peak that thus appears in the cross section, surmounting a much less conspicuous broad hump, is termed a quasiresonance (Lynn, 1966b).

Numerical methods have been developed for determining the S-matrix poles for several R-matrix levels. These involve finding the zeros in the complex energy plane of the determinant of the level matrix $\mathbf{C}$ [Eq. (3.129c)], followed by numerical integration of the collision matrix around a small circular contour surrounding the poles thus determined. Examples of the results of such procedures have been presented by Lynn (1969).

4. Introduction of phenomenological aspects of fission into the formal reaction theory

a. The double-humped fission barrier

The potential $\upsilon(\eta)$ of the deformation Hamiltonian defined in Sec. III.C.1 [Eq. (3.65)] cannot, as yet, be calculated from first principles. It is necessary to deduce it by using theories that have some phenomenological aspects. The original theory of this kind was the liquid drop model (see Sec. II). If this is taken to provide the classical analog of the term $T_\xi(\eta)+V(\eta,\xi)$ of Eq. (3.63), which is just $\varepsilon_0(\eta)$ [$\equiv\upsilon(\eta)$] in the classical limit, it gives a function for υ that has a minimum at values of η corresponding to the sphere, rises and passes through a maximum (the fission barrier) for prolate, axially symmetric deformations, and finally reaches (asymptotically, for the separation into two smaller particles) a value that is considerably lower than the spherical value (for nuclei heavier than iron).

Particle shell effects are added in a semiempirical way to the liquid drop mass in the model of Myers and Swiatecki (1966) (see also Sec. II). These are at maximum for the sphere and are attenuated for larger distortions. They affect the position and magnitude of the ground-state minimum of $\upsilon(\eta)$ but do not affect the barrier.

Shell effects have a much more dramatic influence on υ (so far as fission effects are concerned) in the theory of Strutinsky (1967a, b) as described in Sec. II. The principal term of $T_\xi(\eta)+V(\eta,\xi)$ is taken to be the static liquid drop energy for deformation η. To this is added the sum of single-particle energies computed on the assumption that $V(\eta,\xi)$ is a static, single-particle potential well of fixed deformation η, and from it is sub-

tracted a similar sum computed over a suitably "smoothed-out" (shell-averaged) single-particle spectrum. That this procedure gives a qualitatively reasonable picture of the behavior of $\varepsilon_0(\eta)$ has been checked by Vautherin and Brink (1972) who calculate this quantity directly from the Hamiltonian term $T_\xi(\eta)+V(\eta,\xi)$ by a Hartree–Fock method with the constraint of fixed quadrupole moment. The Strutinsky prescription for the deformation potential $\upsilon(\eta)$ results in a double-humped fission barrier for nuclei in the general range of thorium to curium and, to a less dramatic extent, on either side of these limits. It is the purpose of the remainder of this section to survey, using the R-matrix development given above, the more detailed theoretical consequences for fission reactions of this kind of barrier.

It is useful, at this point, to recall the definition of some quantities which can be used to characterize the barrier, at least in an approximate fashion. The value of the potential at η_I is labeled υ_I, at η_A it is υ_A, at η_{II}, υ_{II} and at η_B, υ_B. In the neighborhood of each of these deformations it is generally assumed, for calculational purposes, that the potential energy υ is harmonic, and that the four harmonic segments join smoothly to each other. Thus, in the region of η_I,

$$\upsilon=\upsilon_I+\tfrac{1}{2}C_I(\eta-\eta_I)^2\,,\quad \eta<\eta_x \tag{3.135}$$

around η_A,

$$\upsilon=\upsilon_A-\tfrac{1}{2}C_A(\eta-\eta_A)^2\,,\quad \eta_x\leq\eta<\eta_y \tag{3.136}$$

and similar equations for the regions around η_{II} and η_B have already been given as Eqs. (3.31) [Eq. (3.136) now replaces the first of those equations]. The joining point η_x is given by

$$\eta_x=\eta_A-\left(\frac{2(\upsilon_A-\upsilon_I)C_I}{C_A(C_A+C_I)}\right)^{1/2}, \tag{3.137a}$$

with the condition

$$\eta_I=\eta_x+(C_A/C_I)(\eta_x-\eta_A)\,. \tag{3.137b}$$

The other joining points are given by Eqs. (3.32). The curvature coefficient is seldom referred to directly, but rather through the real or imaginary vibrational frequencies,

$$\hbar\omega_I=[C_I/B_\eta(\eta_I)]^{1/2}\,, \tag{3.138a}$$

$$\hbar\omega_{II}=[C_{II}/B_\eta(\eta_{II})]^{1/2}\,, \tag{3.138b}$$

$$i\hbar\omega_A=[-C_A/B_\eta(\eta_A)]^{1/2}\,, \tag{3.138c}$$

$$i\hbar\omega_B=[-C_B/B_\eta(\eta_B)]^{1/2}\,. \tag{3.138d}$$

The last two appear in the expressions for the transmission coefficient of a wave through an inverted harmonic barrier. For the barriers A and B separately, the relevant transmission coefficients are

$$T_A=\frac{1}{1+\exp\{-[2\pi(E-\upsilon_A)/\hbar\omega_A]\}} \tag{3.139a}$$

$$T_B=\frac{1}{1+\exp\{-[2\pi(E-\upsilon_B)/\hbar\omega_B]\}} \tag{3.139b}$$

and can be used in the semiquantitative discussion of fission rates through the double-humped barrier as parametrized above, provided the energy is not too far below the heights of the barrier peaks.

b. Illustration of vibrational states of the double potential well: class-I and class-II vibrational states

The nature of the wave functions $\Phi(\eta)$ of the quasidiscrete states of the deformation mode that occur for the double potential well that thus appears in the Strutinsky picture of the deformation energy of actinide nuclei is graphically illustrated by numerical calculation for a double rectangular well (bounded by an infinite potential at the inner wall of well I). For wave functions (unnormalized)

$$\begin{aligned}\Phi(\eta)&=\sin K\eta\,,\quad 0<\eta<\eta_1\ \text{(range of well I)}\\&=ae^{-\kappa\eta}+be^{\kappa\eta}\,,\quad \eta_1<\eta<\eta_2\ \text{(range of barrier } A)\\&=c\sin(k\eta+\delta)\,,\quad \eta_2<\eta<\eta_3\ \text{(range of well II)}\\&=de^{-\lambda\eta}\,,\quad \eta_3<\eta\ \text{(range of barrier } B)\end{aligned}$$

the matching conditions are

$$\cot(k\eta_3+\delta)=-\lambda/k\,,$$

$$\cot(k\eta_2+\delta)=\frac{1-\gamma e^{2\kappa(\eta_2-\eta_1)}}{1+\gamma e^{2\kappa(\eta_2-\eta_1)}}\frac{\kappa}{k}\,,$$

$$\gamma\left(\equiv\frac{b}{a}e^{2\kappa\eta_1}\right)=\frac{\kappa+K\cot K\eta_1}{\kappa-K\cot K\eta_1}\,.$$

Numerical solutions of these equations are shown in Fig. 36. The striking degree of clustering of the wave function within either one well or the other leads to the classification of the wave function; those with major amplitude within the deeper, primary well are class-I vibrational states and those concentrated in the secondary well are class-II vibrational states. Note that the energy eigenvalues of states of either class are very little perturbed from the values they would have if the opposite well were filled in. Note also that the *total* number of nodes of the wave function no longer gives the ordering of the vibrational state within its class. Thus the "zero-point" vibration in the class-II well $\Phi_0^{(II)}$ has three nodes, indicating that it is weakly "coupling" with the class-I vibrational state $\Phi_3^{(I)}$.

c. Amplitude relationships of class-I and class-II vibrational states

The numerical illustration of the last section suggests a systematic way of calculating the special features of the vibrational wave functions of a double potential well of more general shape (Lynn, 1968b). From the double well separate primary and secondary wells [denoted by $\upsilon_1(\eta)$ and $\upsilon_2(\eta)$, respectively] are constructed in the manner shown in Fig. 37 so that $\upsilon_1(\eta)+\upsilon_2(\eta)=\upsilon(\eta)$, the origin of the energy scale being taken as zero. The modified asymptotic end-values are equal to the height of the intermediate maximum of the double well. The

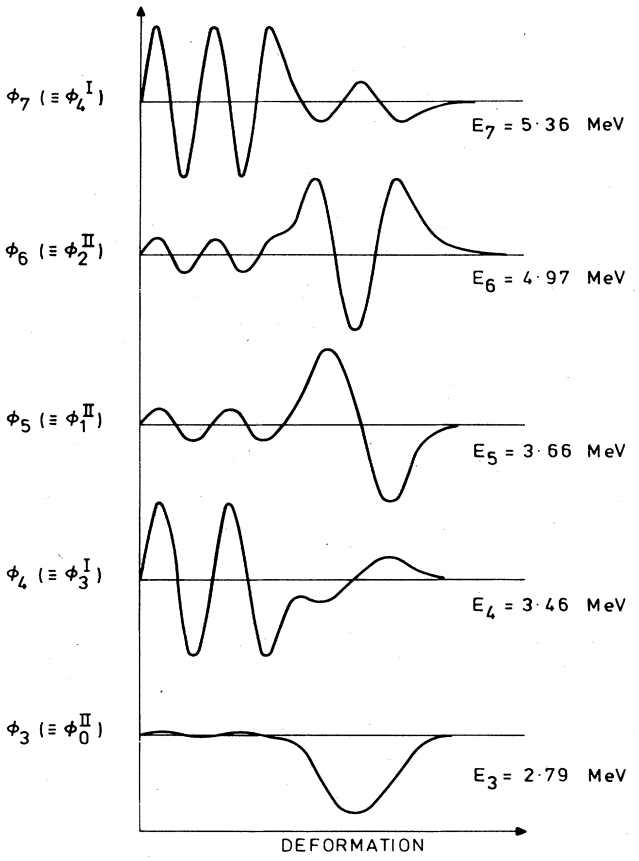

FIG. 36. Eigenfunctions of a double rectangular well with the following specification: $\mathcal{V}_I = 0.0$, $\eta_1 = 0.4$, $\mathcal{V}_A = 6$ MeV, $\eta_2 = 0.5$, $\mathcal{V}_{II} = 2.5$ MeV, $\eta_3 = 0.8$, $\mathcal{V}_B = 6.0$ MeV, $2B/\hbar^2 = 246.5$.

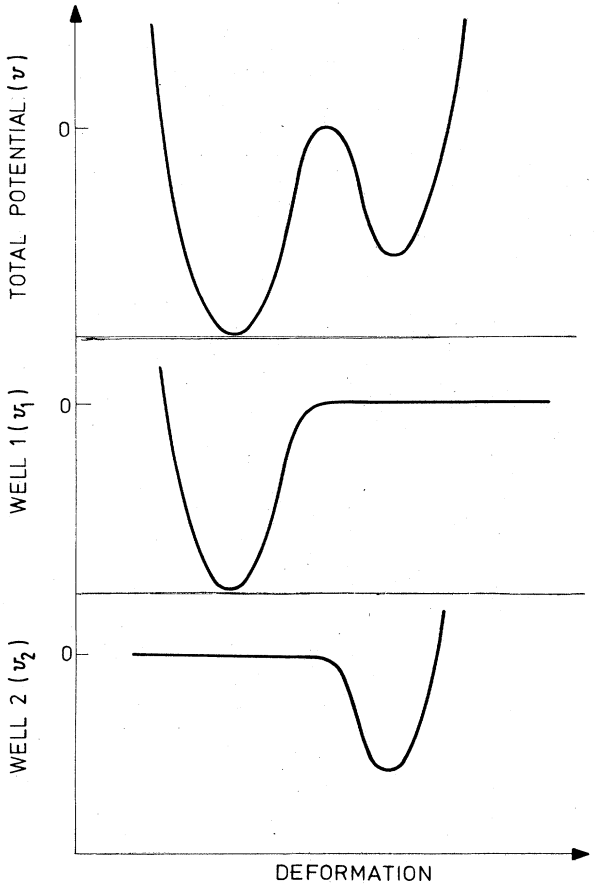

FIG. 37. Construct for separate primary and secondary wells.

eigenvalues $\epsilon_{\nu_n}^{(n)}$ and eigenfunctions $\phi_{\nu_n}^{(n)}$ of the Schrödinger equations for the separated wells n,

$$[T(\eta) + \mathcal{V}_n(\eta)]\phi_{\nu_n}^{(n)}(\eta) = \epsilon_{\nu_n}^{(n)}\phi_{\nu_n}^{(n)}\,, \tag{3.140}$$

are calculated, and the solutions for the Schrödinger equation of the double well are written approximately

$$\Phi_\nu \approx a_\nu \phi_{\nu_1}^{(1)} + b_\nu \phi_{\nu_2}^{(2)}\,, \tag{3.141}$$

the two wave functions appearing on the rhs being (usually) a pair closest in energy. Normally one of the two coefficients a_ν, b_ν is close to unity (giving the class of ϕ_ν) and the other is small. Occasionally more than one of the small amplitude terms will contribute commensurately, and Eq. (3.141) will need to be generalized accordingly; in this case a perturbation treatment will normally suffice.

The determination of the coefficients a_ν, b_ν of Eq. (3.141) can be carried out as follows. The wave function (3.141) is substituted into the Schrödinger equation for the double well, the result is multiplied on the left by $\phi_{\nu_1}^{(1)}$ or $\phi_{\nu_2}^{(2)}$, and integration over the full range of η leads to two equations in a_ν and b_ν which can be diagonalized by the usual method. The result for the eigenvalues is

$$\epsilon_\nu = \epsilon_\nu^{(1)} + \frac{\Delta\epsilon_{\rm mod}}{2} \mp \frac{1}{2}\left[\left((\Delta\epsilon_{\rm mod})^2 - \frac{4\left[\Delta\epsilon\left(\mathcal{V}_{2(11)} - \mathcal{V}_{2(12)}\int d\eta\,\phi_{\nu_1}^{(1)}\phi_{\nu_2}^{(2)}\right) - \mathcal{V}_{1(12)}\mathcal{V}_{2(12)} + \mathcal{V}_{2(11)}\mathcal{V}_{1(22)}\right]}{1 - \left(\int d\eta\,\phi_{\nu_1}^{(1)}\phi_{\nu_2}^{(2)}\right)^2}\right)\right]^{1/2}\,, \tag{3.142a}$$

where

$$\Delta\epsilon = \epsilon_\nu^{(2)} - \epsilon_\nu^{(1)}\,, \tag{3.142b}$$

$$\mathcal{V}_{n(lm)} = \int d\eta\,\phi_{\nu_l}^{(l)}\phi_{\nu_m}^{(m)}\mathcal{V}_n(\eta)\,, \tag{3.142c}$$

$$\Delta\epsilon_{\rm mod} = \frac{\Delta\epsilon + \mathcal{V}_{1(22)} + \mathcal{V}_{2(11)} - (\mathcal{V}_{1(12)} + \mathcal{V}_{2(12)})\int d\eta\,\phi_{\nu_1}^{(1)}\phi_{\nu_2}^{(2)} - \Delta\epsilon\left(\int d\eta\,\phi_{\nu_1}^{(1)}\phi_{\nu_2}^{(2)}\right)^2}{1 - \left(\int d\eta\,\phi_{\nu_1}^{(1)}\phi_{\nu_2}^{(2)}\right)^2}\,. \tag{3.142d}$$

The ratio for the amplitudes is

$$\frac{b_\nu}{a_\nu} = -\frac{\epsilon^{(1)}_{\nu_1} - \epsilon_\nu + \upsilon_{2(11)}}{(\Delta\epsilon + \epsilon^{(1)}_{\nu_1} - \epsilon_\nu)\int d\eta\, \phi^{(1)}_{\nu_1}\phi^{(2)}_{\nu_2} + \upsilon_{1(12)}}, \tag{3.143a}$$

$$\frac{b_\nu}{a_\nu} = -\frac{(\epsilon^{(1)}_{\nu_1} - \epsilon_\nu)\int d\eta\, \phi^{(1)}_{\nu_1}\phi^{(2)}_{\nu_2} + \upsilon_{2(12)}}{\Delta\epsilon + \epsilon^{(1)}_{\nu} - \epsilon_\nu + \upsilon_{1(22)}}. \tag{3.143b}$$

If ν signifies a class-I vibrational state, the eigenvalue is approximately

$$\epsilon_\nu \approx \epsilon^{(1)}_\nu + \upsilon_{2(11)} - \upsilon_{2(12)}\int d\eta\, \phi^{(1)}_{\nu_1}\phi^{(2)}_{\nu_2} - \frac{\upsilon_{1(12)}\upsilon_{2(12)} - \upsilon_{2(11)}\upsilon_{1(22)}}{\epsilon^{(2)}_{\nu_2} - \epsilon^{(1)}_{\nu_1}}, \tag{3.144a}$$

if the matrix elements (3.142c) and overlap quantities are small compared to $\Delta\epsilon$. The amplitude ratio, from Eq. (3.143a), is then

$$\frac{b_\nu}{a_\nu} \approx -\frac{\upsilon_{2(12)}}{\Delta\epsilon}, \tag{3.144b}$$

if terms of second order in T_A, the transmission coefficient through the intermediate barrier (see Sec. III.C.4.a), are dropped.

Similar equations hold for a class-II vibrational state:

$$\epsilon_\nu = \epsilon^{(2)}_{\nu_2} + \upsilon_{1(22)} - \upsilon_{1(12)}\int d\eta\, \phi^{(1)}_{\nu_1}\phi^{(2)}_{\nu_2} + \frac{\upsilon_{1(12)}\upsilon_{2(12)} - \upsilon_{2(11)}\upsilon_{1(22)}}{\Delta\epsilon}, \tag{3.145a}$$

$$\frac{a_\nu}{b_\nu} \approx \frac{\upsilon_{1(12)}(\epsilon^{(2)}_{\nu_2} - \epsilon^{(1)}_{\nu_1})\int d\eta\, \phi^{(1)}_{\nu_1}\phi^{(2)}_{\nu_2} - \upsilon_{1(12)}\upsilon_{2(12)}}{\left(\epsilon^{(2)}_{\nu_2} - \epsilon^{(1)}_{\nu_1}\right)^2 \int d\eta\, \phi^{(1)}_{\nu_1}\phi^{(2)}_{\nu_2} - (\epsilon^{(2)}_{\nu_2} - \epsilon^{(1)}_{\nu_1})\upsilon_{2(12)}}, \tag{3.145b}$$

which is just $\upsilon_{1(12)}/(\epsilon^{(2)}_{\nu_2} - \epsilon^{(1)}_{\nu_1})$. When $\epsilon^{(1)}_{\nu_1}$ and $\epsilon^{(2)}_{\nu_2}$ are very close

$$(|\epsilon^{(2)}_{\nu_2} - \epsilon^{(1)}_{\nu_1}| \lesssim |\upsilon_{1(12)}|)$$

it is clear that $a_\nu \approx b_\nu$, and there is no obvious categorization as a class-I or class-II state. However, for the range of inertial and potential parameters that are relevant for the actinide fission barriers, this kind of degeneracy is extremely unlikely. The band widths within which the closeness condition, given above, is fulfilled, are approximately proportional to $(T_A)^{1/2}$. The constant of proportionality is the square root of the constant given in Eq. (3.148) below in connection with the amplitude of mixing of type 1 and 2 states. For an intermediate quadratic barrier with $\hbar\omega_A \sim 1.0$ MeV [see Eq. (3.138c)] this bandwidth is already only a few keV for states 1 MeV below the barrier and is rapidly attenuating (by a factor ~30/MeV); this is to be compared with an expected spacing, the β-phonon energy, ~0.5–1.0 MeV for the basis states.

In the approximate solution of the Schrödinger equation with the wave function in the normal case the values of the coefficients a_ν and b_ν are very close to the values given by first-order perturbation theory. For a class-I vibrational state, $a_\nu \approx 1$, and

$$b_\nu \approx \frac{\langle \phi^{(1)}_{\nu_1} | \upsilon_2 | \phi^{(2)}_{\nu_2} \rangle}{\epsilon^{(1)}_{\nu_1} - \epsilon^{(2)}_{\nu_2}} \tag{3.146}$$

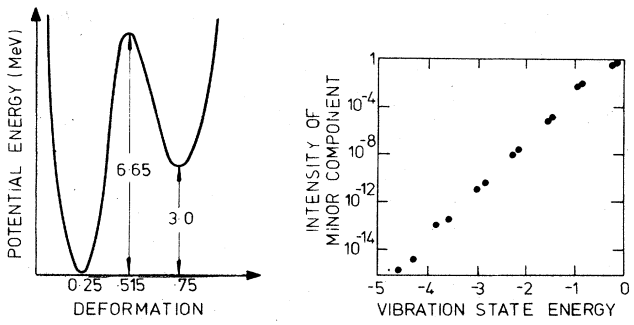

FIG. 38. Intensity of the minor component (tail in opposite well) of class-I and class-II vibrational wave functions of the double-well potential shown in the left-hand part of the figure. The basic phonon frequency in both wells is $\hbar\omega = 0.8$ MeV.

[in agreement with Eq. (3.144b)]. For a class-II vibrational state, $b_\nu \approx 1$, and

$$a_\nu \approx \frac{\langle \phi^{(2)}_{\nu_2} | \upsilon_1 | \phi^{(1)}_{\nu_1} \rangle}{\epsilon^{(2)}_{\nu_2} - \epsilon^{(1)}_{\nu_1}}. \tag{3.147}$$

The small contributions to the wave function that might arise from other states of the potential υ_n can clearly be calculated in the same way.

The matrix elements of υ_n are quite readily and accurately calculable by straightforward digitial computer methods. From the WKB approximation to the wave function $\phi^{(1)}_{\nu_1}$ and $\phi^{(2)}_{\nu_2}$ in the barrier region it can be shown that the strongest factor in the amplitude expressions of Eqs. (3.146) and (3.147) is the square root of the transmission coefficient through the intermediate barrier [refer to Sec. III.A.1 and Eq. (3.139)]. This is borne out by the numerical computations[2]. A graphical display of the matrix elements required for Eqs. (3.146) and (3.147) for all the eigenvalues of a typical double potential well is shown in Fig. 38. If the empirical results are expressed in the form

$$b^2_\nu \approx \frac{KT_A}{(\epsilon^{(1)}_{\nu_1} - \epsilon^{(2)}_{\nu_2})^2} \tag{3.148a}$$

for class-I states and

$$a^2_\nu \approx \frac{KT_A}{(\epsilon^{(2)}_{\nu_2} - \epsilon^{(1)}_{\nu_1})^2} \tag{3.148b}$$

for class-II states, the constant K is found to have the empirical value 0.006, which is close to the expected "statistical" value of $\hbar\omega_{II}(\hbar\omega_<)^2/32\pi$, where $\hbar\omega_<$ is the smaller of $\hbar\omega_I$ and $\hbar\omega_{II}$. In general, for other wells with less uniformity among $\hbar\omega_{II}$, $\hbar\omega_I$, and $\hbar\omega_A$, it is found that K lies within a factor of 2 of this "statistical" value.

d. Boundary conditions; shift and penetration factors

The discussion above of class-I and class-II vibrational states in the deformation potential $\upsilon(\eta)$ for the double potential well feature of the fission barrier was made with the assumption that these states are dis-

[2]For precise computation Equation (3.143b) should be used for class-I states and equation (3.143a) for class-II states.

crete. To employ these, as is done in the next section, in the formal reaction theory to calculate cross sections through the fission barrier, it is necessary to introduce the discreteness through the imposition of a formal boundary condition at the entrance to the deformation channel (see Sec. III.C.3.*b*). This should be real to ensure reality of the vibrational states.

Physically, the most natural boundary condition to choose if a vibrational state in a particular energy region is of principal interest is one that is equal to the shift factor in the deformation channel at an outgoing wave energy that is very close to the vibrational state eigenvalue. In this way level shifts in resonance cross-section formulas become small or negligible [see Sec. III.C.3.*g*, especially Eq. (3.128) and (3.130)].

The calculation of the shift and penetration factors in a deformation channel has already been considered in Sec. III.C.3.*f*. For the main development of the reaction theory in relation to the double-humped barrier, as pursued in the next section, it is clear that the normal choice of channel entrance will be close to the outer peak at η_B in the potential energy wave. The shift factor S then has a (negative) value close to the reciprocal attenuation distance κ at $\eta_B (S=-\kappa=-[2B(\epsilon-\mathcal{V}_B)/\hbar^2]^{1/2})$, while the penetration factor P is exponentially decreasing with decreasing energy ϵ.

There are special situations, however, in which it is useful to be able to set the channel entrance at the inner barrier η_A. The structure of class-I and class-II vibrational wave functions does not then enter the development of the reaction theory, but the shift and penetration factors carry the physics implications of the secondary well. The form of the shift and penetration factors in this case are considered by Lynn (1973). Numerical calculation of these factors can be achieved by the inward potential step method described in Sec. III.C.3.*f*. Typical results are shown in Fig. 39. These have a resonance or "dispersive" character, and the dispersion anomalies occur close to the positions of vibrational states in the secondary well. This is illustrated by the superposition on these figures of the transmission coefficient (as defined in Sec. III.A.2) through the same double-humped barrier; there is always close correspondence in energy. Note however that whereas the transmission coefficient can approach, but never exceed, the value of unity, the penetration factor can peak to much larger values.

A more analytical calculation of the shift and penetration factors employs Eqs. (3.119)–(3.124) of Sec. III.C.3.*f* simplified for a single deformation channel (we are not at this stage considering the possibility of interactions between the deformation and other degrees of freedom in the secondary well). The boundaries of the intermediate zones described in Sec. III.C.3.*f* are η_A and η_B (substituted for η_c, η_d, respectively). If the eigenstates set up in the intermediate zone are to have reasonably uniform properties the poles of the expression obtained for the logarithmic derivative from Eq. (3.124) must be located approximately midway between the eigenvalues F_λ. In a uniform model for these eigenstates, the poles occur at energies $e_\nu \approx \frac{1}{2}(F_\lambda + F_{\lambda+1})$ and their residues are $d_\lambda^2/\pi^2 V_\lambda^2(\eta_A)$, where d_λ is the spac-spacing of the states F_λ. The imaginary component w_ν of the pole energy e_ν is the mean of that of the eigenvalues F_λ and $F_{\lambda+1}$, and this is interpreted as the half-width for decay of an intermediate state at energy e_ν through the outer barrier B. In the region of the pole $e_\nu = \epsilon_\nu - iw_\nu$, the shift and penetration factors thus have the form

$$S+iP \approx S_b + \frac{d_\lambda^2}{\pi^2 V_\lambda^2(\eta_A)} \frac{(\epsilon_\nu-\epsilon)}{(e_\nu-\epsilon)^2+w_\nu^2} + \frac{id_\lambda^2}{\pi^2 V_\lambda^2(\eta_A)} \frac{w_\nu}{(e_\nu-\epsilon)^2+w_\nu^2}, \tag{3.149}$$

where S_b is a smoothly varying background term. This accounts for the "dispersion" character of these factors that appears in the numerical calculations described in the last paragraph. The result (3.149) can be written in terms of the reduced widths $\gamma_\nu^2(\eta_A)$ of vibrational states of the secondary well, which are defined with a boundary condition $D_\nu(\eta_A)/V_\nu(\eta_A) = [2B(\epsilon - V_A)/\hbar^2]^{1/2} \equiv \kappa_A$, rather than with the intermediate zone condition $\mathfrak{B} = -\kappa_A$, which is natural for setting up the conditions appropriate to the internal region ($\eta < \eta_A$). The modified result is

$$S+iP \approx S_b + \frac{4\kappa_A^2 \gamma_\nu^2(\eta_A)(\epsilon_\nu-\epsilon)}{(\epsilon_\nu-\epsilon)^2+w_\nu^2} + \frac{i4\kappa_A^2\gamma_\nu^2(\eta_A)w_\nu}{(\epsilon_\nu-\epsilon)^2+w_\nu^2}. \tag{3.150}$$

5. Specialization of the reaction theory to the double-humped barrier

a. Class-I and class-II compound R-matrix states

The form of the double-humped potential energy barrier in the elongation mode lends itself readily to special treatment within the extended R-matrix reaction

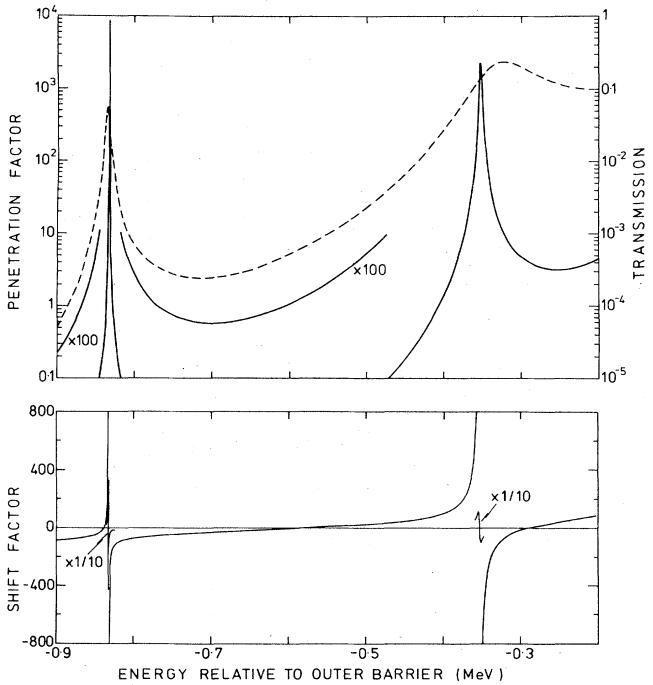

FIG. 39. Shift and penetration factors calculated within the inner peak of a double-humped barrier. The parameters of the barrier are (in MeV): $\mathcal{V}_I = -6.52$ MeV, $\hbar\omega_I = 0.85$ MeV, $\mathcal{V}_A = -0.2$ MeV, $\hbar\omega_A = 1.06$ MeV, $\mathcal{V}_{II} = -2.04$ MeV, $\hbar\omega_{II} = 0.608$ MeV, $\mathcal{V}_B = 0.2$ MeV, $\hbar\omega_B = 0.8$ MeV. The deformation parameters are: $\eta_B = 0.9$, $\eta_A = 0.5845$, channel deformation $\eta_\mu = 0.34$. The transmission coefficient of the barrier is also shown (dashed curve).

theory outlined above. In this the R-matrix internal eigenstates, as defined in Sec. III.C.3.*b*, are expanded in terms of two auxiliary sets of eigenstates, the class-I and class-II states. In this treatment the channel deformations are chosen close to the outer barrier B. Physically, the class-I states are largely confined to deformations within the region of the primary well of the double-humped barrier, and the class-II states are similarly located within the region of the secondary well.

Formal definition of these auxiliary states follows from the expansion of the R-matrix internal states in terms of vibrational wave functions as in Eq. (3.96):

$$X_\lambda = \sum_{\mu,\nu} C^\lambda_{\mu\nu}\chi_\mu\Phi_{\nu(\mu)}\,, \tag{3.151}$$

with the χ_μ being defined as intrinsic states of the intrinsic Hamiltonian for channel deformation η_μ (see Sec. III.C.1). Here, the vibrational wave functions $\Phi_{\nu(\mu)}$, unlike the free wave function $\Phi^{(\eta)}_\mu$ of Eq. (3.96), are subject to a real energy-independent boundary condition at the selected channel deformations η_μ and this can depend on the channel label μ; the vibrational wave functions $\Phi_{\nu(\mu)}$ are themselves discrete, and if their eigenvalues ϵ_ν are lower than the intermediate barrier of the double-humped barrier, they fall into the classes I and II described in Sec. III.C.4.*c*. The class-I and class-II R-matrix states are therefore conveniently defined by the incomplete expansions,

$$X^{(\mathrm{I})}_{\lambda_\mathrm{I}} = \sum_{\mu,\nu} C^{\lambda_\mathrm{I}}_{\mu\nu}\chi_\mu\Phi^{(\mathrm{I})}_{\nu(\mu)}\,, \tag{3.152}$$

$$X^{(\mathrm{II})}_{\lambda_\mathrm{II}} = \sum_{\mu,\nu} C^{\lambda_\mathrm{II}}_{\mu\nu}\chi_\mu\Phi^{(\mathrm{II})}_{\nu(\mu)}\,, \tag{3.153}$$

with eigenvalues $E_{\lambda_\mathrm{I}}, E_{\lambda_\mathrm{II}}$ respectively.

To be formally complete the expansion (3.151) must include unbound intrinsic states χ_μ. R-matrix theory is normally confined to the energy region in which only two-body reactions are possible. With this limitation the terms in (3.151) that include unbound χ_μ will be coupled with Φ_μ with vanishingly small amplitude at the channel deformation η_μ. Such terms can be regarded as giving rise to waves in the simpler particle channels and can be written alternatively as an explicit expansion involving states of the residual nuclei involved in these channels, analogous to Eq. (3.88), leaving only couplings involving bound χ_μ in the explicit sum over $\mu\nu$ in Eq. (3.151).

Physical properties of the class-I and class-II compound states follow quite simply from the expansions (3.152) and (3.153). Class-I states can be expected to contain significant amounts of components $\chi_\mu\Phi^{(\mathrm{I})}_{0(\mu)}$, where $\Phi^{(\mathrm{I})}_{0(\mu)}$ corresponds to zero-point vibrational motion within the primary well and the χ_μ are highly excited intrinsic states. The latter will include unbound states corresponding to the motion of free neutrons or protons, or more complex particles such as α particles, against the appropriate residual nucleus, and the zero-point vibrational state becomes an essential part of the description of the ground (or even a low excited state) of the residual nucleus. Thus class-I states will have neutron and proton reduced widths for decay into these particular channels. They will also have reduced widths for alpha decay to the ground and low excited states. The limitation of the expansion to class-I vibrational states with (extremely likely) very small amplitudes at the channel deformation η_μ, even for comparatively high quantum numbers ν', also implies that the class-I states have very small, although not quite negligible, fission widths.

By contrast, the class-II states, by virtue of their components of class-II vibration, particularly those of high quantum number ν'', have much larger reduced fission widths, but have zero reduced nucleon widths to ground and normal low-lying states of residual nuclei. Another important difference for fission barrier potentials calculated for actinide nuclei by the Strutinsky method lies in the density of the two kinds of state (for the same available excitation energy). This arises from the density of the basis product states $\chi_\mu\Phi^{(\mathrm{I})}_{\nu(\mu)}$ and $\chi_\mu\Phi^{(\mathrm{II})}_{\nu(\mu)}$. The intrinsic states can be envisaged as combinations of single-particle or hole states with spacing of the order of 100 keV. Furthermore, rotational bands with spacings of the same order will be built on them. By contrast, the vibrational states will have separations of the order of 1 MeV. Thus the principal contribution to density of class-I and class-II levels will come from the combinations $\chi_\mu\Phi^{(\mathrm{I})}_{0(\mu)}$ and $\chi_\mu\Phi^{(\mathrm{II})}_{0(\mu)}$, respectively. For the actinides the potential energy calculations (see Sec. II) and the experimental evidence of spontaneously fissioning isomers (see Sec. IV) and fission cross-section intermediate structure (see Sec. VI) indicate that the secondary well is at least about 2 MeV above the primary well, so that this amount of excess energy is tied up in the vibrational state $\Phi^{(\mathrm{II})}_{0(\mu)}$ and is not available for the excitation of intrinsic degrees of freedom in the class-II compound states. Consequently the density of class-II states can be expected to be some 2 or more orders of magnitude lower than the class-I density.

b. Final R-matrix compound states

The final R-matrix states X_λ can now be constructed from the auxiliary class-I and class-II compound states according to the procedure described by Lynn (1968b). The expansion (3.151) is substituted into the Schrödinger equation

$$HX_\lambda = E_\lambda X_\lambda \tag{3.154}$$

in the internal region of configuration space (defined in Sec. III.C.3.*a*). Both sides are multiplied by $\chi^*_\mu\Phi^*_\nu$ and integration over all variables gives

$$(\epsilon_\nu + \mathcal{E}_\mu - E_\lambda)C^\lambda_{\mu\nu} + \sum_{\mu'\nu'} C^\lambda_{\mu'\nu'} \times \langle\chi_\mu\Phi_{\nu(\mu)}|H_c|\chi_{\mu'}\Phi_{\nu'(\mu)}\rangle = 0\,, \tag{3.155}$$

using the split of the Hamiltonian into deformation, intrinsic and coupling (H_c) terms as defined in Eq. (3.64). This is a representative row of a matrix equation, the eigenvalues of which are determined from the secular equation

$$\det(H_{\mu\nu,\mu'\nu'} - E_\lambda\delta_{\mu\nu,\mu'\nu'}) = 0\,. \tag{3.156}$$

The determination of the eigenvalues of the matrix H is also conventionally expressed as finding the unitary matrix U, which transforms H by the operation $\mathbf{UHU}^{-1}$

into the diagonal form E. We now specifically consider only the eigenstates of a particular set of good quantum numbers (these are normally total angular momentum J and parity π).

The matrix H can now be partitioned into submatrices depending on whether the index ν of an element refers to a class-I (ν_I) or class-II (ν_{II}) vibrational function. Thus,

$$\mathbf{H}=\begin{pmatrix}\mathbf{H}_{I,I} & \mathbf{H}_{I,II}\\ \mathbf{H}_{II,I} & \mathbf{H}_{II,II}\end{pmatrix}. \tag{3.157}$$

The submatrices $\mathbf{H}_{I,I}$ and $\mathbf{H}_{II,II}$ may now be separately diagonalized by operation with matrices

$$\begin{pmatrix}\mathbf{S} & 0\\ 0 & \mathbf{T}\end{pmatrix} \quad \text{and} \quad \begin{pmatrix}\mathbf{S}^{-1} & 0\\ 0 & \mathbf{T}^{-1}\end{pmatrix},$$

where S and T are unitary operators within the subspace of functions of classes-I and II, respectively. So we have

$$\begin{pmatrix}\mathbf{S} & 0\\ 0 & \mathbf{T}\end{pmatrix}\begin{pmatrix}\mathbf{H}_{I,I} & \mathbf{H}_{I,II}\\ \mathbf{H}_{II,I} & \mathbf{H}_{II,II}\end{pmatrix}\begin{pmatrix}\mathbf{S}^{-1} & 0\\ 0 & \mathbf{T}^{-1}\end{pmatrix}$$

$$=\begin{pmatrix}\mathbf{S}\,\mathbf{H}_{I,I}\,\mathbf{S}^{-1} & \mathbf{S}\,\mathbf{H}_{I,II}\,\mathbf{T}^{-1}\\ \mathbf{T}\,\mathbf{H}_{II,I}\,\mathbf{S}^{-1} & \mathbf{T}\,\mathbf{H}_{II,II}\,\mathbf{T}^{-1}\end{pmatrix}. \tag{3.158}$$

The eigenvalues of $\mathbf{H}_{I,I}$ are just the class-I compound states defined in Eq. (3.152), and those of $\mathbf{H}_{II,II}$ are the class-II compound states of Eq. (3.153). The unitary matrices S and T required to effect this subspace diagonalization are themselves the expansion coefficients of the class-I and class-II compound states, respectively:

$$S_{\lambda_I,\mu\nu_I}=\langle\lambda_I|\,\mu\nu_I\rangle\equiv C^{\lambda_I}_{\mu\nu_I}$$

$$T_{\lambda_{II},\mu\nu_{II}}=\langle\lambda_{II}|\,\mu\nu_{II}\rangle\equiv C^{\lambda_{II}}_{\mu\nu_{II}}. \tag{3.159}$$

Thus the submatrices $\mathbf{S}\,\mathbf{H}_{I,II}\mathbf{T}^{-1}$ and $\mathbf{T}\,\mathbf{H}_{II,I}\mathbf{S}^{-1}$ have elements of the form

$$(\mathbf{S}\,\mathbf{H}_{I,II}\mathbf{T}^{-1})_{\lambda_I\lambda_{II}}=\sum_{\mu''\nu_{II}}\sum_{\mu'\nu_I}\langle\lambda_I|\,\mu'\nu_I\rangle\langle\mu'\nu_I|H_c|\,\mu''\nu_{II}\rangle\langle\mu''\nu_{II}|\,\lambda_{II}\rangle=\langle X^{(I)}_{\lambda}|H_c|X^{(II)}_{\lambda_{II}}\rangle, \tag{3.160a}$$

$$(\mathbf{T}\,\mathbf{H}_{II,I}\mathbf{S}^{-1})_{\lambda_{II}\lambda_I}=\langle X^{(II)}_{\lambda_{II}}|H_c|X^{(I)}_{\lambda_I}\rangle. \tag{3.160b}$$

For compound states rather lower in energy than the intermediate maximum A in the deformation potential energy barrier, it is expected that the admixture of vibrational states Φ from above the maximum, with comparable amplitude in both regions of deformation I and II, will be very small. In this case the matrix elements of Eq. (3.160) are very small because of the attenuation of the vibrational components through the intermediate peak. At low enough energies it is clearly possible for these matrix elements describing the coupling between class-I and class-II states to be so small that the eigenstates X_λ can be described to a very good approximation as being either class-I or class-II states. Good physical examples of such a clean separation are provided by the slow neutron resonances in the cross sections of ^{240}Pu (see Sec. VI.E.1.*a*) and ^{238}U (see Sec. VI.E.1.*b*).

Very rough estimates of the magnitude of the coupling matrix elements can be made from Eq. (3.160) for the slow neutron case (resonance states at an excitation energy of ~5 MeV with a density $D_I^{-1}\sim 10^5$ MeV^{-1}). Observations of the neutron-induced fission cross sections of fissile nuclei indicate that the high vibrational states (quantum number $\nu\sim 5$–10) are mixed fairly uniformly over the compound states. The magnitude of the matrix element for mixing of a vibrational state into a class-I state in the absence of attenuation through the intermediate barrier can thus be deduced from the spreading width value $W\gtrsim\hbar\omega_I$ (see Sec. III.C.5.*c*(*iii*) for discussion of Lorentzian mixing) to be $\gtrsim(D_I\hbar\omega_I/2\pi)^{1/2}$. The attenuation through the intermediate barrier will reduce this by a factor $(T_A/2\pi)^{1/2}$. The fractionation of a class-II vibrational state into the class-II compound states will be given by

$$\langle\mu\nu_{II}|\,\lambda_{II}\rangle\sim(D_{II}/\hbar\omega_{II})^{1/2},$$

where D_{II} is the class-II compound state spacing. Thus

$$|\langle X^{(I)}_{\lambda_I}|H_c|X^{(II)}_{\lambda_{II}}\rangle|\sim\left(\frac{D_I D_{II}}{2\pi}\,\frac{T_A}{2\pi}\right)^{1/2}. \tag{3.161}$$

Vibrational states ν_I,ν_{II} that are very close in energy, and thus, according to the discussion of Sec. III.C.4.*c*, would be of comparable amplitude in both wells, might be expected to make a large contribution to the admixture coefficients described by Eq. (3.160). Such a situation could cause a breakdown of the weak coupling theory here being developed. In fact this will not happen because the components in the two wells will have opposite relative sign in the two vibrational wave functions (one has an extra node). This will lead to major cancellation in the matrix element of H_c.

c. *Specific coupling modes of class-I and class-II states*

With small matrix elements in the off-diagonal submatrices for coupling class-I and class-II states the final diagonalization of the Hamiltonian of Eq. (3.159), and the insertion of the resulting eigenstates into the R-matrix reaction theory, becomes possible by a number of methods corresponding to distinct physical situations. In most of these the approximation is made that the coupling matrix elements are sufficiently small that the effects of all but one class-II state on a localized group of class-I states can be neglected.

(i) Very weak coupling; narrow class-II states. Here narrowness of the class-II state is defined by the product of penetrability and squared amplitude at the channel deformation (the fission width) being much smaller than the energy interval δ between the class-II state and its nearest class-I neighbor. (It will be shown in Sec. III.C.5.*c*(*v*) that although this condition does not affect the diagonalization of H it has a drastic effect

on the properties of the resonances in the cross section.) Very weak coupling is defined as the average magnitude of the coupling matrix element $\langle \lambda_I | H_c | \lambda_{II} \rangle$ being much smaller than the energy interval δ. This condition allows the Hamiltonian of (3.159) to be diagonalized by perturbation theory. Second-order perturbation theory in the region of a single class-II state gives

$$X_{\lambda'} \approx \left[1 - \frac{\langle X^{(I)}_{\lambda_I} | H_c | X^{(II)}_{\lambda_{II}} \rangle^2}{2(E_{\lambda_I} - E_{\lambda_{II}})^2}\right] X^{(I)}_{\lambda_I} + \frac{\langle X^{(I)}_{\lambda_I} | H_c | X^{(II)}_{\lambda_{II}} \rangle}{(E_{\lambda_I} - E_{\lambda_{II}})} X^{(II)}_{\lambda_{II}} + \sum_{\lambda'_I \neq \lambda_I} \frac{\langle X^{(I)}_{\lambda'_I} | H_c | X^{(II)}_{\lambda_{II}} \rangle \langle X^{(II)}_{\lambda_{II}} | H_c | X^{(I)}_{\lambda'_I} \rangle}{(E_{\lambda_I} - E_{\lambda'_I})(E_{\lambda_I} - E_{\lambda_{II}})}, \tag{3.162a}$$

$$E_{\lambda'} \approx E_{\lambda_I} + \frac{\langle X^{(I)}_{\lambda_I} | H_c | X^{(II)}_{\lambda_{II}} \rangle^2}{E_{\lambda_I} - E_{\lambda_{II}}}, \tag{3.162b}$$

for the states that remain essentially class I in character, and

$$X_{\lambda''} \approx \left[1 - \sum_{\lambda_I} \frac{\langle X^{(I)}_{\lambda_I} | H_c | X^{(II)}_{\lambda_{II}} \rangle^2}{2(E_{\lambda_{II}} - E_{\lambda_I})^2}\right] X^{(II)}_{\lambda_{II}} + \sum_{\lambda_I} \frac{\langle X^{(I)}_{\lambda_I} | H_c | X^{(II)}_{\lambda_{II}} \rangle}{E_{\lambda_{II}} - E_{\lambda_I}} X^{(I)}_{\lambda_I}, \tag{3.163a}$$

$$E_{\lambda''} \simeq E_{\lambda_{II}} + \sum_{\lambda_I} \frac{\langle X^{(II)}_{\lambda_{II}} | H_c | X^{(I)}_{\lambda_I} \rangle^2}{E_{\lambda_{II}} - E_{\lambda_I}}, \tag{3.163b}$$

for the remaining state. From these relations simple results are obtained for the resonance widths [see Sec. III.C.3.g.(ii)]. If $\Gamma_{\lambda_{II}(f)}$ is the fission width that an unperturbed class-II state would have if it appeared as a resonance in a suitable cross section and the fission widths for unperturbed class-I states are assumed to be negligible, we have immediately that

$$\Gamma_{\lambda'(f)} \simeq \frac{\langle X^{(I)}_{\lambda_I} | H_c | X^{(II)}_{\lambda_{II}} \rangle}{(E_{\lambda_I} - E_{\lambda_{II}})^2} \Gamma_{\lambda''_{II}}(f), \tag{3.164}$$

for quasi-class-I resonance states, while

$$\Gamma_{\lambda''}(f) \simeq \left[1 - \sum_{\lambda_I} \frac{(H_c)^2_{\lambda_I \lambda_{II}}}{(E_{\lambda_I} - E_{\lambda_{II}})^2}\right] \Gamma_{\lambda_{II}}(f) \tag{3.165a}$$

$$= \Gamma_{\lambda_{II}}(f) - \sum_{\lambda'(\neq \lambda'')} \Gamma_{\lambda'(f)} \tag{3.165b}$$

is the fission width of the quasi-class-II resonance.

Exactly similar relations hold for the partial radiation widths for electromagnetic transitions to lower class-II states, so we see that each admixed level has exactly the same pattern, in terms of relative intensities, of class-II spectrum superimposed on the normal class-I spectrum. This "fingerprint" spectrum could be used to identify the second minimum phenomenon in resonance behavior when the class-II states themselves cannot fission (because the saddle point is too high). The fingerprint behavior is of course quite different from the normal spectrum behavior that varies strongly (at least in the high transition energy region where discrete transitions can be observed) from one resonant state to the next. Each class-II fingerprint spectrum will also vary strongly from one class-II group of resonances to the next group. Radiative transitions are treated in greater detail in Sec. VI.D.

Neutron (or other particle) widths cannot be given so unambiguously. The expressions for reduced neutron widths (in the experimenters' convention: neutron width divided by a factor proportional to the penetration factor) are

$$\Gamma^{(0)}_{\lambda''(n)} \simeq \left[\left(1 - \frac{\langle X^{(I)}_{\lambda_I} | H_c | X^{(II)}_{\lambda_{II}} \rangle}{2(E_{\lambda_I} - E_{\lambda_{II}})^2}\right)(\Gamma^{(0)}_{\lambda_I(n)})^{1/2} + \sum_{\lambda'_I (\neq \lambda_I)} \frac{\langle X^{(I)}_{\lambda'_I} | H_c | X^{(II)}_{\lambda_{II}} \rangle \langle X^{(II)}_{\lambda_{II}} | H_c | X^{(I)}_{\lambda_I} \rangle}{(E_{\lambda_I} - E_{\lambda'_I})(E_{\lambda_I} - E_{\lambda_{II}})} (\Gamma^{(0)}_{\lambda'_I(n)})^{1/2}\right]^2, \tag{3.166}$$

$$\Gamma^{(0)}_{\lambda''_I(n)} \simeq \left(\sum_{\lambda_I} \frac{\langle X^{(I)}_{\lambda_I} | H_c | X^{(II)}_{\lambda''_I} \rangle}{E_{\lambda_{II}} - E_{\lambda_I}} (\Gamma^{(0)}_{\lambda_I(n)})^{1/2}\right)^2, \tag{3.167}$$

where $\Gamma^{(0)}_{\lambda(n)} = 2P_n$ (at 1 eV) $\gamma^2_{\lambda(n)}$. The terms raised to one-half power (the reduced width amplitudes) are random from one resonant state to another, and generally will be unknown. This gives a number of possibilities for the value of $\Gamma_{\lambda''(n)}$ in relation to the values of the $\Gamma_{\lambda'(n)}$. A maximum value of $\Gamma_{\lambda''(n)}$ can be stated for a finite number of admixed class-I states (this would occur if the signs of the $\sqrt{\Gamma_{\lambda_I(n)}}$ were fully correlated) and a mean expected value of this width can also be given; the latter is

$$\langle \Gamma^{(0)}_{\lambda''(n)} \rangle \approx \sum_{\lambda'(\neq \lambda'')} \frac{\Gamma_{\lambda'(f)} \Gamma^{(0)}_{\lambda'(n)}}{\Gamma_{\lambda_{II}(f)}}. \tag{3.168}$$

Physical examples of such coupling between class-I and class-II states are to be found in the slow neutron cross sections of ^{240}Pu and ^{238}U. In the former, three now well-studied class-II states occur below a neutron energy of 2000 eV, and in this energy range the average class-I level spacing is ~14 eV. For each of the class-II states, identified by the comparatively high fission cross sections of the resonances in their immediate vicinity (see Fig. 7), the class-II fission width is about 2 eV. In two of the cases (at 800 and 1900 eV) the bulk of this fission width is to be found in a single weak, but broad, resonance at the center of a cluster of strong fission resonances. The quasi-class-II resonance thus identified has a reduced neutron width less than one-tenth of the average value of its neighbors. Further details are to be found in Sec. VI.E.1.

(ii) Very weak coupling with accidental degeneracy. The perturbation theory of subsection (i) above does not cover the possibility of an accidental degeneracy or near-degeneracy between a class-I state and a class-II state. This situation, with weak coupling to the remaining class-I states, can be dealt with quite easily. The subsection H_s of the Hamiltonian matrix around a given class-II state (moved into the row 1, column 1 position)

is

$$\begin{bmatrix} E_{1_{II}} & \langle X_1^{(II)}|H_c|X_2^{(I)}\rangle & \langle X_1^{(II)}|H_c|X_3^{(I)}\rangle & \cdots \\ \langle X_2^{(I)}|H_c|X_1^{(II)}\rangle & E_{2_I} & 0 & \\ \langle X_3^{(I)}|H_c|X_1^{(II)}\rangle & 0 & E_{3_I} & 0\cdots \\ \cdot & 0 & 0 & \cdot \\ \cdot & \cdot & \cdot & \cdot \\ \cdot & \cdot & \cdot & \cdot \end{bmatrix} \tag{3.169}$$

Here, E_{2_I} is the nearly degenerate class-I eigenvalue. The top left-hand submatrix of order two can be diagonalized by a matrix with a unitary submatrix W in that position and partitioned otherwise as

$$\begin{bmatrix} W & 0 \\ 0 & 1 \end{bmatrix}.$$

By operating with this matrix and its reciprocal on the submatrix H_S we obtain

$$\begin{bmatrix} E_1' & 0 & W_{11}\langle X_1^{(II)}|H_c|X_3^{(I)}\rangle & \cdots \\ 0 & E_2' & W_{21}\langle X_1^{(II)}|H_c|X_3^{(I)}\rangle & \cdots \\ \langle X_3^{(I)}|H_c|X_1^{(II)}\rangle(W^{-1})_{II} & \langle X_3^{(I)}|H_c|X_1^{(II)}\rangle(W^{-1})_{12} & E_3 & 0\cdots \\ \langle X_4^{(I)}|H_c|X_1^{(II)}\rangle(W^{-1})_{11} & \langle X_4^{(I)}|H_c|X_1^{(II)}\rangle(W^{-1})_{12} & 0 & E_4 \\ \cdot & \cdot & \cdot & \\ \cdot & \cdot & \cdot & \\ \cdot & \cdot & \cdot & \end{bmatrix}. \tag{3.170}$$

Here (dropping Roman subscripts, where their implied presence is obvious, for convenience)

$$E_1' = \tfrac{1}{2}\{(E_1+E_2)+[(E_1-E_2)^2+4\langle X_2^{(I)}|H_c|X_1^{(II)}\rangle^2]^{1/2}\} \tag{3.171a}$$

$$E_{2'} = \tfrac{1}{2}\{(E_1+E_2)-[(E_1-E_2)^2+4\langle X_2^{(I)}|H_c|X_1^{(II)}\rangle^2]^{1/2}\}. \tag{3.171b}$$

The eigenfunctions corresponding to these are

$$X_{1'}' = W_{11}X_1^{(II)} - W_{21}X_2^{(I)}, \tag{3.171c}$$

$$X_{2'}' = W_{21}X_1^{(II)} + W_{22}X_2^{(I)}, \tag{3.171d}$$

where

$$W_{11} = \frac{\langle X_1^{(II)}|H_c|X_2^{(I)}\rangle}{[((E_1-E_{1'})^2+\langle X_1^{(II)}|H_c|X_2^{(I)}\rangle^2)]^{1/2}} = W_{22}, \tag{3.172a}$$

$$W_{21} = \frac{(E_{1'}-E_1)}{[((E_1-E_{1'})^2+\langle X_1^{(II)}|H_c|X_2^{(I)}\rangle^2)]^{1/2}} = -W_{12}. \tag{3.172b}$$

By perturbation theory we find

$$E_{1''} \approx E_{1'} + W_{11}^2 \sum_{\lambda_I(\neq 1,2)} \frac{\langle X_1^{(II)}|H_c|X_{\lambda_I}^{(I)}\rangle^2}{E_{1'}-E_{\lambda_I}}, \tag{3.173a}$$

$$X_{1''} \approx \left[1 - \frac{W_{11}^2}{2}\sum_{\lambda_I(\neq 1,2)} \frac{\langle X_{\lambda_I}^{(I)}|H_c|X_1^{(II)}\rangle^2}{(E_{1'}-E_{\lambda_I})^2}\right]X_{1'} + W_{11}\sum_{\lambda_I(\neq 1,2)} \frac{\langle X_{\lambda_I}^{(I)}|H_c|X_1^{(II)}\rangle}{E_{1'}-E_{\lambda_I}}X_\lambda^{(I)} + W_{21}W_{11}\sum_{\lambda_I(\neq 1,2)} \frac{\langle X_1^{(II)}|H_c|X_{\lambda_I}^{(I)}\rangle^2}{(E_{1'}-E_{\lambda_I})(E_{1'}-E_{2'})}X_{2'}, \tag{3.173b}$$

$$E_{2''} \approx E_{2'} + W_{21}^2 \sum_{\lambda_I(\neq 1,2)} \frac{\langle X_1^{(II)}|H_c|X_{\lambda_I}^{(I)}\rangle^2}{E_{2'}-E_{\lambda_I}}, \tag{3.173c}$$

$$X_{2''} \approx \left[1 - \frac{W_{21}^2}{2}\sum_{\lambda_I(\neq 1,2)} \frac{\langle X_{\lambda_I}^{(I)}|H_c|X_1^{(II)}\rangle^2}{(E_{2'}-E_{\lambda_I})^2}\right]X_{2'} + W_{21}\sum_{\lambda_I(\neq 1,2)} \frac{\langle X_{\lambda_I}^{(I)}|H_c|X_1^{(II)}\rangle}{E_{2'}-E_{\lambda_I}}X_\lambda^{(I)} + W_{21}W_{11}\sum_{\lambda_I(\neq 1,2)} \frac{\langle X_1^{(II)}|H_c|X_{\lambda_I}^{(I)}\rangle^2}{(E_{2'}-E_{\lambda_I})(E_{2'}-E_{1'})}X_{1'}, \tag{3.173d}$$

for the near-degenerate states, and

$$E_\lambda \approx E_{\lambda_I} + W_{11}^2\frac{\langle X_{\lambda_I}^{(I)}|H_c|X_1^{(II)}\rangle^2}{E_{\lambda_I}-E_{1'}} + W_{21}^2\frac{\langle X_{\lambda_I}^{(I)}|H_c|X_1^{(II)}\rangle^2}{E_{\lambda_I}-E_{2'}}, \tag{3.174a}$$

$$X_\lambda \approx \left[1 - \frac{W_{11}^2}{2}\frac{\langle X_1^{(II)}|H_c|X_{\lambda_I}^{(I)}\rangle^2}{(E_{\lambda_I}-E_{1'})^2} - \frac{W_{21}^2}{2}\frac{\langle X_1^{(II)}|H_c|X_{\lambda_I}^{(I)}\rangle^2}{(E_{\lambda_I}-E_{2'})^2}\right]X_{\lambda_I}^{(I)} + \langle X_1^{(II)}|H_c|X_{\lambda_I}^{(I)}\rangle\left[\frac{W_{11}X_{1'}'}{E_{\lambda_I}-E_{1'}} + \frac{W_{21}X_{2'}'}{E_{\lambda_I}-E_{2'}}\right] + \sum_{\lambda_I'(\neq 1,2)} \frac{\langle X_{\lambda_I'}^{(I)}|H_c|X_1^{(II)}\rangle\langle X_1^{(II)}|H_c|X_{\lambda_I}^{(I)}\rangle}{E_{\lambda_I}-E_{\lambda_I'}}\left[\frac{W_{11}^2}{(E_{\lambda_I}-E_{1'})} + \frac{W_{21}^2}{(E_{\lambda_I}-E_{2'})}\right]X_{\lambda_I'}^{(I)}, \tag{3.174b}$$

for the remaining quasi-class-I states.

The corresponding expressions for fission widths of the narrow resonances appearing in the cross section are

$$\Gamma_{1''(f)} \approx \left[1 - W_{11}^2 \sum_{\lambda_I(\neq 1,2)} \frac{\langle X_{\lambda_I}^{(I)} | H_c | X_1^{(II)} \rangle^2}{(E_{1'} - E_{\lambda_I})^2}\right] \Gamma_{1'(f)} + 2W_{21}^2 \sum_{\lambda_I(\neq 1,2)} \frac{\langle X_1^{(II)} | H_c | X_{\lambda_I}^{(I)} \rangle^2}{(E_{1'} - E_{\lambda_I})(E_{1'} - E_{2'})} \Gamma_{1'(f)}, \tag{3.175a}$$

$$\Gamma_{2''(f)} \approx \left[1 - W_{21}^2 \sum_{\lambda_I(\neq 1,2)} \frac{\langle X_{\lambda_I}^{(I)} | H_c | X_1^{(II)} \rangle^2}{(E_{2'} - E_{\lambda_I})^2}\right] \Gamma_{2'(f)} + 2W_{11}^2 \sum_{\lambda_I(\neq 1,2)} \frac{\langle X_1^{(II)} | H_c | X_{\lambda_I}^{(I)} \rangle^2}{(E_{2'} - E_{\lambda_I})(E_{2'} - E_{1'})} \Gamma_{2'(f)}, \tag{3.175b}$$

for the resonance corresponding to the two nearly degenerate states, and

$$\Gamma_{\lambda(f)} \approx \left[\frac{W_{11}^2 \Gamma_{1''(f)}}{(E_\lambda - E_{1'})^2} + \frac{W_{21}^2 \Gamma_{2''(f)}}{(E_\lambda - E_{2'})^2} + \frac{2W_{11} W_{21} (\Gamma_{1''(f)} \Gamma_{2''(f)})^{1/2}}{(E_\lambda - E_{1'})(E_\lambda - E_{2'})}\right] \langle X_1^{(II)} | H_c | X_\lambda^{(I)} \rangle^2 \tag{3.175c}$$

for the remaining quasi-class-I resonances. In these equations the fission widths of the diagonalized pair of nearly degenerate states are given by their amplitudes

$$\Gamma_{1'(f)}^{1/2} = W_{11} \Gamma_{1_{II}(f)}^{1/2}, \tag{3.176a}$$

$$\Gamma_{2'(f)}^{1/2} = W_{21} \Gamma_{1_{II}(f)}^{1/2}. \tag{3.176b}$$

In first approximation the reduced neutron width amplitudes of the nearly degenerate resonance states are

$$\Gamma_{1'(n)}^{(0)1/2} = -W_{21} \Gamma_{2_I(n)}^{(0)1/2}, \tag{3.177a}$$

$$\Gamma_{2'(n)}^{(0)1/2} = W_{11} \Gamma_{2_I(n)}^{(0)1/2}. \tag{3.177b}$$

After perturbation by the remaining class-I states, these two states can no longer be assigned precise estimates for their neutron widths. To first order the expectation values of the reduced neutron widths are

$$\langle \Gamma_{1''(n)}^{(0)} \rangle \approx \left[1 - 2W_{11}^2 \sum_{\lambda_I(\neq 1,2)} \frac{\langle X_1^{(II)} | H_c | X_{\lambda_I}^{(I)} \rangle^2}{(E_{1'} - E_{\lambda_I})(E_{1'} - E_{2'})} - W_{11}^2 \sum_{\lambda_I(\neq 1,2)} \frac{\langle X_{\lambda_I}^{(I)} | H_c | X_1^{(II)} \rangle^2}{(E_{1'} - E_{\lambda_I})^2}\right] \Gamma_{1'(n)}^{(0)} + W_{11}^2 \sum_{\lambda_I(\neq 1,2)} \frac{\langle X_{\lambda_I}^{(I)} | H_c | X_1^{(II)} \rangle^2}{(E_{1'} - E_{\lambda_I})^2} \Gamma_{\lambda_I(n)}^{(0)}, \tag{3.178a}$$

$$\langle \Gamma_{2''(n)}^{(0)} \rangle \approx \left[1 - 2W_{21}^2 \sum_{\lambda_I(\neq 1,2)} \frac{\langle X_1^{(II)} | H_c | X_{\lambda_I}^{(I)} \rangle^2}{(E_{2'} - E_{\lambda_I})(E_{2'} - E_{1'})} - W_{21}^2 \sum_{\lambda_I(\neq 1,2)} \frac{\langle X_{\lambda_I}^{(I)} | H_c | X_1^{(II)} \rangle^2}{(E_{2'} - E_{\lambda_I})^2}\right] \Gamma_{2'(n)}^{(0)} + W_{21}^2 \sum_{\lambda_I(\neq 1,2)} \frac{\langle X_{\lambda_I}^{(I)} | H_c | X_1^{(II)} \rangle^2}{(E_{2'} - E_{\lambda_I})^2} \Gamma_{\lambda_I(n)}^{(I)}. \tag{3.178b}$$

These results are to be substituted into the resonance cross-section formulas, e.g., the single-level formula Eq. (3.125) or a many-level formula of Sec. III.C.3.g.(ii) or (iii). The sign of the first-order level-level interference between the quasidegenerate resonances is implied unambiguously by the diagonalization treatment above. Neglecting the perturbation of the levels λ'', the substitution of the width amplitudes of Eqs. (3.176) and (3.177) into Eq. (3.131) gives

$$\sigma_{nf,\text{int}} = -\frac{\pi}{k_n^2} g_J 2W_{11}^2 W_{21}^2 \Gamma_{1_{II}(f)} \Gamma_{2_I(n)} \times \left(\frac{(E_{1'} - E)(E_{2'} - E) + \frac{1}{4}\Gamma_{1'} \Gamma_{2'}}{[(E_{1'} - E)^2 + \frac{1}{4}\Gamma_{1'}^2][(E_{2'} - E)^2 + \frac{1}{4}\Gamma_{2'}^2]}\right). \tag{3.179}$$

This is positive (constructive) between the two resonances and destructive outside.

A perfect example of accidental degeneracy between a class-II and a class-I level is provided in the fission cross section of ^{240}Pu. The group of resonances centered at 1405 eV neutron energy (shown in Fig. 115) is dominated by two resonances of very similar parameters, sharing between them a total fission width of 3.5 eV. The constructive interference effect is very clear. A full analysis of this group is given in Sec. VI.E.1.

(iii) Moderately weak coupling: narrow class-II states. Moderately weak coupling may be defined as occurring when the magnitude of the coupling matrix elements lies within the range

$$D_I^2 \lesssim \overline{\langle \lambda_I | H_c | \lambda_{II} \rangle^2} \lesssim D_I D_{II}. \tag{3.180}$$

With these conditions it is a good approximation to consider only the mixing of a single class-II state with a group of class-I states in its vicinity. However, the coupling is too strong to permit a perturbation treatment.

The limitation to a single class-II state allows the diagonalization of the matrix on the right-hand side of Eq. (3.158) to be reduced to the solution of

$$C_{\lambda_I}^\lambda (E_{\lambda_I} - E_\lambda) + C_{\lambda_{II}}^\lambda \langle \lambda_I | H_c | \lambda_{II} \rangle = 0,$$

$$\sum_{\lambda_I} C_{\lambda_I}^\lambda \langle \lambda_{II} | H_c | \lambda_I \rangle + C_{\lambda_{II}}^\lambda (E_{\lambda_{II}} - E_\lambda) = 0, \tag{3.181}$$

for a single class-II state λ_{II}, together with the normalization condition

$$(C_{\lambda_{II}}^\lambda)^2 + \sum_{\lambda_I} (C_{\lambda_I}^\lambda)^2 = 1. \tag{3.182}$$

Here the $C_{\lambda_I}^\lambda$, $C_{\lambda_{II}}^\lambda$ are the expansion coefficients of the class-I and class-II states in the diagonalized states λ:

$$X_\lambda = \sum_{\lambda_I} C_{\lambda_I}^\lambda X_{\lambda_I}^{(I)} + C_{\lambda_{II}}^\lambda X_{\lambda_{II}}^{II}. \tag{3.183}$$

The solution of these equations (see, e.g., Lynn, 1968b; Bohr and Mottelson, 1969) is

$$C_{\lambda_I}^\lambda = -\frac{\langle \lambda_I | H_c | \lambda_{II} \rangle}{E_{\lambda_I} - E_\lambda} \cdot C_{\lambda_{II}}^\lambda, \tag{3.184a}$$

$$E_{\lambda_{II}} - E_\lambda = \sum_{\lambda_I} \frac{\langle \lambda_I | H_c | \lambda_{II} \rangle^2}{E_{\lambda_I} - E_\lambda}, \tag{3.184b}$$

$$(C^\lambda_{\lambda_{II}})^2 = \left(\sum_{\lambda_I} \frac{\langle \lambda_I | H_c | \lambda_{II} \rangle^2}{(E_{\lambda_I} - E_\lambda)^2} + 1 \right)^{-1}. \tag{3.184c}$$

This result is exact and incorporates the results of perturbation theory for the very weak coupling case. Equations (3.184) are most easily surveyed for the uniform, or picket fence, model of level structure. Class-I levels are assumed to be equally spaced (with interval D_I) and the squared matrix element of H_c is assumed to be independent of λ_I. Thus

$$E_{\lambda_{II}} - E_\lambda = -\frac{\pi H_c^2}{D_I} \cot\left(\frac{\pi E_\lambda}{D_I}\right), \tag{3.185a}$$

(the origin of the energy scale coinciding with a class-I level) and

$$(C^\lambda_{\lambda_{II}})^2 = \frac{H_c^2}{(E_{\lambda_{II}} - E_\lambda)^2 + \frac{\pi^2 H_c^4}{D_I^2} + H_c^2}. \tag{3.185b}$$

In the familiar Lorentzian form of Eq. (3.185b) the half-width of the profile of squared admixture coefficients (defined as half-width at half-maximum) is

$$W = \frac{\pi H_c^2}{D_I} \left(1 + \frac{D_I^2}{\pi^2 H_c^2}\right)^{1/2}. \tag{3.186}$$

The first factor is the well-known "golden rule," and for all but very weak coupling the second factor is nearly unity. It must be remembered, however, that, according to Eq. (3.185a), eigenvalues are densest close to the spreading class-II state λ_{II} [Fig. 40 is a schematic diagram of the solution (3.185a)], hence the half-width of suitably averaged strength of the mixing $(C^\lambda_{\lambda_{II}})^2/D$ as a function of energy is less than the result given in Eq. (3.186). In fact it has been shown (Lane *et al.*, 1974) that $W = \pi H_c^2/D_I$ is the exact result if the average mixing of λ_{II} into the states λ is defined by an ensemble procedure in which the members of the ensemble are all possible patterns of E_λ and $(C^\lambda_{\lambda_{II}})^2$ resulting from prescribed mean values and statistical distributions of the class-I level spacings and the matrix elements (for further discussion of these distributions see Sec. VI). The strength function $\bar{s}(E)$ for spreading of the state λ_{II} is defined in terms of the probability $P(\gamma^2, E)dE\,d\gamma^2$ for finding, amongst the ensemble of these patterns, a total admixture coefficient $(C^\lambda_{\lambda_{II}})^2$ lying between γ^2 and $\gamma^2 + d\gamma^2$ in value in the energy interval E to $E + dE$. Then

$$\bar{s}(E)dE = dE \int_0^\infty \gamma^2 P(\gamma^2, E) d\gamma^2. \tag{3.187}$$

In the uniform model class-I spacings and matrix elements do not fluctuate about their mean values, and the only quantity that varies among the members of the ensemble is the interval between the class-II state and the nearest class-I state at higher energy. The evaluation of the strength then gives exactly

$$\bar{s}(E) = \frac{1}{D_I} \frac{H_c^2}{(E_{\lambda_{II}} - E)^2 + \pi^2 H_c^4 / D_I^2}. \tag{3.188}$$

An estimate of the value to be expected for the Lorentzian half-width in terms of the intermediate barrier transmission coefficient T_A can be obtained from Eqs. (3.186) and (3.181), with the result

$$2W \approx \frac{D_{II}}{2\pi} T_A. \tag{3.189}$$

The coefficients of mixing of the class-II state, into the states λ, as expressed by Eq. (3.184c), can be used immediately to give the fission widths in the narrow resonance approximation;

$$\Gamma_{\lambda(f)} = (C^\lambda_{\lambda_{II}})^2 \Gamma_{\lambda_{II}(f)}. \tag{3.190}$$

In the uniform model the resonance fission widths would therefore follow the Lorentzian profile of Eq. (3.185b). Entrance channel widths must be deduced from the coefficients of Eq. (3.184a). Far from the class-II state the entrance channel widths are very little disturbed from the original pattern possessed by the class-I states. Near the original class-II states there is considerable dislocation of the original pattern, but, except in the case of very weak coupling, there will be no strong reduction in expected value, and anticorrelation between fission width and entrance channel width will only be weak.

For nonuniform distributions of level spacings and matrix elements (particularly useful for situations where long-range energy variations might be involved) another variation of the locally averaged strength of admixing of the special state may be employed (Bohr and Mottelson, 1969). The locally averaged admixture coefficient $\langle (C^\lambda_{\lambda_{II}})^2 \rangle_E$ is defined as the weighted average

$$\langle (C^\lambda_{\lambda_{II}})^2 \rangle_E = \sum_\lambda \omega(E_\lambda - E)(C^\lambda_{\lambda_{II}})^2, \tag{3.191a}$$

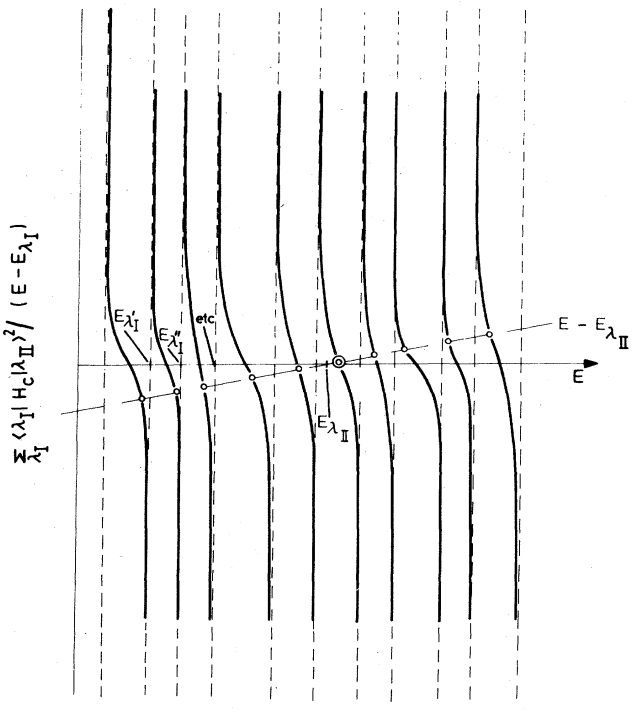

FIG. 40. Schematic diagram of the solution of the eigenvalue Eq. (3.184b) for mixing of a single class-II state with many class-I states. Circles give the eigenvalue solutions E_λ.

where $\omega(x)$ has the Cauchy form

$$\omega(x) = \frac{1}{2\pi}\frac{\Delta}{x^2 + (\Delta/2)^2}. \tag{3.191b}$$

The right-hand side of Eq. (3.191a) is in the form of the sum of residues of a contour integral which can be alternatively evaluated as the sum of residues of the two poles $E + i\Delta/2$, $E - i\Delta/2$, giving

$$\langle (C^{\lambda}_{\lambda_{II}})^2 \rangle_E = \frac{1}{2\pi}\frac{\Gamma + \Delta}{(E_{\lambda_{II}} + \Delta E_{\lambda_{II}} - E)^2 + \frac{1}{4}(\Gamma + \Delta)^2}, \tag{3.192a}$$

with

$$\Gamma = \Delta \sum_{\lambda_I} \frac{\langle \lambda_{II} | H_c | \lambda_I \rangle^2}{(E - E_{\lambda_I})^2 + (\Delta/2)^2}, \tag{3.192b}$$

$$\Delta E_{\lambda_{II}} = \sum_{\lambda_I} \frac{\langle \lambda_{II} | H_c | \lambda_I \rangle^2 (E - E_{\lambda_I})}{(E - E_{\lambda_I})^2 + (\Delta/2)^2}. \tag{3.192c}$$

Physical examples of moderately weak coupling have been observed in the fission reaction in a few cases. The best explored is the slow-neutron-induced fission cross section of ^{234}U (James *et al.*, 1977). Fission and neutron widths have been measured for all the resonances in the region of 550 eV and the former show (Fig. 116) a Lorentzian type of profile about this energy, but with very considerable scatter about the ideal form (see Sec. VI.E.3.b). The half-width of the profile has been assessed as 68 eV, a factor of ~7 times the mean class-I level spacing ($D_I = 10.3$ eV). Further analysis of these data is discussed in Sec. VI.D.3.b. Another example, in which the fine structure resonances have not been experimentally resolved, occurs in the fission cross section (see Fig. 84) for neutrons bombarding ^{230}Th (James *et al.*, 1972). In this case the class-II state appears to be of particularly simple character (see Sec. V.B.5.a.).

(iv) Class-I background effects in moderately weak coupling. So far in this section the assumption has been made that the fission width of the fine-structure resonances arises only from their admixture of class-II compound state. However, a weak contribution to the fission width can also come from the many-phonon class-I vibrational state admixtures in the class-I compound states. The importance of this contribution is assessed here [the discussion is based on an unpublished report (Lynn, 1974a)].

From Eq. (3.183) the reduced width amplitude of final R-matrix state λ for a fission channel μ is

$$\gamma_{\lambda(\mu)} = C^{\lambda}_{\lambda_{II}} \gamma_{\lambda_{II}(\mu)} + \sum_{\lambda_I} C^{\lambda}_{\lambda_I} \gamma_{\lambda_I(\mu)}. \tag{3.193}$$

the class-II and class-I reduced width amplitudes being evaluated from Eqs. (3.152), (3.155), and (3.101a), their essential values being

$$\gamma_{\lambda_{II}(\mu)} \approx \left(\frac{\hbar^2}{2B\eta_\mu}\right)^{1/2} C^{\lambda_{II}}_{\mu\nu''} \Phi^{(II)}_{\nu''}(\eta_\mu), \tag{3.194}$$

$$\gamma_{\lambda_I(\mu)} \approx \left(\frac{\hbar^2}{2B\eta_\mu}\right)^{1/2} C^{\lambda_I}_{\mu\nu'} \Phi^{(I)}_{\nu'}(\eta_\mu), \tag{3.195}$$

where ν'', ν' are the highest appreciably admixed vibrational states in the class-II and class-I compound states under consideration. Clearly these vibrational states will be comparatively close in energy, hence an estimate of the ratio of their wave-functions at η_μ can be obtained from Sec. III.C.4.*d* [Eq. (3.148)]. This is

$$\left|\frac{\Phi^{(I)}_{\nu'}(\eta_\mu)}{\Phi^{(II)}_{\nu''}(\eta_\mu)}\right|^2 \approx \frac{1}{2\pi} T_A \tag{3.196}$$

for separation of the class-I and class-II states by the average value $\frac{1}{4}\hbar\omega$ (the simplifying assumption $\hbar\omega_I \approx \hbar\omega_{II} \equiv \hbar\omega$ is made here). The coefficients $C^{\lambda_{II}}_{\mu\nu''}$ and $C^{\lambda_I}_{\mu\nu'}$ can be evaluated on the assumption of strong mixing of the vibrational modes into the respective class of compound states as

$$(C^{\lambda_{II}}_{\mu\nu''})^2 \approx \frac{D_{II}}{\hbar\omega_{II}}, \tag{3.197}$$

$$(C^{\lambda_I}_{\mu\nu'})^2 \approx \frac{D_I}{\hbar\omega_I}. \tag{3.198}$$

Thus, for moderately weak coupling,

$$\gamma^2_{\lambda(\mu)} \approx \frac{\gamma^2_{II(\mu)} D_{II}}{2\pi}\left[\frac{2W}{(E_\lambda - E_{\lambda_{II}})^2 + W^2} + \frac{2\pi}{D_{II}}\left(\frac{T_A}{2\pi}\right)\frac{\hbar\omega_{II}}{\hbar\omega_I}\right], \tag{3.199}$$

using Eqs. (3.185b) and (3.193–198), and the assumptions that $\sum_{\lambda_I}(C^{\lambda}_{\lambda_I})^2 \approx 1$ (reasonably well satisfied for all λ if the coupling is not very weak) and that there is no correlation in sign amongst the coupling matrix elements. Substitution of Eq. (3.189) into (3.199) shows that at the class-II resonance energy the class-I contribution to the fission width is negligible (fractional contribution $\approx T_A^2/8\pi$).

Far away from resonance the contribution of other class-II compound states has to be included. Perturbation theory expressions can be used for this, giving

$$X_\lambda \approx X^{(I)}_{\lambda_I} + \sum_{\lambda_{II}} \frac{\langle \lambda_I | H_c | \lambda_{II} \rangle}{E_{\lambda_{II}} - E_{\lambda_I}} X_{\lambda_{II}}, \tag{3.200a}$$

$$\therefore \gamma_{\lambda(\mu)} \approx \gamma_{\lambda_I(\mu)} + \sum_{\lambda_{II}} \frac{\langle \lambda_I | H_c | \lambda_{II} \rangle}{E_{\lambda_{II}} - E_{\lambda_I}} \gamma_{\lambda_{II}(\mu)}. \tag{3.200b}$$

In a picket-fence model of uniform class-II levels the sum of the class-II contributions to the reduced width, under the assumption of no correlations in sign among the matrix elements, is just

$$\sum_{\lambda_{II}} \frac{\overline{\langle H_c \rangle^2}}{(E_{\lambda_{II}} - E_\lambda)^2}\overline{\gamma^2_{\lambda_{II}(\mu)}} = \frac{\overline{\pi^2 \langle H_c \rangle^2 \gamma^2_{\lambda_{II}(\mu)}}}{D^2_{II}}\left[1 + \tan^2\left(\frac{\pi E}{D_{II}}\right)\right], \tag{3.201}$$

the energy being measured from a point midway between two class-II levels. Again this can be expressed in terms of the transmission coefficient T_A, from Eq. (3.189), and the result

$$D_I \overline{\gamma^2_{\lambda_{II}(\mu)}}\, T_A/4D_{II}$$

(at $E = 0$) is to be compared with the class-I contribution the second term on the right-hand side of Eq. (3.199), which equals

$$D_I \overline{\gamma^2_{\lambda_{II}(\mu)}}\, T_A/2\pi D_{II}.$$

In this midway situation it is apparent that the class-I contribution to the fission width is comparable to that from the class-II states.

(v) Very weak coupling: broad class-II states. The definition of broadness here is that the fission width of the state, as computed from Eq. (3.126) with appropriate reduced width amplitudes at the channel deformation and penetration factor through the outer barrier, is of the order of or larger than the class-I level spacing. The extremely strong level-level interference that can now occur can completely reorganize the fine-structure resonance patterns from those predicted by the straightforward application of the formulae of the preceding

section into the Breit–Wigner single-level form. This broadness of the class-II state can effectively decouple to a large degree the mixing of class-I and class-II states that occurs when they are confined to the internal region. (The same kind of decoupling effect has already been seen in the statistical treatment of Sec. III.B when the outer barrier B is lower than the intermediate barrier A.)

The effect is most simply illustrated by treating the case of accidental degeneracy of a class-II and class-I level. In Sec. III.C.5.*c*.(ii) the formulas for eigenvalues of the internal R-matrix states that result from the degeneracy are given [Eq. (3.173)]. These are substituted in the level-matrix formulation of R-matrix theory [Sec. III.C.3.*g*.(*ii*)]. With the neglect of radiative capture and retention of a single entrance (neutron, in this example) and fission channel, the resulting two-level matrix [Eq. (3.129c)] is

$$\mathbf{C}=\begin{pmatrix} E_{\lambda'}-E-\frac{1}{4}i(\Gamma_{\lambda_{II}(f)}+\Gamma_{\lambda_I(n)}) & -\frac{1}{4}i(\Gamma_{\lambda_{II}(f)}-\Gamma_{\lambda_I(n)}) \\ -\frac{1}{4}i(\Gamma_{\lambda_{II}(f)}-\Gamma_{\lambda_I(n)}) & E_{\lambda'}+2|\langle\lambda_I|H_c|\lambda_{II}\rangle|-E-\frac{1}{4}i(\Gamma_{\lambda_{II}(f)}+\Gamma_{\lambda_I(n)}) \end{pmatrix}. \tag{3.202}$$

The poles of the S matrix [see Sec. III.C.3.*g*(*iv*)], which give the positions and widths of fine-structure resonances, are determined by solving the secular equation for this matrix, with the result

$$E_l^{(H)}-\tfrac{1}{2}i\Gamma_l^{(H)}=E_{\lambda'}-\tfrac{1}{4}i(\Gamma_{\lambda_{II}(f)}+\Gamma_{\lambda_I(n)})+|\langle\lambda_I|H_c|\lambda_{II}\rangle| \mp[(\langle\lambda_I|H_c|\lambda_{II}\rangle^2-\tfrac{1}{16}(\Gamma_{\lambda_{II}(f)}-\Gamma_{\lambda_I(n)})^2)]^{1/2}. \tag{3.203}$$

If $(\Gamma_{\lambda_{II}(f)}-\Gamma_{\lambda_I(n)})^2\gg 16\langle\lambda_I|H_c|\lambda_{II}\rangle^2$ then the approximate positions and widths of the fine-structure resonances are

$$E_1^{(H)}=E_2^{(H)}=E_{\lambda'}+|\langle\lambda_I|H_c|\lambda_{II}\rangle|, \tag{3.204a}$$

$$\Gamma_1^{(H)}\approx\Gamma_{\lambda_{II}(f)}-\frac{4\langle\lambda_I|H_c|\lambda_{II}\rangle^2}{\Gamma_{\lambda_{II}(f)}-\Gamma_{\lambda_I(n)}}, \tag{3.204b}$$

$$\Gamma_2^{(H)}\approx\Gamma_{\lambda_I(n)}+\frac{4\langle\lambda_I|H_c|\lambda_{II}\rangle^2}{\Gamma_{\lambda_{II}(f)}-\Gamma_{\lambda_I(n)}}. \tag{3.204c}$$

The residues of the poles may be factorized into the partial width quantities:

$$G_{1(f)}^2\exp(2i\xi_{1(f)})\approx\Gamma_{\lambda_{II}(f)}\left(1+\frac{4\langle\lambda_I|H_c|\lambda_{II}\rangle^2}{(\Gamma_{\lambda_{II}(f)}-\Gamma_{\lambda_I(n)})^2}\right), \tag{3.205a}$$

$$G_{1(n)}^2\exp(2i\xi_{1(n)})\approx\Gamma_{\lambda_I(n)}\frac{4\langle\lambda_I|H_c|\lambda_{II}\rangle^2}{(\Gamma_{\lambda_{II}(f)}-\Gamma_{\lambda_I(n)})^2}, \tag{3.205b}$$

$$G_{2(f)}^2\exp(2i\xi_{2(f)})\approx(i)^2\Gamma_{\lambda_{II}(f)}\frac{4\langle\lambda_I|H_c|\lambda_{II}\rangle^2}{(\Gamma_{\lambda_{II}(f)}-\Gamma_{\lambda_I(n)})^2}, \tag{3.205c}$$

$$G_{2(n)}^2\exp(2i\xi_{2(n)})\approx\Gamma_{\lambda_I(n)}\left\{1+\frac{4\langle\lambda_I|H_c|\lambda_{II}\rangle^2}{(\Gamma_{\lambda_{II}(f)}-\Gamma_{\lambda_I(n)})^2}\right\}. \tag{3.205d}$$

These results may be applied to the interesting physical situation that may occur when the excitation energy of the compound nucleus is of the order of or greater than the saddle-point energy but much lower than the intermediate potential energy maximum. In this case $\Gamma_{\lambda_{II}(f)}$ may be very large, perhaps as great as or greater than the spacing of the class-I states. With very weak coupling and accidental degeneracy between a class-I and a class-II state, the two R-matrix internal states have nearly equal fission and neutron widths, and the resonant structure due to these has the form of a narrow resonance with strong neutron width and small fission width superposed on and interfering with a very low, broad background resonance term with small neutron width and large fission width. If the spacing between the class-II state and the next neighbor class-I states is greater than $\Gamma_{\lambda_{II}(f)}$, we note [from Eq. (3.175c)] that the fission widths of the next-neighbor resonances are approximately

$$\langle\lambda_I|H_c|\lambda_{II}\rangle^2\Gamma^{II}_{\lambda''(f)}/(E^I_{\lambda'}-E^{II}_{\lambda''})^2.$$

If the fission width of the class-II state is only slightly less than the class-I level spacing, we see that the next-neighbor resonance fission widths ($G^2_{\lambda''(f)}$) are nearly of the same order as that of the sharp component of the quasiresonance. We have here an example of the qualitative result [also discussed by Weigmann (1968)] that if we consider the class-II state as first coupled to the continuum, giving a broad resonance, then, even though the coupling of the class-II state to the class-I states may be very weak, this coupling is spread over the width of the class-II resonance. This is quite distinct from the case of coupling of discrete states in which the spreading of the class-II state is governed by the coupling strength alone. The simple approximate expression for the fission widths of the fine-structure resonances is

$$\Gamma_{\lambda(f)}\approx\frac{\langle\lambda_I|H_c|\lambda_{II}\rangle^2\Gamma_{\lambda_{II}(f)}}{(E_\lambda-E_{\lambda_{II}})^2+\frac{1}{4}\Gamma^2_{\lambda_{II}(f)}}. \tag{3.206}$$

The deduction of Eq. (3.206) follows (Lynn, 1968b) from an elaboration of the level-matrix method of R-matrix theory [see Sec. III.C.3.*g*(*ii*)]. In this method [due to Lane and Thomas (1958)] the internal R-matrix states [the X_λ of Eq. (3.151)] are divided into two groups, and the R matrix is correspondingly split into two parts, R^0 and R', each consisting of a sum over one group of levels. It can be shown that the collision matrix now has the form

$$U_{ab}=e^{-i(\phi_a+\phi_b)}\left\{\delta_{ab}+2iP_a^{1/2}[(1-i\mathrm{R}^0\mathrm{P})^{-1}\mathrm{R}^0]_{ab} +2i\sum_{\lambda\mu}P_a^{1/2}\alpha_{\lambda(a)}P_b^{1/2}\alpha_{\mu(b)}A'_{\lambda\mu}\right\}, \tag{3.207}$$

where P_c denotes the penetration factor for channel c. The new inverse level matrix $\mathbf{A}'$ now refers only to the levels contained in the section $\mathbf{R}'$ of the R matrix, and the elements of its reciprocal $\mathbf{A}^{-1}$ are

$$(\mathbf{A}^{-1})_{\lambda\lambda'} = (E_\lambda - E)\delta_{\lambda\lambda'} - i\sum_{c,c'} P_c[(1-i\mathbf{R}^0\mathbf{P})^{-1}]_{cc'}\gamma_{\lambda(c')}\gamma_{\lambda'(c')}, \tag{3.208}$$

while the quantities α are modified reduced width amplitudes

$$\alpha_{\lambda(c)} = [(1-i\mathbf{R}^0\mathbf{P})^{-1}]_{cc'}\gamma_{\lambda(c')}. \tag{3.209}$$

If $\mathbf{R}^0$ consists of a single level the matrix $1-i\mathbf{R}^0\mathbf{P}$ is readily inverted giving

$$[(1-i\mathbf{R}^0\mathbf{P})^{-1}]_{cc'} = \delta_{cc'} + \frac{iR^0_{cc'}P_{c'}}{1-T}, \tag{3.210a}$$

where

$$T = i\sum_c \gamma^2_{0(c)}P_c/(E_0-E) = \tfrac{1}{2}i\Gamma_0/(E_0-E). \tag{3.201b}$$

Equation (3.210a) can be substituted in Eqs. (3.208) and (3.209) which in turn are substituted in Eq. (3.207). Rather than write out this general expression we consider only the case where R' consists only of narrow levels so that A'^{-1} and hence A' are approximately diagonal. The collision matrix for this case is

$$U_{ab} \approx e^{i(\phi_a+\phi_b)}\delta_{ab} + \frac{\frac{1}{2}i\Gamma^{1/2}_{0(a)}\Gamma^{1/2}_{0(b)}}{E_0-E-\frac{1}{2}i\Gamma_0} + \frac{1}{2}i\sum_\lambda \frac{1}{E_\lambda - E - \frac{1}{2}i\Gamma'_\lambda} \times \left(\Gamma^{1/2}_{\lambda(a)}\Gamma^{1/2}_{\lambda(b)} + \frac{\frac{1}{2}i(\Gamma^{1/2}_{\lambda(a)}\Gamma^{1/2}_{0(b)} + \Gamma^{1/2}_{0(a)})\Gamma^{1/2}_{\lambda(b)}\sum_c \Gamma^{1/2}_{0(c)}\Gamma^{1/2}_{\lambda(c)}}{E_0-E-\frac{1}{2}i\Gamma_0} - \frac{\frac{1}{4}\Gamma^{1/2}_{0(a)}\Gamma^{1/2}_{0(b)}(\sum_c \Gamma^{1/2}_{0(c)}\Gamma^{1/2}_{\lambda(c)})^2}{(E_0-E-\frac{1}{2}i\Gamma_0)^2}\right), \tag{3.211a}$$

where

$$\Gamma'_\lambda = \sum_c \Gamma_{\lambda(c)} + \frac{\frac{1}{2}i\sum_c(\Gamma^{1/2}_{0(c)}\Gamma^{1/2}_{\lambda(c)})^2}{E_0-E-\frac{1}{2}i\Gamma_0}. \tag{3.211b}$$

For the very weak coupling situation (ignoring now the possibility of accidental degeneracy between a class-I and class-II level) the level in $\mathbf{R}^0$ is taken to be the quasi-class-II level $E_0 \approx E_{\lambda II}$; its width is very nearly the class-II fission width in the circumstances in which we are interested—$\Gamma_{\lambda\,II(f)}$ comparable to or larger than $\bar{D}_I$. The poles corresponding to the other levels are now easily estimated from Eq. (3.211): they are at the complex energies $E_l^{(H)} - \frac{1}{2}i\Gamma_l^{(H)}$, where

$$E_l^{(H)} = E_\lambda + \frac{\frac{1}{4}(\sum_c \Gamma^{1/2}_{0(c)}\Gamma^{1/2}_{\lambda(c)})^2(E_0-E_l^{(H)})}{(E_0-E_l^{(H)})^2 + \frac{1}{4}(\Gamma_0-\Gamma_l^{(H)})^2}, \tag{3.212a}$$

$$\Gamma_l^{(H)} = \Gamma_\lambda - \frac{\frac{1}{4}(\sum_c \Gamma^{1/2}_{0(c)}\Gamma^{1/2}_{\lambda(c)})^2(\Gamma_0-\Gamma_l^{(H)})}{(E_0-E_l^{(H)})^2 + \frac{1}{4}(\Gamma_0-\Gamma_l^{(H)})^2}. \tag{3.212b}$$

The residues of these poles may be factorized into partial width and phase factors

$$G^2_{l(a)}e^{2i\xi_{l(a)}} = \Gamma_{\lambda(a)} - \frac{\frac{1}{2}(\Gamma_0-\Gamma_l^{(H)})\Gamma^{1/2}_{\lambda(a)}\Gamma^{1/2}_{0(a)}\sum_c\Gamma^{1/2}_{\lambda(c)}\Gamma^{1/2}_{0(c)}}{(E_0-E_l^{(H)})^2+\frac{1}{4}(\Gamma_0-\Gamma_l^{(H)})^2} - \frac{\frac{1}{4}\Gamma_{0(a)}(\sum_c\Gamma^{1/2}_{0(c)}\Gamma^{1/2}_{\lambda(c)})^2[(E_0-E_l^{(H)})^2-\frac{1}{2}(\Gamma_0-\Gamma_l^{(H)})^2]}{[(E_0-E_l^{(H)})^2+\frac{1}{4}(\Gamma_0-\Gamma_l^{(H)})^2]^2} + \frac{i\Gamma^{1/2}_{\lambda(a)}\Gamma^{1/2}_{0(a)}\sum_c\Gamma^{1/2}_{0(c)}\Gamma^{1/2}_{\lambda(c)}(E_0-E_l^{(H)})}{(E_0-E_l^{(H)})^2+\frac{1}{4}(\Gamma_0-\Gamma_l^{(H)})^2} - \frac{\frac{1}{4}i\Gamma_{0(a)}(\sum_c\Gamma^{1/2}_{0(c)}\Gamma^{1/2}_{\lambda(c)})^2(E_0-E_l^{(H)})(\Gamma_0-\Gamma_l^{(H)})}{[(E_0-E_l^{(H)})^2+\frac{1}{4}(\Gamma_0-\Gamma_l^{(H)})^2]^2}. \tag{3.213}$$

In the condition of very weak coupling we have, from Eqs. (3.162) and (3.163)

$$\Gamma^{1/2}_{\lambda(f)} \approx \frac{\langle\lambda_{II}|H_c|\lambda_I\rangle}{E_\lambda - E_{\lambda_{II}}}\Gamma^{1/2}_{\lambda_{II}(f)},\ \Gamma^{1/2}_{0(f)} \approx \Gamma^{1/2}_{\lambda_{II}(f)},\ \Gamma^{1/2}_{0(n)} \approx \sum_{\lambda'}\frac{\langle\lambda_{II}|H_c|\lambda_I\rangle}{E_0-E_{\lambda'}}\Gamma^{1/2}_{\lambda'(n)}, \tag{3.214}$$

and therefore (ignoring other possible open channels such as radiative capture)

$$\sum_c \Gamma^{1/2}_{\lambda(c)}\Gamma^{1/2}_{0(c)} \approx \frac{\langle\lambda_{II}|H_c|\lambda_I\rangle}{E_\lambda - E_0}\Gamma_{\lambda_{II}(f)} + \sum_{\lambda'}\frac{\langle\lambda_{II}|H_c|\lambda_I\rangle}{E_0-E_{\lambda'}}\Gamma^{1/2}_{\lambda'(n)}\Gamma^{1/2}_{\lambda(n)} \tag{3.215}$$

for fission summed over channels μ. With $\Gamma_{\lambda_{II}(f)} \gtrsim D_I$ it is clear that only the first term on the right-hand side is important. It is now apparent, from Eq. (3.212), that the magnitudes of $E_l^{(H)} - E_\lambda$ and $\Gamma_l^{(H)} - \Gamma_\lambda$ are small compared to $E_0 - E_l^{(H)}$ and $\Gamma_0 - \Gamma_l^{(H)}$, respectively, except in the case of accidental degeneracy. We can therefore approximate E_λ by $E_l^{(H)}$ and neglect $\Gamma_l^{(H)}$ in comparison with Γ_0 in finding an approximate expression for the partial width quantity $G^2_{l(f)}$ from Eq. (3.213). After some manipulation the result for $G^2_{l(f)}$ is found to be

$$G^2_{l(f)} = \frac{\langle\lambda_{II}|H_c|\lambda_I\rangle^2\Gamma_{\lambda II(f)}}{(E_0-E_l^{(H)})^2+(\frac{1}{2}\Gamma_{\lambda_{II}(f)})^2} \tag{3.216a}$$

[cf. Eq. (3.185)]. The phase factor is given by

$$\exp(2i\xi_{l(f)}) = \arctan\left[\frac{\Gamma_{\lambda_{II}(f)}(E_0-E_l^{(H)})}{(E_0-E_l^{(H)})^2-(\frac{1}{2}\Gamma_{\lambda_{II}(f)})^2}\right]. \tag{3.216b}$$

Equation (3.213) with the extra conditions (3.214) also allows us to see that the neutron partial width quantity $G^2_{l(n)}$ is very close to $\Gamma_{\lambda(n)}$.

To find the parameters of the broad resonance term, the roles of R^0 and R' can be reversed; the latter now includes only the level at E_0. In the same way as before we now find that the width of the pole associated with the broad resonance is, approximately,

$$\Gamma_0^{(H)} \approx \Gamma_{\lambda_{II}(f)}\left(1 - \frac{\overline{\pi\langle\lambda_{II}|H_c|\lambda_I\rangle^2}}{\bar{D}_I^2}\right), \tag{3.217}$$

while its neutron partial width and phase quantities have an *expectation value* of

$$G^2_{0(n)}\exp(2i\xi_{0(n)}) \approx -\pi\frac{\overline{\Gamma_{(n)}\langle\lambda_{II}|H_c|\lambda_I\rangle^2}}{\bar{D}_I\Gamma_{\lambda_{II}(f)}}. \tag{3.218}$$

A simpler treatment of the broad class-II level can be made by use of the extended penetration factor described in Sec. III.C.4.*d*. The deformation channel boundaries are set close to the intermediate maximum A. Because of the compound states associated with the secondary well the penetration and shift factors to these intermediate channel deformations have a dispersion form:

$$L_\mu \equiv S_\mu + iP_\mu = S_{b\mu} + \sum_l \frac{G_l}{\mathcal{F}_l - E - i\mathcal{W}_l}, \tag{3.219}$$

where $S_{b\mu}$ is a background term comparatively slowly varying with energy, and the residues G_l of the poles $\mathcal{F}_l - i\mathcal{W}_l$ vary similarly with energy (roughly speaking as the transmission coefficient T_A through the intermediate barrier). The half-widths $\mathcal{W}_l$ also vary with energy (as the transmission coefficient T_B). The R-matrix internal states are confined to the primary well region of deformation and are expected to have no features that relate to intermediate structure, i.e., their reduced widths and energy levels will vary over considerable energy regions only in a way characteristic of statistical scatter. The properties of the fine-structure resonances in the cross section are found by studying the S matrix. If it is assumed that particle channel widths are all small it is sufficient to do this for the one-channel (deformation) S matrix, which is just

$$1 - U_{\mu\mu} = \frac{-2iP_\mu R_{\mu\mu}}{1 - \hat{L}_\mu R}, \tag{3.220}$$

where $\hat{L}_\mu = L_\mu - \mathcal{B}_\mu$. With the dispersive form for $\hat{L}_\mu$ (limited to one pole) this becomes

$$1 - U_{\mu\mu} = \frac{-2iG_l\mathcal{W}_l R_{\mu\mu}}{(\mathcal{F}_l - E - i\mathcal{W}_l)[(1-\hat{S}_{b\mu})(\mathcal{F}_l - E - i\mathcal{W}_l) - G_l R_{\mu\mu}]}, \tag{3.221}$$

with poles $E_m^{(H)} - \frac{1}{2}i\Gamma_m^{(H)}$ given by

$$(\mathcal{F}_l - E_m^{(H)} + \tfrac{1}{2}i\Gamma_m^{(H)} - i\mathcal{W}_l)(1-\hat{S}_{b\mu}) - G_l R_{\mu\mu} = 0, \tag{3.222}$$

which can be further simplified by putting $\hat{S}_{b\mu} = 0$ through arranging the boundary condition $\mathcal{B}_\mu$ at the channel entrance to be equal to $S_{b\mu}$. If the compound state associated with the secondary well that is responsible for the dispersion form of the logarithmic derivative L_μ is broad [this is defined by the conditions

$$2G\overline{\gamma_{\lambda(\mu)}^2}\mathcal{W}_l D_\lambda \ll 1$$

and $\mathcal{W}_l \gg D_\lambda$, where $\gamma_{\lambda(\mu)}^2$ are the reduced widths of the internal levels and D_λ their spacing], the fine-structure resonances appear at energies

$$E_m^{(H)} = E_\lambda + \Delta_\lambda, \tag{3.223a}$$

the level shifts Δ_λ being

$$\Delta_\lambda \approx \frac{G_l\gamma_{\lambda(\mu)}^2(\mathcal{F}_l - E_\lambda)}{(E_\lambda - \mathcal{F}_l)^2 + \mathcal{W}_l^2}, \tag{3.223b}$$

and have widths

$$\Gamma_m^{(H)} \approx \frac{2G_l\mathcal{W}_l\gamma_{\lambda(\mu)}^2}{(E_\lambda - \mathcal{F}_l)^2 + \mathcal{W}_l^2}. \tag{3.223c}$$

These equations are of the same basic form as Eq. (3.212). In addition to these poles an additional pole with $E_m^{(H)} \approx \mathcal{F}_l$ and $\Gamma_m^{(H)} \approx 2\mathcal{W}_l$ can be found, corresponding to the class-II state.

It is also to be noted that this treatment reproduces the results for a narrow class-II state. If $\mathcal{W}_l$ is vanishingly small the approximate solution of the pole equation is

$$\mathcal{F}_l - E_m^{(H)} \approx G_l \sum_\lambda \frac{\gamma_{\lambda(\mu)}^2}{E_\lambda - E_m^{(H)}}, \tag{3.225a}$$

$$\Gamma_m^{(H)} \approx \frac{2\mathcal{W}_l}{G_l\sum_\lambda[\gamma_\lambda(\mu)^2/(E_\lambda - E_m^{(H)})^2] + 1}. \tag{3.225b}$$

The disadvantage of these results compared with those previously derived is that numerical estimates of the important quantity G_l, which in conjunction with the reduced widths $\gamma_{\lambda(\mu)}^2$ plays the role of the squared coupling matrix elements, are not so straightforwardly obtained.

(vi) Stronger class-I–class-II coupling (with weak coupling to the continuum). Physical situations in which more than one class-II state must be simultaneously considered have received little study. When the spreading widths [as defined by Eq. (3.186)] are much smaller than the spacing of class-II states, perturbation treatments are valid [as exemplified in Sec. III.C.5.*c*(*i*)]. When the spreading widths are as large or larger than the class-II spacings (moderate to strong coupling) numerical methods must in general be employed in diagonalizing the matrix. Some special cases have been treated however. One is the case of a damped vibrational resonance (Back, 1974), which is discussed in Sec. V.C.2.*c*. Another case is that in which only two class-II states are overlapping (Lynn, 1974a).

When only two class-II states are involved the matrix (3.157) can be diagonalized in the following way. The eigenvalues and admixture coefficients resulting from the coupling of the class-I states to one of the class-II states (e.g., called N) are first found from Eq. (3.184); these coupled states are called λ'. The matrix elements coupling these new states to the second class-II state M are

$$\langle\lambda'|H_c|M\rangle = \sum_{\lambda_I} C_{\lambda_I}^{\lambda'}\langle\lambda_I|H_c|M\rangle = -\sum_{\lambda_I}\frac{C_N^{\lambda'}\langle\lambda_I|H_c|N\rangle\langle\lambda_I|H_c|M\rangle}{E_{\lambda_I} - E_{\lambda'}} \tag{3.226}$$

[substituting Eq. (3.184a)]. The product $\langle\lambda_I|H_c|N\rangle \times \langle\lambda_I|H_c|M\rangle$ can be expected to have uniform sign from one class-I level to another in the case of sub-barrier coupling; if the intrinsic states χ_μ are defined at the deformation of intermediate barrier A, then

$$\langle\lambda_I|H_c|N\rangle\langle\lambda_I|H_c|M\rangle = \sum_{\nu_I\mu}(C_{\nu_I\mu}^{\lambda_I})^2 \sum_{\nu'_{II}\mu',\nu''_{II}\mu''_{II}} C_{\nu'_{II}\mu'}^{N} C_{\nu''_{II}\mu''}^{M}\langle\nu_I\mu|H_c|\nu'_{II}\mu'\rangle\langle\nu_I\mu|H_c|\nu''_{II}\mu''\rangle$$
$$\approx (C_{\nu_I\mu}^{\lambda_I})^2 C_{\nu'_{II}\mu'}^{N} C_{\nu'_{II}\mu'}^{M}\langle\nu_I\mu|H_c|\nu'_{II}\mu'\rangle^2, \tag{3.227}$$

the modes $\nu_I\mu$ and $\nu'_{II}\mu'$ being taken to be the only ones contributing appreciably in magnitude to the coupling. Thus the matrix element $\langle\lambda'|H_c|M\rangle$ can be written approximately, in the general case of statistically scattered squared matrix elements $\langle\lambda_I|H_c|\lambda_{II}\rangle^2$, and exactly, in the uniform case of equal squared matrix elements, as

$$\langle\lambda'|H_c|M\rangle = \pm\frac{C_{\nu'_{II}\mu}^{M}}{C_{\nu'_{II}\mu}^{N}} C_N^{\lambda'}(E_N - E_{\lambda'}), \tag{3.228}$$

[from Eq. (3.184b)] with the sign being determined by the product

$$-C^N_{\nu^f_{II}\mu'} C^M_{\nu^f_{II}\mu'}.$$

The expectation value of squared matrix element therefore has, instead of the essential independence of energy of the $\langle\lambda_I|H_c|M\rangle^2$, a strong energy dependence of the form

$$\mathrm{Ex}(\langle\lambda'|H_c|M\rangle^2) = (C^M_{\nu^f_{II}\mu}/C^N_{\mu'_{II}\mu})^2 \frac{\overline{\langle\lambda_I|H_c|N\rangle^2}(E_N - E_{\lambda'})^2}{(E_N - E_{\lambda'})^2 + W_N^2}, \tag{3.229}$$

where $W_N = \pi\langle\lambda_I|H_c|N\rangle^2/D_I$.

The result of coupling the states λ' to the class-II state M with the matrix elements of Eq. (3.228) can be written in the generalized Lorentzian form described in Sec. III.C.5.*c.(iii)*, giving the admixture coefficients $(C^\lambda_M)^2$ of M into the final eigenstate λ, averaged over a Cauchy weighting function. With the matrix element substituted into the width expression it appears that if the class-II state M lies much closer to N than the half-width W_N, the effective width of the central states λ close to N is much smaller than the value deduced from the matrix element $\langle\lambda_I|H_c|M\rangle$. Well away from the center, however, the wings will be more nearly the value expected for a simple Lorentzian. Thus the appearance of a narrow peak superimposed on a broader base begins to appear.

In studying the behavior of the fission widths of the final states, the contribution of the state N must also be included. Expressions for the coefficients of admixture N can be derived just as for M, but now the states λ' are obtained by coupling M to the λ_I. It now has to be decided whether the contributions $C_{\lambda(M)}\gamma_{M(f)}$ and $C_{\lambda(N)}\gamma_{N(f)}$ to the fission width amplitudes of the final states are to be added in a coherent or incoherent manner (on the average). This can be answered by deducing the coefficients $C_{\lambda(N)}$ in the following manner:

$$C_{\lambda(\lambda')} = -\frac{C_{\lambda(M)}\langle\lambda'|H_c|M\rangle}{E_{\lambda'} - E_\lambda},$$

[see Eq. (3.184a)]

$$\therefore C_{\lambda(N)} = -C_{\lambda(M)} \sum_{\lambda'} \frac{\langle\lambda'|H_c|M\rangle C_{\lambda'(N)}}{E_{\lambda'} - E_\lambda}. \tag{3.230}$$

The sum of $C_{\lambda(M)}$ and $C_{\lambda(N)}$ is, therefore,

$$C_{\lambda(M)} + C_{\lambda(N)} = C_{\lambda(M)}\left[1 - \sum_{\lambda'} \frac{\langle\lambda'|H_c|M\rangle C_{\lambda'(N)}}{E_{\lambda'} - E_\lambda}\right]$$

$$= C_{\lambda(M)}\left[1 \pm \sum_{\lambda'} \frac{C^2_{\lambda'(N)}(E_N - E_{\lambda'})}{E_{\lambda'} - E_\lambda}\right], \tag{3.231}$$

by Eq. (3.228), showing the existence of either complete coherence or anticoherence.

In Fig. 41 the locally averaged admixture coefficient $\langle C^2_{\lambda(M)}\rangle_{\mathrm{av}}$ is shown for the case

$$E_M - E_N = 0.5D_I, \langle\lambda_I|H_c|M\rangle^2 = \langle\lambda_I|H_c|M\rangle^2 = D_I,$$

the nearest class-I level to E_N is $0.25D_I$ above E_N (i.e., midway between E_N and E_M), and the width of the averaging function Δ is just D_I. At the peak energy the width is $0.458D_I$, and the level shift ΔE_M is $0.246D_I$. These properties are reflected approximately in the peak of Fig. 41, which has a measured half-width of $\approx 1.3D_I$, corresponding to $\Gamma + \Delta$, and is centered about $E_M + 0.22D_I$ (the fact that the peak of Fig. 41 is narrower than expected from the calculated Γ is due to the rapid energy variation of the level shift). If the fission width associated with the level E_N is negligible compared with that of E_M, the curve of Fig. 41 is proportional simply to the locally averaged fission widths of the final eigenstates of the system.

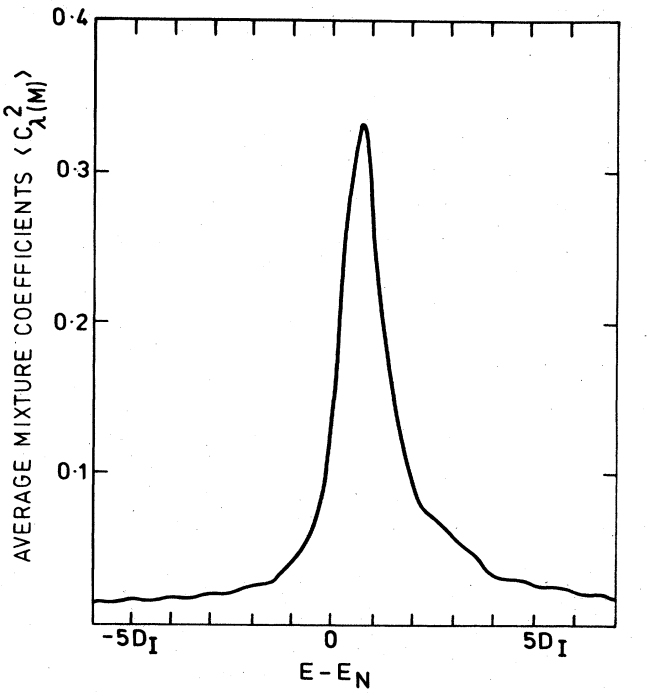

FIG. 41. The locally averaged admixture coefficient $\langle C^2_{\lambda(M)}\rangle_{\mathrm{av}}$ for the coupling of a class-II state M into the final eigenstates λ of a picket-fence system of class-I levels coupled to two very close class-II levels of which M is one.

(vii) Overlap of class-II levels with broad resonance. The appearance of a narrow peak in the profile of admixture coefficients resulting from "overlap" of two class-II states is analogous to the formation of quasi-resonances in interference of fine-structure resonances (Lynn, 1964, 1966b).

In the last section this effect was seen for the case in which the class-II states lie within their coupling half-widths. The effect can also be demonstrated for overlap within the decay widths of the class-II states over the outer barrier B. A simulated numerical example (Lynn, 1974a) is shown in Fig. 42. In this example the class-II R-matrix state parameters (relative to the class-I state spacings D_I) are

$$E^{II}_2 - E^{II}_1 = 12D_I, \quad \Gamma^{II}_{1(f)} = 20D_I, \quad \Gamma^{II}_{2(f)} = 28D_I,$$

and the mean squared coupling matrix element

$$\langle\lambda_I|H_c|\lambda_{II}\rangle^2 = 1.4D_I^2/2\pi.$$

With these parameters the matrix (3.157) has been diagonalized and the resulting eigenstates substituted into the collision matrix (3.117). The poles of the collision matrix are determined by numerical methods [see Sec. III.C.3.*g.(iv)*]. From the residues of the poles [see Eq. (3.134)] the fission strength $G^2_{m(f)}$ is determined and the plot of these quantities is shown in Fig. 42. The broad and narrow intermediate resonances in the pattern of fine-structure resonances is easily apparent, while the background class-II resonances are also indicated.

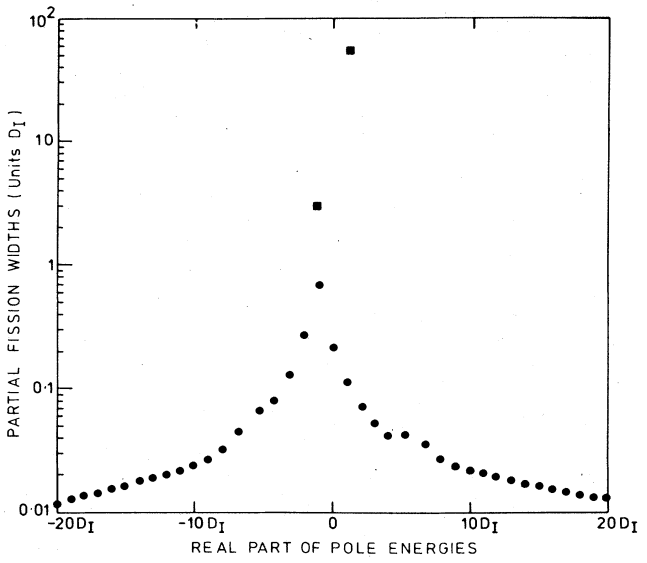

FIG. 42. The partial fission width quantities $G^2_{m(f)}$ of the S-matrix poles resulting from the coupling of a picket-fence set of class-I R-matrix levels to two overlapping class-II levels. The envelope of these pole strengths is analogous to quasiresonance profiles that can occur in fine-structure cross-section curves. Circles correspond to poles that will appear as comparatively narrow resonance peaks in the cross section, while the squares correspond to the poles of the underlying class-II quasiresonances.

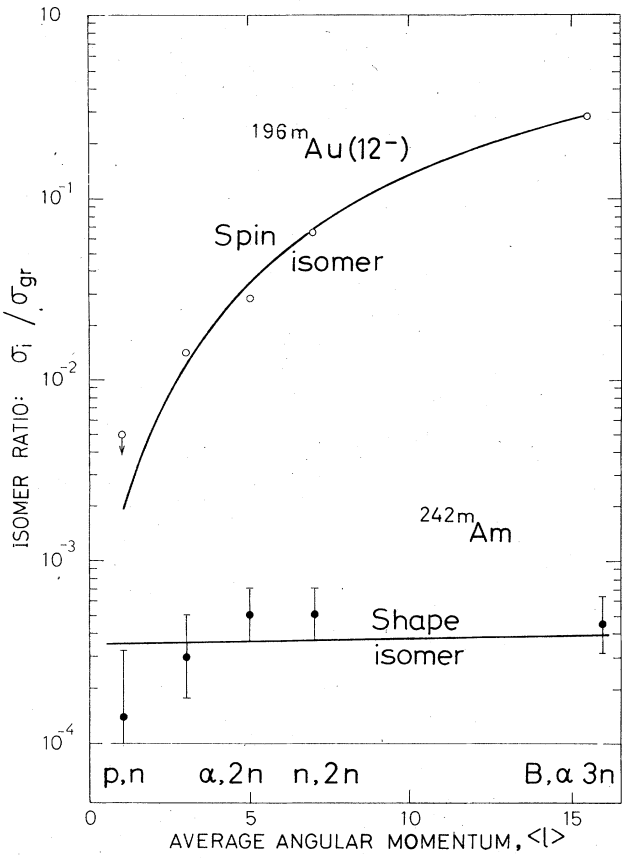

FIG. 43. The isomeric yield ratio for a typical spin isomer ^{196}Au with $I = 12^-$, as compared to the isomer yield ratio for ^{242m}Am. Flerov *et al.* (1968).

IV. SHAPE ISOMERS

A. Early developments

1. Discovery

The discovery of the shape isomers, or spontaneously fissioning isomers, is now history. As such it is a classic example of how an unexpected side effect turned out to be more interesting than the primary effect for which the initial experiment was designed.

In 1961 the search for new elements had been pushed to $Z = 101$, mendelevium, and beyond. There was controversy about the properties of element 102 (nobelium) but enough was known to realize that spontaneous fission was likely to be the dominating decay mode for heavier elements such as element 104. Liquid drop theory, together with half-life systematics, suggested spontaneous fission lifetimes in the millisecond range. In an effort to synthesize and identify the new element 104, Flerov and his co-workers in Dubna bombarded a plutonium target ($Z = 94$) with neon ions ($Z = 10$) to make element 104.

$$^{242}_{94}\mathrm{Pu} + ^{22}_{10}\mathrm{Ne} = ^{260}104 + 4n\,.$$

The detectors indeed registered a radioactive substance decaying by spontaneous fission with a half-life of 14 milliseconds. As a test, designed to rule out lighter elements as the source of the spontaneously fissioning activity, a control experiment was performed

$$^{238}_{92}\mathrm{U} + ^{22}_{10}\mathrm{No} \neq ^{260}104 + 4n\,.$$

Unexpectedly, the 14 msec activity reappeared! (Polikanov *et al.*, 1962). In subsequent experiments, including fast neutron activation of ^{243}Am, the activity was soon tracked down to ^{242m}Am (Flerov and Polikanov, 1964). Thereby a range of completely new questions arose.

2. Approaching an explanation

How was it possible for an excited state in a nucleus to resist gamma decay for more than 14 msec and at the same time undergo spontaneous fission at a rate which meant a dramatic reduction of the fission barrier by comparison to ^{242}Am in its ground state? The possibility of explaining the stability towards gamma decay by ascribing a very high spin value to the isomeric level was soon ruled out by the observation that the yield of the isomer, compared to the ground state yield, was virtually the same whether it had been produced in a heavy ion reaction, bringing 20–25 units of angular momentum into the system, or by a (p,n) reaction at the Coulomb barrier where there is barely any angular momentum brought in (Fig. 43). If high spin cannot explain the stability towards gamma decay, would it be possible that the isomer was lying quite close to the ground state? It would then be necessary to explain how the fission barrier could be penetrated so exceptionally fast.

This interesting possibility was explored by Urin and Zaretsky (1966). It is a fact that the inertial parameters B_q required, according to Eq. (2.16), to explain the

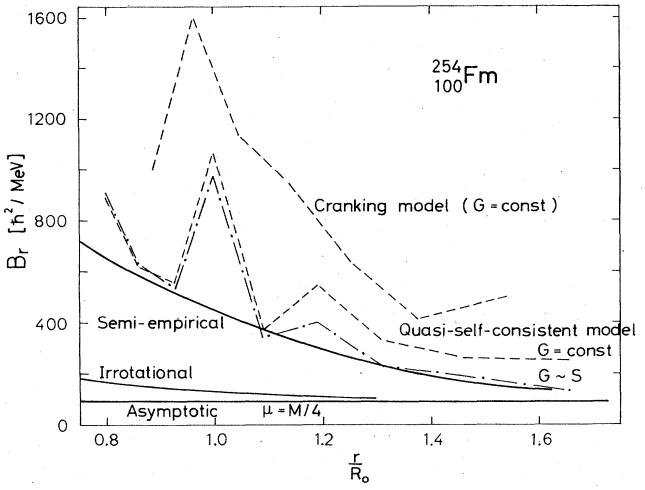

FIG. 44. Comparison of various inertial-mass functions B_r (here shown for ^{254}Fm). The lower curve represents the irrotational-flow calculation, while the kinked upper curves correspond to various microscopic models. The smooth curve in between is the determined best one-parameter semiempirical inertial-mass function. From Randrup *et al.* (1973).

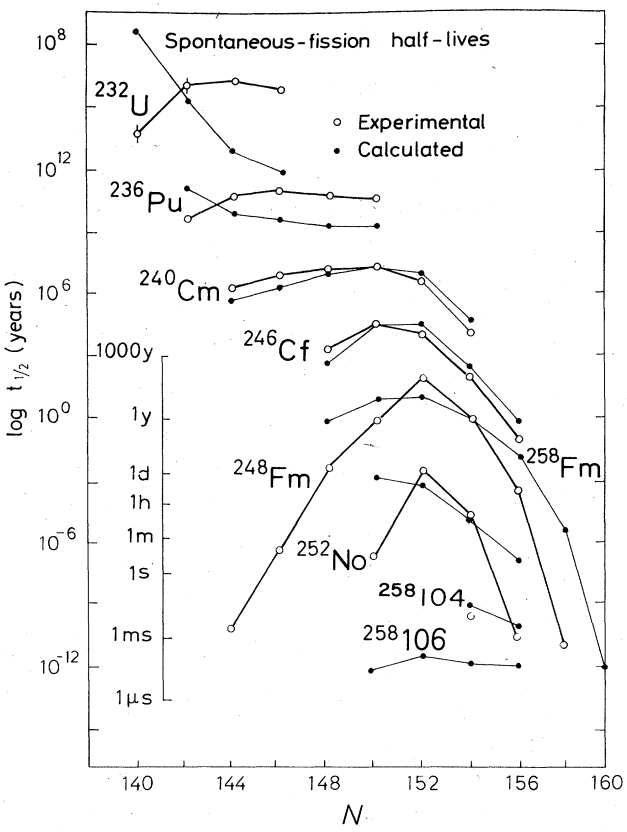

FIG. 45. Ground-state spontaneous-fission half-lives. Open circles: experimental values. Full circles: calculated values with the determined semiempirical inertial-mass function shown in Fig. 44. From Randrup *et al.* (1973).

ordinary spontaneous fission half-lives, are quite large compared to the minimum inertia one could envisage in the case of nuclear matter behaving as an irrotational, nonviscous fluid during the shape changes which lead to fission. For a sphere this minimum inertia is 32/15 = 2.13 times greater than the reduced mass of the nucleus, considered as two solid half-spheres. (For larger distortions the irrotational mass approaches the reduced mass value.) In ordinary spontaneous fission the inertial parameters required to explain the observed half-lives are five to ten times larger than the reduced mass values; see Figs. 44 and 45. If the new isomer were a piece of nuclear matter in a special hyperfluid state with an inertial parameter some four times smaller than that of ordinary nuclear matter, tunneling through the same energy barrier would take place at a rate characterized by a penetration factor of 10^{-18}, as observed for the 14 msec isomer, rather than by a factor 10^{-30}–10^{-40}, which is typical of ordinary spontaneous fission in this region of A. In such a case the isomer could be very close to the ground state in energy, whereby the problem of understanding the stability towards gamma decay would be eliminated.

This hypothesis failed to find support from subsequent reaction threhsold measurements (Bjørnholm *et al.*, 1967), which showed that the isomer excitation energy was of the order of 3 MeV. Now speculations about special hyperfluid nuclear matter had again to yield to ways of explaining the striking stability towards gamma decay of a 3 MeV excited state in a doubly odd heavy nucleus and with low spin. Clearly, a new selection rule was operating here.

3. Shape isomerism

The idea of nuclear shape isomerism, which implied that the isomer was lodged in an intermediate energy minimum, was advanced as one of several possible explanations by Polikanov *et al.* (1962) and by Flerov and Druin (1966). A breakthrough occurred in 1966 when the idea received independent support from the theoretical side. Myers and Swiatecki's work (1966) on the incorporation of shell effects into the liquid drop description of nuclear masses and fission barriers had focused attention on shell effects. This inspired several attempts to replace the first schematic description of these by one based on the actual shell model diagrams of the single-particle levels as a function of deformation (Nilsson diagrams). In this way one could hope to obtain better accuracy in the calculation of ground state masses and barriers. The general method along these lines that was developed by Strutinsky proved to be particularly fruitful (see Sec. II). In 1966 the first numerical results were obtained (Strutinsky, 1967a). They immediately showed (Fig. 46) that the liquid drop fission barrier for a certain region of nuclei among the actinides was split into two by a large negative shell correction; and ^{242}Am lay in that region. Similar results, based on a somewhat different theoretical approach were obtained at the same time by Gustafson *et al.* (1967).

Experiments with isomeric fission now became focused by these ideas. One obvious consequence, namely that all the nuclides in the region, rather than a few odd ones, ought to exhibit fission isomerism, was soon confirmed by Lark *et al.* (1969), as techniques for detecting isomers with half-lives shorter than milliseconds and microseconds were developed.

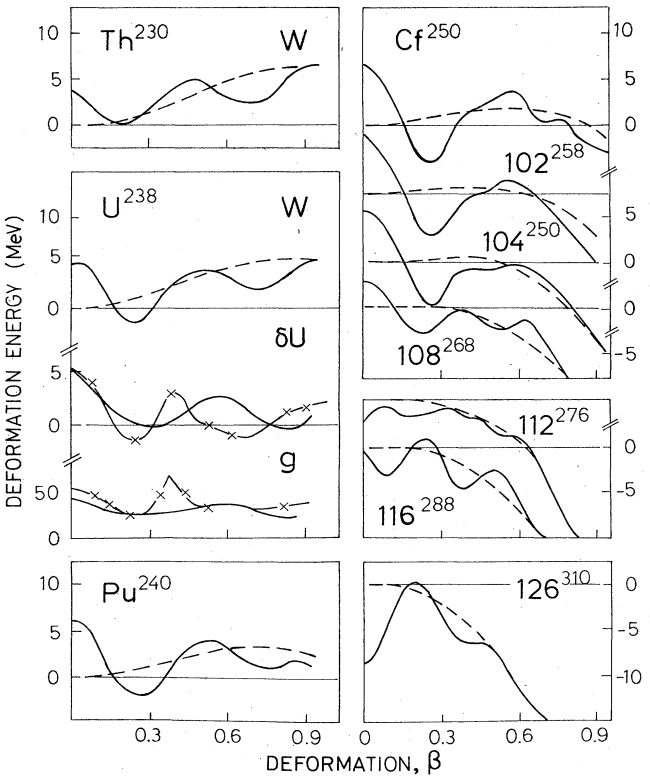

FIG. 46. The first calculations of fission barriers based on the liquid drop model (dashed lines) with inclusion of shell effects (full lines). Strutinsky (1967ab).

The interpretation of the isomers as the lowest state of the intermediate minimum between two barriers, which the theoretical calculations suggest, leads to a host of very specific predictions of the properties of the isomeric states and of the collective and individual particle excitations which can be built on these. In Sec. IX these particular aspects, including the appearance of two isomers in the same nucleus, are examined in greater detail.

B. Islands of shape isomers and decay modes

1. The uranium-berkelium island

The occurrence and half-lives of presently known isomers are illustrated in Fig. 47 and listed in Table II. They form an island around a midpoint of maximum stability. This is most readily seen when even, odd-A and doubly odd nuclides are examined separately. These are three groups with half-lives increasing stepwise as one goes from one to the next. Within each group the longest half-lives occur for isotopes with neutron number around 146–148. This special stability is evidence of a neutron shell with the magic number around 146–148. Strictly speaking it is evidence of a minimum in the transmission coefficient, Eq. (1.6), for spontaneous fission as a function of neutron number. It requires independent measurements of the isomer energy E_{II} and the height of the outer barrier E_B with high accuracy to establish at which shape the magic number applies. There must necessarily be a strong shell effect for those shapes which we identify with the isomers, in order to have shape isomerism at all. It is therefore generally assumed that the magic neutron numbers apply to this shape; but some influence from an antishell effect at the outer barrier may well play a role (see Sec. VIII.E).

The variation of half-lives with proton number is monotonic and seems to be dominated by the general decrease in stability towards spontaneous fission with increasing nuclear charge.

The extension of the island of shape isomers towards the "north" and the "east" (increasing Z and N, respectively), is thus readily understood. To the "south" and "west" the island appears to be limited, not by the filling of the shell minimum, but by a shift in the relative importance of the inner and outer barrier. Spontaneous fission gives way to gamma decay as the dominating decay mode. This is seen indirectly from an abnormal decrease in the partial cross section for observation of the spontaneous fission mode in ^{236}U and ^{238}U, as shown by Pedersen and Rasmussen (1972) and by Wolf and Unik (1973) in the case of ^{237}Np. This general trend is entirely in agreement with expectation, but it would be highly desirable to obtain more details. Here, one runs into the fundamental difficulty of devising methods with a sensitivity that is sufficient for the identification of weakly populated gamma decaying isomers. For the spontaneous fission mode the problem is much simpler. In no case has a shape isomer been identified through its delayed gamma rays, and only in one case, namely ^{238}U, has it been possible to measure delayed gamma transitions after the isomer was identified through its (weak) spontaneous fission decay branch (see Fig. 48).

It has been possible to discover the island of shape isomers in the actinide region thanks to the specificity of the spontaneous fission decay mode. On the other hand, cross sections are small in this region because of the competing prompt fission reaction. This also renders detection of delayed gamma rays particularly difficult.

It is unlikely, as demonstrated by the studies of Borggreen *et al.* (1973), that the "south western" coast line of the island of shape isomers around the magic neutron number 144–148 will readily be mapped. This is unfortunate, for it may help resolve the puzzle of the ^{231}Th resonance at 5.83 MeV excitation energy, which is a candidate for the lowest-lying state in the second minimum, or alternatively, as proposed by Möller and Nix (1974), of a third minimum present in these light nuclei at still larger elongation. A systematic mapping of the shape isomer family in the region between ^{238}U and ^{230}Th would definitely help to clarify the situation and test the prediction of a rapidly decreasing inner barrier as ^{230}Th is approached.

2. Other islands?

In addition to the magic island of shape isomers with $N = 141$–151 there are other regions with a different set of magic numbers, where shell effects will stabilize a particular shape. Most prominent among these is the island of superheavy elements characterized by spherical shapes and magic numbers $(Z, N) = (114, 184)$, which

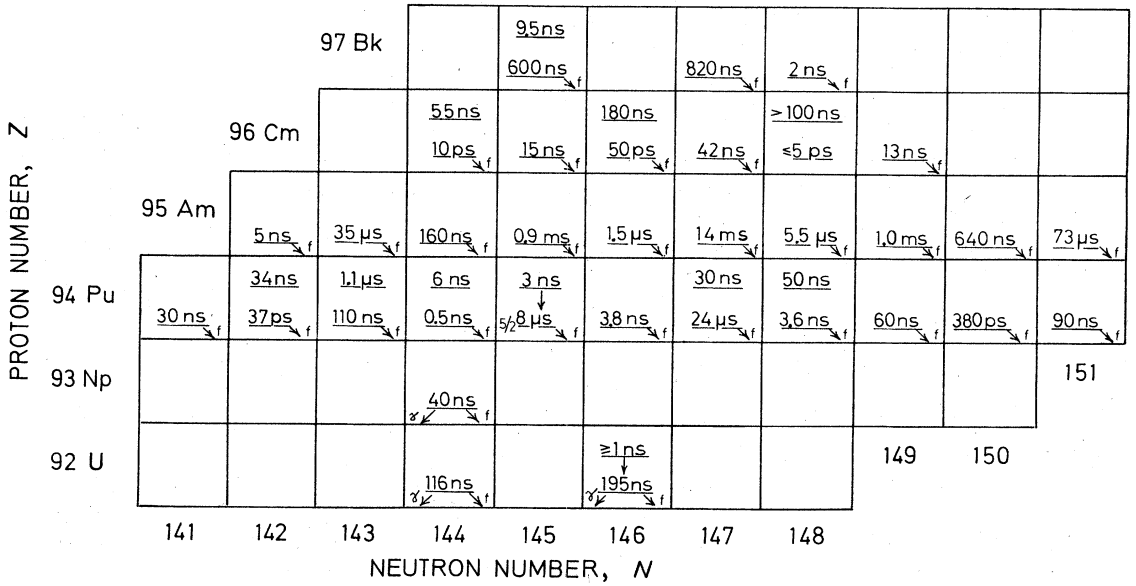

FIG. 47. The island of shape isomers in the actinide region of the isotope chart. From Metag (1980).

is of course the higher homolog of the well-known (spherical) shell model nuclei. Below the actinide region, nonspherical shapes are stabilized by shell effects for nuclei with (Z,N) close to (84, 118), i.e., ^{202}Po. Detailed calculation of deformation energy curves have been performed by Pashkevich (1969b) and Tsang and Nilsson (1970); see Fig. 49. It is apparent that the inner barrier is considerably smaller than the outer barrier and thus gamma-ray emission is the most likely decay mode according to the calculations. So far, it has not been possible to identify this additional island of shape isomers. Early experimental indications of delayed fission from reaction recoils with mass numbers near to ^{202}Po (Ruddy and Alexander, 1969) could not be confirmed (Bjørnholm *et al.*, 1970). The more recent interest focuses on the detection of gamma rays, but no definite indications have been obtained about the existence of this magic island.

TABLE II. Occurrence and half-life of fission isomers. In a number of nuclei there are two decay periods. The one that is listed as number two is presumably due to an excited state in the second minimum. For the even isotopes of plutonium (except ^{242}Pu) and curium, and for ^{237}Pu, this is substantiated by measurements of excitation functions near threshold. Reference 1 is Britt (1973); more recent results are taken from Ref. 2 (Metag, 1974) and Ref. 3 (Metag, 1980).

Nucleus	$t_{1/2}$	Ref.	Nucleus	$t_{1/2}$	Ref.
^{236}U	125 ± 15 nsec	1	^{237}Am	5 ± 2 nsec	1
^{238}U	195 ± 30 nsec	1	^{238}Am	35 ± 4 μsec	1
	>1 nsec	3	^{239}Am	163 ± 12 nsec	1
^{237}Np	40 ± 12 nsec	1	^{240}Am	0.91 ± 0.07 msec	1
^{235}Pu	30 ± 5 nsec	1	^{241}Am	1.5 ± 0.6 μsec	1
^{236}Pu	40 ± 15 psec	2	^{242}Am	14 ± 0.7 msec	1
	34 ± 8 nsec	1	^{243}Am	5.5 ± 0.5 μsec	1
^{237}Pu	110 ± 12 nsec	1	^{244}Am	1.0 ± 0.15 msec	1
	1.1 ± 0.08 μsec	1	^{245}Am	640 ± 60 nsec	1
^{238}Pu	0.5 ± 0.2 nsec	1	^{246}Am	73 ± 10 μsec	1
	6.0 ± 1.5 nsec	1	^{240}Cm	10 ± 2 psec	3
^{239}Pu	8.1 ± 0.8 μsec	1		55 ± 5 nsec	3
	3.0 ± 2 nsec	3	^{241}Cm	15 ± 1 nsec	1
^{240}Pu	3.8 ± 0.3 nsec	1	^{242}Cm	40 ± 15 psec	2
^{241}Pu	24 ± 1 μsec	1		180 ± 70 nsec	1
	30 ± 5 nsec	1	^{243}Cm	42 ± 6 nsec	1
^{242}Pu	3.6 ± 0.6 nsec	2	^{244}Cm	<5 psec	2
	50 ± 30 nsec	1		>100 nsec	1
^{243}Pu	60 ± 15 nsec	2	^{245}Cm	13 ± 2 nsec	1
^{244}Pu	0.4 ± 0.1 nsec	2	^{242}Bk	600 ± 100 nsec	1
^{245}Pu	90 ± 30 nsec			9.5 ± 2 nsec	1
			^{243}Bk	5 ± 2 nsec	2
			^{244}Bk	820 ± 60 nsec	1
			^{245}Bk	2 ± 1 nsec	1

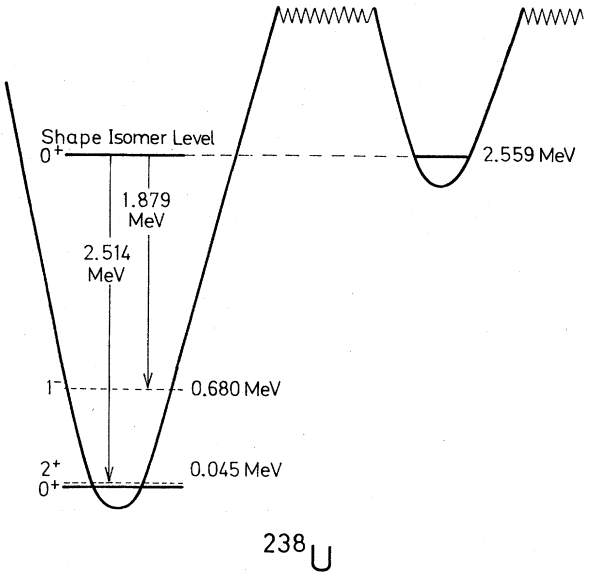

FIG. 48. The gamma decay of the ^{238}U shape isomer. Russo, Petersen, and Vandenbosch (1974, 1975).

3. Unobserved decay modes

So far we have discussed the decay of a shape isomer by barrier penetration only, i.e., by spontaneous fission or by gamma decay. In addition to this, the isomers may, in principle, decay in the same way as the ground state undergoes radioactive alpha or beta decay to a daughter nucleus. If the radioactive decay proceeds in complete analogy, that is, without shape change, then the Q values and hence half-lives will be comparable to those of the ground-state decay, and this means lifetimes of the order of minutes to thousands of years. In this case, since the longest observed total lifetime is 14 msec, it is not surprising that attempts to observe alpha or beta branches from the shape isomers have failed. It is true that alpha emission from the tips of an elongated shape is enhanced because the interplay of the nuclear and Coulomb potentials that determine the heights of the barrier against alpha decay diminishes the barrier at the tips, but this effect is not strong enough to offset the influence of the initially very long alpha half-lives. The effect is likely to be less than a factor of 100 in decay probability, as can be seen from the fact that in the general alpha decay systematics there are no signs of an enhancement of the alpha transitions between (normally) deformed nuclei as compared to spherical alpha emitters (Lederer *et al.*, 1967).

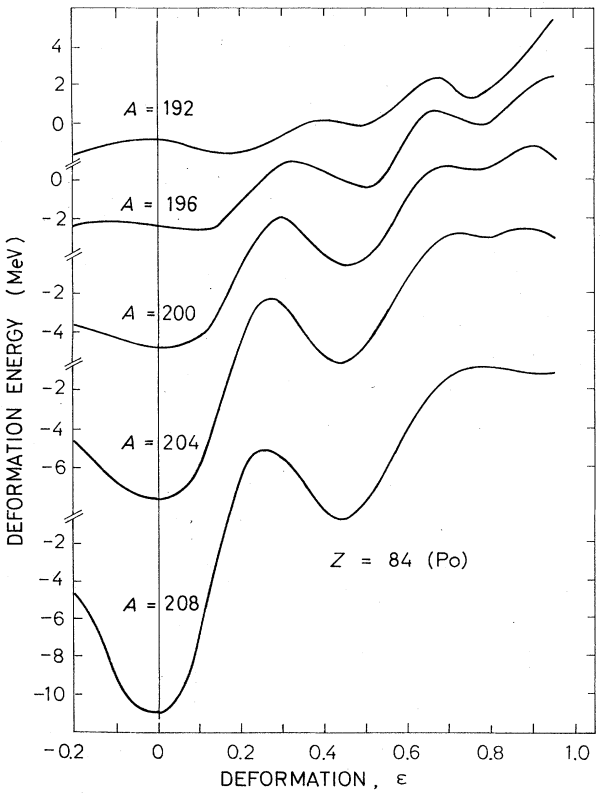

FIG. 49. Shape isomers with a deformation parameter $\epsilon = 0.4$ are predicted in the region of Z near 84, and N near 118. From Tsang and Nilsson (1970).

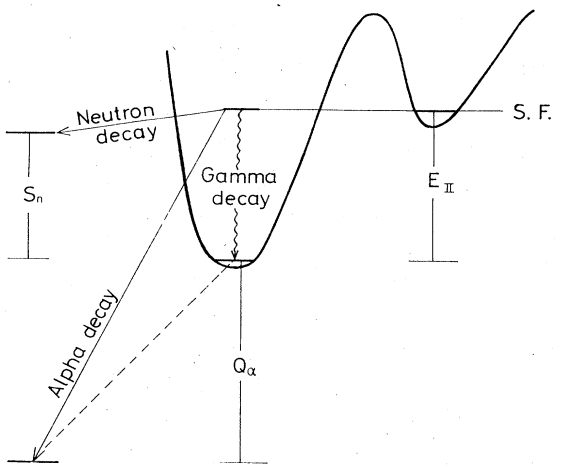

FIG. 50. Several decay channels are open to a shape isomer when its energy E_{II} is sufficiently high compared to the neutron separation energy S_n, or when the alpha decay Q value, $(Q_{\alpha_0} + E_{II})$, is large, e.g., greater than 12 MeV.

In the case of an alpha (or beta) transition from a shape isomeric state directly to the normally deformed daughter ground state the Q value is increased by the isomer excitation energy E_{II}. A 2-MeV increase in Q value will speed up the alpha decay by a very large factor of the order of 10^{10} [see Lederer *et al.* (1967)]. This is the maximum to expect, since the poor spatial overlap between initial and final states will lead to a reduction of the order of the transmission coefficient of the inner barrier. For ^{238}U an isomer with 2.5 MeV excitation energy will have a partial alpha half-life longer than 10^2 sec, to be compared to the actual isomer lifetime of 2×10^{-7} sec. Similarly an isomer in ^{242}Cm with 2.0 MeV excitation energy will have a partial alpha half-life exceeding 10^{-2} sec, to be compared to an actual decay period of 4×10^{-11} sec. Clearly, possible long-range alpha groups from shape isomers in the actinide region will be extremely weak. Beta decay branches are even more unlikely.

Long-range alpha groups could be found, however, among lighter nuclides. For example, long-range alpha particles are emitted from the excited states of ^{212}Po, which has an exceptionally high ground-state Q value

($Q_\alpha = 8.95$ MeV) and a ground-state half-life of 3×10^{-7} sec. Therefore, alpha emission from excited states competes successfully with gamma-ray emission. If shape isomers in the region of highly unstable alpha emitters exist, which means the region above ^{208}Pb with $Z > 84$ and $N > 128$, the shape isomeric state would contain, by barrier penetration, some elements of these excited, alpha emitting states and would correspondingly have a significant chance of itself decaying by long-range alpha emission. This possibility remains to be explored. According to Tsang and Nilsson (1970) one should expect shape isomers in this region, which is part of the $Z \approx 84$, $N \approx 118$ magic island (Fig. 49).

An interesting decay mode that is related to gamma decay appears possible if the isomer excitation energy exceeds the neutron separation energy from the first well. In this case penetration of the inner barrier leads to an unbound state and delayed neutron emission can occur. This may be a sensitive way of detecting shape isomers in the Po region. The isomers must, however, lie at such high energies in this case that the formation cross section is likely to be quite low.

The decay modes discussed in this section are illustrated in Fig. 50.

C. Half-life systematics and odd-even effects

1. Spontaneous fission half-lives

The majority of known shape isomers decay predominantly by spontaneous fission; the measured half-lives thus relate directly to the penetration of the outer barrier. In a few cases, namely, ^{236}U, ^{238}U, and ^{237}Np, the decay probability has to be corrected for the gamma decay mode, which dominates in these cases, as revealed by abnormally low partial reaction cross sections for observation of the delayed fission mode. In all other cases the cross sections follow a regular and reasonably well-understood pattern, which is compatible with a negligible gamma branch and hence a total lifetime equal to the partial spontaneous fission lifetime. The observed regularity in the formation cross sections makes it very unlikely that gamma decay could play a role; this decay mode would invariably change from case to case because of the discrete nature of states in the first well influencing the decay probability in an erratic way.

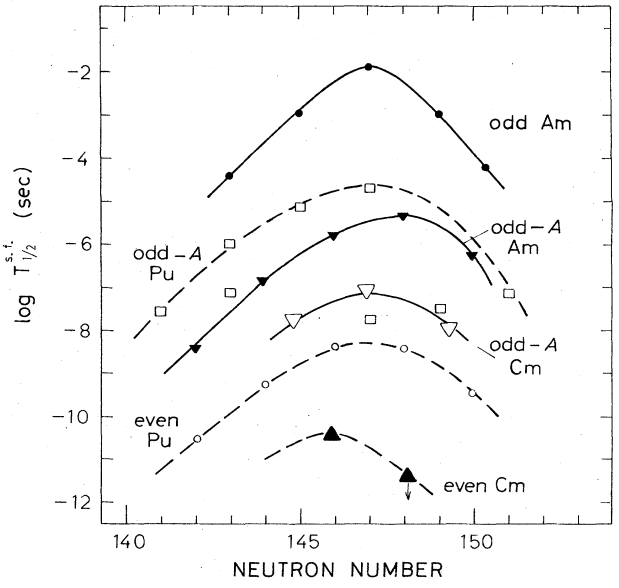

FIG. 51. Isomeric half-lives show a strong neutron dependence and a strong odd-even effect. Based on Metag (1974).

The spontaneous fission half-lives are plotted in Fig. 51 as function of neutron number and in Fig. 52 as function of proton number. The difference is striking; a strong shell effect in the neutron dependence is contrasted to a monotonic, liquid-drop-type dependence on proton number. A pure liquid drop dependence would give nearly horizontal lines for the neutron dependence and strongly sloping lines in the Z diagram. It is the changing slopes for neutrons and the constancy of the slopes for protons that constitute the real difference between the two cases, representing the most direct evidence for a neutron shell effect centered around $N = 144-148$.

In addition to this, the half-lives fall into groups according to the odd-even character of the decaying nucleus. On the average, the lifetime increases by some 3–5000 times as one goes from an even nucleus to an odd-A nucleus and by a similar factor during the next step to doubly odd species. This is equivalent to a nearly 25% increase, for each step, in the magnitude of the penetration integral [Eq. (2.16)].

It should be noted that the odd-even effect is erratic to some degree. The numbers given above apply to the most extreme cases, which form the largest group including all even nuclides, but there are a few excep-

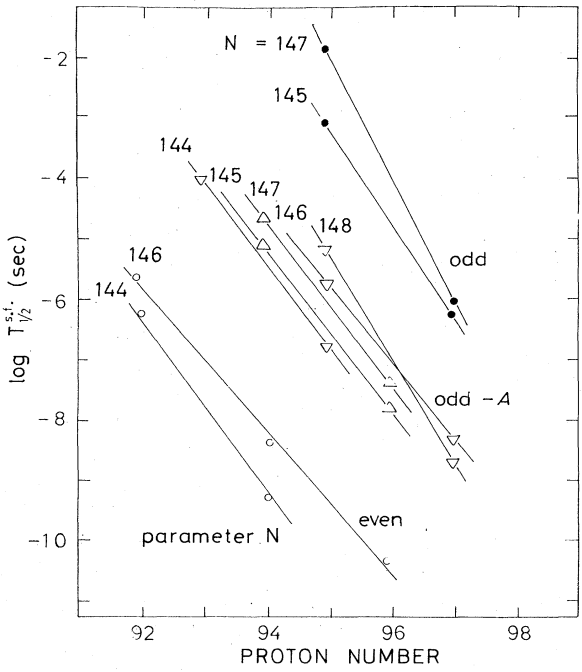

FIG. 52. Half-life for spontaneous fission as a function of proton number. For the two isomers of uranium ($Z = 92$) and for ^{237}Np ($Z = 93$) the spontaneous fission lifetime is much longer than the directly observed half-life, because gamma decay dominates, as evidenced by "missing cross section." From Metag (1974).

tions with short half-lives, for example, the 9.5 nsec isomer ^{242m}Bk, the 110 nsec isomer ^{237m}Pu and the more or less well established isomers, ^{241m}Pu (35 nsec) and ^{243m}Pu (60 nsec). It could be argued that these isomers represent excited states in the second well which consequently have to penetrate a lower barrier. In the case of ^{237m}Pu this is definitely not so (Vandenbosch *et al.*, 1973) and in the other three cases the formation cross sections are quite normal in magnitude. If these isomers were excited states in the second well with excitation energies 0.3–0.7 MeV, as required to explain the reduction in half-life, then a considerable reduction in formation probability would be expected.

2. The odd-even effect

There are three separate effects contributing to the odd-even differences in the lifetimes

(i) An increase in *inertial parameter* and hence a decrease in $\hbar\omega_B$ value with the number of unpaired nucleons. As mentioned earlier, the effective inertia associated with the barrier penetration exceeds the minimum value consistent with the physical separation of the nucleus into two halves; see Fig. 44. Griffin (1971) has shown that the inertia associated with the separation of a system of virtually independent particles would be even larger by several orders of magnitude. The pair correlations facilitate the inertial response to shape changes, although they do not reduce the inertia to the minimum possible value. Accordingly, systems with unpaired nucleons will have increased inertia. Urin and Zaretsky (1966) and Sobiczewski *et al.* (1969a) have made theoretical estimates of the increase due to one unpaired particle and found it to be of the order of 25% in the inertia, and therefore of the order of 12% in the value of $\hbar\omega_B$. Other things being equal this will increase a spontaneous fission half-life typically by a factor of one hundred to one thousand. This is the general order of magnitude, but considerable variations are to be expected depending on which particular orbital the unpaired particle occupies.

(ii) An increase in the *pairing gap* at the barrier top compared to the gap at the shape isomeric "ground" state. Just as the magnitude of the pairing gap is measured by the odd-even differences of the ground state masses, a difference in pairing gap will be revealed by an odd-even staggering in the barrier heights. Here, the barrier and the ground state are defined as the lowest-lying state, whatever its spin and parity. Since the barrier height is a measure of the energy difference between a minimum and a maximum in the potential energy curve, one might expect shell effects of opposite sign at the two points and hence a systematic difference in the pairing gap also. This view is open to question, however, because the barrier can also be considered as a minimum in a many-dimensional energy landscape of all the variables except one. There is, in fact, a large negative shell effect at the asymmetric outer barrier. On the other hand, if the pairing energy is dependent upon surface area, even with a negative shell effect one may expect an increased pairing gap (Sec. VIII.D). As defined here the odd-even differences in the pairing gap can be small or large, but they are likely to be systematic in nature.

(iii) Specialization energy. This is the extra energy required to find a transition state at the barrier with quantum numbers matching those of the shape isomeric ground state. The minimum and absolute requirement is for the transition state to have spin and parity $I\pi$ equal to that of the initial state. If this is all, then the specialization energy is likely to be low because rotational levels with appropriate spin and parity are in general easy to find at the asymmetric outer barrier. Requiring also that the spin projection K be conserved narrows the choice. From what is known about Coriolis mixing of K quantum numbers, one should indeed expect spin projection to be conserved during the tunneling motion, provided the nuclear shape preserves axial symmetry. According to theory this is not the case for the inner barrier, but it seems to hold for the outer one (see Sec. II). Even so, the K quantum number is not an absolute constant. Admixtures are nevertheless likely to be small so that the fission probability, by virtue of such admixtures, is expected to be cut down by a factor of 100 or more. There can also be restrictions on the intrinsic radial and orbital angular momentum quantum numbers of the individual particle that will further increase the effective specialization energy. Finally, for doubly odd nuclei, preservation of the quantum numbers of each of the two unpaired nucleons individually will lead to a specialization energy that is the sum of the individual specialization energies. This is equivalent to the assumption of completely independent motion of the two particles. Spectroscopic evidence from normally deformed nuclei does not give much support to such a stringent assumption, since mixing of two-quasiparticle configurations with the same total K values appears to be very strong in many cases. It is characteristic of the specialization energy that it depends strongly on the properties of the initial single-particle state; it may be large but it can also be zero.

The three contributions to the odd-even effect are illustrated schematically in Fig. 53.

3. Shell effects

Metag (1974) has made a phenomenological analysis of the neutron shell effect and of the odd-even effects based on all the known spontaneous fission half-lives of shape isomers. The exponent in the penetration integral [Eq. (2.16)] is expressed in the following way:

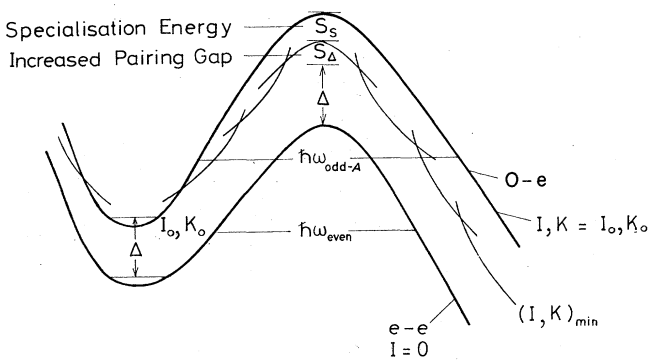

FIG. 53. Compared to the barrier of an even nucleus (with spin zero) an odd-A shape isomer sees an increased barrier: (i) the inertia may increase to decrease the $\hbar\omega$ value; (ii) the pairing gap Δ may be larger at the barrier by an amount S_Δ, compared to the minimum; (iii) the lowest-lying transition state with $(I, K)^\pi$ value equal to that of the isomeric state may lie on amount S_s above the lowest transition state.

$$\frac{2\pi}{\hbar\omega_B}(E_B - E_{II}) = \frac{2\pi}{\hbar\omega}\left[aX + b + c(N - N_0)^2 + S\right], \tag{4.1}$$

where

$$\hbar\omega = \hbar\omega_0 \begin{cases} 1/f \text{ for odd nuclei} \\ 1.0 \text{ for odd-}A\text{ nuclei} \\ f \text{ for even nuclei} \end{cases}$$

and

$$S = \begin{cases} 2S_0 & \text{for odd nuclei} \\ S_0 & \text{for odd-}A\text{ nuclei} \\ 0 & \text{for even nuclei.} \end{cases}$$

The quantity X is the fissility parameter [Eq. (1.5)] and the term $aX + b$ accounts for the smooth liquid drop dependency. The term $c(N - N_0)^2$ describes the neutron shell effect, whereas the odd-even variation of inertial coefficients is expressed through the parameter f which multiplies $\hbar\omega_B$, and the odd-even effect on the barrier height is reflected through the energy S, which is then the sum of a possible systematic difference in energy gap S_Δ and specialization energy S_s.

Equation (4.1) expresses the main systematic effects. Provided these effects are strong compared to the scatter caused by individual particle effects, a fit to the known half-lives serves to determine the parameters N_0, c, S_0, f, and $\hbar\omega_0$ in a meaningful way.

Figure 54 shows a least-square fit to the parameter N_0, the magic neutron number. The value $N_0 = 146$ is clearly preferred. This reflects the weighted shell effects for all shapes across the outer barrier. It is not certain that $N_0 = 146$ is the magic number for the isomeric shape as such, although it is suggested (compare though, Sec. VIII.E). The strength of the shell effect is expressed by the parameter c, for which Metag (1974) obtains 0.04 $\hbar\omega$, or 0.024 MeV for $\hbar\omega_0 = 0.6$ MeV.

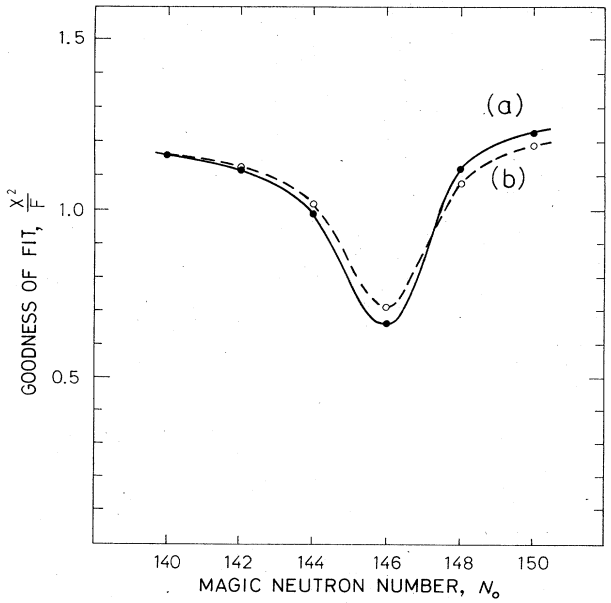

FIG. 54. Determination of the magic neutron number N_0 from a least-squares fit to the half-lives using Eq. (4.1). Curve (a) corresponds to $S = 0$, curve (b) corresponds to $f = 1, S = 0$. From Metag (1974).

4. The $\hbar\omega_B$ values

A separate determination of f and S is virtually impossible on the basis of the available lifetimes, essentially because of the scatter in the actual decay rates. This is very clearly brought out by Vandenbosch's (1974) discussion of the data, shown on Fig. 55. As can be seen, it is equally possible to throw the entire odd-even effect into the barrier height S or into the inertia through the $\hbar\omega_B$ values.

The resolution of this ambiguity remains a challenge.

Figure 56 shows one of the Metag (1974) fits to the spontaneous fission half-lives. With 5.5×10^{-21} sec as the half-life for zero barrier height, he obtains the following values:

$$\begin{aligned} a &= (-49.4 \pm 5.2)\hbar\omega_0, \\ b &= (46.0 \pm 4.4)\hbar\omega_0, \\ c &= (-3.9 \pm 0.4) \cdot 10^{-2}\hbar\omega_0, \\ S_0 &= (0.43 \pm 0.26)\hbar\omega_0, \\ f &= 1.16 \pm 0.08. \end{aligned} \tag{4.2}$$

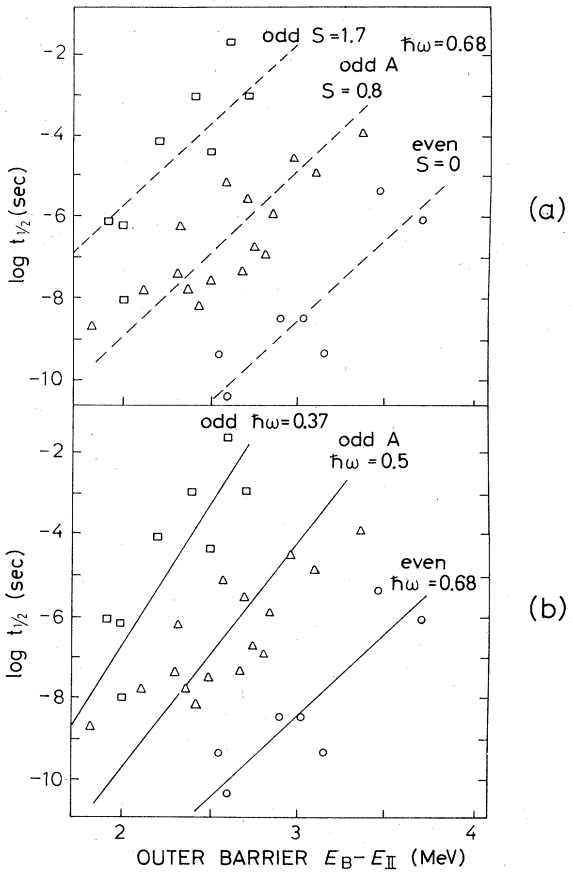

FIG. 55. In both parts of the figure the experimental spontaneous fission half-lives are plotted against the theoretically calculated height of the outer barrier, assuming no odd-even effect. From part (a) the maximum value of the specialization energy, $S = S_\Delta + S_s$, is derived by assuming $\hbar\omega = 0.68$ for all nuclear types. In part (b) S is assumed to be zero and the maximum variation in $\hbar\omega$ value is derived. From Vandenbosch (1974).

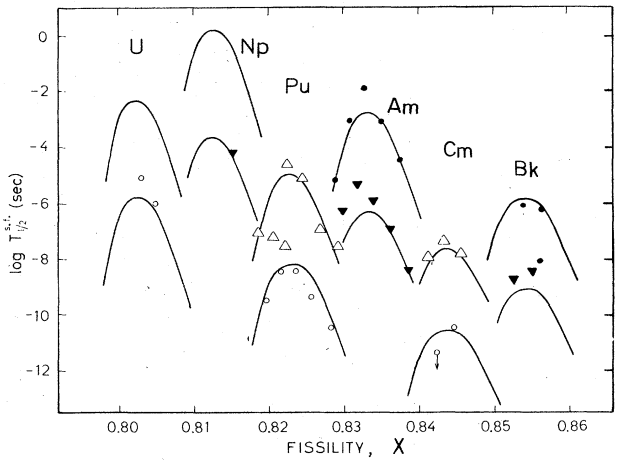

FIG. 56. Simple phenomenological description of spontaneous fission half-lives including the effect of a magic neutron number and the odd-even effect. The full drawn curves are the predictions of Eq. (4.1) with parameters adjusted to give a best fit. Points are experimental values. From Metag (1974).

(Other fits with either $S_0 = 0$ or $f = 1.0$ are equally satisfactory; compare Fig. 55.) From the experimental barrier heights ($E_B - E_{II}$) and the half-lives of ^{238}U, ^{238}Pu, and ^{240}Pu, a value of $\hbar\omega_B = (0.65 \pm 0.05)$ MeV results. With this value the results can be summarized as in Table III.

The average behavior of inertial effects and increases of the barrier heights will lie between the extremes I and III. The analysis of odd-even effects, Sec. VIII. D.2, points to a pairing energy difference of the order of 0.25 MeV; thus case I is definitely ruled out. Whether case II, based on Metag's (1974) suggestion, has struck the right balance still remains to be seen. In addition, a glance at Figs. 55 and 56 clearly shows that the idea of defining average quantities such as $\langle\hbar\omega_B\rangle$ and $\langle S\rangle$ in an unambiguous way is of limited usefulness.

5. Theoretical half-life estimates

First, a remark on the relation between isomer and ground-state spontaneous fission half-lives is in order. This aspect has been explored in particular by Randrup *et al.* (1973), by Pauli and Ledergerber (1974), and again by Randrup *et al.* (1976). Randrup *et al.* (1973) derive a phenomenological inertial coefficient that exceeds the reduced mass by a factor of 6.5 more than the irrotational, nonviscous, mass coefficient does; see Fig. 44. They obtained this number through a fit to all the known ground-state spontaneous fission half-lives of even nuclei, using the then-best calculated barrier, Fig. 45. When this phenomenological inertial coefficient was used to estimate isomeric decay, half-lives that were too long resulted. Pauli and Ledergerber (1974) find theoretical half-lives based on microscopically calculated inertial parameters and barriers in good agreement with experiment for the (even) ground states as well as for (even) isomers, see Figs. 21 and 22. This requires, however, a rather arbitrary Z-dependent readjustment of the liquid drop parameters. Without this readjustment calculated and measured lifetimes still agree within 2–3 orders of magnitude, which is not bad for a process characterized by penetration factors of 10^{-20}–10^{-40}. Returning to the problem, Randrup *et al.* (1976) estimate half-lives using both phenomenological and microscopical inertial coefficients. At the same time new barriers are calculated with the inclusion of further shape degrees of freedom. Good fits are obtained in both cases. The factor multiplying the mass excess compared to irrotational flow is now 11.5 instead of 6.5, and the microscopically calculated inertias are reduced 20%. The isomer half-lives are now satisfactorily reproduced, especially when the microscopic inertial coefficients are used.

The ground-state spontaneous fission is also strongly influenced by the presence of an unpaired particle. For the heavier elements, Pu to Fm, the hindrance factor is about 10^5 (Randrup *et al.*, 1973) to be compared with a hindrance of $(3–5) \times 10^3$ for isomer fission. For ground-state fission it is not possible to discern a tendency towards proportionality between the penetration exponent and the logarithm of the hindrance factor as one would expect from Eq. (4.1) for constant f and a constant increase S in barrier height. The barrier height is known to remain almost constant from Th to Fm; therefore a constant increase (in MeV) is also a constant relative increase. This failure can to some degree be attributed to the influence of the individual unpaired particle, but not entirely. Puzzlingly, the most stable elements long appeared to be the least hindered by the presence of the odd particle. Thus the hindrance factor for ^{233}U is quoted to be HF = 10 and for ^{235}U, HF = 40. This problem has been taken up by Grütter *et al.* (1974) who attempted to remeasure the spontaneous fission rate of ^{235}U and found the hindrance factor to be unmeasurably large and at least ten times greater than previously believed. When the difficulties of measuring these weak fission rates are considered,

TABLE III. Three different hypotheses relating the penetration factor $\hbar\omega_B$ with the magnitude of pairing and specialization energy to explain isomer half-lives.

	Case I		Case II		Case III	
	Pairing and specialization energy $\langle S\rangle$ (MeV)	$\langle\hbar\omega_B\rangle$ (MeV)	Pairing and specialization energy $\langle S\rangle$ (MeV)	$\langle\hbar\omega_B\rangle$ (MeV)	Pairing and specialization energy $\langle S\rangle$ (MeV)	$\langle\hbar\omega_B\rangle$ (MeV)
$e-e$	0	0.65	0	0.65	0	0.65
$o-e$	0	0.51	0.25	0.56	0.8	0.65
$o-o$	0	0.40	0.50	0.48	1.6	0.65

together with the problem of obtaining samples sufficiently free of contaminating impurities of neighboring even isotopes, it appears reasonable to discard the problem and attribute the situation as being due to experimental difficulties. The same may apply to the ^{242}Am ground-state spontaneous fission branch, which experimentally appears to be less hindered than the decay from the odd-A neighbors.

The fact that as a rule the hindrance factors for doubly odd isomers are closely equal to the product of the odd-A hindrance factors indicates independent contributions from each particle. This is expected for the inertial and pairing gap effect. To the extent that the specialization energy contributes in a major way to the hindrance, this also means that not only is the total spin projection K conserved during tunneling, but each individual component Ω_1 and Ω_2 of two particles is conserved too ($K=\Omega_1+\Omega_2$).

On the basis of an observed hindrance due to a single particle of $\approx 3\times10^3$ for the shape isomeric fission with a typical penetration factor of 10^{-14} it would be reasonable to expect hindrance factors in excess of 10^7 for ground-state spontaneous fission of odd-A nuclei in the Cm–Fm region where penetration factors are of the order of 10^{-28} and smaller. The fact that the observed hindrance is less, typically 10^4–10^5, has been interpreted by Nilsson (1969) as indicative of a barrier penetration process where not just one but several shape degrees of freedom come into play. The thicker the barrier to be penetrated, the greater freedom there is to find a way through the multidimensional deformation energy landscape and thus to minimize the penetration integral. Alternatively, the axial asymmetry at the inner barrier may ease the problem of matching the quantum numbers at the inner barrier to those of the initial state, in this way easing the hindrance due to the odd particle.

Summarizing, the predominant features of spontaneous fission from the ground state and from the isomeric state can be understood within the same conceptual framework of tunneling through a two-humped fission barrier. Both barrier heights and inertial effects are increased by the presence of one or several unpaired particles. This picture, partly phenomenological, leads to an understanding of tunneling rates with an accuracy of 10–20% in the penetration exponent.

D. Shape isomer formation yields and excitation functions

More specific information on the barriers containing the shape isomer, particularly on the isomer excitation energy and on the outer barrier, can be obtained from the experimental data on the cross sections for formation of the isomer, and especially from the dependence of such cross sections on excitation energy. Specifically, it is expected that extrapolation backwards of a sharply rising excitation curve to its threshold point will yield the isomer excitation energy, while the maximum value of the excitation curve, in the case of neutron evaporation reactions, will give information on the relative transmission coefficients (and hence barrier heights) of the inner and outer barriers of the penultimate nucleus in the evaporation process (i.e., that nucleus with one more neutron than that of the shape isomer itself); and the drop in yield with further increasing excitation energy ought to be governed by the outer barrier of the final nucleus.

1. Threshold excitation curves from neutron evaporation theory

Most of the experimental data on shape isomer excitation curves are from neutron evaporation reactions; a highly excited nucleus is formed, usually from charged particle bombardment, and the isomer results from this after emission of a specified number of neutrons. The relevant width (or more accurately transmission coefficient) for the last stage neutron evaporation leading to the states in the final nucleus that feed the isomer is expected to be very small in comparison with the total for all other modes of decay. It is then possible to derive simple statistical theory expressions that describe to first order the expected feature of the excitation curve in the neighborhood of its threshold (Jägare, 1970; Vandenbosch, 1972). These are related to the features of (xn) evaporation reactions first discussed in terms of the statistical theory by Jackson (1956).

a. The one-neutron evaporation process

The case treated here is for an initial nucleus of mass number A excited by a monoenergetic reaction to a precise excitation energy E^* and total angular momentum and parity J^π. The evaporation of a neutron from this excited nucleus is treated in the statistical theory, originally formulated by Weisskopf (1973), by the use of the transmission coefficients for formation of the compound nucleus by neutrons as defined in Eq. (3.41). From this expression, by summing over all possible angular momenta, a simplified expression can be obtained for the neutron transmission coefficient for specific neutron energy ϵ connecting the compound nucleus to a single state of the residual nucleus and summed over all orbital angular momenta:

$$\sum_{l=0}^{\infty}(2l+1)T_{(l)}(\epsilon)=\frac{2m\epsilon\sigma_{n(\mathrm{CN})}(\epsilon)}{\pi\hbar^2}, \tag{4.3}$$

where m is the reduced mass of neutron and nucleus. If the level density of the residual nucleus is assumed to depend on total angular momentum J simply as $2J+1$, a simple expression for the summed transmission coefficient for total first-stage neutron emission from the nucleus may be obtained from Eq. (4.3); this is,

$$T_{J^\pi(n,\,\mathrm{tot})}(E^*)=\frac{2m}{\pi\hbar^2}(2J+1)\times\int_0^{E^*-S_1}d\epsilon\,\sigma_{n(\mathrm{CN})}(\epsilon)\epsilon\rho_{\mathrm{eff}}^{(1)}(E^*-S_1-\epsilon), \tag{4.4}$$

where $\rho_{\mathrm{eff}}^{(1)}$ is the level density of the residual nucleus $A+x-1$ for an effective angular momentum of zero and both parities and S_1 is the neutron separation energy of a neutron from the nucleus A. In the use of Eqs. (4.3) and (4.4) the compound nucleus formation cross section by neutrons, $\sigma_{n(CN)}$, is generally assumed to be independent of the neutron energy ϵ.

A more accurate representation of the spin dependence of the level density is

$$\rho(U,I)=\rho_{\mathrm{eff}}(U)(2I+1)\exp\left(-\frac{(I+\frac{1}{2})^2}{2\sigma^2}\right), \tag{4.5}$$

where σ is a spin dispersion coefficient. The use of this form of the level density excludes a simple derivation of Eq. (4.4), but a modified form can be obtained (Lynn, 1974b) containing an additional factor $f_{\rm eff}(J,\epsilon)$ in the integrand. For approximate calculations a simple prescription for $f_{\rm eff}(J,\epsilon)$ is to compute it in terms of a related function $f(J,l)$:

$$f(J,l)=\frac{\sum_{I=(J-1)}^{J+1}(2I+1)\exp[-(I+\tfrac{1}{2})^2/2\sigma^2]}{(2J+1)(2l+1)}. \tag{4.6}$$

The required factor $f_{\rm eff}(J,\epsilon)$ is simply set equal to the weighted average of $f(J,l_<)$ and $f(J,l_>)$, where $l_<$ and $l_>$ are the orbital angular momentum values bracketing the average orbital angular momentum of the contributions to the compound nucleus formation cross section as expressed in Eq. (4.3). This will vary somewhat with energy, and to remove $f_{\rm eff}(J,\epsilon)$ from the integrand of the modified Eq. (4.4) $l_{\rm av}$ should be calculated for the approximate mean energy $\bar{\epsilon}$ of neutron emission. If the level density energy variation can be described by a simple exponential formula with constant temperature θ then $\bar{\epsilon}$ is just 2θ. The factor $f_{\rm eff}(J,2\theta)$ will not be included explicitly in the equations given in this section, but should be understood to be included as a multiplying constant in more detailed work.

Equations (4.3) and (4.4) are applicable to special states that might feed a specific isomer as well as to the totality of states of the residual nucleus. For the application of Eq. (4.4) to such a special state their level density is labeled by the extra superscript s, and the same factorization as in Eq. (4.5) is adopted:

$$\rho^{(1,s)}(U,I)=\rho_{\rm eff}^{(1,s)}(U)(2I+1)\exp[-(I+\tfrac{1}{2})^2/2\sigma^2]. \tag{4.7}$$

Thus the transmission coefficient summed over the special states is

$$T_{J^\pi(n,s)}(E^*)=\frac{2m}{\pi\hbar^2}(2J+1)\times\int_0^{E^*-S_1}d\epsilon\,\sigma_{n(\rm CN)}(\epsilon)\epsilon\rho_{\rm eff}^{(1,s)}(E^*-S_1-\epsilon). \tag{4.8}$$

The evaluation of the integrals in Eqs. (4.4) and (4.8) is particularly simple if, as well as making the assumption that $\sigma_{n(\rm CN)}$ is constant, it is assumed that the level density has the simple exponential form with constant temperature:

$$\rho_{\rm eff}^{(1)}(U)=\rho_{\rm eff}^{(1)}(0)e^{U/\theta_1} \tag{4.9a}$$

$$\rho_{\rm eff}^{(1,s)}(U_s)=\rho_{\rm eff}^{(1,s)}(0)e^{U_s/\theta_1^{(s)}}. \tag{4.9b}$$

Here U_s is an effective excitation energy for the special states and may differ from the true excitation energy of the residual nucleus by an isomer excitation energy E_s. Similarly, the temperature $\theta_1^{(s)}$ may be one that is appropriate only to the special states. Substitution of Eq. (4.9b) into Eq. (4.8) gives

$$T_{J^\pi(n,s)}(E^*)=\frac{2m\sigma_{n(\rm CN)}\rho_{\rm eff}^{(1,s)}(0)\theta_1^{(s)}}{\pi\hbar^2}(2J+1)\times[\theta_1^{(s)}e^{(E^*-S_1-E_s)/\theta_1^{(s)}}-(E^*-S_1-E_s+\theta_1^{(s)})]. \tag{4.10}$$

Thus the excitation function for the population of a specific state that is fed by the set of special states s (with no branching elsewhere) is given by the ratio $T_{J^\pi(n,s)}/T_{J^\pi(T)}$, where $T_{J^\pi(T)}$ is the summed transmission coefficient over all possible decay processes. If these are effectively limited to neutron emission then

$$T_{J^\pi(T)}(E^*)=T_{J^\pi(n,\rm tot)}(E^*)=\frac{2m\sigma_{n(\rm CN)}\rho_{\rm eff}^{(1)}(0)\theta_1}{\pi\hbar^2}(2J+1)[\theta_1e^{(E^*-S_1)/\theta_1}-(E^*-S_1+\theta_1)]. \tag{4.11}$$

If the isomer excitation energy E_s is appreciably greater than the residual nucleus temperature θ_1, the second factor in the square bracket of Eq. (4.11) is unimportant in the evaluation of the excitation function, which becomes

$$Y_s(E^*)=\frac{T_{J^\pi(n,s)}(E^*)}{T_{J^\pi(n,\rm tot)}(E^*)}=\frac{\rho_{\rm eff}^{(1,s)}(0)\theta_1^{(s)2}}{\rho_{\rm eff}^{(1)}(0)\theta_1^2}e^{-E_s/\theta_1^{(s)}}e^{E_1^*(1/\theta_1^{(s)}-1/\theta_1)}\left[1-\left(1+\frac{E^*-S_1-E_s}{\theta_1^{(s)}}\right)e^{-(E^*-S_1-E_s)/\theta_1^{(s)}}\right]. \tag{4.12}$$

For the simple case of $\theta_1^{(s)}=\theta_1$, this function is shown in Fig. 57. By contrast, the excitation function of the ground state of the residual nucleus, on the assumptions that it is fed uniformly from all states reached by neutron evaporation and that there are no competing reactions, is simply a step function at the threshold energy.

b. Two-neutron evaporation process

For isomers reached by a two-stage neutron emission process from the nucleus A the population of states excited in the nucleus $A-1$ by emission of one neutron must first be written down. This is obtained simply from Eqs. (4.3) and (4.4) giving

$$P_1(\mathcal{E}_1)\,d\mathcal{E}_1=\frac{T_{J^\pi(n,\rm tot)}(E^*)}{T_{J^\pi(T)}(E^*)}\frac{(E^*-S_1-\mathcal{E}_1)\rho_{\rm eff}^{(1)}(\mathcal{E}_1)}{\int_0^{E^*-S_1}d\epsilon\,\epsilon\rho_{\rm eff}^{(1)}(E^*-S_1-\epsilon)}\,d\mathcal{E}_1 \tag{4.13}$$

for the probability of exciting states, of all spins, within the interval of excitation energy $d\mathcal{E}$, at energy $\mathcal{E}$, in the residual nucleus. If now the isomer is fed (uniformly) from a set of special states in the residual nucleus $A-2$ reached after emission of a second neutron, and the density of these states is denoted by $\rho^{(2,s)}(U,I)$, the probability of forming the isomer is

$$Y_s(E^*)=\int_{S_2+E_s}^{E^*-S_1}d\mathcal{E}_1\,P_1(\mathcal{E}_1)\frac{T_{(n,s)}(\mathcal{E}_1)}{T_{(T)}(\mathcal{E}_1)}, \tag{4.14}$$

where the transmission coefficients now refer to the compound nucleus $A-1$ and the total angular momentum notation has been dropped (the dependences on angular momentum being assumed to cancel). These again can be readily evaluated under the constant temperature level density assumption to obtain expressions of the kind (4.10) and (4.11), but with the numeral 1 that appears there in superscripts and subscripts being replaced by 2, to indicate quantities referring to

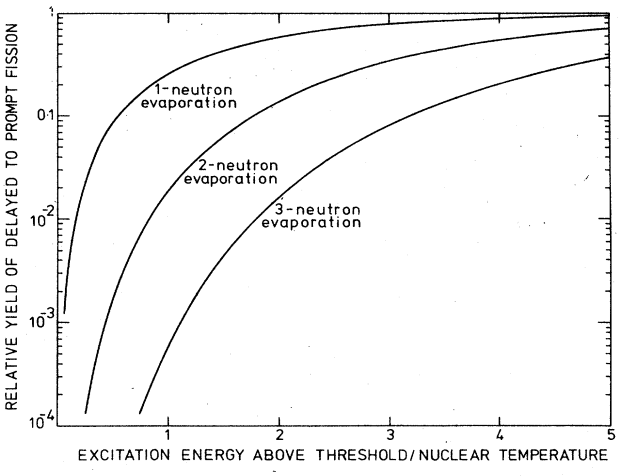

FIG. 57. Isomer excitation functions for one-neutron, two-neutron, and three-neutron evaporation processes in the equi-temperature level density models [from Eqs. (4.12), (4.16), and (4.21)]. The curves are normalized to the factor $[T_{J^\pi(n,\mathrm{tot})}(E^*)\rho_{\mathrm{eff}}^{(n,s)}(0)/T_{J^\pi(T)}(E^*)\rho_{\mathrm{eff}}^{(n)}(0)]\exp(-E_s/\theta_n^*)$.

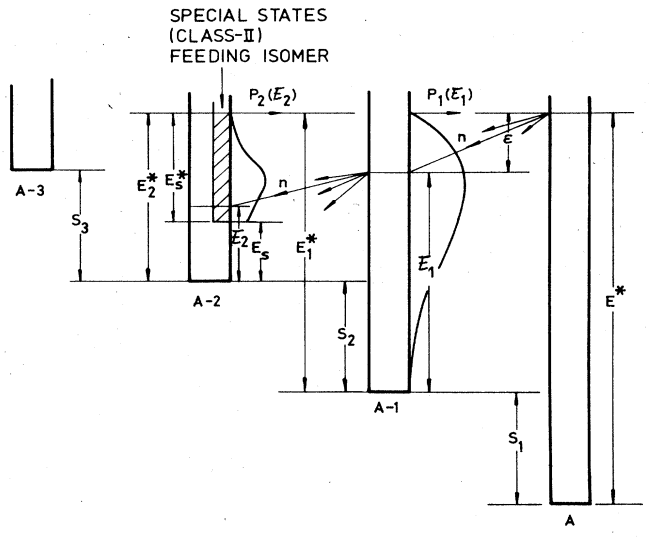

FIG. 58. Diagramatic illustration of energy relationships used in isomer excitation formulas. Neutron separation energies are indicated by S, maximum excitation energies (relative to a ground state or isomer state) by E, neutron energies by ϵ, actual excitation energies (following neutron evaporation) by $\mathcal{E}$. Subscripts indicate the nucleus to which the quantity refers.

the residual nucleus $A-2$, and the excitation energy E^* being replaced by $\mathcal{E}_1$. A diagram showing the relevant energy relationships at a glance is given in Fig. 58. Equation (4.14) then becomes, for the case in which decay processes from the nucleus $(A-1)$ are limited to neutron emission,

$$Y_s(E^*)=\frac{2m\sigma_{n(\mathrm{CN})}\rho_{\mathrm{eff}}^{(1)}(0)(2J+1)}{\pi\hbar^2 T_{J^\pi(T)}(E^*)}\frac{\rho_{\mathrm{eff}}^{(2,s)}(0)\theta_2^{(s)}}{\rho_{\mathrm{eff}}^{(2)}(0)\theta_2}\int_{S_2+E_s}^{E^*-S_1}d\mathcal{E}_1\,\frac{(E^*-S_1-\mathcal{E}_1)e^{\mathcal{E}_1/\theta_1}[\theta_2^{(s)}e^{(\mathcal{E}_1-S_2-E_s)/\theta_2^{(s)}}-(\mathcal{E}_1-S_2-E_s+\theta_2^{(s)})]}{[\theta_2 e^{(\mathcal{E}_1-S_2)/\theta_2}-(\mathcal{E}_1-S_2+\theta_2)]}\,. \tag{4.15}$$

With the simplifying assumptions that all temperatures occurring in the integral of Eq. (4.15) are equal, and that E_s/θ_2 is considerably greater than unity so that only the exponential term in the denominator of the integrand need be retained, the expression for the excitation curve simplifies to

$$Y_s(E^*)\approx\frac{T_{J^\pi(n,\mathrm{tot})}(E^*)}{T_{J^\pi(T)}(E^*)}\frac{\rho_{\mathrm{eff}}^{(2,s)}(0)}{\rho_{\mathrm{eff}}^{(s)}(0)}e^{-E_s/\theta_2}\left\{1-\left[1+\frac{E_s^*}{\theta_2}+\frac{1}{2}\left(\frac{E_s^*}{\theta_2}\right)^2+\frac{1}{6}\left(\frac{E_s^*}{\theta_2}\right)^3\right]e^{-E_s^*/\theta_2}\right\}, \tag{4.16}$$

where $E_s^*=E^*-S_1-S_2-E_s$. This function is shown in Fig. 56.

By contrast, the excitation function for forming the ground state of the nucleus $A-2$ in the absence of reactions competing strongly with neutron decay [which can be found by equating $T_{(n,s)}/T_{(T)}$ to unity in the integral of Eq. (4.14)] has the functional form of Eq. (4.12) with E_s set equal to S_2 and $\theta_1^{(s)}$ replaced by θ_1; Eq. (4.12), the isomer yield curve for one-neutron evaporation, has in fact the functional form first given by Jackson (1956) for two-neutron evaporation to the nucleus $(A-2)$. Excitation curves for two-neutron evaporation to the ground state can, however, have the functional form given in Eq. (4.16) (which has the Jackson three-neutron evaporation form for excitation of the nucleus $A-3$) provided there is a predominant competing reaction with exponentially increasing transmission coefficient. Such competition could be provided, for example, by fission from the nucleus $A-1$, the effective fission barrier being considerably lower than the neutron threshold (Metag *et al.*, 1973).

Generally, it is expected that the temperature associated with the level density of the first-stage nucleus $A-1$ will differ considerably from the temperature of the final nucleus; for the range of excitation energies of interest in the analysis of spontaneous fission isomerism calculations based on the assumption of an independent-particle model (Fermi gas) kind of level density indicate that the former temperature may be ~25% higher than that of the $A-2$ nucleus. Equation (4.15) may be integrated for this more general case, the result being

$$Y_s(E^*)=\frac{T_{J^\pi(n,\mathrm{tot})}(E^*)}{T_{J^\pi(T)}(E^*)}\frac{\rho_{\mathrm{eff}}^{(2,s)}(0)}{\rho_{\mathrm{eff}}^{(2)}(0)}\frac{\theta_2^{(s)2}\Theta^2}{\theta_2^2\theta_1^2}e^{E_2^*[1/\theta_2^{(s)}-1/\theta_2]}e^{-E_s/\theta_2(s)}$$
$$\times\left(1-\left(1+\frac{E_s^*}{\Theta}\right)e^{-E_s^*/\theta}-\left\{\frac{\Phi^2}{\Theta^2}\left(1+\frac{E_s^*}{\theta_2^{(s)}}\right)\left[1-\left(1+\frac{E_s^*}{\Phi}\right)e^{-E_s^*/\Phi}\right]-\frac{\Phi^3}{\theta_2^{(s)}\Theta^2}\left[2-\left(\frac{E_s^{*2}}{\Phi^2}+\frac{2E_s^*}{\Phi}+2\right)e^{-E_s^*/\Phi}\right]\right\}e^{-E_s^*/\theta_2^{(s)}}\right) \tag{4.17}$$

where Θ here denotes the quantity $(\theta_2^{(s)-1}+\theta_1^{-1}-\theta_2^{-1})^{-1}$ and Φ denotes $(\theta_1^{-1}-\theta_2^{-1})^{-1}$. The form of this equation for some typical temperatures is shown in Fig. 59.

c. *Three-neutron evaporation processes*

To calculate the excitation curve for isomers reached by three-stage neutron emission from the nucleus A the population of states excited in the nucleus $A-2$ by emission of two neutrons must first be evaluated. This is obtained from the population at the previous stage, Eq. (4.13), by multiplying by the branching ratio to states at excitation energy $\mathcal{E}_2$ in $A-2$ and integrating over $\mathcal{E}_1$:

$$P_2(\mathcal{E}_2)d\mathcal{E}_2 = d\mathcal{E}_2 \int_{S_2+\mathcal{E}_2}^{E^*-S_1} d\mathcal{E}_1 P_1(\mathcal{E}_1) \times \frac{2m\sigma_{n(CN)}}{\pi\hbar^2}\,\frac{(\mathcal{E}_1-S_2-\mathcal{E}_2)\rho_{\mathrm{eff}}^{(2)}(\mathcal{E}_2)}{T_{(T)}(\mathcal{E}_1)}. \tag{4.18}$$

With the previous assumptions of no significant competition against fission decay and equal temperatures in the $A-1$ and $A-2$ level density laws this again can be evaluated very simply for values of the excitation energy such that $\mathcal{E}_2/\theta_2 \gg 1$. The range of excitation energies in the nucleus $A-2$ in which we are interested well satisfy this condition. The result is

$$P_2(\mathcal{E}_2)\,d\mathcal{E}_2 = \frac{T_{J^\pi(n,\mathrm{tot})}(E^*)}{T_{J^\pi(T)}(E^*)} \times \frac{1}{6\theta}\left(\frac{E_2^*-\mathcal{E}_2}{\theta}\right)^3 e^{-(E_2^*-\mathcal{E}_2)/\theta} d\mathcal{E}_2 . \tag{4.19}$$

The isomer yield curve is

$$Y_s(E^*) = \int_{S_3+E_s}^{E^*-S_1-S_2} d\mathcal{E}_2\, P_2(\mathcal{E}_2)\,\frac{T_{(n,s)}(\mathcal{E}_2)}{T_{(T)}(\mathcal{E}_2)}, \tag{4.20}$$

and substitution of the relevant quantities under the constant temperature level density assumption gives

$$Y_s(E^*) = \frac{T_{J^\pi(n,\mathrm{tot})}(E^*)}{T_{J^\pi(T)}(E^*)}\,\frac{\rho_{\mathrm{eff}}^{(3,s)}(0)}{\rho_{\mathrm{eff}}^{(3)}(0)}\,e^{-E_s/\theta}\left[1-\left(1+\frac{E_s^*}{\theta}+\frac{E_s^{*2}}{2\theta^2}+\frac{E_s^{*3}}{6\theta^3}+\frac{E_s^{*4}}{24\theta^4}+\frac{E_s^{*5}}{120\theta^5}\right)e^{-E_s^*/\theta}\right], \tag{4.21}$$

where, as before, E_s^* is the maximum excitation energy of the system relative to the isomer, i.e., $E_s^* = E^* - S_1 - S_2 - S_3 - E_s$. This excitation function is shown in Fig. 57.

The important case in which the temperature of the special states feeding the isomer differs from the other temperatures can also be derived very simply. The result is

$$Y_s(E^*) = \frac{T_{J^\pi(n,\mathrm{tot})}(E^*)}{T_{J^\pi(T)}(E^*)}\,\frac{\rho_{\mathrm{eff}}^{(3,s)}(0)}{\rho_{\mathrm{eff}}^{(3)}(0)}\left(\frac{\theta_3^{(s)}}{\theta}\right)^6 \exp\left[-E_3^*\left(\frac{1}{\theta}-\frac{1}{\theta_3^{(s)}}\right)\right] \times e^{-E_s/\theta_3^{(s)}}\left[1-\left(1+\frac{E_s^*}{\theta_3^{(s)}}+\frac{E_s^{*2}}{2\theta_3^{(s)2}}+\frac{E_s^{*3}}{6\theta_3^{(s)3}}+\frac{E_s^{*4}}{24\theta_3^{(s)4}}+\frac{E_s^{*5}}{120\theta_3^{(s)5}}\right)e^{-E_s^*/\theta_3^{(s)}}\right], \tag{4.22}$$

shown for various ratios of $\theta_3^{(s)}$ to θ in Fig. 60.

The leading term in Eqs. (4.22) and (4.21) for small $E_s^*/\theta_3^{(s)}$ has the form $(E_s^*/\theta)^6$ at large values of $E_s^*/\theta_3^{(s)}$ the term $\exp[-E_3^*(1/\theta-1/\theta_3^{(s)})]$ becomes dominant in Eq. (4.22). Thus, if the special states have a high temperature,

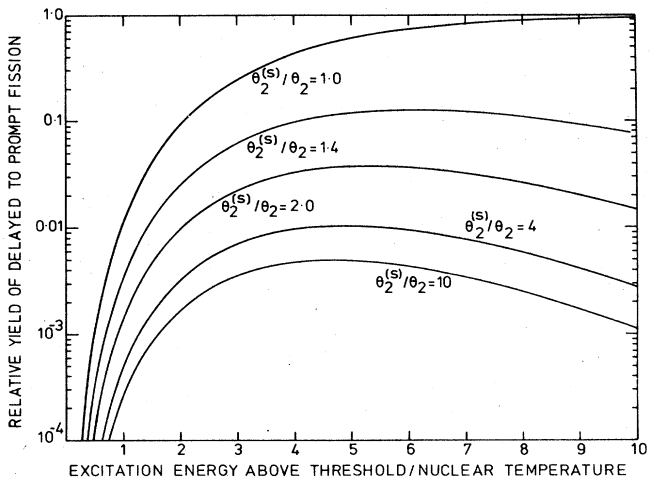

FIG. 59. Isomer excitation function for two-neutron evaporation process, with different temperatures for the level densities in the different states. The curves are normalized as in Fig. 57. Curves are labeled by values of $\theta_2^{(s)}/\theta_2$. For every curve $\theta_1/\theta_2=1.4$, $E_s/\theta_2=4$.

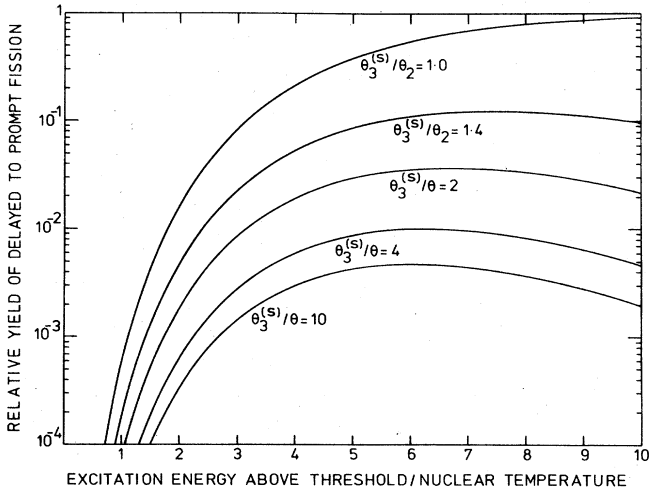

FIG. 60. Isomer excitation function for three-neutron evaporation process, with the temperature of the isomer-feeding states differing from the temperature of the overall level density law. The curves are normalized as in Fig. 57 and are labeled by values of $\theta_3^{(s)}/\theta$.

such as might be employed phenomenologically to represent the sparsely occurring levels in an energy gap region, the rising excitation curve above the threshold becomes rapidly damped and can be expected to fall away rapidly in due course. The same feature is found in the expressions (4.12) and (4.17) for isomers formed from one- and two-neutron evaporation. In the first case, the leading term is proportional to $(E_s^*/\theta_1)^2$, but the term $\exp[-E_1^*(1/\theta_1 - 1/\theta_1^{(s)})]$ becomes dominant at high energies for differing temperatures; while in the two-neutron evaporation case the leading term is $(E_s^*/\theta_2)^4$.

The general result for the three-neutron evaporation case, with all temperatures being different, is

$$
\begin{aligned}
Y_s(E^*) = {} & \frac{T_{J^\pi(n_{\rm tot})}(E^*)}{T_{J^\pi(T)}(E^*)} \frac{\rho_{\rm eff}^{(3,s)}(0)}{\rho_{\rm eff}^{(3)}(0)} \frac{\theta_3^{(s)2}\Theta^2}{\theta_3^2\theta_2^2\theta_1^2} e^{-E_s^*/\theta_3} \\
& \times \{ e^{E_s^*/\theta_3^{(s)}} [\zeta^2(1-e^{-E_s^*/\zeta}) - 2\zeta\Theta - \zeta(E_s^* - 2\Theta)e^{-E_s^*/\zeta} + \Pi^2(1-e^{-E_s^*/\Pi}) + 2\Pi\Theta - \Pi(E_s^* + 2\Theta)e^{-E_s^*/\Pi}] \\
& + [\Phi^2(1 + 2\Theta/\theta_3^{(s)} - E_s^*/\theta_3^{(s)}) + \Phi(E_s^* - 2\Theta)] e^{-E_s^*/\Phi} \\
& + (2\Phi^3/\theta_3^{(s)})(1 - e^{-E_s^*/\Phi}) - \Phi^2(1 + 2\Theta/\theta_3^{(s)} + E_s^*/\theta_3^{(s)}) + 2\Phi\Theta(1 + E_s^*/\theta_3^{(s)}) \\
& + [\Lambda^2(1 - 2\Theta/\theta_3^{(s)} - E_s^*/\theta_3^{(s)}) + \Lambda(E_s^* + 2\Theta)] e^{-E_s^*/\Lambda} \\
& + (2\Lambda^3/\theta_3^{(s)})(1 - e^{-E_s^*/\Lambda}) - \Lambda^2(1 - 2\Theta/\theta_3^{(s)} + E_s^*/\theta_3^{(s)}) - 2\Lambda\Theta(1 + E_s^*/\theta_3^{(s)}) \} ,
\end{aligned}
$$

where

$$
\Theta^{-1} = \theta_1^{-1} - \theta_2^{-1}, \quad \Phi^{-1} = \theta_2^{-1} - \theta_3^{-1}, \quad \Pi^{-1} = \theta_1^{-1} - \theta_3^{-1} + \theta_3^{(s)-1}, \quad \Lambda^{-1} = \theta_1^{-1} - \theta_3^{-1}, \quad \zeta^{-1} = \theta_2^{-1} - \theta_3^{-1} + \theta_3^{(s)-1}. \tag{4.23}
$$

d. General remarks

It is apparent from the above equations and the illustrating diagrams (Figs. 57, 59, and 60) that a variety of shapes of isomer excitation curves can occur, even for reactions of a specified number of neutron evaporation stages. Care must be taken therefore when the excitation curve is analyzed to deduce the isomer energy E_s. The most common assumption that is made is the equitemperature one. This is probably quite adequate in the analysis of data leading to isomers occurring in doubly odd nuclei. It is fraught with considerable uncertainty, however, in dealing with the spontaneously fissioning isomers of even- and odd-A nuclei. In these cases the special levels (which are the class-II levels of the secondary well in the fission barrier) are expected to be spasmodically placed in an energy gap with no strong overall energy variation, which is then followed by a normal level density region characterized by a typical temperature. An approximation to the excitation curve could be achieved by summing a curve calculated with a very high (or perhaps even negative) "temperature" built on the isomer state, with an equitemperature curve built on an effective isomer energy placed at the top of the energy gap. This could possibly introduce some structure into an otherwise monotonic excitation curve with a smoothly varying derivative. Some evidence for this kind of picture emerges from the data on excitation of the ^{238}U shape isomer through the (n,n') reaction [Wolf and Meadows (1974) and private communication]; attempts to fit these data with the simple equitemperature one-stage evaporation model of Eq. (4.12) have not been very successful (Fig. 61).

Further modification of the excitation curves discussed above might occur with relaxation of the restriction that decay of the compound nuclei in all but the initial state is through neutron emission processes only. Fission is the major competitive reaction, of course.

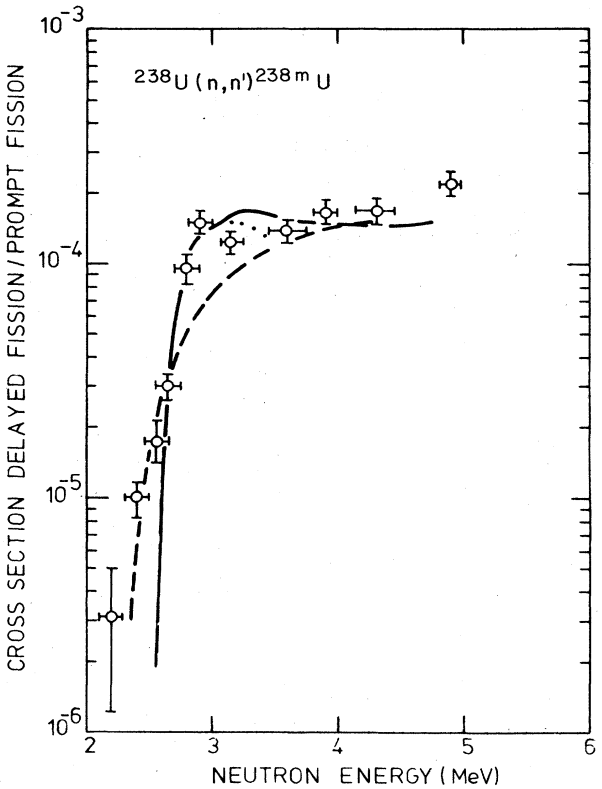

FIG. 61. Data for excitation of ^{238m}U shape isomer by the (n,n') reaction (Wolf and Meadows, 1974 and private communication). The broken curve is a statistical calculation based on constant temperature level density models ($\theta_1 = 0.5$ MeV, $\theta_1^{(s)} = 0.53$ MeV, $E_{II} = 2.35$ MeV). The full curve treats the class-II state spectrum as having an energy gap ($2\Delta = 1.2$ MeV) containing rotational bands based on $K^\pi = 0^+$ ground state, a $K^\pi = 0^-$ vibration at 0.5 MeV higher, and a $K^\pi = 2^+$ vibration at 1 MeV higher. The isomer energy is 2.56 MeV. The dotted curve shows the effect of omitting the $K^\pi = 0^-$ band.

As long as the fission transmission coefficient has a similar dependence on excitation energy as the total neutron transmission coefficient (as suggested by the near constancy of neutron-induced fission cross sections at energies above the fission barrier; see Sec. VII), the shapes of the excitation curves presented above will remain essentially unchanged, but the magnitude will be reduced by a product of factors representing the ratio of neutron to total transmission coefficient at each stage of evaporation. Proximity of a fission barrier to an excitation threshold could alter the shapes very considerably, but assessment of all the known shape isomer data shows that this does not appear to occur in any known case. It can affect the shape of a ground-state excitation curve quite severely, however, as in the case of two-neutron evaporation to ^{240}Cm (Metag *et al.*, 1973).

Discussion of the detailed analysis of isomer threshold data is given in Sec. IV.D.3.

2. Absolute strengths of excitation curves

Some of the factors governing the absolute values, as distinct from the shapes, of the excitation curves for shape isomers have already been discussed. Some of these factors are included explicitly in the equations already given, notably the probability of first neutron emission from the initial compound nucleus, and level density ratios between isomer-feeding states and the totality of residual states in the final nucleus. Extra multiplying factors that have to be introduced into the isomer yield functions are the probabilities of second and subsequent neutron emission, the overall factor being approximately

$$\prod_{p=1}^{x-1} \frac{T_{(n,\mathrm{tot})}^{(A-p)}(E_p^* - 2p\theta)}{T_{(T)}^{(A-p)}(E_p^* - 2p\theta)} \tag{4.24}$$

for an (xn) evaporation process. As stated at the end of Sec. IV.D.1.*d*, fission is normally expected to be the major reaction competing with neutron evaporation.

So far in this section we have not considered the implications of the double-humped fission barrier for shape isomer yield except insofar as the secondary minimum of the barrier provides the mechanism for the existence of the class-II states that feed the isomer after final neutron emission. The formulas given so far are implicitly for an outer barrier very much higher than the inner barrier. When the outer barrier is comparable with or lower than the inner barrier there is a decoupling effect on transition processes from a nucleus effectively in a normal shape to states in a differently deformed shape. This effect has already been discussed in Sec. III B.1, and the relevant reduction factor for states of class I decaying to states of class II is given by Eq. (3.50). This implies a further multiplying factor, approximately

$$\frac{T_{(A)}^{(A-x+1)}[E_{x-1}^* - 2(x-1)\theta]}{T_{(A)}^{(A-x+1)}[E_{x-1}^* - 2(x-1)\theta] + T_{(B)}^{(A-x+1)}[E_{x-1}^* - 2(x-1)\theta]} \tag{4.25}$$

where $T_{(A)}$, $T_{(B)}$ are the transmission coefficients across the inner and outer barriers, respectively, for the final stage of decay at the nucleus $A-x+1$, the isomer being found in the nucleus $A-x$.

For analysis of the shape isomer excitation curves, information on the product (4.24) is to be obtained, directly or indirectly, from experimental data such as neutron-induced fission cross sections up to excitation energies of some 20 MeV. At these higher energies the data are somewhat indirect because they contain contributions from (xnf) reactions as well as immediate fission, and an assessment of the relative importance of the contributions from each process has to be made; at the present state of knowledge this is largely subjective. For the highly fissile nuclei—Pu and up—there are good reasons to think that first chance fission dominates. Data on relative neutron and fission transmission coefficients are given by Huizenga and Vandenbosch (1962), and a further discussion of these topics is given in Sec. VII of the present review. Where experimental data do not exist on the relative neutron to fission emission probabilities for particular nuclei these have to be deduced from systematic trends.

Apart from determining the isomer excitation energy it is also a prime aim of the analysis of isomer excitation data to deduce the factor (4.25); this gives information on the height of the outer barrier relative to the inner barrier in the nucleus $A-x+1$. How far this can be successfully accomplished will be dealt with in the detailed analysis of data in Sec. IV.D. 3.

Most measurements of shape isomer excitation curves have been made by detecting the delayed spontaneous fission of the isomer relative to the prompt fission yield. Such a measurement introduces another possible factor into the analysis of the data, namely the branching ratio between decay of the isomer by spontaneous fission and by gamma cascades through lower class-I states to the ground state of the residual nucleus. The gamma branch of the isomer decay is very difficult to measure, and has in fact been observed in only one case, namely, from the shape isomer of ^{238}U (Russo *et al.*, 1974). Although the difficulty of the measurement suggests that the sparsity of data on the gamma branch may not reflect an intrinsic improbability in this mode of decay, the systematic behavior of the spontaneous fission yield from most isomers strongly supports the belief that for most of the presently known shape isomers the gamma-decay branch is negligible.

At higher excitation energies the shape and magnitude of the isomer excitation curve becomes distorted by additional effects. The first of these is the possibility of fission decay, through the outer barrier, of the higher class-II states that feed the isomer (Britt *et al.*, 1971). Here, the competition between gamma decay and fission must be calculated from a model of the radiation process and the Hill–Wheeler penetrability factor through the outer barrier [see Eq. (3.17)]. The outer barrier height can be left as an adjustable parameter in fitting the curve over an extended energy range [as was attempted by Britt *et al.* (1971, 1973)] or can be assessed from other data. In the two papers of Britt *et al.* (1971, 1973) the radiation transmission coefficient to lower class-II states was calculated from a simple strong coupling dipole model in which the gamma-ray strength is simply assumed to be proportional to the cube of the gamma-ray energy and the proportionality

constant is obtained from neutron resonance radiation width data in the actinide region. In some of the numerical analysis given below in Sec. IV.D. 3 a more elaborate giant-dipole resonance model has been used; this is described in more detail in Sec. VII. For the analysis of plutonium and americium isomer data the basic analysis is not too greatly dependent on the treatment of the radiation process (typical calculations of the transmission coefficients for radiation and fission are shown in Fig. 62, but in the curium isomers, where the outer barrier appears to be rather low, this competition is more difficult to assess; in these nuclei class-II states not far above the energy gap could be decaying appreciably by fission, and the radiation properties of such states will be particularly difficult to compute reliably with a statistical model.

The net effect of this fission competition in the decay of the class-II states is to attenuate the isomer excitation curve at higher energies, causing it to fall away from the asymptotic values indicated in the idealized formulas (4.12), (4.16), and (4.21). Tending to compensate this effect, however, is another route for feeding the class-II states. In this final neutron evaporation is to highly excited class-I states of the final nucleus; these are coupled, relatively strongly above the intermediate barrier, and much more weakly below, to the class-II states which can then feed the isomer by gamma cascades (see Fig. 63). These class-II states suffer strongly from the fission attenuation effect, of course, but in the neutron evaporation process the class-I states of the final nucleus are so much more strongly populated than the class-II states that the route can be an appreciable one at higher excitation energies. Britt *et al.* (1971) estimate that this route can be the predominant one at an excitation energy of 5 MeV above the isomer threshold. These calculations were very schematic, however, assuming a sharp cutoff energy, for example, below which coupling between class-I and class-II states was negligible. More realistic calculations made for the present review with reassessed empirical level density functions for normally deformed nuclei and for the barriers (see Sec. VII) indicate that even for energies greater than about 7 MeV above the threshold the contribution from the class-I route is of the order of 10–20% of that from direct neutron evaporation to the class-II states. At these higher energies, however, other processes even more difficult to assess quantitatively come into play, such as neutron emission in a preequilibrium mode rather than compound nucleus evaporation (Britt *et al.*, 1973), and although it is encouraging that the overall shape of the excitation curve can be accounted for, not much reliance can be placed on parameters deduced from the higher energy reaches.

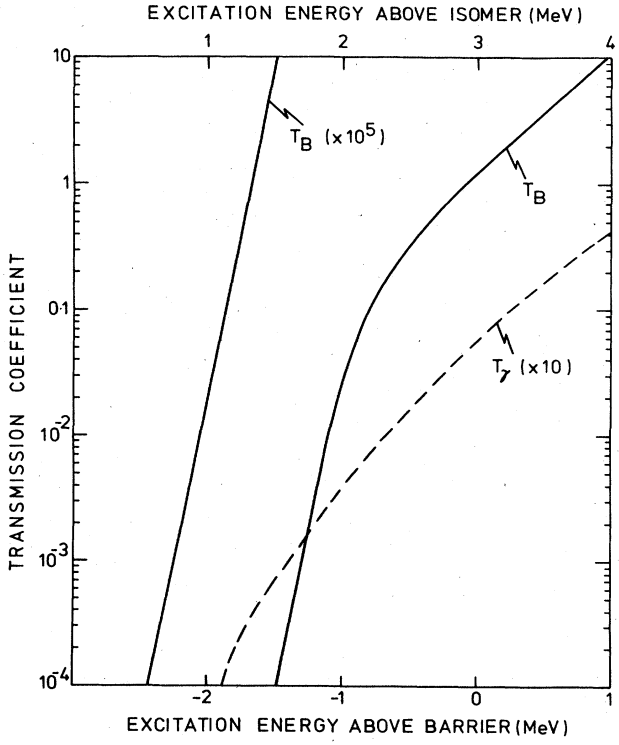

FIG. 62. Transmission coefficients for radiation and fission of class-II states above the shape isomer.

3. Experimental data on isomer excitation

Most experimental data on excitation of spontaneously fissioning isomers exist for the Pu, Am, and Cm nuclides. In Secs. IV.D. 1 and 2 it was remarked that analysis of the excitation curves is probably least complicated for double odd nuclei. For this reason the study of the experimental data is begun with the americium series.

a. Americium shape isomers

(i) ^{242}Am. The most important data available on the excitation function of the 14-msec isomer of this nucleus are those due to Flerov *et al.* (1967) using the ^{243}Am$(n, 2n)$ reaction. There are also data on the ^{242}Pu$(d, 2n)$ reaction (Britt *et al.*, 1971), which do not reach to such a low energy as the former, but are believed to give more accurate values of the overall mag-

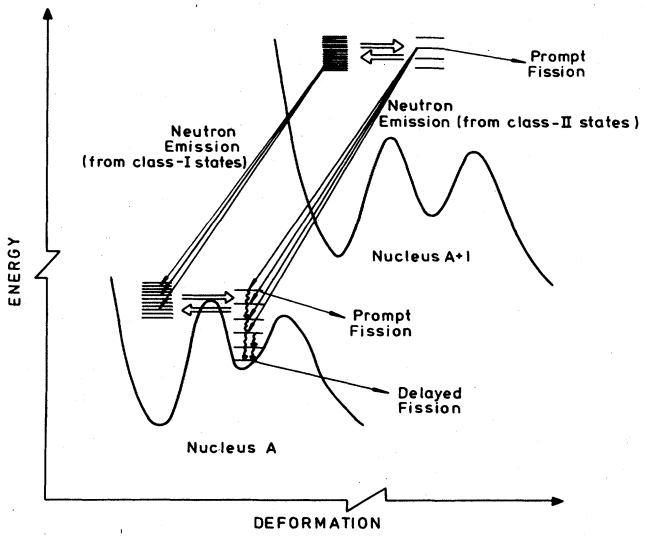

FIG. 63. Schematic diagram of population routes for the shape isomer.

nitude of the yield. If the $(n, 2n)$ data are normalized to the $(d, 2n)$ data (which are given as the ratio of delayed fission cross section to prompt fission cross section), they must be approximately doubled in value.

These data are plotted in Fig. 64. A number of fitted curves and calculated points from the theory described in Secs. IV.D. 1 and 2 are shown in comparison. In the first of these (long-dashed curve) the level density temperatures assumed are $\theta_1 = 0.65$ MeV (for ^{243}Am), $\theta_2 = 0.528$ MeV (for ^{242}Am), and $\theta_2^{(s)} = 0.5$ MeV (for class-II states of ^{242}Am). The numerical values of temperature are discussed in Sec. VII. All class-II states excited in ^{242}Am are assumed to decay to the isomer. The fitted curve shown is for parameters $E_{II} = 2.5$ MeV, and a normalization constant

$$N = \exp(-E_{II}/\theta_2^{(s)}) \frac{\rho_{\text{eff}}^{(2,s)}(0)}{\rho_{\text{eff}}^{(2)}(0)} \frac{P_{2n}}{P_f} \frac{T_A^{(A-1)}}{T_A^{(A-1)} + T_B^{(A-1)}} \tag{4.26}$$

with value 1.5×10^{-4}. In the expression for N, P_n is the probability of two-neutron evaporation and P_f the accumulated prompt fission probability (in this case the sum of f, $n'f$, and, at the highest energies, $2nf$ processes), while $T_A^{(A-1)}$, $T_B^{(A-1)}$ are the barrier transmission coefficients for the nucleus one neutron higher than the isomer [see Eq. (4.25)]. The fission and neutron-evaporation data reviewed in Sec. VII indicate that $P_{2n}/P_f \sim 0.23$ for ^{244}Am, and, with the assumption that $\rho_{\text{eff}}^{(2,s)}(0) = \rho_{\text{eff}}^{(2)}(0)$, this fit determines $T_A/(T_A + T_B) \approx 0.074$ for ^{243}Am. Using the behavior of fission barrier level densities as reviewed in Sec. VII this quantity indicates a barrier difference $V_A - V_B \approx 1.5$ MeV for ^{243}Am.

The dot-dashed curve and the short-dashed curves are for different assumptions of temperature, while the continuous curve is an example of a fit making allowance in a simplified way for higher class-II states to decay by fission over the outer barrier. With an assumed height for the outer barrier the energy in the secondary minimum at which the class-II radiation coefficient T_γ equals the outer barrier transmission coefficient can be determined on the basis of models (see Fig. 62 based on the considerations of Sec. VII). Class-II states below this energy are assumed to decay completely by radiation to the isomer and above this energy by fission over the outer barrier. This approximation is intuitively justified by the very rapid change with energy of the barrier transmission coefficient below the barrier energy. The population distribution of states in the second well following two-neutron evaporation is shown in Fig. 65.

A summary of the parameters of all the fits is given in Table IV. This demonstrates the range of variation in deduced values of the parameters resulting from reasonable assumptions about some of the other nuclear parameters. It does not include any variation due to experimental error. The most reasonable set of assumptions is probably incorporated in the solid curve shown in Fig. 63 [for a discussion of V_B for ^{242}Am see subsection (*ii*) below], and the values of E_{II} and $V_B^{(A-1)}$ deduced from this are taken as the most likely values of these parameters. The errors (from parametrization) appear to be of the order of ±0.2 MeV and ±0.3 MeV, respectively.

Data from the ^{242}Pu$(t, 3n)$ reaction (Britt *et al.*, 1972) seem to confirm approximately the value of V_B for ^{243}Am. With a generalized multitemperature model for the three-neutron evaporation (temperatures of $\theta_1 = 0.83$

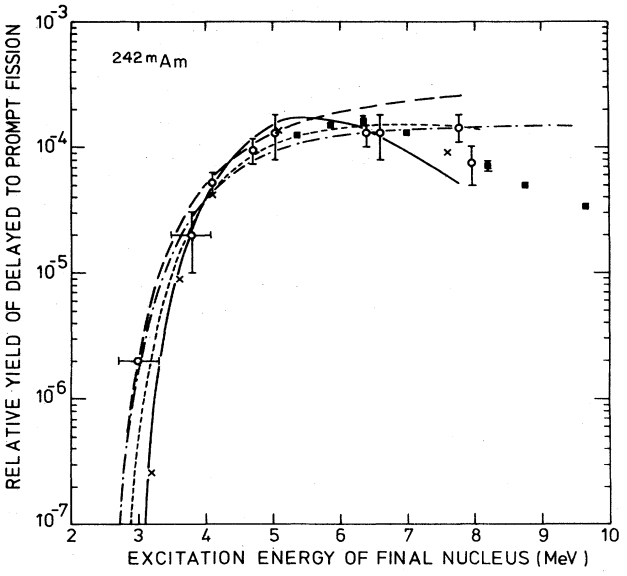

FIG. 64. Excitation of 14 msec isomer of ^{242}Am through $(n, 2n)$ (Flerov *et al.*, 1967) and $(d, 2n)$ (Britt *et al.*, 1971) reactions. The fitted curves are explained in the text and in Table IV. Circles are experimental points due to Flerov *et al.* (1967), squares are experimental data of Britt *et al.* (1971) and crosses are detailed statistical theory computer calculations.

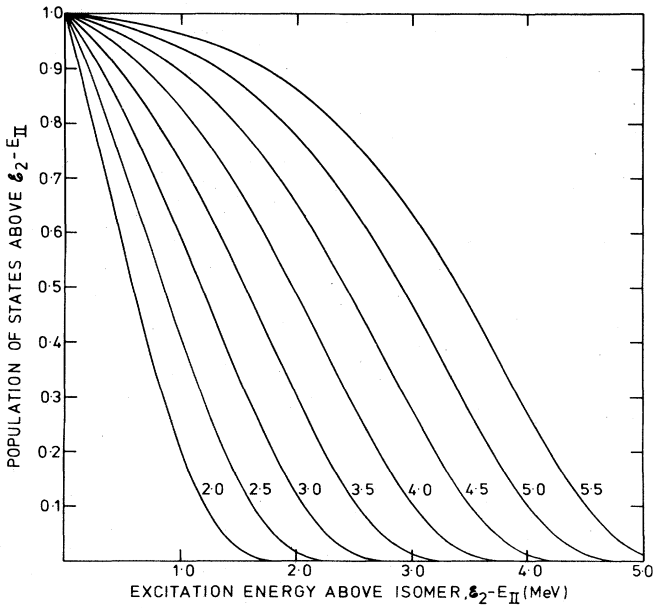

FIG. 65. Cumulative population distribution of states in secondary minimum following two-neutron evaporation to odd residual nucleus. Temperature θ_1 for first-stage evaporation is assumed to be 0.65 MeV and $\theta_2^{(s)}$ for second-stage evaporation is 0.528 MeV. Curves are labeled by the amount of (initial) excess energy above the Q value for reaching the isomeric state in a two-neutron evaporation reaction, $E_2^* - E_{II}$.

TABLE IV. Fits to excitation function data for 14 msec shape isomer of ^{242}Am. In deduction of $U_B^{(A-1)}$, the value of U_A for ^{243}Am was taken to be 6.25 MeV. The points X are full statistical theory numerical calculations of the isomer excitation for the parameters shown. See Fig. 64.

Curve	θ_1 (MeV)	θ_2 (MeV)	$\theta_2^{(s)}$ (MeV)	$U_B^{(A-2)}$	E_{II}	N	$\frac{T_A^{(A-1)}}{T_A^{(A-1)}+T_B^{(A-1)}}$	$U^{(A-1)}$
Long dash	0.65	0.528	0.500	High	2.5	1.5×10^{-4}	0.074	4.75
Dot–dash	0.65	0.528	0.528	High	2.5	1.5×10^{-4}	0.074	4.75
Short–dash	0.65	0.528	0.528	High	2.7	2.7×10^{-4}	0.15	5.05
Solid	0.65	0.528	0.528	5.3	2.9	3.2×10^{-4}	0.34	5.55
Not shown	0.65	0.528	0.528	5.6	2.8	2.5×10^{-4}	0.22	5.25
Not shown	0.65	0.528	0.558	5.3	3.0	5.0×10^{-4}	0.47	5.75
X		0.528	0.528	5.7	3.0			5.45

MeV, $\theta_2 = 0.63$ MeV, $\theta_3 = \theta_3^{(s)} = 0.52$ MeV are deduced from the level density parameters recommended in Sec. VII), with E_{II} fixed at 2.9 MeV and $P_{3n}/P_f = 0.17$, these data yield ~0.9 MeV for the barrier height difference in ^{243}Am. The quality of these data are relatively poor, however, covering only one decade in relative range. In particular the isomer excitation energy is ill determined, a perfectly adequate fit being possible with E_{II} ~ 2.3 MeV, for example.

(ii) ^{241}*Am.* Data on the excitation of this isomer through the ^{242}Pu$(p,2n)$ reaction are due to Lark *et al.* (1969), and are shown in Fig. 66. Fits with simple constant-temperature level density models tend to give low values of E_{II} and $V_B^{(A-1)}$. As explained in Sec. IV.D. 2 more realistic level density models should be used in the odd-A (or even) case. The actual fits shown here employ an energy gap $2\Delta^{(s)}$ in the level density of the secondary minimum, within which the density is constant (assumed equal to 1.2 MeV^{-1} for $J = \frac{1}{2}$ states of one parity in the odd-A case) and above which the density has a constant temperature rather similar to the temperature of the class-I states in the corresponding energy region. If, for the level density above the gap, $\rho_{\text{eff}}^{(2,s)}(0) = \rho_{\text{eff}}^{(2)}(0)$, only poor fits are possible (for a reasonable value of the gap, say $2\Delta^{(s)} = 1.2$ MeV); and a fit is shown by the dashed curve in Fig. 66 (parameters are $E_{II} = 1.8$ MeV, $V_B^{(A-2)} = 5.3$ MeV, $T_A^{(A-1)}/(T_A^{(A-1)} + T_B^{(A-1)}) = 0.011$. Better fits are achieved if $\rho_{\text{eff}}^{(2,s)}(0)$ is rather lower than $\rho_{\text{eff}}^{(2)}(0)$ (by a factor ~2), or $\theta_2^{(s)}$ is rather higher than θ_2 (by perhaps 10%). With such fits, an example of which is shown by the continuous curve of Fig. 66, higher values of V_B for ^{242}Am, more in accord with other evidence, are achieved. The parameters for the continuous curve are: $\theta_1 = 0.65$ MeV, $\theta_2^{(s)} = \theta_2 = 0.518$ MeV, $2\Delta^{(s)} = 1.2$ MeV, $\rho_{\text{eff}}^{(2,s)}(0) = 0.5\,\rho_{\text{eff}}^{(2)}(0) = 0.9$ MeV^{-1}, $E_{II} = 2.2$ MeV, $V_B^{(A-2)} = 5.0$ MeV, $P_{2n}/P_f = 0.303$, $T_A^{(A-1)}/(T_A^{(A-1)} + T_B^{(A-1)}) = 0.058$. With a value of $V_A = 6.5$ MeV for ^{242}Am (see Sec. VII) this last value can be interpreted to give $V_B = 5.3$ MeV for ^{242}Am.

(iii) ^{240}*Am.* Important data on the threshold excitation curve of the 0.9 msec isomer of ^{240}Am are available from the ^{241}Pu$(p,2n)$ reaction (Bjørnholm *et al.*, 1967). The absolute magnitude of the curve is confirmed by results from the ^{240}Pu$(d,2n)$ reaction (Britt *et al.*, 1971). These data are shown in Fig. 67.

The analysis of the data carried out for this review is similar to that described for ^{242}Am. A typical fitted curve is shown in Fig. 67. The parameters for this are: $\theta_1 = 0.65$ MeV, $\theta_2 = 0.528$ MeV, $\theta_2^{(s)} = 0.558$ MeV,

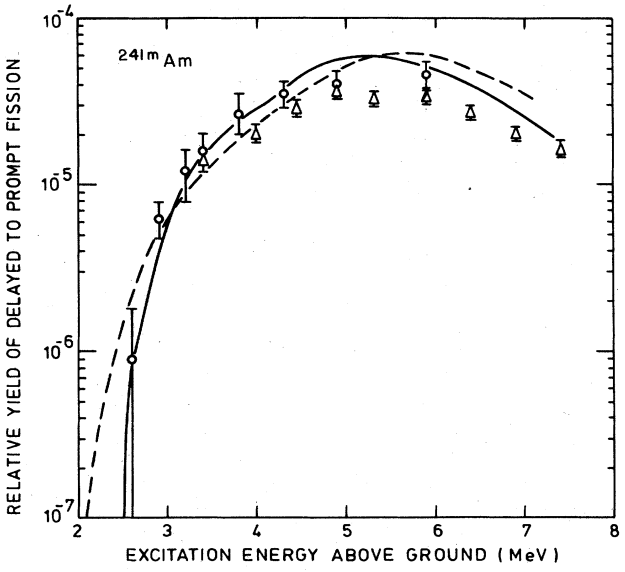

FIG. 66. Excitation of 1.5 μsec isomer of ^{241}Am through ^{242}Pu$(p,2n)$ reaction, circles are due to Lark *et al.* (1969) and triangles to Britt *et al.* (1972). The parameters for two possible fits are described in the text.

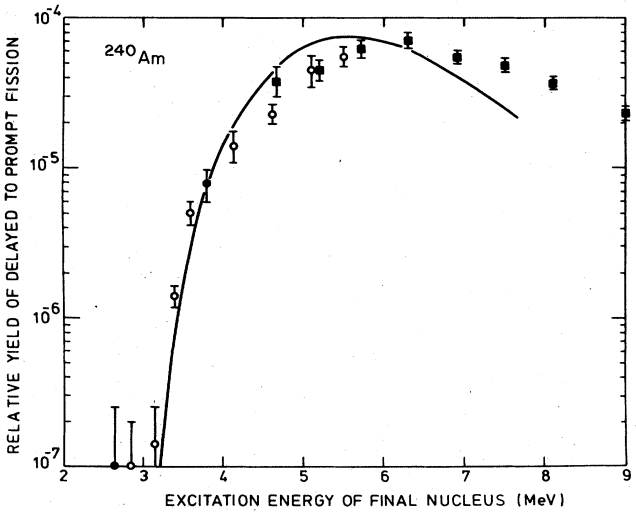

FIG. 67. Excitation of 0.9 msec isomer of ^{240}Am. Circles are data from the ^{241}Pu$(p,2n)$ reaction (Bjørnholm *et al.*, 1967) and squares are from the ^{240}Pu$(d,2n)$ reaction (Britt *et al.*, 1971).

$V_B^{(A-2)} = 5.3$ MeV, $E_{II} = 3.0$ MeV, $N = 2 \times 10^{-4}$. From this (with $P_{2n}/P_f = 0.2$) it is deduced that $T_A^{(A-1)}/(T_A^{(A-1)} + T_B^{(A-1)}) = 0.2$ and hence that V_B is ~0.9 MeV lower than V_A for ^{241}Am.

The rather poor data from the ^{240}Pu$(t, 3n)$ reaction (Britt *et al.*, 1972) indicate a barrier height difference of about 1.5 MeV for ^{241}Am, if the isomer energy is fixed at 3.0 MeV.

(iv) ^{239}*Am.* Data on the excitation of the 0.163 msec isomer of ^{239}Am are available from three reactions, the ^{240}Pu$(p, 2n)$ reaction (Lark *et al.*, 1969; Britt *et al.*, 1972), the ^{237}Np$(\alpha, 2n)$ reaction, and the ^{239}Pu$(d, 2n)$ reaction (Britt *et al.*, 1971). Data on the ^{237}Np$(\alpha, 2n)$ reaction are also given by Fleury *et al.* (1973). These data, shown in Fig. 68, illustrate the consistency, and hence the experimental uncertainty, connected with this kind of work; it is apparent that systematic shifts in normalization (by up to 30%) and/or energy (by up to 0.2 MeV) are required to bring the data from the different reactions into juxtaposition.

Examples of three fits to the data are shown. The continuous curve is the fit of Britt *et al.* (1971). This was a computer program calculation based on statistical theory and the level density functions used were those of Gilbert and Cameron (these are essentially constant temperature forms below about 4 MeV); the relevant parameters are $E_{II} = 2.5$ MeV, $V_B^{(A-2)} = 5.2$ MeV, $V_A^{(A-1)} - V_B^{(A-1)} = 1.2$ MeV. The dashed curve is based on a level density model with energy gap as described for ^{241}Am; the parameters are $\theta_1 = 0.65$ MeV, $\theta_2 = \theta_2^{(s)} = 0.518$ MeV, $E_{II} = 2.4$ MeV, $V_B^{(A-2)} = 5.2$ MeV, $P_{2n}/P_f = 0.1$ (assumed), $T_A^{(A-1)}/(T_A^{(A-1)} + T_B^{(A-1)}) = 0.044$, giving $V_B = 5.2$ for $V_A = 6.5$ MeV in ^{240}Am. The dot-dash curve is due to Britt *et al.* (1973) and is based on a model in which all relevant level densities (including barrier densities) and hence transmission coefficients are calculated from the deformed nucleus single-particle level schemes of Bolsterli *et al.* (1972) (these do not show energy gap features). This model allows for prequilibrium neutron emission (which has the effect, mainly, of not allowing the isomer yield to drop too rapidly at high excitation energies) but the absolute fraction of preequilibrium component in the excited populations is adjusted to the data. The parameters deduced from the fit are $E_{II} = 2.5$ MeV, $V_F^{(A-2)} = 4.65$ MeV, $V_B^{(A-1)} = 5.6$ MeV (with $V_A^{(A-1)} = 6.45$ MeV).

(v) ^{244}*Am.* The data available on the excitation of the 1 msec isomer are from the ^{244}Pu$(t, 3n)$ reaction (Britt *et al.*, 1972). Two typical fits are shown in Fig. 69. The parameters for the dashed curve are: $\theta = 0.7$ MeV (for the residual nuclei in the first two evaporation stages), $\theta_3 = 0.5$ MeV (final stage), $V_B^{(A-3)} - E_{II} \sim 2.5$ MeV, $E_{II} = 2.8$ MeV, $V_A^{(A-2)} - V_B^{(A-2)} \sim 1.2$ MeV (assuming $P_{3n}/P_f = 0.45$). Higher values of the outer barrier are deduced from a more general multitemperature model. The full curve employs for the first-stage evaporation, $\theta_1 = 0.83$ MeV, for the second stage, $\theta_2 = 0.63$ MeV, and, again $\theta_3 = \theta_3^{(s)} = 0.5$ MeV for the final stage. With $E_{II} = 2.8$ MeV, $V^{(A-2)} - V_B^{(A-2)} \sim 1.0$ MeV. Considerable variation in these parameters is possible; E_{II} could be lowered to ~2.5 MeV and $V_B^{(A-2)}$ by 0.3–0.4 MeV.

(vi) Data from (n, γ) *reactions.* Two of the isomers discussed above (those of ^{242}Am and ^{244}Am) have been formed also by the (n, γ) reaction, the neutron energy varying between thermal and ~2 MeV. The reaction yields as a function of neutron energy have been compared with the results of gamma-ray cascade

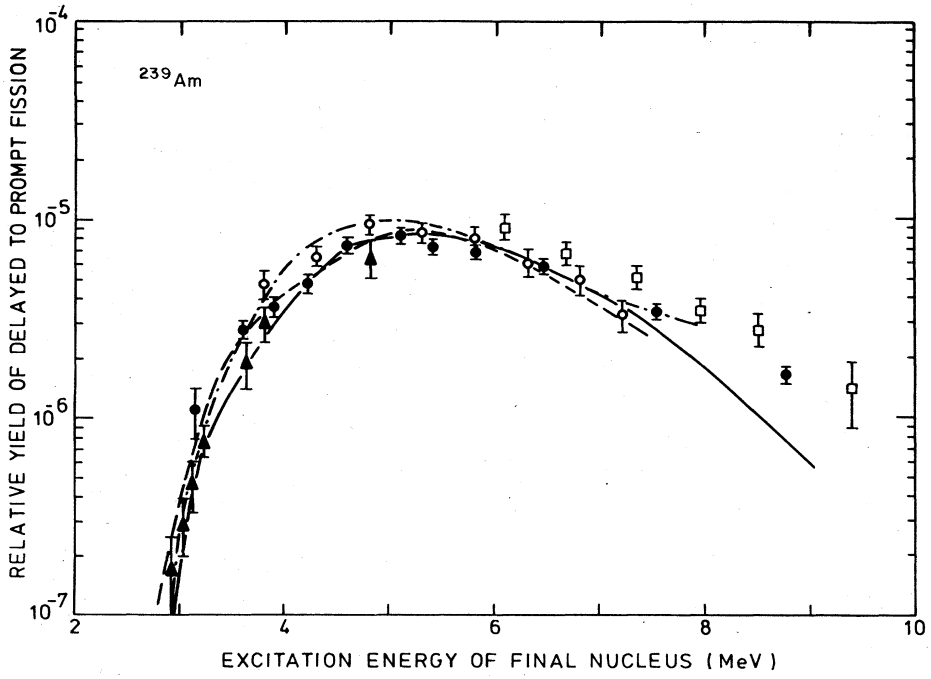

FIG. 68. Excitation of the 0.163 μsec isomer of ^{239}Am. Triangles are ^{240}Pu$(p, 2n)$ data (Lark *et al.*, 1969), closed circles are ^{237}Np$(\alpha, 2n)$ data, squares are ^{239}Pu$(d, 2n)$ data [both from Britt *et al.* (1971)], and open circles are ^{240}Pu$(p, 2n)$ data by Britt *et al.* (1972). The fitted curves are described in the text.

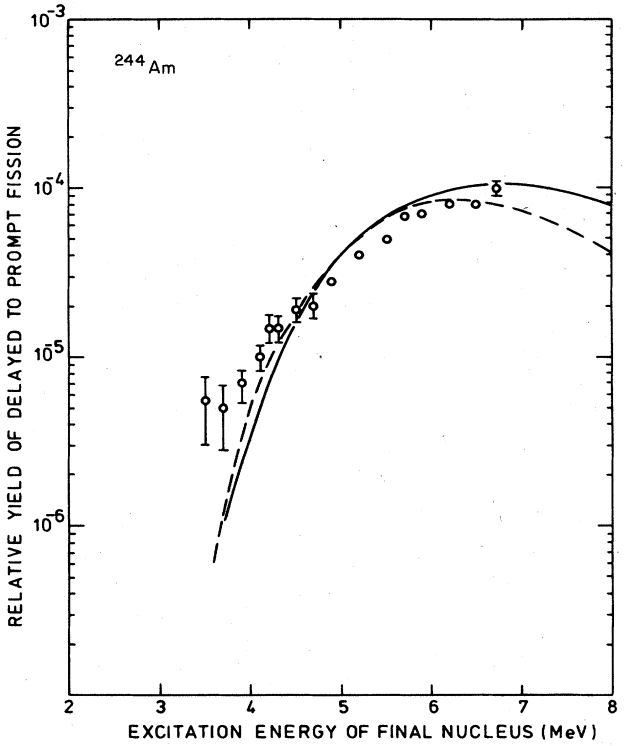

FIG. 69. Excitation of the 1 msec isomer of ^{244}Am by means of the ^{244}Pu(t, $3n$) reaction (Britt *et al.*, 1972). Parameters for the fitted curve are given in the text.

calculations modeling the transition schemes between primary and secondary well with neutron and fission competition. The transition scheme is shown in Fig. 70. In this, the nucleus is assumed to be formed in class-I states at an excitation energy equal to the neutron energy plus neutron separation energy. These states are mixed with class-II states (the mixing can be considered as a shape transition across the intermediate barrier), the mixing strength being given by the statistical formulae of Sec. III. B, if the excitation energy is above the intermediate barrier, or by the formulas for mixing of discrete states (see Sec. III. C. 5) if otherwise. The class-II components of the mixed states can decay by fission over barrier B or by radiative transitions to lower states in the secondary well.

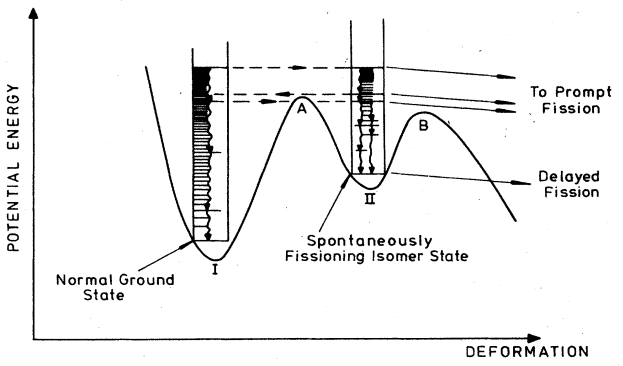

FIG. 70. Transition scheme for formation of shape isomer by cascade radiation.

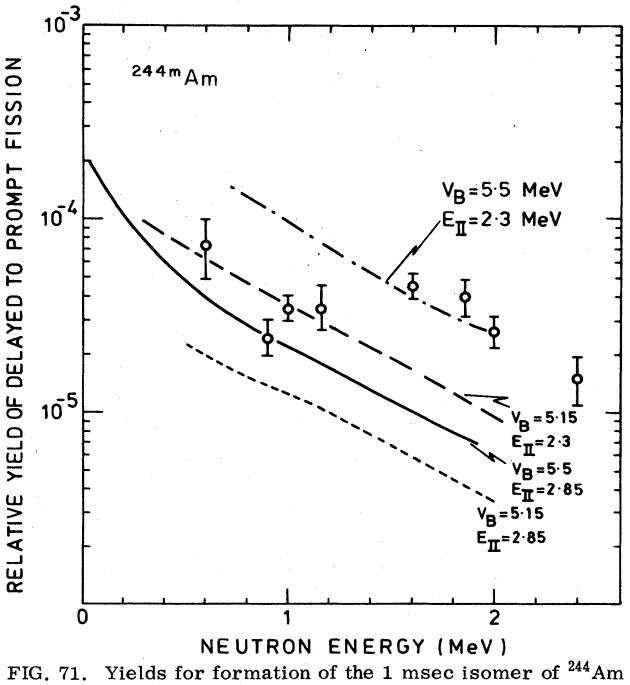

FIG. 71. Yields for formation of the 1 msec isomer of ^{244}Am by the ^{243}Am(n, γ) reaction (Boca *et al.*, 1969). The curves are calculated results from the radiation cascade model.

These lower class-II states can either mix with class-I states allowing further radiative deexcitation to states of normal shape, or fission, or deexcite radiatively to still lower class-II states. The main class-I component of the original excited state can decay either by neutron emission or radiation to lower class-I states which themselves have a (generally smaller) class-II component mixed with them. The complete cascade is very expensive to follow in full numerical detail on an electronic digital computer but Monte Carlo treatments of

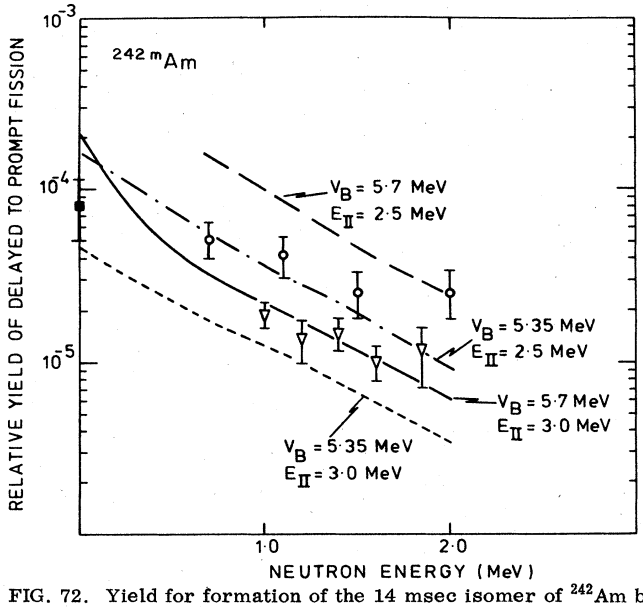

FIG. 72. Yield for formation of the 14 msec isomer of ^{242}Am by the ^{241}Am(n, γ) reaction. Experimental points are: □ Dahlsuren *et al.* (1969), ○ Boca *et al.* (1969), ▽ Nagy *et al.* (1970).

TABLE V. Double-barrier parameters of americium nuclei as deduced from experimental data on shape isomer excitation functions. The level density parameters employed are those given in Sec. VII for class-I states and barrier deformations. For class-II states of odd-A nuclei, the level density parameters are described under Section IV.B.3.*a*. U_A values, where appropriate, are taken from Sec. VII. The table is to be taken as an attempt to achieve consistent parameters through the whole chain of nuclides downwards from ^{245}Am. Bracketed values are assumed from other evidence than the stated reaction for the purpose of obtaining a fit.

Nuclide	Reaction Data	Ref.	E_{II} (MeV)	U_A (MeV)	U_B (MeV)	Remarks
^{245}Am	^{244}Pu(t, $3n$)^{244}Am	Britt *et al.* (1972)		6.15	5.2	~±0.3–0.5 MeV uncertainty on U_B
^{244}Am	ditto	ditto	2.8		(5.3)	~±0.3–0.5 MeV uncertainty on E_{II}
	^{243}Am(n, γ)^{244m}Am	Boca *et al.* (1969)	(2.8)		5.5	U_B deduced with assumed E_{II}
	^{244}Pu(p, $2n$)^{243m}Am	Britt *et al.* (1972)		6.37	5.3	
^{243}Am	ditto	ditto	2.3		(5.0)	~±0.3–0.4 MeV uncertainty on E_{II}
	^{243}Am(n, $2n$)^{242m}Am	Flerov *et al.* (1968)				
	^{242}Pu(d, $2n$)^{242m}Am	Britt *et al.* (1971)		6.25	5.55	
	^{242}Pu(t, $3n$)^{242m}Am	Britt *et al.* (1972)			5.3	Value deduced if E_{II} for ^{242}Am assumed to be 2.9 MeV
^{242}Am	^{243}Am(n, $2n$)^{242m}Am	Flerov *et al.* (1968)				
	^{242}Pu(d, $2n$)^{242m}Am	Britt *et al.* (1971)	2.9		(5.3)	
	^{242}Am(n, γ)^{242m}Am	Dahlsuren *et al.* (1969) Boca *et al.* (1969) Nagy *et al.* (1970)	(2.9)		~5.5	U_B deduced with assumed E_{II}
	^{242}Pu(p, $2n$)^{241m}Am	Lark *et al.* (1969) Britt *et al.* (1972)		6.5	5.3	
^{241}Am	Ditto	Ditto	2.2		(5.0)	
	^{241}Pu(p, $2n$)^{240m}Am	Bjørnholm *et al.* (1967)				
	^{240}Pu(d, $2n$)^{240m}Am	Britt *et al.* (1971)		6.2	5.3	
	^{240}Pu(t, $3n$)^{240m}Am	Britt *et al.* (1972)			~4.7	Value deduced if E_{II} for ^{240}Am assumed to be 3.0 MeV
^{240}Am	^{241}Pu(p, $2n$)^{240m}Am	Bjørnholm *et al.* (1967)	3.0		(5.3)	
	^{240}Pu(p, $2n$)^{239m}Am	Lark *et al.* (1969)				
		Britt *et al.* (1972)		6.5	5.2	
	^{237}Np(α, $2n$)^{239m}Am	Britt *et al.* (1971)				
	^{239}Pu(d, $2n$)^{239m}Am	Ditto				
^{239}Am	Ditto	Ditto	2.4		(~5.2)	Assumed value for U_B
	^{239}Pu(p, $2n$)^{238m}Am	Sletten and Jørgensen (private commun.)		6.0	~4.5	
^{238}Am	Ditto	Ditto	2.6		(~5.0)	Assumed value for U_B
	^{238}Pu(p, $2n$)^{237m}Am	Polikanov and Sletten (1970)		$U_A - U_B$ ~1.2		
^{237}Am	Ditto	Ditto	2.4		(~5.0)	Assumed value for U_B

the model have been devised.

Comparisons between calculations and observation for the ^{244}Am isomer are shown in Fig. 71, and for the ^{242}Am isomer in Fig. 72. In both cases it is apparent that these (n, γ) data are in reasonable agreement (at least in order of magnitude) with the parameters necessary to achieve fits for the excitation by neutron evaporation reactions.

(vii) General remarks. Data on other americium isomers (^{243}Am, ^{238}Am, ^{237}Am) are also available. The deductions from these and all the above-mentioned data, using the present analysis, are collected in Table V. It will be seen from the discussions of specific cases given in the subsections above that the error due to uncertainties from the analysis alone (due to uncertainties in the choice of theoretical parameters) seems generally to be of the order of 0.2–0.3 MeV in the quantities E_{II} and V_B, and experimental uncertainties are probably of similar magnitude. In some cases the data are considerably poorer or more limited in range than the average case; for these the extent of the uncertainty in analysis is indicated in the "remarks" column of Table V.

b. Plutonium shape isomers

The analysis of these isomers for this review follows the same general lines already described for the odd-A americium isomers [see particularly the discussion of ^{241}Am under Sec. IV.D.3. *a. (ii)*]. For even nuclei the constant level density within the energy gap of the class-II level system is assumed to be 0.45 MeV^{-1}, and it is also assumed that the exponentially rising component of the class-II level density is half the magnitude of the corresponding class-I component.

A typical example of analysis of plutonium data is given in Fig. 73. The data are from the ^{235}U$(\alpha, 2n)$ and ^{237}Np$(d, 2n)$ reactions for excitation of the shape isomers of ^{237}Pu (Britt *et al.*, 1971). The model parameters for the continuous curve are $\theta_1 = 0.65$ MeV, $\theta_2^{(s)} = \theta_2 = 0.5$ MeV, $2\Delta^{(s)} = 1.2$ MeV, $\rho_{\text{eff}}^{(2,s)}(0) = 0.5\,\rho_{\text{eff}}^{(2)}(0)$, $E_{II} = 2.8$ MeV, $V_B^{(A-2)} = 5.3$ MeV, $P_{2n}/P_f = 0.12$, $T_A^{(A-1)}/(T_A^{(A-1)} + T_B^{(A-1)}) = 0.34$, implying that $V_B = 4.9$ MeV with $V_A = 5.5$ MeV for ^{238}Pu. The ^{236}U$(\alpha, 3n)$ data of Wolf and Unik [referred to by Britt *et al.*, (1972)] support an outer barrier height that may be ~0.3 MeV lower than this.

The collected results of analysis of plutonium isomer data on the present scheme are presented in Table VI. The remarks given above Table IV are relevant to this table also.

The data referred to in Table VI do not exhaust the available experimental information on excitation functions of plutonium shape isomers. The 8.5 μsec isomer of ^{239}Pu has been observed by the ^{240}Pu(γ, n) reaction (Gangrskii *et al.*, 1973). The nature of the energy dependence of the bremsstrahlung source adds a further complication to the analysis of this kind of reaction. From their analysis Gangrskii *et al.* report a number of values of E_{II} ranging around 3.0 MeV, and therefore in qualitative agreement with the value given in Table V. The photoneutron reaction has also been used to investigate the excitation of the 24 μsec isomer of ^{241}Pu (Gangrskii *et al.*, 1970). In this case the ratio of delayed fission to prompt fission (>10^{-3} at maximum bremsstrahlung energy of 12.5 MeV) seems very high. The isomer energy is given as 2.9 MeV for a nuclear level density temperature of 0.7 MeV.

c. Curium shape isomers

The principles for analysis of curium isomer data are the same as those described for the plutonium isomers. In the curium case much of the evidence rests on three-neutron evaporation data, so a typical example of this, for excitation of the ^{245}Cm isomer, is shown in Fig. 74. Here the fit is for an energy-gap model as described in Sec. IV.D.3. *b* with temperatures $\theta_1 = 0.83$ MeV, $\theta_2 = 0.63$ MeV, $\theta_3 = \theta_3^{(s)}$ (above the energy gap) $= 0.5$ MeV. The isomer energy $E_{II} = 2.1$ MeV, and with the assumption $P_{3n}/P_f = 0.06$ it turns out that $V_A - V_B$

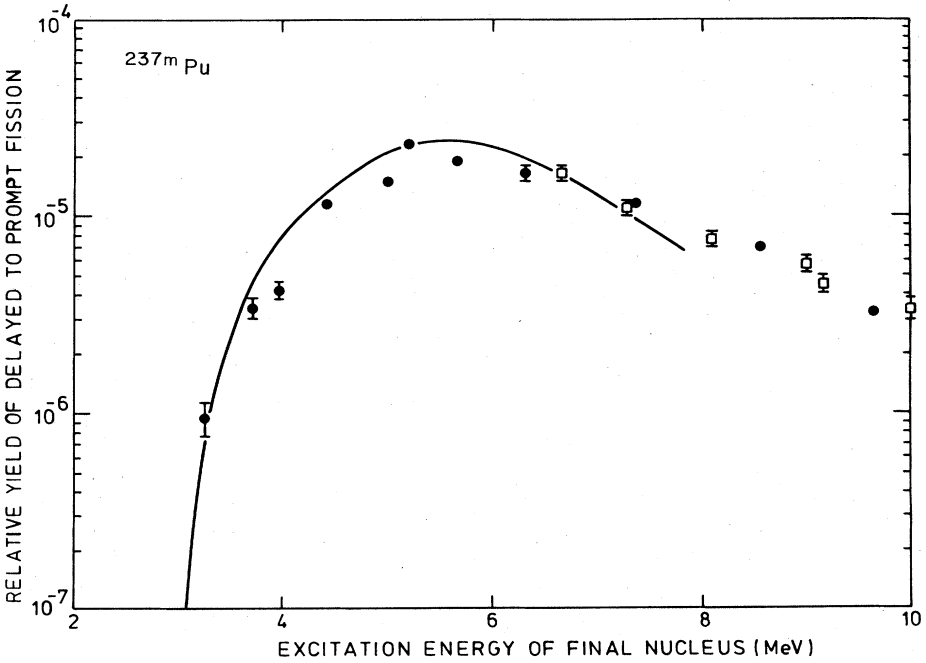

FIG. 73. Excitation of the 0.11 and 1.1 μsec isomers of ^{237}Pu. Circles are the ^{235}U$(\alpha, 2n)$ reaction and squares the ^{237}Np$(d, 2n)$ reaction. [From Britt *et al.* (1971)].

TABLE VI. Double-barrier parameters of plutonium nuclei as deduced from shape isomer excitation functions.

Nuclide	Reaction data	Ref.	E_{II} (MeV)	V_A (MeV)	V_B (MeV)	Remarks
^{241}Pu	^{238}U(α, $2n$)^{240m}Pu	Britt *et al.* (1971) Namboodiri *et al.* (1973) Gangrskii *et al.* (1972)		6.14	~5.4	±0.5 MeV uncertainty depending on value of E_{II} selected for ^{240}Pu. Note data of 2nd ref. ~60% lower than that of 1st
^{240}Pu	Ditto ^{238}U(α, $3n$)^{239m}Pu	Ditto Britt *et al.* (1971) Wolf and Unik (1972)	~2.3	5.57	~5.0	±0.5 MeV uncertainty
^{239}Pu	Ditto ^{236}U(α, $2n$)^{238m}Pu	Ditto Limkilde and Sletten (1973)	2.7	6.26	(5.2) 5.6	
^{238}Pu	Ditto	Ditto	2.7		(~5.0)	
	^{235}U(α, $2n$)^{237m}Pu ^{237}Np(d, $2n$)^{237m}Pu	Britt *et al.* (1971)		5.5	4.9	
	^{236}U(α, $3n$)^{237m}Pu	Wolf and Unik, see Britt *et al.* (1972)			~4.6	V_B deduced for E_{II} of ^{237}Pu = 2.8 MeV
^{237}Pu	^{235}U(α, $2n$)^{237m}Pu ^{237}Np(d, $2n$)^{237m}Pu	Britt *et al.* (1971)	2.8		(5.3)	
^{236}Pu	^{233}U(α, $2n$)^{235m}Pu	Britt *et al.* (1971)		~5.2	~4.5	
^{235}Pu	Ditto	Ditto	2.6		(5.1)	±0.3–0.5 MeV uncertainty

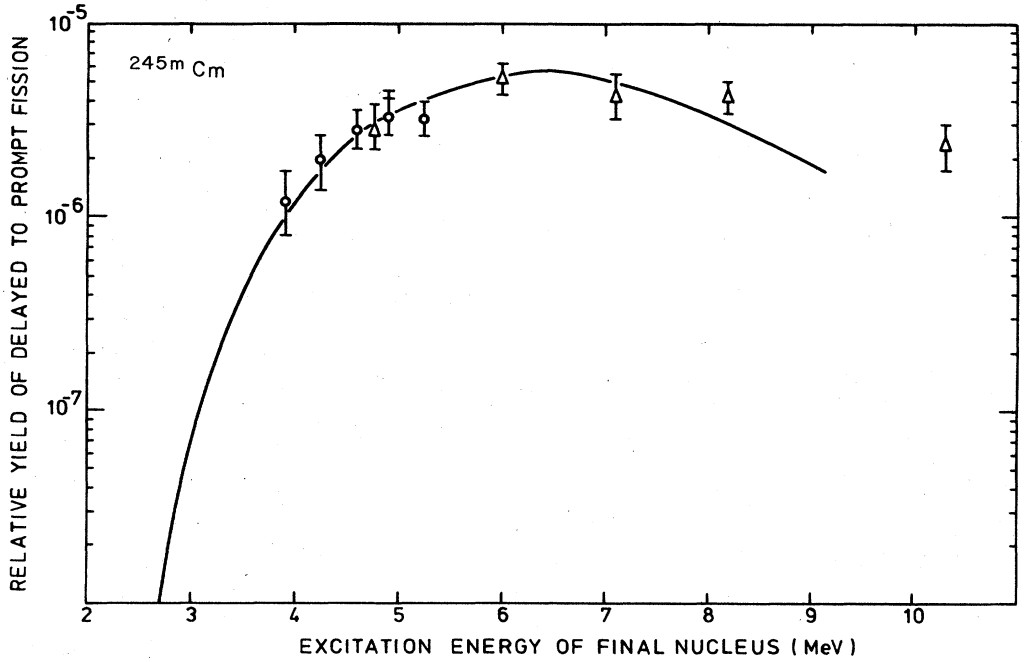

FIG. 74. Excitation of the 13 nsec isomer of ^{245}Cm by the ^{244}Pu(α, $3n$) reaction; circles are from Britt *et al.* (1971); and triangles are results of Wolf and Unik (1972), communicated privately to Britt *et al.* (1971).

~1.6 MeV for ^{246}Cm.

Collected double-barrier parameters for curium nuclei are given in Table VII. The deductions obviously have very great uncertainties associated with them, but the trend, in comparison with Pu and Am isomers, is clear; both the E_{II} values and the V_B values are considerably lower than the correspondingly values for the lower-Z nuclei.

d. Shape isomers of other nuclei

While shape isomers of nuclei other than the isotopes of Pu, Am, and Cm are known, and in some cases their excitation functions have been measured, these do not add significantly to the body of systematic quantitative information on barrier parameters assembled in Tables V to VII. This is for a variety of reasons; in some cases the data are too limited in range to provide reliable estimates of such quantities as the isomer energy, in other cases information is lacking on other nuclear parameters (such as neutron evaporation probability), sometimes the isomer formation results from a reaction chain that involves charged particle emission and is thus of a predominantly direct or preequilibrium character, and finally, for nuclei of lower charge than plutonium, it is believed that the isomer may have a significant branching ratio for decay by gamma emission (cascading through class-I states associated with the primary well). These "nonsystematic" cases are dealt with below.

(*i*) *Berkelium isomers.* Three fission isomers of Berkelium have been reported by Wolf and Unik (1972). Two having half-lives of 600 and 9.5 nsec belong to ^{242}Bk, and the third, half-life 820 nsec, belongs to ^{244}Bk. All are excited by the $(\alpha, 3n)$ reaction. Excitation curves have been measured by these authors, but the cross sections are low and the range of the data is too limited for reliable analysis. The yields are about 1 order of magnitude (or more) lower than those of similar reactions leading to isomers of Pu, Am, and Cm. Although part of this factor may be accounted for by greater fissionability in the berkelium chains, the results do seem to provide qualitative evidence for a continued decrease in both isomer energy and outer barrier height with the extra increase in proton number.

Isomers of ^{243}Bk (5 nsec) and ^{245}Bk (2 nsec) have been reported by Gangrskii *et al.* (1972). These were formed by $(\alpha, 2n)$ reactions and very low cross sections of 0.48 and 0.25 μb, respectively, were measured.

(*ii*) ^{236}U. Several observations have been made of this spontaneously fissioning isomer, the most precise value of the half-life of which has been quoted as 116 ± 7 nsec (Christiansen *et al.*, 1975). The reactions used to investigate it have been ^{235}U(d,p), ^{235}U(n,γ) (for both thermal neutrons and fast neutrons up to ~2 MeV), and ^{236}U(d,pn). All except the fast neutron reactions, for which there are special experimental difficulties, agree in establishing the cross section for delayed fission to be rather low. Christiansen *et al.* (1975) report the ratio of delayed fission yield to prompt fission to be $(1.24 \pm 0.6) \times 10^{-5}$ at deuteron energy 11 MeV, Britt and Erkilla (1971) report $(8.7 \pm 1.3) \times 10^{-5}$ for the same quantity at 12 MeV, and Wolf *et al.* (1970) give the isomer ratio (relative to formation of the ground state) as 1.3×10^{-5} at 13 MeV deuteron energy. Wolf *et al.* (1970) also measured the isomer ratio for the ^{236}U(d,pn) reaction at 21 MeV deuteron energy; the result quoted is 9×10^{-5}, whereas a value of more than 10^{-3} might have been expected for a shape isomer at about 3 MeV excitation energy.

Probably the most detailed study of the formation of the ^{236}U shape isomer has been carried out by Pedersen and Rasmussen (1972). This was also a study of the (d,p) reaction but the delayed fission was measured in coincidence with the proton energy (at deuteron energy of 11 MeV), and thus the delayed fission cross section was established as a function of excitation energy in ^{236}U. The data were analyzed by Pedersen and Rasmussen on the assumption that class-I states were excited by the (direct) (d,p) reaction and these could decay by gamma emission to the isomer, or by prompt fission, by coupling to class-II states (for a discussion of the theory of this coupling, see Sec. III. C.5). Assumptions of either complete damping of class-II vibrational states into the class-II compound states, or of only partial damping, could lead to reasonable reproduction of the observed coincidence spectrum (see Fig. 75), using the following barrier parameters: $\upsilon_A = 6.1$ MeV, $\hbar\omega_A = 1.0$ MeV, $\upsilon_B = 5.8$ MeV, $\hbar\omega_B = 0.7$ MeV, and a reasonable spectrum for the low-lying barrier states. With these same parameters the total cross section for formation of the isomer was estimated to lie between 6 and 20 μb, whereas the observed cross section for delayed fission was only 1.0 ± 0.5 μb. The discrepancy suggests that the γ-decay branch of the isomer (through low-lying class-I

TABLE VII. Double-barrier parameters of curium nuclei as deduced from shape isomer excitation functions.

Nuclide	Reaction data	Ref.	E_{II} (MeV)	υ_A (MeV)	υ_B (MeV)	Remarks
^{246}Cm	^{244}Pu$(\alpha, 3n)^{245m}$Cm	Britt *et al.* (1971) Wolf and Unik (1972)		5.65	4.05	
^{245}Cm	Ditto	Ditto	2.1		(4.6)	
^{244}Cm	^{242}Pu$(\alpha, 3n)^{243m}$Cm	Ditto		5.8	4.3	
^{243}Cm	Ditto	Ditto	1.9		(4.4)	
^{242}Cm	^{239}Pu$(\alpha, 2n)^{241m}$Cm	Britt *et al.* (1971)		6.0	~4.0	~±0.5 MeV uncertainty
^{241}Cm	Ditto	Ditto	2.1		(~4.3)	Ditto

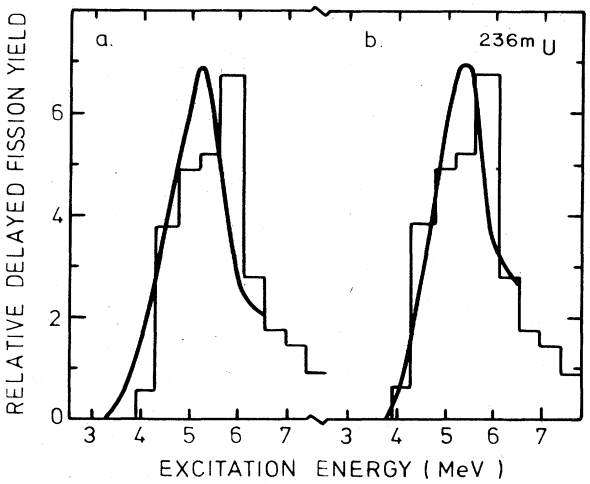

FIG. 75. Relative delayed fission yield (measured in coincidence with proton yield from the d,p reaction) of ^{236}U (histogram). Part (a) shows calculation of yield assuming complete damping of class-II vibrational states into class-II compound states, and part (b) is a calculation for partial damping [from Pedersen and Rasmussen (1972)].

states) is about 1 order of magnitude stronger than the fission branch, and this is qualitatively supported by the results of the other measurements referred to above.

(iii) ^{238}U. A spontaneously fissioning isomer of ^{238}U with half-life ~200 ns has been observed by means of the (d,pn) reaction (Polikanov and Sletten, 1970; Wolf *et al.*, 1970) and the (n,n') reaction [Wolf and Meadows (1974) and private communication]. Cross sections for the first reaction are quoted as 0.4 μb at deuteron energy of 13 MeV and a few μb at 21 MeV. The excitation curve for the (n,n') reaction is shown in Fig. 61; its analysis by use of Eqs. (4.12), (4.23), and (4.25), yields an isomer energy of ~2.3 MeV and an outer barrier height of ~4.5 MeV for ^{239}U (assuming $\upsilon_A = 6.4$ MeV; see Sec. VII). This outer barrier appears to be very much lower than its assessment from other evidence (Secs. VI and VII), and the isomer therefore appears to be a candidate, like ^{236}U, for appreciable competition from a gamma-decay branch. Direct observation of this branch has been made by Russo *et al.* (1975) using the (d,pn) reaction at a deuteron energy of 18 MeV; see Fig. 48 and Sec. IV.B.1. This gamma-ray transition scheme establishes the isomer excitation energy as 2.559 MeV. There is conflict here with the results from the (n,n') reaction (see Fig. 61). The simple temperature model fit shown in that diagram gives $E_{II} = 2.35$ MeV, and with a higher temperature fit Wolf and Meadows (private communication) obtain $E_{II} = 2.0$–2.2 MeV; this rests strongly on the experimental separation of the two lowest points of the curve from background. If these two points are ignored then the data can be fitted rather well with a more elaborate model that represents the states within the energy gap as rotational bands based on the ground state and one or two vibrational states, plus a normal exponentially rising continuum of states above the gap. The full curve of Fig. 61 is based on an isomer excitation energy of $E_{II} = 2.56$ MeV.

The observations of Russo *et al.* are supported by measurements of the nuclear radiative decay of muonic atoms of ^{238}U (Fromm *et al.*, 1977). These authors interpreted a group of gamma rays with decay half-life 9 ± 2 nsec as feeding the low-lying vibrational and rotational states of ^{238}U from an isomeric state at 3.176 MeV. They accounted quantitatively for the shortened half-life and increased energy relative to the observations of Russo *et al.* by the distortion of the fission barrier due to the energy shift of the bound muon.

(iv) ^{237}Np. Despite many attempts and some false attributions later retracted, it was not until 1973 that reliable evidence for the existence of a spontaneously fissioning isomer in any neptunium isotope was published. The isomer then reported was found to have a half-life of 40 ± 12 nsec and belong to ^{237}Np (Wolf and Unik, 1973). The reaction employed was ^{238}U$(p,2n)$, and the excitation curve is shown in Fig. 76. The curve fitted by Wolf and Unik, using Eq. (4.16) for a simple single temperature model, gives an isomer energy of 2.7 ± 0.3 MeV. An energy-gap model, as described in Sec. IV.D.1.*d.*, gives an E_{II} value in the range ~1.5–2.8 MeV. The ratio of the cross sections for delayed fission to prompt fission is the lowest ever measured, and if this were interpreted simply as a measure of the value of $T_A/(T_A + T_B)$ for ^{238}Np it would imply an outer barrier several MeV below the intermediate barrier. It is clear from the evidence of intermediate structure in the neutron-induced fission cross sections of ^{237}Np that this cannot be so (see Sec. VI.E.3.*c.*). It is inferred therefore that this isomer has a very strong gamma decay branch through class-I states, and that the branching ratio for fission is only of the order of 10^{-3} (for E_{II} ~ 2.8 MeV). The existence of this isomer has been confirmed by Migneco *et al.* (1977), who measured a half-life of 45 ± 5 nsec and an excitation energy of 2.85 ± 0.4 MeV, and deduced a branching ratio of 1.9×10^{-3}.

e. Summary of barrier information from isomer excitation functions

The properties of the double-humped barrier deduced from the measured excitation functions are summarized in Table VIII for the Pu, Am, and Cm isomers. This is a comparison of the results of three independent sets of

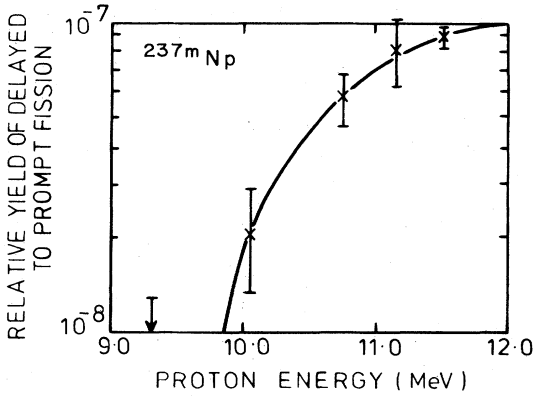

FIG. 76. Excitation of the ^{237}Np shape isomer by the ^{238}U$(p,2n)$ reaction [after Wolf and Unik (1973)]. The curve shown is Wolf and Unik's fit for $E_{II} = 2.7$ MeV.

analyses. In Table VIII the values of V_A that are employed to deduce outer barrier heights, but are themselves generally deduced from other information, are shown in the first three columns. The column labeled by the figure (3) lists our own recommendations as discussed in Sec. VII. The column labeled (1) lists the more crudely assessed values of V_A (generally from the same experimental sources, such as fast neutron fission cross sections (d,pf) yields, etc., as used in the work of Britt *et al.* (1971), in which a systematic effort to analyze the excitation data on many isomers was first made. The column labeled (2) is from the analysis by Britt *et al.* (1973) in which all the relevant data (fission cross sections as well as isomer excitation functions) were analyzed using a computation of level densities (both at barriers and in the potential mixing) based on the single-particle level schemes calculated by Bolsterli *et al.* (1972); this was an approach distinct from the earlier one, which employed the empirical level density parameters of Gilbert and Cameron, and in many cases it appears that the V_A values differ appreciably from the values either recommended by ourselves or quoted by Britt *et al.* (1971). This could be due in part to the fact that the level densities calculated by Britt *et al.* (1973) contain no enhancement factor to allow for the collective states (particularly the rotational bands) built on the independent quasiparticle states of that calculation, and therefore do not allow for the variations in these rotational enhancement factors with the changing asymmetry in nuclear shape that follows changing nuclear deformation [Bjørnholm *et al.* (1974); see Sec. VII].

The next three columns give the values of the shape isomer excitation energy E_{II} for E_s as deduced from the measured excitation functions. The numerals (1), (2), and (3) have the same connotation as above. The final three columns give the information on outer barrier heights deduced from the excitation functions and the values of V_A listed in the relevant one of the first three columns. Again, in both sets of numbers there is very considerable variation, by up to 0.5 MeV for the E_{II} values and in some cases even more for the V_B values. In general, there is rather close agreement between the E_{II} values of Britt *et al.* (1971) and ourselves [columns labeled (1) and (3)], but there seems to be better agreement on the V_B values between Britt *et al.* (1973) and ourselves [columns labeled (2) and (3)]. These differences can be taken as a measure of the uncertainty still remaining in our knowledge of these barrier parameters.

TABLE VIII. Barrier parameters deduced for plutonium, americium, and curium nuclides with the aid of shape isomer excitation data. Numbers in columns labeled (1) are from Britt *et al.* (1971), in columns labeled (2) from Britt *et al.* (1973), and in columns labeled (3) the results from our analysis are presented.

	V_A (MeV)			E_{II} (MeV)			V_B (MeV)		
Nuclide	(1)	(2)	(3)	(1)	(2)	(3)	(1)	(2)	(3)
^{235}Pu	5.8	(4.7)		2.4	1.7	2.6	5.0	4.6	(5.1)
^{236}Pu		(5.04)	~5.2						~4.5
^{237}Pu	5.8	(5.27)		2.9	2.3	2.8	5.4	5.4	(5.3)
^{238}Pu		(5.26)	5.5		2.4	2.7		5.35	4.9
^{239}Pu	5.8	(6.27)	6.3	2.6	2.2	2.7		5.15	5.6
^{240}Pu	5.8	(6.00)	5.6	2.6	2.4	~2.3	5.35	5.35	~5.0
^{241}Pu		(5.95)	6.1	2.6					~5.4
^{237}Am	6.4	(5.09)		2.4	2.1	2.4		4.8	(~5.0)
^{238}Am	6.4	(6.4)	~6.2	2.7	2.3	2.6		5.4	(~5.0)
^{239}Am	6.4	(5.8)	6.0	2.5	2.5	2.4	5.4	4.65	~4.5
^{240}Am	6.4	(6.45)	6.5	3.0	2.6	3.0	6.05	5.5	5.2
^{241}Am	6.4	(5.7)	6.2	2.2	2.2	2.2		4.55	5.3
^{242}Am	6.4	(6.4)	6.5	2.9	2.3	2.9	6.0	4.95	5.3
^{243}Am		(5.75)	6.3		2.0	2.3		4.9	5.5
^{244}Am		(6.25)	6.4			2.8			5.3
^{245}Am			6.1						5.2
^{241}Cm	6.2	(5.05)		2.3	2.0	2.1	5.0	4.2	(~4.3)
^{242}Cm			6.0						~4.0
^{243}Cm	6.2	(5.8)		2.0	1.5	1.9	4.8	4.0	(4.4)
^{244}Cm			5.8						4.3
^{245}Cm	6.2	(6.3)		2.4	1.7	2.1	4.9	4.4	(4.6)
^{246}Cm			5.7						4.1

V. VIBRATIONAL RESONANCES IN FISSION CROSS SECTIONS

A. Introduction

Structure in fast neutron-induced fission cross sections had been observed at a compartively early stage in fission physics. For example, unpublished measurements at Los Alamos dating from about 1950 show clear structure in the fission cross section of ^{232}Th for neutrons above 1 MeV energy (see Fig. 77). This structure certainly had nothing to do with resonance fine structure, the energy resolution of these measurements being about 4 orders of magnitude coarser than the expected resonance fine spacing. First published explanations[3] of the effect were based on an extension of A. Bohr's (1956) ideas of channels over the fission barrier for the fission process (see Sec. I.B). The simple Hauser–Feshbach (1952) type of expression, based on the statistical theory of nuclear reactions, for the fission cross section is

$$\sigma_{cF} = \sigma_{c\,(CN)} \frac{T_{(f)}}{\sum_{c'} T_{(c')}} \,. \tag{5.1}$$

The compound nucleus formation cross section $\sigma_{c\,(CN)}$ is itself proportional to the transmission coefficient for the entrance channel c [see Eq. (3.41)]. The fission transmission coefficient $T_{(f)}$ is the sum over all Bohr fission channels μ, and the sum in the denominator is taken over all particle and fission channels. From Eq. (5.1) it is easily seen that the fission cross section will rise as a distinct fission channel opens in accordance with an expression such as Eq. (3.17) or (3.18) and tends to an asymptotic value (modulated only by the assumed gentle energy variation of $\sigma_{c\,(CN)}$ as the opening becomes complete, only to fall after an inelastic scattering threshold for a particle channel c' is crossed.

At later dates structure was also found in the fission yield of certain (d,pf) reactions. In this reaction the proton energy following the deuteron stripping process

[3]The original explanation appears to have been due to Mottelson (unpublished) but was developed and popularized by Wheeler (1956).

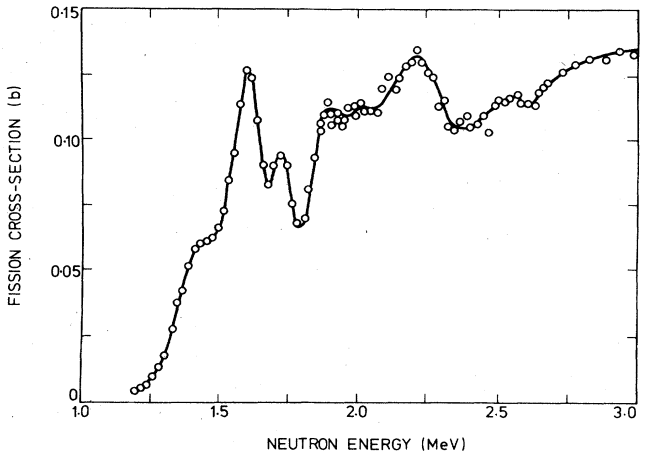

FIG. 77. Neutron-induced fission cross sections of ^{232}Th. From Henkel and Smith (1956).

is measured so that the excitation energy of the resulting fissioning nucleus is known. The reaction is particularly useful for observing fission in the barrier region of even compound nuclei in which the barrier lies below the neutron separation energy. In this situation the only competition against the fission process is the electromagnetic deexcitation and it has a very weak energy dependence without structure. Early observations of the structure (Northrop *et al.*, 1959) suggested a series of steps and plateaus, and these were explained as the effect of the initial channel opening for a set of states of particular spin and parity. Later observations (Britt *et al.*, 1968) showed that some of these "plateau" levels really dipped with increasing excitation, and the explanation was advanced that this was due to structure [probably residual single particle effect (Specht *et al.*, 1966)] in the (d,p) formation probability for states of the same spin and parity as the opening fission channel.

Changes in the angular distributions of fission products with changing excitation energy in such reactions were also held to be manifestations of the channel structure of the fission barrier [see, e.g., Huizenga (1965)].

Later observations and more quantitative analysis, particularly of the structure in fast neutron-induced fission cross sections, showed such explanations to be virtually untenable. The principle evidence came from measurements of the fission cross section of ^{230}Th (Gokhberg *et al.*, 1959b, Evans and Jones, 1965). This showed a distinct peak in the cross section at a neutron energy of 720 keV; in the higher resolution measurements of Evans and Jones the peak cross section was observed to be about four times higher than the minimum value at higher neutron energy (see Fig. 8). At these comparatively low neutron energies for bombardment of an even target nucleus, there is only a very limited possibility of inelastic scattering thresholds. On the basis of very plausible assumptions about the residual states in ^{230}Th for inelastic scattering, it was computed on the competition theory (Lynn, 1966) that the fission cross section should only drop at most some 10% below the peak value (see Fig. 78); the peak in this curve was clearly a resonance effect of some kind. An analysis of the peaks in the fission cross section at higher neutron energies (~1.4 MeV) in the cross section of ^{232}Th showed that there would have to be a very strong onset of states in ^{232}Th above 1.5 MeV for them to be explained by the channel competition theory; the density of states above this energy would have to increase at a rate about five times greater than acceptable on current knowledge of level densities, and it was also established experimentally (Holmberg *et al.*, 1969) that no strong onset of inelastic scattering occurred at that energy.

Channel analysis of angular distributions of the fission products released in fast neutron-induced fission had fallen into similar difficulties. Sharp changes in the angular distribution with changing neutron energy were attributed to new fission channels opening but an attempt at quantitative analysis for the ^{234}U target nucleus by Vandenbosch (1967) showed that the various channels would need to have very different tunneling characteristics ($\hbar\omega$ ranging from 12 keV to ~1.5 MeV).

It was apparent therefore that intermediate reson-

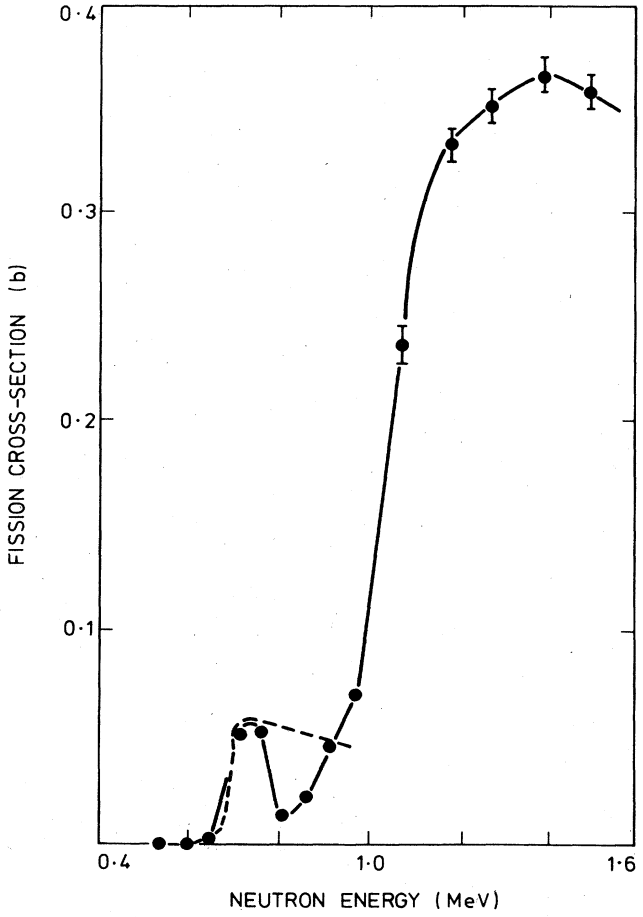

FIG. 78. Neutron-induced fission cross-section of ^{230}Th [data of Evans and Jones (1965)]. Calculations of the fission cross sections on the assumption that any structure is due entirely to single barrier penetration and competition from inelastic scattering; the K^{π} value of the fission channel was assumed to be $\frac{7}{2}^-$, fission following excitation by neutron f waves.

ance effects existed in the fission transmission coefficient, the structure not being attributable to the neutron entrance channel, since no sign of systematically related structure existed in other fast neutron reactions on these nuclei. An optical model of the inverse fission process was introduced (Lynn, 1966a), the variable of the complex potential well being the prolate deformation parameter, and this served to show that the imaginary component of such a potential would have to be of the order of 50 keV or less to obtain resonance effects in the fission mode transmission coefficient as strong as those observed. Contrasted with the imaginary potential value of a few MeV routinely found in optical model analyses of nucleon scattering data, this suggested surprisingly weak coupling of the deformation mode with the compound nucleus motion, and raised a number of questions. One of these was, why was there no suggestion of such structure in the slow neutron cross sections of fissile nuclei (particularly in the fine-structure resonances where the fission widths appeared to show the characteristic features of strong mixing into the compound nucleus). Another important question was raised by the stipulation that the resonant mode in such a model should be a many-phonon beta vibration; the zero-point vibration and one-phonon beta state are well known in the nuclear spectroscopy of even nuclei, but the higher beta vibrations have never been observed, suggesting that they may be quite appreciably damped by coupling with the other degrees of freedom of the compound nucleus.

The theoretical work of Strutinsky introducing the double-humped fission barrier of the actinide nuclei provided answers for these questions. The weakly damped beta-vibrational states responsible for the resonance structure in the fission transmission coefficient could be explained, not indeed as a many-phonon state in the oscillator well centered on the normal beta deformation associated with the nuclear ground state, but as a few-phonon state oscillating about the mean deformation value of the secondary well. The weak damping observed is due to the combination of the low effective excitation energy available in the secondary well and the inhibition provided by the intermediate barrier. When this barrier is energetically overcome, as it is for the slow neutron cross sections of the fissile nuclei, there is a dramatic increase in the mixing of this special vibrational state into the normal states of the compound nucleus, and the broad resonance features in the fission transmission coefficient largely disappear. In this picture, the dramatic changes in angular distribution of fission products with changing excitation energy that are often observed are due more to the dominance of individual vibrational resonances, each associated with spin-parity quantum numbers given by coupling with simple states in the other degrees of freedom (single-particle, gamma vibrations, rotations, etc.), rather than the opening of fresh fission channels at the barrier. The "steps" in the fission probability curves measured from (d,pf) and similar reactions are now also largely understood as vibrational resonances, rather than the energies at which the lowest channel of each spin and parity become effectively open at the barrier (see also Sec. IX, Fig. 152).

B. Pure vibrational resonances

1. Definition as barrier transmission resonances

When there is no damping of the vibrational motion by the other degrees of freedom, the vibrational resonances can be treated by the simple transmission theory of Sec. III.A.2. The fission transmission coefficient to be substituted in the cross section, Eq. (5.1), is calculated directly from the flux transmitted through the double-humped barrier if an incident wave of unit flux progressing from low to higher deformation is incident on the barrier. It is found for a symmetric barrier that the narrow peaks in the transmission coefficient reach a value of unity. The resonant condition is given approximately by Eq. (3.21). For a harmonic oscillator form of potential for the secondary well, $\upsilon = \upsilon_{II} + \frac{1}{2}C_{II}\eta^2$, and an inertial parameter independent of deformation this gives the familiar beta-phonon condition $E - \upsilon_{II} = (n+\frac{1}{2})\hbar\omega$. Forms for the transmission coefficient in the region of resonance are given by Eq. (3.23a), and from this it can be shown [Eq. (3.26)] that the resonance width is proportional to the sum of the transmission coefficients T_A and T_B through the inner and outer barrier, respectively, considered as separate entities, and is also proportional to the oscillation frequency between the two barriers:

$$\Gamma \approx (T_A + T_B)\hbar\omega_{II}/2\pi \ . \tag{5.2}$$

The peak transmission at the resonance is

$$T_{res} \approx \frac{4T_AT_B}{(T_A+T_B)^2} \ . \tag{5.3}$$

Between vibrational resonances the transmission reaches a low value of

$$T_{min} \approx \frac{T_AT_B}{4} \ . \tag{5.4}$$

These formulas were first given by Ignatyuk *et al.* (1969).

Examples of calculated transmission curves have been shown in Figs. 31 and 34. These certainly bear a close qualitative resemblance to the best experimental examples of vibrational resonances (cf. the neutron fission cross section of ^{230}Th, Fig. 6). Considerable use has been made of the simple transmission theory in analyzing such data. A typical early attempt is to be found in the paper of Britt *et al.* (1969) in which the fissioning compound nucleus ^{240}Pu is studied. An indication of a resonance at about 5 MeV excitation energy in the fission transmission coefficient of this nucleus had been noticed in the (d,pf) reaction (Britt *et al.*, 1968; Wolf *et al.*, 1968). This was investigated further by means of the ^{240}Pu$(p,p'f)$ reaction in which the reappearance of the resonance confirmed that it was associated with the fission exit channel and not the entrance channel as first suggested by Pedersen and Kuzminov (1969). The energy variation of the fission yields in both reactions could be reasonably well reproduced by the transmission model, if allowance is made for resolution broadening or damping of the resonance (Back *et al.*, 1969, 1971). The basic vibrational res-

onance was deduced to be at an excitation of 4.91 MeV in a double-humped barrier with $\upsilon_A = 5.95$ MeV, $\hbar\omega_A = 1.3$ MeV, $\upsilon_{II} = 2.1$ MeV, $\hbar\omega_{II} = 2.00$ MeV, $\upsilon_B = 5.25$ MeV, $\hbar\omega_B = 0.48$ MeV (these parameters should be compared with those in Sec. V.C.4.*a*). These parameters also reproduce reasonably well the spontaneous fission half-lives of the ground state of ^{240}Pu (7×10^{12} y) and its shape isomer (4 nsec). Later experimental work has shown the 5 MeV resonance to have considerable substructure (Specht et al., 1969; Glässel et al., 1976; see Sec. V.C.4.*a*). This can be explained as simple coupling to excited intrinsic states (see Sec. V.B.2) or (more likely) as evidence for damping of the vibrational resonance; this is treated in Sec. V.C.2.

Another example of the use of the transmission theory is provided by analysis of sub-barrier photofission of ^{238}U (Alm *et al.*, 1974). The fission yield for asymmetric fission is shown in Fig. 79. Because of the nature of the incident bremsstrahlung gamma-ray spectrum structural features are not strongly pronounced but the inflexion at around 5 MeV maximum gamma-ray energy does indicate a strong resonance feature. Comparison of barrier models with the experimental data is made by calculating the expression for photofission yield,

$$Y(E_{\gamma,\max}) \propto \int_0^{E_{\gamma,\max}} dE_\gamma \sigma_{\gamma(CN)} \frac{T_{(f)}}{\sum_{c'} T_{(c')}} n(E_\gamma, E_{\gamma,\max}) \tag{5.5}$$

embodying the Hauser–Feshbach expression for the photofission cross section [see Eq. (5.1)] and the bremsstrahlung spectrum yield $n(E_\gamma, E_{\gamma\max})$ of photons of energy E_γ from incident electrons of energy $E_{\max}$. In the photofission cross-section calculation photons of electric dipole character dominate, exciting compound nucleus states in ^{238}U of spin and parity $J^\pi = 1^-$. The photofission cross section that fits the data is shown in Fig. 80; it includes weak quadrupole fission. Below the neutron emission threshold at 6.14 MeV in ^{238}U, gamma-ray emission is the only process competing with fission. The barrier parameters found for the fission transmission coefficient are $\upsilon_A = 6.1$ MeV, $\hbar\omega_A = 1.0$ MeV, $\upsilon_B = 6.05$ MeV, $\hbar\omega_B = 0.9$ MeV, $\upsilon_{II} = 2.9$ MeV, $\hbar\omega_{II} = 3.2$ MeV. These barrier heights for ^{238}U are about 400 keV higher than those deduced from analysis of other data (see Sec. VII); this is expected for the inner barrier since the 1^- channel will be somewhat above the 0^+ channel defining the barrier, but at the reflection-asymmetric outer barrier the 1^- channel should be much closer to the barrier peak. The discrepancy may be accounted for by the high value of $\hbar\omega_B$ adopted in the above analysis.

Indications of vibrational resonances at much lower energies have been found by Zuchko *et al.* (1978b) in the photofission of ^{238}U and ^{236}U (see Figs. 128 and 161).

2. Barrier transmission resonances coupled with excited intrinsic states

It is to be expected that fission cross-section or yield curves should show considerably more structure, though probably on a satellite scale, than that apparent in a

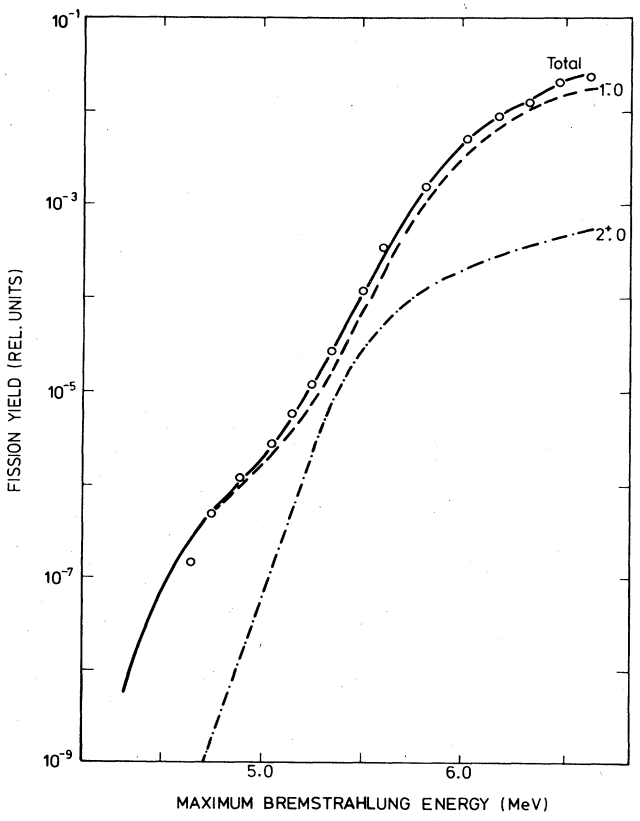

FIG. 79. Points, measured sub-barrier photofission yield for asymmetric fission of ^{238}U as a function of the end-point energy of the bremsstrahlung spectrum. The full line is a calculated yield curve composed of a dipole fission contribution (dashed curve) and a quadrupole contribution (dot-dashed curve). From Alm *et al.* (1974).

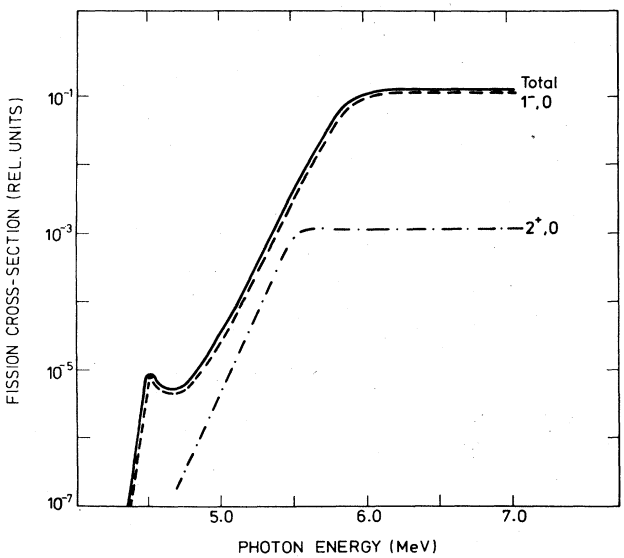

FIG. 80. Calculated photofission cross sections as in Fig. 79, but here plotted directly as a function of the photon energy. This makes the resonance structure near 4.5 MeV readily visible. From Alm *et al.* (1974).

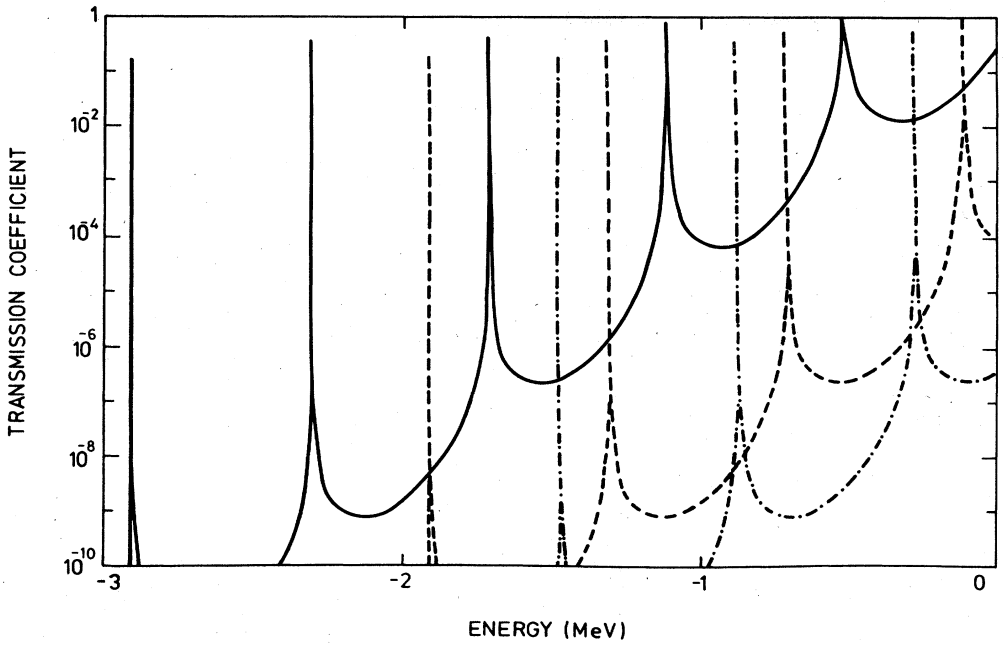

FIG. 81. Schematic energy dependence of fission transmission coefficient allowing for excitation in the intrinsic degrees of freedom (uncoupled to the fission mode). Two intrinsic excitations are shown, with 1 MeV excitation (--- curve) and 1.5 MeV excitation (-·-·- curve).

simple transmission curve such as Fig. 31. Such a transmission curve completely ignores all degrees of freedom other than the deformation mode, whereas it should be interpreted as the transmission curve for all intrinsic degrees of freedom in the lowest state of excitation. If the intrinsic degrees of freedom are in an excited state, a corresponding fission transmission coefficient will exist, similar to the original one but raised in energy by an amount equal to the intrinsic excitation; this is shown schematically in Fig. 81. Ultimately there will be an infinite superposition of such curves constituting the total fission transmission coefficient, but the structure of all but the lowest of these will be lost at energies not far above the barrier among the high, structureless contributions from the lowest intrinsic excitations. Below the barrier the extra resonances that occur will be much narrower than those related to the lowest one or two intrinsic states, and will normally be suppressed by experimental resolution. This picture assumes, of course, that within the entire barrier region there is no mixing between the deformation and intrinsic degrees of freedom.

Evidence for the coupling of higher intrinsic states with vibrational resonances is sparse. The most thoroughly investigated example is the fission cross section of ^{230}Th in the neutron energy range 0.7–1.4 MeV (James *et al.*, 1972). In this case the vibrational resonances coupled to different intrinsic excitations are hardly at all resolved, but the main peak of 720 keV has been interpreted as a superposition of vibrational resonances each comprising a vibrational state coupled to a member of a rotational band, while in the region of the rising cross section around 1 MeV the strong change in angular distribution of fission products is inferred as a vibrational state coupled to an intrinsic excitation of different single-particle character from that in the 720-keV resonance. The ^{230}Th cross section and analysis is discussed in greater detail in Sec. V.B.5.*a*).

The fission cross section of ^{231}Pa (Muir and Veeser, 1971) shows structure that appears complicated enough to demand an explanation based on at least a few intrinsic states. Much improved measurements of this cross section (higher energy resolution, better angular distributions) are desirable to enable a careful analysis to be made; studies by Sicre *et al.* (1976, 1979) have gone a considerable way to meeting this need.

Some early attempts at analysis of the (d, pf) resonance found at 5.0 MeV excitation energy in ^{240}Pu were also based on the idea of a pure transmission resonance with satellites representing coupling to intrinsic states (Back *et al.*, 1969). In the measurements reported in this paper structure was observed on the high-energy side of the resonance. This could be qualitatively reproduced with a rotational band of intrinsic states carrying spin-projection quantum number $K^\pi = 0^+$, while subsidiary structure at a slightly higher energy was ascribed to a $K^\pi = 1^-$ (bending vibration) rotational band. Barrier parameters for the model were $\upsilon_A = 6.0$ MeV, $\hbar\omega_A = 1.3$ MeV, $\upsilon_B = 5.8$ MeV, $\hbar\omega_B = 1.3$ MeV, $\upsilon_{II} = 2.3$ MeV, $\hbar\omega_{II} = 2.0$ MeV. The intermediate barrier height is very similar to that of Britt *et al.* (1969) but the outer barrier parameters are rather different. Our assessment (see Sec. VII) is a few hundred keV lower, but again penetrability parameters ($\hbar\omega_A$, $\hbar\omega_B$) are also considerably lower.

3. Formal definition of vibrational states in R-matrix theory

The comprehensive formal reaction theory for treating fission cross sections expounded in Sec. III. C.5 includes the special case of pure vibrational resonances. The R-matrix theory described there is based on the concept of eigenstates of the internal region of the reaction system. It was shown that if the fission barrier is of double-humped character the R-matrix internal eigenstates can be constructed from two auxiliary sets of states with only a limited degree of coupling between them. The second set of these states, the class-II states associated with vibrational motion mostly within the secondary well, are largely responsible for governing the magnitude of the fission cross section.

The class-II internal states are defined in Eq. (3.153) in terms of the vibrational and intrinsic wave functions of the components of the Hamiltonian introduced in Sec. III. C.1 [Eqs. (3.64–67)]. It is immediately apparent that a sufficient condition for a class-II state of a pure vibrational nature is that it contains only one term in the expansion (3.153), namely

$$X^{(\mathrm{II})}_{\lambda_{\mathrm{II}}} \approx \chi_\mu \Phi^{(\mathrm{II})}_{\nu(\mu)} \ , \tag{5.6}$$

with eigenvalue

$$E_{\lambda_{\mathrm{II}}} \approx \epsilon_\nu + \mathcal{E}_\mu \ . \tag{5.7}$$

For a physically observable resonance the distribution of energy here should be high for the vibration and low for the intrinsic state. The wave function χ_μ describing the state of motion in the intrinsic degrees of freedom is defined at a fixed value of deformation η_0, generally taken to be the channel deformation close to the outer barrier B. In the case of an absolutely pure vibrational state this choice of deformation is not important, because the coupling term H_c in the Hamiltonian [Eq. (3.67)] must then vanish, implying that the intrinsic term H_{int} is independent of deformation. This can never be completely true of course, or fission would be practically unobservable in particle-induced reactions. There must at least be considerable interaction in the primary well region. It is to be expected in a number of situations that Eq. (5.5) might be very nearly satisfied for intrinsic states defined at a deformation η_0 near the center of the secondary well, but nevertheless the description in terms of a basis defined at the outer or inner barrier might be more fragmented. Thus a nearly pure vibrational state in the configurational sense may not be outstanding in its fission strength. The criteria for the appearance of pure vibrational fission resonances in fission cross sections or yield curves are clearly very tight; they demand the near fulfilment of Eq. (5.6) at both the inner and outer barriers so that the coupling width as well as fission width is maximized. It is to be expected that such resonances will normally be found only at energies equivalent to excitations in the second well that are within the energy gap for even nuclei or that are very close to "ground" in odd-A and odd nuclei. Some numerical studies of models of configuration mixing relating to fission strength are described in Sec. V. C. 1 on damped vibrational states.

Although it is the vibrational factor in Eq. (5.6) that governs the magnitude of the cross section resulting from the class-II internal state, the nature of the intrinsic states entering the expansion is important for special features of the fission process such as the angular distribution of the fission products. Analysis of angular distributions for the observed case of fast neutron-induced fission of ^{230}Th is described in Sec. V.B.5.a.

4. Cross sections in the region of vibrational resonances

With the definition of the vibrational state as a relatively simple type of class-II auxiliary R-matrix state [Eq. (5.6)] all cross-section formulas resulting from coupling this class-II state to the much denser and more complex class-I auxiliary states, associated with normal deformation, to give the complete R-matrix states can be taken over from Sec. III.5. All degrees of coupling strength are possible in principle, but only one—moderately weak coupling—has been reasonably well established by observation; this is the ^{230}Th neutron-induced fission cross section.

The magnitude of the matrix element for the coupling of the vibrational state to the class-I states is given immediately by Eq. (3.161) with $D_{\mathrm{II}} = \hbar\omega_{\mathrm{II}}$ where ω_{II} is the circular frequency of vibrations in the secondary well. The result for the matrix element is

$$\left| \langle X^{(\mathrm{I})}_{\lambda_{\mathrm{I}}} | \, H_c \, | X^{\mathrm{II}}_{\nu_{\mathrm{II}}} \rangle \right| \sim \frac{1}{2\pi} \left(D_{\mathrm{I}} \hbar\omega_{\mathrm{II}} T_A \right)^{1/2} , \tag{5.8}$$

and the coupling width of the Lorentzian profile for admixture of the vibrational states into the complete compound nucleus states is [from Eqs. (3.185), (3.186)]

$$\Gamma_{\nu_{\mathrm{II}}(c)} = 2W \approx \frac{\hbar\omega_{\mathrm{II}}}{2\pi} \, T_A \ . \tag{5.9}$$

The actual profile of fission widths of the fine-structure resonances that appear in fission yields or cross sections of reactions that are initiated by populating the class-I states depends also on the fission width of the vibrational state. The estimate for this is commonly based on the statistical theory methods of Wigner (1938) or Blatt and Weisskopf (1952) [see Sec. I, Eq. (1.9)], giving

$$\Gamma_{\nu_{\mathrm{II}}(f)} \approx \frac{\hbar\omega_{\mathrm{II}}}{2\pi} \, T_B \ . \tag{5.10}$$

This estimate is borne out by numerical computations based on the formal R-matrix expression for the fission width in terms of reduced widths and penetration factor [Eq. (3.126)]. The penetration factor P, along with the shift factor S, can be computed numerically by integrating an outgoing wave in the deformation mode through an inverted harmonic oscillator barrier up to the barrier deformation η_B to determine its logarithmic derivative there (the method is described more fully in Sec. III.C.3.f). The reduced width can be computed by numerical integration of the vibrational wave function in a well composed of normal and inverted harmonic oscillator segments smoothly connected [see Eq. (3.31) in Sec. III. A.2.b], so that it matches the shift factor (taken to be the natural boundary condition ⊛) at η_B; the value of the wave function at η_B gives the reduced width on substitution in Eq. (3.99).

To illustrate the magnitudes involved the following examples may be quoted. A secondary well of depth $\hbar\omega_{II} = 0.7$ MeV and bounded by barriers with $\hbar\omega_A = 0.8$ MeV, $\hbar\omega_B = 0.6$ MeV has eigenvalues (above the zero-point vibration) of −2.45 MeV (for $\mathcal{B} = -38$), −1.75 MeV (for $\mathcal{B} = -32$), −1.07 MeV ($\mathcal{B} = -23.6$), −0.5 MeV ($\mathcal{B} = -13.3$). The reduced width amplitudes γ_ν at the outer barrier deformation are 0.0022, 0.015, 0.097, 0.51, respectively, and the penetration factors P at these energies are 0.0047, 0.048, 0.46, 2.6. These values give fission widths $2P\gamma_\nu^2$ for the vibrational states of 3.8×10^{-11}, 1.8×10^{-8}, 7.2×10^{-6}, and 1.13×10^{-3} MeV, respectively. Comparison with Eq. (5.10) for the fission widths suggests that the latter underestimates the widths of the vibrational states by a factor ranging from about unity for the high-lying states near the top of the fission barrier to about 100 for the states 3 MeV below the barrier.

Depending on the relative magnitude of $\Gamma_{\nu_{II}(c)}$ and $\Gamma_{\nu_{II}(f)}$ with each other and with the class-I (fine-structure) level spacing D_I, different formulas from Sec. III.C.5 are applicable. We summarize them here. If both the coupling width and fission width of the vibrational state are much smaller than the class-I level spacing, then the perturbation formulas, Eqs. (3.165) and (3.166), are applicable to the partial widths that describe the resonance fine structure through the Breit–Wigner formula [Eq. (3.125)] or a many-level formula [Eqs. (3.129)–(3.131) of Sec. III.C.3.*g*]. If the coupling width is much larger than the class-I level spacing and the fission width $\Gamma_{\nu_{II}(f)}$, then the Lorentzian form of Eqs. (3.185) and (3.190) determines the fission widths for the resonance fine structure. The third major case that is likely to occur is the dominance of $\Gamma_{\nu_{II}(f)}$ with respect to both D_I and $\Gamma_{\nu_{II}(c)}$. In this case the fission widths of the fine-structure resonances in the cross section are given by Eq. (3.204) which is essentially identical in form to Eq. (3.185), if the total vibrational width is substituted in the Lorentzian denominator. In intermediate situations ($\Gamma_{\nu_{II}(c)} \sim \Gamma_{\nu_{II}(f)}$) Lorentzian patterns of widths in the fine structure are not expected, even as an average "ideal" representation. Numerical studies of such cases reveal considerable enhancement of the fission widths at the center of the vibrational resonance above the Lorentzian profile. Examples of such patterns can be found in the literature [see, e.g., Lynn (1973)]; see also Sec. VI.E.4.*a*).

No example of resonance fine structure in the cross section through a pure vibrational resonance has yet been observed. Consequently cross-section formulas that describe the local average over the resonance fine-structure are of more immediate interest for analyzing experimental data. If the vibrational state is coupled strongly enough with the fine-structure levels ($\Gamma_{\nu_{II}(c)} \gg D_I$) it is sufficient to find the local variation of the fission strength function $\overline{\Gamma}_{\lambda(\mu)}/\overline{D}_\lambda$ through the vibrational resonance. The extended penetration factor method described in Sec. III.C.4.*d* can be employed for this. The logarithmic derivative for the outgoing wave function through the secondary well can be written in dispersive form [see Eq. (3.150)], and this can be employed directly in one-channel reduced R-matrix theory (Thomas, 1955) [see Sec. III.C.3.*g*(*iii*)] provided that the partial widths in all eliminated channels are small ($\Gamma_{\lambda(e)} \ll D_\lambda$). The collision function in Thomas' theory is just $U_{\mu\mu} = \exp(2i\phi_\mu)\,(1-\hat{L}_\mu^* R)/(1-\hat{L}_\mu R)$, where $\hat{L}_\mu = L_\mu - \mathcal{B}_\mu = \hat{S}_\mu + iP_\mu$. The R function is $R = \sum_\lambda \gamma_{\lambda(\mu)}^2/(E_\lambda - E - iW_\lambda)$, where $W_\lambda = \frac{1}{2}\sum_e \Gamma_{\lambda(e)}$ is the sum over the partial half-widths of eliminated channels. For uniform overlapping R-matrix levels ($W_\lambda \gg D_\lambda$) the R function is just $i\pi s_\mu$, s_μ being the reduced strength function $s_\mu = \gamma_{\lambda(\mu)}^2/D_\lambda$. The absorption cross section

$$\sigma_{abs} = \pi\lambda\!\!\!^{-2}_\mu (1 - |U_{\mu\mu}|^2) \tag{5.11}$$

becomes

$$\sigma_{abs} = \pi\lambda\!\!\!^{-2}_\mu \frac{4\pi s_\mu P_\mu}{|1-\hat{L}R|^2} = \pi\lambda\!\!\!^{-2}_\mu \frac{4\pi s_\mu G_\mu \mathcal{W}_l (1+\hat{S}_{b\mu}\pi^2 s_\mu^2)^{-1}}{[\mathcal{F}_l + \pi^2 G_l \hat{S}_{b\mu} s_\mu^2/(1+\pi^2\hat{S}_{b\mu}^2 s_\mu^2) - E]^2 + [\mathcal{W}_l + \pi G_l s_\mu/(1+\pi^2\hat{S}_{b\mu}^2 s_\mu^2)]^2}\,, \tag{5.12}$$

where $\hat{S}_{b\mu} = S_{b\mu} - \mathcal{B}_\mu$ is the smoothly varying background component of $\hat{L}_\mu$. In the uniform model (Lane and Thomas, 1958) the absorption cross section can be written in terms of the local strength function as

$$\sigma_{abs} = 2\pi^2\lambda\!\!\!^{-2}_\mu \frac{\overline{\Gamma}_{\lambda(\mu)}}{\overline{D}_\lambda} \frac{1-\exp(-4\pi W_\lambda/D_\lambda)}{1-\exp(-4\pi W_\lambda/D_\lambda)(1-2\pi\Gamma_{\lambda(\mu)}/D_\lambda)}\,. \tag{5.13}$$

With the above conditions, the equality of the right-hand sides of the equations gives

$$\frac{\overline{\Gamma}_{\lambda(\mu)}}{D_\lambda} = \frac{1}{2\pi} \frac{\Gamma_{l(c)}\Gamma_{l(\mu)}}{(\mathcal{F}_l + \Delta_l - E)^2 + \frac{1}{4}(\Gamma_{l(c)} + \Gamma_{l(\mu)})^2}\,, \tag{5.14}$$

with $\Gamma_{l(\mu)} = 2\mathcal{W}_l$, $\Gamma_{l(c)} = 2\pi s_\mu G_l/(1+\pi^2\hat{S}_{b\mu}^2 s_\mu^2)$, $\Delta_l = \pi^2 s_\mu^2 G_l \hat{S}_{b\mu}/(1+\pi^2\hat{S}_{b\mu}^2 s_\mu^2)$ for the fission width, coupling width, and shift factor of the vibrational resonance l, appearing as an anomaly about energy $\mathcal{F}_l$ in the extended penetration factor. The fission strength function (multiplied by 2π) can be used directly as the appropriate transmission coefficient in average cross sections of the Hauser–Feshbach type [see Eq. (5.1) of Sec. V.A].

A more direct calculation of the fission cross section through a vibrational resonance can be obtained by using two-channel reduced R-matrix theory. We now consider an entrance channel different from the fission channel. (We assume in the notation below that this is a neutron channel, labeled n.) The fission cross section through channel μ is

$$\sigma_{n\mu} = \pi\lambda\!\!\!^{-2}_n g_J |U_{n\mu}|^2\,, \tag{5.15}$$

with

$$U_{n\mu} = 2i P_n^{1/2} P_\mu^{1/2} \mathcal{R}_{n\mu} d^{-1}\,, \tag{5.16}$$

the two-channel reduced R-matrix being

$$\mathcal{R}_{cc'} = \sum_{\lambda} \frac{\gamma_{\lambda(c)}\gamma_{\lambda(c')}}{E_\lambda - E - \frac{1}{2}i\Gamma_{\lambda(e)}} , \tag{5.17}$$

and d is the determinant of $(1 - L\mathcal{R})$. For the fission channel the dispersive logarithmic derivative of Eq. (3.150) is again adopted. The cross-section expression is tractable if there is complete lack of correlation among the partial widths; this is defined by

$$\overline{\sum_{\lambda,\lambda' \neq \lambda} \gamma_{\lambda(n)}\gamma_{\lambda(n')}\gamma_{\lambda(\mu)}\gamma_{\lambda'(\mu)}} = 0 . \tag{5.18}$$

The $\mathcal{R}^2_{n\mu} = 0$, so that $d = (1 - \hat{L}_n\mathcal{R}_{nn})(1 - \hat{L}_\mu\mathcal{R}_{\mu\mu})$. For uniform overlapping R-matrix levels ($\Gamma_{\lambda(e)} \gg D_\lambda$, giving $\sum_\lambda \gamma^2_{\lambda(n)}/(E_\lambda - E - \frac{1}{2}i\Gamma_{\lambda(e)}) = i\pi s_n$, $\sum_\lambda \gamma^2_{\lambda(\mu)}/(E_\lambda - E - \frac{1}{2}i\Gamma_{\lambda(e)}) = i\pi s_\mu$

$$d^{-1} = \frac{\mathcal{F}_l - E - i\mathcal{W}_l}{(1+\pi P_n s_n)(1 - i\pi\hat{S}_\mu s_\mu)[\,\mathcal{F}_l - E + \pi^2 G\hat{S}_\mu s^2_\mu/(1+\pi^2\hat{S}^2_\mu s^2_\mu) - i\mathcal{W}_l - i\pi G_l s_\mu/(1+\pi^2\hat{S}^2_\mu s^2_\mu)]} \tag{5.19}$$

and

$$|\,2iP_n^{1/2}P_\mu^{1/2}\mathcal{R}_{n\mu}|^2 = 4P_nP_\mu|\,\mathcal{R}_{n\mu}|^2 = \frac{4P_nG_l\mathcal{W}_l s_n s_\mu}{(\mathcal{F}_l - E)^2 + \mathcal{W}_l^2} \quad \frac{2\pi D_\lambda}{\Gamma_{\lambda(e)}} . \tag{5.20}$$

The final expression for the cross section is

$$\sigma_{n\mu} = \pi\lambda\!\!\!^{-2} g_J \frac{T_{(n)}T_{(\mu)}}{T_{(e)}} , \tag{5.21}$$

where

$$T_{(\mu)} = \frac{\Gamma_{l(\mu)}\Gamma_{l(c)}}{(\mathcal{F}_l + \Delta_l - E)^2 + \frac{1}{4}(\Gamma_{l(\mu)} + \Gamma_{l(c)})^2} , \tag{5.22}$$

in agreement with Eq. (5.14). The other transmission coefficients in Eq. (5.21) are defined as

$$T_{(n)} = 4\pi P_n s_n/(1 + \pi P_n s_n)^2 , \tag{5.23}$$

$$T_{(e)} = 2\pi\Gamma_{\lambda(e)}/D_\lambda . \tag{5.24}$$

The form of the neutron transmission coefficient allows for the contribution of many-level interference effects which do not cancel in the average cross section when the narrow-level expression for T_n (namely, $4\pi P_n s_n$) approaches unity.

The formula obtained for the fission strength function $\Gamma_{\lambda(\mu)}/D_\lambda$ or the transmission coefficient, $T_\mu = 2\pi\Gamma_{(\mu)}/D_\lambda$, can be applied directly to obtaining the fission probability P_f, the quantity that is normally measured in fission induced by particle transfer reactions. It is simply

$$P_f = \frac{\sum_\mu T_{(\mu)}}{\sum_\mu T_{(\mu)} + \sum_c T_{(c)}} , \tag{5.25}$$

where $T_{(c)}$ denotes the transmission coefficients for other channels, such as radiative decay and neutron emission.

The angular distribution of fission products resulting from nuclear reactions plays an important role in analyzing the data on vibrational resonances. The expression for this angular distribution up to excitation energies not much greater than the barrier height is based on the idea of Bohr (1956) that the fissioning nucleus in transition over the barrier, being "cold" insofar as intrinsic excitations are concerned, can be in a transition state in which the projection of total angular momentum on the cylindrical symmetry axis K is a good quantum number. The angular behavior of the wave function of the fissioning nucleus is then described by the wave function of a symmetric top (Wigner, 1959):

$$D^J_{MK}(\theta, \phi, \chi) = d^J_{MK}(\theta)\epsilon^{iM\phi}e^{iK\chi}$$

$$d^J_{MK}(\theta) = \sum_n \frac{(-)^n\{(J+K)!(J-K)!(J+M)!(J-M)!\}^{1/2}}{(J-M-n)!(J+K-n)!n!(n+M-K)!}$$

$$\times \cos^{2J+K-M-2n}(\tfrac{1}{2}\theta)\sin^{2n+M-K}(\tfrac{1}{2}\theta) , \tag{5.26}$$

(where the integer n takes values such that the factorial arguments are not negative) with J being the total angular momentum and M its projection on a laboratory-fixed axis; θ and ϕ are the polar and azimuthal angles, respectively, of the symmetry axis of the top in the laboratory frame and χ is the angle of rotation of the top about its symmetry axis. After the nucleus has passed through the fission barrier it is assumed that the direction of this symmetry axis, along which the recoiling fission products ultimately emerge, remains undisturbed. The fission product angular distribution is therefore just the squared modulus of $d^J_{MK}(\theta)$ weighted by the distribution of J and M:

$$W(\theta) = \sum_{JM}\sigma_f(J^\pi, M)W_{JKM}(\theta)$$

$$W_{JKM}(\theta) \propto |\,d^J_{MK}(\theta)|^2 + |\,d^J_{M-K}(\theta)|^2 . \tag{5.27}$$

This formula was first applied by Bohr (1956) to the special case of photofission of an even target nucleus. Since the spin projection M on the beam direction carried by photons is zero, Eq. (5.27) reduces simply to

$$W(\theta) = \frac{3\sin^2\theta}{4\pi} \tag{5.28}$$

for $K = 0$ channels, and to

$$W(\theta) = \frac{3(1+\cos^2\theta)}{4\pi} \tag{5.29}$$

for $K = 1$; these formulas are sufficient for dipole radiation. Comparison with experiment [photofission of ^{238}U, Winhold *et al.* (1952)] demonstrated the preponderance of the $K = 0$ channel at energies just above the fission barrier. At higher energies a falling-away from sideways peaking of the fission product distribution to a more isotropic form demonstrated the opening of a

$K=1$ channel.

For particle-induced reactions going through a compound nucleus state of definite total angular momentum J and parity π, the projection of the orbital angular momentum of the incident particle is zero, and this can in many cases simplify the M distribution and hence the angular distribution expression. In particular, for nucleons incident on a zero-spin target nucleus (in which case $|M|$ can only be $\frac{1}{2}$) the angular distribution is (Wilets and Chase, 1956):

$$W_{J=K,K}(\theta)=\frac{(2K)!}{[(K-\frac{1}{2})!]^2 2^{2K}}\sin^{2K-1}\theta\,,$$

$$W_{J=K+1,K}(\theta)=\frac{(2K+1)!}{[(K+\frac{1}{2})!]^2 2^{2K+2}}\sin^{2K-1}\theta[1+4K(K+1)\cos^2\theta]\,, \tag{5.30}$$

$$W_{J=K+2,K}(\theta)=\frac{(2K+3)!}{(K+\frac{1}{2})!(K+\frac{3}{2})!\,2^{2K+4}}\sin^{2K-1}\theta[1-4K\cos^2\theta+4K(K+2)\cos^4\theta]\,,$$

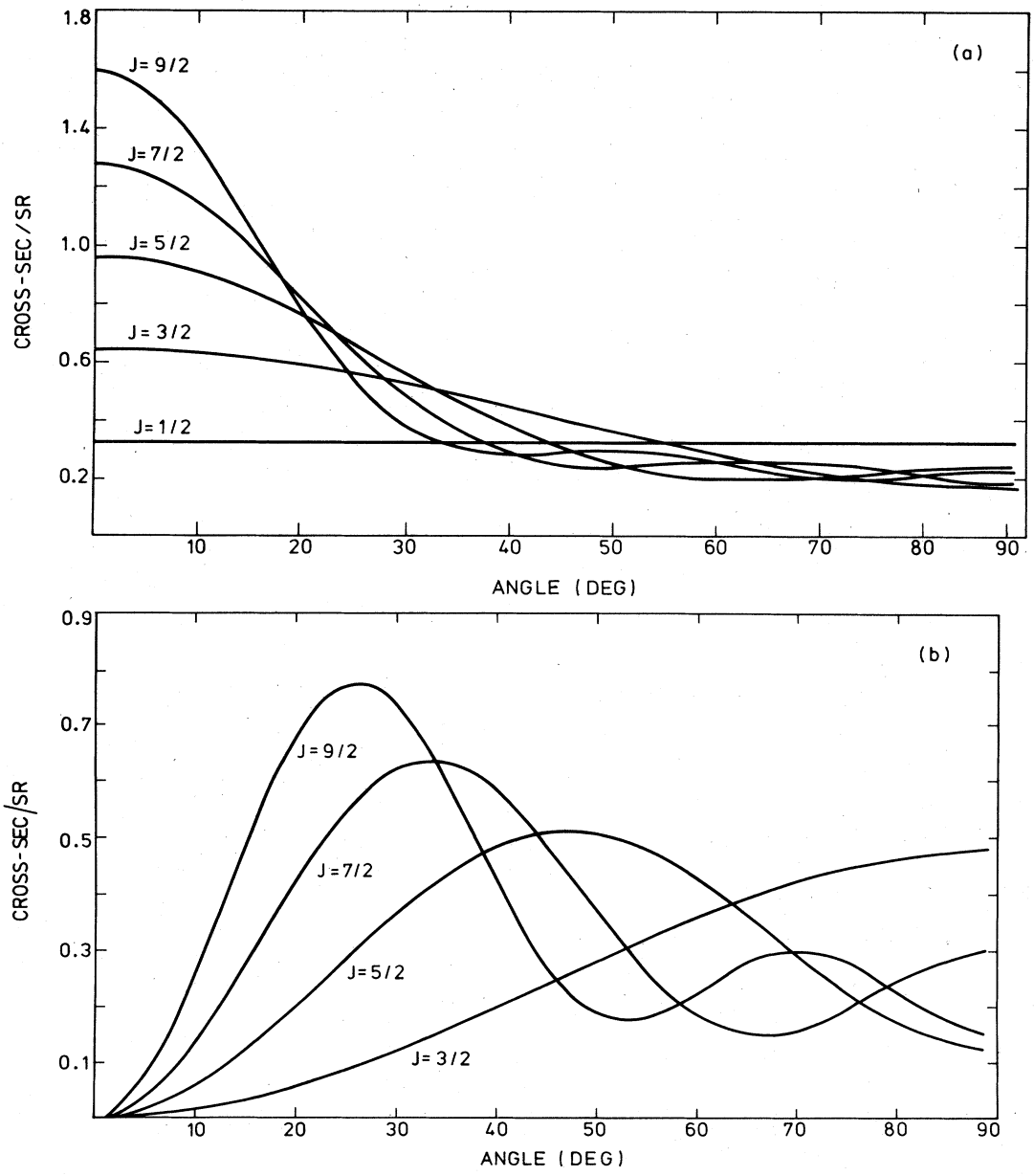

FIG. 82. Angular distribution of fission products following nucleon-induced fission of a zero-spin nucleus (Wilets and Chase, 1956). (a) gives curves for $K=\frac{1}{2}$, (b) $K=\frac{3}{2}$.

for the three lowest values of J. This expression is shown graphically in Fig. 82. For nonzero values of I the angular distribution functions for many special cases are presented by Wheeler (1963). Calculations of the distribution for unoriented target nuclei with $I \neq 0$ are shown in Fig. 83.

The M distribution resulting from reactions of the particle-transfer type is more complicated (Britt *et al.*, 1965; Specht *et al.*, 1966). In this case the laboratory-fixed direction is generally chosen to be that of the outgoing particle immediately prior to the fission of the residual excited nucleus, i.e., the angular correlation between this particle and the fission products is computed. For a stripping or pickup reaction leading to the fissioning compound state via a single-particle or hole state of orbital angular momentum l, total spin j, and spin projection m, coupled to an unexcited core state (the target nucleus) of angular momentum and projection I, M_I the amplitude $A(ljm; IM_I; JM; \mathbf{k}_p)$ for emitting the final particle with momentum $\mathbf{k}_p$ has to be computed by a suitable method (such as distorted wave Born approximation). If more than one single-particle (or hole) state contributes to the reaction the appropriate amplitudes are summed after multiplying by the reduced width amplitude $\gamma_{\lambda(lj)}$ for entering the compound nucleus state λ; the states λ thus reached are the fine-structure states λ discussed formally in Sec. III.C.3. For narrow levels λ it can be assumed that they are formed and decay independently of each other. The probability of fission of a level λ through channel μ, projection K is

$$P_{\lambda(\mu K)} = \frac{\Gamma_{\lambda(\mu)}}{\Gamma_{\lambda(\mu)} + \sum_c \Gamma_{\lambda(c)}} . \tag{5.31}$$

The angular correlation between $\mathbf{k}_p$ and the fission products can be written in terms of the above quantities as

$$W(\theta_f) \propto \sum_{M_I} w(M_I) \sum_{J,M,\lambda} \left| \sum_{ljm} A(ljm; IM_I; JM; \mathbf{k}_p) \gamma_\lambda(lj) \right|^2$$

$$P_{\lambda(\mu K)} \{ |d^J_{MK}(\theta_f)|^2 + |d^J_{M-K}(\theta_f)|^2 \} . \tag{5.32}$$

This is normally expanded into a sum of Legendre polynomials with coefficients A_L:

$$W(\theta_f) = \sum_L A_L P_L(\cos\theta_f) . \tag{5.33}$$

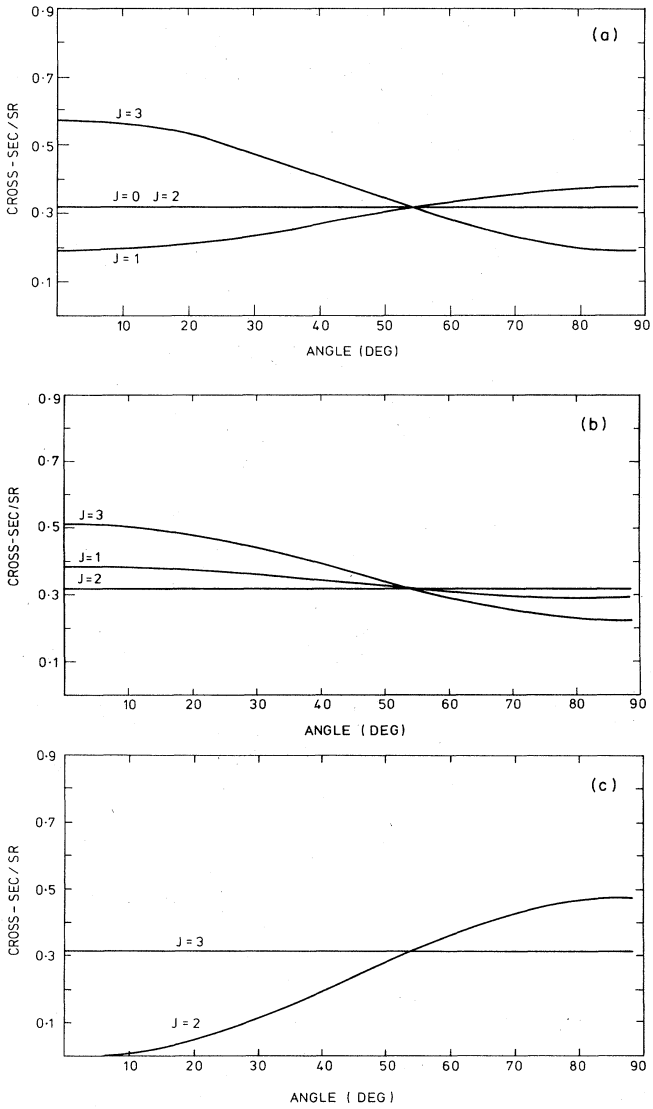

FIG. 83. Angular distribution of fission products following nucleon-induced fission of target nuclei with spin $I = \frac{3}{2}$ and nucleon $l = 1$. (a) is for $K = 0$, (b) for $K = 1$, (c) for $K = 2$.

5. Experimental data on pure vibrational resonances

No experimental evidence on broad resonance behavior in fission cross sections or fission probabilities has so far been found that is completely conclusive in proving the existence of a pure vibrational state. Nevertheless we shall summarize here the data in a number of likely cases without prejudice to the eventual interpretation.

a. ^{231}Th

The most carefully studied candidate as a pure vibrational resonance is undoubtedly ^{231}Th in the region of 5.85 MeV excitation. Data on neutron-induced fission of ^{230}Th have been measured by Yuen *et al.* (1971) and James *et al.* (1972) and analyzed by the latter authors. Very recent measurements by Blons *et al.* (1978, 1980) are discussed in Sec. X.B.2.*a*. In this cross section the resonance occurs at a neutron energy of 720 keV, and is apparently about 30-keV wide; this is about 4 orders of magnitude greater than the resonance fine spacing expected in the cross section at this energy. A feature of the experimental studies is that the angular distribution of fission products with respect to the incident neutron beam direction has been measured at various energies across the resonance. The forward peaking of the angular distribution right across the resonance indicates that the intrinsic state (defined at the outer barrier η_B) in the resonance configuration [Eq. (5.6)] has angular momentum projection $K = \frac{1}{2}$ on the symmetry axis [see Eq. (5.30) of Sec. V.B.4]. The analysis of the data proceeds on the assumption that the observed resonance is a composite of peaks, each of $K = \frac{1}{2}$ but with different total angular

momentum J, forming a rotational band of intrinsic states.

On this assumption the cross section has been calculated using the Hauser–Feshbach formula (5.1) and the fission transmission coefficient for a vibrational resonance, Eq. (5.14). The major competition against fission in the decay of the compound nucleus is provided by elastic and inelastic scattering of neutrons to known and inferred rotational bands in ^{230}Th. Strength functions for the calculation of these neutron transmission coefficients were taken from the known s- and p-wave neutron strength functions determined by low-energy neutron studies. At 700-keV neutron energy the main neutron entrance channels to the compound nucleus are provided by s-, p-, and d-wave neutrons (exciting total angular momenta and parity $J^\pi = \frac{1}{2}^+, \frac{1}{2}^-, \frac{3}{2}^-, \frac{3}{2}^+, \frac{5}{2}^+$) and somewhat more weakly by f-wave neutrons ($J^\pi = \frac{5}{2}^-, \frac{7}{2}^-$). From the calculation of the various spin-parity components of the cross section the angular distribution of fission products is obtained by the use of Eq. (5.30).

The main variables in fitting the data are the parity of the intrinsic state in the vibrational resonance configuration, and the effective moment of inertia $\mathcal{I}$ and decoupling parameter a that govern the relative spacings of the members of the $K = \frac{1}{2}$ rotational band:

$$E_{\lambda_{II}(JK)} = E_{\lambda_{II}(KK)} + \frac{\hbar^2}{2\mathcal{I}}\left[J(J+1) - K(K+1) + \delta_{K,1/2} a_{1/2} (-)^{J+1/2}(J+\tfrac{1}{2})\right]. \quad (5.34)$$

The best fit to the data of James *et al.* (1972) and Yuen *et al.* (1971) was achieved with odd parity and with $(\hbar^2/2\mathcal{I})$ lying between 1.8 and 2.7 keV and $a_{1/2}$ between −2.0 and −2.3 (see Figs. 84 and 85 and Table IX). The value of the moment of inertia thus determined is more than twice that observed for any normally observed rotational bands in odd-A actinide nuclei, and this provided one of the first direct indications that the shape of the nucleus in the intermediate states acting in fission was indeed much different from normal, as postulated by the double-humped barrier theory. The lower bound 1.8 keV leads actually to a moment of inertia that exceeds the rigid value for a deformation corresponding to the normal isomeric state by 30%. It may be taken as indication of the resonances in ^{231}Th being located in a third minimum of still higher deformation (see Sec. II.A.1.*d*., also Sec. VII.D.3., Sec. IX.C.3., and especially Sec. X.B.2.*a*).

What are the reasons for believing this remarkable resonance phenomenon to be a nearly pure vibrational resonance as distinct from a damped vibrational resonance as described in Sec. V.C? Mainly, that it is very smooth. With neutron energy resolution of a few keV it is to be expected that any class-II compound state structure would not occur with a frequency greater than a few class-II states per resolution interval, and, because of the statistical fluctuations in strength and width inherent in compound states, this would cause large variations about any smooth curve that would describe the envelope of the vibrational resonance. On the other hand, there is a feature in the fit to the data that suggests damping is playing a role. This is the variation in width and strength of the different spin components of the resonance (other than variations due to penetration through the centrifugal barrier). If the strength of a vibrational resonance of given spin J is defined by

$$S_{J(f)} = \frac{\Gamma_{J(c)}\Gamma_{J(f)}}{\Gamma_{J(c)} + \Gamma_{J(f)}}, \quad (5.35)$$

where $\Gamma_{(c)}$ is the coupling width of the vibrational res-

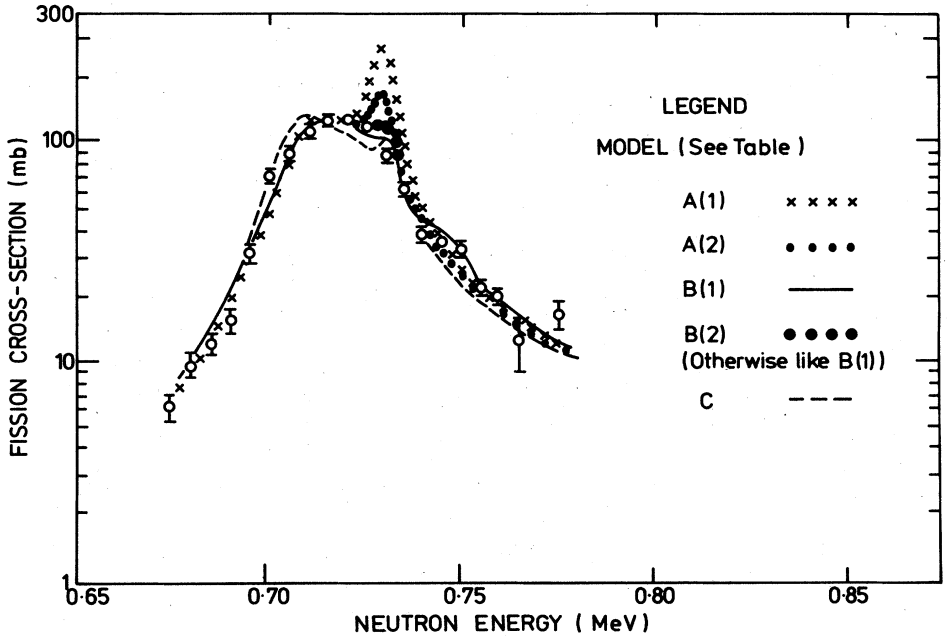

FIG. 84. Comparisons of the fission cross section of ^{230}Th with models of the rotational band associated with the class-II vibrational state (James *et al.*, 1972). Details of the model are given in Table IX.

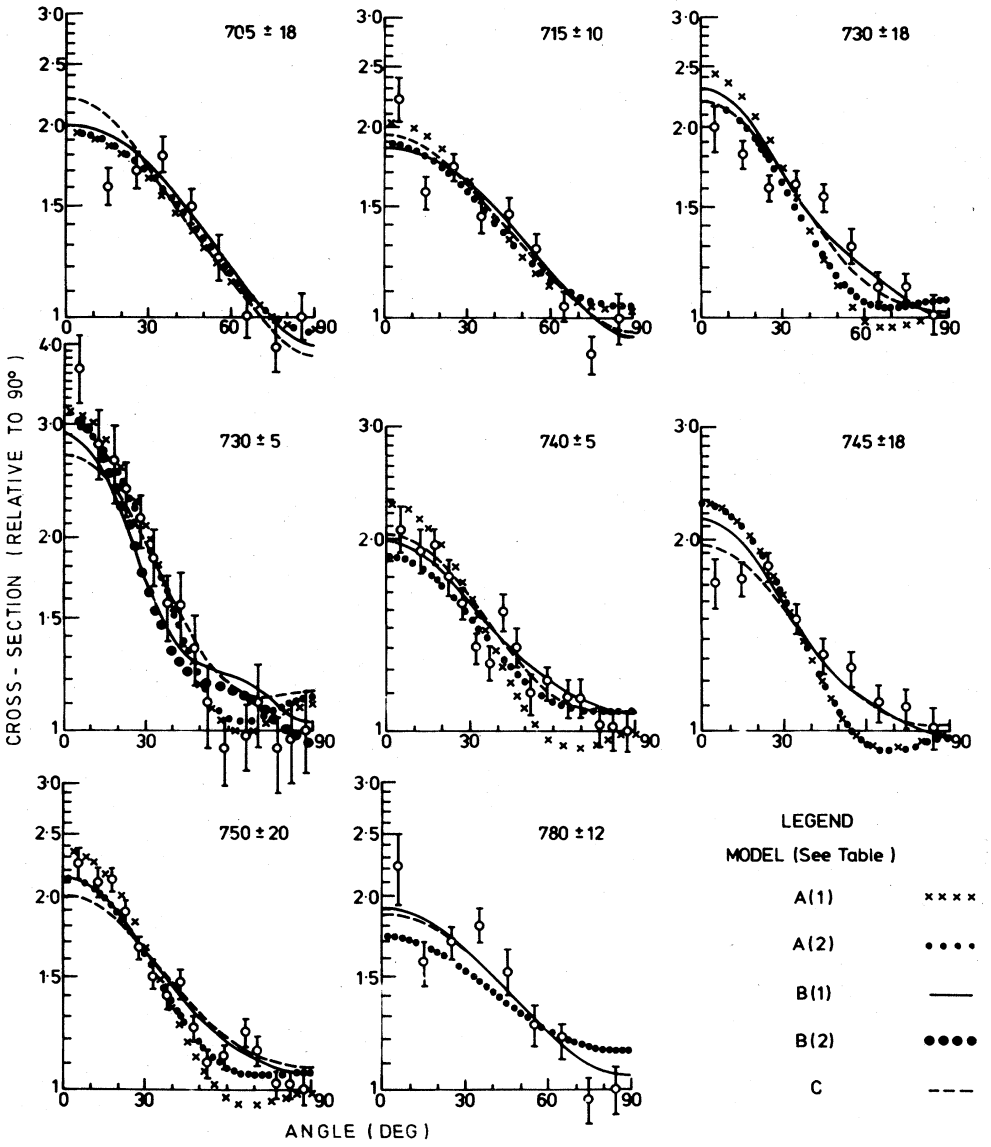

FIG. 85. Comparison of fission product angular distribution from the reaction ^{230}Th(n,f) with the models of Table IX (James *et al.*, 1972).

onance, then in the ^{231}Th best fit the ratio of strengths is

$$S_{1/2(f)} : S_{3/2(f)} : S_{5/2(f)} : S_{7/2(f)} = 1 : 0.5 : 0.2 : 0.4. \quad (5.36)$$

Strictly speaking these variations arise, in the analysis, from the neutron fission cross section of each component, and could be attributed to the variation of neutron strength function with spin, but this appears unlikely. The question is discussed further in Sec. V.C.

Recent high-resolution work on the neutron fission cross section of ^{230}Th in the region of 720 keV has shown that there is more structure than can be accounted for by a single rotational band (Veeser, 1976; Blons *et al.*, 1978). One suggestion (Blons *et al.*, 1978) is that there are two rotational bands of $K=\frac{1}{2}$ and opposite parity, lending support, again, to the idea of a third minimum, but this requires further investigation (see also Sec. V.C.4.*e*, Sec. IX.C and Sec. X.B.2.*a*).

At higher energies in ^{231}Th no more peaks appear in the cross section, but the angular distribution of fission products undergoes marked variations in character with changing neutron energy, becoming considerably sideways-peaked with respect to neutron direction at about 960 keV and forward-peaked again at 1060 keV. The sideways peaking is attributed by James *et al.* (1972) to a $K=\frac{3}{2}$ intrinsic state coupled to a much broader vibrational resonance. The general behavior of the $K=\frac{1}{2}$ component of the cross section both at the sharp resonance at 720 keV and at higher energies can be satisfactorily explained by the choice of barrier parameters:

$$\upsilon_A \approx 6.02 \text{ MeV}, \quad \hbar\omega_A \sim 0.9 \text{ MeV},$$

$$\upsilon_B \approx 6.27 \text{ MeV}, \quad \hbar\omega_B \sim 0.57 \text{ MeV}.$$

TABLE IX. Parameters for models of the rotational band associated with the class-II vibrational resonance of ^{231}Th. In column 5 the coupling or fission width is examined, whichever is the smaller.

Model	J	$E_{\lambda_{II}(JK)}$ (keV)	$\Gamma^{(JK)}_{\nu_{II}}$ (keV)	$\Gamma^{(JK)}_{\nu_{II}(c \text{ or } f)} / \Gamma^{(KK)}_{\lambda_{II}(c \text{ or } f)}$
$A(1)$: $\pi = +$	$\frac{1}{2}$	718	26	1
$\Gamma^{(KK)}_{\nu_{II}(c \text{ or } f)} = 2.16$ keV	$\frac{3}{2}$	709	14	1
	$\frac{5}{2}$	729	3.5	1
$A(2)$: $\pi = +$	$\frac{1}{2}$	718	26	1
$\Gamma^{(KK)}_{\nu_{II}(c \text{ or } f)} = 2.16$ keV	$\frac{3}{2}$	709	14	1
	$\frac{5}{2}$	729	3.5	0.5
$B(1)$: $\pi = -$	$\frac{1}{2}$	720	26	1
$\Gamma^{(KK)}_{\nu_{II}(c \text{ or } f)} = 1.27$ keV	$\frac{3}{2}$	712	14	0.5
	$\frac{5}{2}$	747	7	0.2
	$\frac{7}{2}$	729	3.5	0.4
$B(2)$: $\pi = -$	$\frac{1}{2}$	720	26	1
$\Gamma^{(KK)}_{\nu_{II}(c \text{ or } f)} = 1.27$ keV	$\frac{3}{2}$	712	14	0.5
	$\frac{5}{2}$	747	7	0.2
	$\frac{7}{2}$	729	3.5	0.6
C: $\pi = -$	$\frac{1}{2}$	720	26	1
$\Gamma^{(KK)}_{\nu_{II}(c \text{ or } f)} = 1.2$ keV	$\frac{3}{2}$	710	14	0.5
	$\frac{5}{2}$	732	7	0.8
	$\frac{7}{2}$	708	3.5	0.4

b. ^{233}Th

Early work (Henkel and Smith, 1956) showed the rich structure in the fast neutron fission cross section of ^{232}Th and the work of Henkel and Brolley (1956) revealed the strong fission product angular distributions associated with it. Recent work on the fission vibrational resonances of ^{233}Th has concentrated on finding substructure within the main resonances (Blons *et al.*, 1975), and on improving the energy resolution of the angular distribution information (Caruana *et al.*, 1977).

Blons *et al.* (1975 a, b) have attempted to use both sets of information for an analysis akin to that described in the section on ^{231}Th. Some of the substructure found on the main resonance peaks has spacing patterns akin to that of a simple rotational band (see Fig. 86); simple because, as proved by the sideways peaking of the angular distribution on these main peaks (see Fig. 87), the intrinsic states at the head of the bands have spin projection quantum number $K \geq \frac{3}{2}$, and the pattern is therefore not complicated by the decoupling parameter occurring in Eq. (5.34). However, the conclusion is contentious because other groups of substructure do not fall into a simple rotational pattern, and a quantitative fit to the magnitude of the cross section that includes the detailed structure has not been achieved [see Caruana *et al.*, (1977)]. Proof would require a measurement of the angular distribution with sufficiently fine resolution to isolate the individual peaks of the substructure.

The deduced moment of inertia of the rotational bands is on average larger even than that found for ^{231}Th, and this has led Blons *et al.* (1975a) to suggest that this is evidence for a tertiary well in the region of the "conventional" second barrier peak, splitting the fission barrier into three peaks. Although the hypothesis has attractions on theoretical grounds concerning the calculation of fission barriers (see Sec. II), and for the explanation of some trends in the systematics of fission cross sections (see Sec. VII and also the caption to Fig. 87) and barrier heights (see Sec. VIII. F), it cannot be regarded as conclusive.

c. ^{232}Pa

The fission of this nucleus has been explored principally in a series of measurements of the neutron interaction with ^{231}Pa, including angular distribution of the fission products (Sicre, 1976; Sicre *et al.*, 1979). Measurements of the fission cross section with high-energy resolution have been made by James *et al.* (1979) and Plattard *et al.* (1979). The considerable structure observed in the fission cross section measured with about 10-keV resolution is shown in Fig. 88. The analysis of the cross section and, more especially, the angular distribution data are complicated by the nonzero spin of the target nucleus ($I^\pi = \frac{3}{2}^-$). Hence the range of M quantum numbers extends from -2 to 2 and implies much less dramatic features in the angular distribution. On the other hand, the rather low neutron energies of the resonances limit the orbital angular momentum that can be brought effectively into the compound nucleus. Only neutron s and p waves will give appreciable cross sections for compound nucleus formation, allowing excitation of states of total angular momentum and parity $J^\pi = 1^-, 2^-$ and $J^\pi = 0^+, 1^+, 2^+, 3^+$, respectively. In spite of the undramatic angular distributions Sicre found that the data could not be reproduced by a model based on a unique K value for each resonance. Rotational bands based on $K^\pi = 2^-$ and 3^- were required for the 200-keV resonance and on $K^\pi = 0^-$ and 3^+ for the 330-keV resonance, as shown in Fig. 88. Measurements with higher energy resolution (~ 2 keV) reveal that the 200-keV resonance does have in fact a narrow component (width considerably less than 2 keV) at 160 keV (Fig. 89), and angular distribution measurements (rather strongly sideways peaked; see, e.g., Fig. 90) confirm that $J, K = 3$. The likelihood of odd parity (excitation by neutron d waves) is almost ruled out by the peak cross section [80 mb, according to Plattard *et al.* (1979), to be contrasted with an expected maximum value of about 60 mb).

On the assumption that these resonances are all of pure vibrational character, Sicre gives possible barrier heights that will represent the data. They are fairly close to the values

$$\upsilon_A = 5.95 \text{ MeV}, \quad \hbar\omega_A = 0.9 \text{ MeV},$$

$$\upsilon_B = 6.15 \text{ MeV}, \quad \hbar\omega_B = 0.4 \text{ MeV}$$

that also give a reasonable representation of the fission

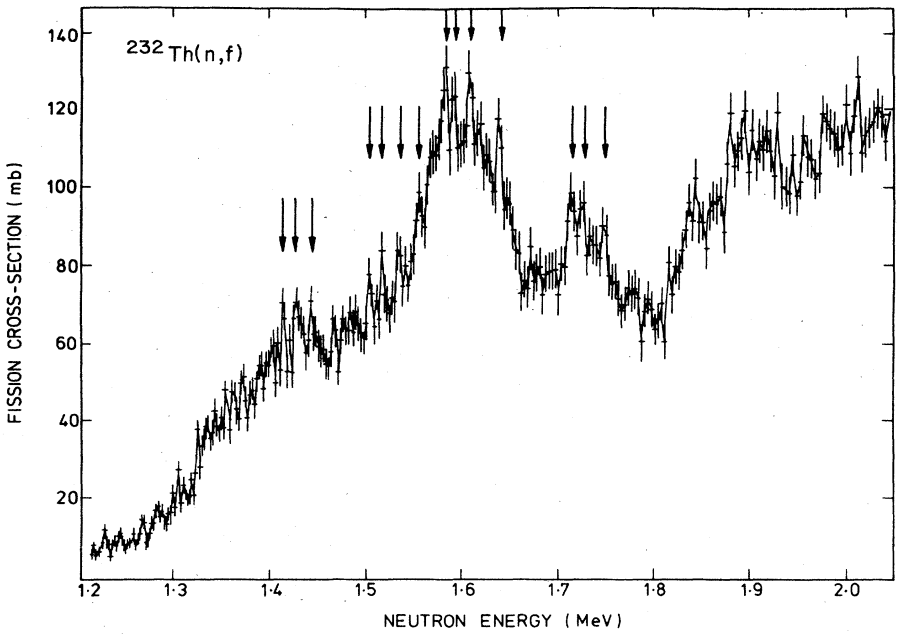

FIG. 86. High-resolution cross-section measurements of the neutron-induced fission cross section of ^{232}Th (Blons *et al.*, 1975a) with possible rotational bands indicated.

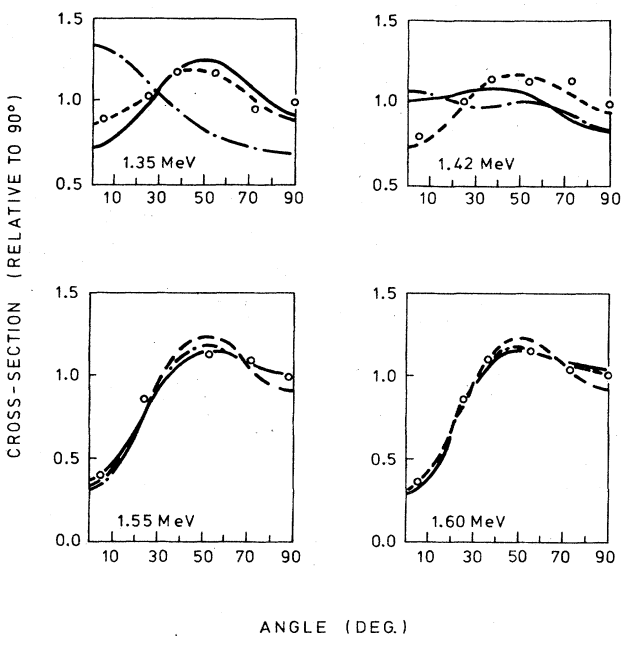

FIG. 87. Fission product angular distributions from the reaction ^{232}Th(n,f) [Caruana *et al.* (1977); see also Androsenko *et al.* (1969)]. The energy resolution is 50 keV. The dashed, dash-dot, and continuous curves are attempted fits to the data by Caruana *et al.* For the continuous curve, the lowest vibrational resonance was assumed to be associated with $K^{\pi}=\frac{3}{2}^{+}$, while the barrier parameters were considerably higher than normally assumed for the actinides, viz. $\mathcal{U}_A = 6.2$ MeV, $\hbar\omega_A = 1.4$ MeV, $\mathcal{U}_B = 7.0$ MeV, $\hbar\omega_B = 0.7$ MeV. These parameters also provided a fit to the cross-section data of Fig. 86. Simultaneous fits to the angular distribution data and the cross section using more conventional parameters for the barrier were not achieved.

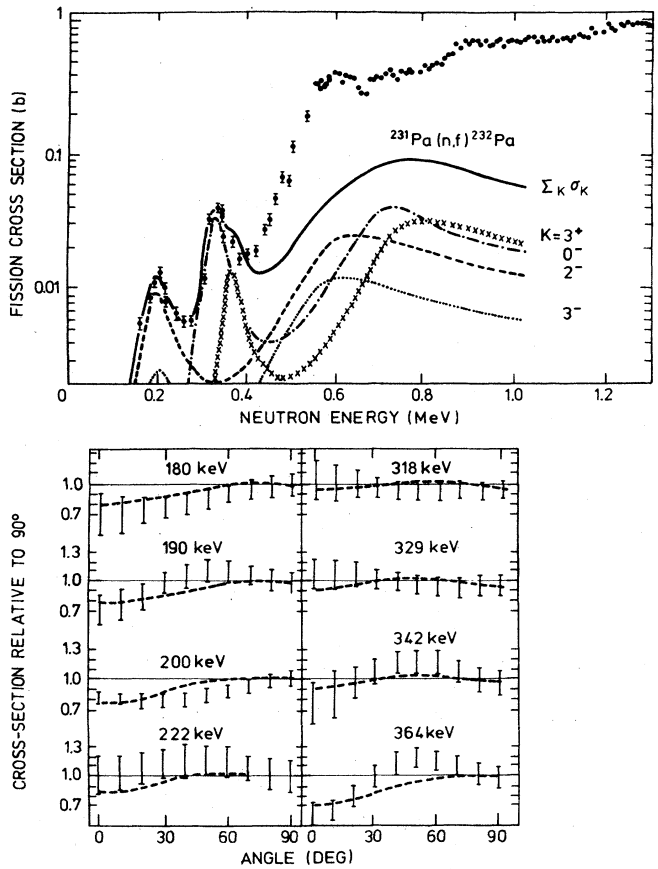

FIG. 88. Above; fission cross section of ^{231}Pa (Sicre, 1976). The curves are calculations of the cross section based on vibrational resonances with the stated K values. Below; fragment angular distributions; the curves are calculated with the same parameters as above.

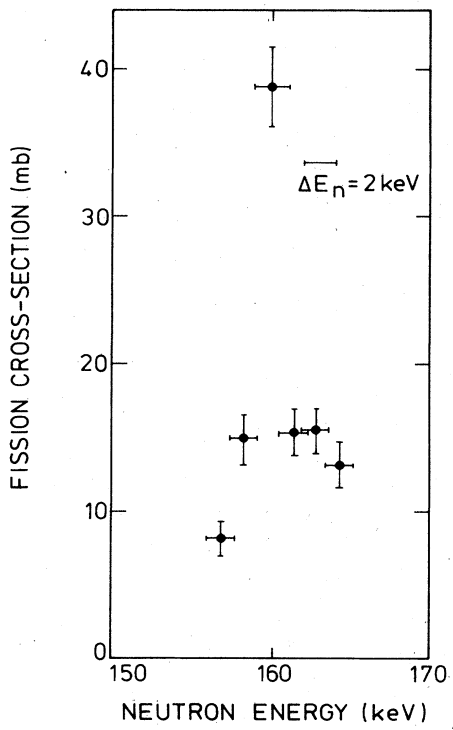

FIG. 89. Fission cross section of ^{231}Pa (Sicre, 1976) in the region of 160 keV neutron energy. Energy resolution is ~2 keV.

cross section at higher energies using a strong coupling model.

d. ^{234}Th

In the (t, pf) reaction on ^{232}Th Back *et al.* (1974a) have observed marked structure at an excitation energy of 5.5–5.8 MeV and broader structure at 6.5 MeV. The fission probability curve (see Fig. 91) up to 6 MeV has been fitted with barrier parameters:

$$\mathcal{U}_A = 6.15 \text{ MeV}, \quad \hbar\omega_A = 1 \text{ MeV},$$

$$\mathcal{U}_B = 6.52 \text{ MeV}, \quad \hbar\omega_B = 0.75 \text{ MeV}.$$

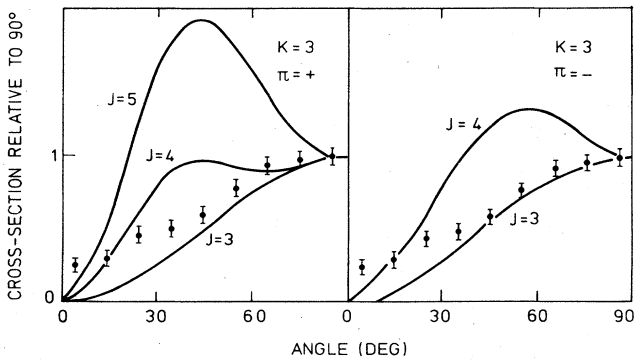

FIG. 90 Angular distribution of fission products from neutron-induced fission of ^{231}Pa at neutron energy 160 keV. The smooth curves are the theoretical ones for particular combinations of J, K, and π (implying different M weightings).

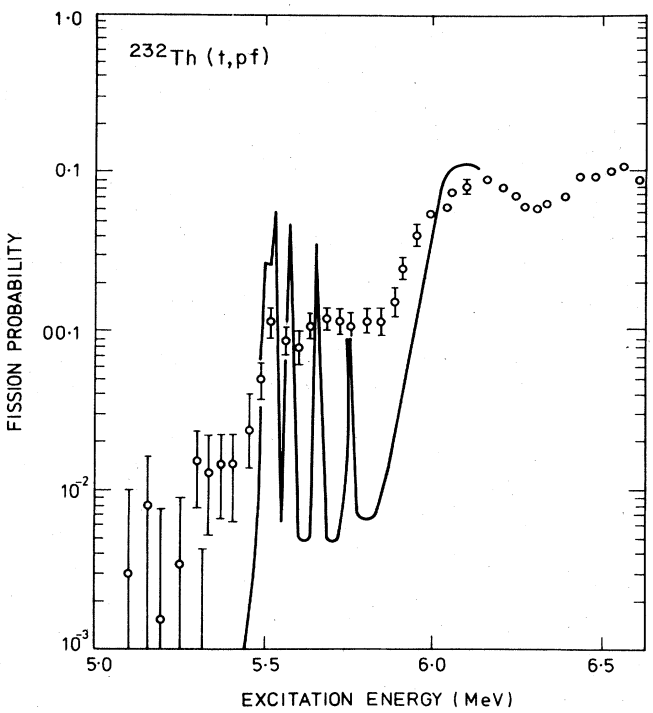

FIG. 91. Fission probability for ^{234}Th as function of excitation energy from the reaction ^{232}Th(t, pf) (Back *et al.*, 1974a). The full curve is an attempted fit with a pure vibrational resonance carrying a rotational band, no resolution broadening included.

e. Other nuclei

Other nuclei showing structure which may be due to more or less pure vibrational resonances are ^{238}U [from the ^{236}U(t, pf) reaction] showing a considerable peak at 5.1 MeV, ^{240}U [from ^{238}U(t, pf)] with a less significant peak at 5.3 MeV, and ^{234}U [from ^{233}U(d, pf)] with some structure at 4.9 and 5.4 MeV excitation [Back *et al.* (1974a)]. All have been analyzed with pure vibrational models, as described in Sec. V.B.1 and Sec. III.A.2, giving barrier heights of about 6 MeV.

C. Damped vibrational resonances

1. Schematic models of damping

In this section we study some schematic models, based on the Hamiltonian, Eq. (3.64), introduced in Sec. III.C.1. We recall that the Hamiltonian is split into three components, viz., a deformation-dependent part, an intrinsic part (defined at fixed deformation η_0), and a coupling term, which allows for the change in the intrinsic part with changing deformation about η_0:

$$H = H_\eta + H_{\text{int}}(\xi, \eta_0) + H_c(\eta, \xi; \eta_0), \tag{5.37}$$

where

$$H_\eta = T_\eta + \mathcal{U}(\eta),$$

$$H_{\text{int}}(\eta_0) = T_\xi(\eta_0) - \varepsilon_0(\eta_0) + V(\eta_0, \xi),$$

$$H_c = T_\xi(\eta) - \varepsilon_0(\eta) + V(\eta, \xi) - H_{\text{int}}(\eta_0).$$

The eigenvalues of $T_\xi(\eta) + V(\eta, \xi)$ at fixed η are labeled $\varepsilon_\mu(\eta)$ and those of $H_{\text{int}}(\eta)$ are $\mathcal{E}_\mu(\eta) = \varepsilon_\mu(\eta) - \varepsilon_0(\eta)$. The

potential energy of deformation $\mathcal{V}(\eta)$ is just the "ground"-state energy $\varepsilon_0(\eta)$.

In the numerical models presented below a limited number of vibrational states (depending only on the deformation) and a limited number of intrinsic states (at fixed deformation) are combined to form the basis states, and the mixing of these through the coupling term into final eigenstates is studied. Although the models must be considered as schematic ones developed to gain insight into the mixing process and the effect on fission and coupling widths, some attempt has been made to introduce quantities that give them some bearing on realistic physical situations.

a. Single-particle models

The dependence of the intrinsic states on deformation is taken to be qualitatively similar to that determined by the single nucleon states in a deformed potential well of the Nilsson type. In the Nilsson model levels are labeled by harmonic oscillator quantum numbers and the projection Ω of the nucleon total angular momentum on the cylindrical symmetry axis of the potential well: the energy of such a level depends strongly on deformation, generally (though not always) decreasing for low Ω and increasing for high Ω. A schematic nuclear intrinsic state is constructed by filling single-particle states until the appropriate numbers N and Z of neutrons and protons occupy the level scheme. For low-lying states paired particles are made to occupy the lowest orbits and are then regarded as a vacuum, while the last unpaired neutron or proton occupies any appropriate higher orbit, the energy above the Fermi energy (defined here as the highest pair-occupied level) giving the excitation energy of the state. As an orbit occupied by a single particle sinks into the "Fermi sea" with changing deformation, a "hole" state can appear, carrying the same configuration, by displacing two paired particles from its orbit into the next available unoccupied orbit. For the present schematic model this behavior in energy is represented by a parabola, one branch representing the particle state in an orbit above the Fermi level and the other branch representing its reemergence as a hole state in the Fermi sea.

In realistic Nilsson model calculations the potential well is never a perfect harmonic oscillator. The difference between the latter and the actual potential causes mixing and repulsion when two labeled orbits of the same spin projection and parity intersect. In the work of Möller and Nix (1974), for example, the matrix element for this interaction between the harmonic oscillator orbits is of the order of 0.1 MeV; a typical diagram of level behavior with this effect included is shown in Fig. 92.

Residual internucleon forces that cannot be included in a smooth potential well description will also affect the repulsion between levels at orbital crossings. This can be included in the method of calculation described below. However, its extreme manifestation in the pairing correlation force is not included, but it is hoped that nothing essential for the results of the present study is thereby omitted.

In this model the residual interaction, as described above, between the orbitals is assumed to be independent of deformation. Also the wave function of a given harmonic oscillator orbital is assumed to be dependent on deformation in only a very slow and non-essential way, which is henceforth neglected. In this way the coupling term of Eq. (5.37) can be written

$$H_c(\eta, \xi; \eta_0) = H_p(\xi, \eta) - H_p(\xi, \eta_0), \tag{5.38}$$

where $H_p(\eta, \xi)$ is the Hamiltonian for the single-particle oscillator orbits. The eigenvalues and eigenstates of H_p are denoted by $\mathcal{E}_\mu^{(p)}, \chi_\mu^{(p)}$. The Hamiltonian for the intrinsic states is

$$H_{\rm int}(\xi, \eta_0) = H_p(\xi, \eta_0) + v_{\rm res}, \tag{5.39}$$

where $v_{\rm res}$ is the residual interaction between orbitals. Since the matrix element

$$\langle \mu' | H_p(\xi, \eta_0) | \mu \rangle = \mathcal{E}_\mu^{(p)}(\eta_0)\delta_{\mu'\mu}, \tag{5.40}$$

$$\therefore \langle \mu' | H_c(\eta, \xi; \eta_0) | \mu \rangle = [\mathcal{E}_\mu^{(p)}(\eta) - \mathcal{E}_\mu^{(p)}(\eta_0)]\delta_{\mu'\mu}. \tag{5.41}$$

The diagonalization of

$$H = H_\eta + H_p(\eta_0) + v_{\rm res} + H_c \tag{5.42}$$

is accomplished by using the basis states $\phi_\nu(\eta)\chi_\mu^{(p)}(\eta_0)$ in the expression

$$\psi_\lambda = \sum_{\nu\mu} c_{\nu\mu(p)}^{(\lambda)} \phi_\nu \chi_\mu^{(p)}(\eta_0). \tag{5.43}$$

By the usual technique of multiplication by $\phi_{\nu'}^*\chi_{\mu'}^*$, after operation on ψ_λ by H, and integration, the coupled equations

$$c_{\nu'\mu'(p)}^{(\lambda)}[\epsilon_{\nu'} + \mathcal{E}_{\mu'}^{(p)}(\eta_0)] + \sum_\mu c_{\nu'\mu(p)}^{(\lambda)} \langle \chi_{\mu'}^{(p)} | v_{\rm res} | \chi_\mu^{(p)} \rangle + \sum_\nu c_{\nu\mu'(p)}^{(\lambda)} \langle \nu' | [\mathcal{E}_{\mu'}^{(p)}(\eta) - \mathcal{E}_{\mu'}^{(p)}(\eta_0)] | \nu \rangle = E_\lambda c_{\nu'\mu'(p)}^{(\lambda)} \tag{5.44}$$

are obtained. If we limit ourselves first to simple harmonic oscillator behavior of the deformation potential, with its center being taken as the origin of the deformation scale,

$$\mathcal{V}(\eta) = \tfrac{1}{2}C\eta^2 = \tfrac{1}{2}B\omega^2\eta^2,$$

and the intrinsic orbits are assumed to have the quadratic behavior (as discussed above)

$$\mathcal{E}_\mu^{(p)}(\eta) = \mathcal{E}_{0\mu}^{(p)} + D_\mu^{(p)}\eta + A_\mu^{(p)}(\eta - b_\mu^{(p)})^2$$

the Eqs. (5.44) reduce to

$$c_{\nu\mu(p)}^{(\lambda)}[\epsilon_\nu + \mathcal{E}_{0\mu}^{(p)} + A_\mu^{(p)}b_\mu^{(p)2} - E_\lambda] + \sum_{\mu'} c_{\nu\mu'(p)}^{(\lambda)} v_{\mu\mu'} + \sum_{\nu'} c_{\nu'\mu(p)}^{(\lambda)} \left[\frac{A_\mu^{(p)}}{\alpha^2}\left(\frac{1+2\nu}{2}\right)\delta_{\nu\nu'} + \frac{A_\mu^{(p)}}{2\alpha^2}\{[\nu(\nu-1)]^{1/2}\delta_{\nu\nu'+2} + [(\nu+2)(\nu+1)]^{1/2}\delta_{\nu\nu'-2}\}\right.$$
$$\left. + \frac{D_\mu^{(p)} - 2A_\mu^{(p)}b_\mu^{(p)}}{\alpha}\{\sqrt{\tfrac{1}{2}\nu}\,\delta_{\nu\nu'+1} + \sqrt{\tfrac{1}{2}\nu + \tfrac{1}{2}}\,\delta_{\nu\nu'-1}\}\right] = 0, \tag{5.45}$$

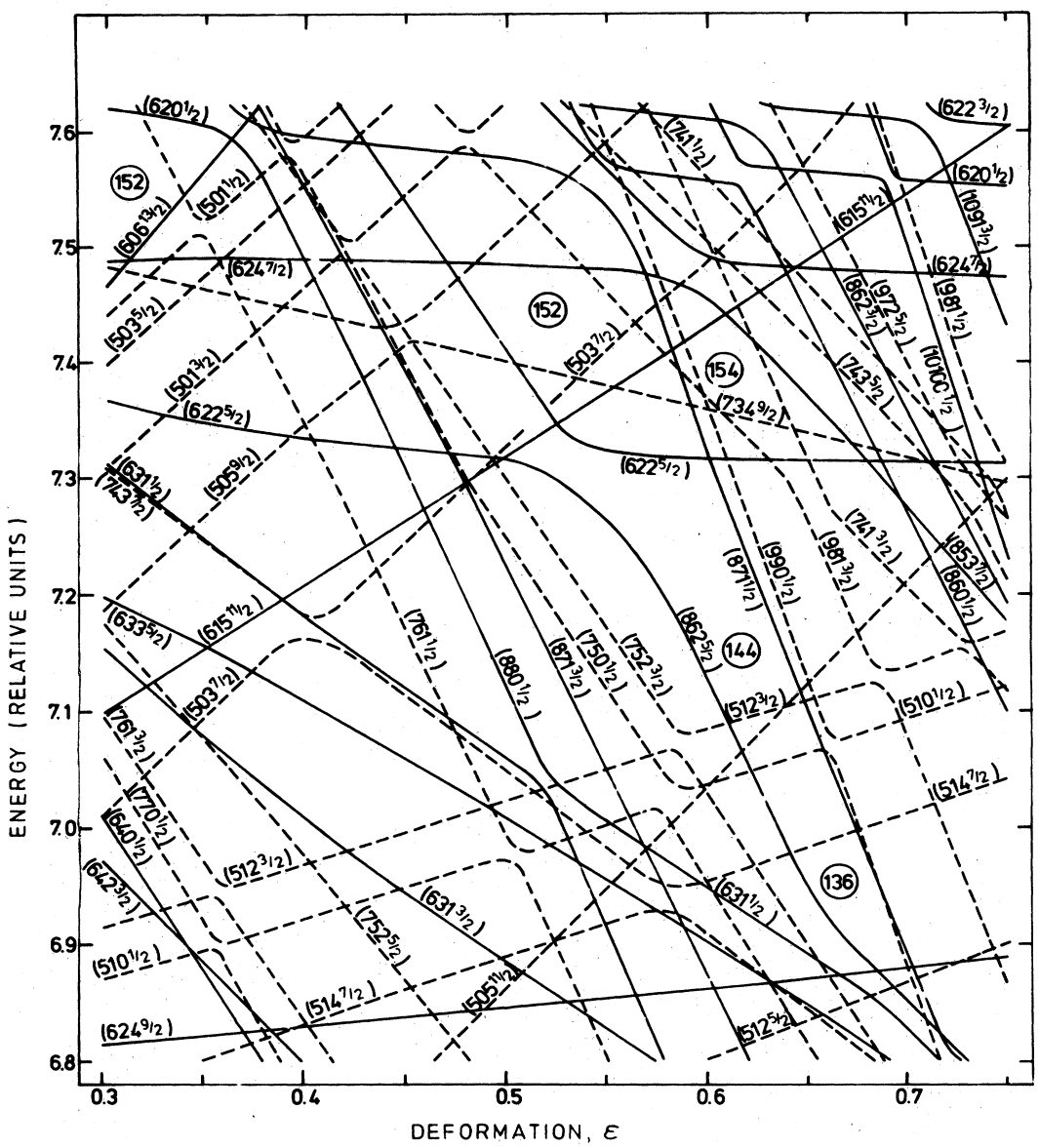

FIG. 92. Behavior of single-particle orbits (neutrons) as a function of deformation with residual interaction effects included [from Nilsson *et al.* (1969)]. Numbers in circles indicate number of neutrons required to fill all lower orbits.

where $v_{\mu\mu'}$ (taken to be $v[1-\delta_{\mu\mu'}]$ in the calculations below) represents $\langle\mu|v_{\rm res}|\mu'\rangle$ and $\alpha=(B\omega/\hbar)^{1/2}$. The harmonic oscillator quantum numbers ν have the usual convention of being enumerated from zero upwards.

After diagonalization of the Eqs. (5.45) the eigenfunctions ψ_λ must be rewritten in the basis $\phi_\nu\chi_\mu(\eta_0)$ with expansion coefficients $c_{\nu\mu}^{(\lambda)}$, where the $\chi_\mu(\eta_0)$ are the intrinsic eigenfunctions of $H_{\rm int}(\eta_0)=H_p(\eta_0)+v_{\rm res}$. This is simply accomplished by diagonalizing the equations

$$\mathcal{E}_\mu^{(p)}(\eta_0)-\mathcal{E}_K(\eta_0)+\sum_{\mu'}v_{\mu\mu'}=0 \tag{5.46}$$

in the basis $\chi_\mu^{(p)}(\eta_0)$, the expansion coefficients $\langle\chi_K(\eta_0)|\chi_\mu^p(\eta_0)$ being used to make the transformation in the expansion of ψ_λ.

In this model the harmonic oscillator potential can be taken to represent the secondary well in the fission barrier, and η_0 can be chosen as a channel deformation near η_B, or at the center of the oscillator (in order to define the configuration mixing in the most obvious way), or at a lower deformation towards the intermediate barrier η_A in order to obtain a measure of the coupling width that the eigenstates will have. By estimating amplitudes of the vibrational wave functions ϕ_ν at the channel deformation and intermediate barrier deformation, quantities proportional to the fission reduced width amplitude and coupling reduced width amplitude for the different channels μ can be obtained:

$$\gamma_{\lambda(\mu)}^{(A,B)}\propto\sum_\nu\phi_\nu(\eta_0)c_{\nu\mu}^{(\lambda)}, \tag{5.47a}$$

depending on the choice of η_0. The new expansion coefficients are

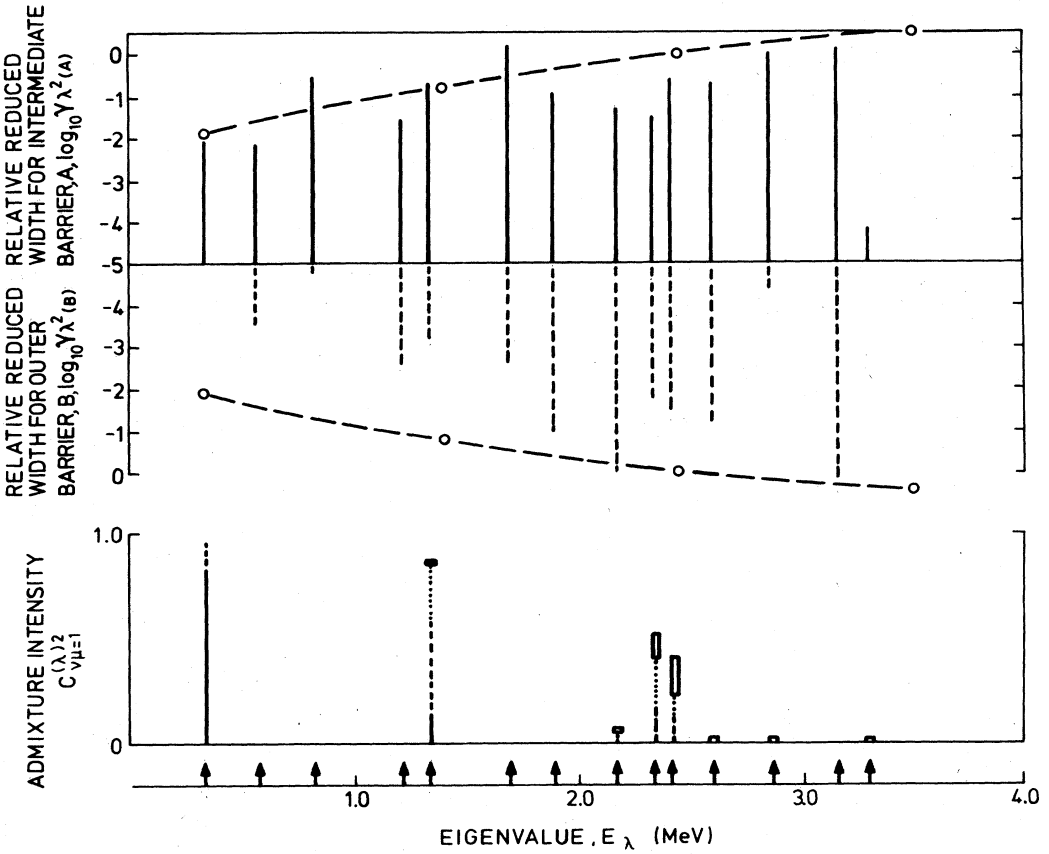

FIG. 93. Numerical model of vibrational damping of lowest states of an odd-mass nucleus. The lower part of the diagram shows the conventional vibrational admixture intensities for vibrations coupled to the lowest intrinsic state ($\mu=1$) as defined at the mean deformation of the vibrating nucleus. Zero-point vibrations are indicated by continuous vertical lines, one-phonon by dashed vertical lines, two-phonon by dotted vertical lines, and three-phonon by a vertical rectangle. Eigenvalues are indicated by arrows on the energy scale. The upper part of the diagram shows relative reduced widths for transmission through the two barriers, respectively, via the lowest intrinsic states at the two chosen barrier deformations. The envelopes of these quantities for pure vibrational states are also shown. Note the logarithmic scale.

$$c^{(\lambda)}_{\nu\mu} = \sum_{\mu'} c^{(\lambda)}_{\nu\mu'}\, {}_{(p)}\langle \chi_\mu(\eta_0) | \chi^{(p)}_{\mu'}(\eta_0)\rangle \,. \qquad (5.47b)$$

The results of a numerical example are presented in Fig. 93 for the parameters of Table X; this is a basis limited to four vibrational states ($\nu=0$–3), with phonon energy equal to 0.7 MeV, and six states of the particle potential well ($\mu=1$–6). While the first five particle states have the parabolic behavior schematically assigned to single-particle states as described above, the sixth is given no deformation dependence but is intended to allow for the mixing in of more complex states above the energy gap. The residual interaction matrix element between all particle states is taken as 0.1 MeV.

In the lower part of Fig. 93 a conventional measure of the vibrational strength of the first 14 calculated eigenstates is shown; these are the squared admixture coefficients $C^{(\lambda)2}_{\nu\mu}$ for the basis components with $\mu=1$, the lowest intrinsic state, defined at the central deformations of the well (denoted here by η_{II}). Different phonon components are denoted by various forms of vertical line measure, as indicated in the figure caption. Vibrational strength as thus defined is obviously quite well localized, although the weighted mean strength for different phonon components is not separated by the starting phonon energy of 0.7 MeV but by an "effective" phonon energy of 1.0 MeV.

In the upper part of Fig. 93 the relative reduced widths calculated at deformations $\eta_A=\eta_{II}-0.13$ and $\eta_B=\eta_{II}+0.13$ are shown for the lowest channel. Because the logarithms are presented in this diagram the relative differences are visually underemphasized, but it is apparent that there is no marked correlation either of

TABLE X. Parameters describing the deformation dependence of schematic single-particle levels in numerical model of vibration damping (energies in MeV). All values of $D^{(p)}_\mu$ are set to zero.

$\mu\,(p)$	$\mathcal{E}^{(p)}_{0\mu}$	$A^{(p)}_\mu$	$b^{(p)}_\mu$
1	0.0	154	−0.24
2	0.0	72	−0.125
3	0.0	130	−0.06
4	0.0	500	0.04
5	0.0	55	0.23
6	1.2	0.0	0.0

the reduced widths with each other or with the conventional vibrational strength. The reason for the lack of correlation is, of course, that the intrinsic states defining the lowest channels at the chosen intermediate and outer barrier deformations have essentially different particle state structures from each other and from the intrinsic state defined at η_{II}. The last is essentially 94% of $\mu_p = 3$, while the lowest channel at η_A is composed of 97.6% of $\mu_p = 2$ (and only 1.7% $\mu_p = 3$), and the lowest channel at η_B is 98% of $\mu_p = 5$.

The envelopes of possible reduced widths for pure vibrational states are shown by dashed curves in the upper part of Fig. 93. It is apparent that none of these eigenstates would have nearly the full fission strength that our simple conception of a vibrational resonance would lead us to expect. A single quantitative measure of fission strength for the eigenstates cannot be given since it would involve the barrier penetrabilities which are independent of the mixing model, but for reasonably similar values of P_A and P_B (the condition under which fission vibrational resonances are most likely to be apparent), the greatest strength will fall short of a pure vibrational fission strength by more than an order of magnitude. The fission strength is here defined by

$$S_{\lambda(\mu)} = \frac{\Gamma^{(A)}_{\lambda(\mu)}\Gamma^{(B)}_{\lambda(\mu)}}{\Gamma^{(A)}_{\lambda(\mu)} + \Gamma^{(B)}_{\lambda(\mu)}} = \frac{(2P_A\gamma^2_{\lambda(\mu)})(2P_B\gamma^2_{\lambda(\mu)})}{2P_A\gamma^{(A)2}_{\lambda(\mu)} + 2P_B\gamma^{(B)2}_{\lambda(\mu)}}, \qquad (5.48)$$

which is proportional to the integrated cross section across a fission resonance.

Finally it should be noted that the chosen input parameters for this calculation were not entirely arbitrary; they very approximately describe the single-particle states with odd parity and spin projection $\frac{1}{2}$ for a 141 neutron system in the region of the secondary well deformation ($\eta \equiv \epsilon \sim 0.65$) as deduced from the diagram of Nilsson *et al.* (1969). The lack of a clearcut contender with outstanding fission strength in the spectrum of Fig. 93 (particularly among the lower states, below, say, 1.5 MeV excitation energy) throws doubt on the interpretation of the resonance in ^{231}Th as a pure vibrational resonance, as discussed in Sec. V.B.5.*a*. The state with greatest potential fission strength (that at 2.59 MeV) has in fact over 80% of $\mu_p = 6$ in its structure, which implies that it is very likely further damped into a great many more complex states. Further discussion of the ^{231}Th case is given in Sec. V.C.4 and Sec. X.B.2.*a*.

b. Single-particle models with rotation and Coriolis coupling

The kind of model described in the previous subsection is appropriate for the low-lying states in odd-A nuclei with spin $\frac{1}{2}$. Higher spin states of single-particle character are expected to have similar density, eventually falling away in a Gaussian manner as the spin exceeds a dispersion value σ_k of order 3–3.5 in actinide nuclei. These higher-spin single-particle states would also couple with members of the rotational bands built on lower spin states. For an axially symmetric nucleus, the residual interaction mechanism for this coupling is the Coriolis force

$$H_{\rm cor} = -\frac{\hbar^2}{2\mathcal{I}}(2\mathbf{I}\cdot\mathbf{j}), \qquad (5.49)$$

where **j** is the intrinsic spin of the single particle. In first order the Coriolis coupling connects states which differ by unity in the spin projection K on the symmetry axis. The matrix element for the coupling of two intrinsic states is [see, e.g., Bohr and Mottelson (1975)]

$$\langle\chi_{\mu(I,K+1)}|H_{\rm cor}|\chi_{\mu'(I,K)}\rangle = -[(I-K)(I+K+1)]^{1/2}A_K, \qquad (5.50)$$

where

$$A_K = \frac{\hbar^2}{2\mathcal{I}}\langle K+1|j_\perp|K\rangle,$$

and $j_\perp$ is the component of the nucleon spin perpendicular to the symmetry axis. For ^{235}U the magnitude of A_K is observed from interband electric quadrupole transition strengths to be ≈ 25 keV in the normally deformed nucleus.

The Coriolis force can also operate in second order between states differing by 2 in K. But the appropriate matrix elements are expected to be an order of magnitude smaller.

It is clear that Coriolis coupling will significantly increase the fragmentation of vibrational fission states with spin greater than $\frac{1}{2}\hbar$. The already fragmented configuration of spin-$\frac{1}{2}$ single-particle states given in the example at the end of the previous subsection will be reflected in the spin-$\frac{3}{2}$ components of their rotational bands, and these will be further fragmented by Coriolis coupling with single-particle states with $\Omega = \frac{3}{2}$. Numerical models demonstrating the effect in a weaker way, and how it might apply to ^{231}Th, are given in Sec. V.C.4.

c. Even nucleus

A simple model for an even nucleus is to postulate a lowest intrinsic state (the fully pair-correlated state) with a wave function that is assumed to be invariant to deformation, and higher intrinsic states that are composed of two single-particle states or holes. The higher states are built up from configurations with energies that have a parabolic dependence on deformation, as described in Sec. V.C.1.*a*, with residual interaction matrix elements coupling them. The minimum energies of the higher states are greater than or equal to the energy gap (2Δ), relative to the lowest intrinsic state.

A schematic numerical model of this system has been solved with three vibrational states and eight intrinsic states. The lowest intrinsic state has zero energy and no dependence on deformation while the remaining seven have quadratic coefficients $A^{(p)}_\mu$ ranging between 300 and 400 MeV, and minimum energies (2Δ) of about 1.2 MeV (within the range 1.15–1.25 MeV) occurring at deformation $b^{(p)}_\mu$ of ranging from about −0.15 to 0.15 at intervals of approximately 0.05, relative to the center of the deformation well. The residual matrix element coupling all the intrinsic states (including the lowest) has been taken to be 0.1 MeV.

The result, as shown in Fig. 94, is that the coupling and fission widths for the lowest channel are correlated not only with each other, but with the vibrational configuration as defined at the center of the deformation well, and this is true not only for the main fission res-

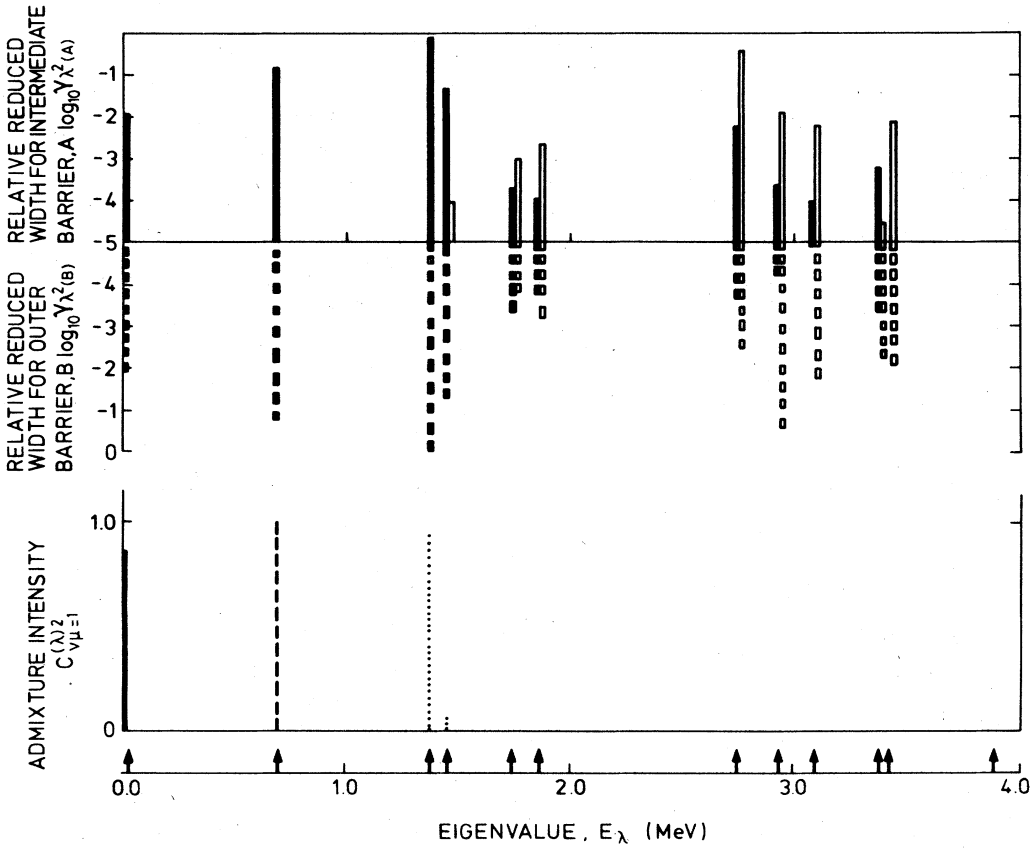

FIG. 94. Numerical model of vibrational damping of lowest states of an even nucleus. The layout of the figure and the key are as in Fig. 93 with the addition that reduced widths for the next available channel at the two barriers are also shown; these are denoted by open continuous and broken vertical blocks on the right-hand side of the solid blocks showing the reduced widths for the principal channels at each eigenvalue.

onances at 0.0, 0.7, and 1.4 MeV excitations (corresponding very precisely to 0, 1, and 2 phonons coupled to the lowest intrinsic state) but, to some degree, for the higher states as well. However, the fission and coupling widths of the higher states through the lowest channels are so small that the contributions of higher channels to the widths must be taken into account. The reduced widths for the next channel are therefore shown on Fig. 94 also. For these it is apparent that there is little sign of correlation. This is because the channel intrinsic states at the inner and outer deformation have a quite different configuration.

2. Detailed resonance structure of damped vibrational resonances

The results of the schematic models discussed in the last section show us that among states of fairly simple character some states with high fission strength do occur, but, except in even nuclei, these are not usually states of strong vibrational character in the conventional sense. Furthermore, states can occur with particularly high fission or coupling width, but not necessarily both, and these will not always appear with particularly strong fission character. Nevertheless, such states will be treated in this section as vibrational resonances in considering the mixing of relatively simple states with a dense background of much more complicated states (class-II compound states), but in doing this the possibility of their having nonideal properties must be considered. After dissolution of its fission strength in an incomplete way among the neighboring class-II compound states, the vibrational resonance is coupled to the class-I compound states to give an idealized situation which is indicated schematically in Fig. 95 [from Lynn (1970)]. Below, the possible detailed properties

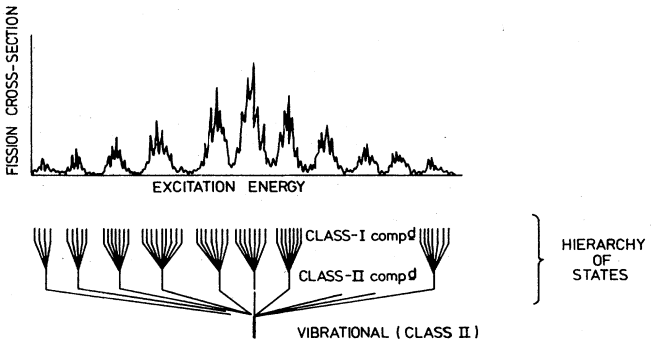

FIG. 95. Schematic illustration of the damping of a vibrational resonance into class-II, and ultimately class-I compound states.

of this three-stage hierarchy of structure are considered.

a. Resonance widths and cross sections

(*i*) *Damping of a state with ideal vibrational character.* A considerable amount can be learnt about the detailed structure of resonance widths and cross sections by simple use of the formulas for the coupling of class-I and class-II states given in Sec. III.C.5. To use these formulas it is only necessary to assume that there is no overlapping of the class-II states that constitute a damped vibrational resonance. In the ideal situation (the uniform model with equal matrix elements connecting the isolated vibrational state to its neighboring class-II compound states) the fission widths of the class-II (R-matrix auxiliary) states will be given by

$$\frac{\Gamma_{\lambda_{II}(f)}}{D_{II}} = \frac{1}{2\pi} \frac{\Gamma_{v(D)}\Gamma_{v(f)}}{(E_v - E_{\lambda_{II}})^2 + (\frac{1}{2}\Gamma_{v(D)})^2}, \tag{5.51}$$

where $\Gamma_{v(D)}$ and $\Gamma_{v(f)}$ are the damping and fission widths of the vibrational state at E_v; the coupling widths are given by a similar formula. The condition that class-II states of maximum width at the center of the damped vibrational resonance do not overlap is equivalent to

$$\Gamma_{v(f)} \ll \Gamma_{v(D)}, \quad \Gamma_{v(c)} \ll \Gamma_{v(D)}.$$

The choice of formula for coupling the class-II and class-I compound states will depend on the magnitude of $\Gamma_{\lambda_{II}(c)}$ and $\Gamma_{\lambda_I(f)}$ at each class-II state. One reasonable case is to assume that the class-II coupling widths $\Gamma_{\lambda_{II}(c)}$ are much greater than the class-I level spacing at the center. The formula for moderately weak coupling [Eq. (3.185)] then applies. Notice that as long as $\Gamma_{\lambda_{II}(c)} \gg D_I$, as we move away in energy from the center of the damped vibration the fine-structure fission widths (of R-matrix states) at the center of each class-II intermediate resonance remain constant at the value

$$\Gamma_{\lambda(f)} \approx \frac{2D_I}{\pi} \frac{\Gamma_{v(f)}}{\Gamma_{v(c)}}. \tag{5.52}$$

Thus a profile of the vibrational resonance drawn through the peaks of the fission widths at the class-II states will be much broader than the nominal width $\Gamma_{v(D)}$; this width will be reflected in the rapidly decreasing widths of the class-II states, as illustrated in Fig. 96. At sufficient energy from the center of the vibrational state, however, the coupling widths of the class-II resonances become less than the class-I level spacing, and then the perturbation formulas applicable to very weak coupling [Eqs. (3.162)–(3.167)] are applicable. A quasi-class-II state can then be identified in each intermediate group, carrying the bulk of the class-II fission width

$$\Gamma_{\lambda'' (f)} \approx \frac{D_{II}}{2\pi} \frac{\Gamma_{v(f)}\Gamma_{v(D)}}{(E_v - E_{\lambda_{II}})^2 + (\frac{1}{2}\Gamma_{v(D)})^2}. \tag{5.53}$$

The profile, rather than the widths of the intermediate groups, then shows the wing attenuation of the vibrational resonance.

The features of the cross section to be expected across a damped vibrational resonance are more complicated than this. Here we shall not discuss the precise shape (width and peak cross section) of each fine-structure resonance but only the locally averaged fission cross section across the fine-structure line, i.e.,

$$\langle \sigma_{\lambda(f)} \rangle \propto \frac{\Gamma_{\lambda(e)}\Gamma_{\lambda(f)}}{\Gamma_\lambda}, \tag{5.54}$$

where $\Gamma_{\lambda(e)}$ is the entrance channel width and Γ_λ is the total resonance width that includes all reaction channels in addition to entrance and exit channels. The equations expressing the entrance channel width, when this, as will normally be the case, is a process carried only by the class-I compound states, have been given for perturbation theory (very weak coupling between class-I and class-II states) in Sec. III [Eq. (3.167)]; a quasi-class-II state will carry only a small fraction of class-I admixture and its entrance channel width is correspondingly smaller than its quasi-class-I neighbors (this topic is discussed in more detail with examples in Sec. VI). When somewhat stronger coupling applies, the admixture coefficients $C^2_{\lambda(\lambda_{II})}$ carrying the fraction of class-II state in the fine-structure states λ become small, even at the center of the class-II intermediate resonance, and in the uniform model there is no marked fluctuation of the expected entrance channel width

$$\Gamma_{\lambda(e)} = (1 - C^2_{\lambda(\lambda_{II})})\langle \Gamma_{\lambda_I(e)} \rangle \tag{5.55}$$

in crossing the intermediate resonance.

Reaction channels can be characteristic of either class-I or class-II compound states. For the most part, in the excitation energy ranges in which structured fission phenomena are likely to occur, particle emission processes, such as inelastic neutron scattering, are likely to be confined to class-I compound states and will have the same properties relating to the intermediate resonances as the entrance channel widths. On the other hand, electromagnetic radiation widths are likely to be of the same order of magnitude for class-II compound states as class-I states (see Sec. VI.D.2 for a discussion). Thus we may write in general

$$\Gamma_{\lambda(\gamma)} = (1 - C^2_{\lambda(\lambda_{II})})\Gamma_{\lambda_I(\gamma)} + C^2_{\lambda(\lambda_{II})}\Gamma_{\lambda_{II}(\gamma)}. \tag{5.56}$$

Thus the factors that determine the appearance of the cross section across a damped vibrational resonance depend not only on the vibrational state widths $\Gamma_{v(D)}, \Gamma_{v(c)}, \Gamma_{v(f)}$, but also on the magnitude of the class-I entrance channel width and on the magnitude and nature of the reaction widths. Some examples of the effect of the magnitude of the competition factors are shown in Figs. 96, *a*, *b*, *c*, *d*, and *e*.

(*ii*) *Damping of vibrational states with nonideal character.* The ideal vibrational resonance discussed above is that of a single state with particularly strong fission and coupling width embedded (before mixing) in a dense forest of compound class-II states with fission and coupling widths that are small enough to be neglected. The discussion of Sec. V.C.1 makes it apparent that nonideal situations can occur in which, for example, two comparatively simple states may be situated quite close together, one carrying a strong coupling width and the other a strong fission width. The background class-II states will pick up elements of both, with the result

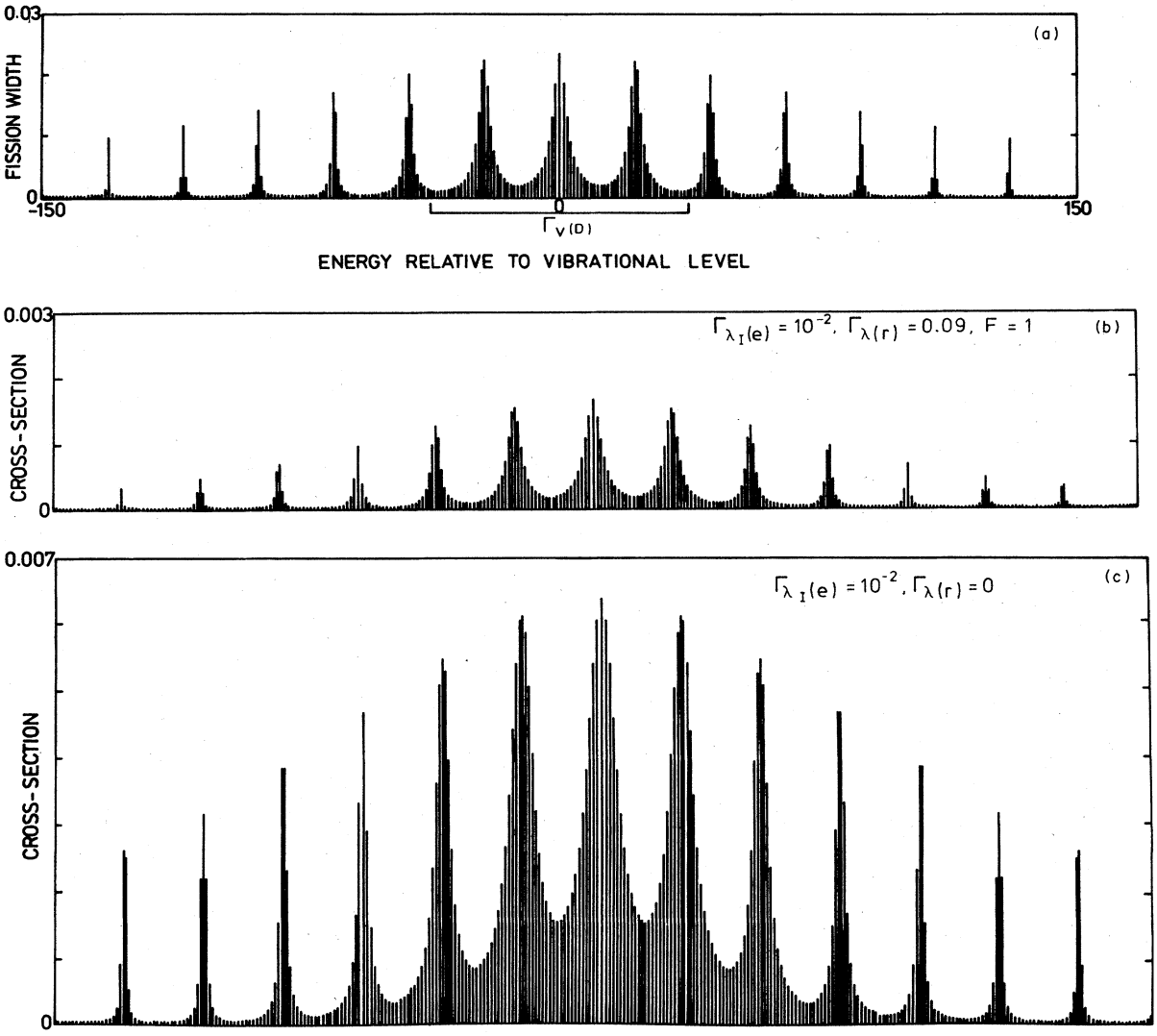

FIG. 96. Fission widths and cross sections of the fine-structure resonances across a damped vibrational resonance, with parameters $\Gamma_{\nu(f)} = 1$ unit, $\Gamma_{\nu(c)} = 25$, $\Gamma_{\nu(D)} = 75$, $D_I = 1$, $D_{II} = 21.7$. The top part of the diagram presents the widths and illustrates the flattening of the profile through the peaks of the class-II states. Lower diagrams show the cross section (averaged over an energy interval D_I across each fine structure resonance) for different choices of the entrance channel width and reaction width. Note: energy eigenvalues have been diagonalized only approximately.

that in the region of one state (say that one with the strong fission width) the fission widths of the class-II states will have the typical Lorentzian character of Eq. (5.51), but the coupling widths will show relatively little change with energy; this is shown schematically in Fig. 97. In this nonideal case the fine-structure width and cross-section profiles will show quite different features from those described in the previous subsection.

The simplest assumption is that the class-II state coupling width (or alternatively the fission width) is effectively constant across the vibrational resonance. As in the previous subsection we shall confine our discussion to the properties of R-matrix states, which means that the simple cross section deductions from the partial widths are only applicable when the class-II coupling width always exceeds the fission width. Then the fission width profile is (for moderately weak coupling)

$$\Gamma_{\lambda(f)} = \frac{D_I}{(2\pi)^2} \frac{\Gamma_{\nu(D)}\Gamma_{\nu(f)}D_{II}\Gamma_{II(c)}}{[(E_{\lambda_{II}} - E_\nu)^2 + (\tfrac{1}{2}\Gamma_{\nu(D)})^2][(E_\lambda - E_{\lambda_{II}})^2 + (\tfrac{1}{2}\Gamma_{II(c)})^2]} . \tag{5.57}$$

At the center of each class-II resonance the fission width of fine-structure levels is

$$\Gamma_{\lambda(f)}(E_\lambda \sim E_{\lambda_{II}}) = \frac{1}{\pi^2} \frac{D_I}{\Gamma_{II(c)}} \frac{\Gamma_{\nu(D)}\Gamma_{\nu(f)}D_{II}}{(E_{\lambda_{II}} - E_\nu)^2 + (\tfrac{1}{2}\Gamma_{\nu(D)})^2} . \tag{5.58}$$

Thus the profile through the peaks of the intermediate resonances reproduces that of the vibrational state with its characteristic damping width. The widths of the

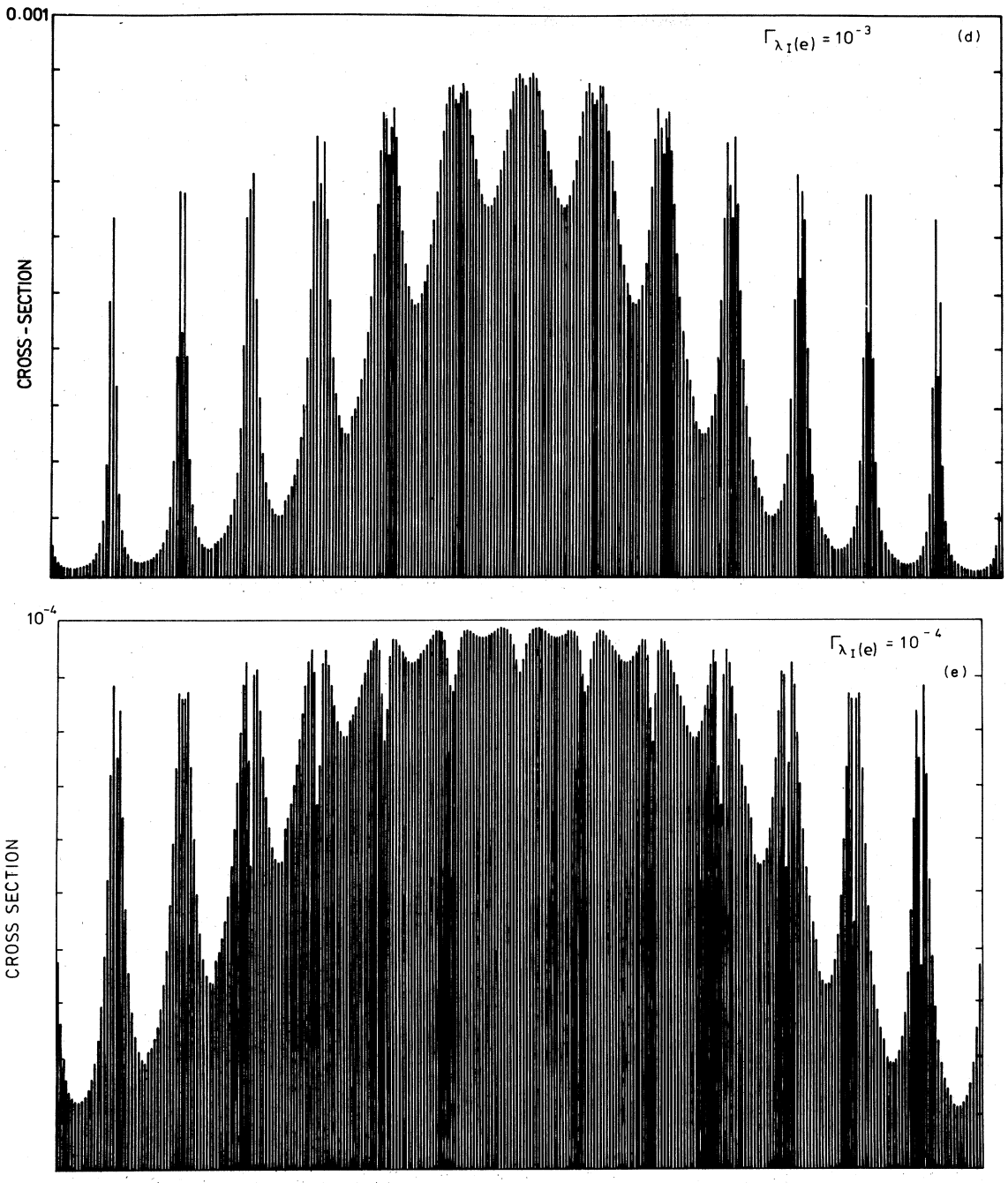

FIG. 96. (*Continued*)

intermediate resonances are constant, on the other hand, at the value $\Gamma_{II(c)}$. These features are illustrated in Fig. 98.

(*iii*) *Cross-section properties where class-II fission widths exceed coupling widths.* In this section the discussion may be based on the widths associated with the poles of the collision matrix. The relevant equations for coupling of a single class-II state with many class-I compound states are given in Sec. III.C.5 [Eq. (3.206)].

From Eq. (3.206) it can be seen that the main difference that accrues in the profile of observed resonance widths when the fission width of the vibrational level is much greater than its coupling width is that the two widths interchange their roles. Thus for the case of the ideal vibrational resonance the fission widths in the central region are

$$\Gamma_{\lambda(f)} \approx \frac{2D_I}{\pi} \frac{\Gamma_{\nu(c)}}{\Gamma_{\nu(f)}} \tag{5.59}$$

for the poles that carry significant partial width in the entrance channel and hence appear as significant fine-structure resonances in the cross section. In addition to these there is a pole with fission width approaching in value to the full fission width of the class-II reso-

nance but with very small entrance channel width; it will not normally be observable as a resonance in the cross section, but if it is included in the pattern of fission widths, it will introduce a very sharp distinction from the case discussed in Sec. V.C.2*a* (*i*); this is illustrated in Figs. 99 *a*, *b*, *c*, and *d*.

At the fringes of the vibrational resonance the class-II fission width eventually becomes less than the class-I level spacing, and perturbation theory again becomes applicable. The central resonance will have a fission width given by Eq. (5.53) and its immediate (quasi-class-I) neighbors have the values

$$\Gamma_{\lambda(f)} \approx \frac{2}{\pi}\frac{\Gamma_{\lambda_{II}(c)}\Gamma_{\lambda_{II}(f)}}{D_I} = \frac{1}{2\pi^3 D_I}\frac{\Gamma^2_{\nu(D)}\Gamma_{\nu(c)}\Gamma_{\nu(f)}}{[(E_{\lambda_{II}}-E_\nu)^2+(\frac{1}{2}\Gamma_{\nu(D)})^2]^2}. \quad (5.60)$$

In the cross section the central resonance, being narrower than the fine-structure spacing, will now, in principle, be observable, but its entrance channel width, being governed by the quantity $(1-C^2_{\lambda(\lambda_{II})})$, will be smaller, by a very considerable factor than in the corresponding case described in Sec. V.C.2.*a*(*i*).

In the case of the nonideal vibrational resonance, there is no longer even an approximate simple exchange of roles between the fission width and coupling width. We present here the general formulae for the fission width of fine-structure resonances ignoring the contribution of poles corresponding to very broad quasi-class-II states.

When the coupling width of the class-II states is essentially constant and only their fission widths follow the vibrational resonance profile, the required expression is

$$\Gamma_{\lambda(f)} = \frac{D_I}{4\pi^2}\frac{D_{II}\Gamma_{II(c)}\Gamma_{\nu(D)}\Gamma_{\nu(f)}[(E_{\lambda_{II}}-E_\nu)^2+\frac{1}{4}\Gamma^2_{\nu(D)}]}{(E_\lambda-E_{\lambda_{II}})^2[(E_{\lambda_{II}}-E_\nu)^2+\frac{1}{4}\Gamma^2_{\nu(D)}]^2+\frac{1}{4}\left\{\frac{D_{II}}{2\pi}\Gamma_{\nu(f)}\Gamma_{\nu(D)}+\Gamma_{II(c)}[(E_{\lambda_{II}}-E_\nu)^2+\frac{1}{4}\Gamma^2_{\nu(D)}]\right\}^2}, \quad (5.61)$$

provided class-II fission widths are greater than class-I level spacings [otherwise Eqs. (5.57), (5.58) are valid]. If the class-II fission widths remain essentially constant and Lorentzian behavior is confined to the coupling widths

$$\Gamma_{\lambda(f)} = \frac{D_I}{4\pi^2}\frac{D_{II}\Gamma_{II(f)}\Gamma_{\nu(D)}\Gamma_{\nu(c)}[(E_{\lambda_{II}}-E_\nu)^2+\frac{1}{4}\Gamma^2_{\nu(D)}]}{(E_\lambda-E_{\lambda_{II}})^2[(E_{\lambda_{II}}-E_\nu)^2+\frac{1}{4}\Gamma^2_{\nu(D)}]^2+\frac{1}{4}\left\{\frac{D_{II}}{2\pi}\Gamma_{\nu(c)}\Gamma_{\nu(D)}+\Gamma_{II(f)}[(E_{\lambda_{II}}-E_\nu)^2+\frac{1}{4}\Gamma^2_{\nu(D)}]\right\}^2} \quad (5.62)$$

b. Interference effects

Interference effects in the neighborhood of a class-II compound state forming a component of a damped vibrational resonance can be brought out by using perturbation theory (Lynn, 1974). In the neighborhood of a class-II state λ_{II} the contribution of all other class-II states λ'_{II} to the wave function of a fine-structure compound state at energy E_λ is

$$\sum_{\lambda'_{II}}\frac{\langle\lambda_I|H_c|\lambda'_{II}\rangle}{E_{\lambda'_{II}}-E_\lambda}X_{\lambda'_{II}} = \sum_{\lambda'_{II}}\sum_{\nu'_{II}\mu'}\frac{\langle\lambda_I|H_c|\nu'_{II}\mu'\rangle}{E_{\lambda'_{II}}-E_\lambda}\langle\lambda'_{II}|\nu'_{II}\mu'\rangle\langle\lambda'_{II}|\nu_{II}\mu\rangle\Phi_{\nu_{II}}\chi_\mu \quad (5.63)$$

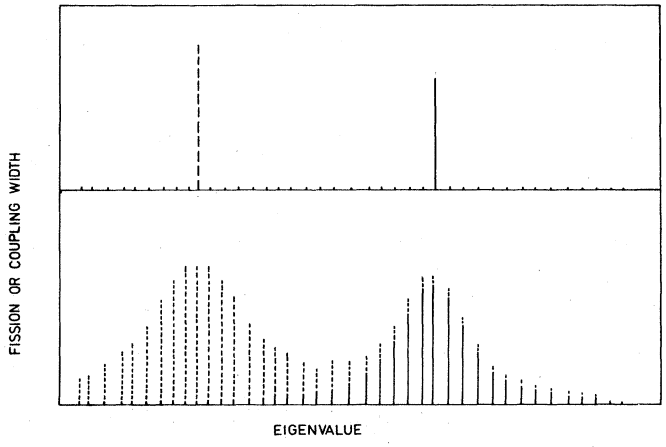

FIG. 97. Damping of nonideal vibrational states into class-II compound states. The upper part of the diagram shows two such states, one with strong coupling width (indicated by the broken vertical line), the other with strong fission width (indicated by the solid vertical line). Background class-II states are indicated by dots. In the lower part of the diagram the result after Lorentzian mixing of each special state into the background states is shown, coupling widths being indicated by dotted line and fission widths by solid lines.

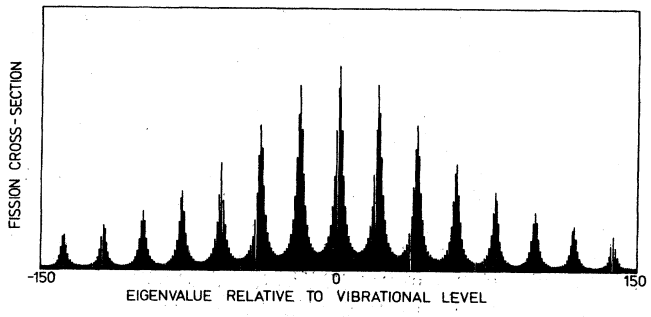

FIG. 98. Fission cross sections of fine-structure resonances across a damped vibrational resonance of nonideal properties, the class-II fission width having Lorentzian behavior and the class-II coupling width being independent of energy. Parameters are: $D_I = 1$ unit, $D_{II} = 19.7$, $\Gamma_{\nu(D)} = 100$, $\Gamma_{\nu(f)} = 3$, $\Gamma_{I(n)} = 0.15$, $\Gamma_{II(c)} = 0$.

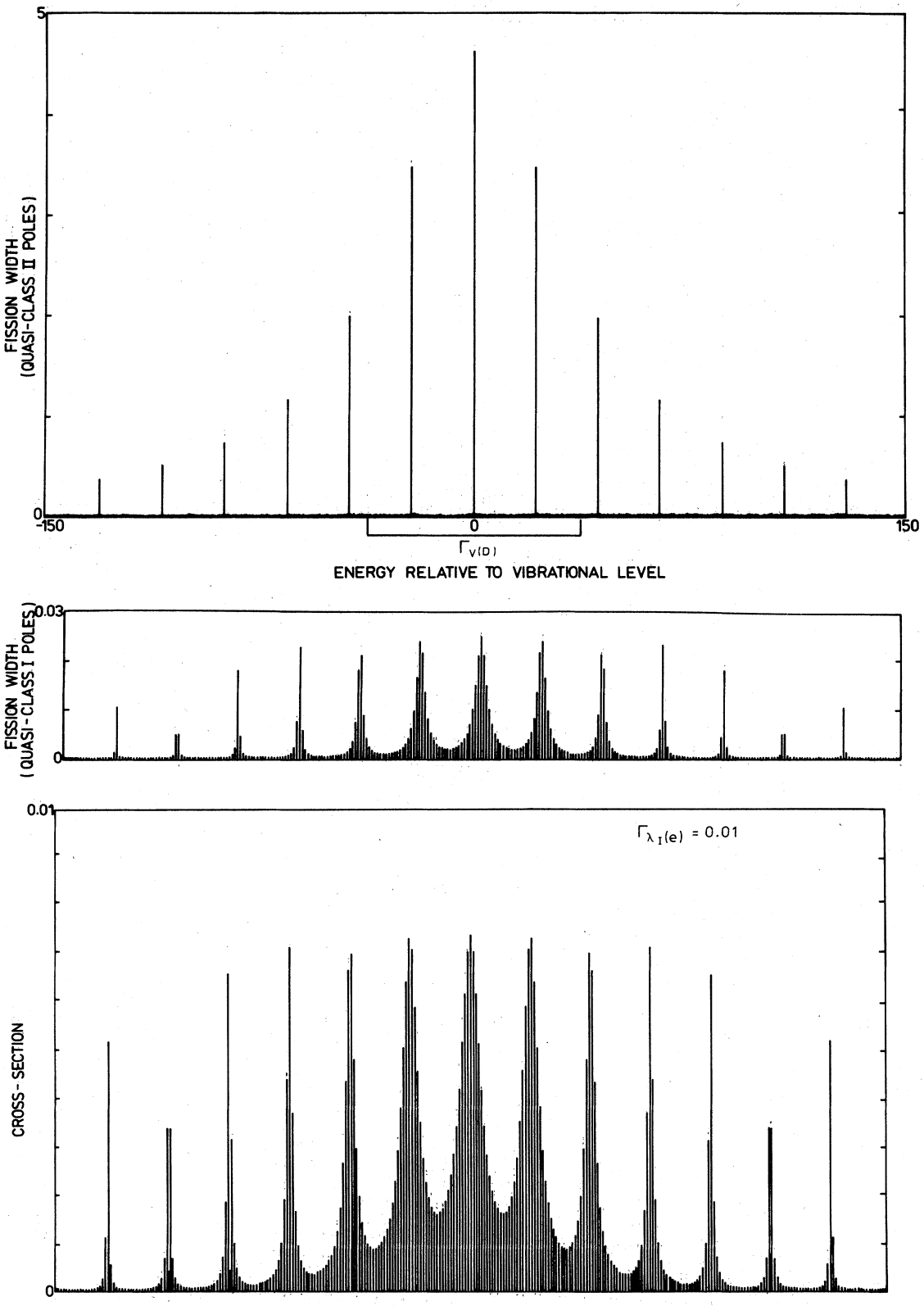

FIG. 99. Fission widths and cross sections related to the collision matrix poles across a damped vibrational resonance with fission width exceeding the coupling width. The parameters of the vibrational level are $\Gamma_{\nu(e)}=1$ unit, $\Gamma_{\nu(f)}=25$, $\Gamma_{\nu(D)}=75$, $D_{\mathrm{I}}=1$, $D_{\mathrm{II}}=21.7$. The top part of the diagram shows all the fission widths including the poles corresponding to class-II levels; this illustration effectively suppresses the widths of the fine structure resonances. The part diagram below is on a scale which shows the latter, the widths of the class-II poles being removed.

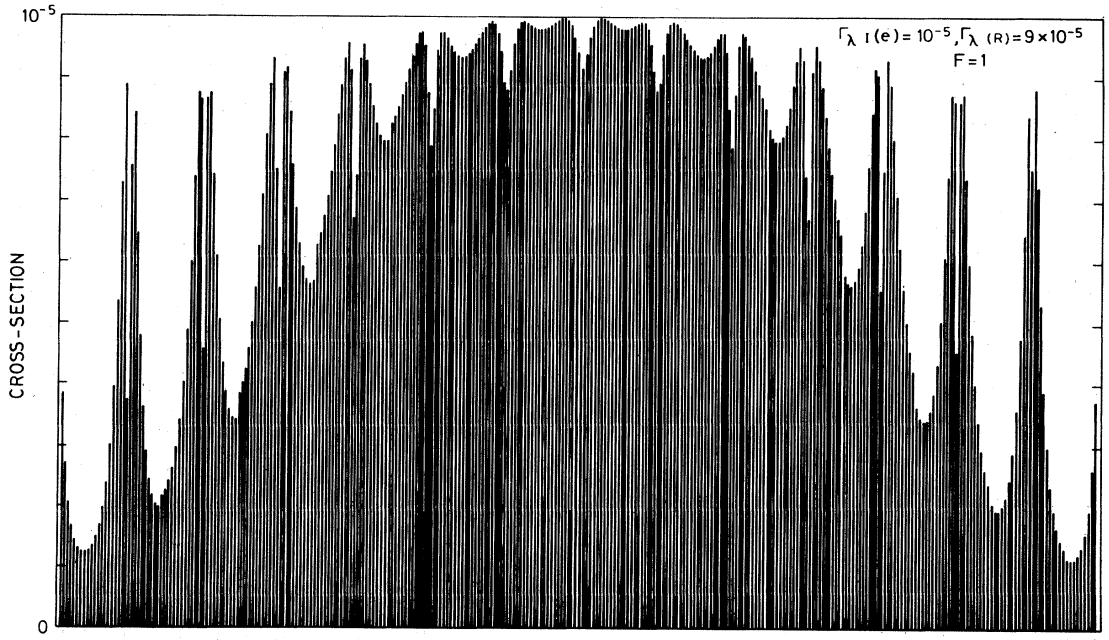

FIG. 99. (*Continued.*)

for the projection on the fission vibrational mode $\Phi_{\nu_{II}}\chi_\mu$. With the assumption of the Lorentzian expression the coefficients $\langle\lambda'_{II}|\nu_{II}\mu\rangle^2$ giving the damping (with half-width $W_{\nu_{II}\mu} = \frac{1}{2}\Gamma_{\nu_{II}\mu\,(d)}$) of the vibrational state into the states λ'_{II}, the "diagonal" term in this expression can be evaluated as

$$\frac{\pi\langle\lambda_I|H_c|\nu_{II}\mu\rangle\overline{\langle\lambda'_{II}|H_c|\nu_{II}\mu\rangle^2}}{D_{II}W_{\nu_{II}\mu}}\left[\frac{E_{\nu_{II}\mu}-E+iW_{\nu_{II}\mu}}{(E_{\nu_{II}\mu}-E)^2+W^2_{\nu_{II}\mu}}\right]\Phi_{\nu_{II}}\chi_\mu\,. \tag{5.64}$$

The contribution from the state λ_{II} to the same projection of the wave function can be written

$$\sum_{\nu'_{II}\mu'}\frac{\langle\lambda_I|H_c|\nu'_{II}\mu'\rangle\langle\nu'_{II}\mu'|\lambda_{II}\rangle\langle\lambda_{II}|\nu_{II\mu}\rangle}{E_{\lambda_{II}}-E_\lambda-iW_{\lambda_{II}}}\Phi_{\nu_{II}}\chi_\mu\,, \tag{5.65}$$

the half-width of the class-II state λ_{II} being $W_{\lambda_{II}} = \frac{1}{2}\Gamma_{\lambda_{II}(c)}$. Thus besides the Lorentzian contribution to the fission width of a fine-structure (R-matrix) state λ from the nearest class-II state there is an interference term (changing sign across the intermediate resonance) and a background term from other class-II states:

$$\Gamma_{\lambda(f)} = \frac{\langle\lambda_I|H_c|\lambda_{II}\rangle^2\Gamma_{\lambda II(f)}}{(E_\lambda-E_{\lambda_{II}})^2+W^2_{\lambda_{II}}} + 2\Re\,|\langle\lambda_I|H_c|\lambda_{II}\rangle\langle\lambda_I|H_c|\lambda_{II}\rangle|$$
$$\times\left\{\frac{(E_{\nu_{II}\mu}-E_\lambda)(E_{\lambda_{II}}-E_\lambda)+W_{\nu_{II}\mu}W_{\lambda_{II}}}{[(E_{\nu_{II}\mu}-E)^2+W^2_{\nu_{II}\mu}][(E_{\lambda_{II}}-E_\lambda)^2+W^2_{\lambda_{II}}]}\right\}\Gamma^{1/2}_{\lambda_{II}(f)}\Gamma^{1/2}_{\nu_{II}\mu\,(f)} + \frac{\langle\lambda_I|H_c|\nu_{II}\mu\rangle^2\Gamma_{\nu_{II}\mu(f)}}{(E_{\nu_{II}\mu}-E_\lambda)^2+W^2_{\nu_{II}\mu}}\,. \tag{5.66}$$

These expressions are derived on the assumption that cross-terms in $\nu'_{II}\mu'$ not equal to $\nu_{II}\mu$ vanish. The degree of correlation between inner barrier coupling and outer barrier fission modes (expressing the purity of the initial vibrational configuration; see Sec. V.C.1) is given by the term $\Re$:

$$\Re = \left|1 - \sum_{\nu'_{II}\mu'\neq\nu_{II}\mu}\frac{\langle\lambda_I|H_c|\nu'_{II}\mu'\rangle\langle\nu'_{II}\mu'|\lambda_{II}\rangle}{\langle\lambda_I|H_c|\lambda_{II}\rangle}\right|. \tag{5.67}$$

c. Closed expression for an idealized damped vibrational resonance

A closed expression for the mixing of an idealized vibrational configuration into class-II and class-I states has been obtained by Back (1974). The basic assumption made in deriving this expression is that only the vibrational configuration $\Phi_{\nu_{II}}\chi_\mu$ couples to the class-I compound states (through the matrix element $\langle\lambda_I|H_c|\nu_{II}\mu\rangle$); the matrix elements between class-I states and all other configurations of the type $\Phi'_{\nu_{II}}\chi_{\mu'}$ are zero. Physically, this corresponds to the ideal vibrational state with full correlation of amplitude and intrinsic wave function at the inner and outer barriers. The nonzero matrix elements $\langle\lambda^{(q)}_{II}|H_c|\nu_{II}\mu\rangle$ give the damping of the vibrational state among the other class-II states $\lambda^{(q)}_{II}$ which are obtained by diagonalization among all class-II configurations $\nu'_{II}\mu'$ except $\nu_{II}\mu$.

The uniform picket-fence model (see Sec. III.C.5) may be adapted to deal with this situation. Two sets of uniform spacings and matrix elements are postulated. The eigenvalues of the fine-structure R-matrix states are (in general) given by

$$E_\lambda - E_{\nu_{II}} = \sum_{\lambda_I}\frac{\langle\lambda_I|H_c|\nu_{II}\mu\rangle^2}{E_\lambda-E_{\lambda_I}} + \sum_{\nu'_{II}\mu'}\frac{\langle\lambda^{(q)}_{II}|H_c|\nu_{II}\mu\rangle^2}{E_\lambda-E^{(q)}_{\lambda_{II}}}\,. \tag{5.68}$$

Admixture coefficients for:

(i) states λ_I into fine-structure states are

$$C_{\lambda(\lambda_I)} = \frac{\langle \lambda_I | H_c | \nu_{II}\mu\rangle}{E_\lambda - E_{\lambda_I}} C_{\lambda(\nu_{II}\mu)}, \tag{5.69}$$

(ii) quasi-class-II states $\lambda_{II}^{(q)}$ into fine-structure states

$$C_{\lambda(\lambda_{II}^{(q)})} = \frac{\langle \lambda_{II}^{(q)} | H_c | \nu_{II}\mu\rangle}{E_\lambda - E_{\lambda_I}^{(q)}} C_{\lambda(\nu_{II}\mu)}, \tag{5.70}$$

(iii) the vibrational state into fine-structure states

$$C^2_{\lambda(\nu_{II}\mu)} = \left[1 + \sum_{\lambda_I} \frac{\langle \lambda_I | H_c | \nu_{II}\mu\rangle^2}{(E_\lambda - E_{\lambda_I})^2} + \sum_{\lambda_{II}^{(q)}} \frac{\langle \lambda_{II}^{(q)} | H_c | \nu_{II}\mu\rangle^2}{(E_\lambda - E_{\lambda_{II}^{(q)}})^2}\right]^{-1}. \tag{5.71}$$

In the picket-fence model the last expression becomes

$$C^2_{\lambda(\nu_{II}\mu)} \approx \frac{D_I}{2\pi} \frac{\Gamma_{\nu_{II}(c')}}{\left(E_\lambda - E_{\nu_{II}\mu} - \frac{1}{2}\Gamma_{\nu_{II}(D)} \cot\frac{\pi E_\lambda}{D_{II}}\right)^2 + \frac{1}{4}\left(\Gamma^2_{\nu_{II}(c')} + \Gamma_{\nu_{II}(c')}\Gamma_{\nu_{II}(D)}(D_I/D_{II})\csc^2\frac{\pi E_\lambda}{D_{II}}\right)} \tag{5.72}$$

where

$$\Gamma_{\nu_{II}(c')} = \frac{2\pi\langle \lambda_I | H_c | \nu_{II}\mu\rangle^2}{D_I} \tag{5.73}$$

is the coupling width for the vibrational state directly into the class-I compound states, and

$$\Gamma_{\nu_{II}(D)} = \frac{2\pi\langle \lambda_{II}^{(q)} | H_c | \nu_{II}\mu\rangle^2}{D_{II}} \tag{5.74}$$

is the damping width of the vibrational state into the quasicomplete class-II set.

The eigenvalue equation in the picket-fence model becomes

$$E_\lambda - E_{\nu_{II}\mu} = \frac{1}{2}\Gamma_{\nu_{II}(c')} \cot\frac{\pi E_\lambda}{D_I} + \frac{1}{2}\Gamma_{\nu_{II}(D)} \cot\frac{\pi(E_\lambda - \delta)}{D_{II}}, \tag{5.75}$$

the original spacings being

$$E_{\lambda_I} = \lambda_I D_I, \quad E^{(q)}_{\lambda_{II}} = \lambda_{II} D_{II} + \delta. \tag{5.76}$$

A numerical example of the admixture coefficients of Eq. (5.72) is shown in Fig. 100. This should be compared with Fig. 96 in which the coefficients have been computed with overlap, but not interference, of the class-II intermediate resonances.

3. Average fission strength functions and cross sections over a damped vibrational resonance

a. Strength function for a single vibrational level (with weak coupling to the fission continuum)

If an individual class-II state λ_{II} is considered after damping of the vibrational state ν_{II}, the fission strength function averaged over the class-II intermediate resonance is [see Sec. V.C.2.*a*.(*i*)]

$$\left\langle \frac{\Gamma_{\lambda(f)}}{D} \right\rangle = \frac{\Gamma_{\lambda_{II}(e)}\Gamma_{\lambda_{II}(f)}}{D_{II}(\Gamma_{\lambda_{II}(e)} + \Gamma_{\lambda_{II}(f)})}. \tag{5.77}$$

If it is assumed that the admixture of the vibrational state gives the coupling width as well as the fission width to the class-II compound states, then simple Lorentzian expressions for these properties can be written down (assuming that these widths add a negligible amount to the damping of the vibrational state and that

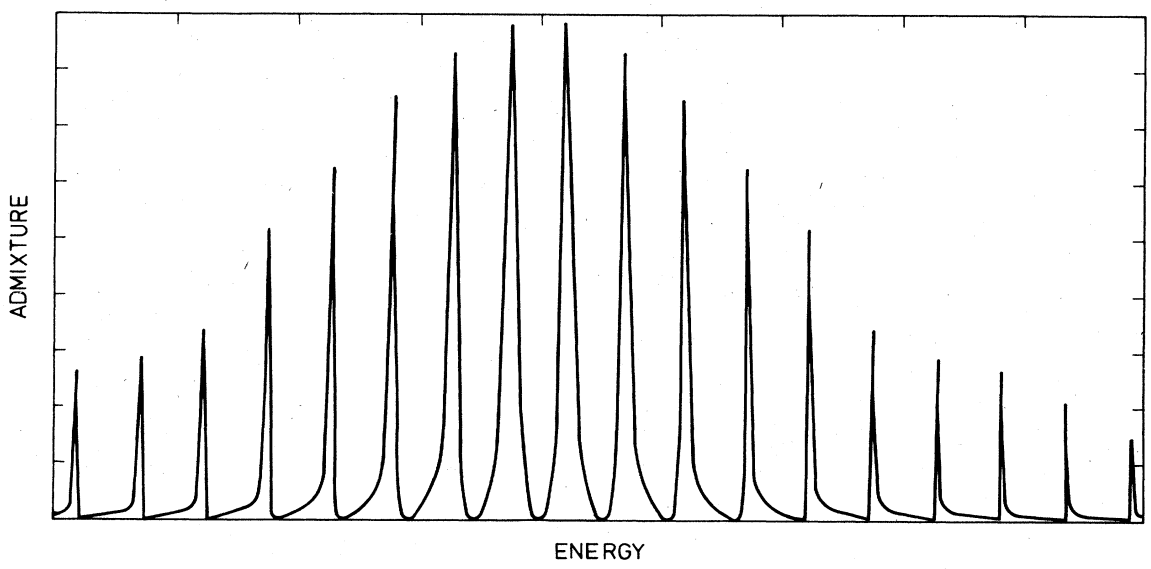

FIG. 100. An exact uniform model calculation of profile of admixture coefficients for the R-matrix eigenstates across a damped vibrational resonance [due to Back (1974)]. Parameters are $D_I = 1$, $D_{II} = 21.7$, $2\pi\langle \lambda_I | H_c | \upsilon_{II}\mu\rangle^2/D_I = 25$, $2\pi\langle \lambda_{II} | H_c | \upsilon_{II}\mu\rangle^2/D_{II} = 75$.

$\Gamma_{\lambda_{II}(c)} \gg \Gamma_{\lambda_{II}(f)}$):

$$\Gamma_{\lambda_{II}(c)} = \frac{D_{II}}{2\pi} \frac{\Gamma_{\nu_{II}(D)}\Gamma_{\nu_{II}(c)}}{(E_{\lambda_{II}} - E_{\nu_{II}})^2 + \frac{1}{4}\Gamma^2_{\nu_{II}(D)}}, \tag{5.78}$$

$$\Gamma_{\lambda_{II}(f)} = \frac{D_{II}}{2\pi} \frac{\Gamma_{\nu_{II}(D)}\Gamma_{\nu_{II}(f)}}{(E_{\lambda_{II}} - E_{\nu_{II}})^2 + \frac{1}{4}\Gamma^2_{\nu_{II}(D)}}, \tag{5.79}$$

where $\Gamma_{\nu_{II}(D)}$ is the damping width of the vibrational state into the class-II compound states. Substitution of these expressions into (5.77) gives

$$\left\langle \frac{\Gamma_{\lambda(f)}}{D_\lambda} \right\rangle \approx \frac{1}{2\pi} \frac{\Gamma_{\nu_{II}(D)}\Gamma_{\nu_{II}(f)}}{(E - E_{\nu_{II}})^2 + \frac{1}{4}\Gamma^2_{\nu_{II}(D)}}. \tag{5.80}$$

If none of the fine-structure (R-matrix) levels resulting from the mixing of a vibrational level, first into class-II states, and from these into class-I states, has a fission width of the order of or greater than the class-I level spacing, a superior treatment, based on Bohr and Mottelson's (1969) expression [Eqs. (3.192)] for the energy-dependent average properties of a Lorentzian line, can be given. As in Back's fine-structure treatment, given above in Sec. V.C.2.*c*, two kinds of matrix element coupling the vibrational level to the class-I states $H_{\lambda_I \nu_{II}}$ and to the background class-II states, $H_{\lambda_{II}^{(b)}\nu_{II}}$ are recognized. Then the expression for the effective width [Eq. (3.192b)] becomes

$$\Gamma_{\rm eff}(E) \approx \int \frac{dE_\lambda}{D_I} \frac{H^2_{\lambda_I \nu_{II}}}{(E - E_{\lambda_I})^2 + (\frac{1}{2}\Delta)^2} + \sum_{\lambda_{II}} \frac{H^2_{\lambda_{II}^{(b)}\nu_{II}}}{(E - E^{(b)}_{\lambda_{II}})^2 + (\frac{1}{2}\Delta)^2} \tag{5.81}$$

if a Cauchy averaging function of width Δ, is employed. If the second term on the right-hand side of this expression is evaluated at energy E equal to a given $E_{\lambda_{II}}$ the result in the uniform approximation is

$$\sum_{\lambda_{II}^{(b)}} \frac{H^{(b)}_{\lambda_{II}\nu_{II}}}{(E - E_{\lambda_{II}})^2 + (\frac{1}{2}\Delta)^2} = \frac{2\pi H^2}{D_{II}\Delta} \coth \frac{\pi\Delta}{2D_{II}} = \frac{2\pi H^2_{\lambda_{II}^{(b)}\nu_{II}}}{D_{II}} \mathcal{S}, \tag{5.82}$$

with $\mathcal{S} = 1.0903$ for $\Delta = D_{II}$ and approaching unity for $\Delta \gg D_{II}$. The same term at energy midway between two class-II levels is

$$\sum_{\lambda_{II}^{(b)}} \frac{H^2_{\lambda_{II}^{(b)}\nu_{II}}}{(E - E_{\lambda_{II}})^2 + (\frac{1}{2}\Delta)^2} = \frac{2\pi H^2_{\lambda_{II}^{(b)}\nu_{II}}}{D_{II}\Delta} \tanh \frac{\pi\Delta}{2D_{II}} = \frac{2\pi H^2_{\lambda_{II}^{(b)}\nu_{II}}}{D^2_{II}} \mathcal{S}, \tag{5.83}$$

with $\mathcal{S} = 0.0171$ for $\Delta = D_{II}$ and again approaching unity for $\Delta \gg D_{II}$. Evaluation of the first term gives

$$\int \frac{dE_\lambda}{D_I} \frac{H^2_{\lambda_I \nu_{II}}}{(E - E_{\lambda_I})^2 + (\frac{1}{2}\Delta)^2} = \frac{2\pi H^2_{\lambda_I \nu_{II}}}{D_I \Delta}. \tag{5.84}$$

The result is that $\Gamma_{\rm eff}$ for the locally averaged, damped vibrational resonance is

$$\Gamma_{\rm eff} = \frac{2\pi H^2_{\lambda_I \nu_{II}}}{D_I} + \frac{2\pi H^2_{\lambda_{II}^{(b)}\nu_{II}}}{D_{II}} \mathcal{S}, \tag{5.85}$$

which is approximately the sum of the widths for coupling the vibrational level to the class-I and background class-II states directly and alone, $\Gamma_{\nu_{II}(c)}$ and $\Gamma_{\nu_{II}(D)}$ respectively. The expression for the fission strength function through channel μ is, therefore,

$$\left\langle \frac{\Gamma_{\lambda(\mu)}}{D_\lambda} \right\rangle \approx \frac{1}{2\pi} \frac{(\Gamma_{\nu_{II}(c)} + \Gamma_{\nu_{II}(D)} + \Delta)\Gamma_{\nu_{II}(\mu)}}{(E_{\nu_{II}} - E)^2 + \frac{1}{4}(\Gamma_{\nu_{II}(c)} + \Gamma_{\nu_{II}(D)} + \Delta)^2}. \tag{5.86}$$

Note that this treatment explicitly achieves the extra spreading of the vibrational state due to coupling with class-I states across the intermediate barrier. In this way it is superior to the first treatment presented. The price paid for the simplicity of treatment is the neglect of any contribution to the coupling with class-I states that may come from the background class-II states [see also Sec. V.C.2.*a*.(*ii*)].

b. Energy-independent coupling to class-I states

An alternative assumption to that presented in the previous subsection is that the coupling width for each class-II compound state is effectively constant. The mechanism for this possibility is that the source of the coupling width does not come from the vibrational level that provides the fission width. Examples of this possibility were seen in the schematic models of Sec. V.C.1 and discussed in more detail in Sec. V.C.2.*a*(*ii*). If we think of these models as giving the configurations only of the simplest (class-II) states, which then have to be coupled to a denser background of more complex (class-II) states, then we see that in certain cases (such as the single-particle models for odd-A nuclei) there may be little or no correlation between the coupling and fission widths of the "simple" states. We can find examples in those models of a state with considerable fission width and small coupling width being neighbor to one with negligible fission width but very large coupling width. It is apparent then that the class-II compound states in the neighborhood of the first state may nearly satisfy the assumption of energy-independent coupling.

With this assumption and the use of Eqs. (3.185b) and (5.53) it is found that

$$\left\langle \frac{\Gamma_{\lambda(f)}}{D_\lambda} \right\rangle \approx \frac{1}{2\pi} \frac{\Gamma_{\nu_{II}(D)}\Gamma_{\nu_{II}(f)}}{\left[(E - E_{\nu_{II}})^2 + \frac{1}{4}\left(\Gamma^2_{\nu_{II}(D)} + \frac{2D_{II}\Gamma_{\nu_{II}(D)}\Gamma_{\nu_{II}(f)}}{\pi\Gamma_{\lambda_{II}(c)}}\right)\right]}. \tag{5.87a}$$

Thus the effective width of the vibrational resonance is

$$\left(\Gamma^2_{\nu_{II}(D)} + \frac{2D_{II}\Gamma_{\nu_{II}(D)}\Gamma_{\nu_{II}(f)}}{\pi\Gamma_{\lambda_{II}(c)}}\right)^{1/2}. \tag{5.87b}$$

c. Non-Lorentzian fission width behavior

Yet again, the class-II coupling widths may have the Lorentzian form of the vibrational resonance while their fission widths have different energy behavior. The form of the fission strength function is then

$$\left\langle \frac{\Gamma_{\lambda(f)}}{D_\lambda} \right\rangle \approx \frac{1}{2\pi} \frac{\Gamma_{\nu_{II}(D)}\Gamma_{\nu_{II}(c)}}{\left[(E - E_{\nu_{II}})^2 + \frac{1}{4}\left(\Gamma^2_{\nu_{II}(D)} + \frac{2D_{II}\Gamma_{\nu_{II}(D)}\Gamma_{\nu_{II}(c)}}{\pi\Gamma_{\lambda_{II}(f)}}\right)\right]}. \tag{5.88}$$

d. Fission probability and fission cross section

If the widths of class-II compound states are greater than the class-II level spacing the expressions for the

fission strength discussed in Secs. V.C.3.*a* and *b* may be used directly in computations of fission probability or fission cross section [see Eqs. (5.1) and (5.25)], the fission transmission coefficient being

$$T_f = 2\pi\left\langle\frac{\Gamma_{\lambda(f)}}{D_\lambda}\right\rangle . \tag{5.89}$$

These expressions are not valid if the intermediate structure is not washed out in this way. Consider the situation in which the transmission coefficient for competitive processes (such as radiative capture) T' is much smaller than the fission coefficient. If the energy dependence of the latter is modulated across the class-II resonances there will be regions between the resonances where the fission probability is much smaller than indicated by the ratio of the average transmission coefficients, and in consequence the true average fission probability is also smaller than this ratio; the factor between the two can be large. No exact treatment of the problem is available for the class-II structure across a damped vibrational resonance, but treatments for local levels and a sequence of uniform levels are described in Sec. VI.C.2.*c*. Application of these formulas to the damped vibrational resonance results in line shapes for the fission probability that are similar in width to that of the original fission transmission coefficient although the half-widths of the intermediate structures in the fission probability are much broader than the corresponding widths in the transmission coefficient [see Eq. (6.87)]. The expression for the fission probability averaged over energy intervals equal to the class-II level spacing as deduced from Eqs. (5.25), (5.78), and (5.79) for isolated class-II states is:

$$\langle P_f\rangle_{D_{II}} = \frac{\frac{1}{2}\Gamma_{\nu_{II}(D)}}{[(E-E_{\nu_{II}})^2+\frac{1}{4}\Gamma^2_{\nu_{II}}]} \times \frac{\Gamma_{\nu_{II}(c)}\Gamma_{\nu_{II}(f)}}{[T'\Gamma_{\nu_{II}(c)}\Gamma_{\nu_{II}(f)}+\frac{1}{4}T'^2(\Gamma_{\nu_{II}(c)}+\Gamma_{\nu_{II}(D)})^2]^{1/2}} . \tag{5.90}$$

The conditions for the validity of this are that $\Gamma_{\nu_{II}(f)}$ and $\Gamma_{\nu_{II}(c)}$ are much smaller than $\Gamma_{\nu_{II}(D)}$ and that $\Gamma_{\nu_{II}(c)}\Gamma_{\nu_{II}(f)}/\Gamma^2_{\nu_{II}(D)} \ll T'$. This expression is illustrated for certain choices of parameters in Fig. 101 and compared with the shape that would be deduced if the class-II intermediate structure were not taken into account:

$$\text{“}P_f\text{”} = \frac{\Gamma_{\nu_{II}(D)}\Gamma_{\nu_{II}(c)}\Gamma_{\nu_{II}(f)}}{\Gamma_{\nu_{II}(D)}\Gamma_{\nu_{II}(c)}\Gamma_{\nu_{II}(f)}+T'(\Gamma_{\nu_{II}(c)}+\Gamma_{\nu_{II}(f)})[(E-E_{\nu_{II}})^2+\frac{1}{4}\Gamma^2_{\nu_{II}}]} . \tag{5.91}$$

4. Examples of damped vibrational resonances

a. ^{240}Pu

The classic example of a damped vibrational fission resonance occurs at 5 MeV excitation energy in the compound nucleus ^{240}Pu and has been studied by many workers (Back *et al.*, 1969; Specht *et al.*, 1969; Britt *et al.*, 1969; Back *et al.*, 1974b; Glässel *et al.*, 1976). The most definitive work has been done by Glässel *et al.* (1976), who have measured the fission yield curve of the ^{239}Pu(d,pf) reaction with energy resolution of 3 keV, thus revealing structure (presumably class-II intermediate reasonances) within the damped vibrational resonance, and also the angular distribution of fission fragments about the classical recoil axis. Their

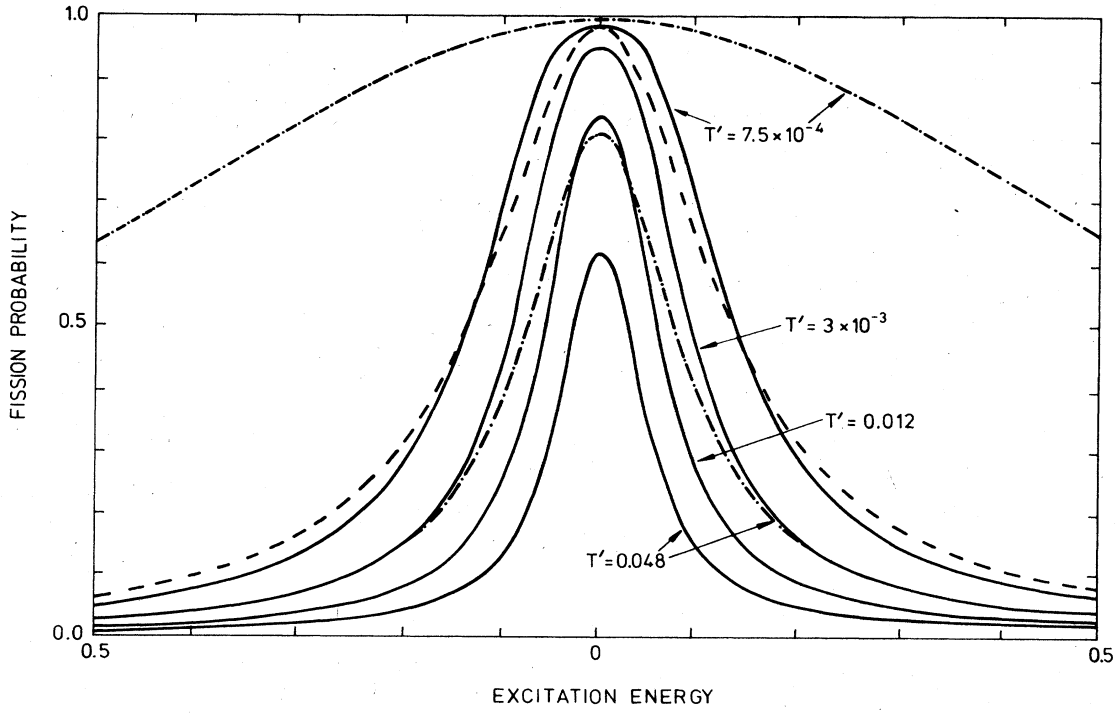

FIG. 101. Fission probability, averaged across energy interval of the order of the class-II level spacing, for a damped vibrational resonance. In this example the parameters are $\Gamma_{\nu_{II}(D)} = 0.05$, $\Gamma_{\nu_{II}(A)} = 0.02$, $\Gamma_{\nu_{II}(B)} = 0.01$. Dot-dash curves do not include effect of class-II structure. Dashed curve is a Lorentzian for comparison with the $\Gamma = 7.5\times10^{-4}$ full drawn curve.

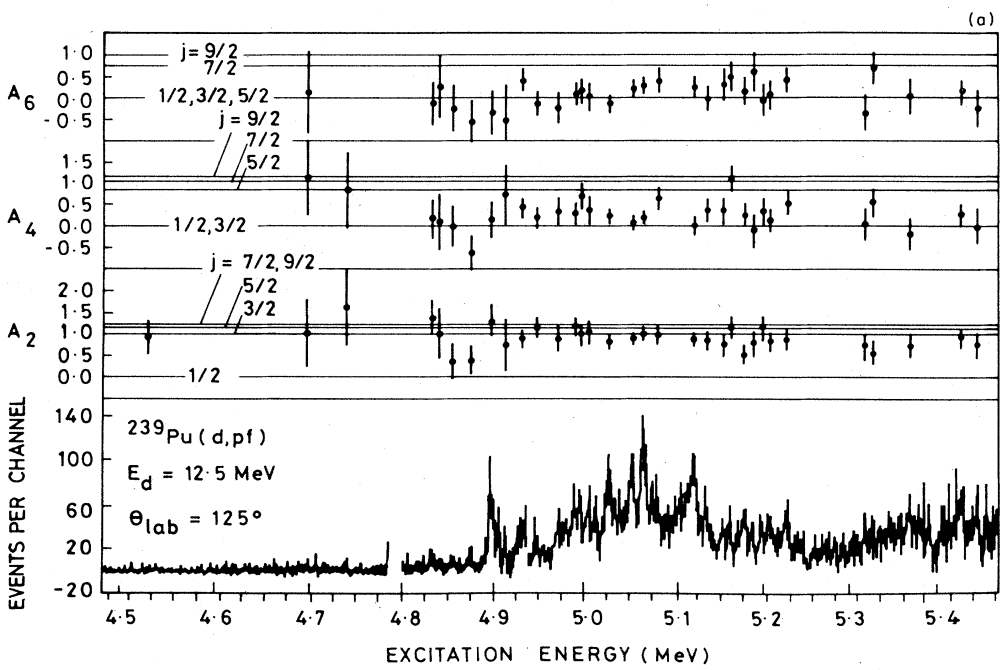

FIG. 102a. High-resolution (~3 keV) proton spectrum from the (d,pf) coincidence experiment by Glässel *et al.* (1976), below. Above are the measured fission fragment angular distribution coefficients A_λ [Eq. (5.92)]. Horizontal lines are theoretical coefficients for states of a $K=0$ rotational band populated through a neutron transfer to the $j=\frac{1}{2}$ ^{239}Pu target with neutron j values as indicated.

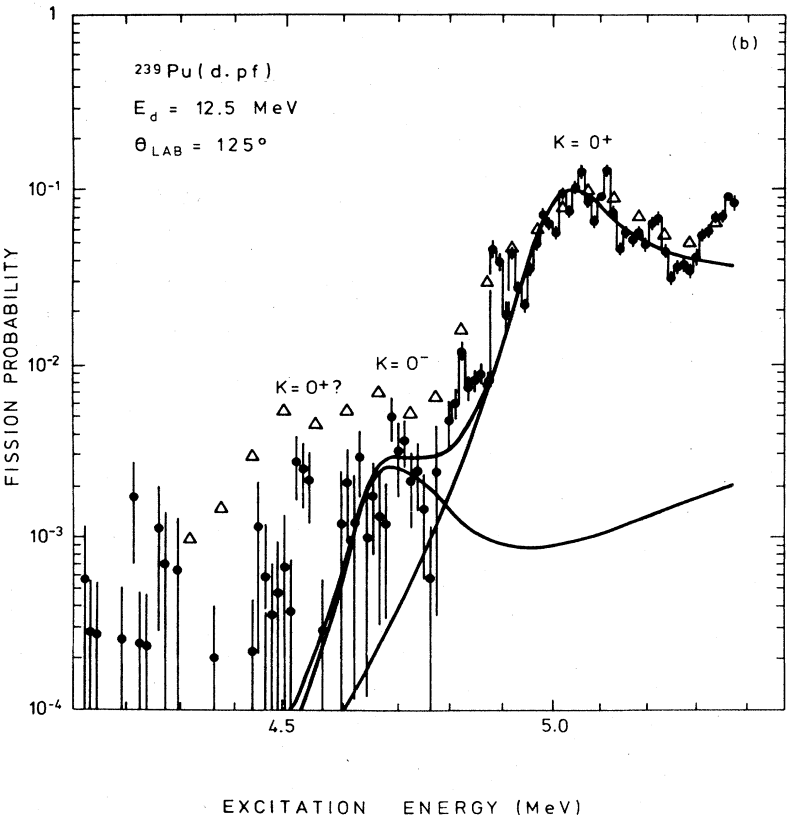

FIG. 102b. Fission probability of ^{240}Pu in the region of 5 MeV, determined from the ^{239}Pu(d,pf) reaction and a model fit to the data. Barrier parameters used are given in the text (Glässel *et al.*, 1976).

results are shown in Fig. 102a. The coefficients A_λ are those describing an expansion of the angular distribution in Legendre polynomials

$$W_K^{J\pi f}(\theta) = \sum_\lambda A_\lambda P_\lambda(\cos\theta) . \tag{5.92}$$

The interpretation of the data centers around the assumption [supported by photofission data of Rabotnov *et al.*, (1970)] that the fission channels have spin projection along the fissioning axis $K^\pi = 0^+$. The average branching ratios (or fission probabilities)

$$P_f(J^\pi, K) = \frac{T_f(J^\pi, K)}{T(J^\pi)} \tag{5.93}$$

for the different total angular-momentum components of the fissioning nucleus can then be deduced, the relative compound nucleus formation cross sections for these components being calculated from distorted wave Born approximation and the Nilsson scheme of neutron levels. The branching ratios found at 5 MeV are:

$$P_f(0^+, 0) = 0.63 ,$$

$$P_f(2^+, 0) = 0.50 ,$$

$$P_f(4^+, 0) = 0.20 .$$

The high average branching ratios found for the lower angular-momentum values imply that the widths of intermediate structures in the fission probability curve approach the class-II intermediate level spacing, in fact about 40% and 60% of the respective D_{II} values, while the width of the spin 4 structures will be about 12% of D_{II}. The actual intermediate structure resonances observed in the vibrational resonance are nearly all $J^\pi = 2^+$, giving $D_{II}(J^\pi = 2^+) = 10.8$ keV. The expected widths (in the probability curve) for these resonances is therefore about 4 keV, i.e., close to the resolution width and agreeing with observation. The level spacing for $J^\pi = 0^+$ states is expected to be about five times greater than the $J^\pi = 2^+$ spacing, thus implying a width ≈30 keV for any intermediate resonances with $J^\pi = 0^+$. These would therefore be hidden by the superimposed $J^\pi = 2^+$ resonances, and it is therefore not surprising that they are not observed. The widths of the $J^\pi = 4^+$ resonances on the other hand are much smaller than the resolution width, and their strength is about one order of magnitude lower (per resonance) than the 2^+ resonances; therefore, because of finite instrumental sensitivity, they will not be observed.

A model fit (which cannot be unique) to the data is also shown in Fig. 102b; it incorporates a hypothetical $K^\pi = 0^-$ vibrational resonance at 4.65 MeV. The barrier parameters are $\upsilon_A = 5.65$ MeV, $\hbar\omega_A = 0.82$ MeV, $\upsilon_B = 5.3$ MeV, $\hbar\omega_B = 0.6$ MeV, $\hbar\omega_{II} = 0.8$ MeV, while the damping width $\Gamma_{\nu_{II}(D)} = 0.12$ MeV. It does appear that a better fit could be achieved with a slightly larger damping width and a lowering of one or both barriers. Otherwise the intermediate resonances at 4.9 MeV are probably excessively high; they do in fact seem to suggest a fragmentation of the vibrational strength between two subsidiary states before the operation of the more general Lorentzian damping amongst the class-II compound states.

The more recent evidence also indicates that the vibrational resonances of ^{240}Pu are "nonideal" in character. Goerlach *et al.* (1978) have measured the prompt and delayed (shape isomeric) fission as a function of excitation energy using the ^{239}Pu(d,pf) reaction. Both forms of fission show resonancelike structure but the energies of the peaks are uncorrelated. This can be explained on the assumption that the prompt fission is associated mainly with states (before damping into the class-II compound states) having strong fission widths and moderate to weak coupling widths, whereas delayed fission, which follows the radiative decay of the class-II compound states, will then be inhibited by competition due to the large prompt fission widths. Thus delayed fission may exhibit peaking in other energy regions where there are underlying states enhancing the coupling width but having very weak fission width.

In these circumstances the barrier parameters of ^{240}Pu deduced from the prompt fission probability should be reinterpreted. The relevant equation for describing the data is (5.87a). In fact, owing to the dominance of the damping width, the outer barrier is only lowered very slightly (≈15 keV) as a result of this analysis.

b. ^{238}U

A number of other even nuclei exhibit structure in their curves of fission probability versus energy that has been interpreted as damped vibrational resonance structure. The compound nucleus ^{238}U, explored by means of the ^{236}U(t,pf) reaction (Back *et al.*, 1974a), is typical of these. The data are shown in Fig. 103. These data have been fitted on the assumption of a vibrational state (for angular momentum $J^\pi = 0^+$) associated with

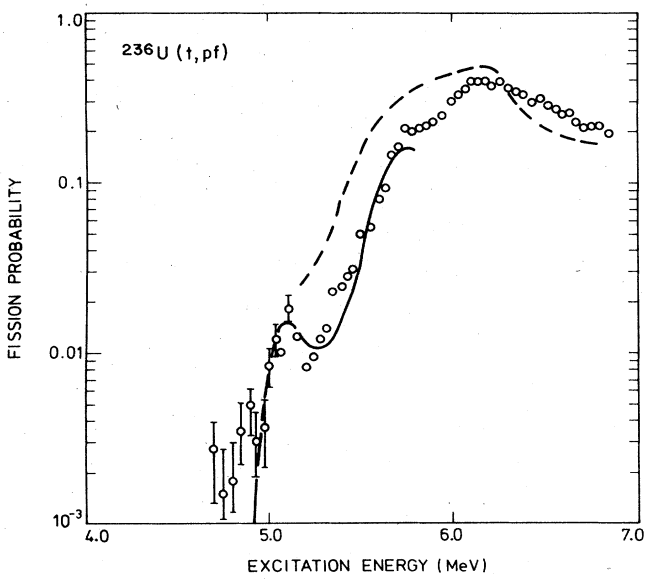

FIG. 103. Fission probability of ^{238}U as a function of excitation energy as measured in the ^{236}U(t,pf) reaction (Back *et al.*, 1974a). The fitted curve full line assumes a vibrational level (for $J^\pi = 0^+$) at 4.98 MeV carrying a rotational band. The dashed curve is a calculation from statistical representation of level densities and is appropriate above the barrier region (see Sec. VII).

the secondary well at an excitation energy of 4.98 MeV carrying a rotational band of similar levels, the rotational parameter being $\hbar^2/2\vartheta \approx 3$ keV. The damping width for the fit was $\Gamma_{\nu(D)} \approx 0.1$ MeV, and the barrier parameters were chosen as $\upsilon_A = 5.68$ MeV, $\hbar\omega_A = 1.0$ MeV, $\upsilon_B = 5.67$ MeV, and $\hbar\omega_B = 0.6$ MeV. In this calculation full account was taken of the effect on average fission probability of the underlying class-II structure in the damped vibration (see Sec. V.C.3.*d*), including also the Porter–Thomas fluctuations of the widths of the class-II intermediate resonances (see Sec. VI.C. 3.*c*).

c. ^{242}Pu

Another good example of a vibrational resonance revealed by the (t,pf) reaction occurs in ^{242}Pu (Back *et al.*, 1974). Data and fit are shown in Fig. 104. The vibrational-rotational band starts at 4.53 MeV and a damping width $\Gamma_{\nu(D)} = 0.2$ MeV was used in the fit (Lynn and Back, 1974); this is apparently a little high. Barrier parameters for the fit are $\upsilon_A = 5.55$ MeV, $\hbar\omega_A = 1.0$ MeV, $\upsilon_B = 5.05$ MeV, $\hbar\omega_B = 0.7$ MeV.

d. ^{235}U

The best studied example of a "classical" damped vibrational resonance in an odd-mass nucleus is found in ^{235}U and has been explored by means of the $^{234}U(n,f)$ reaction. The basic resonancelike feature at 300 keV neutron energy has been known for a long time (Lamphere, 1962) but was long believed to be explicable as competition between successive opening of fission and inelastic scattering channels (see Sec. V.A). The attempt to investigate the class-II intermediate structure within the vibrational resonance has been made by James *et al.* (1977). Individual class-II compound structure could not be observed at such high neutron energies with the available energy resolution (~1 keV to be compared with expected class-II state spacing of ~0.2 keV). However, very considerable fluctuations of the data points about any possible smooth curve through the vibrational resonance were observed. This was attributed to the limited number (~5) of class-II states to be found in any one resolution interval and the fluctuations of their strengths due to the Porter–Thomas distribution expected for their widths (see Sec. VI.B.3). The degree of fluctuation of the cross-section data was particularly determined and found to be consistent with observations on individual class-II states at low neutron energies (see Sec. VI.E.3.*b*) and a modeling of the vibrational resonance (see Fig. 105) with the following parameters:

$$\upsilon_A = S_n + 0.101 \text{ MeV},$$
$$\hbar\omega_A = 1 \text{ MeV},$$
$$\upsilon_B = S_n + 0.674 \text{ MeV},$$
$$\hbar\omega_B = 0.56 \text{ MeV},$$
$$\Gamma_{\nu_{II}(D)} = 0.05 \text{ MeV},$$
$$\hbar\omega_{II} = 0.5 \text{ MeV},$$

where the neutron separation energy $S_n = 5.31$ MeV.

The barrier heights resulting from this analysis require a comment. They are considerably different from the values that would be required to explain the behavior of the fission cross section at higher energies, and also from values required by the systematic behavior of barrier parameters of neighboring nuclei (see Sec. VII.D.2). The reason for this appears to be the choice of behavior for the coupling width in the parametrization given by James *et al.* The class-II coupling width has been assumed *not* to have vibrational resonance behavior in the region of 300 keV, and this is consistent with nonideal behavior described in Sec. V.C.2.*a*.(*ii*). The hypothesis of ideal behavior (vibrational resonance behavior in both the coupling and fission widths of the class-II states) can be accomodated within their parametrization. In Sec. V.C.3.*b*. the ef-

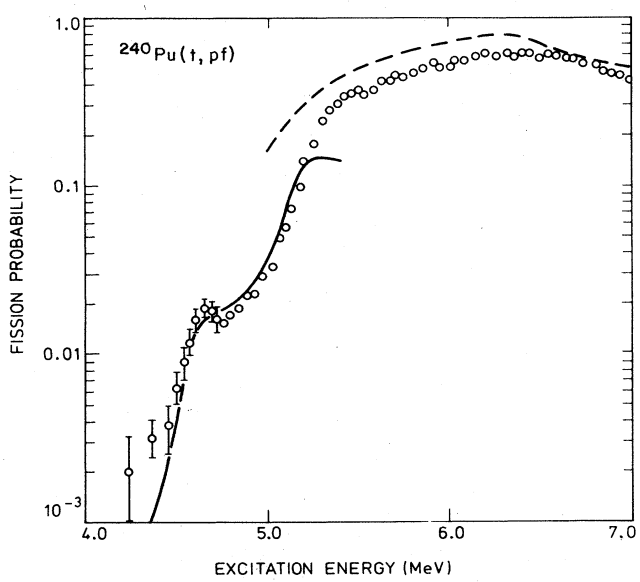

FIG. 104. Fission probability of ^{242}Pu as a function of excitation energy as measured in the $^{240}Pu(t,pf)$ reaction (Back *et al.*, 1974a). The fitted curve full line assumes a vibrational level (for $J^\pi = 0^+$) at 4.53 MeV carrying a rotational band. Dashed curve as in Fig. 103.

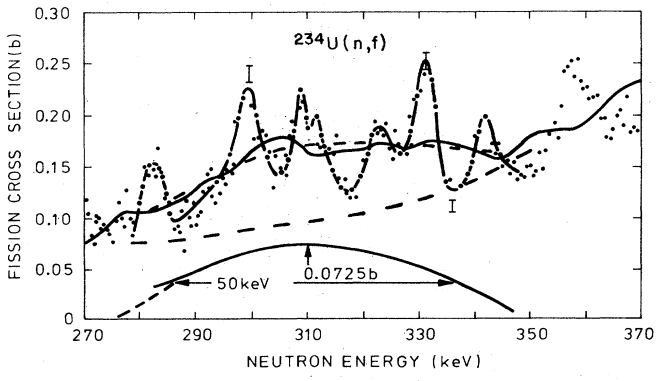

FIG. 105. Neutron-induced fission cross section of ^{234}U in the region of the 300 keV vibrational resonance (James *et al.*, 1977). The curve below is the fit of the authors using the parameters described in the text, after subtracting a background cross section indicated by the broken curve.

fective width of a nonideal vibrational resonance is given [Eq. (5.87)]. We can equate this (substituting the parameters of James *et al.*) to the width of an ideal vibrational resonance with modified barrier parameters, so that

$$\Gamma_{\nu_{II}(c)}^{(\mathrm{mod})}=\left(\Gamma_{\nu_{II}(D)}^{2}+\frac{2D_{II}\Gamma_{\nu_{II}(D)}\Gamma_{\nu_{II}(f)}}{\pi\Gamma_{\lambda_{II}(c)}}\right)^{1/2}-\Gamma_{\nu_{II}(D)}-\Gamma_{\nu_{II}(f)}. \tag{5.94}$$

This will lead to a modified barrier parameter $v_A = S_n + 0.44$ MeV with $\hbar\omega_A = 1.0$ MeV in the present case.

e. ^{231}Th

This case was treated as a pure vibrational resonance in Sec. V.B but the discussion in Sec. V.C.1 on schematic models for incipient damping indicated that pure vibrational resonances are unlikely to occur in odd-mass nuclei; some observable degree of fragmentation of the vibrational strength is to be expected. This conclusion is particularly reinforced by the numerical model given in Sec. V.C.1.*a* in which basic parameters simulating the Nilsson level scheme in the region of the secondary well deformation were used; no level with outstanding fission properties resembling that known in the ^{230}Th neutron fission cross section at 720 keV was found. This suggests indeed that the model of vibrational resonances in a secondary well in the curve of potential energy of deformation cannot provide an explanation of the distinctive features of the ^{230}Th fission cross section, and that the theoretical suggestions (Möller and Nix, 1974) of a third well at the deformation associated with the outer barrier (see Sec. II.A.1.*d*) should be further explored.

Parameters that describe schematically the behavior with deformation of the single-neutron levels in a system of 141 neutrons at deformations in the region of the second barrier have been taken from the work of Möller and Nix (1974); they are shown in Table XI [but the $\mu(p)=6$ is meant to be representative of more complex intrinsic states at the head of the energy gap]. These levels coupled with vibrational levels with a spacing of 0.8 MeV provide the basis for the diagonalization of the Schrödinger equation (5.37) as described in Sec. V.C.1.*a*. Reduced widths can be calculated by projecting the wave functions onto intrinsic states defined at deformations equivalent to a barrier position on either side of the assumed tertiary well at η_B. For angular momentum $J^\pi=\frac{1}{2}^-$ states (arising from only the $\Omega^\pi=\frac{1}{2}^-$ states in Table XI) it appears that the lowest channel at an inner deformation η_{B_1} (chosen here as $\eta_{B_1}=\eta_B-0.12$) has a configuration containing ~99% of the state $\mu(p)=5$ as listed in Table XI. The next lowest channel is about 1 MeV higher in intrinsic excitation energy. At an outer deformation $\eta_{B_2}(\eta_{B_2}=\eta_B+0.12)$ the lowest channel has a configuration containing 95.5% of $\mu(p)=1$ and is 0.43 MeV lower than the next channel state. With these very different configurations for inner (governing coupling to complex class-II and hence to class-I states) and outer channels (governing fission widths) any correlation between the reduced width amplitudes for coupling and fission is unlikely.

The reduced coupling and fission widths are shown in Fig. 106. From this it can be seen that strong candidates for fission resonances are the eigenstates $\lambda=4$, $\lambda=5$, $\lambda=6$, and $\lambda=7$. The relative importance of these will depend on the ratio of the barrier penetrability

TABLE XI. Parameters (in MeV) describing the deformation dependence of schematic neutron single-particle levels in a system of 141 neutrons [taken from Möller and Nix (1974)] at a deformation equal to that of the normal outer barrier in the thorium region. These are used in the model of vibration damping used to explain the resonance feature at 720 keV in the neutron fission cross section of ^{230}Th.

$\mu(p)$	$\mathcal{E}_{0\mu}^{(p)}$	$A_\mu^{(p)}$	$b_\mu^{(p)}$	$D_\mu^{(p)}$
$\Omega^\pi=\frac{1}{2}^-$				
1	0.0	242	0.053	0
2	1.4	63	0.053	0
3	4.1	0	0	17.5
4	1.8	0	0	2.5
5	0.0	450	−0.1	0
6	0	0	0	0
$\Omega^\pi=\frac{3}{2}^-$				
7	0.0	47	0.06	0
8	0.0	417	−0.06	0
9	2.6	0	0	3.75
$\Omega^\pi=\frac{5}{2}^-$				
10	0.0	31	0.02	0
11	0.0	150	0.08	0
12	0.95	105	0.02	0

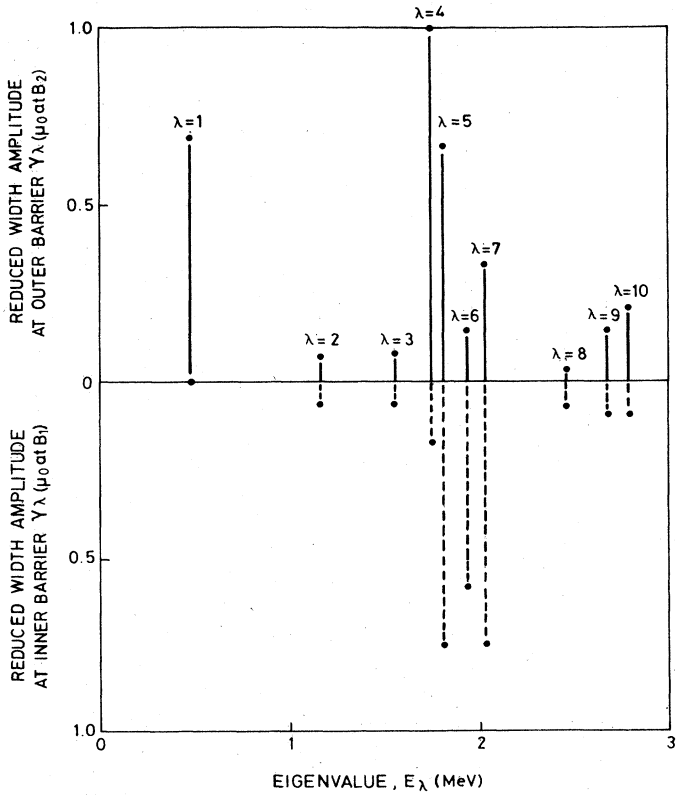

FIG. 106. Reduced width amplitudes (relative scale) for a model of $J^\pi=\frac{1}{2}^-$ eigenstates at a tertiary minimum deformation of a 141 neutron system.

TABLE XII. Fission strengths of $J^\pi = \frac{1}{2}^-$ states resulting from diagonalization of $N = 141$ system as described in text. Barrier penetrabilities are chosen to give widths for the $\lambda = 5$ state that are in the ratio of about 20:1 (as observed for the $J^\pi = \frac{1}{2}^-$ component of the 720 keV resonance in the reaction ^{230}Th(n,f).

λ	E_λ (MeV)	$\gamma_\lambda(B_1, \mu = 1)$ (rel.)	$\gamma_\lambda(B_2, \mu = 1)$ (rel.)	S_f $(P_{B_1} > P_{B_2})$	S_f $(P_{B_1} < P_{B_2})$
4	1.755	−0.173	−1.01	0.371	0.030
5	1.816	0.749	−0.670	0.430	0.527
6	1.945	0.578	0.144	0.021	0.182
7	2.036	−0.740	−0.334	0.110	0.437

factors P_{B1} and P_{B2}, but on any reasonable choice of these $\lambda = 5$ is always strong in fission. If P_{B_1} and P_{B2} are adjusted to give for this state the observed ratio of coupling and fission widths for the $J^\pi = \frac{1}{2}^-$ component of the ^{231}Th resonance (see Table IX), the fission strengths of the eigenvalues in the region of $\lambda = 5$ have the values shown in Table XII. The fission strengths quoted are relative values, but are otherwise defined according to Eq. (5.48).

The two choices for the penetration factors give results that begin to have some qualitative resemblance to the ^{231}Th observations. If the basic parameters of the single particle states were to be adjusted slightly so that the $\lambda = 4$ state moved away from $\lambda = 5$ and lost strength, or alternatively moved closer and merged with $\lambda = 5$, the $P_{B1} > P_{B2}$ case would be a favored solution. This is particularly so because the admixture of $\mu(p) = 6$ (representing a thicket of complex intrinsic states) into $\lambda = 5$ is only ~1%, whereas it is ~33% into $\lambda = 7$ (more than 200 keV higher), so the strength of the latter is likely to be more dispersed than the schematic calculation suggests.

The diagonalization of $J^\pi = \frac{3}{2}^-$ state involves the $\Omega^\pi = \frac{3}{2}^-$ intrinsic states of Table XI and the $I = \frac{3}{2}$ members of the rotational bands based on the $\Omega^\pi = \frac{1}{2}^-$ states. The two sets are coupled by the Coriolis force as described in Sec. V.C.1.*b*. With the Coriolis coupling term A_K [Eq. (5.50)] set at a somewhat exaggerated value of 40 keV, the following picture emerges for the $J^\pi = \frac{3}{2}^-$ states. First, the lowest channel at the inner barrier has the same character as in the $J^\pi = \frac{1}{2}^-$ case, i.e., it is a $K = \frac{1}{2}$ channel. Second, the lowest channel at the outer barrier is now almost pure $K = \frac{3}{2}$ and lies a few hundred keV below the $K = \frac{1}{2}$ channel considered for the $J^\pi = \frac{1}{2}^-$ states. If the penetration factor for the former channel is assumed to be a factor of 20 greater than that for the latter then the fission strengths for the two outer barrier channels have the values given in Table XIII. In this grouping only one new state (at 2.09 MeV) appears; its wave function contains over 90% of admixture of $\Omega^\pi = \frac{3}{2}^-$ basis states. The other states contain very small admixtures of $\Omega^\pi = \frac{3}{2}^-$ (the largest admixture is ~5% in the 2.03 MeV state) and can therefore be regarded structurally as members of rotational bands built on the $K = \frac{1}{2}$ states in Table XII. Nevertheless their fission strengths demonstrate considerable fission decay through the $K = \frac{3}{2}$ channel. The candidate for the strong vibrational resonance at 1.81 MeV has an 18% component of $K = \frac{1}{2}$ decay, while the other strong fissioning state at 200 keV higher has a 93% probability of $K = \frac{3}{2}$ decay.

TABLE XIII. Fission strengths of $J^\pi = \frac{3}{2}^-$ states resulting from diagonalization of $N = 141$ system as described in text.

λ	E_λ (MeV)	Γ_λ (rel.)	$S_{f(\mu=1)}^{K=3/2}$ (rel.)	$S_{f(\mu=2)}^{K=1/2}$ (rel.)	$\frac{S_{f(\mu=1)}}{S_{f(\text{total})}}$
7	1.75	20.9	0.0016	0.027	0.057
8	1.81	11.2	0.097	0.433	0.184
9	1.94	1.67	0.184	0.095	0.659
10	2.03	36.7	0.456	0.032	0.935
11	2.09	588	0.031	8×10^{-7}	1.0

Similar trends are revealed for the $J^\pi = \frac{5}{2}^-$ states. For these the basis states are the $\Omega^\pi = \frac{5}{2}^-$ state of Table XI and members of rotational bands based on both $\Omega^\pi = \frac{3}{2}^-$ and $\frac{1}{2}^-$ states. A second-order Coriolis coupling strength of $A_K = 4$ keV is assumed for the coupling of the latter to the intrinsic states. Again the coupling channel through the inner barrier is unchanged, but two (very close) channels below the $K = \frac{1}{2}$ channel now appear for the outer barrier. One of these is $K = \frac{3}{2}$ and the other $K = \frac{5}{2}$. The total fission strength of the three principal states (at 1.81, 1.94, and 2.03 MeV) are almost the same as in the $J = \frac{1}{2}$ and $\frac{3}{2}$ cases, but a greater fraction of the fission strength of the 1.81 MeV state (22%) goes through the higher K channels, and most of this is fractionated in favor of $K = \frac{5}{2}$.

These calculations account, in a qualitative way, for the observations on the ^{230}Th(n,f) reaction and its analysis described in Sec. V.B.5.*a*. One essential feature of the analysis of the 720 keV resonance was the reduction in widths (and hence strength) of the higher spin components. This would not have been necessary if, as suggested by the present schematic model, part of the strength of the higher spin components had been assumed to be routed through higher K channels, thus damping the forward peaking in the angular distribution.

It is also to be noted that a model of incipient damping of this type, and based, in this case, on the hypothesis of a third minimum in the potential energy curve, would allow the explanation of substructure within the 720-keV peak, some suggestion of which has been observed by Veeser (1976) and Blons *et al.* (1978). For example, adjustment of the basic parameters to move the 1.755-MeV state (see Table XII) much closer to the 1.816-MeV state could give rise to this effect (for a discussion of the role of decoupling with pairs of $\frac{1}{2}$ states of opposite parity (see Sec. IX.C.1).

f. ^{233}Th

This compound nucleus has also been described as a candidate for pure vibrational fission resonances (see Sec. V.B.5.*b*) but the richness of main structure and substructure suggest that it is more likely to fall in the class of incipient damping as described above for ^{231}Th. The same degree of detailed analysis has not been carried out on ^{233}Th, and hence it has not been thought worthwhile yet to explore a detailed model of incipient damping. It is to be noted, however, that the presence of two additional neutrons in this system will reduce the number of easily available $\Omega^\pi = \frac{1}{2}^-$ orbitals and give rise to a greater dominance of fission through higher K channels, as observed.

VI. NARROW INTERMEDIATE STRUCTURE IN FISSION CROSS SECTIONS

A. Introduction

The discovery of narrow intermediate structure in the slow neutron fission cross sections of ^{237}Np (Paya *et al*, 1968) and ^{240}Pu (Migneco and Theobald, 1968) (see Fig. 7) provided important evidence for the Strutinsky theory of the double-humped fission barrier in nuclei of the actinide series. The existence of spontaneously fissioning isomers and a gross resonance structure in fission cross sections could already be explained by the model of the double-humped barrier, but the new phenomenon, the recurrence of narrow groups of fine-structure resonances, only a few in number with considerable fission strength interspaced by tens or hundreds of resonances with negligible fission strength, was seen to provide vital corroboration of the picture of a double-humped barrier with a secondary minimum of considerable depth (Lynn, 1968 a,b,c; Weigmann, 1968).

The narrow intermediate resonances are interpreted as class-II compound nucleus states associated with a range of nuclear deformation within the secondary minimum of the barrier, unlike the normal, much denser, fine-structure resonances associated with class-I compound states, for which the nuclear deformation is much less elongated, being close to that of the ground state of the nucleus. Because the secondary well is shallower than the primary well in the deformation energy, the class-II states have less energy available for excitation of intrinsic modes and hence are considerably less dense than the class-I states. Being associated with a much more elongated form, they clearly have much larger fission widths than the class-I states; hence their characteristic fission signature.

Since the original discovery of the intermediate structure in the cross sections of ^{237}Np and ^{240}Pu, many nonfissile, and some fissile, actinide nuclei have been found to exhibit the phenomenon of narrow intermediate structure. In some cases it is clear that the intermediate structure is associated with the gross structure due to damped vibrational resonances as described in Sec. V; the picture here is of a simple vibration mode (which carries the bulk of the fission strength) in the secondary well being incompletely mixed into the class-II compound states. In some cases there is no evidence for narrow intermediate structure, and gross structure in the cross section is interpreted as being due to a pure vibrational state, no mixing occurring because the secondary well is so shallow that there are no nearby states with which the vibrations can mix; in this case the gross structure also represents the intermediate structure insofar as it is an actual state associated with the secondary well, albeit of much simpler structure than is usual.

In this section we analyze the data on narrow intermediate structure to give quantitative information on the double barrier. The basic theory necessary for this analysis has been presented in Sec. III.C.5 and needs little or no further development here, except for the treatment of average cross sections including the effects due to fluctuations in the properties of the fine-structure and intermediate-structure levels. We describe the expected statistical properties of class-II compound states in Sec. VI.B. In Sec. VI.C we present expressions for the area of intermediate fission resonances, and from these we also derive average cross sections under different assumptions about the strength of coupling and of fission decay; these will be employed in the analysis of average fission cross-section data in Sec. VII. We discuss electromagnetic radiation properties in Sec. VI.D, outline the possibilities of observing such radiation, and discuss the implications on observations of fission cross sections through the two-stage (γf) exit process. Finally, we give examples of intermediate structure for different conditions of coupling and fission decay in Sec. VI.E and analyze them by appropriate methods.

B. Statistical properties of class-II states

1. Mean values of fission and coupling widths

The formal expression from R-matrix theory for the width of a state is given in terms of a penetration factor P, and a reduced width amplitude $\gamma_{\lambda(c)}$ (see Sec. III.C.3.*e*)

$$\Gamma_{\lambda(c)} = 2P_c\gamma^2_{\lambda(c)} . \tag{6.1}$$

In the case of fission widths no formal calculations have been based on this expression. Rather, the usual approach to calculating fission widths is to consider a pure vibrational state of frequency ω_{II}; in classical terms this reproduces its configuration at the edge of the well (i.e., the entrance to the barrier region) $\omega_{II}/2\pi$ times per second. The probability of the wave being transmitted through the barrier from this state of deformation, rather than being reflected to continue the vibration, is taken from the simple theory of Sec. III.A.1 for the transmission of a traveling wave through a single peaked barrier. This is denoted by T_B and the Hill-Wheeler expression for transmission through an inverted harmonic oscillator form of barrier is given in Eq. (3.140) of Sec. III.C.4.*a*. Thus the probability that the vibrational state decays through the outer barrier is $\omega_{II}T_B/2\pi$ per second; therefore its half-life τ for this decay is $(2\pi/\omega_{II}T_B)$, and its fission width is

$$\Gamma_{\nu_{II}(f)} = \frac{\hbar}{\tau} = \frac{\hbar\omega_{II}T_B}{2\pi} . \tag{6.2}$$

From this expression for the fission width of a vibra-

tional state, the fission width of a class-II state is derived by determining the fraction of the vibrational mode in the configuration of the class-II state. This is given in Sec. III.C.5.*a*, Eq. (3.153). If the predominant mode for fission decay (defined at a deformation close to the barrier) is $\chi_\mu \Phi_{\nu_{II}}$, the class-II state fission width is

$$\Gamma_{\lambda_{II}(f\equiv\mu\nu)} = \frac{(C^{\lambda_{II}}_{\mu\nu})^2 \hbar\omega_{II} T_B}{2\pi} . \tag{6.3a}$$

Expressions for $(C^{\lambda_{II}}_{\mu\nu})^2$ in the case of damped vibrational resonances are given in Sec. V.C, but here we are more concerned with the complete damping case, which we simplify by assuming that the vibrational state is spread uniformly over an energy interval equal to the spacing between two vibrational states $\hbar\omega_{II}$. Thus $(C^{\lambda_{II}}_{\mu\nu})^2 \approx D_{II}/\hbar\omega$ and

$$\Gamma_{\lambda_{II}(f=\mu\nu)} = (D_{II}/2\pi) T_B . \tag{6.3b}$$

In this equation, the penetrability T_B is calculated for the energy of the class-II state rather than the vibrational state; this is in the spirit of the expression (6.1). All kinetic energies with respect to the barrier must be adjusted for any excitation energy carried by the intrinsic state μ.

The magnitude of the coupling matrix element has already been discussed in Sec. II.C.5.*b*. Equation (3.161) gives

$$(H_c)^2_{\lambda_I \lambda_{II}} \approx \frac{D_I D_{II} T_A}{4\pi^2} . \tag{6.4}$$

The coupling width is therefore

$$\Gamma_{\lambda_{II}(c)} = \frac{2\pi \overline{(H_c)^2_{\lambda_I \lambda_{II}}}}{D_I} \approx \frac{D_{II}}{2\pi} T_A . \tag{6.5}$$

2. General remarks on statistical fluctuations

If the excitation energy of the compound nucleus is not much higher than the secondary minimum in the deformation energy, statistical treatments of the class-II states are inappropriate; detailed nuclear structure considerations become paramount, and our state of knowledge in this respect has been reviewed in Sec. IV on spontaneously fissioning isomers and in Sec. V on vibrational resonances; Sec. IX is also devoted to this subject. At higher excitation energies it is to be expected that the properties of class-II states will be governed to an increasing extent by the statistical phenomena that have been well explored for highly excited states of normally deformed nuclei, such as fine-structure neutron resonances. Also, of course, any hint of departure from idealized statistical behavior is of great interest, and this is likely to occur, given the comparatively modest excitation energies involved when the fission intermediate structure is found.

Statistical fluctuation of the properties of compound nucleus states is best discussed in terms of the formal R-matrix states described in Sec. III.C. This is because the R-matrix states are defined completely by the nuclear Hamiltonian within the nuclear internal region (with energy-independent boundary conditions to establish their discreteness), whereas the S-matrix poles [Sec. III.C.3.*g*(*iv*)], which underlie resonance properties, are in addition governed significantly by conditions in the external region.

The differences that can occur between the statistics of R-matrix states and of S-matrix poles can be illustrated by a numerical example. We took a set of R-matrix states, their individual properties (consisting of reduced width amplitudes for entrance and exit channels and energy eigenvalue) being chosen at random from Gaussian distributions with zero mean for the amplitudes and a Wigner distribution [see Eq. (6.1) below] for the spacings between eigenvalues. To calculate the collision matrix we chose a small penetration factor for the entrance channel c and a large one for the exit channel c' so that the average widths of the final R-matrix state width distributions was

$$\langle \Gamma_{(c)} \rangle \ll \langle D \rangle \quad \langle \Gamma_{(c')} \rangle = \langle D \rangle / 2\pi ,$$

$\langle D \rangle$ being the average R-matrix state spacing. We calculated poles of the resulting collision matrix by numerical methods. Distributions of the real components of the pole positions $E_l^{(H)}$ (see Sec. III.C.3.*g*(*iv*) for definitions), the width amplitude quantities, $G^{(H)}_{l(c')}$, and the phase factors $\xi_{l(c')}$ are shown in Figs. 107–109 in comparison with the distributions expected for narrow resonances (very small penetration factors in all channels). As can be seen from this numerical example distinct differences occur.

3. Class-II level spacing statistics

a. Intermediate structure groups

The distribution of eigenvalues of R-matrix levels has been discussed in a long series of papers stemming from an original suggestion by Wigner (1956). For a review of this topic see Lynn (1968a). The basic idea is that randomly distributed off-diagonal matrix elements of the Hamiltonian matrix cause repulsion of its eigenvalues. The distribution of spacings between nearest levels that results from this is remarkably close (within a few percent) to the simple expression that Wigner deduced from the consideration of two levels alone:

$$p(D)dD = \frac{\pi D}{2\langle D \rangle^2} \exp\left[-\frac{\pi D^2}{4\langle D \rangle^2}\right] dD . \tag{6.6}$$

The important extra result that has been deduced from the study of the diagonalization of Hamiltonians of higher order is that the positions of distant levels are correlated. To state this more precisely, the distribution of higher-order spacings, defined as the spacing between a level and the distant neighbor separated from the first by a specified number of nearer levels, has a much smaller variance than would be deduced from the addition of the specified number (plus one) of nearest neighbor spacings drawn randomly from the Wigner distribution, Eq. (6.6). The degree of correlation is very considerable. For large order spacings, the variance in the number of levels expected to be found in an energy interval of n mean level spacings is (Dyson and Mehta, 1963)

$$V = \frac{2}{\pi^2}\left[\ln(2\pi n) + 1 + \gamma - \tfrac{1}{8}\pi^2\right] , \tag{6.7}$$

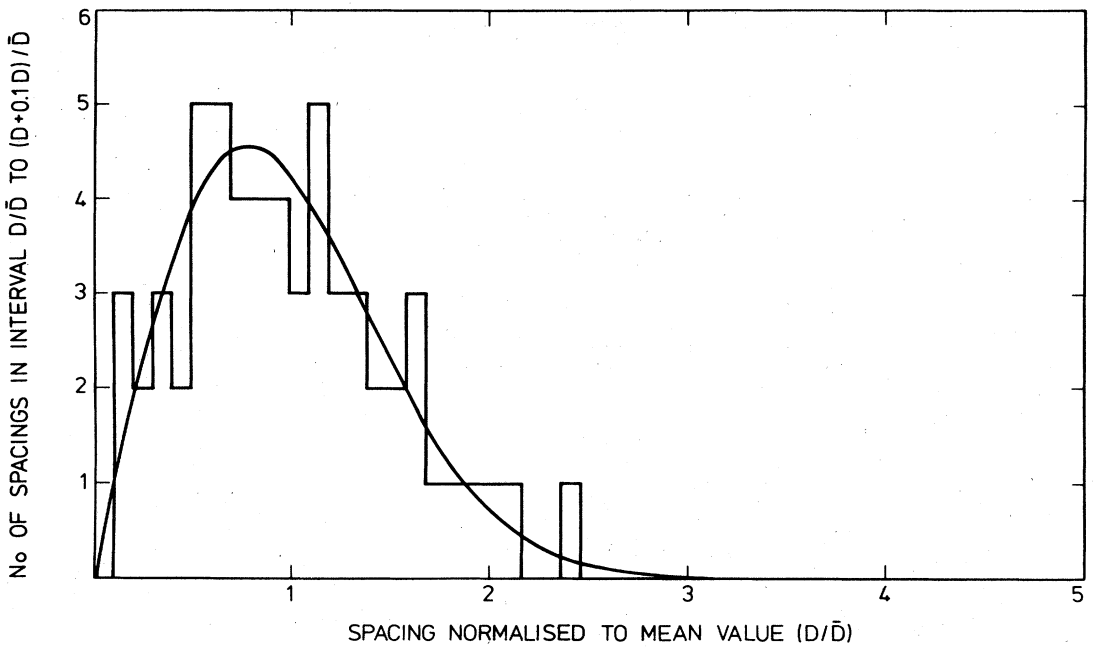

FIG. 107. Distribution in histogram form of real components of S-matrix pole separations in many-level case described in text. Full curve is the Wigner distribution normalized to 59 spacings.

where $\gamma(=0.5772)$ is Euler's constant. [This is to be contrasted with the random superposition of Wigner spacings, $V=0.273n$. For $n=100$, this is 27.3, whereas Eq. (6.7) gives $V=1.4$.] These long-range correlation properties have been used in statistical schemes for testing long sequences of neutron resonances to determine such things as (a) the existence of hidden quantum numbers, (b) the absence of levels from what otherwise appears to be a complete sequence, or (c) the presence of levels that are not of the same kind (having the same set of good quantum numbers) as the remainder of the sequence.

These statistical properties of level spacings are expected to hold good for most cases of narrow intermediate structure, in which class-II levels are dense enough that it is obvious that considerable intrinsic excitation energy is available. In only one case, to date, are there sufficient data available to make any significant test of the expected statistics, or to make deductions on the purity of the level sequence involved; this is the structure in the cross section of the ^{237}Np (n,f) reaction.

b. *Impact on fine-structure spacing correlations*

It is of considerable interest to consider the effect of coupling class-II levels with class-I levels on the spacing distributions of the fine-structure levels. We restrict the discussion to narrow levels, and hence to observable resonances with properties that can be related immediately to those of the R-matrix states. If coupling is very weak, as described in Sec. III.C.5.*c*(*i*), a sequence of class-I R-matrix levels becomes interspersed with occasional levels that are of nearly pure class-II character with very little disturbance of their original eigenvalues [unless there is accidental degeneracy; Sec. III.C.5.*c*(*ii*), in which case rather more dislocation occurs owing to level repulsion between the degenerate class-I and class-II levels]. Application of sophisticated statistical tests as described, for example, by Rahn *et al.* (1972) to a complete series of resonances of one angular momentum in, say, a total cross section, should reveal the class-II interlopers. Slightly stronger coupling, which spreads the class-II state appreciably into a modest number of class-I states [see Sec. III.C.5.*c*(*iii*)] will preclude the identification of individual interlopers but nevertheless should cause some dislocation of the correlation properties of the original class-I series. Simple application of the statistical tests of Dyson and Mehta (1963) should reveal a considerably increased variance due to this effect; the variance on the number of levels n to be found in a given energy interval becomes

$$V=\frac{4}{\pi^2}[\ln(2\pi n)+1+\gamma-\tfrac{1}{8}\pi^2]+\frac{2}{\pi^2}\left[\ln\frac{\langle D\rangle}{\langle D_{\mathrm{I}}\rangle}+\ln\frac{\langle D\rangle}{\langle D_{\mathrm{II}}\rangle}\right], \tag{6.8}$$

where $\langle D\rangle$ is the mean spacing of all states and $\langle D_{\mathrm{I}}\rangle$, $\langle D_{\mathrm{II}}\rangle$ the mean spacings of class-I and class-II states, respectively. This is to be compared with Eq. (6.7). To the best of our knowledge no applications of these tests to samples of experimental data have yet been reported.

4. Statistical properties of class-II fission widths

The statistical properties of fission and coupling widths of class-II states follow from the theory of level width statistics pioneered by Porter and Thomas (1956) with reference to neutron resonance spectroscopy in

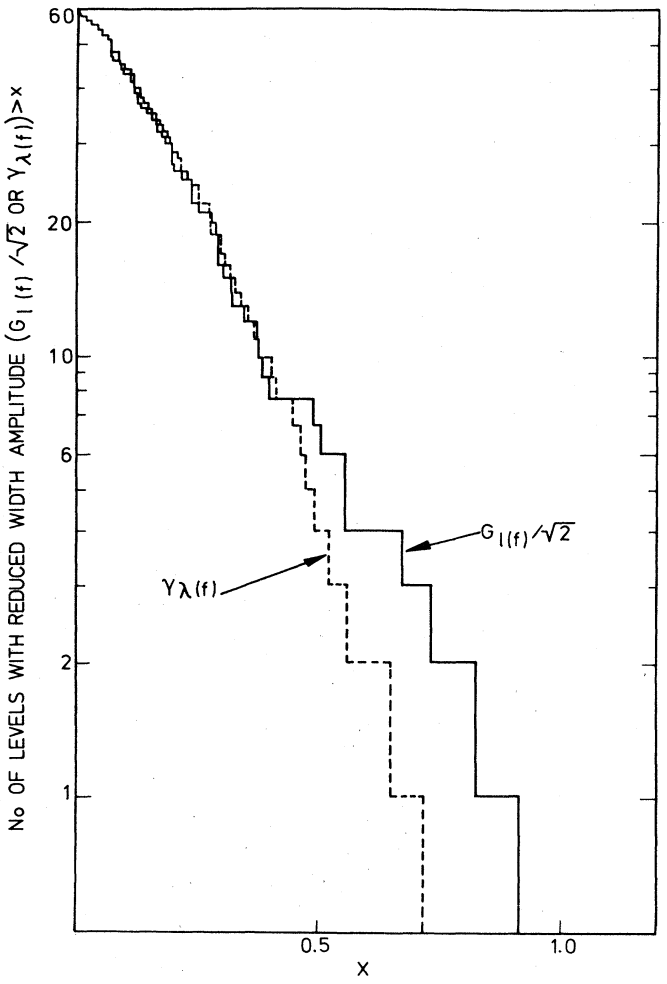

FIG. 108. Distribution of S-matrix partial width amplitudes ($G_{1(f)}/2^{1/2}$) compared with R-matrix reduced width amplitudes ($\gamma_{\lambda(f)}$) in many-level case described in text.

particular. The basic ideas follow from Eq. (3.153). Let us suppose that this expansion is based on a deformation close to the outer barrier for the definition of the intrinsic states χ_μ. Then a particular component $\chi_{\mu'}\Phi^{(II)}_{\nu'(\mu')}$ (where μ' will normally be a low-lying intrinsic state and ν' a high phonon number) will define the wave function for the fission channel. For class-II states of considerable excitation there will be very many terms in the expansion (3.153) and it is then to be expected that the expansion coefficients $C^{\lambda_{II}}_{\mu\nu}$ will have a Gaussian distribution with zero mean to a very good approximation. Thus the projection of the class-II state wave function $X^{(II)}_{\lambda_{II}}$ on the channel wave function $\chi_{\mu'}\Phi^{II}_{\nu'(\mu')}$, and hence the reduced width amplitude for fission through this channel, will have the same Gaussian distribution

$$p(\gamma^{(II)}_{(\mu')})d\gamma^{(II)}_{(\mu')} = \frac{1}{(2\pi\overline{\gamma^{(II)2}_{(\mu')}})^{1/2}} \exp\left(-\frac{\gamma^{(II)2}_{(\mu')}}{2\overline{\gamma^{(II)2}_{(\mu')}}}\right) d\gamma^{(II)}_{(\mu')} . \tag{6.9}$$

Transformation of this distribution to that for the widths gives

$$p(\Gamma^{(II)}_{(\mu')})d\Gamma^{(II)}_{(\mu')} = \frac{1}{(2\pi\Gamma^{(II)}_{(\mu')}\overline{\Gamma^{(II)}_{(\mu')}})^{1/2}} \exp\left(-\frac{\Gamma^{(II)}_{(\mu')}}{2\overline{\Gamma^{(II)}_{(\mu')}}}\right) d\Gamma^{(II)}_{(\mu')} , \tag{6.10}$$

which is the Porter–Thomas distribution.

If more than one deformation channel μ' contributes to the fission width it is to be expected that the partial widths are uncorrelated and hence the total fission width will have a distribution with lower variance than the Porter–Thomas one. For a number of deformation channels with mean widths that are not too different an effective number of channels ν_{eff} can be defined. The definition is based on the variance of the fission width distribution:

$$\frac{\mathrm{var}\Gamma^{(II)}_{(f)}}{\overline{\Gamma^{II\,2}_{(f)}}} = \frac{2}{\nu_{eff}} . \tag{6.11a}$$

This gives (the variance of each deformation channel width being $2\overline{\Gamma^{(II)}_{(\mu')}}^2$)

$$\nu_{eff} = \left(\sum_{\mu'} \overline{\Gamma^{(II)}_{(\mu')}}\right)^2 \Big/ \sum_{\mu'} \overline{\Gamma^{(II)}_{(\mu')}}^2 . \tag{6.11b}$$

For equal partial widths the fission width distribution will be the member of the χ^2 family with ν_{eff} degrees of freedom:

$$P_{\nu_{eff}}(\Gamma_{(f)})d\Gamma_{(f)} = \Gamma^{-1}(\tfrac{1}{2}\nu_{eff})(\nu_{eff}/2\overline{\Gamma}_{(f)})^{\nu_{eff}/2} \times \Gamma^{(\nu_{eff}-2)/2}_{(f)} e^{-\nu_{eff}\Gamma_{(f)}/2\overline{\Gamma}_{(f)}} d\Gamma_{(f)} . \tag{6.11c}$$

5. Statistics of coupling matrix elements

The coupling matrix elements linking the fine-structure resonances with the class-II intermediate states, and defined by Eq. (3.160), are subject to a bivariate form of distribution. In the double sum in Eq. (3.160a), the coefficients

$$\langle \lambda_I | \mu'\nu_I \rangle \equiv C^{\lambda_I}_{\mu'\nu_I} \quad \text{and} \quad \langle \mu''\nu_{II} | \lambda_{II} \rangle \equiv C^{\lambda_{II}}_{\mu''\nu_{II}}$$

are expected to have separately the Gaussian distribution form of Eq. (6.9) with zero mean. If more than one term in the sum over $\mu'\nu_I$ and $\mu''\nu_{II}$ in Eq. (3.160a) is significant, the form of distribution is unaffected, although the dispersion, and hence the mean of the squared matrix element, is the sum of the squared individual terms. Thus, if we consider only the distribution relating to class-I levels (for a given class-II level), the resulting form is the Porter–Thomas one

$$p[(H_c)^2_{\lambda_I\lambda_{II}}]d(H_c)^2_{\lambda_I\lambda_{II}} = \frac{1}{[2\pi(H_c)^2_{\lambda_I\lambda_{II}}\overline{(H_c)^2_{\lambda_I\lambda_{II}}}]^{1/2}} \exp\left[-\frac{(H_c)^2_{\lambda_I\lambda_{II}}}{2\overline{(H_c)^2_{\lambda_I\lambda_{II}}}}\right] d(H_c)^2_{\lambda_I\lambda_{II}} ,$$

where

$$(H_c)^2_{\lambda_I\lambda_{II}} = \sum_{\mu'\nu_I} \overline{(C^{\lambda_I}_{\mu'\nu_I})^2} \sum_{\mu''\nu_{II}} \langle \mu'\nu_I | H_c | \mu''\nu_{II} \rangle^2 (C^{\lambda_{II}}_{\mu''\nu_{II}})^2 ,$$

the bars referring to averages with respect to class-I states only. The usual expression for the coupling width of the given class-II state can therefore be written

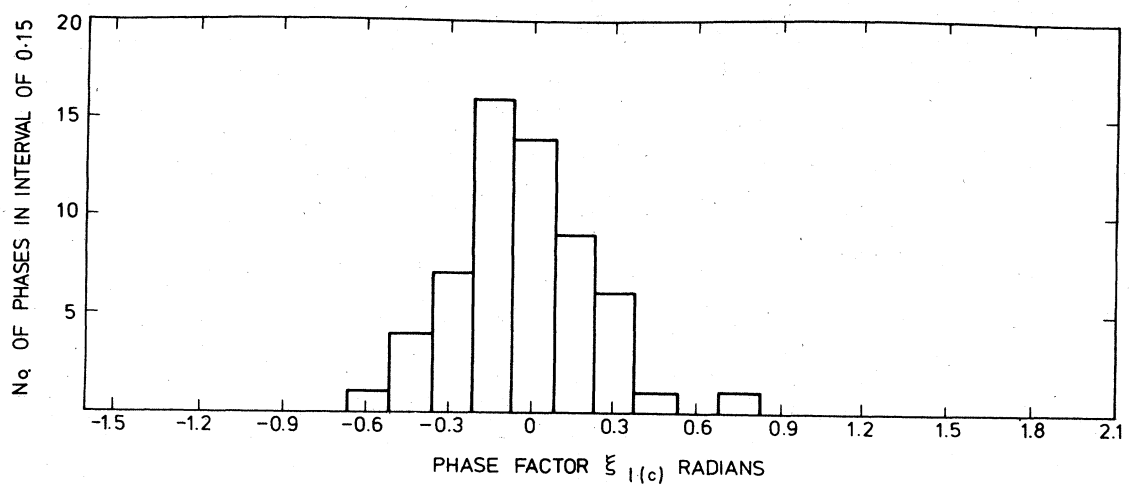

FIG. 109. Distribution of S-matrix phase factors for exit channel $\xi_{I(c')}$.

$$\Gamma_{\lambda_{II}(c)} = 2\pi\overline{(H_c)^2_{\lambda_I\lambda_{II}}}\Big/D_I = 2\pi\sum_{\mu'\nu_I}\overline{(C^{\lambda_I}_{\mu'\nu_I})^2}\sum_{\mu''\nu_{II}}\langle\mu'\nu_I|H_c|\mu''\nu_{II}\rangle^2(C^{\lambda_{II}}_{\mu''\nu_{II}})^2\Big/D_I . \tag{6.12}$$

Because of the Gaussian distribution of the coefficients $C^{\lambda_{II}}_{\mu''\nu_{II}}$ over class-II levels, it is immediately obvious that the distribution of the coupling width thus defined also has the Porter-Thomas form,

$$p(\Gamma_{\lambda_{II}(c)})d\Gamma_{\lambda_{II}(c)} = \frac{1}{(2\pi\Gamma_{\lambda_{II}(c)}\langle\Gamma_{\lambda_{II}(c)}\rangle)^{1/2}} \times\exp\left(-\frac{\Gamma_{\lambda_{II}(c)}}{2\langle\Gamma_{\lambda_{II}(c)}\rangle}\right)d\Gamma_{\lambda_{II}(c)} \tag{6.13}$$

the triangular bracket referring to the mean over class-II levels

$$\langle\Gamma_{\lambda_{II}(c)}\rangle = 2\pi\sum_{\mu''\nu_{II}}\sum_{\mu'\nu_I}\langle\mu'\nu_I|H_c|\mu''\nu_{II}\rangle^2\langle(C^{\lambda_{II}}_{\mu''\nu_{II}})^2\rangle\overline{(C^{\lambda_I}_{\mu'\nu_I})^2}\Big/D_I . \tag{6.14}$$

There could be special circumstances in which a channel effect appears, and as a result the coupling width distribution could be that of a set of superimposed Porter–Thomas distributions with smaller variances. This can happen, for example, if the matrix elements $\langle\mu'\nu_I|H_c|\mu''\nu_{II}\rangle$ are nonzero only if $\mu'\equiv\mu''$, and the significant values are limited, by tunneling, to very few values of ν_I,ν_{II}. Hence

$$\overline{(H_c^2)}_{\lambda_I\lambda_{II}} \approx \sum_{\mu'\nu_I}\overline{(C^{\lambda_I}_{\mu'\nu_I})^2}(C^{\lambda_{II}}_{\mu'\nu_{II}})^2\langle\mu'\nu_I|H_c|\mu'\nu_{II}\rangle^2$$

and

$$\langle\Gamma_{\lambda_{II}(c)}\rangle \approx 2\pi\sum_{\mu'\nu_I}\overline{(C^{\lambda_I}_{\mu'\nu_I})^2}\langle(C^{\lambda_{II}}_{\mu'\nu_{II}})^2\rangle\langle\mu'\nu_I|H_c|\mu'\nu_{II}\rangle^2/D_I . \tag{6.15}$$

6. Correlations between fission and coupling widths of class-II states

The question of a possible correlation between coupling and fission widths of class-II states must be raised here. Superficially, the fission width expression of Eq. (6.3) and the coupling matrix element of Eq. (3.160a) involve the same significant expansion coefficient $C^{\lambda_{II}}_{\mu\nu_{II}}$ for a many-phonon vibration mode, and the two would therefore seem to be correlated. This could, in fact, be the case when pure vibration modes uncoupled to other degrees of freedom retain their identity in a special way after coupling is introduced, so that the vibration is mixed into a dense background of compound states without any further major adjustments at a more elementary level. This could be the case in an even nucleus, and the vital factor that the discussion of Sec. V.C.1 brings out is that the intrinsic wave function χ_μ defining the lowest channel at both the inner and outer barrier deformations has the same, or a very similar, configuration. That discussion also shows that even the simplest low-lying states in odd-A nuclei have quite uncorrelated fission and coupling widths, because the intrinsic channels are so different in these nuclei, and it is therefore very unlikely that any pattern of correlation will be carried over to the compound class-II states unless there are very marked effects of damped vibrational resonances.

C. Average cross sections over intermediate resonances

1. Area of intermediate fission resonances

When we come to examine the experimental data (Sec. VI.E) we shall find that there are many observations of intermediate fission resonances in which the fine structure has not been resolved. Nevertheless, valuable information can still be obtained from such structure.

The area of the neutron cross section under an intermediate resonance is the sum of the area of its component fine-structure resonances. Each of these has an area

$$A_\lambda = 2\pi^2\lambda^2 g(J)\Gamma_{\lambda(n)}\Gamma_{\lambda(f)}/\Gamma_\lambda . \tag{6.16a}$$

Therefore,

$$A_{\lambda_{II}} = 2\pi^2\lambda^2 g(J)\sum_\lambda \Gamma_{\lambda(n)}\Gamma_{\lambda(f)}/\Gamma_\lambda . \tag{6.16b}$$

The sum has to be computed taking into account the

variation of the fission width across the intermediate resonance, and the Porter–Thomas fluctuations of the partial widths both in the entrance and the deformation channels.

a. Moderately weak coupling: general expression with neglect of fluctuations

The fine-structure fission widths of Eq. (6.16) are represented by a Lorentzian [Eq. (3.185b)]. In addition to the neutron and fission widths, an additional reaction width $\Gamma_{\lambda(r)}$ is included in the total width. Normally, for low-energy neutron reactions the neutron width is just the total radiation width. We replace the sum by an integral in Eq. (6.16) and obtain, for a well isolated class-II resonance,

$$\sum_{\lambda}\frac{\Gamma_{\lambda(n)}\Gamma_{\lambda(f)}}{\Gamma_{\lambda}}\approx\Gamma_{(n)}\frac{\Gamma_{\lambda_{II}(c)}\Gamma_{\lambda_{II}(f)}}{(\Gamma_{(n)}+\Gamma_{(r)})}\times\left(\frac{\pi(\Gamma_{(n)}+\Gamma_{(r)})}{(\Gamma_{\lambda_{II}(c)}+\Gamma_{\lambda_{II}(f)})^2(\Gamma_{(n)}+\Gamma_{(r)})\pi+2D_I\Gamma_{\lambda_{II}(c)}\Gamma_{\lambda_{II}(f)}}\right)^{1/2}. \tag{6.17}$$

This is to be contrasted with the expression that would be obtained if the class-II fission width were spread uniformly over all fine-structure resonances in an energy interval D_{II}:

$$\sum_{\lambda}\frac{\Gamma_{\lambda(n)}\bar{\Gamma}_{\lambda(f)}}{\bar{\Gamma}_{\lambda}}\approx\Gamma_{(n)}\frac{\Gamma_{\lambda_{II}(c)}\Gamma_{\lambda_{II}(f)}D_{II}}{(\Gamma_{\lambda_{II}(c)}+\Gamma_{\lambda_{II}(f)})(\Gamma_{(n)}+\Gamma_{(r)})D_{II}+\Gamma_{\lambda_{II}(c)}\Gamma_{\lambda_{II}(f)}D_I}. \tag{6.18}$$

The value of the right-hand side of Eq. (6.17) is smaller than that of Eq. (6.18).

The area under an intermediate resonance in a neutron fission cross section is, therefore, neglecting fluctuations,

$$A_{\lambda_{II}}=2\pi^2\lambda^2 g(J)\frac{\Gamma_{(n)}}{\Gamma_{(n)}+\Gamma_{(r)}}\Gamma_{\lambda_{II}(c)}\Gamma_{\lambda_{II}(f)}\times\left(\frac{\pi(\Gamma_{(n)}+\Gamma_{(r)})}{(\Gamma_{\lambda_{II}(c)}+\Gamma_{\lambda_{II}(f)})^2(\Gamma_{(n)}+\Gamma_{(r)})\pi+2D_I\Gamma_{\lambda_{II}(c)}\Gamma_{\lambda_{II}(f)}}\right)^{1/2}. \tag{6.19}$$

Notice that this expression is general for any Lorentzian form of the fine-structure fission widths and thus encompasses the case of very weak coupling to a class-II level with broad fission width.

When the fission widths of the fine-structure resonances at the center of the intermediate resonance are much smaller than the total widths

$$(\Gamma_{\lambda_{II}(f)}D_I/\Gamma_{\lambda_{II}(c)}\ll\Gamma_{(n)}+\Gamma_{(r)}),$$

the intermediate area is approximately

$$A_{\lambda_{II}}\approx 2\pi^2\lambda^2 g(J)\frac{\Gamma_{(n)}}{\Gamma_{(n)}+\Gamma_{(r)}}\Gamma_{\lambda_{II}(f)} \tag{6.20}$$

in the limiting case $\Gamma_{\lambda_{II}(f)}\ll\Gamma_{\lambda_{II}(c)}$.

b. Moderately weak coupling with fluctuations of fine structure

Analytical expressions for intermediate resonance areas that take account of the fluctuations in the widths of the fine-structure resonances are available only for some simplified cases.

(i) $\Gamma_{\lambda(f)}\ll\Gamma_{\lambda}$. Firstly, we consider the case in which the fine-structure fission widths are always much smaller than the total widths. The individual terms in the sum in Eq. (6.16) are to be averaged over Porter–Thomas distributions $p(x)dx$ [see Eq. (6.10)]. Thus, on the assumption that the reaction width $\Gamma_{\lambda(r)}$ is uniform,

$$\left\langle\frac{\Gamma_{\lambda(n)}\Gamma_{\lambda(f)}}{\Gamma_{\lambda}}\right\rangle\approx\left\langle\frac{\Gamma_{\lambda(n)}\Gamma_{\lambda(f)}}{\Gamma_{\lambda(n)}+\Gamma_{\lambda(r)}}\right\rangle\approx\iint d\Gamma_{(n)}d\Gamma_{(f)}p(\Gamma_{(n)})p(\Gamma_{(f)})\frac{\Gamma_{(n)}\Gamma_{(f)}}{\Gamma_{(n)}+\Gamma_{(r)}}=\bar{\Gamma}_{(f)}\int d\Gamma_{(n)}p(\Gamma_{(n)})\frac{\Gamma_{(n)}}{\Gamma_{(n)}+\Gamma_{(r)}}. \tag{6.21}$$

The last integral is well known from the theory of neutron capture reactions (Lane and Lynn, 1957), so we obtain the result

$$A_{\lambda_{II}}=2\pi^2\lambda^2 g(J)\frac{\bar{\Gamma}_{(n)}}{\bar{\Gamma}_{(n)}+\Gamma_{(r)}}s_{nr}\sum_{\lambda}\Gamma_{\lambda(f)}, \tag{6.22a}$$

where

$$s_{nr}=(1+\Gamma_{(r)}/\bar{\Gamma}_{(n)})\left\{1-\frac{\Gamma_{(r)}}{\bar{\Gamma}_{(n)}}\left[1-\left(\frac{\pi\Gamma_{(r)}}{2\bar{\Gamma}_{(n)}}\right)^{1/2}\exp\left(\frac{\Gamma_{(r)}}{2\bar{\Gamma}_{(n)}}\right)\operatorname{erfc}\left(\frac{\Gamma_{(r)}}{2\bar{\Gamma}_{(n)}}\right)^{1/2}\right]\right\}, \tag{6.22b}$$

and the sum $\sum_{\lambda}\Gamma_{\lambda(f)}\approx\Gamma_{\lambda_{II}(f)}$ if $\Gamma_{\lambda_{II}(f)}\ll\Gamma_{\lambda_{II}(c)}$.

(ii) Reaction width negligible. If only the entrance channel width and fission width are substantial the average value of $\Gamma_{\lambda(n)}\Gamma_{\lambda(f)}/\Gamma_{\lambda}$ becomes

$$\left\langle\frac{\Gamma_{\lambda(n)}\Gamma_{\lambda(f)}}{\Gamma_{\lambda(n)}+\Gamma_{\lambda(f)}}\right\rangle=\frac{\bar{\Gamma}_{(n)}\bar{\Gamma}_{(f)}}{(\bar{\Gamma}_{(n)}^{1/2}+\bar{\Gamma}_{(f)}^{1/2})^2} \tag{6.23}$$

for Porter–Thomas fluctuations. The ratio

$$s_{nf}=\frac{\bar{\Gamma}_{(n)}\bar{\Gamma}_{(f)}}{(\bar{\Gamma}_{(n)}^{1/2}+\bar{\Gamma}_{(f)}^{1/2})}\Big/\frac{\bar{\Gamma}_{(n)}\bar{\Gamma}_{(f)}}{(\bar{\Gamma}_{(n)}+\bar{\Gamma}_{(f)})} \tag{6.23b}$$

is shown in Fig. 110 as a function of the ratio $\bar{\Gamma}_{(n)}/\Gamma_{(f)}$.

To obtain the intermediate resonance area the expression (6.23) must be integrated over the Lorentzian energy dependence for the fission width:

$$\sum_{\lambda}\frac{\Gamma_{\lambda(n)}\Gamma_{\lambda(f)}}{\Gamma_{\lambda(n)}+\Gamma_{\lambda(f)}}\approx\frac{1}{2\pi}\Gamma_{\lambda_{II}(c)}\Gamma_{\lambda_{II}(f)}\bar{\Gamma}_{(n)}\int_{-\infty}^{\infty}d\varepsilon\frac{1}{\bar{\Gamma}_{(n)}(\varepsilon^2+W^2)+2\left[\frac{\bar{\Gamma}_{(n)}\Gamma_{\lambda_{II}(c)}\Gamma_{\lambda_{II}(f)}D_I}{2\pi}(\varepsilon^2+W^2)\right]^{1/2}+\frac{\Gamma_{\lambda_{II}(c)}\Gamma_{\lambda_{II}(f)}D_I}{2\pi}}\,, \tag{6.24}$$

with half-width $W=\frac{1}{2}(\Gamma_{\lambda_{II}(c)}+\Gamma_{\lambda_{II}(f)})$. The ratio of this quantity to the expression (6.17), which we label $\mathrm{Int}s_{nf}$,

$$\mathrm{Int}s_{nf}=\pi^{-1}(W^2+U)^{1/2}\times\int_{-\infty}^{\infty}d\varepsilon\frac{1}{\varepsilon^2+W^2+2[U(\varepsilon^2+W^2)]^{1/2}+U}$$

depends only on the parameter $W/\sqrt{U}$ where $U=\Gamma_{\lambda_{II}(c)}\Gamma_{\lambda_{II}(f)}D_I/2\pi\Gamma_{I(n)}$. This functional dependence is shown in Fig. 111.

c. Moderately weak coupling: fluctuation of intermediate areas

Fluctuations in the areas of intermediate resonances are due in principle to fluctuations in the widths of the fine-structure resonances as well as to fluctuations in the widths of the class-II states. In practice, when the half-width of the intermediate resonance encompasses several fine-structure resonances on average, the effect of the former is small and only fluctuations of the class-II widths need be considered.

(i) $\Gamma_{\lambda(f)}\ll\Gamma_{\lambda}$. This is the simplest case to consider. The expression for the area is given by Eq. (6.20). The fluctuations in the intermediate area are just those in the class-II fission width, i.e., they are governed by the Porter–Thomas distribution Eq. (6.10) in the case of a single deformation channel. The variance associated with this distribution is twice the square of the mean value.

(ii) $\Gamma_{\lambda(f)}\sim\Gamma_{\lambda}$ *in central resonances.* In this extreme the expression for the intermediate resonance is [from Eq. (6.19)]

$$A_{\lambda_{II}}=2\pi^2\lambda^2 g(J)\frac{\Gamma_{(n)}}{\Gamma_{(n)}+\Gamma_{(r)}}\left(\frac{\pi(\Gamma_{(n)}+\Gamma_{(r)})\Gamma_{\lambda_{II}(c)}\Gamma_{\lambda_{II}(f)}}{2D_I}\right)^{1/2}, \tag{6.25}$$

in the absence of fluctuations. With independent Porter–Thomas fluctuations of both the coupling and fission widths the mean value of $A_{\lambda_{II}}$ will be

$$\bar{A}_{II}=2A_{II,un}/\pi\,, \tag{6.26}$$

where the "uniform model" value of the area $A_{II,un}$ is just Eq. (6.25) with the mean values of the class-II widths substituted for $\Gamma_{\lambda_{II}(c)},\Gamma_{\lambda_{II}(f)}$.

The variance in the intermediate area is also easily computed for Eq. (6.25); it is

$$\mathrm{var}A_{II}=\bar{A}_{II}^2\left(\frac{\pi^2-4}{\pi^2}\right). \tag{6.27}$$

This is considerably lower than case *(i)*, by a factor of about 3.

In general, because of fluctuations, intermediate areas will cover a range between cases *(i)* and *(ii)* and the variance will lie between the limits established for the two cases.

d. Very weak coupling of narrow class-II states

(i) Areas in the uniform model. This degree of coupling is analysed using perturbation theory in Sec.III.5.*c*(*ii*). From that discussion it is clear that two kinds of term contribute to the intermediate resonance area of Eq. (6.16), the single quasi-class-II level and the many quasi-class-I levels. The area of the quasi-class-II resonance is

$$A_{\lambda''}\approx 2\pi^2\lambda^2 g(J)\frac{\left(\sum_{\lambda_I}\frac{H_{c(\lambda_I,\lambda_{II})}\Gamma^{1/2}_{\lambda_I(n)}}{E_{\lambda_I}-E_{\lambda_{II}}}\right)\Gamma_{\lambda_{II}(f)}\left(1-\sum_{\lambda_I}\frac{H^2_{c(\lambda_I,\lambda_{II})}}{(E_{\lambda_I}-E_{\lambda_{II}})^2}\right)}{\left(\sum_{\lambda_I}\frac{H_{c(\lambda_I,\lambda_{II})}\Gamma^{1/2}_{\lambda_I(n)}}{E_{\lambda_I}-E_{\lambda_{II}}}\right)^2+(\Gamma_{\lambda_{II}(f)}+\Gamma_{\lambda_I(r)})\left(1-\sum_{\lambda_I}\frac{H^2_{c(\lambda_I,\lambda_{II})}}{(E_{\lambda_I}-E_{\lambda_{II}})^2}\right)+\sum_{\lambda_I}\frac{H^2_{c(\lambda_I,\lambda_{II})}\Gamma_{\lambda_I(r)}}{(E_{\lambda_I}-E_{\lambda_{II}})^2}}\,. \tag{6.28}$$

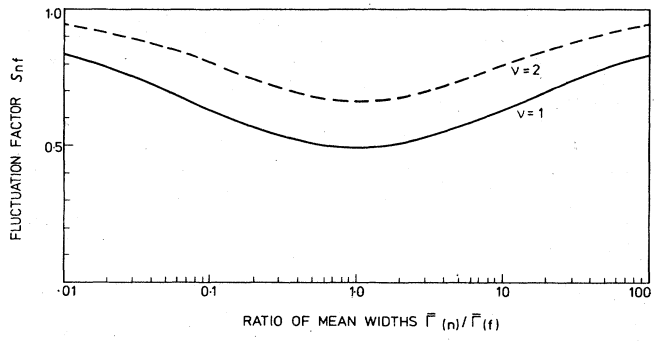

FIG. 110. The fluctuation factor S_{nf} for Porter–Thomas fluctuations. The full curve labeled $\nu=1$ is the factor calculated from Eq. (6.23b) for Porter–Thomas distributions of neutron widths. The broken curve ($\nu=2$) is for exponential distributions.

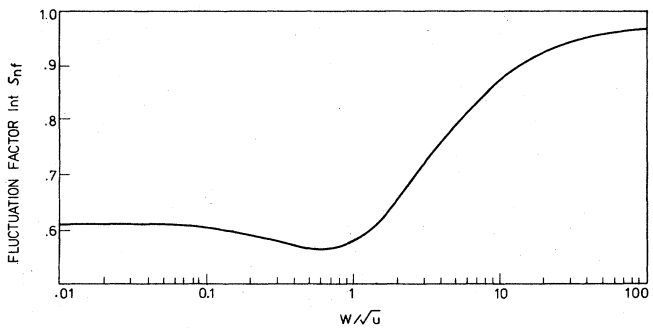

FIG. 111. The fluctuation factor Int S_{nf} as a function of the parameter $W/\sqrt{U}$.

The first term in the denominator is the quasi-class-II resonance neutron width, the second includes reaction processes from the class-II state (principally fission and radiation), and the third is the contribution to reaction processes from class-I levels. The last is assumed to comprise very many incoherent channels (as in radiative capture).

The contribution to the area from the quasi-class-I resonance is

$$A_{\lambda'} \approx 2\pi^2 \lambda^2 g(J) \sum_{\lambda_I} \Gamma_{\lambda_{I(n)}} \frac{H^2_{c(\lambda_I,\lambda_{II})} \Gamma_{\lambda_{II(f)}}}{(E_{\lambda_{II}} - E_{\lambda_I})^2} \Big/ \left[\Gamma_{\lambda_{I(n)}} + \Gamma_{\lambda_{I(r)}} + \frac{H^2_{c(\lambda_I,\lambda_{II})} (\Gamma_{\lambda_{II(f)}} + \Gamma_{\lambda_{II(r)}})}{(E_{\lambda_{II}} - E_{\lambda_I})^2} \right]. \tag{6.29}$$

Expectation values of the total area

$$A_{\lambda_{II}} = A_{\lambda''} + A_{\lambda'} \tag{6.30}$$

can be calculated on the assumption of a uniform model for spacings, class-I partial widths and coupling matrix elements. Let us assume that the class-II level lies at energy xD_I from the nearest class-I level. Then the sum

$$\sum_{\lambda_I} \frac{1}{(E_{\lambda_I} - E_{\lambda_{II}})^2} = \frac{1}{D_I^2} \sum_{n=-\infty}^{\infty} \frac{1}{(n-x)^2} = \frac{\pi^2}{D_I^2} \csc^2 \pi x . \tag{6.31}$$

Applying this to Eq. (6.28), with the assumption of completely random sign in the matrix elements and reduced neutron width amplitudes $\Gamma^{1/2}_{\lambda_{I(n)}}$, we find

$$A_{\lambda''} = \frac{2\pi^2 \lambda^2 g(J)(\pi^2 H^2 \Gamma_{I(n)} \Gamma_{\lambda_{II(f)}} / D_I^2)[1 - (\pi^2 H^2 / D_I^2) \csc^2 \pi x] \csc^2 \pi x}{(\pi^2 H^2 / D_I^2)\Gamma_I \csc^2 \pi x + [1 - (\pi^2 H^2 / D_I^2) \csc^2 \pi x] \Gamma_{\lambda_{II}}} \tag{6.32}$$

(where $\Gamma_I = \Gamma_{I(n)} + \Gamma_{I(r)}$ and $\Gamma_{\lambda_{II}} = \Gamma_{\lambda_{II(f)}} + \Gamma_{\lambda_{II(r)}}$).

For the same uniform model we can derive

$$A_{\lambda'} = 2\pi^2 \lambda^2 g(J) \frac{H^2 \Gamma_{I(n)} \Gamma_{\lambda_{II(f)}}}{D_I^2 \Gamma_I} \sum_{n=-\infty}^{\infty} \frac{1}{(n-x)^2 + H^2 \Gamma_{\lambda_{II}} / D_I^2 \Gamma_I} . \tag{6.33}$$

We find a lower limit for this by putting $x = \frac{1}{2}$:

$$A_{\lambda'} \gtrsim 2\pi^2 \lambda^2 g(J) \frac{H^2 \Gamma_{I(n)} \Gamma_{\lambda_{II(f)}}}{D_I^2 \Gamma_I} \left(\frac{\pi^2 D_I^2 \Gamma_I}{H^2 \Gamma_{\lambda_{II}}} \right)^{1/2} \tanh \left(\frac{\pi^2 H^2 \Gamma_{\lambda_{II}}}{D_I^2 \Gamma_I} \right)^{1/2} . \tag{6.34}$$

An upper limit is found by neglecting the class-II contribution to the denominator in Eq. (6.29):

$$A_{\lambda'} \lesssim 2\pi^2 \lambda^2 g(J) \frac{\pi^2 H^2 \Gamma_{I(n)} \Gamma_{\lambda_{II(f)}}}{D_I^2 \Gamma_I} \csc^2 \pi x . \tag{6.35}$$

For very weak coupling the argument of the hyperbolic tangent in Eq. (6.34) is very small, so the hyperbolic tangent is well approximated by its argument. Within this approximation Eq. (6.34) is the same as Eq. (6.35), so we can adopt the latter in forming the final expression for $A_{\lambda_{II}}$:

$$A_{\lambda_{II}} \approx 2\pi^2 \lambda^2 g(J) \frac{\pi^2 H^2 \Gamma_{I(n)} \Gamma_{\lambda_{II(f)}}}{D_I^2} \csc^2 \pi x \left\{ \frac{[1 - (\pi^2 H^2 / D_I^2) \csc^2 \pi x]}{(\pi^2 H^2 / D_I^2)\Gamma_I \csc^2 \pi x + \Gamma_{\lambda_{II}} [1 - (\pi^2 H^2 / D_I^2) \csc^2 \pi x]} + \frac{1}{\Gamma_I} \right\}. \tag{6.36}$$

The median value of x is $\frac{1}{4}$, for which

$$A_{\lambda_{II}}(\text{med}) \approx 2\pi^2 \lambda^2 g(J) \frac{2\pi^2 H^2 \Gamma_{I(n)} \Gamma_{\lambda_{II(f)}}}{D_I^2} \left\{ \frac{1 - 2(\pi^2 H^2 / D_I^2)}{(2\pi^2 H^2 / D_I^2)\Gamma_I + (1 - 2\pi^2 H^2 / D_I^2)\Gamma_{\lambda_{II}}} + \frac{1}{\Gamma_I} \right\}. \tag{6.37}$$

(ii) Fluctuations. Fluctuations in the area are much more sensitive to the fluctuation in the class-I levels in this case, and also to the relative position x of the class-II level in relation to the nearest class-I level. Indeed the sensitivity of the expression (6.36) to the x parameter renders it impossible to derive from it a true expectation value. For very small values of x the physical case is that of accidental degeneracy, treated in Sec. III.C.5.*c.*, in which the most important contributions to the area come from two fine-structure resonances sharing almost equally nearly all of the class-II fission width and the neutron width of the degenerate class-I level. If we make the assumption that the level repulsion is much greater than their widths $2|H| \gg \frac{1}{2}(\Gamma_{\lambda_{II}} + \Gamma_{\lambda_I})$ (so that the coherent interference in the cross section need not be taken into account) the intermediate resonance area is simply

$$A_{\lambda_{II}}(\text{deg}) \approx 4\pi^2 \lambda^2 g(J) (\tfrac{1}{2}\Gamma_{\lambda_{I(n)}})(\tfrac{1}{2}\Gamma_{\lambda_{II(f)}}) / [\tfrac{1}{2}(\Gamma_{\lambda_I} + \Gamma_{\lambda_{II}})] , \tag{6.38a}$$

and this is the true upper limit of Eq. (6.36) for small x. Equation (6.38) will replace Eq. (6.36) for small x below a transitional region around $x \sim 2|H|/D_I$. Integration of the leading terms of Eq. (6.36) from this transitional value of x to $x = 0.5$ allows us to find very approximate values for the mean value and variance (due to the x parameter alone) of the intermediate area. They are

$$\bar{A}_{\lambda_{II}} \approx 2\pi^2 \lambda^2 g(J) \frac{\overline{|H|}}{D_I} \bar{\Gamma}_{I(n)} \bar{\Gamma}_{\lambda_{II(f)}} \left\{ \frac{1}{\bar{\Gamma}_{II}} + \frac{1}{\bar{\Gamma}_I} \right\}, \tag{6.39}$$

$$\text{var} A_{\lambda_{II}} \approx \bar{A}^2_{\lambda_{II}} \frac{D_I}{6\pi \overline{|H|}} . \tag{6.40a}$$

For weak enough coupling, the factor $D_I / 6\pi \overline{|H|}$ in the variance can be very much greater than the typical value of 2 due to Porter–Thomas fluctuations in widths. Extra quantities of this order must be multiplied into this factor to account for fluctuations in $\Gamma_{I(n)}$, $\Gamma_{\lambda_{II(f)}}$, and $|H|$ in the expression (6.39).

The contribution from degenerate levels should be

added to the mean value of Eq. (6.39), giving

$$\bar{A}_{\lambda_{II}} \approx 2\pi^2 \lambda\!\!\!^{-2} g(J) \frac{\overline{|H|}}{D_I} \bar{\Gamma}_{I(n)} \bar{\Gamma}_{\lambda_{II}(f)} \times \left\{ \frac{1}{\bar{\Gamma}_{II}} + \frac{1}{\bar{\Gamma}_I} + \frac{4}{(\bar{\Gamma}_I + \bar{\Gamma}_{II})} \right\} . \quad (6.41a)$$

A modification to these considerations arises from the possibility that the class-II fission width (and/or class-I neutron width) is greater than the modulus of the coupling matrix element. Then, if accidental degeneracy nearly occurs, the fine structure resonances do not have parameters identical to the R-matrix levels as we have assumed so far; their areas must be determined from the parameters of the S-matrix poles. We presented the appropriate S-matrix parameters in Sec. III.C.5.$c(v)$ [see Eqs. (3.204),(3.205)]. Using these we find

$$A_{\lambda_{II}}(\text{deg}) \approx 2\pi^2 \lambda\!\!\!^{-2} g(J) \frac{4H^2}{(\Gamma_{\lambda_I(n)} - \Gamma_{\lambda_{II}(f)})^2} \Gamma_{\lambda_I(n)} \Gamma_{\lambda_{II}(f)} \left\{ \frac{1}{\Gamma_{\lambda_{II}}} + \frac{1}{\Gamma_{\lambda_I}} \right\} , \quad (6.38b)$$

if the class-I and class-II reaction widths are equal.

This is lower than the right-hand side of Eq. (6.38a) by the factor

$$4H^2(\Gamma_{\lambda_I} + \Gamma_{\lambda_{II}})^2 / (\Gamma_{\lambda_I(n)} - \Gamma_{\lambda_{II}(f)})^2 \Gamma_{\lambda_I} \Gamma_{\lambda_{II}} .$$

Equation (6.38b) is expected to be crudely valid for $x = 0$ to

$$x \sim \{ [(\Gamma_{\lambda_{II}} + \Gamma_{\lambda_I})/2D_I]^2 - 4H^2 \}^{1/2} .$$

The expectation value of the intermediate area becomes, in consequence,

$$\bar{A}_{\lambda_{II}} \approx 2\pi^2 \lambda\!\!\!^{-2} g(J) \frac{4H^2}{D_I} \Gamma_{I(n)} \Gamma_{\lambda_{II}(f)} \times \left\{ \frac{1}{\Gamma_I \Gamma_{II}} + 2 \left(\frac{\Gamma_I + \Gamma_{II}}{\Gamma_I - \Gamma_{II}} \right)^2 \frac{1}{\Gamma_I \Gamma_{II}} \right\} . \quad (6.41b)$$

This bears the ratio to the rhs of (6.41a) of roughly $8|H|(\Gamma_I + \Gamma_{II})/(\Gamma_I - \Gamma_{II})^2$.

By similar arguments as before the variance is at least

$$\text{var} A_{\lambda_{II}} \approx \bar{A}^2_{\lambda_{II}} \frac{2D_I}{3\pi(\Gamma_{I(n)} + \Gamma_{II(f)})} . \quad (6.40b)$$

2. Average fission cross sections

a. Moderate to strong coupling and/or very broad fission width

This is the limiting case in which intermediate structure is barely or not at all perceivable. To a good approximation the average fission cross section is just the normal expression from statistical compound nucleus theory:

$$\sigma_f = \sigma_{CN} \frac{\bar{\Gamma}_{(f)}}{\bar{\Gamma}} , \quad (6.42)$$

neglecting fine-structure width fluctuations. For incoming neutrons the compound nucleus formation cross section σ_{CN} is

$$\sigma_{CN} = 2\pi^2 \lambda\!\!\!^{-2} g(J) \frac{\bar{\Gamma}_{(n)}}{\bar{D}_I} . \quad (6.43)$$

The mean fission width is obtained by averaging over the class-II levels. For a single class-II level,

$$\langle \Gamma_{(f)} \rangle_{\text{loc}} \approx \frac{D_I}{D_{II}} \frac{\Gamma_{\lambda_{II}(c)} \Gamma_{\lambda_{II}(f)}}{(\Gamma_{\lambda_{II}(c)} + \Gamma_{\lambda_{II}(f)})} \quad (6.44)$$

(which is just the result from pure statistical theory, Sec. III.B.1.). The average of expression (6.44) over a sequence of class-II levels with coupling and fission widths independently distributed in the Porter–Thomas manner is

$$\bar{\Gamma}_{(f)} = \frac{D_I}{D_{II}} \frac{\bar{\Gamma}_{\lambda_{II}(c)} \bar{\Gamma}_{\lambda_{II}(f)}}{(\bar{\Gamma}^{1/2}_{\lambda_{II}(c)} + \bar{\Gamma}^{1/2}_{\lambda_{II}(f)})^2} . \quad (6.45)$$

The ratio $\bar{\Gamma}_{(f)}/\langle \Gamma_{(f)} \rangle_{\text{loc}}$ [with average values of the class-II width substituted in Eq. (6.44)] is denoted by $s^{(II)}_{cf}$, and a perfectly analogous quantity is shown in Fig. 110.

The fluctuation factor $s^{(II)}_{cf}$ is closer to unity if more than one deformation channel is open at the barriers. For example, with two equally open channels at the outer barrier and coupling that is strong enough to give moderate overlap ($\Gamma_{II} \approx D_{II}$) of neighboring intermediate resonances the effective statistical distributions can be assumed to be approximately exponential, and the average fission width becomes

$$\bar{\Gamma}_{(f)} = \frac{D_I}{D_{II}} \frac{\bar{\Gamma}_{\lambda_{II}(c)} \bar{\Gamma}_{\lambda_{II}(f)}}{(\bar{\Gamma}_{\lambda_{II}(c)} - \bar{\Gamma}_{\lambda_{II}(f)})^3} \left[\bar{\Gamma}^2_{\lambda_{II}(c)} - \bar{\Gamma}^2_{\lambda_{II}(f)} - 2\bar{\Gamma}_{\lambda_{II}(c)} \bar{\Gamma}_{\lambda_{II}(f)} \ln \left(\frac{\bar{\Gamma}_{\lambda_{II}(c)}}{\bar{\Gamma}_{\lambda_{II}(f)}} \right) \right] . \quad (6.46)$$

The corresponding graph of $s^{(II)}_{cf}$ is also shown in Fig. 110. For more details of the fluctuation factor $s^{(II)}_{cf}$ see Lynn (1980).

Evaluation of the fluctuation factor s_{nf}, which must be multiplied into the simple statistical form (6.42) to allow for fine-structure width fluctuations in the neutron fission cross section, must be obtained in general by numerical integration. With the definition

$$s_{nf} = \left\langle \frac{\Gamma_{\lambda(n)} \Gamma_{\lambda(f)}}{\Gamma_\lambda} \right\rangle \Big/ \frac{\bar{\Gamma}_{(n)} \bar{\Gamma}_{(f)}}{\bar{\Gamma}}$$

the general integral to be calculated is (Dresner, 1957)

$$s_{nf} = \left(\frac{\Gamma_{(\gamma)}}{2} \right)^{n/2+1} \frac{\bar{\Gamma}}{(\bar{\Gamma}_{(n)} \bar{\Gamma}_{(f)})^{3/2} (\bar{\Gamma}_{(a)} \cdots \bar{\Gamma}_{(x)})^{1/2}} \times \int_0^\infty dx \frac{e^{-x}}{(x + \Gamma_{(\gamma)}/2\bar{\Gamma}_{(n)})^{3/2} (x + \Gamma_{(\gamma)}/2\bar{\Gamma}_{(f)})^{3/2} [(x + \Gamma_{(\gamma)}/2\Gamma_{(a)}) \cdots (x + \Gamma_{(x)}/2\bar{\Gamma}_{(x)})]^{1/2}} \quad (6.47)$$

with Porter–Thomas fluctuations in n channels, including the entrance and exit channels, together with reaction channels labeled here by a to z in addition to a non-fluctuating radiation width $\Gamma_{(\gamma)}$.

b. Fluctuations in the broadly modulated fission cross section

Although the narrow intermediate structure will not be dramatic when the class-II levels are broad (whether due to coupling or to fission) the locally averaged fission cross section (in the sense of averaging over an energy interval of order D_{II}) will show fluctuations due to the width fluctuations of class-II levels, if the coupling is still sufficiently moderate that a single class-II level will dominate the fission strength function in its immediate vicinity. We have evaluated the variance of the expression (6.44) for Porter–Thomas distributions of the class-II coupling and fission widths; it is

$$\mathrm{var}\langle\Gamma_{(f)}\rangle_{\mathrm{loc}} = 2\bar{\Gamma}^2_{(f)} . \tag{6.48}$$

We must make approximations in applying this to the local average cross-section fluctuations. If fission is weak in the deexcitation of the compound nucleus, then

$$\mathrm{var}\langle\sigma_f\rangle_{\mathrm{loc}} \approx 2\bar{\sigma}_f^2 . \tag{6.49}$$

If fission predominates, on the other hand, the cross-section fluctuations are greatly reduced. We analyze this crudely by making the expansion

$$\langle\sigma_f\rangle_{\mathrm{loc}} = 2\pi^2\lambda\!\!\!^{-2} g(J)\,\frac{\bar{\Gamma}_{(n)}}{D}\,\frac{(\bar{\Gamma}_{(f)}+\delta\Gamma_{(f)})}{\bar{\Gamma}(1+\delta\Gamma_{(f)}/\bar{\Gamma})}$$
$$= \bar{\sigma}_f\left[1+\delta\Gamma_{(f)}\left(\frac{1}{\bar{\Gamma}_{(f)}}-\frac{1}{\bar{\Gamma}}\right)-\frac{(\delta\Gamma_{(f)})^2}{\bar{\Gamma}}\left(\frac{1}{\bar{\Gamma}_{(f)}}-\frac{1}{\bar{\Gamma}}\right)+\cdots\right]. \tag{6.50}$$

Only second-order terms are retained. The average of $(\delta\Gamma_{(f)})^2$ is just $\mathrm{var}\langle\Gamma_{(f)}\rangle_{\mathrm{loc}}$, and we can deduce

$$\mathrm{var}\langle\sigma_f\rangle_{\mathrm{loc}} = \overline{\langle\sigma_f\rangle^2_{\mathrm{loc}}} - \overline{\langle\sigma_f\rangle_{\mathrm{loc}}}^{\,2}$$
$$\approx [\bar{\sigma}_f(\sigma_{\mathrm{CN}}-\bar{\sigma}_f)]^2\,\frac{\mathrm{var}\langle\Gamma_{(f)}\rangle_{\mathrm{loc}}}{\bar{\Gamma}^2_{(f)}} . \tag{6.51}$$

c. Moderately weak coupling and/or moderate class-II fission widths

The average neutron fission cross section can be deduced immediately from the expression for the area over an intermediate resonance, Eq. (6.19). This is spread over the energy interval D_{II} to give the average (local) cross section,

$$\langle\sigma_{nf}\rangle_{\mathrm{loc}} = 2\pi^2\lambda\!\!\!^{-2} g(J)\,\frac{\Gamma_{(n)}}{\Gamma_{(n)}+\Gamma_{(r)}}\,\frac{\Gamma_{\lambda_{II}(c)}\Gamma_{\lambda_{II}(f)}}{D_{II}}$$
$$\times\left[\frac{\pi(\Gamma_{(n)}+\Gamma_{(r)})}{(\Gamma_{\lambda_{II}(c)}+\Gamma_{\lambda_{II}(f)})^2(\Gamma_{(n)}+\Gamma_{(r)})\pi+2D_I\Gamma_{\lambda_{II}(c)}\Gamma_{\lambda_{II}(f)}}\right]^{1/2}, \tag{6.52}$$

on the assumption that fluctuations in the fine-structure widths can be ignored. The same assumptions as in Sec. VI.C.1.*b* must be made to obtain analytical expressions that include the effects of fluctuations. If the fine-structure fission widths are all much less than the total widths, the rhs of Eq. (6.52) must be multiplied by the fluctuation factor $\mathcal{S}_{nr}$ [Eq. (6.22b)] (or a generalization if there is one or more inelastic scattering channels included in the reaction width). If the reaction width is negligible the multiplying factor is $\mathcal{S}_{nf}$ [Eq. (6.23b)], suitably integrated over the Lorentzian profile (see Fig. 110).

If the class-II width approaches the order of magnitude of the class-II level spacing the expression (6.52) is found to be inaccurate and can exceed the value of the compound nucleus formation cross section. This is because the fission competition factor is unduly weighted far out on the wings of the intermediate resonance, beyond the energy limits $|E-E_{\lambda_{II}}| = \frac{1}{2}D_{II}$, where the other intermediate resonances become dominant, thus depressing the effectiveness of fission in the competition process. This effect can be compensated partially by limiting the integration to the energy interval D_{II}, in which case

$$\langle\sigma_{nf}\rangle_{\mathrm{loc}} = 2\pi^2\lambda\!\!\!^{-2} g(J)\,\frac{\Gamma_{(n)}\Gamma_{\lambda II(c)}\Gamma_{\lambda II(f)}}{(\Gamma_{(n)}+\Gamma_{(r)})D_{II}}\left[\frac{\pi(\Gamma_{(n)}+\Gamma_{(r)})}{(\Gamma_{\lambda_{II}(c)}+\Gamma_{\lambda_{II}(f)})^2(\Gamma_{(n)}+\Gamma_{(r)})\pi+2D_I\Gamma_{\lambda_{II}(c)}\Gamma_{\lambda_{II}(f)}}\right]^{1/2}$$
$$\times\frac{2}{\pi}\arctan\left[D_{II}\left(\frac{\pi(\Gamma_{(n)}+\Gamma_{(r)})}{(\Gamma_{\lambda_{II}(c)}+\Gamma_{\lambda_{II}(f)})^2(\Gamma_{(n)}+\Gamma_{(r)})\pi+2D_I\Gamma_{\lambda_{II}(c)}\Gamma_{\lambda_{II}(f)}}\right)^{1/2}\right]. \tag{6.53}$$

More accurately, the contribution of the wings of the other class-II levels within the energy interval D_{II} can be taken into account. An exact expression can be found within the uniform (picket-fence) model (Lynn and Back, 1974):

$$\bar{\sigma}_{nf} = \langle\sigma_{nf}\rangle_{\mathrm{loc}} = 2\pi^2\lambda\!\!\!^{-2} g(J)\,\frac{\Gamma_{(n)}}{D_I}$$
$$\times\left\{1+R^2+2R\coth\left[\frac{\pi(\Gamma_{II(c)}+\Gamma_{II(f)})}{D_I}\right]\right\}^{-1/2}, \tag{6.54}$$

where $R = (\Gamma_{(n)}+\Gamma_{(r)})(\Gamma_{II(c)}+\Gamma_{II(f)})D_{II}/(\Gamma_{II(c)}\Gamma_{II(f)}D_I)$.

The "smooth-average" fission cross section (averaged over many energy intervals of D_{II}) is subject also to fluctuations in the class-II widths. When the fine-structure fission widths are always much smaller than the total widths the appropriate multiplicative factor $\mathcal{S}^{(II)}_{cf}$ is just unity. The final approximate expression for the cross section is in this case

$$\bar{\sigma}_{nf} \approx 2\pi^2\lambda\!\!\!^{-2} g(J)\,\frac{\Gamma_{(n)}}{\Gamma_{(n)}+\Gamma_{(r)}}\mathcal{S}_{nr}\,\frac{\bar{\Gamma}_{II(f)}}{D_{II}} . \tag{6.55}$$

Alternatively, if the class-II fission width is much greater than the coupling width, $\bar{\Gamma}_{II(c)}$ replaces $\bar{\Gamma}_{II(f)}$ in Eq. (6.55).

On the other hand, if fission saturates the center of the intermediate resonances [$\Gamma_{\lambda(f)} \sim \Gamma_\lambda$; Eq. (6.25) then applies to the intermediate areas], the fluctuation factor $S_{cf}^{(II)} \approx 2/\pi$. Hence

$$\bar{\sigma}_{nf} \approx 2\pi^2 \lambda\!\!\!^{-2} g(J) \frac{\Gamma_{(n)}}{\Gamma_{(n)}+\Gamma_{(r)}} \times \left[\frac{2(\Gamma_{(n)}+\Gamma_{(r)})\bar{\Gamma}_{II(c)}\bar{\Gamma}_{II(f)}}{\pi D_I}\right]^{1/2} \frac{1}{D_{II}} S_{nr} . \tag{6.56}$$

Again, fluctuations must be expected in the local average cross section. In the former case ($\Gamma_{\lambda(f)} \ll \Gamma_\lambda$) these fluctuations will be of the Porter–Thomas type, so

$$\mathrm{var}\langle\sigma_{nf}\rangle_{loc} \approx 2\bar{\sigma}_{nf}^2 . \tag{6.57}$$

In the second case ($\Gamma_{\lambda(f)} \sim \Gamma_\lambda$ at the center of intermediate resonances)

$$\mathrm{var}\langle\sigma_{nf}\rangle_{loc} \approx \left(\frac{\pi^2-4}{\pi^2}\right)\bar{\sigma}_{nf}^2 . \tag{6.58}$$

d. Very weak coupling

The local average fission cross section is obtained from Eq. (6.36):

$$\langle\sigma_{nf}\rangle_{loc} \approx 2\pi^2 \lambda\!\!\!^{-2} g(J) \frac{\pi^2 H^2 \Gamma_{I(n)} \Gamma_{\lambda II(f)}}{D_I^2 D_{II}} \csc^2\pi x \left\{\frac{[1-(\pi^2H^2/D_I^2)\csc^2\pi x]}{(\pi^2H^2/D_I^2)\Gamma_I \csc^2\pi x + \Gamma_{\lambda_{II}}[1-(\pi^2H^2/D_I^2)\csc^2\pi x]} + \frac{1}{\Gamma_I}\right\} \tag{6.59}$$

As discussed in Sec. VI.C.1.*d* the variance of this quantity is high.

The average fission cross section over a large number of class-II spacings is [see Eq. (6.41a)]

$$\bar{\sigma}_{nf} \approx 2\pi^2 \lambda\!\!\!^{-2} g(J) \frac{\overline{|H|}}{D_I} \frac{\bar{\Gamma}_{I(n)}\bar{\Gamma}_{II(f)}}{D_{II}} \times \left\{\frac{1}{\bar{\Gamma}_{II}} + \frac{1}{\bar{\Gamma}_I} + \frac{4}{(\bar{\Gamma}_I+\bar{\Gamma}_{II})}\right\} . \tag{6.60}$$

Note that this is higher by a factor $D_I/2\pi^2\overline{|H|}$ than the expression one would obtain from a picket-fence model, with the class-II state always at the median position ($\frac{1}{4}D_I$) with respect to the nearest class-I level.

If the mean class-II or class-I width is greater than the modulus of the coupling matrix element we must derive the average cross section from Eq. (6.41b); it is

$$\bar{\sigma}_{nf} \approx 2\pi^2 \lambda\!\!\!^{-2} g(J) \frac{4H^2}{D_I} \frac{\bar{\Gamma}_{I(n)}}{D_{II}} \bar{\Gamma}_{II(f)} \times \left\{\frac{1}{\bar{\Gamma}_I\bar{\Gamma}_{II}} + 2\left(\frac{\bar{\Gamma}_I+\bar{\Gamma}_{II}}{\bar{\Gamma}_I-\bar{\Gamma}_{II}}\right)^2 \frac{1}{\bar{\Gamma}_I\bar{\Gamma}_{II}}\right\} . \tag{6.61}$$

D. The class-II radiation width and fission by the two-step (γf) process

1. General remarks

In the interpretation of the fission cross section observed in intermediate structure phenomena and in analyzing the class-II level parameters that are obtained due allowance must be made for the radiative deexcitation of the class-II level. This enters not only as a competition factor, but may also lead to delayed fission following radiative cascades to the class-II shape isomer (or isomers). It depends on the half-life of the shape isomer and the method of measurement whether or not this two-step fission process will contribute to the measured cross section. If it does contribute then an assessment of its importance must be made before an interpretation of the outer barrier parameters can be deduced from the prompt fission width.

If measurements of the fission yield are made using time-independent processes, i.e., the incident beam is monoenergetic, or the method of analysis (as in bremsstrahlung experiments) can give an effectively monoenergetic result, the delayed fission contribution is completely contained within the measured yield. Most neutron fission cross sections are measured with pulsed neutron beams and time-of-flight methods, however. In such measurements delayed fission will be contained completely within the total fission yield only if the half-life of the shape isomeric state is much less than the time resolution interval of the neutron energy determination or the time-interval equivalent of the resonance width (whichever is the greater). If the shape isomer half-life is much greater than the time resolution then the delayed fission yield will almost certainly be lost in the background effects, unless special care is taken to suppress instrumental background and prompt fission is very weak compared with delayed fission. If the shape isomer half-life is roughly equivalent to the time resolution or resonance width, delayed fission will be observable as a tail or skew effect in the resonances in the time-of-flight spectrum.

Alternatively, it may be possible with careful measurements (no successes have been definitively reported to date) to observe the gamma-ray transitions between the class-II levels directly. These will mostly be prompt, of course, and the complete cascade of gamma rays will show a spectrum quite different from that of the class-I transitions; the maximum energy will be lower than that of a class-I spectrum by the excitation energy of the shape isomer, and discrete primary gamma rays will be observable at energies which only show a dense effective continuum in the class-I spectrum. The difficulties of measuring such a spectrum will depend on the magnitude of prompt fission deexciting the initial class-II state and on the degree of admixture of the class-II state into the class-I states. Gamma rays accompanying the prompt fission will tend to mask the characteristic class-II spectrum, as will gamma rays from the deexcitation of admixed class-I states into a quasi-class-II resonance.

2. Magnitude of the class-II radiation width

Estimates of radiation widths depend on theoretical models of the radiative transition matrix element and the level density of final states. For a review of the

topic see Lynn (1968a). Two relatively simple models of the radiative transition process are commonly favored. In both, electric dipole transitions are normally assumed to be predominant. In the strong coupling dipole model due to Blatt and Weisskopf (1952) the transition matrix element is assumed to be independent of the energy ε_γ of the transition and proportional to the level spacing of the initial state. Thus the energy dependence of the radiative width for the transition is proportional to the phase-space factor ε_γ^3. In the giant dipole resonance model the same dependence on level spacing is assumed, but the energy dependence is that required to give the form of the photonuclear cross section according to the Goldhaber–Teller (1948) collective model. Combined with the phase-space factor the radiative width becomes

$$\Gamma_{\lambda(\gamma)}(\varepsilon_\gamma)=\frac{4}{3\pi}\frac{NZ}{A}\frac{e^2}{\hbar c}\frac{(1+0.8x)}{Mc^2}\times\frac{\Gamma_G\varepsilon_\gamma^4}{(\varepsilon_\gamma^2-E_G^2)^2+(\Gamma_G\varepsilon_\gamma)^2}D_\lambda\,, \tag{6.62}$$

where N, Z, and A are the neutron, charge, and mass numbers of the nucleus, respectively, M is the nucleon mass, E_G is the energy of the giant resonance (of the order of 13 MeV for very heavy nuclei), and Γ_G is the width of the giant resonance (~4 MeV). The quantity x is the fraction of exchange force in the internucleon force (Levinger and Bethe, 1950). It is normally assumed to be 0.5, but there is some evidence that it may be lower.

Two relatively simple level density formulations are also adopted. In the constant temperature form a pure exponential rise of level density with excitation energy is assumed:

$$\rho(E^*)=D^{-1}(U)=C\exp(E^*/\theta)\,. \tag{6.63}$$

C is a simple proportionality constant. Alternatively, the Fermi gas form is favored, in which the nuclear states are assumed to be built from a superposition of independent particles moving in a potential field:

$$\rho(E^*)=\frac{1}{12\sqrt{2}}\frac{1}{\sigma^3}\frac{e^{2(aE^*)^{1/2}}}{a^{1/4}E^{*5/4}}\,. \tag{6.64}$$

The excitation energy E^* is usually adjusted to an effective value according to the parity of the nucleon numbers; this is a semiempirical adjustment to allow for the highly correlated nature of the nucleon ground state due to pairing interactions among the nucleons. The Fermi gas parameter a is proportional to the density of single-particle states at the Fermi energy of the unexcited nucleus. Normally parameters like a, C, and the temperature θ are adjusted so that the chosen formulation reproduces observed level densities at low excitation energies and at the neutron separation energy, where neutron resonances give convenient reference data. The difficulty of fitting data at widely different excitation energies has given rise to the use of hybrid models [see, e.g., Gilbert and Cameron (1965)] in which the constant temperature model is used for the first few MeV of excitation, above which the Fermi gas formula follows without discontinuity. The dependence of level density on spin is a common choice to most work:

$$\rho(J^\pi)=\frac{1}{2}(2J+1)\exp\left[-\frac{(J+\frac{1}{2})^2}{2\sigma^2}\right]\rho(E^*)\,. \tag{6.65}$$

The spin dispersion coefficient σ has values of the order of 6 for actinide nuclei.

Simple estimates of class-II radiation widths are obtained from the combination of the strong coupling dipole model and the constant temperature level density model. The total radiation width depends on excitation energy and temperature according to

$$\Gamma_{\lambda(\gamma)}\propto 6\theta^4-e^{-E^*/\theta}\{\theta E^{*3}+3\theta^2E^{*2}+6\theta^3E^*+6\theta^4\}\,. \tag{6.66}$$

The effective excitation energy of class-II states is lower than the true excitation energy by the energy of the class-II shape isomer, E_{II}. If the effective excitation energy is considerably greater than the temperature the class-II radiation width is essentially equal to the class-I radiation width unless the temperature for the class-I and class-II radiation widths differ.

If the Fermi-gas model is adopted for the level density we may still employ Eq. (6.66) to obtain a rough estimate of the class-II radiation width relative to the class-I width. The effective temperature to be substituted in Eq. (6.66) is $\theta\approx 2(E^*/a)^{1/2}$. Therefore,

$$\Gamma_{\lambda_{II}(\gamma)}\approx\left(\frac{E^*-E_{II}}{E^*}\right)^2\frac{a_I}{a_{II}}\Gamma_{\lambda_I(\gamma)}\,. \tag{6.67}$$

For low to moderate energy transitions the energy dependence of the partial radiation width in the giant resonance model lies between ε_γ^4 and ε_γ^5. Thus the leading term in the radiation width dependence approaches $120\theta^6$, and, for the Fermi-gas model, the total radiation width of class-II states is more nearly represented by

$$\Gamma_{\lambda_{II}(\gamma)}\approx\left(\frac{E^*-E_{II}}{E^*}\right)^3\left(\frac{a_I}{a_{II}}\right)^{3/2}\Gamma_{\lambda_I(\gamma)}\,. \tag{6.68}$$

More exact calculations of the class-II radiation width require numerical integration. A detailed survey of data on the actinide nuclei (Lynn, 1974b) leads to the conclusion that the giant dipole resonance model in conjunction with a constant temperature level density model ($\theta\approx 0.5$ MeV) up to a few MeV excitation followed by the independent particle model can give a good representation of the deexcitation of these nuclei. From this representation we have calculated some typical results on the value of the class-II radiation width and show them in Table XIV. In all cases we have assumed that the level density parameters of the class-II states are the same as those of the class-I states. The details of the level density parameters that we have adopted [from Lynn (1974b)] are given in Sec. VII.

3. The class-I radiation width to class-II final states

Cross transitions from class-I states to class-II states may also lead to prompt or delayed fission and contribute to any background fission observed between intermediate resonances. Such transitions have been considered by Lynn (1969). The electromagnetic perturbation operator in the Hamiltonian may be split into a collective part and a single-particle operator. Tran-

TABLE XIV. Total radiation widths calculated on the giant dipole resonance model [parameters given in report by Lynn (1974b)] over a range of effective excitation energies appropriate to class-II states.

Effective excitation energy E^*-E_{II} (MeV)	Typical even nucleus (^{240}Pu) $\Gamma_{(\gamma T)}$ (meV)	Typical odd-A nucleus (^{239}U) $\Gamma_{(\gamma T)}$ (MeV)	Typical odd nucleus (^{238}Np) $\Gamma_{(\gamma T)}$ (meV)
1.0			2.0
1.5	0.1	2.6	8.0
2.0	1.9	6.1	17.4
2.5	7.5	12.0	27.5
3.0	15.5	19.5	36.7
4.0	32.1	24.1	48.9
5.0	34.2		54.5

sitions involving the latter are not allowed because of the orthogonality of the vibrational states of the basis. Collective transitions of the electric monopole type between vibrational state components or electric quadrupole type between members of the rotational bands based on such vibrational states are allowed but are weaker, by a factor of the order of the transmission coefficient across the inner barrier T_A, Eq. (3.139), than the corresponding transitions within the set of class-I states.

The simple factor T_A was estimated on the assumption that only the "tail" of the final vibrational wave function, having similar character to the main part of the initial wave function within the primary well, would contribute significantly to the matrix element

$$\int d\eta\, \Phi\nu_{\rm I}(\eta)\eta\Phi\nu_{\rm II}(\eta)\,.$$

We have checked this assumption numerically by investigating these matrix elements within a double potential built up from rectangular components. The difference between primary and secondary well depth was postulated to be 3 MeV, the barrier between them was 6 MeV above the primary well, the barrier width $\Delta\eta_A = 0.38$, and the width of each well $\Delta\eta_{\rm I} = \Delta\eta_{\rm II} = 0.19$. The inertial parameter B was chosen so that $2B/\hbar^2 = 1156.4$ with the energy in MeV units. We calculated the lowest class-I vibrational states to have eigenvalues 0.209, 0.834, 1.869, and 3.297 MeV. The eigenvalues of the two lowest class-II states are 2.674 and 3.199 MeV. Calculations of the matrix element between the 2.674 and 1.869 MeV states and the 3.297 and 3.199 MeV states compared with a standard class-I transition between the 3.292 and 1.869 MeV states show one to two orders of magnitude increase in radiative strength over the value estimated on the simple assumption. This can be attributed to the contribution from the wave function in the barrier region. This result still implies that at sub-barrier energies cross transitions can normally be neglected.

4. Branching ratio of the shape isomer

In Sec. IV.D.3.*d* we presented examples of shape isomer decay in which there is clear evidence that the predominant mode of decay is electromagnetic radiation to lower states of class-I character rather than fission. Here we indicate how the radiation strength, and hence the branching ratio to fission, is quantitatively related to the barrier parameters.

If we assume that the isomer state is described by a wave function of the type

$$X_0 \approx \Phi_0^{\rm II}\chi_0 \tag{6.69}$$

it has the possibility of decaying to lower class-I states by collective $E0$ or $E2$ transitions through the beta-vibration-rotation bands, the relevant matrix elements being of the type

$$\langle \Phi_0^{\rm II} | \eta | \Phi_\nu^{\rm I} \rangle\,. \tag{6.70}$$

A contribution to this matrix element will come from the primary well region I of the deformation parameter, where the wave function $\Phi_0^{\rm II}$ has a very weak tail of class-I type ($\Phi_0^{\rm II} \sim c\Phi_\nu^{\rm I}$ in region I; see Sec. III.C.4.*c*). The intensity of this tail c^2 is estimated as being of the order of the transmission coefficient T_A [Eq. (3.148b)]. From this component alone we estimate the radiative half-life of the isomer as

$$\tau_{(\gamma(E2))} \approx 10^{-11} T_A \text{ (sec)}\,. \tag{6.71}$$

Numerical studies of the matrix element (6.70) in a rectangular well model (see Sec. III.C.4.*b* and Sec. VI.D.3) show that the barrier region also gives a major contribution to the matrix element, and the transitions of this type can be 1 to 2 orders of magnitude faster than the estimate (6.71).

The isomeric wave function will contain very small components of nearby class-I states owing to the coupling term H_c in the Hamiltonian, Eq. (3.64) (Lynn, 1971). The mixing process will be one of extremely weak coupling and is described by the perturbation theory of Sec. III.C.5.*c*(*i*). The isomeric wave function is thus

$$\chi_{\rm is} \approx \Phi_0^{\rm II}\chi_0 + \sum_\lambda \frac{\langle \Phi_0^{\rm II}\chi_0 | H_c | X_\lambda^{\rm I}\rangle}{E_{\lambda_{\rm I}} - E_0^{\rm II}} X_\lambda^{\rm I}\,. \tag{6.72}$$

The small class-I terms give a contribution to the radiation width of

$$\Gamma'_{{\rm is}(\gamma)} \approx \sum_{\lambda_{\rm I}} \frac{\langle \Phi_0^{\rm II} | H_c | X_\lambda^{\rm I}\rangle^2}{(E_{\lambda_{\rm I}} - E_0^{\rm II})^2} \Gamma_{\lambda_{\rm I}(\gamma T)}\,, \tag{6.73}$$

and the class-I radiative transitions comprised in $\Gamma_{\lambda_{\rm I}(\gamma T)}$ will normally contain electric dipole as well as magnetic and higher multipolarities. Because of the statistically fluctuating character of both the coupling matrix element and the energy denominator in this equation the isomer radiation width is expected to fluctuate strongly from one nucleus to another (to a considerably greater extent than the fission width). Most

fluctuation comes from the energy denominator. If x denotes the separation of the isomer from the nearest class-I state relative to the mean class-I spacing $D_{\rm I}$,

$$\Gamma'_{{\rm is}(\gamma)} \approx \frac{\pi^2 \Gamma_{\lambda_{\rm I}(\gamma T)} \overline{H_c^2}}{D_{\rm I}^2} \csc^2 \pi x \,. \tag{6.74}$$

For the median value of x ($x = \frac{1}{4}$), $\Gamma'_{{\rm is}(\gamma)} \approx 2\pi^2 H_c^2 \Gamma_{\lambda_{\rm I}(\gamma T)} / D_{\rm I}^2$, but this is not the expectation value. An expectation value cannot be calculated from Eq. (6.74) alone, consideration of the possibility of accidental degeneracy between the isomer and a class-I state being necessary. If accidental degeneracy occurs the value of the isomer radiation width is $\frac{1}{2}\Gamma_{\lambda_{\rm I}(\gamma T)}$. This is the approximate value of $\Gamma'_{{\rm is}(\gamma)}$ to be expected within the range of x from zero to $2|H_c|/D_{\rm I}$, Eq. (6.74) being relevant (approximately) in the region $x > 2|H_c|/D_{\rm I}$ to $x = \frac{1}{2}$. The expectation value of $\Gamma'_{{\rm is}(\gamma)}$ is, therefore,

$$\Gamma'_{{\rm is}(\gamma)} \approx \frac{3\overline{|H_c|}}{D_{\rm I}} \Gamma_{\lambda_{\rm I}(\gamma T)} \,, \tag{6.75}$$

with variance

$$\mathrm{var}\Gamma'_{{\rm is}(\gamma)} \approx \overline{\Gamma'^2_{{\rm is}(\gamma)}} \frac{D_{\rm I}}{6\pi \overline{|H_c|}} \,, \tag{6.76}$$

which is expected to be very large.

This "mixing" contribution to the shape isomer radiative width is much greater than the pure collective component, Eq. (6.71), even at the "median" level. The dependence of the isomer partial half-lives (including fission) on energy and barrier parameters is shown in Fig. 112. The coupling matrix element is deduced from the strong coupling model in terms of the transmission coefficient T_A through the intermediate barrier [see Eq. (3.161)]. Mean class-I level spacings and radiation widths are deduced from the recommended level density parameters discussed in Sec. VII. Note that the "median" value of the half-life shown in Fig. 112 is also the expectation value (to a good approximation). The variance of the half-life is just half the square of the median value.

5. The two-step (γf) process through class-I states

The two-step (γf) process was recognized before the concept of the double-humped barrier as a possible, though rather weak, fission decay mechanism of the compound nucleus (Lynn, 1965). The primary γ-ray transition takes place through compound nucleus states of normal deformation (now described as class-I states). This is not related to the intermediate structure phenomena of course. The fission decay of the final state reached in the gamma-ray transition is governed by the nature of the fission barrier. Intermediate structure phenomena may be involved if the final state lies below the barrier peaks. Intermediate resonance phenomena as such will not be observable in this reaction (except, in principle, by very sophisticated experimental methods not yet undertaken), but the probability of the fission stage of deexcitation may be affected appreciably by such structure. In the uniform picket-fence model of the final states after gamma-ray deexcitation the branching ratio for fission is (Lynn and Back, 1974)

$$P_f(E) = \left\{1 + \frac{T_{\rm I}^2 (T_A + T_B)^2}{T_A^2 T_B^2} + 2\frac{T_{\rm I}(T_A + T_B)}{T_A T_B} \coth\left[\tfrac{1}{2}(T_A + T_B)\right]\right\}^{-1/2} , \tag{6.77a}$$

where T_A, T_B are the transmission coefficients [Eqs. (3.139) and (3.140)] for a state at excitation energy E across the inner and outer barriers, and $T_{\rm I}$ is the class-I transmission coefficient in the absence of fission

$$T_{\rm I} = \frac{2\pi\Gamma_{\rm I}}{D_{\rm I}} \,. \tag{6.77b}$$

This fission probability is to be integrated over the primary gamma-ray deexcitation spectrum to obtain the width for the (γf) process:

$$\Gamma_{\lambda_{\rm I}(\gamma f)} = \int_0^E d\varepsilon_\gamma \, \Gamma_{\lambda_{\rm I}(\gamma)}(\varepsilon_\gamma) \rho_{\rm I}(E - \varepsilon_\gamma) P_f(E - \varepsilon_\gamma) \,. \tag{6.77c}$$

There is some experimental evidence for the $(n, \gamma f)$ reaction. Ryabov *et al.* (1973) have measured the mean energy of gamma rays and the mean number $\bar{\nu}$ of prompt neutrons emitted in association with fission for several of the slow neutron resonances in the neutron cross section of ^{239}Pu, and have correlated the results with the resonance fission widths. For resonances identified as being $J^\pi = 1^+$, apparent linear relationships between these quantities and the reciprocal fission width were observed, the mean total gamma-ray energy increasing from 13.8 MeV for resonances with large fission width to 14.7 MeV for those with very small $\Gamma_{(f)}$, and $\bar{\nu}$ decreasing from 2.87 (very large $\Gamma_{(f)}$) to 2.65 (very small $\Gamma_{(f)}$).

These results can be interpreted as evidence for the $(n, \gamma f)$ reaction as follows. The total energy $E_\gamma^{(P)}$ of the gamma rays emitted by fission products is known to be

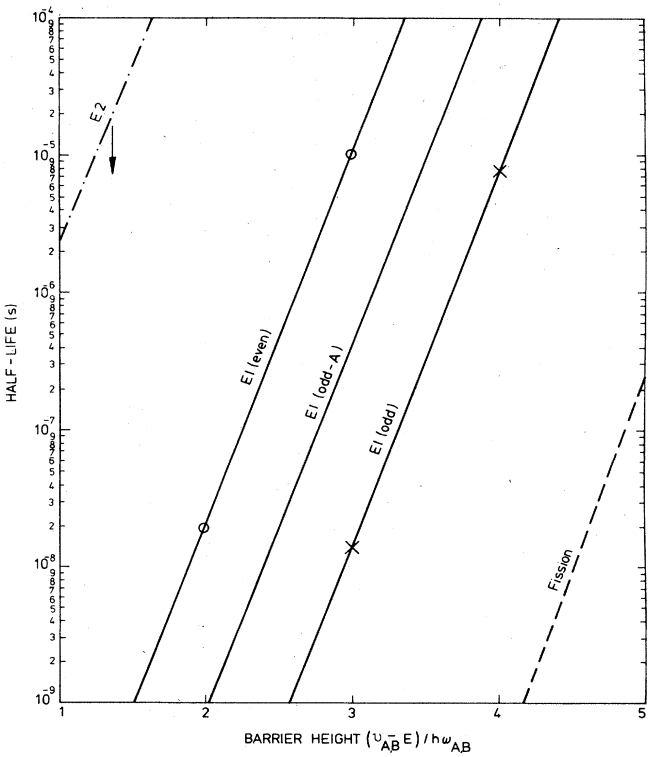

FIG. 112. Median estimates of shape isomer radiative and fission half-lives.

comparatively insensitive to the excitation energy of the fissioning compound nucleus. The variation in gamma-ray energy observed in these measurements can therefore be attributed to the primary gamma rays of mean energy $\bar{\varepsilon}_\gamma$ emitted in the part of the total fission occurring by the (γf) route, giving

$$\bar{E}_\gamma = \frac{E_\gamma^{(P)}\Gamma_{(f)} + (E_\gamma^{(P)} + \bar{\varepsilon}_\gamma)\Gamma_{(\gamma f)}}{\Gamma_{(f)} + \Gamma_{(\gamma f)}} = E_\gamma^{(P)} + \frac{\bar{\varepsilon}_\gamma \Gamma_{(\gamma f)}}{\Gamma_{(f,\mathrm{eff})}},$$

where $\Gamma_{(f,\mathrm{eff})}$ is the (observed) total effective fission width, $\Gamma_{(f)} + \Gamma_{(\gamma f)}$. The neutron emission number does depend appreciably on the excitation energy of the fissioning nucleus. If this dependence is assumed to be linear, as observed in neutron-induced fission at higher energies,

$$\bar{\nu}_{\mathrm{obs}} = \frac{\nu(S_n)\Gamma_{(f)} + [\nu(S_n - \bar{\varepsilon}_\gamma)]\Gamma_{(\gamma f)}}{\Gamma_{(f)} + \Gamma_{(\gamma f)}}$$

$$= \nu(S_n) - \frac{\bar{\varepsilon}_\gamma (d\nu/dE)\Gamma_{(\gamma f)}}{\Gamma_{(f,\mathrm{eff})}}.$$

The experimental results can therefore be analyzed to give the quantity $\bar{\varepsilon}_\gamma \Gamma_{(\gamma f)}$. For $J^\pi = 1^+$ resonances of ^{240}Pu it is 4.6 ± 0.4 MeV.meV (Shackleton, 1974). The minimum observed resonance fission width is $\Gamma_{(f,\mathrm{eff})} = 3.5 \pm 0.6$ meV (for the 35.5 eV resonance), giving an upper limit for the (γf) width of $\Gamma_{(\gamma f)} \lesssim 3.5$ meV, and a mean primary gamma-ray energy of $\bar{\varepsilon}_\gamma \gtrsim 1.3$ MeV. (The earlier results of Ryabov *et al.* gave $\Gamma_{(\gamma f)} = 4.1 \pm 0.9$ meV. $\bar{\varepsilon}_\gamma = 800 \pm 90$ keV.)

If only electric dipole primary gamma-ray emission is assumed then fission will take place through intermediate states of spin and parity $J^\pi = 0^-, 1^-, 2^-$, and of these the $J^\pi = 1^-$ states are expected to have the lowest fission barrier. The barrier parameters for $J^\pi = 1^-$ are expected to be $v_A(1^-) \sim v_A(0^+) + 1.0$ MeV, $v_B(1^-) \sim v_B(0^+)$. Using the 0^+ barrier parameters assessed in Sec. VII we have done cascade calculations [based on Eq. (6.77c)] of the partial γf width of the 1^+ resonances of ^{239}Pu $+n$. If the primary gamma-ray deexcitation is assumed to be by the giant dipole resonance mechanism (see Sec. VII.B.2) the result is $\Gamma_{(\gamma f)} = 1.0$ meV, and the mean primary gamma-ray energy $\bar{\varepsilon}_\gamma = 0.83$ MeV.

It is known, however, that magnetic dipole primary transitions are quite significant in the deexcitation of neutron resonance states of heavy nuclei (to the order of 10%). In this case the intermediate fission states can have spin and parity $J^\pi = 0^+, 1^+, 2^+$. Hence fission is especially favored. The primary gamma-ray $M1$ strength was assumed proportional to the cube of the gamma-ray energy in our cascade calculation for this process. The partial width was calculated to be $\Gamma_{(\gamma f)} = 2.4$ meV ($E1 + M1$) and the mean primary gamma-ray energy $\bar{\varepsilon}_\gamma = 0.98$ MeV. These values are a little lower than the experimental data suggest, but this could reflect a deficiency in our understanding of the primary gamma-ray deexcitation mechanism rather than uncertainty in the fission barrier parameters.

Attempts to make more direct measurement of the primary gamma rays emitted in the $(n, \gamma f)$ reaction have been reported (Dlouhy *et al.*, 1976). A small fraction of the primary radiative transitions will undergo electron conversion, and these are detected by observation of the sequential characteristic K x-rays in coincidence with fission. Measurements of this kind on the neutron resonances of ^{235}U suggested a correlation of the intensity of each coincidence with the reciprocal fission width, but unfortunately the statistical significance of the correlation is weak.

E. Experimental data on intermediate structure and its analysis

1. Very weak coupling

The formal treatment of very weak coupling between class-I states and narrow class-II states has been described in Sec. III.C.5.*c*(*i*). The treatment is by perturbation theory, and the significant feature of the fine-structure resonance pattern that emerges is the occurrence in each intermediate group of a single state, carrying the bulk of the class-II strength, with large fission width and small neutron width; a few neighboring levels, all essentially class-I in nature, have significant, but comparatively small fission widths and normal neutron widths.

a. Intermediate structure in ^{241}Pu

A particularly good example of the phenomenon is found in the slow neutron fission cross section of ^{240}Pu (Fig. 7). The intermediate structure in this cross section was originally discovered by Migneco and Theobald (1968). The original resonance parameters that they deduced from their data allowed a range of interpretations. One was indeed the weak coupling phenomenon, a few of the intermediate groups having a resonance with fission width of the order of 100 meV (but with large standard errors) dominating its neighbors. In some analyses, however, the widths of the groups were found to be consistent with values of the order of 20–50 eV, and this was held to be evidence of either moderate coupling [see Sec. III.C.5.*c*(*iii*)] or very weak coupling to a broad class-II state. An intermediate case was possible (Lynn, 1968b) in which the quasi-class-II level with a width of the order of a few eV lay unidentified, because of its relative weakness as a peak, among the observed structure.

In the most definitive data to date (Auchampaugh and Weston, 1975) the last possibility has proved to be the correct one. The three lowest intermediate resonances (at 782, 1405 and 1936 eV) were measured with high resolution and sensitivity in both total and fission cross sections. The measurements on the 1405-eV group confirmed the observation of Migneco and Theobald that the bulk of the fission strength in the group was divided roughly equally between the 1402 and 1408 eV resonances but the fission widths of these are much larger (~2 eV) than originally believed; this is in fact a case of accidental degeneracy (Lynn, 1968b). The measurements on the other two groups (see, e.g., Fig. 113) revealed resonances that were missed in the earlier work; in each group a resonance with large fission width (~2 eV) and weak neutron width was revealed, ideal candidates for the role of the quasi-class-II state.

We have analyzed the data for the 782 and 1936 eV groups using the perturbation theory of Sec. III.C.5.*c*(*i*).

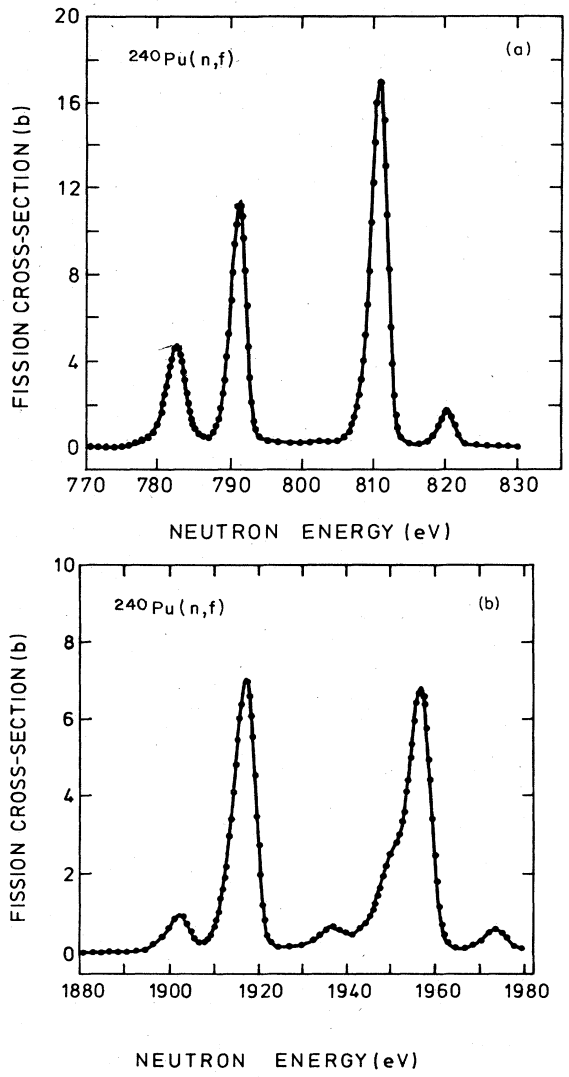

FIG. 113. Intermediate structure in the slow neutron fission cross section of ^{240}Pu in the regions of 782 and 1936 eV [from Auchampaugh and Weston (1975)].

In each group we summed the fission widths of observed resonances to give the best estimate of the class-II fission width [Eq. (3.165b)]. We used them to find the coupling matrix elements [Eq. (3.169)] and finally, from Eq. (3.167) and the values of reduced neutron widths of the quasi-class-I levels, we deduced a range of possible values of the reduced neutron width of the quasi-class-II level and compared this with the experimentally measured value.

The results of the analysis are shown in Table XV. We analyzed 16 quasi-class-I levels in each group. The mean squared coupling matrix element for each class-II level is represented in the table in the form of the coupling width

$$\Gamma_{\lambda_{II}(c)} = 2\pi\overline{(H_c)^2_{\lambda_I\lambda_{II}}}/D_I .$$

From the total cross-section resonances D_I has been found to be 15 eV. The possible values of the reduced neutron width of the quasi-class-II level were found, as expected, to have a distribution highly skewed in favor of very small values (resembling a Porter–Thomas distribution). The mean of the possible values (the expectation value), and the maximum value possible (all contributions to the amplitude from the 16 analyzed class-I levels having the same sign) are quoted in the table, and it is apparent that for both cases the observed width is of the order of the expected value and much less than the maximum possible value, lying in fact in the center two quartiles of the distribution; these values are very much smaller than the mean reduced neutron width of class-I levels, i.e., 15×10^{-4} eV.

The following information on barrier heights can be deduced from the information in Table XV. By substitution of the mean class-II fission width $\Gamma_{\lambda_{II}(f)} = 2.5$ eV into Eq. (6.3) with the Hill–Wheeler barrier penetrability formula [Eq. (3.140)] for T_B, we find the value of $2\pi(V_B - S_n)/\hbar\omega_B$ to be 3.6. Here, S_n is the neutron separation energy. The assumption of $\hbar\omega_B = 0.52$ MeV, which is the consensus of evidence described in Sec. VII.D.1, gives $v_B = 5.54$ MeV. Note that this is the barrier height for fission channels of total angular momentum and parity $J^\pi = \frac{1}{2}^+$ and may not be the nominal barrier height for the lowest channels. Similarly, from Eq. (6.5) the inner barrier (for $J^\pi = \frac{1}{2}^+$) has the numerical relation $2\pi(v_A - S_n)/\hbar\omega_A = 3.8$, which, for $\hbar\omega_A = 0.8$ MeV yields $v_A = 5.73$ MeV. As can be seen from the data on barrier heights compiled in Sec. VII, the values of v_A and v_B for $J^\pi = \frac{1}{2}^+$ channels are quite consistent with the overall picture.

Several intermediate resonances have been observed in the fission cross section of ^{240}Pu at neutron energies greater than 2 keV, but the fine structure of these has not been measured in any detail. Because the class-II fission widths appear to be so very large it is clear that analysis of the areas of these higher energy intermediate resonances will not give any extra useful information.

From the density of class-II states we infer the ex-

TABLE XV. Weak coupling analysis of intermediate structure of the neutron fission cross section of ^{240}Pu. Data from Auchampaugh and Weston (1975). For completeness, details of the 1405 eV class-II level (analyzed as an accidental degeneracy in Sec. VI.E.2 has been included in this table. Units are eV.

	Quasi-class-II level				Class-II level	
	Observed properties		Calculated neutron width		Deduced properties	
$E_{\lambda''}$	$\Gamma_{\lambda''(f)}$	$\Gamma^{(0)}_{\lambda''(n)}$	$\langle\Gamma^{(0)}_{\lambda''(n)}\rangle_{exp}$	$(\Gamma^{(0)}_{\lambda''(n)})_{max}$	$\Gamma_{\lambda_{II}(f)}$	$\Gamma_{\lambda_{II}(c)}$
782.4	1.45	1.3×10^{-4}	0.84×10^{-4}	3.3×10^{-4}	1.53	1.60
1936	2.2	4.5×10^{-5}	1.2×10^{-4}	5.7×10^{-4}	2.4	3.7
(1405)					3.54	1.5

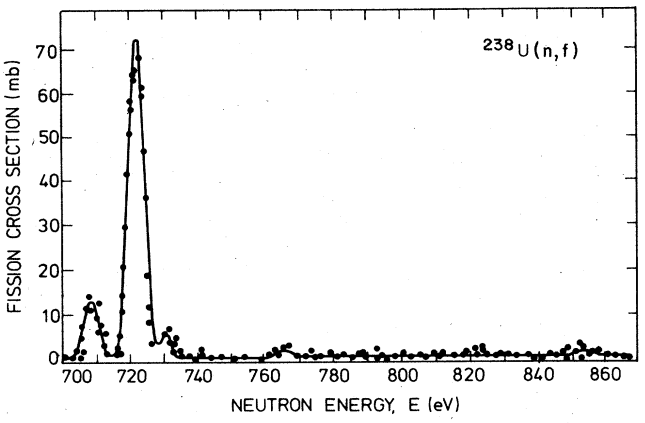

FIG. 114. Intermediate structure in the slow neutron fission cross section of ^{238}U in the region of 720 eV [from Difillipo *et al.* (1977)].

citation energy of the lowest state of the secondary well to be 1.85 MeV. This is based on the assumption that the level density law of class-II states is similar to that of class-I states; the parameters for the latter can be found in Sec. VII.B.3.

b. *Intermediate structure in ^{239}U*

Because of the known fact that barrier height(s) in ^{239}U are much higher relative to the neutron separation energy than those of ^{241}Pu it was expected that fission intermediate structure in the cross section ^{238}U at low neutron energies would be much weaker in magnitude than that of ^{240}Pu. This is indeed so, and it took many years of searching before definitive evidence was discovered, commencing with a crude resolution measurement (using a lead slowing down spectrometer on the electron linac of the Rensselaer Polytechnic Institute) and measurements of fine-structure resonance parameters appearing later from RPI (Block *et al.*, 1973) and Oak Ridge (Difilippo *et al.*, 1977).

Below 60 keV neutron energy 28 groups of fission resonances have been discovered. Seven of these lie below 10 keV, giving a mean spacing for class-II states of ~1.4 keV. Only for the groups at 720 and 1213 eV has the resonance fine structure been partly elucidated (Difillipo *et al.*, 1977); it is shown in Fig. 114 for the 720 eV group and resonance parameters are given in Table XVI. We can make alternative deductions about the properties of the class-II state; one deduction depends on the hypothesis that the resonance at 720 eV in the fission cross section is different from the resonance observed at about the same energy in the total cross section, and the other is that they are identical. The data of Difillipo *et al.* (1977) and De Saussure *et al.* (1978) indicate that there may be about 0.5 eV discrepancy between the observed resonance at this energy in total and fission cross sections when the energy scales of the other resonances are matched.

For the first hypothesis our analysis of the data suggests that $\Gamma_{\lambda_{II}(f)}$ lies between 23 meV and about 500 meV, the maximum value being governed by the resolution width, while the minimum value is derived from the area of the fission resonance and the experimental upper limit for the neutron width of a resonance that would be unobservable in the total cross section. The mean squared matrix element will lie between about 0.37 and 0.02 eV^2, and hence the coupling width $\Gamma_{\lambda_{II}(c)}$ lies between 0.13 and 0.05 eV. For the second hypothesis, $\Gamma_{\lambda_{II}(f)} = 1.6$ meV, $\Gamma_{\lambda_{II}(c)} = 2.5$ eV.

The first hypothesis indicates barrier heights for states of total angular momentum and parity $J^\pi = \frac{1}{2}^+$, as $\upsilon_A \sim 1.0$ MeV (for $\hbar\omega_A = 0.8$ MeV), $\upsilon_B \sim 0.75$ MeV ($\hbar\omega_B = 0.52$ MeV) relative to the neutron separation energy. The second hypothesis indicates $\upsilon_A \sim 0.6$ MeV, $\upsilon_B \sim 1$ MeV. Both these sets or parameters are considerably lower [by about $\frac{1}{2}$ MeV on hypothesis (i), and up to 1 MeV on hypothesis (ii)] than those assessed for ^{238}U + n by fitting the fast neutron fission cross section (see Sec. VII).

There are two possibilities for explaining this discrepancy. One is that the class-II states at low neutron energy in the cross section of ^{238}U may be considerably

TABLE XVI. Resonance parameters of fine-structure resonances in the fission cross section of ^{238}U—721 eV group. Units are eV or eV^2 (last two columns).

E_λ	$\Gamma_{\lambda(f)}$	$\Gamma^{(0)}_{\lambda(n)}$	Remarks	$H^2_{c,\lambda_I\lambda_{II}}$ ($\Gamma_{\lambda_{II}(f)} = 0.023$) (i)	$H^2_{c,\lambda_I\lambda_{II}}$ (ii)
708.3	2.4×10^{-5}	8.2×10^{-4}		0.18	2.7
721.0	$\lesssim 1.4\times10^{-4}$	6.4×10^{-5}	Hypothesis (i)		
721.6	>0.023	$<3.7\times10^{-6}$	—quasi-class-II	$<1.8\times10^{-3}$	—
	<0.5	$>1.7\times10^{-7}$	level unobserved in total cross section.	$\equiv\lambda_{II}$	
721.6	1.4×10^{-3}	6.4×10^{-5}	Hypothesis (ii)— quasi-class-II level with neutron width as observed in total cross section	—	$\equiv\lambda_{II}$
730.1	1.2×10^{-4}	3.6×10^{-5}		0.36	5.4
765.0	6.1×10^{-6}	2.8×10^{-4}		0.49	7.3
856.0	1.1×10^{-6}	2.9×10^{-3}		0.84	12.7

enhanced in strength by a damped vibrational resonance effect. The other explanation concerns the possibility of shape isomeric fission. This is not expected to be observed in the neutron time-of-flight measurements of the fission cross section if either the branching ratio for fission (in competition with gamma-ray decay to the normal ground state) is very small or the half-life of the isomeric state is very much greater than the effective time resolution of the measurement (which was about 0.25 μsec). If neither of these conditions are fulfilled then the expected magnitude of the class-II state radiation width (~20 meV on the giant dipole resonance model, described in Sec. VI.D.1) implies that delayed fission from the isomer as well as prompt fission is contributing to the observed cross sections. The true class-II fission width will therefore be less, probably much less, than the values deduced above, and barrier B will consequently be much higher. To account fully for the discrepancies both possibilities are probably required. It does seem, however, that hypothesis (i) is greatly favored if isomeric fission does indeed constitute the bulk of the observed fission, the inner barrier height being nearer to the value required by the statistical analysis of fast neutron cross sections by some 400 keV. In this case the fission branching ratio of the shape isomer is about unity. On hypothesis (ii) the branching ratio will be about 0.1.

Information may also be obtained from the areas of the intermediate resonances at higher energies. As explained above, the hypothesis (i) employed in the analysis of the 721 eV intermediate resonance leads to the further hypothesis that most of the observed fission is delayed fission following class-II radiation and the branching ratio for fission at the isomer state is almost unity. With this assumption we can analyze the areas using the very weak coupling formula, Eq. (6.36), substituting $\Gamma_{\lambda_{II}} = \Gamma_{\lambda_{II}(\gamma)} \approx 0.023$ eV. Because the areas of the intermediate resonances up to 25 keV or so do not appear to fluctuate abnormally we do not use the expectation value formula derived from Eq. (6.36), i.e., Eq. (6.41a), which is dominated by the effect of near degeneracy, but rather the median formula, Eq. (6.37). The intermediate resonance areas and the deduced coupling widths $\Gamma_{\lambda_{II}(c)} = 2\pi H_c^2/D_I$ are listed in Table XVII. The mean value of the coupling width (including the 721 eV group) is 0.012 eV, which implies a barrier height $\upsilon_A \sim 1.25$ MeV.

The second hypothesis that may be adopted in the analysis of these areas is that moderately weak coupling applies, in which case Eq. (6.20) may be employed to give the class-II fission width. These fission widths are also listed in Table XVII. The mean value is $\overline{\Gamma}_{\lambda_{II}(f)} = 3.9 \times 10^{-4}$, which implies an outer barrier height of $\upsilon_B \sim 1.1$ MeV. These widths may still be interpreted as the class-II state radiation width multiplied by the isomer branching ratio. Although the fluctuation of the values appears at first sight to rule out this interpretation it is possible that the fluctuations are determined by the fluctuations of the neutron widths of the few resonances in each group carrying significant fission strength. For sufficiently strong coupling to allow the validity of Eq. (6.20), the quasi-class-II state must pick up a neutron width of normal value from its class-I neighbors, and this implies $2\pi^2 H_c^2/D_I^2 \gtrsim 1$. From this condition the mean coupling width should be at least 6 eV, implying an inner barrier height, $\upsilon_A \sim 0.45$ MeV, which is certainly much too low and indicates that the first hypothesis is more satisfactory.

TABLE XVII. Analysis of intermediate resonance areas in the neutron fission cross section of ^{238}U. Hypothesis (i): very weak coupling with class-II fission widths composed predominantly of the radiation width leading to delayed fission. Hypothesis (ii): moderately weak coupling.

$E_{\lambda_{II}}$ (eV)	$A_{\lambda_{II}}$ (b.eV)	Hypothesis (i) $\Gamma_{\lambda_{II}(c)}$ (eV)	Hypothesis (ii) $\Gamma_{\lambda_{II}(f)}$ (eV)
1213	0.221	4.75×10^{-3}	1.07×10^{-4}
5715	0.0134	6.9×10^{-4}	2.4×10^{-5}
7090	0.0382	2.2×10^{-3}	8.3×10^{-5}
7430	0.094	5.6×10^{-3}	2.1×10^{-4}
7804	0.093	5.7×10^{-3}	2.2×10^{-4}
9358	0.025	1.7×10^{-3}	6.9×10^{-5}
11432	0.199	1.5×10^{-2}	6.7×10^{-4}
14479	0.031	2.7×10^{-3}	1.3×10^{-4}
15228	0.223	1.96×10^{-2}	9.7×10^{-4}
15558	0.189	1.68×10^{-2}	8.4×10^{-4}
18119	0.0405	3.9×10^{-3}	2.1×10^{-4}
23067	0.029	3.2×10^{-3}	1.9×10^{-4}

The spacing of the class-II states suggests that the "ground" state of the secondary well is about 1.85 MeV above true ground. This is considerably lower (by ~0.7 MeV) than the shape isomer state of the neighboring nucleus ^{238}U.

c. *Intermediate structure in ^{243}Pu*

Intermediate structure in the neutron fission cross section of ^{242}Pu was first discovered by James (1969) who found weak fission groups at 767 eV and 29 keV. Auchampaugh *et al.* (1971) and Bergen and Fullwood (1971) were able to make much more sensitive measurements with higher energy resolution and discovered many more fission groups, giving an estimate for the class-II level spacing of about 720 eV. Auchampaugh and Bowman (1973) deduced parameters of the fine-structure resonances in the five lowest energy groups with the aid of high resolution total cross-section measurements. The parameters of the quasi-class-II levels apparently revealed by these data are not as definitive as those for the ^{240}Pu cross section; the deduced properties of the class-II states, with comments, are given in Table XVIII.

It is apparent that the properties of only the lowest two class-II levels are reasonably well established. From these we deduce that the mean class-II fission width, $\Gamma_{\lambda_{II}(f)} \sim 0.3$ eV, and the coupling width, $\Gamma_{\lambda_{II}(c)} \sim 2.7$ eV. These values (with class-II spacing ~900 eV) would correspond to barrier heights $\upsilon_A, \upsilon_B \sim 0.5$ MeV above the neutron separation energy of ^{243}Pu (assuming $\hbar\omega_A = 0.8$ MeV and $\hbar\omega_B = 0.52$ MeV), and these are reasonably consistent with the parameters established in Sec. VII.

Intermediate resonances at higher energies do not completely confirm the above coupling width. If the areas are analyzed using the formula for moderately

TABLE XVIII. Deductions on properties of class-II levels revealed in cross section for ^{242}Pu(n,f). Based on resonance parameters of Auchampaugh and Bowman (1973). Units are eV.

$E_{\lambda_{II}}$	$\Gamma_{\lambda_{II}(f)}$	$\Gamma_{\lambda_{II}(c)}=\frac{2\pi\overline{H_c^2}}{D_I}$	Comment
762.5	>0.26	<1.1	Neutron width $\Gamma_{\lambda''(n)}$ of quasi-class-II resonance satisfies constraints of perturbation theory by factor 2 below maximum for $\Gamma_{\lambda_{II}(f)}=0.26$ $\therefore \Gamma_{\lambda_{II}(f)}\gtrsim 0.5$ $\Gamma_{\lambda_{II}(c)}\lesssim 0.5$
1836	>0.11	<4.4	$\Gamma_{\lambda''(n)}$ very close to maximum allowed by perturbation theory $\therefore$ stated limits are probably very close to actual values
2741	~0.002	~60	Has the quasi-class-II resonance been observed?
3112	>0.021	<30	Do these contribute one or two class-II levels?
3568	>0.015	<70	
3670	~0.007	~60	

weak coupling, Eq. (6.20), as the value of 2.7 eV for the coupling width suggests they could be, the deduced fission widths of the 1836 and 3112 eV class-II states are 4 and 2.5 meV, respectively, in disagreement with the values given in Table XVIII. The reason is that the neutron widths of the quasi-class-II resonances in these groups are much lower than the average class-I neutron widths, thus showing that the coupling is not strong enough, in these two cases at least, for the application of Eq. (6.20) to be valid. The mean class-II fission width deduced in this way from the areas up to 30 keV is 15 meV. Much of the contribution to this average value comes from a group of three strong intermediate resonances around 28 keV.

To use the very weak coupling formula for the intermediate resonance areas, Eq. (6.27), we need to have an estimate of the class-II fission width. With an assumed value of $\Gamma_{\lambda_{II}(f)}=0.2$ eV the mean value of the coupling width is $\Gamma_{\lambda_{II}(c)}\approx 0.14$ eV and with $\Gamma_{\lambda_{II}(f)}=0.025$ eV it is 0.28 eV. With this value of the coupling width the inner barrier height v_A is 0.8 MeV above the neutron separation energy.

d. *Intermediate structure in ^{245}Pu*

Intermediate structure is apparent in the cross sections of ^{244}Pu (Auchampaugh *et al.*, 1971), but this is too weak, and the first group at too high an energy, for it to have been possible to investigate the underlying fine structure in any detail. The areas of the intermediate resonances up to 20 keV have been measured, however. On the assumption that very weak coupling is operating we have analyzed these areas using the "median" formula, Eq. (6.27). The value of the fission width was assumed to be (i) 0.025 eV (i.e., class-II radiation followed by delayed fission) and (ii) 0.2 eV in turn. The results for the coupling widths $\Gamma_{\lambda_{II}(c)}=2\pi\overline{H_c^2}/D_I$ are shown in Table XIX. The mean values are 0.21 and 0.1 eV for the two cases, respectively. With a class-II level spacing of 2.7 keV, this implies $(v_A-S_n)/\hbar\omega_A\simeq 1.21$, 1.34, or $v_A-S_n\sim 1.0$, 1.07 MeV, respectively, for $\hbar\omega_A=0.8$ MeV.

2. Very weak coupling with accidental degeneracy

The formal theory for accidental degeneracy is described in Sec. III.C.5.*c*(*ii*). There is now one well-established example of the phenomenon, already mentioned, the 1405 eV intermediate resonance in the cross section of ^{240}Pu (Fig. 115). Here, two fine-structure resonances at 1402.2 and 1408.3 eV share almost equally a large total fission width of ~3.5 eV. All neighboring resonances have fission widths no larger than 5 meV, so it is clear that these two resonances share almost equally the bulk of the class-II state wave function. This can be attributed to the accidental degeneracy (or very near degeneracy) of a class-I and class-II level, the actual levels that are the result of diagonalization being repelled by the coupling interaction.

The actual analysis of the 1405 eV intermediate resonance, based on Eq. (3.170) onward, can be simplified by noting that the sum of the fission widths of all other resonances in the group is only of the order of 1% of those of the two central resonances and therefore forms an extremely weak perturbation. Our approach is to assume that the class-II level has been diagonalized with all class-I levels except the nearly degenerate one, and we now consider the diagonalization of this approximate class-II level denoted by $\lambda'_{II}=1'(II)$ with its degenerate class-I neighbor, denoted by $\lambda_I=2(I)$.

TABLE XIX. Intermediate resonance areas in the fission cross section of ^{244}Pu. Analysis is on the assumption of very weak coupling [Eq. (6.27)].

$E_{\lambda_{II}}$ (eV)	$A_{\lambda_{II}}$ (b.eV)	$\Gamma_{\lambda_{II}(c)}$ (eV) Assn. (i) $\Gamma_{\lambda_{II}(f)}=0.025$	$\Gamma_{\lambda_{II}(c)}$ (eV) Assn. (ii) $\Gamma_{\lambda_{II}(f)}=0.2$
1650	6.4	0.146	0.050
5500	5.1	0.24	0.098
7700	3.6	0.20	0.088
11300	0.94	0.065	0.031
12000	1.9	0.135	0.064
15600	1.2	0.10	0.050
18000	6.4	0.58	0.30

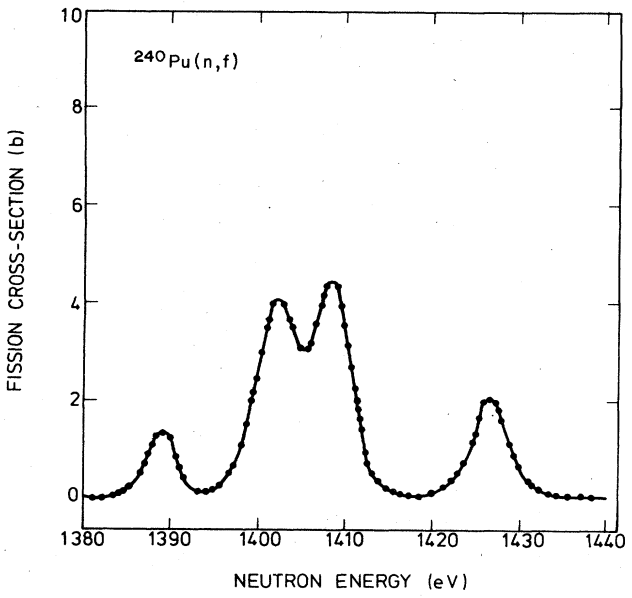

FIG. 115. The 1405 eV intermediate resonance in the neutron fission cross section of ^{240}Pu showing two fine-structure resonances interpreted as being due to the accidental degeneracy of a class-I with a class-II level. Data are from Auchampaugh and Weston (1975).

We obtain the mixing coefficients W_{11}, W_{12} from the values of $\Gamma_{\lambda(f)}$ using Eq. (3.173b), by the use of

$$\frac{\Gamma_{1(f)}}{\Gamma_{1(f)}+\Gamma_{2(f)}}=W_{11}^2\,, \tag{6.78a}$$

$$\frac{\Gamma_{2(f)}}{\Gamma_{1(f)}+\Gamma_{2(f)}}=W_{12}^2\,. \tag{6.78b}$$

Thus, from Eq. (3.172), the repulsion $\Delta(=E_{\lambda_{II}}-E_{\lambda=1})$ is related to the coupling matrix element between the class-II state and the state $\lambda_I=2(I)$ by

$$\frac{\Delta^2}{H_{12}^2}=\frac{W_{12}^2}{W_{11}^2}=\frac{\Gamma_{2(f)}}{\Gamma_{1(f)}}\,. \tag{6.79}$$

We deduce the separation of the class-II and class-I state from Eq. (3.171), giving

$$\frac{(E_{2(I)}-E_{1'(II)})^2}{H_{12}^2}=\frac{\Gamma_{1(f)}}{\Gamma_{2(f)}}\left(1-\frac{\Gamma_{2(f)}}{\Gamma_{1(f)}}\right)^2\,. \tag{6.80}$$

By successive approximations, starting with $|\Delta|\sim 3$ eV, $\Gamma_{1(f)}=2.0$ eV, $\Gamma_{2(f)}=1.5$ eV, it turns out that $H_{c(12)}^2=9.8(\pm 0.5)$ eV^2 and $E_{2(I)}-E_{1'(II)}=0.9$ eV with an accuracy of the order of 20%.

We deduce the reduced neutron width of the approximate class-II level from

$$\Gamma_{1(n)}^{(0)1/2}=W_{11}\Gamma_{1'(II)(n)}^{(0)1/2}-W_{21}\Gamma_{2(I)(n)}^{(0)1/2}\,, \tag{6.81a}$$

$$\Gamma_{2(n)}^{(0)1/2}=W_{21}\Gamma_{1'(II)(n)}^{(0)1/2}+W_{11}\Gamma_{2(I)(n)}^{(0)1/2}\,, \tag{6.81b}$$

giving

$$\Gamma_{1'(II)(n)}^{(0)1/2}=W_{11}\Gamma_{1(n)}^{(0)1/2}+W_{21}\Gamma_{2(n)}^{(0)1/2}\,. \tag{6.82}$$

The observed values of the reduced neutron widths are 0.22×10^{-4} and 0.23×10^{-4} eV$^{1/2}$, giving possible values of 3.1×10^{-6} and 4.5×10^{-4} eV$^{1/2}$ for $\Gamma_{1'(II)(n)}^{(0)1/2}$. This reduced width can only be picked up by the very weak mixing with the remaining class-II levels, and therefore the lower value is likely to be the valid one.

Our analysis of the remaining fine-structure resonances follows the perturbation procedure outlined in the previous section, the quasi-class-II level being set at 1405.3 eV with a fission width of 3.5 eV. The average squared matrix element $H_{c,\lambda_I\lambda_{II}}^2$ (including the nearly degenerate class-I level) is found to be 3.6 eV^2 and hence the class-II coupling width $\Gamma_{\lambda_{II}(c)}=1.5$ eV. The expectation value of the reduced neutron width of the approximate class-II level is 1.4×10^{-5} eV$^{1/2}$; this is to be compared with the value of 3.1×10^{-6} eV$^{1/2}$ inferred above, which is in fact quite close to the median value for the distribution of possible reduced width values.

One more interesting comparison can be made between the degeneracy analysis and the cross section data. This concerns the interference to be expected between the two central resonances in the cross section. From the two-level analysis we have

$$\Gamma_{1(f)}^{1/2}=W_{11}\Gamma_{1'(II)(f)}^{1/2}\,, \tag{6.83a}$$

$$\Gamma_{2(f)}^{1/2}=W_{21}\Gamma_{1'(II)(f)}^{1/2}\,. \tag{6.83b}$$

From these expressions and the corresponding ones for the neutron widths [Eq. (6.81)] we have

$$\Gamma_{1(n)}^{1/2}\Gamma_{1(f)}^{1/2}=W_{11}^2\Gamma_{1'(II)(f)}^{1/2}\Gamma_{1'(II)(n)}^{1/2}-W_{11}W_{21}\Gamma_{1'(II)(f)}^{1/2}\Gamma_{2(I)(n)}^{1/2} \tag{6.84a}$$

$$\Gamma_{2(n)}^{1/2}\Gamma_{2(f)}^{1/2}=W_{21}^2\Gamma_{1'(II)(f)}^{1/2}\Gamma_{1'(II)(n)}^{1/2}+W_{11}W_{21}\Gamma_{1'(II)(f)}^{1/2}\Gamma_{2(I)(n)}^{1/2}\,. \tag{6.84b}$$

The deduced value of $\Gamma_{1'(II)(n)}^{1/2}$ $[3.1\times10^{-6}(E_{1'(II)}\text{ eV})]$ implies that the first term on the rhs of these two equations can be neglected, giving opposite signs for the two products that control the interference; hence constructive interference is expected for the fission cross section between the resonances [destructive outside: see Eq. (3.131)]. This is in agreement with Auchampaugh and Weston's multilevel fit to their data.

3. Moderately weak coupling

a. Analysis procedures

For narrow class-II states (fission widths much less than the class-I state spacing) moderately weak coupling is defined by the spreading of the class-II state into the neighboring states to sufficient extent that no single state carries the bulk of the original class-II state. However, there is insufficient spreading to allow comparable and significant amounts of two or more class-II states to be found in the final states. The mathematical formulation of this mixing problem was outlined in Sec. III.C.5. The condition for the matrix elements was shown to be

$$D_I<\frac{2\pi\overline{H_c^2}}{D_I}\ll D_{II}\,.$$

For an idealized picket-fence model with uniform class-I level spacing and uniform squared matrix elements the pattern of fission widths for the resonant states is Lorentzian [see Eq. (3.185)], and most analyses of data are based on this fact, the assumption being made that

in a realistic case the actual fission widths of the resonances will fluctuate according to a Porter–Thomas distribution [see Eq. (6.10)] about a Lorentzian profile. While this assumption is certainly reasonable in practice for the values far out on the wings of the Lorentzian (and can be demonstrated on the more basic assumption of Gaussian behavior of the matrix elements) it is much more questionable near the center of the group, particularly if it is rather narrow; the individual distributions are truncated (maximum value is the class-II fission width) unlike the Porter–Thomas distribution, which extends to infinity, and there must be some degree of correlation amongst the widths.

The most straightforward approach to analysis of this kind of data is a "differential" one. The fission widths of the resonances are treated as experimental observations of the Lorentzian function, and the parameters of the latter (centroid energy, peak height, and half-width) are determined by fitting a curve to the "observations" using the method either of least squares or of maximum likelihood. Because of the highly skewed distribution function of the "observations" relative to the ideal profile, the latter method is the more satisfactory. The procedure has been described by Werz *et al.* (1973) and James *et al.* (1977).

Differential fits turn out to be unsatisfactory if there are only a few levels within the half-width of the Lorentzian profile. This is because the strong central levels dominate the fit (the faraway levels only determine the product $\Gamma_{\lambda_{II}(f)}\Gamma_{\lambda_{II}(c)}$) and these few can be wildly untypical owing to the Gaussian spread of the small number of matrix elements that govern their properties. Numerical tests of the fitting procedure based on stochastically generated simulations of resonance widths (Lynn, 1972) indicate that little confidence can be placed in the method.

Fitting procedures of an "integral" kind turn out to be better (Lynn, 1972; Lane *et al.*, 1974). The cumulative sum of fission widths is plotted as a function of energy. This "staircase" function is then fitted by an idealized smooth function derived from a Lorentzian:

$$\frac{\Gamma_{\lambda_{II}(f)}\Gamma_{\lambda_{II}(c)}}{2\pi}\int_{-\infty}^{E} dE_\lambda \frac{1}{(E_\lambda - E_{\lambda_{II}})^2 + W^2} = \left[\frac{1}{2}+\frac{1}{\pi}\arctan\left(\frac{E-E_{\lambda_{II}}}{W}\right)\right]\frac{\Gamma_{\lambda_{II}(f)}\Gamma_{\lambda_{II}(c)}}{2W}, \tag{6.85}$$

where $W=\frac{1}{2}\Gamma_{\lambda_{II}(c)}$. Numerical trials on simulated level sequences show that the square root of the variance in the determination of the width ranges from about 50% for $\Gamma_{\lambda_{II}(c)}/D_I=1.5$ to about 30% for $\Gamma_{\lambda_{II}(c)}/D_I=12.5$.

The concept of the coupling width is more of an aid to discussion than a physical reality. The quantity that we really wish to know is the mean squared matrix element for the coupling. It is just this quantity that is extracted from the data on very weak coupling, by the determination of the individual matrix elements. It is also possible, in principle, to extract the individual matrix elements from data on moderately weak coupling. The equations to be solved are (3.184b) and (3.184c) [substituted into Eq. (3.190)] together with the sum rule $\sum_\lambda \Gamma_{\lambda(f)} = \Gamma_{\lambda_{II}(f)}$ to give the unknowns E_{λ_I}, $E_{\lambda_{II}}$, $\Gamma_{\lambda_{II}(f)}$, and $\langle\lambda_I|H_c|\lambda_{II}\rangle^2$, exactly equal in number to the observed quantities E_λ and $\Gamma_{\lambda(f)}$. A numerical procedure has been established for doing this (Lynn and Moses, 1980). From the basic Eqs. (3.181) for the mixing of a class-II state with a set of N class-I states, together with the normalization conditions, (3.182) and

$$\sum_\lambda C^2_{\lambda(\lambda_I)} = 1, \quad \lambda_I = 1-N$$

$$\sum_\lambda C^2_{\lambda(\lambda_{II})} = 1,$$

we obtain

$$\langle\lambda_I|H_c|\lambda_{II}\rangle^2 = \frac{1}{\sum_\lambda C^2_{\lambda(\lambda_{II})}/(E_{\lambda_I}-E_\lambda)^2}, \tag{6.86a}$$

$$\sum_\lambda \frac{C^2_{\lambda(\lambda_{II})}}{E_{\lambda_I}-E_\lambda} = \frac{1}{\langle\lambda_I|H_c|\lambda_{II}\rangle^2}\left[E_{\lambda_I} - \sum_\lambda E_\lambda C^2_{\lambda(\lambda_I)}\right], \tag{6.86b}$$

$$E_{\lambda_{II}} - \sum_\lambda E_\lambda C^2_{\lambda(\lambda_{II})} = \sum_{\lambda_I}\left[E_{\lambda_I} - \sum_\lambda E_\lambda C^2_{\lambda(\lambda_I)}\right]. \tag{6.86c}$$

The sum $r(E)\equiv\sum_\lambda C^2_{\lambda(\lambda_{II})}/(E-E_\lambda)$, which features on the lhs of Eq. (6.86b) for $E=E_{\lambda_I}$, has $N+1$ poles at $E=E_\lambda$. These, by Eq. (3.184b), are also the poles of the function

$$\frac{f(E)}{E-E_{\lambda_{II}}+\sum_{\lambda_I}\langle\lambda_I|H_c|\lambda_{II}\rangle^2/(E_{\lambda_I}-E)},$$

[$f(E)$ being regular], and hence this may be identified with $r(E)$. By Liouville's theorem $f(E)$ must then be a constant and it turns out to be unity by calculating the residue of $r(E)$ at any pole E_λ. Thus

$$\sum_\lambda \frac{C^2_{\lambda(\lambda_{II})}}{(E-E_\lambda)} = \frac{1}{E-E_{\lambda_{II}}+\sum_{\lambda_I}\langle\lambda_I|H_c|\lambda_{II}\rangle^2/(E_{\lambda_I}-E)},$$

giving

$$\sum_\lambda \frac{C^2_{\lambda(\lambda_{II})}}{E_{\lambda_I}-E_\lambda} = 0. \tag{6.86d}$$

Substituted into Eq. (6.86b) this gives the sum rule

$$E_{\lambda_I} = \sum_\lambda E_\lambda C^2_{\lambda(\lambda_I)}, \tag{6.86e}$$

which in turn in (6.86c) gives

$$E_{\lambda_{II}} = \sum_\lambda E_\lambda C^2_{\lambda(\lambda_{II})}. \tag{6.86f}$$

These two sum rules and the normalization conditions lead to

$$\sum_\lambda E_\lambda - \sum_{\lambda_I} E_{\lambda_I} = E_{\lambda_{II}}. \tag{6.86g}$$

In practice the class-I eigenvalues are found from the numerical solution of Eq. (6.86d). Once these are determined the matrix elements can be calculated from Eq. (6.86a) and the class-II eigenvalue from Eq. (6.86f). A check on the convergence of the numerical process can be provided by evaluating

$$\chi^2 = \sum_\lambda \frac{1}{\sigma^2_\lambda}\left[\frac{\Gamma_{\lambda_{II}(f)}}{\sum_{\lambda_I}\langle\lambda_I|H_c|\lambda_{II}\rangle^2/(E_{\lambda_I}-E_\lambda)^2+1} - \Gamma_{\lambda(f)}\right]^2,$$

where the σ_λ are the experimental errors on the observed fission widths. The procedure has been tested on simulated resonance parameter sets, including sets with stochastically generated errors. The recovery of the initial values of the matrix elements has been shown to be remarkably good.

b. *Intermediate structure in ^{235}U*

Narrow intermediate structure was discovered in the neutron fission cross section of ^{234}U by James and Rae (1968). The first attempt at determining the resonance parameters in the lowest intermediate resonance was made by James and Slaughter (1969), and a much more comprehensive study of the cross section was later carried out by James *et al.* (1977).

The intermediate resonance at 580 eV in this cross section seems to be the best known example of moderately weak coupling between a class-II state and its class-I neighbors. The fission widths of the fine-structure resonances up to 1000 eV total 190 meV, while the largest individual value is 8.7 meV (for the resonance at 515.9 eV). There are several more individual fission widths of similar magnitude, e.g., 4.1 meV (at 455.3 eV), 4.0 meV (at 518.9 eV), 5.0 meV (at 560.9 eV), 7.0 meV (at 582.4 eV), 5.0 meV (at 643.5 eV), 5.1 meV (at 690.0 eV), and 4.9 meV (at 726.1 eV). A tight cluster of strong fission resonances around 1100 eV appears to constitute a second, narrower, intermediate resonance.

In analyzing the data James *et al.* (1977) employed both the method of least-squares fitting to a cumulative sum of fission widths and the differential fitting method with maximum likelihood. They improved the latter method by weighting the likelihood function for each individual fission width according to the experimental uncertainty in the value of that width. In applying the maximum likelihood method they tested the hypothesis that two class-II levels are present as well as the hypothesis of a single class-II level. The former hypothesis is indicated at a significance level of 98.7%. Fits to the data are shown in Fig. 116.

The parameters deduced for the class-II level are given in Table XX. The width of the resonance at 580 eV encompasses 13 class-I levels ($D_I = 10.6 \pm 0.6$ eV), and it can be presumed in consequence that the differential method of fitting these data is fairly sound. The parameters of the 1227-eV level must be considered much more doubtful, because, in particular, a moderately strong fission resonance observed at 1134 eV has not been seen in transmission and its fission width could therefore be much more substantial than the value assigned to it in the analysis.

James *et al.* have also observed intermediate structure at higher energies (see Fig. 117). Assignment of individual class-II levels is difficult, because two or more observed groups may belong to the same class-II state owing to the fluctuation phenomenon (see, e.g., the clusters between 4.0 and 4.6 keV, which probably constitute one or at most two class-II states). James *et al.* give an upper limit of 2.1 keV for the class-II spacing. Using Eq. (6.19) with an additional fluctuation factor [Eq. (6.22b)] the class-II fission widths can be extracted from the areas of the intermediate fission resonances. These values are listed in Table XX. The mean class-II fission width of 81 meV, together with the class-II spacing, imply, on the strong damping assumption, barrier parameters of

$$(V_B - S_n)/\hbar\omega_B = 1.32$$

($V_B - S_n = 0.7$ MeV, on the assumption that $\hbar\omega_B = 0.52$ MeV).

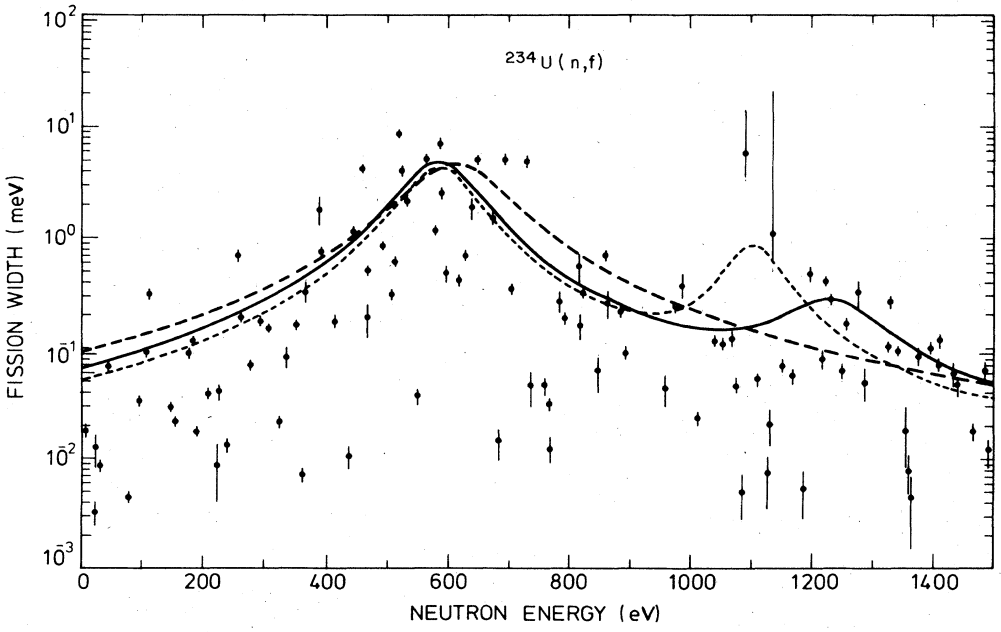

FIG. 116. Fission width in the neutron fission cross section of ^{234}U as a function of neutron energy. The full curve is a fit using experimentally weighted maximum likelihood, and the dotted curve is based on unweighted maximum likelihood (giving a width for the higher class-II state 40% lower than that from the "weighted" analysis). Data and fit from James *et al.* (1977).

TABLE XX. Properties of class-II levels in the cross section for $^{234}U(n,f)$. From James *et al.* (1977) (an arithmetical error occurred in this paper and has been corrected in the values listed below, supplied by G. D. James).

$E_{\lambda_{II}}$ (eV)	$\Gamma_{\lambda_{II}(f)}$ (meV)	$\Gamma_{\lambda_{II}(c)}$ (eV)	Comments
580 ± 16	85 ± 20	136 ± 20	Analysis by Lorentzian fitting to fission width of fine-structure resonances.
1227 ± 65	$5.1^{+3.3}_{-2.2}$	174^{+34}_{-26}	Ditto
3100	15		Value obtained from area of intermediate structure resonance (neutron width assumed constant).
4575	50		Ditto
7845	263		Ditto
11886	58		Ditto
13076	130		Ditto

The much sparser data on the coupling width suggest that

$$(\upsilon_A - S_n)/\hbar\omega_A \approx 0.25 ,$$

allowing for an effective number of transition states at the inner barrier of ~2.4 (see Sec. VII.C.1.). Analysis of the overall features of the fast fission cross section (see Sec. VII) suggests that the inner barrier is much higher than this. It would appear therefore that a damped vibrational resonance may be enhancing the coupling width in the slow neutron energy region.

c. *Intermediate structure in ^{238}Np*

The neutron fission cross section of ^{237}Np was the first in which narrow intermediate structure was discovered (Paya *et al.*, 1968; Fubini *et al.*, 1968). Since the first measurement a great deal of precise work has been done (Paya *et al.*, 1969; Brown *et al.*, 1970; Kolar *et al.*, 1971; Keyworth *et al.*, 1973; Plattard *et al.*, 1976), so that by now many intermediate resonances have been observed and the fine-structure resonance parameters of the group at lowest energy are almost completely known.

The remaining uncertainties in the lowest energy group, at 39.9 eV (shown in Fig. 118), are such, however, that it is not clear whether this group should fall into the classification of very weak coupling or that of moderately weak coupling. The fission cross section is dominated by a resonance at 39.9 eV with a fission width of 3.3 meV (Plattard *et al.*, 1976); the neighboring resonances have fission widths of the order of 0.4 meV at most. But a careful examination of the shape of the central resonances has revealed another weak unresolved resonance with a fission width similar to or greater than that at 39.9 eV; the magnitude of this width appears crucial to the interpretation of the intermediate resonance. The analysis of Plattard *et al.* suggests that the fission width of the resonance at 39.7 eV is ~1.6 meV; with this value the fission width of the resonance at 39.9 eV is reduced to ≈0.9 meV.

The spacing of the resonance fine structure is 0.69 eV (Paya *et al.*, 1968) for s-wave resonances of both spins. It is fundamental to the theory of fission intermediate structure as developed in this article that the total angular momentum of each class-II state, like that of each class-I state, is a good quantum number, and no coupling between the two classes of states can violate this property. It has been checked that the important fission resonances in the region of 40 eV do have the same spin (Keyworth *et al.*, 1973) and its value is $J = 3$. Hence, the relevant class-I spacing $D_I(J = 3^+) = 1.17$ eV (spin and parity of ^{237}Np are $I^\pi = \frac{5}{2}$). It is clear from the dominance of the fission widths of the two central resonances that the width of the intermediate resonance

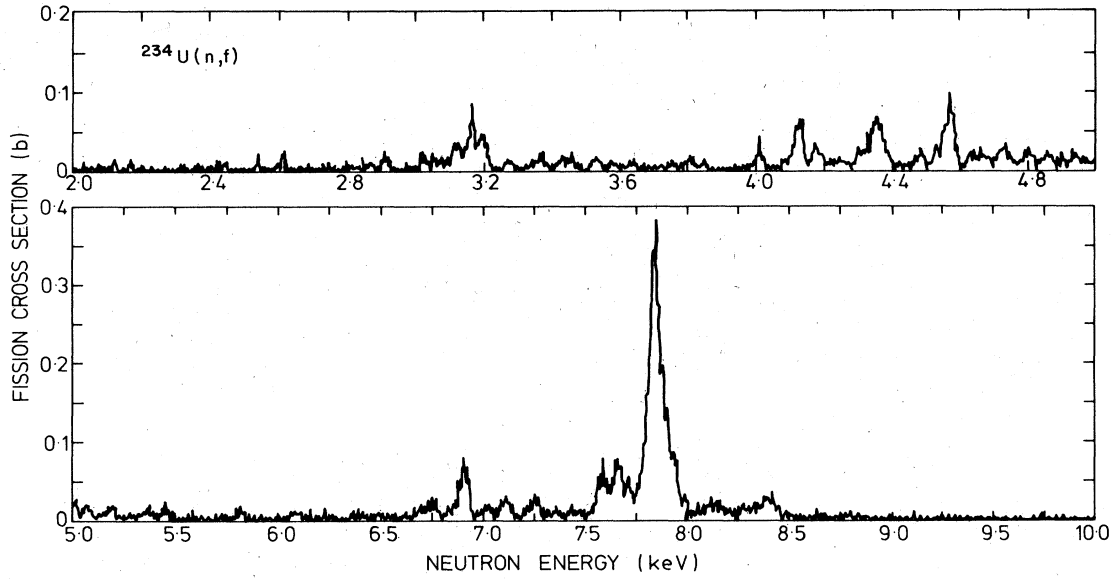

FIG. 117. Neutron fission cross section of ^{234}U above 2 keV neutron energy. From James *et al.* (1977).

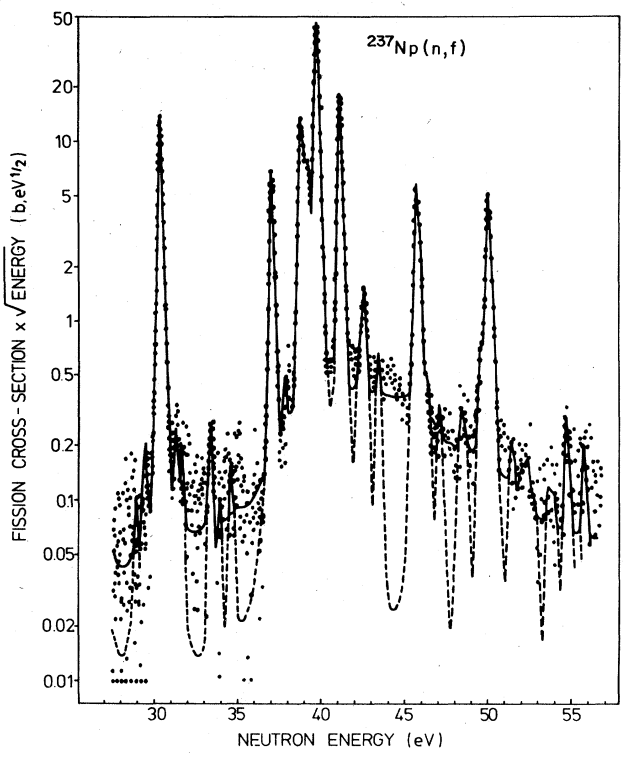

FIG. 118. Neutron fission cross section of ^{237}Np in region of 40 eV. Data from Paya *et al.* (1969). For explanation and discussion of the curves see reference.

cannot be much greater than the class-I spacing.

A very rough and simple analysis of the data confirms this. We have extracted the product $\langle\lambda_I|H_c|\lambda_{II}\rangle^2 \Gamma_{\lambda_{II}(f)}$ for all the $J=3$ resonances from 20 to 55 eV (together with a few of unknown spin but significant fission width) using the simple Lorentzian formula, Eq. (3.185), for a class-II level at 39.7 eV, and two assumptions about the half-width W, i.e., (i) $W=0$ and (ii) $W=1.5$ eV. With assumption (i) we find that $2\pi\langle\lambda_I|H_c|\lambda_{II}\rangle^2\Gamma_{\lambda_{II}(f)}/D_I = 8.4\times10^{-3}$ eV^2, and with assumption (ii) the same quantity $=10\times10^{-3}$ eV^2. The smaller of the two widths $\Gamma_{\lambda_{II}(c)}$, $\Gamma_{\lambda_{II}(f)}$ should equal 5.3 meV (the sum of the observed fine-structure fission widths) and this indicates $2W\approx1.7$ eV for either assumption (i) or (ii). Notice that no *a priori* assumption about moderately weak coupling of a narrow (fission width) class-II level or of very weak coupling of a broad class-II level [see Sec. III.C.5.$c(v)$] has been made.

Apart from the disagreement between the initial input ($W=0$) and the result, assumption (i) would be untenable on statistical grounds; the central ten resonances give a mean squared coupling matrix element only one quarter of that from the full range. The probability of this, or a smaller value, occurring can be calculated from the χ^2 distribution with 10 degrees of freedom; it is $\sim10^{-4}$.

The data have also been analyzed by fitting an integrated Lorentzian curve to the cumulative sum of the fission widths (Moses, 1976). The result depends on the value assumed for the fission width of the 39.7 eV resonance, ranging from $2W=1.3$ eV for very small values through $2W=0.55$ eV for $\Gamma_{\lambda(f)}=1.5$ meV to $2W=0.18$ eV for $\Gamma_{\lambda(f)}=9$ meV. The overall error in these results due to experimental uncertainties in the fission widths of the other resonances is of the order of 10%. It is clear from the variations in the extracted values of the envelope width $2W$ that the central widths are unduly affecting the determination of the required quantity. In the procedure of Lynn and Moses (1980), which is least sensitive to the details of the central levels, $2W$ is 1.88 eV for the data of Plattard *et al.* (1976).

Some other interesting properties of the 40 eV intermediate resonance have been measured. Kiuken *et al.* (1972) measured the angular distribution of fission products from the (n,f) reaction with the target nuclei aligned. They attempted to interpret these data in terms of unique values of total angular momentum J and projection of angular momentum K along the cylindrical symmetry axis of the nucleus as it passes through the deformation channel at the outer barrier. The pair of values implied by experimental data were $J=2, K=2$. The J value is in conflict with that of Keyworth *et al.* (1973) determined by polarization methods. The discrepancy can be resolved if it is assumed that two or more deformation channels, with different K values, are about equally penetrable at this excitation energy. This accords with current ideas on the density of deformation channels at the outer barrier of an odd nucleus (Lynn, 1974b). An expression for the effective number of available channels at given excitation energy below the barrier energy is given in Sec. VII.C.1. [Eq. (7.30)]. With the barrier level density parameters also given in that section this number is 3.6 in the present case.

This factor for the effective number of channels must also be taken into account in interpreting the intermediate structure parameters in terms of barrier heights. If the average value of $\Gamma_{\lambda_{II}(f)}$ is assumed to be 5.3 meV (and this value appears to be borne out by the approximate fission widths deduced from the areas of the higher-energy intermediate resonances) and the class-II level spacing for one spin only is taken as 80 eV (twice the observed spacing (Paya *et al.*, 1969); see Fig. 119), the outer barrier height relative to the neutron separation energy is

$$(U_B - S_n)/\hbar\omega_B = 1.43\ ,$$

giving $U_B - S_n = 0.65$ MeV for $\hbar\omega_B = 0.45$ MeV. Note that in this interpretation it has been assumed that the observed fission width is entirely due to prompt fission. The smallness of its value does put this assumption in doubt. The observation could be that of delayed fission from the shape isomer of ^{238}Np (if its half-life is substantially less than 1 μsec), but this is not likely because the observed isomer of the neighboring nucleus of ^{237}Np only has a branching ratio to fission of $\sim10^{-3}$. In interpreting the value of the coupling width an even larger number of effective channels (7.2) must be allowed for the inner barrier (see Sec. VII.C.2.). With this the barrier height relation is

$$(U_A - S_n)/\hbar\omega_A = 0.72\ ,$$

giving $U_A - S_n = 0.47$ MeV for $\hbar\omega_A = 0.65$ MeV. These

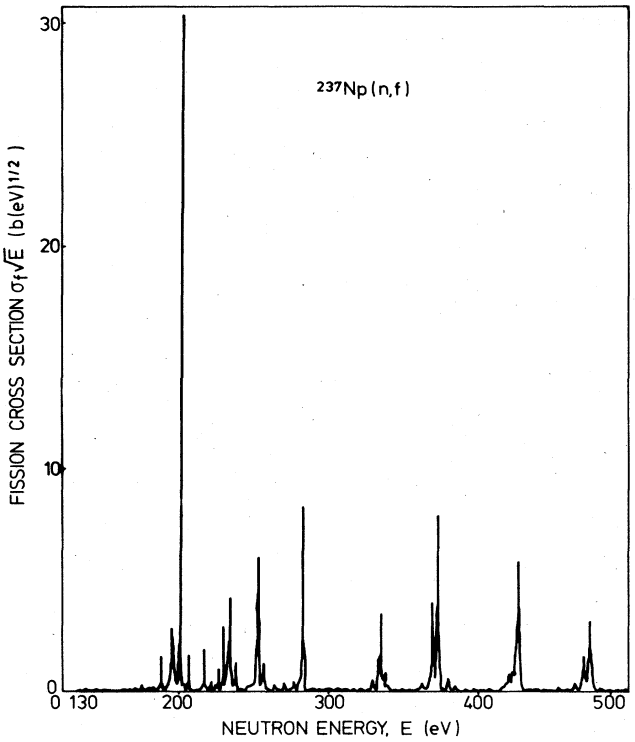

FIG. 119. Neutron fission cross section of ^{237}Np in region 100–500 eV [from Plattard *et al.* (1976)].

barrier heights both lie within 300 keV of the values required to fit the fast neutron cross section (Sec. VII).

If the roles of the barrier heights are reversed [i.e., the intermediate resonances are interpreted as very weak coupling of the class-I states to a broad class-II level as described in Sec. III.C.5.*c*(*v*)] the discrepancy with barrier parameters required to fit the fast neutron fission cross section becomes very much worse.

It should be noted that the above interpretation, in which it is assumed that both possible angular momentum states for s-wave neutron resonances $J^\pi = 2^+, 3^+$ are about equally fissionable on account of the density of deformation channels available for odd nuclei, is in some conflict with observations on the distribution of spacings of the intermediate resonances at higher energies (Fubini *et al.*, 1968). This appears to satisfy the Wigner relationship for a single set of levels with good quantum numbers [Eq. (6.6)]. However, because of the Porter–Thomas fluctuations of the fine-structure components, there is a clear conceptual difficulty in distinguishing uniquely one intermediate resonance from another. Further development of methods to assign "signatures" of class-II states to the individual fine-structure resonances (e.g., of the type mentioned above in which the angular distribution of fission products is measured) will be required to resolve this question.

TABLE XXI. Areas of intermediate resonances in the fission cross section of ^{237}Np [data from Plattard (1973)] and analysis.

$E_{\lambda_{II}}$ (eV)	$A_{\lambda_{II}}$ (b.eV)	$\Gamma_{\lambda_{II}(c)}$ (eV) (assuming $\Gamma_{\lambda_{II}(f)} = 0.003$ eV, $\Gamma_{\lambda_{II}} = 0.03$ eV)
119	0.78	0.061
200	1.6	0.17
233	0.49	0.054
253	0.50	0.058
283	0.43	0.055
335	0.31	0.043
372	0.74	0.11
426	0.50	0.076
474	0.34	0.056
553	0.13	0.023
584	0.26	0.048
669	0.52	0.105
719	0.41	0.083
808	0.51	0.11

We have analyzed the areas of the intermediate resonances at higher energy as measured by Plattard (1973), see Table XXI. Because the data on the 40 eV intermediate resonance indicate that this is an intermediate case between moderately weak coupling and very weak coupling we have in the first place used the very weak coupling area formula, Eq. (6.37), for the median position of the class-II level. We have assumed a class-II radiation width of 0.027 eV and a class-II fission width of 0.003 eV in this analysis. The average value of the coupling width, including the value of 0.55 eV for the 40 eV group, is 0.107 eV. This leads to the value

$$(v_A - S_n)/\hbar\omega_A \approx 1.12$$

(allowing seven effective channels), or $v_A - S_n \approx 0.73$ MeV (assuming $\hbar\omega_A = 0.65$ MeV).

4. Weak coupling to class-II states with broad fission width

a. General

This case bears many similarities to that of moderately weak coupling to a class-II state with narrow fission width. In particular the pattern of fine-structure fission widths is expected to be basically Lorentzian (with Porter–Thomas fluctuations about the Lorentzian envelope). In fact there is better justification for this expectation than there is in the alternative case. The areas of intermediate resonances are expected to be governed by the same general formulas (see Sec. VI.C.1.*a*).

The differences should be found, in principle, in the details of the microscopic cross section. The presence of another S-matrix pole, in addition to those governing the fine-structure resonances, lying at a comparatively large distance below the real axis in the complex energy plane, must give rise to some interference effects. In practice such interference effects can hardly be observable in any but the most precise of measurements and analysis. This is illustrated in Fig. 120 in which are shown the cross sections calculated from a simulated set of R-matrix parameters generated from a stochastic set of class-I parameters and coupling matrix elements and a postulated class-II state. The details of some of the class-I and R-matrix parameters are given in Table XXII together with parameters of the S-matrix poles to which they give rise. As expected

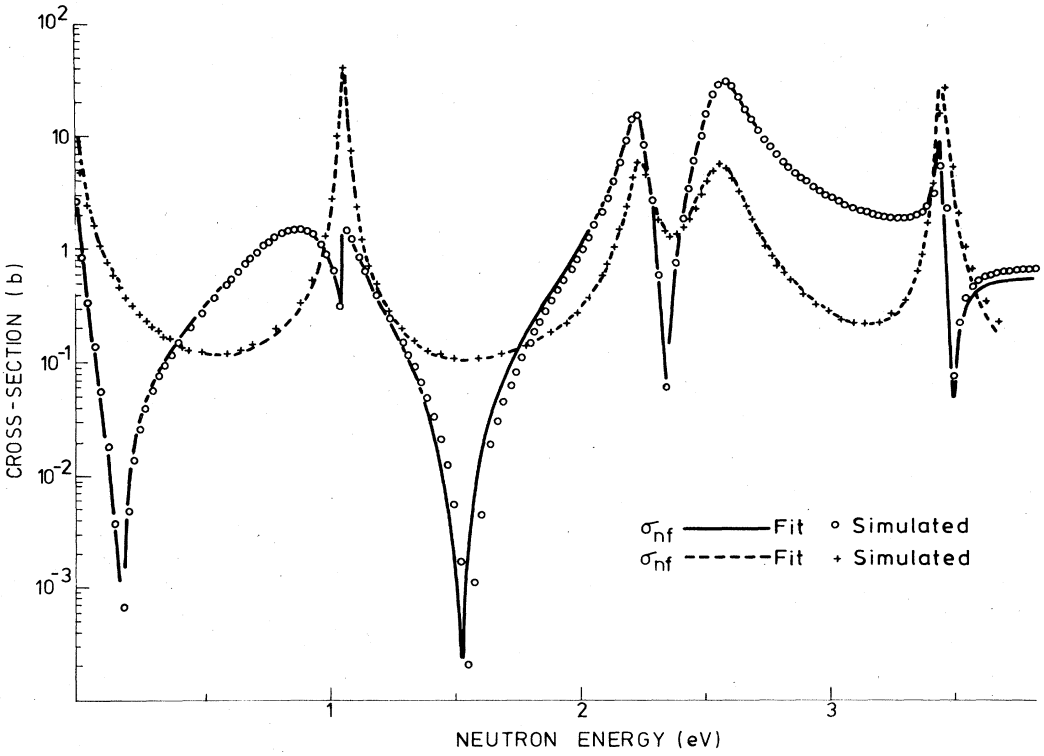

FIG. 120. Simulated cross sections and fits for weak coupling of class-I states to a class-II state with large fission width ($\Gamma_{\lambda_{II}(f)} \gg D_I$). Parameters are given in Table XXII.

the R-matrix and S-matrix parameters have little resemblance. An R-matrix fit to the cross section leads to a set of R-matrix parameters which are similar to the S-matrix poles, except that the distant pole is absent. The fit is good and the similarity between the fitted R matrix and the S matrix indicates that the cross section has almost the exact appearance of moderately weak coupling.

Effects that obviously cannot be described by a simple R-matrix fit based only on the apparent fine-structure resonances do occur if the class-II coupling and fission widths are comparable in size. A simulated example is shown in Fig. 121 with parameters listed in Table XXIII. The fit shown in Fig. 121 was the best that could be procured and shows considerable discrepancy with the simulated cross section.

We conclude therefore that the interpretation of broad intermediate resonances ($\Gamma_{II} \gg D_I$) is generally ambiguous and is likely to remain so for some time in the present state of the experimental art. There are some data extant, however, for which there seem to be good reasons for interpreting as weak coupling, strong fission rather than vice versa.

b. *Intermediate structure in ^{239}Pu*

The neutron fission cross section of ^{238}Pu has been measured in the low- and medium-energy ranges by

TABLE XXII. Part of the set of level parameters describing the simulated cross sections of Fig. 120. The class-II state has fission and coupling widths $\Gamma_{\lambda_{II}(f)} = 20$, $\Gamma_{\lambda_{II}(c)} = 4.3$. The unit for all parameters is the mean class-I level spacing D_I.

Class I			Coupled			Poles		Cross-section fit		
E_{λ_I}	$\Gamma_{\lambda_I(n)}$	$H^2_{\lambda_I\lambda_{II}}$	E_λ	$\Gamma_{\lambda(n)}$	$\Gamma_{\lambda(f)}$	$E_m^{(H)}$	$\Gamma_m^{(H)}$	E'_λ	$\Gamma'_{\lambda(n)}$	$\Gamma'_{\lambda(f)}$
−0.932	0.0070	0.387	−1.011	0.0089	0.299	−0.947	0.091	−0.947	0.0077	0.0665
−0.037	0.0147	0.032	−0.056	0.0156	0.222	−0.038	0.041	−0.037	0.0182	0.0050
			0.256	0.(3)3	2.813	0.792	15.154			
0.928	0.0022	1.89				0.903	0.414	0.928	0.0024	0.390
1.072	0.0051	0.0056	1.072	0.0048	0.(3)57	1.072	0.025	1.072	0.0048	0.009
			1.934	0.0046	2.574					
2.246	0.0070	0.274				2.250	0.082	2.25	0.0070	0.053
			2.369	0.(3)2	0.605					
2.585	0.0248	0.577				2.577	0.164	2.58	0.0259	0.125
			3.141	0.0353	4.503					
3.465	0.0051	0.015	3.478	0.0016	0.255	3.465	0.028	3.47	0.0049	0.0036
4.632	0.0158	0.066	4.649	0.0130	0.084	4.635	0.047	4.64	0.0128	0.0125

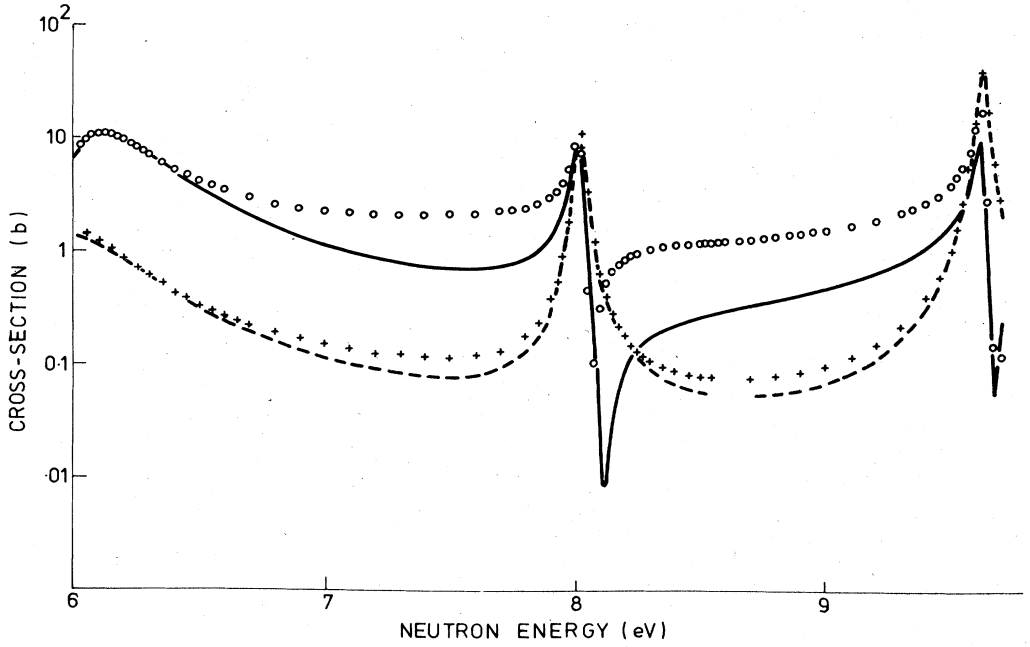

FIG. 121. Simulated cross sections and fits for coupling of class-I states to a class-II state when the coupling and fission widths are of comparable magnitude. Parameters are given in Table XXIII.

Silbert *et al.* (1973). At low energies (to a few hundred eV) the capture cross section has also been measured and this has enabled Silbert and Berreth (1973) to analyze the fine-structure resonance parameters across the intermediate resonance at 285 eV.

The central resonance in this group, at 285 eV, has a fission width $\Gamma_{\lambda(f)} \approx 3.5$ eV. The other resonances all have fission widths of the order of or less than 100 meV, the two largest being at 192 eV ($\Gamma_{\lambda(f)} = 130$ meV) and 300 eV ($\Gamma_{\lambda(f)} = 102$ meV). This case could apparently be one of very weak coupling analyzable with first-order perturbation theory (see Sec. VI.E.1). We have carried out an analysis of this kind over the central 16 resonances, and this results in an estimate of the coupling width

$$\Gamma_{\lambda_{II}(c)} = 2\pi\overline{H_c^2}/D_I = 17 \text{ eV},$$

which is a little too large for very weak coupling to be a good description. More importantly, however, this detailed analysis gives $\Gamma^{(0)}_{\lambda''(n)} = 1.46 \times 10^{-3}$ eV$^{1/2}$ for the maximum value of the reduced neutron width of the hypothesized quasi-class-II resonance, 3.06×10^{-4} eV$^{1/2}$ for its expectation value, and 1.7×10^{-4} eV$^{1/2}$ for the median value of the distribution of possible reduced neutron widths. The observed value for the 285 eV resonance is 1.54×10^{-3} eV$^{1/2}$, which seems to rule out the very weak coupling interpretation.

The hypothesis of a broad class-II fission width therefore seems the only tenable one. The 285 eV resonance would then be interpreted as essentially a class-I resonance close to the class-II state and having a large coupling matrix element to yield a fission width with a value that has fluctuated well above the expectation value at that energy. The appearance of the next two substantial fission resonances at a separation of the order of 100 eV suggests that the Lorentzian, hence

TABLE XXIII. Part of the set of level parameters describing the simulated cross-section of Fig. 121. The class-II state has fission and coupling widths of $\Gamma_{\lambda_{II}(f)} = 20$, $\Gamma_{\lambda_{II}(c)} = 17$; the unit for all parameters is the mean class-I level spacing D.

Class I		Coupled			S-matrix poles				Attempted fit		
E_{λ_I}	$\Gamma_{\lambda_I(n)}$	E_λ	$\Gamma_{\lambda(n)}$	$\Gamma_{\lambda(f)}$	$E_m^{(H)}$	$\Gamma_m^{(H)}$	$G^2_{m(n)}$	$G^2_{m(f)}$	E_χ	$\Gamma_{\chi(n)}$	$\Gamma_{\chi(f)}$
2.822	0.0110	2.822	(−)0.0112	0.(4)5	2.822	0.031	0.012	0.(4)7	2.82	0.011	0.(4)4
3.895	0.0114	5.601	0.0797	0.146	5.632	0.132	0.081	0.023	5.63	(−)0.114	0.011
5.626	0.0980	5.655	(−)0.0263	0.134	5.706	0.241	0.0044	0.296			
5.788	0.0006	6.055	0.0146	0.306	6.053	0.419	0.024	0.589	6.1	(−)0.019	0.379
6.421	0.0217	7.788	(−)0.0142	1.490	7.622	2.153	0.0075	3.5			
8.015	0.0036	8.047	0.(3)3	0.202	8.019	0.038	0.0034	0.017	8.02	0.003	0.018
8.596	0.(7)4	8.598	(−)0.(5)4	0.(3)2	8.598	0.035	0.(4)2	0.(3)1			
9.247	0.0135										
9.638	0.0087	9.624	0.0129	0.0104	9.627	0.041	0.012	0.009	9.62	0.012	0.009
10.267	0.0158	10.267	0.0055	1.455	9.853	1.210	0.0077	1.62	9.87	0.0039	0.791
11.657	0.0097	11.667	(−)0.0079	0.066	11.651	0.071	0.0086	0.042	11.65	(−)0.0088	0.040
12.167	0.(6)23	12.178	0.(4)4	0.037	12.170	0.047	0.(4)7		12.18	0.(4)3	0.027

class-II, width approaches this order of magnitude. A reasonable guess at the parameters of the Lorentzian might be $\langle\Gamma_{\lambda(f)}\rangle(E_{\lambda_{II}}) \sim 400$ meV, $\Gamma_{\lambda_{II}(f)} \sim 50$ eV, giving

$$\overline{H_c^2} \sim 7.5 \text{ eV}^2, \quad \Gamma_{\lambda_{II}(c)} \sim 4.5 \text{ eV}.$$

The fitting procedure of Lynn and Moses (1980) yields $\Gamma_{\lambda_{II}(c)} = 4.3$ eV, $\Gamma_{\lambda_{II}(f)} = 28$ eV.

Silbert and Berreth (1973) point out that the overall statistical distribution of fission widths in this intermediate group is peaked (at about 5 meV). This suggests that the distribution of squared coupling matrix elements may not be as broad as a Porter–Thomas form, and this could be explained by the hypothesis that there is more than one effective "channel" for coupling across the intermediate barrier. (Note, however, that this is a physical concept that is *not* contained naturally within the theoretical development of the coupling matrix element, as outlined in Sec. III.C.5.*b*). The low-lying density of $J^\pi = \frac{1}{2}^+$ states at the inner barrier is expected to be about 14 MeV^{-1}, and the effective channel number [see Eq. (7.30), Sec. VII.C.1) might therefore be expected to be ~2.4. However, if the measured fission widths from 18 to 500 eV are divided by the Lorentzian expectation curve with the parameters given above, the peak in the distribution reported by Silbert and Berreth is largely washed out, and the distribution is not too dissimilar from a Porter–Thomas form. Therefore this case does not provide us with definitive evidence of "multichannel coupling."

The areas and widths of the intermediate resonances at higher energies have been determined from the data of Silbert (1969). From the evidence of the detailed fine structure of the 285 eV intermediate resonance as well as the apparent size of the higher resonances, it is clear that fission usually saturates at their center. Therefore the apparent width of these resonances is not their true width. The true width is given by the expression

$$\Gamma_{\lambda_{II}(app)} \approx 2\left[\tfrac{1}{4}(\Gamma_{\lambda_{II}(c)} + \Gamma_{\lambda_{II}(f)})^2 + \frac{\Gamma_{\lambda_{II}(c)}\,\Gamma_{\lambda_{II}(f)}}{2\pi(\Gamma_{\lambda_I(n)} + \Gamma_{\lambda_I(r)})}\right]^{1/2}, \tag{6.87}$$

which is obtained by substituting a Lorentzian form for the fission width into the competition expression $\Gamma_{\lambda(f)}/\Gamma_\lambda$.

Another relation between the coupling and fission widths of the class-II states is obtained from the intermediate resonance areas by use of Eq. (6.19), together with a fluctuation factor for which we have adopted Eq. (6.24b). The results of the complete analysis are shown in Table XXIV. The mean coupling width $\overline{\Gamma}_{\lambda_{II}(c)} = 7.1$ eV; this yields (with $D_{II} \sim 900$ eV)

$$(\upsilon_A - S_n)/\hbar\omega_A = 0.48,$$

or $\upsilon_A - S_n = 0.38$ MeV if $\hbar\omega_A = 0.8$ MeV. The mean fission width $\overline{\Gamma}_{\lambda_{II}(f)} = 180$ eV is sufficiently large to suggest that the outer barrier for spin $J^\pi = \frac{1}{2}^+$ states is near or lower than the neutron separation energy. These values are in qualitative agreement with the deductions made in Sec. VII from the behavior of the fast neutron fission cross section.

c. *Intermediate structure in ^{240}Pu*

^{239}Pu is normally considered to be fissile by slow neutrons, and as such would not be expected to display narrow intermediate resonances in its neutron fission cross section. Because the compound nucleus ^{240}Pu is even, however, compound nucleus states having certain values of spin and parity may still lie near or below the lowest appropriate deformation channel, at both the inner and outer barriers. The $J^\pi = 1^+$ states, which can be formed by absorption of s-wave neutrons by ^{239}Pu ($J^\pi = \frac{1}{2}^+$), are expected to be such a set. The 1^+ state is not expected as a simple low-lying collective state in the spectrum of an even nucleus for either normal or barrier deformations; the lowest candidate for the intrinsic state in the description of a deformation channel at the barriers is a combination of a mass-asymmetry vibration ($K^\pi = 0^-$) and a bending vibration ($K^\pi = 1^-$), or a two-quasi-particle (broken pair) excitation coupled to $K^\pi = 1^+$.

For this reason intermediate structure in the 1^+ resonances of the ^{239}Pu cross section, overlying the broad 0^+ resonances in which no more than very rudimentary intermediate structure is expected, has been sought (Patrick and James, 1968; Paya *et al.*, 1969). The assumption that the structure is indeed confined to the 1^+ resonances has been confirmed by Trochon *et al.* (1970) who determined resonance spins by measurement of the elastic scattering cross section of ^{239}Pu. The early attempts at analysis employed the autocorrelation method first applied to neutron cross-section data by Egelstaff (1958). In this, a sequence of normalized locally averaged cross sections are defined for a standard energy interval W by

$$a_j(W) = \int_{(j-1)W}^{jW} \left[\frac{\sigma(E)\sqrt{E}}{\langle\sigma(E)\sqrt{E}\rangle} - 1\right] dE, \tag{6.88}$$

and serial correlation coefficients

$$r_k(W) = \frac{\text{cov}[a_j(W); a_{j+k}(W)]}{[\text{var}a_j(W).\text{var}a_{j+k}(W)]^{1/2}} \tag{6.89}$$

are determined. The data can thus be reduced for a

TABLE XXIV. Areas and widths of intermediate resonances in the fission cross section of ^{238}Pu [data from Silbert (1969)].

$E_{\lambda_{II}}$ (eV)	$A_{\lambda_{II}}$ (b.eV)	W_{λ_π} (eV)	$\Gamma_{\lambda_{II}(f)}$ (eV)	$\Gamma_{\lambda_{II}(c)}$ (eV)
2000	965	~400	350	1.8
2900	1340	~170	48	10
3300	706	~300	200	2
4000	950	~100	~15	~25
5600	1200	~300	180	7
6000	560	~100	~17	~11
6200	360	~200	170	1.6
6400	460	~200	160	2.2
6900	630	~200	130	4
8700	1300	~600	440	9
9600	970	~500	370	7

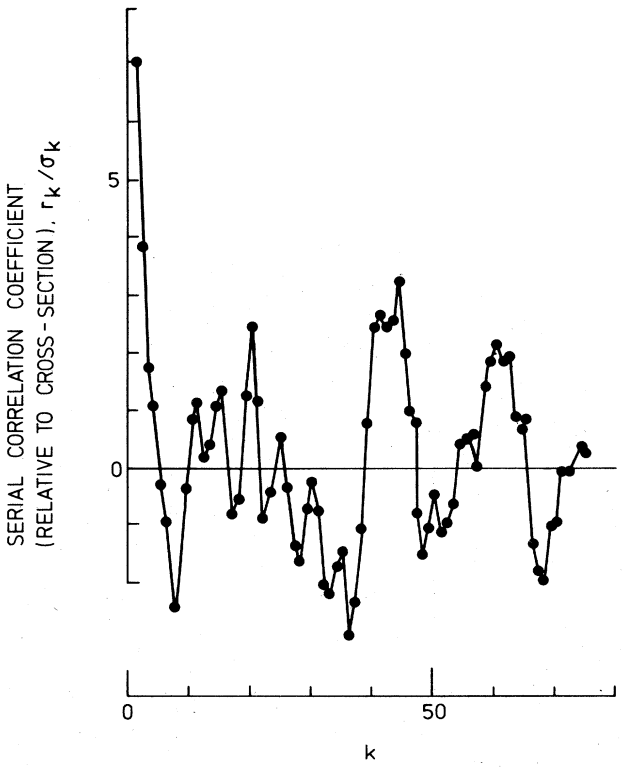

FIG. 122. Autocorrelogram from data on the neutron fission cross section of ^{239}Pu (James and Patrick, 1969). The cross section is averaged over energy intervals of $W = 33.3$ eV.

range of values of W. A typical correlogram thus produced from the ^{239}Pu neutron fission cross section is shown in Fig. 122 for $W = 33.3$ eV. The peaks that appear at energy intervals of typically $\Delta k \cdot W \approx 450$ eV are taken as indications of intermediate resonances with a local spacing of about that value. Perez *et al.* (1969) have shown that this is not a good measure of the average spacing of the intermediate resonances; if the individual spacings are assumed to have a quasi-Wigner distribution with long-range correlations, as described in Sec. VI.B.3, then the correlogram would rise monotonically to an asymptotic value with increasing k.

Nevertheless, Fig. 122 is strongly indicative of intermediate structure, and several of the peak values in the correlogram have a probability of occurring from a purely statistical grouping of fine-structure resonances of less than 0.1%. James and Patrick (1969) have returned to the original cross-section data, averaged in 33.3 eV groups, and attempted to define the intermediate resonances by fitting a curve of the form

$$\langle \sigma_f \sqrt{E} \rangle_{33.3\,\mathrm{eV}} = 70 + \sum_{\lambda_{II}=1}^{10} \frac{K_{\lambda_{II}}}{(E_{\lambda_{II}} - E_\lambda)^2 + (\frac{1}{2}\Gamma_{\lambda_{II},\mathrm{eff}})^2}, \tag{6.90a}$$

where

$$K_{\lambda_{II}} = \pi \lambda_0 g^2(J) \frac{\Gamma_I^{(0)}(n)}{D_I} \frac{\Gamma_{\lambda_{II}(c)} \Gamma_{\lambda_{II}(f)}}{\Gamma_I} \tag{6.90b}$$

$$\Gamma_{\lambda_{II},\mathrm{eff}} = \left(\Gamma_{\lambda_{II}}^2 + \frac{2\Gamma_{\lambda_{II}(c)} \Gamma_{\lambda_{II}(f)} D_I}{\pi \Gamma_I} \right)^{1/2}. \tag{6.90c}$$

The numerical term $70b \cdot \mathrm{eV}^{1/2}$ is an estimate of the contribution from the spin 0 resonances. The parameters of the intermediate resonances are given in Table XXV, and the data are shown in Fig. 123. If the data are divided by the fitted curve, a relatively structureless correlogram is obtained.

The average coupling and fission widths from the data in Table XXV are $\overline{\Gamma}_{\lambda_{II}(c)} = 5.2$ eV, $\overline{\Gamma}_{\lambda_{II}(f)} = 200$ eV. The class-II level spacing is $D_{II} = 515$ eV. These results indicate that the inner barrier for $J^\pi = 1^+$ states is about 0.45 MeV above the neutron separation energy ($S_n = 6.52$ MeV). Reference to the barrier height (for 0^+ states) of ^{240}Pu, quoted in Sec. VII, indicates that the first 1^+ inner barrier state lies ~1.4 MeV above the inner barrier. On the other hand the class-II fission width indicates that there are already about two deformation channels of $J^\pi = 1^+$ fully open over the outer barrier at the neutron separation energy. This indicates that the lowest 1^+ states may occur at a considerably lower energy in the spectrum of states at the outer barrier deformation than at the inner barrier, and may well be related to lack of reflection symmetry in the shape of the nucleus as it passes over the outer barrier (see Sec. VII).

The data on intermediate structure in the neutron fission cross section of ^{239}Pu together with that in the region of 5 MeV excitation energy from the (d,pf) reaction in the same nucleus give fuller evidence on the level density behavior of class-II states than we have for any other nucleus. From the neutron fission cross section we find that the class-II spacing of ^{240}Pu at excitation energy 6.5 MeV is ~500 eV (for spin and parity, $J^\pi = 1^+$). The class-II spacing at 5 MeV in ^{240}Pu is deduced from the intermediate structure to be ~11 keV (Glässel *et al.*, 1976); it is inferred [from the strength of quadrupole fission observed in the angular distribution of photofission products of ^{240}Pu (Rabotnov *et al.*, 1970), and the angular distributions of the d,pf peaks] that the spin and parity of these states is $J^\pi = 2^+$.

If we assume that the dependence of the class-II level density on effective excitation energy is similar to that of class-I levels we can infer (from the level density parameters in Sec. VII.B.3) that the energy of the shape isomer state of ^{240}Pu is $E_{II} \sim 2.6$ MeV.

TABLE XXV. Parameters of intermediate resonances and deduced properties of class-II state in the neutron fission cross section of ^{239}Pu.

$E_{\lambda_{II}}$ (eV)	$\Gamma_{\lambda_{II},\mathrm{eff}}$ (eV)	$K_{\lambda_{II}}$ (b.eV$^{5/2}$)	$\Gamma_{\lambda_{II}(c)}$ (eV)	$\Gamma_{\lambda_{II}(f)}$ (eV)
982	317	372×10^4	6.0	222
1350	133	53×10^4	1.9	102
1800	150	101×10^4	4.2	92
2416	266	154×10^4	2.7	222
2800	266	264×10^4	5.7	185
3200	233	227×10^4	6.2	151
3817	266	248×10^4	5.5	190
4517	600	1140×10^4	11.0	449
5217	200	164×10^4	5.5	131
5617	316	217×10^4	3.7	264

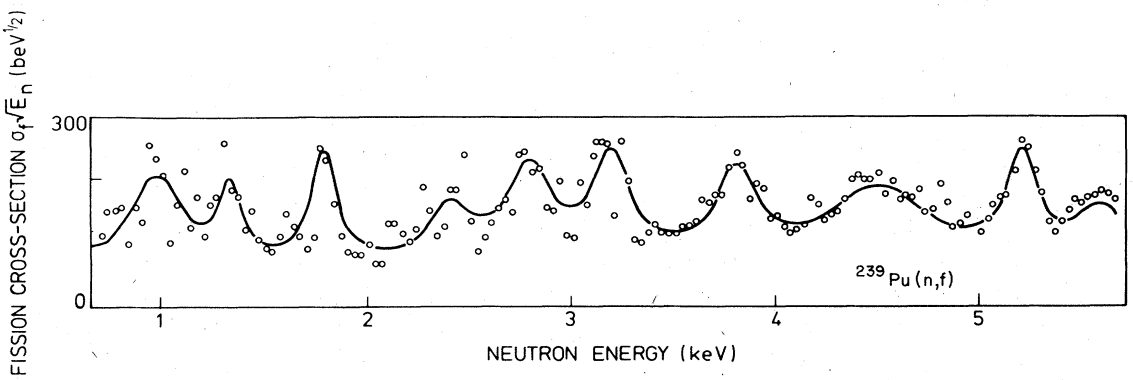

FIG. 123. Neutron fission cross section of ^{239}Pu [averaged over 33.3 eV intervals and fitted according to Eq. (6.90)] with parameters given in Table XXV.

VII. GENERAL TRENDS IN FISSION ABOVE AND BELOW THE BARRIER

A. Introduction

In Secs. IV–VI we have discussed all the special intermediate structure phenomena that can be expected as features of the double-humped barrier, and we have analyzed the considerable amount of data on these. Apart from such data there is a large amount of fission cross-section measurements available that do not show structure related to spectroscopic features of the secondary well, but nevertheless are directly dependent on the double barrier and can be made to yield important information for testing the theoretical development of deformed nuclear structure and for future use in applications of nuclear reaction theory.

Because of the wealth of parameters implied by the double-humped barrier, no single fission cross section and its functional dependence on excitation energy can be made to yield a unique set of barrier parameters for the relevant nucleus. Rather we must assume general trends for the barriers over the full set of actinides, being guided to some extent by the theoretical expectations, and, more importantly, by the deductions already made from the study of structure effects, principally those on yields of spontaneously fissioning isomers. Even with this use of systematic trends we still find it necessary to assume that certain parameters are unchanged over the full range of the actinides. These are principally the barrier penetrabilities ($\hbar\omega_A$ and $\hbar\omega_B$) and the level densities of intrinsic states at the barrier deformations. With this assumption of no variation (other than that due to the odd-even character of the nucleus) the barrier heights of a large number of the actinide series of nuclides can be deduced.

B. Statistical transmission coefficients

1. Elastic and inelastic neutron channels

The general concepts of the statistical treatment of cross sections of reactions that proceed through a compound nucleus mechanism were introduced in Sec. III.B. The simplest form of general equation for a reaction cross section integrated over all angles of emission of the outgoing particle is written in terms of the transmission coefficients introduced there as

$$\sigma_{cc'}^{(J\pi)} = \sigma_{c(\mathrm{CN})}^{J\pi}\frac{T_{(c')}}{\sum_{c''}T_{(c'')}} = \pi\lambda_c^2 g(J)\frac{T_{J\pi(c)}T_{(c')}}{\sum_{c''}T_{(c'')}}, \tag{7.1}$$

where the sum over c'' is to be made over all open channels. In applying this expression to fission cross sections in the barrier region of actinide nuclei the chief competitive processes are neutron emission to the ground and excited states of the target nucleus, and, to a lesser extent, radiative transitions to lower states of the compound nucleus.

If the compound nucleus is excited by the bombardment process to an excitation energy not too much above its neutron separation energy, and the magnitude of the compound nucleus formation cross section for each total angular momentum and parity J^π can be calculated fairly accurately, it is possible to use Eq. (7.1) in a full Hauser–Feshbach (1952) treatment in which the transmission coefficient for each excited state of the target nucleus is calculated from its energy of excitation and spin and parity quantum numbers. The full compound nucleus formation cross section for neutron bombardment at energy E_n of a nucleus of spin I and parity π_I, for example, is

$$\sigma_{n(\mathrm{CN})}(E_n) = \pi\lambda^2\sum_J\sum_{s=|I-1/2|}^{I+1/2}\sum_{l=|J-s|}^{J+s} g(J,I)T_{J\pi(n,ls)}(E_n) \tag{7.2a}$$

from which the components of given J^π are deduced. In Eq. (7.2a) the quantity s is the channel spin in the entrance channel and l is the neutron orbital angular momentum. The parity π of each term within the sum on the rhs of Eq. (7.2) is implied by the condition

$$(-1)^l\pi = \pi_I. \tag{7.2b}$$

The contribution of the neutron channels to the sum in the denominator of Eq. (7.1) is

$$\sum_{n''}T_{(n'')} = \sum_{I''}\sum_{i''}\sum_{s''=|I''-1/2|}^{I''+1/2}\sum_{l''=|J-s''|}^{J+s''} T_{J\pi(i'',l'')}(E_n-\varepsilon_{i''}), \tag{7.3a}$$

where $\varepsilon_{i''}$ is the excitation energy of the state i'' of the residual nucleus defining the channel n'' and I'' is its angular momentum. The sum over orbital angular momenta l'' on the rhs of (7.3) is further limited by the condition

$$(-1)^{l''}\pi = \pi_{i''}, \tag{7.3b}$$

$\pi_{i''}$ being the parity of the excited state of the residual

nucleus. The subscripts i'' and l'', which with s'', collectively define the channel, will often be denoted simply by n''.

Expressions for the individual neutron transmission coefficients can be obtained from R-matrix theory as follows. The basic expression for the ratio of average neutron width (in a single channel) of the R-matrix states to their level spacing is

$$\frac{\overline{\Gamma}_{J^\pi(n)}(E_n)}{D_{J^\pi}} = 2P_l(E_n)s_{JlI}(E_n)\,, \tag{7.4}$$

in which P_l is the penetration factor of Eq. (3.108) governing, in this case, the penetration through the centrifugal barrier, and s_{JlI} is the strength function describing the intensity of the R-matrix states just within the barrier, i.e., ratio of average reduced width $\gamma^2_{\lambda J^\pi(n,lI)}$ to level spacing D_{J^π}; it is governed in principle by the total angular momenta and excitation energies of the compound and target (or residual) nuclei, and the orbital angular momentum of the emitted neutron, but is much less sensitive to these factors than is the penetration factor.

At the relatively low bombarding energies at which cross sections are dominated by narrow resonances the transmission coefficient is deduced by averaging the cross section [of Eq. (3.41)] over the single-level Breit–Wigner form to give

$$T_{J^\pi(n)} = 2\pi\overline{\Gamma}_{J^\pi(n)}/D_{J^\pi}\,. \tag{7.5}$$

In fissile nuclei at low neutron bombarding energies, and at higher energies in other nuclei, the resonances are broader (relative to the level spacing) and the cross sections have interference, or "many-level" terms that lead to the breakdown of the simple linear relation (7.5). From simple considerations of statistical fluctuations in cross sections Feshbach *et al.* (1954) have proposed the expression

$$\sigma^{J^\pi}_{n,\mathrm{CN}} = \pi\lambda^2_n g(J)(1 - |\overline{U}_{nn}|^2) \tag{7.6}$$

for the definition of the compound nucleus formation cross section, $\overline{U}_{nn}$ being the collision matrix element averaged over many levels. If $\overline{U}_{nn}$ is calculated from R-matrix theory, with the possibility of direct reactions being ignored, Eqs. (7.6) and (3.41) lead to

$$T_{J^\pi(n)} = \frac{2\pi\overline{\Gamma}_{J^\pi(n)}/D_{J^\pi}}{(1+\pi\overline{\Gamma}_{J^\pi(n)}/2D_{J^\pi})^2}\,. \tag{7.7}$$

This expression is also obtained by Lane and Thomas (1958) as a result of deriving [using the reduced R-matrix formulation described in Sec.III.C.3.*g*(*iii*)] the average cross section for a specific entrance and exit channel. Their derivation rests on the restrictive assumption that in all other channels c'', which are eliminated from the reduced R matrix, $2\pi\Gamma_{(c'')}/D \ll 1$.

Equation (7.7) is approximated by Eq. (7.5) for small values of $\overline{\Gamma}_{(n)}/D$. Equation (7.7) reaches a maximum value of unity for $2\pi\overline{\Gamma}_{(n)}/D = 4$, and then diminishes to approach the value of $16/(2\pi\overline{\Gamma}_{(n)}/D)$. This asymptotic part of the behavior of the transmission coefficient is still a slightly dubious feature. Moldauer (1967) has examined its behavior through the intermediary of S-matrix theory [see Sec.III.C.3.*g*(*iv*)], calculating it for various simple models of the R-matrix parameters. He finds that relation (7.7) holds for one, two, and three channel models with uniform or harmonic behavior of the reduced widths of the levels. He also finds the relationship

$$T_{(c)} = 1 - \exp\left(-\frac{2\pi\overline{\Gamma}^{(H)}_{(c)}}{D}\right) \tag{7.8}$$

between the transmission coefficient and the S-matrix partial strength function $\overline{\Gamma}^{(H)}_{(c)}/\overline{D}$, giving a connection between S-matrix and R-matrix strength functions:

$$\frac{2\pi|\overline{\Gamma}^{(H)}_{(c)}|}{D} = 4\tanh^{-1}\left(\frac{\pi\overline{\Gamma}_{(c)}}{2D}\right) \quad \text{if } \frac{\pi\overline{\Gamma}_{(c)}}{2D} < 1$$
$$= 4\coth^{-1}\left(\frac{\pi\overline{\Gamma}_{(c)}}{2D}\right) \quad \text{if } \frac{\pi\overline{\Gamma}_{(c)}}{2D} > 1\,. \tag{7.9}$$

Numerical parameters for the transmission coefficients are usually calculated from an optical model of nuclear reactions, often with specific channels included by a coupled channel treatment. There are few experimental data to fully validate such calculations, and since the bulk of our calculations are expected to be rather insensitive to the details of the individual transmission coefficients we have chosen to use certain experimental data directly and apply them to a wider range of nuclides, orbital angular momenta, and excitation energy of the residual nucleus by the simplest possible extrapolation. The chosen experimental data are the neutron strength functions measured in low-energy neutron resonance cross sections of some of the commoner actinides. These are limited to s- and p-wave neutrons and have values of $s_0 = 0.025$ and $s_1 = 0.045$ for an assumed channel radius of 9 fm. For calculations at higher neutron energies, for inelastic channels and for other actinides, we have simply assumed that for all even values of orbital angular momentum the strength functions have the value of s_0 above, and for odd values of l the strength functions take the value of s_1.

At higher neutron energies our knowledge of the spectroscopy of the residual nucleus involved in such processes becomes incomplete or nonexistent except in a statistical sense, describable by a level density function. It is then necessary to make statistical estimates of the sum in Eq. (7.3a). A discussion of such estimates has already been given in Sec.IV.D.1.*a*, in connection with the competitive effects in the process of excitation of shape isomers. The relevant equations for the total transmission coefficient for neutron channels is Eq. (4.4) [note also the extra factor in Eq. (4.6)]. With the common assumption of a constant temperature form for the level density,

$$\rho^{(1)}_{\mathrm{eff}}(U) = C_1\exp(U/\theta_1)\,, \tag{7.10}$$

Equation (4.4) takes the simple form

$$T_{J^\pi(n,\mathrm{tot})} = \frac{2m\sigma_{n(\mathrm{CN})}}{\pi\hbar^2}C_1\theta_1(2J+1)f_{\mathrm{eff}}(J,2\theta_1)$$
$$\times\left[\theta_1\exp\left(\frac{E_n}{\theta_1}\right) - (E_n+\theta_1)\right]. \tag{7.11}$$

The level density parameters to be used in conjunction with these equations are described in Sec.VII.B.3. The value of the compound nucleus formation cross section can be calculated for one (entrance) neutron channel

using the strength functions adopted above; as implied in the derivation of Eq. (4.4) the value of this quantity is essentially constant above neutron energies of about 100 keV, its value being about 2.9 b.

2. Radiative transitions

At the present state of knowledge the competitive role of radiative transitions in the compound nucleus process must be treated entirely on a statistical basis. An individual transmission coefficient for γ-ray emission of energy ε_γ from highly excited states of energy E and total angular momentum and parity J^π can be written

$$T_{J^\pi(\gamma)}(E)=\frac{2\pi\Gamma_{J^\pi(\gamma)}}{D_{J^\pi}}=2\pi F(E,\varepsilon_\gamma)\,, \tag{7.12}$$

where $F(E,\varepsilon_\gamma)$ contains the energy dependence of the transition matrix element as well as the phase space dependence $\varepsilon_\gamma^{2L+1}$ depending on the multipolarity $L\pi_L$ of the transition concerned. The total radiative transmission coefficient is therefore

$$T_{J^\pi(\gamma,\mathrm{tot})}(E)=\frac{2\pi\Gamma_{J^\pi(\gamma,\mathrm{tot})}}{D_{J^\pi}} =\int_0^E d\varepsilon_\gamma F(E,\varepsilon_\gamma)\sum_L\sum_{J_f=|J-L|}^{J+L}\rho^{(c)}(E-\varepsilon_\gamma,J_f^{\pi f})\,, \tag{7.13}$$

in which $\rho^{(c)}(U,J_f^{\pi f})$ is the level density of the normal states of the compound nucleus at excitation U.

There is still a choice of model for the transition matrix element and its related energy dependence $F(E,\varepsilon_\gamma)$. There are two principal models of practical use at the present time.

In the Weisskopf strong coupling (SCD) model it is assumed that the spectral behavior $F(E,\varepsilon_\gamma)$ depends only on the phase space factor, $\varepsilon_\gamma^{2L+1}$. For the purposes of competition by radiation in particle emission and fission reactions we consider only dipole radiation, $L=1$, as being a significant contributor to the radiative process, so we set

$$F(E,\varepsilon_\gamma)=C_\gamma\varepsilon_\gamma^3 \tag{7.14}$$

and calculate the total radiative transmission coefficient from Eq. (7.13). The constant C_γ can be determined for actinides by adjusting the radiation width for slow neutron capture by ^{238}U to the experimental value of 24 meV (s-wave resonances corresponding to levels in ^{234}U with $J^\pi=\frac{1}{2}^+$).

The alternative model that is in general use is the giant dipole resonance (GDR) model. A more plausible model than the SCD, it is based on collective models of the giant dipole resonance observed in photonuclear absorption. From the form of the photonuclear cross section as given by the model of Goldhaber and Teller (1948) it can be deduced that the appropriate spectral factor is

$$F(E,\varepsilon_\gamma)=\frac{8}{3}\frac{NZ}{A}\frac{e^2}{\hbar c}\frac{(1+0.8x)}{mc^2}\frac{\Gamma_G\varepsilon_\gamma^4}{(\varepsilon_\gamma^2-E_G^2)^2+(\Gamma_G\varepsilon_\gamma)^2}\,, \tag{7.15}$$

where e is the electron charge, c the velocity of light, x the fraction of exchange force between neutron and proton in the nuclear Hamiltonian [Levinger and Bethe (1950)], and m the nucleon mass. For uranium and its neighbors the photoresonance parameters have values $E_G\approx 13$ MeV, $\Gamma_G\approx 4$ MeV. A more exact form of the spectral factor that is suitable for deformed nuclei is

$$F(E,\varepsilon_\gamma)=\frac{8}{3}\frac{NZ}{A}\frac{e^2}{\hbar c}\frac{(1+0.8x)}{mc^2}\sum_{i=1}^{2}\left(\frac{i}{3}\right)\frac{\Gamma_{iG}\varepsilon_\gamma^4}{(\varepsilon_\gamma^2-E_{iG}^2)^2+(\Gamma_{iG}\varepsilon_\gamma)^2}\,. \tag{7.16}$$

Veysière *et al.* (1973) give the following parameters for the two dipole components:

$$E_{1G}=11\text{ MeV},\quad \Gamma_{1G}=2.9\text{ MeV}$$
$$E_{2G}=14\text{ MeV},\quad \Gamma_{2G}=4.5\text{ MeV}\,.$$

The two models can be tested by their ability to reproduce the energy dependence of neutron capture cross sections and the capture gamma-ray spectra resulting from thermal neutron capture. However, the choice of level density model and parameters strongly affects the results of the calculations. Hence, the first kind of experimental datum is used to establish the effective temperature θ for the low-energy level densities of actinides (see Sec. VII.B.3), this temperature thus being dependent on the radiative model. It turns out that the SCD model requires a temperature θ of 0.55 MeV to fit the neutron radiative capture cross section of ^{238}U up to 3 MeV neutron energy. The temperature for the GDR model is 0.5 MeV, and this is much closer to the value implied by other evidence on the level density (such as neutron inelastic scattering).

With the appropriate value of the level density temperature taken as a fixed parameter for the model, the gamma-ray spectra can be calculated. In these calculations it is assumed that the secondary gamma-ray transitions of the cascade are governed by the same model as the primary transitions. The calculation for the SCD and GDR models are compared in Fig. 124 with experimental data from thermal neutron capture by ^{238}U. Agreement is not very good for the SCD model, but is distinctly better for the GDR model. Therefore the GDR model is adopted for the purposes of further analysis of fission cross-section data in this review.

3. Level densities for neutron and radiative channels

It is generally believed that the main contribution to the nuclear level density at moderate to high excitation energies comes from the combinations of nucleons (or quasinucleons) independently excited from the nuclear "vacuum" or ground state. To first order the independent-nucleon model gives rise to the well-known Fermi-gas type of level density relation:

$$\rho(U,J^\pi)=\frac{(2J+1)e^{-(J+1/2)^2/2\sigma^2}}{4\sigma^3(2\pi)^{1/2}}\rho(U)\,, \tag{7.17a}$$

$$\rho(U)=\frac{\sqrt{\pi}}{12}\frac{e^{2(aU)^{1/2}}}{a^{1/4}U^{5/4}}\,, \tag{7.17b}$$

$$\sigma^2=0.088a\theta A^{2/3}\,, \tag{7.17c}$$

$$\theta=(U/a)^{1/2}\,, \tag{7.17d}$$

$$a=\pi^2\tilde{\rho}_s/6\,. \tag{7.17e}$$

The predominant parameter here is a, which is related to the average density $\tilde{\rho}_s$ of single-nucleon states around the Fermi energy of the nucleus, the width of the averaging function being of the order of the temper-

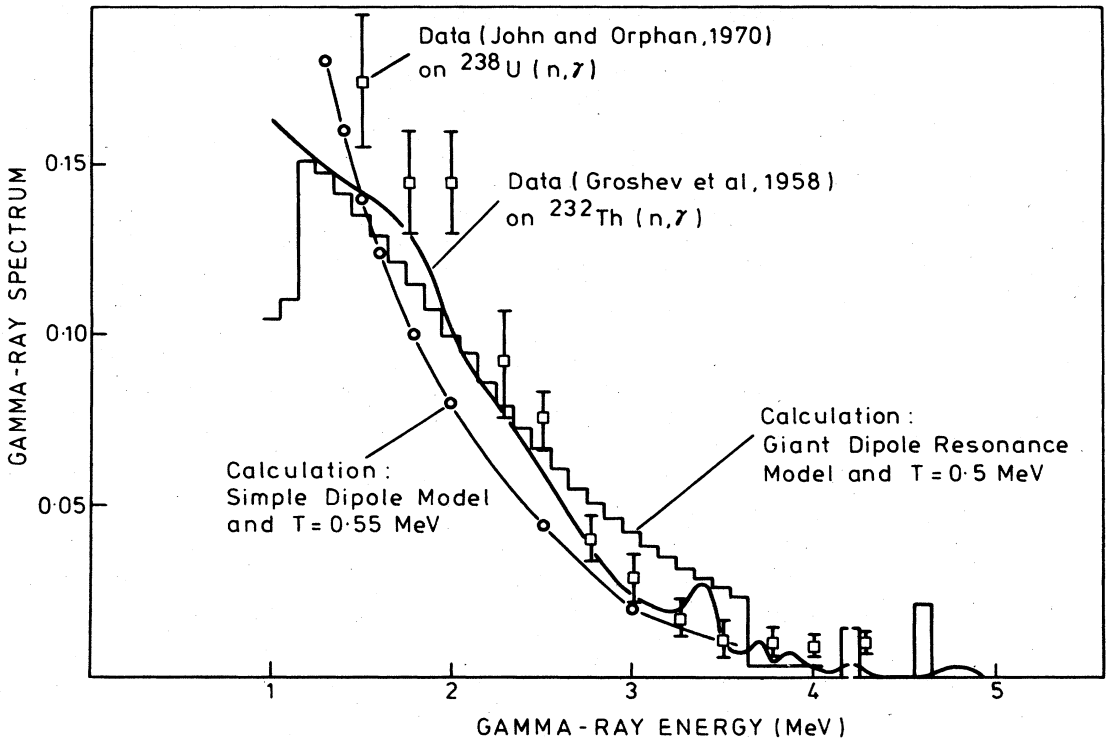

FIG. 124. Gamma-ray spectra resulting from low-energy neutron capture by ^{238}U and ^{232}Th compared with calculations on the strong coupling dipole and the giant dipole resonance model.

ature θ. The spin-dispersion parameter σ is also related to $\tilde{\rho}_s$ as well as to the spin distribution of the single-nucleon states; the numerical coefficient adopted in Eq. (7.17c) comes from a gross assessment of the spins of all the bound single-particle levels and is not expected to be an accurate value for individual nuclides, because the actual coefficient depends most strongly on the spins of the single-particle orbitals around the Fermi level.

The effective excitation energy U appearing in Eqs. (7.17) is adjusted from the true excitation energy E by an amount which depends on the odd or even nature of the nucleus. This adjustment was originally introduced empirically (Hurwitz and Bethe, 1951), but is now understood as an asymptotic consequence of the more realistic model of independent quasinucleons. The quasinucleons emerge as a consequence of the short-range pairing force between nucleons which results in all nucleons paired in single-particle orbitals becoming involved in a correlated motion which depresses the energy of the correlated state. It costs energy to create the quasiparticles by placing unpaired nucleons in particular orbitals. This energy cost is over and above that from the single-particle energies due to different occupation of the orbitals, and at the lowest level it amounts to an energy gap 2Δ. In an even nucleus this gap separates the ground state from the lowest of the noncollective states, which have the character of two quasiparticles. In an odd-mass nucleus it separates single quasiparticles from three quasiparticle states. The availability of an increasing number of quasiparticles to form independent quasinucleon states gives rise to a rapidly increasing density of such states (by simple combinatorial considerations). According to this model there are sudden jumps in density at energy intervals of approximately 2Δ, but numerical calculations indicate that the sharpness of the jumps becomes very much reduced at the higher excitations. Because of this smearing it appears that the level density can be approximated by a constant temperature form, Eq. (7.10). An odd nucleus is already expected to have a high density of two quasiparticle states at very low excitation energy. This density will be roughly equal to that of an even nucleus just above the energy gap at $E = 2\Delta$, although rather lower than that of an odd-mass nucleus at this excitation energy. Thus even at low excitation energies an odd-even effect in level densities, and hence the need for a possible adjustment in effective excitation energy, is found to exist.

At somewhat higher energies a certain "critical energy" is expected in the quasiparticle model, above which the single-particle orbitals around the Fermi energy are mostly occupied (statistically) by unpaired nucleons, and the operation of the pairing interaction in forming a correlated state is thereby inhibited. Above this critical energy the independent-nucleon model, described by Eq. (7.17), of level densities gains a certain validity. However, the depression of the correlated ground state by the pairing force gives rise to a modification of the effective excitation energy to be used in Eq. (7.17). For an even nucleus the effective lowering of the ground-state energy, and hence the correction to be subtracted from the true excitation energy to give the effective excitation energy U, is

$$E - U = \tfrac{1}{4}\tilde{\rho}_s\Delta^2. \qquad (7.18a)$$

TABLE XXVI. Values of empirical even proton and neutron number excitation energy corrections for the independent-particle model level density formulation. Bracketed values are assumptions; other values from Gilbert and Cameron (1965).

Z	$P(Z)$	N	$P(N)$
90	0.78	138	(0.60)
92	0.69	140	0.60
94	0.61	142	0.57
96	0.72	144	0.49
98	(0.78)	146	0.43
		148	0.50
		150	0.39
		152	(0.45)
		154	(0.45)

For odd mass and odd nuclei this correction should be reduced by the amounts Δ and 2Δ, respectively, as discussed above. In practice empirical corrections are usually employed for the effective excitation energy. Gilbert and Cameron (1965) give

$$U = E - P(Z) - P(N), \tag{7.18b}$$

the P functions being zero for odd values of proton and neutron number. The values of P for even Z and N, which we use in our own analyses, are given in Table XXVI. In normal use, the Fermi-gas level density formula employs the effective excitation energy Eq. (7.18b), and the constant a is empirically adjusted to observed level densities from neutron resonance spectroscopy.

Direct numerical calculations of level densities in both the independent nucleon and quasinucleon models have been made, the actual density of combinations from the detailed spectrum of single-particle orbitals being computed. For deformed nuclei such calculations describe the density of intrinsic states; they therefore fall far short of the level density actually observed because there is a large contribution of collective states of rotational character (Bjørnholm, Bohr, and Mottelson, 1974). The contribution of these depends directly on the density of the intrinsic states, the latter being assumed to be the bandhead states of the rotational levels. To obtain the full functional dependence on energy and angular momentum it is necessary to know, or assume, a spin dependence for the bandhead states. In a deformed nucleus with axial symmetry the projection Ω of the angular momentum of a particle or quasiparticle on the symmetry axis is a good quantum number. Several independent particles summing their spin projections in a statistical manner to give a total spin projection K can therefore be expected, to good approximation, to give rise to a Gaussian distribution for the dependence of the bandhead level density on this quantity:

$$\rho_{\mathrm{BH}}(U,K) = \frac{\rho_{\mathrm{BH}}(U)}{\sigma_K(2\pi)^{1/2}}\, e^{-K^2/2\sigma_K^2}. \tag{7.19}$$

In this expression both positive and negative values of K are implied. In fact, for a reflection and axially symmetric nucleus (the latter is a necessary condition for K to be a good quantum number) the allowed states must necessarily be a correctly phased combination of a wave function of positive K and its conjugate form with negative K. By convention these states are assigned positive K values only, and in this case an extra factor of 2 must be included on the right-hand side of Eq. (7.19) to achieve normalization. In the special term with $K=0$ this would seem to imply an imbalance in the density of such states. In fact, the condition of symmetry on rotation through π about an axis perpendicular to the symmetry axis of the nucleus, which is assumed to be a normal condition of the states we are discussing, leads to the omission of every alternate state from the rotational sequence built on the $K=0$ bandhead. Invariance of the eigenstates to the operation of rotation through π implies the existence of a quantum number r with eigenvalues ± 1. The members of the rotational band have allowed angular momentum $(-1)^I = r$. Thus, to a good degree of accuracy, the total density of bandhead and rotational states will be obtained by using Eq. (7.19) for $K=0$ states without the extra factor of 2 required for $K \neq 0$ states by the condition of π-rotational symmetry.

Examination of the Nilsson model of single-particle schemes in the actinide region indicates that for single-particle neutron levels $(\bar{\Omega}_N^2)^{1/2} \approx 3.5$ and for single-particle proton levels $(\bar{\Omega}_p^2)^{1/2} \approx 3.0$. This leads to an estimate of $\sigma_K \sim (2n)^{1/2} \times 3.25$ at about $E \sim (2n+1)\Delta$ for an even nucleus, and at correspondingly lower energies for odd mass and odd nuclei.

The total density of nuclear states as a function of excitation energy and total angular momentum I is finally determined by adding to the bandhead density the contribution of the rotational states:

$$\rho(U,I) = \rho_{\mathrm{BH}}(U, K=I) + \sum_{K=-(I-1)}^{I-1} \rho_{\mathrm{rot}}(U,K,I) \tag{7.20a}$$

$$\rho_{\mathrm{rot}}(U,K,I) = \rho_{\mathrm{BH}}\left[U - \left\{I(I+1) - K^2\right\}\frac{\hbar^2}{2\mathcal{I}}, K\right], \tag{7.20b}$$

where $\mathcal{I}$ is the effective rotational moment of inertia of the nucleus about an axis perpendicular to the symmetry axis. If the bandhead density has a simple constant temperature form [as Eq. (7.10)] then we obtain

$$\rho(U,I) = \frac{Ce^{U/\theta}}{\sigma_K(2\pi)^{1/2}} \exp\left[\frac{-I(I+1)\hbar^2}{2\mathcal{I}\theta}\right] \sum_{K=-(I-1)}^{I-1} \times \exp\left[K^2\left(\frac{\hbar^2}{2\mathcal{I}\theta} - \frac{1}{2\sigma_K^2}\right)\right]. \tag{7.21}$$

For small values of the coefficient $(\hbar^2/2\mathcal{I}\theta - 1/2\sigma_K^2)$ (compared with I^2) this expression tends to the form

$$\rho(U,I) \approx (2I+1)e^{-I(I+1)/2\sigma^2}\rho_0(U), \tag{7.22a}$$

where

$$\sigma = (\mathcal{I}\theta/\hbar^2)^{1/2}, \tag{7.22b}$$

and

$$\rho_0(U) = \frac{C}{\sigma_K(2\pi)^{1/2}}\, e^{U/\theta}. \tag{7.22c}$$

For states of low angular momentum this represents an increase over the density of bandhead states alone by a factor of approximately $2\sigma_K^2$.

With this rotational enhancement effect it is possible to make explicit calculations of level densities from the independent-particle and quasiparticle models that can

be usefully used in analysis of cross-section data. This is the approach adopted in the work of Gavron *et al.* (1976). In our analysis of data for this review we have preferred to adopt empirical information on level density parameters, using the formulations outlined above for purposes of interpolation and extrapolation.

In this spirit we employ a level density analysis based on the approach of Gilbert and Cameron (1965), but with a special treatment of the very low-energy regions of even and odd-mass nuclides. This very low-energy region is just the energy gap $E = 0-2\Delta$. For even nuclides the energy gap contains only a very few levels of collective type, such as beta, gamma, and octupole vibrations with their accompanying rotational bands. The levels of odd-mass nuclei consist mainly of single quasinucleon excitations, again accompanied by rotational bands. A crude level density approximation to these spectra would be, in first order, simply independent of energy, and this we have adopted, except that in very many of our analyses the detailed spectra themselves have been used in this energy gap region. With an energy-independent level density form

$$\rho(U, J^{\pi}) = C(2J+1)e^{-(J+1/2)^2/2\sigma^2}, \tag{7.23}$$

the values of C and σ have been chosen as $C \approx 0.225$ MeV^{-1}, $\sigma \approx 4$ for even nuclides, and $C \approx 0.625$ MeV^{-1}, $\sigma \approx 4.5$ for odd-A nuclides.

At intermediate energies we have adopted Gilbert and Cameron's suggestion of a constant temperature form

$$\rho(E, J^{\pi}) = C(2J+1)e^{-(J+1/2)^2/2\sigma^2}e^{E/\theta}. \tag{7.24}$$

The data required to parametrize this formula for the actinides are very sparse. In particular, for the value of the spin-dispersion coefficient σ we have resorted to calculated estimates as given by the independent-particle formula, Eq. (7.17), and the rotational band enhancement, Eq. (7.21). The consensus of such values is collected in Table XXVII. Some theoretical guidance is necessary for the values of the constant C also. Experimental spectroscopic evidence (which again is much sparser than we would wish) indicates that $C \approx 3.5$ for odd actinides. Our discussion of the quasi-independent nucleon model indicates that this should be reduced by a factor of approximately $e^{-\Delta/\theta}$ for odd-A nuclides and $e^{-2\Delta/\theta}$ for even nuclides. The temperature θ has been determined from a selection of nuclear reactions, subjected to statistical theory analysis. The spectra of inelastically scattered neutrons from ^{238}U and ^{232}Th, with neutron bombarding energies up to 5 MeV, have been measured by Batchelor *et al.* (1965) and analyzed to give $\theta \sim 0.45-0.5$ MeV. We have analyzed the neutron radiative capture cross section of ^{238}U up to 3 MeV [as evaluated by Sowerby *et al.* (1974)]. This depends on the temperature representing the level density of residual states in ^{238}U involved in inelastic neutron competition as well as the temperature of the final states excited by primary radiative transitions in ^{239}U. The calculation of the radiative transmission coefficient from the latter level density also involves an assumption about the radiative mechanism. With the assumption of the GDR model (see Sec. VII B.2) the final (common) temperature for the two level densities that best fits the data is $\theta = 0.5$ MeV. The choice of the SCD model is $\theta = 0.55$ MeV. We consider that the best consensus of experimental data for the actinides yields $\theta = 0.5$ MeV. The collected parameters for this intermediate energy region are given in Table XXVII.

TABLE XXVII. Level density parameters for the actinides at intermediate excitation energies (except where temperatures are modified by Table XXVIII). Constant temperature forms of type $\rho(J^{\pi}) = (2J+1)\, e^{-(J+1/2)^2/2\sigma^2}$. $Ce^{E/\theta}$ are assumed.

Type	Energy range	C (MeV^{-1})	θ (MeV)	σ
Even	1 MeV$-E_{IP}$	0.225	0.5	5.3
Odd-A	1.2$-E_{IP}$	0.9	0.5	6.1
Odd	0$-E_{IP}$	3.75	0.5	6.1

At higher energies the independent-particle model formulation, described by Eqs. (7.17), has been adopted for our analysis. The value of the Fermi-gas parameter a has been fixed by the data from neutron resonance cross sections at an excitation energy equivalent to the neutron separation energy of the compound nucleus. The Fermi-gas parameters of nuclides for which neutron resonance data have not been measured have simply been assumed by extrapolation from neighboring nuclides. We have defined the energy E_{IP} demarcating the intermediate energy regime from the higher-energy regime by the simple condition of equality between the density given by the constant temperature formula to that of the independent-particle formula. In some cases the energy E_{IP} cannot be so defined, the density from the latter formula being everywhere lower than that of the former at excitation energies lower than the neutron separation energy. In these cases we have assumed the intermediate energy region to include the neutron separation energy and we have adjusted the temperature so that Eq. (7.24) reproduces the neutron resonance density. The collected parameters for the actinides are given in Table XXVIII.

C. Transmission coefficients for fission

1. Statistical expressions

The statistical theory for fission decay through the double-humped barrier has been treated in Sec. III.B. From Eq. (3.49) for the fraction of decay by fission we see that the statistical transmission coefficient for fission can be written in terms of transmission coefficients across barriers A and B separately as

$$T_{(f)} = \frac{T_{(A)}T_{(B)}}{T_{(A)} + T_{(B)}} \tag{7.25}$$

(with neglect of the very small transmission coefficient for decay of class-II states by particle or radiative emission). The calculation of the statistical transmission coefficients $T_{(A)}$ and $T_{(B)}$ is based on the original statistical theory of Bohr and Wheeler (1939) and the transmission coefficient of Hill and Wheeler (1953) for quantal tunneling through an inverted parabolic barrier [see Sec. III.A.1.b(*iii*), Eq. (3.17)]. Denoting either A or B by D the required expression is

TABLE XXVIII. Level density parameters for the actinides at higher excitation energies. Bracketed entries of a and E_{IP} are assumed values. Entries labeled + are from Gilbert and Cameron (1965). Neutron separation energies S_n are from the tables of Wapstra and Gove (1971).

Nucleus	I^π (ground state)	θ (MeV)	E_{IP} (MeV)	a (MeV^{-1})	S_n (MeV)	$D(0^+, S_n)$ (eV)	$D_{l=0}(S_n)$ (eV)	$D_{obs}(S_n)$ (eV)
^{228}Th	0^+				7.134			
^{229}Th	$\frac{5}{2}^+$		(3.27)	(31.6)	5.233			
^{230}Th	0^+		4.7	29.31	6.787	4.13	0.39	0.41
^{231}Th	$(\frac{5}{2}^+)$		3.27	31.6	5.129	16.5	8.25	7.7
^{232}Th	0^+		4.45	29.44$^+$	6.431	7.56		
^{233}Th	$(\frac{1}{2}^+)$		3.27	31.6	4.789	36.0	18.0	16.7
^{234}Th	0^+		(4.45)	(29.44)	6.179			
^{231}Pa	$\frac{3}{2}^-$		3.82	28.76$^+$	6.863	(1.033)		
^{232}Pa	(2,3)		3.6	29.0	5.567	3.46	0.46	0.41
^{233}Pa	$\frac{3}{2}^-$		4.0	28.88$^+$	6.511	(1.79)		
^{234}Pa	(4^+)		3.1	29.8	5.197	5.26	0.69	0.69
^{232}U	0^+		5.0	27.97$^+$	7.278	2.41	0.22	
^{233}U	$\frac{5}{2}^+$		4.4	29.05	5.737	(8.54)	4.31	4.1
^{234}U	0^+	0.519		26.79$^+$	6.840	8.43	0.804	0.6
^{235}U	$\frac{7}{2}^-$		4.4	29.05$^+$	5.307	(22.7)	11.5	10.6
^{236}U	0^+		4.17	28.51$^+$	6.536	6.43	0.49	~0.5
^{237}U	$\frac{1}{2}^+$		4.4	29.05	5.129	(32.9)	16.9	17.3
^{238}U	0^+		3.87	28.51	6.144	12.4	3.1	2.5
^{239}U	$\frac{5}{2}^+$		3.36	30.5	4.863	(36.6)	18.3	20.8
^{240}U			(3.87)	(28.51)	5.924			
^{234}Np	(0^+)	(0.518)			6.119	1.98		
^{235}Np	$\frac{5}{2}^+$	(0.5)			6.992			
^{236}Np	(6^-)	(0.518)			5.691	4.53		
^{237}Np	$\frac{5}{2}^+$		5.0	27.37$^+$	6.591	2.6	0.45	
^{238}Np	2^+	0.518		28.0	5.486	6.85	0.59	0.69
^{239}Np	$\frac{5}{2}^+$				6.227			
^{235}Pu	$\frac{5}{2}^+$				6.25			
^{236}Pu	0^+				7.357			
^{237}Pu	$(\frac{7}{2}^-)$				5.859			
^{238}Pu	0^+		3.97	28.51	6.998	2.32		
^{239}Pu	$\frac{1}{2}^+$		5.4	28.0	5.657	14.5	7.3	9.5
^{240}Pu	0^+		4.15	27.41$^+$	6.524	7.99	2.0	2.25
^{241}Pu	$\frac{5}{2}^+$		4.4	28.5	5.243	28	14.0	12.7
^{242}Pu	0^+		3.6	29.0	6.305	7.44	0.67	~0.65
^{243}Pu			3.5	29.5	5.043	29.6	14.8	17
^{244}Pu	0^+		(3.6)	(29.0)	6.018	10.7		
^{245}Pu			2.66	32.0	4.76	23.6	11.8	$\lesssim$14
^{240}Am	(3^-)				5.94			
^{241}Am	$\frac{5}{2}^-$	0.518		26.0	6.66	(2.54)		
^{242}Am	1^- (I.S. 5^-)	0.528		27.2	5.535	7.5	0.75	0.77

TABLE XXVIII. (*Continued.*)

Nucleus	I^π (ground state)	θ (MeV)	E_{IP} (MeV)	α (MeV^{-1})	S_n (MeV)	$D(0^+, S_n)$ (eV)	$D_{I=0}(S_n)$ (eV)	$D_{obs}(S_n)$ (eV)
^{243}Am	$\frac{5^-}{2}$	0.518		26.0	6.425 (+0.049 for ^{242m}Am)	(4.57)	0.33	$\lesssim$0.67 (refers to I.S. target)
^{244}Am		0.509		28.2	5.365	7.07	0.70	0.67
^{245}Am		(0.528)			6.047			
^{246}Am		(0.528)			5.06			
^{247}Am		(0.528)			5.86			
^{241}Cm	$(\frac{1^+}{2})$	(0.521)			6.07	(9.71)		
^{242}Cm	0^+	(0.534)		25.7	6.972	9.53		
^{243}Cm	$\frac{5^+}{2}$	(0.521)		27.5	5.705			
^{244}Cm	0^+	(0.534)		25.7	6.796	13.2		
^{245}Cm	$\frac{7^+}{2}$	0.521		27.5	5.52	28.4	14.2	14.8
^{246}Cm	0^+	0.520		25.7	6.452	18.2	1.54	1.55
^{247}Cm		0.544		27.0	5.156	85.3	42.7	40.8
^{248}Cm	0^+	0.504		26.5	6.209	20.0		1.33
^{249}Cm		0.495		29.5	4.713	81.7	41.3	35
^{250}Cm		(0.504)		26.5	5.91			
^{249}Bk	$\frac{7^+}{2}$	(0.5)			6.214	(4.46)		
^{250}Bk	2^-	(0.5)			4.968	12.9		
^{248}Cf	0^+				7.03			
^{249}Cf	$\frac{9^-}{2}$				5.60			
^{250}Cf	0^+	0.51		27.5	6.62	10.3	0.68	$\lesssim$1.2
^{251}Cf	$\frac{1^+}{2}$				5.11			
^{252}Cf	0^+				6.17			
^{253}Cf	$(\frac{7^+}{2})$		3.4	32.0	4.83	(33.8)	16.9	16.0

$$T_{J^\pi(D)}(E) = \int_0^\infty d\epsilon\, \rho_D(\epsilon, J^\pi)\left[1+\exp\left(-\frac{2\pi(E-\upsilon_D-\epsilon)}{\hbar\omega_D}\right)\right]^{-1}, \tag{7.26}$$

where ρ_D is the density of intrinsic states χ_μ at the barrier deformation η_D. We assume henceforth, unless specifically stated, that this has the constant temperature form

$$\rho_D(U, J^\pi) = C_D(2J+1)e^{-(J+1/2)^2/2\sigma_D^2}e^{U/\theta_D}, \tag{7.27}$$

the effective excitation energy U being measured from the peak barrier potential υ_D.

By using Eq. (7.27) simple approximations can be found for the barrier transmission coefficients. For $E > \upsilon_D$

$$T_{J^\pi(D)} = \theta_D C_D(2J+1)e^{-(J+1/2)^2/2\sigma_D^2}\left\{\left[\exp\left(\frac{E-\upsilon_D}{\theta_D}\right)-1\right]+2\exp\left(\frac{E-\upsilon_D}{\theta_D}\right)\left(\frac{\hbar\omega_D}{2\pi\theta_D}\right)^2[\pi^2/12+\cdots]\right.$$
$$\left.+\left[\sum_{n=1}^{n_{cut}}(-)^{n+1}\frac{\hbar\omega_D}{2\pi n\theta_D+\hbar\omega_D}\exp\left(\frac{-2\pi n(E-\upsilon_D)}{\hbar\omega_D}\right)+\cdots\right]\right\}. \tag{7.28}$$

The terms neglected in the second square bracket of the rhs are of order $(\hbar\omega_D/2\pi\theta_D)^4$ and higher, and those neglected in the third square bracket are those remaining after the practical computational summation at $n=n_{cut}$. For $E<\upsilon_D$

$$T_{J^\pi(D)} = \theta_D C_D(2J+1)e^{-(J+1/2)^2/2\sigma_D^2}\times\sum_{n=1}^{\infty}(-)^{n+1}\frac{\hbar\omega_D}{2\pi n\theta_D-\hbar\omega_D}\exp\left(\frac{2\pi n(E-\upsilon_D)}{\hbar\omega_D}\right). \tag{7.29}$$

If we consider only the leading term of this we see that for $E \ll \mathcal{V}_D$ the transmission coefficient can be described as the product of the Hill–Wheeler transmission factor and an effective number of (degenerate) channels equal to

$$n_{\text{eff}} \approx \rho_D(E - \mathcal{V}_D, J^\pi)\left(\frac{\theta_D \hbar\omega_D}{2\pi\theta_D - \hbar\omega_D}\right). \tag{7.30}$$

2. Level densities of intrinsic states at barrier deformations

It is believed that the density of intrinsic states at extended deformations of the nucleus, such as those of the barriers, can be accounted for by models such as the independent-particle models discussed in Sec. VII.B.3 with the addition of rotational state enhancement. Such models have been used directly in analysis of fission cross-section data, notably by Britt *et al.* (1973), the basic single particle level schemes required for the computations being taken from the work of Bolsterli *et al.* (1972) [described briefly in Sec. III.A.1.*c*(*ii*)].

As a consequence of the Strutinsky theory on nuclear energies as a function of nuclear deformation it is expected that the single-particle state densities at the Fermi energy for the barrier deformations of actinide nuclei should be considerably higher than those at the stable or meta-stable deformations. This has two consequences for the density of intrinsic states. One is that the energy gap in the density of barrier states should be greater than those at stable deformations. The other is a tendency to an increase in the level density owing to the increase in the Fermi-gas parameter a, Eq. (7.17e). Calculations based on the independent quasiparticle model that include both these effects indicate that the net effect is a reduction in level density at the barriers at effective excitation energies up to about 8 MeV (Britt *et al.*, 1973). These effects are expected to be greater at barrier A than at barrier B, at which reflection asymmetric shapes are calculated to have several MeV greater stability than symmetric shapes, with consequent decrease in single-particle state density. At barrier B, therefore, it can be expected that the density of independent quasiparticle states will be quite similar to that of the stable nucleus.

On the other hand, lack of symmetry of the nuclear shape at the barrier deformations can increase the contribution of the rotational states built on each independent particle bandhead (Bjørnholm, Bohr, and Mottelson, 1974). The simplest enhancement of rotational states is exhibited by a deformed shape which violates both the parity operation $\mathcal{P}$ and that of rotation through π about an axis perpendicular to the symmetry axis $\mathcal{R}$, but invariant to the product of these operations, which describes reflection $\mathcal{S}$ in a plane containing the symmetry axis. This invariance implies that eigenstates with K (spin projection on the symmetry axis) = 0 have quantum number $s = \pm 1$. Unlike the states with $\mathcal{R}$ invariance (discussed briefly in Sec. VII.B.3) with quantum number $r = \pm 1$, the rotational bands built on these states have a complete sequence of angular momentum but their parity is constrained by the condition $\pi = s(-1)^I$. States with $K > 0$ also have a complete sequence of angular momenta in the rotational band and also have both parities for each rotational state. Thus the density of rotational states is just twice that in which the nuclear shape is invariant to the $\mathcal{P}$ and $\mathcal{R}$ operations. The nuclear energy calculations described in Sec. II.A.1.*d*(*iii*) indicate that $\mathcal{S}$ invariance but lack of $\mathcal{R}$ invariance is the condition to be expected for the nuclear shape at the outer barrier deformations.

Maximum enhancement of the rotational states is obtained when the nuclear shape is completely lacking in symmetry. In this case the nucleus will be able to make collective rotations about the three (perpendicular) body-fixed axes, with the result that there will be $2I+1$ different states for every value of rotational angular momentum I in each rotational band. If each of these states is labeled by a number τ, the total level density based on a density of bandhead states $\rho_{\text{BH}}(U)$ is

$$\rho(E, I) = \sum_{\tau=1}^{2I+1} \rho_{\text{BH}}[E - E_{\text{rot}}(\tau, I)] \approx (2I+1)\rho_{\text{BH}}(E) \tag{7.31}$$

if $E_{\text{rot}}(\tau, I)$ is much less than the temperature θ of the level density formula for ρ_{BH}. For this expression we note that the density of bandhead states will be approximately double that of axially symmetric nuclei because K is no longer a good quantum number and states of negative K therefore contribute independently to the basis. Equation (7.31) is thus higher by a factor $\sim\sigma_K(8\pi)^{1/2}$ than the density for an axially symmetric nucleus with $\mathcal{R}$ invariance, Eq. (7.21).

The rotational states of the completely asymmetric nucleus can be built up from basis states of specified symmetry with respect to rotations through π about the three body-fixed axes. The quantum numbers for these rotations fall into four sets: $(r_1 r_2 r_3) = (+1, +1, +1)$, $(+1, -1, -1)$, $(-1, +1, -1)$, $(-1, -1, +1)$. Any one of these sets is appropriate for the description of a single rotational band of a nucleus that lacks axial symmetry but otherwise possesses the symmetry of an ellipsoid. This is expected to be the condition of the deformed nucleus as it passes over the inner barrier A. The density of its rotational states therefore is expected to be one quarter of the density for the completely asymmetric nucleus, i.e., $\sigma_K(\pi/2)^{1/2}$ times that of the normally deformed nucleus with axial and $\mathcal{R}$ symmetry [Eq. (7.22)].

These theoretical expectations on the intrinsic state densities at the barrier deformations are at least semiquantitatively confirmed by an analysis of the data on fission cross sections. In this analysis we are guided by the relative heights of barriers A and B as determined by the study of shape isomer yields (Sec. IV.D), and, where these give no information, the calculation of energy surfaces, (Sec. II.A.1). From this evidence it is clear that the outer barrier of Cm, Am, and, to a lesser extent, of Pu, nuclides is much lower than the inner barrier.

The trend of this evidence indicates that the two barriers will be of comparative height for U and Np nuclides. The theoretical evidence indicates a higher outer barrier for the Th nuclides. The magnitudes of the cross section, well above the barrier, depend mainly on the higher barrier, both on its height and the density of intrinsic states. Neutron competition, the main

factor in which is the normal level density, provides the measure of the latter quantity. After making due allowance for the effect of barrier height it appears that the fission cross sections of Th and Pa nuclides are relatively weaker than those of the Pu and higher charge nuclides. The numerical factors for enhancement of the barrier state densities over the level densities of normally deformed nuclei turn out to be ~4 for barrier A and ~2 for barrier B.

Owing to the wide range of numerical parameters, chiefly of the rotational enhancement effects, permitted within our current theoretical understanding of the barrier level densities, we have based our analysis of fission barriers, so far as possible, on experimental evidence for these densities. This experimental evidence is essentially limited to the fission cross sections themselves. But the deduction of such level densities from fission cross sections is very dependent upon assumptions about the barrier height; and to some extent the converse is true—deductions about barrier heights are affected by assumptions about the barrier level densities. For the present work we have attempted to find, for odd and odd-A compound nuclei, simple constant temperature forms that will satisfy a few key cross sections that are well measured. For odd-A nuclides these are the fission cross sections of ^{246}Cm, ^{238}U, and ^{232}Th, and for odd nuclides the fission cross sections of ^{237}Np and ^{241}Am. The cross section of ^{246}Cm is chosen because of the evidence that the outer barrier of ^{247}Cm is some 1.3 MeV below the inner barrier. The cross sections of ^{238}U and ^{232}Th are chosen as being two of the best-known cross sections with rather close barrier peaks but requiring the dominant barrier to be reversed between the two cases; comparison of these two indicates the necessity of the density at deformation B to be lower than that at A.

Barrier densities of even nuclides are assumed to be more complex; an energy gap containing a limited spectrum of collective levels, different for barriers A and B, according to the shape symmetry indicated by theory for the two deformations, is postulated, beyond which a sequence of constant temperature forms is found. At deformation B a vibration-rotation band describing mass asymmetry vibration and carrying quantum number $K^{\pi}=0^{--}$ is assumed to coexist with the "ground" state $K^{\pi}=0^{++}$ band. The only other vibration-rotation band that is believed, possibly, to exist within the energy gap is the gamma vibration with $K^{\pi}=2^{+}$; its excitation energy is placed, arbitrarily, at about 1 MeV, but there is no strong reason why it should be similar to its value at the stable deformation. The other characteristic vibration-rotation band to be found in the spectrum of a normally deformed nucleus is the one-phonon beta vibration, but this expresses excited motion in the deformation degree of freedom η and is not to be counted among the intrinsic states. At deformation A $\mathcal{R}$ symmetry holds but axial asymmetry implies that the gamma vibration near the top of the energy gap is to be replaced by extra rotations in the ground-state band. The members of the rotational band, which has the set of quantum numbers $(r_1r_2r_3)=(+++)$, are as follows: $I=0,\ 2^2,\ 3,\ 4^3,\ 5^2,\ 6^4\ \ldots$. The exact energies of these states will depend on the moments of inertia for rotation about the three principal axes of the nuclear shape. With the low-lying spectra thus postulated and barrier heights roughly fixed from particle-transfer induced fission reactions (which can explore fission from excited states below the neutron separation energy of the compound nucleus) we have determined the constant temperature barrier level densities from the neutron-induced fission cross sections of ^{235}U and ^{239}Pu, two of the most accurately known of all cross sections.

The barrier level density parameters thus determined and used in our analysis of data on other actinide nuclides are presented in Table XXIX. The reference barrier parameters of the compound nuclides ^{236}U and ^{240}Pu are as follows:

$$\begin{aligned} &^{236}\mathrm{U}: \upsilon_A = 5.63\ \mathrm{MeV},\ \hbar\omega_A = 1.04\ \mathrm{MeV},\\ &\upsilon_B = 5.53\ \mathrm{MeV},\ \hbar\omega_B = 0.6\ \mathrm{MeV}\\ &^{240}\mathrm{Pu}: \upsilon_A = 5.57\ \mathrm{MeV},\ \hbar\omega_A = 1.04\ \mathrm{MeV},\\ &\upsilon_B = 5.07\ \mathrm{MeV},\ \hbar\omega_B = 0.6\ \mathrm{MeV}. \end{aligned} \tag{7.32}$$

TABLE XXIX. Barrier level density parameters employed for actinide nuclei. Level densities take the form of Eq. (7.27). The parameters given in the last line (for odd nuclides) are only suggested values; no experimental data have been analyzed beyond 2 MeV.

Type	Energy range (MeV)	C_A (MeV^{-1})	θ_A (MeV)	C_B (MeV^{-1})	θ_B (MeV)	σ
Even	1.0–2.5	0.021 35	0.3005			5.7
	2.5–2.8	1.435×10^{-4}	0.1877			6.0
	2.8–≳5	1.6	0.5			6.3
	1.0 – 1.4			0.021 35	0.3005	5.7
	1.4–2.0			0.198	0.576	5.7
	2.0–3.05			0.009 65	0.308	6.0
	3.05–≳5			0.426 5	0.5	6.3
Odd-A	0–≳3	6.8	0.48	3.4	0.48	6.4
Odd	0–~2	11.5	0.36	5.75	0.36	6.4
	~2–≳5	54.5	0.5	27.2	0.5	6.4
			(Suggested: no data analyzed beyond ~2 MeV)			

The number of parameters available for fitting the cross-section data of these nuclides is excessive for a unique fit. Some of the factors that must be taken into account in assessing the significance of this particular choice are discussed in Sec. VII.D.

3. Effects due to intermediate structure

The effect on fission cross sections of intermediate structure due to the hierarchy of class-II levels associated with the secondary well has already been discussed in detail in Secs. V and VI. Here we summarize the implications for extraction of the fission barrier parameters.

The effects will be confined, in the main, to sub-barrier energies. Above the barrier the fission cross sections can be treated with considerable confidence with the Hauser–Feshbach formula incorporating the statistical fission transmission coefficient described in Sec. VII.C.1. Details of calculation of fluctuation factors to take into account the statistical variation of the underlying class-II states are given by Lynn (1980).

Below the barrier there are two main classes of effect. The first is a "giant resonance" class in which the cross section, even on the large scale observed with comparatively poor experimental resolution, shows structure. For this the data must be analyzed directly using the fission transmission coefficients described in Sec. V.B for pure vibrational resonances, or Sec. V.C for damped vibrations.

The second class of effect is that due to compound class-II states, the density of which is too high to permit observation by experiments with normal resolution. From the point of view of Hauser–Feshbach theory the important result of this class of effect is that the fine-structure resonances are not uniform in their properties. A certain degree of statistical variation in the partial widths can be absorbed within Hauser–Feshbach calculations by the use of the fluctuation factors $\mathcal{G}$ [see, e.g., Eq. (6.22)], but the variation in widths introduced by the coupling between class-II and class-I states is too extreme to be handled within the simple framework of that theory. The modified expressions required for the fission probability and hence the average cross sections can be obtained from Secs. VI.C.1. *a*, *b*, and *c*, and VI.C.2.*c* for moderate coupling between class-I and class-II states, and for the case of the class-II fission width being much greater than the class-I level spacing, and in Secs. VI.C.1.*d* and VI.C.2.*d* for very weak coupling of narrow class-I and class-II states. This class of intermediate structure effect will also be present when there is already grosser structure due to damped vibrational resonances.

The importance and magnitude of these effects are illustrated in Fig. 125. The uppermost curve is the one that would be obtained for a given set of barrier parameters if the Hauser–Feshbach theory were assumed to be completely valid to deep sub-barrier energies. The upper branch of this curve at very low energies is due to the assumption that radiative cascades can depopulate the class-II states and lead (via the shape isomeric state) to delayed fission. There is already a large difference between this statistical theory result and the fission probability calculated on the assumption of moderate to moderately weak coupling; this implies that the incorrect use of statistical theory to analyze data, especially those at excitation energies below the neutron separation energy where weak radiation effects provide the only competition to fission, can lead to large errors in the extraction of barrier heights. At very low energies the very weak coupling mechanism again causes drastic changes in the behavior of the fission probability. The statistical assumptions (discussed in Sec. VI.C.1.*d*) used for estimating the average are quite crucial here, and the two curves shown can be used together as a pictorial representation of the range of fluctuation to be expected for the locally averaged fission probability in this regime, the range of averaging being the class-II level spacing. Over most of the regime delayed fission can be the principal contributor to the total fission yield, especially when spon-

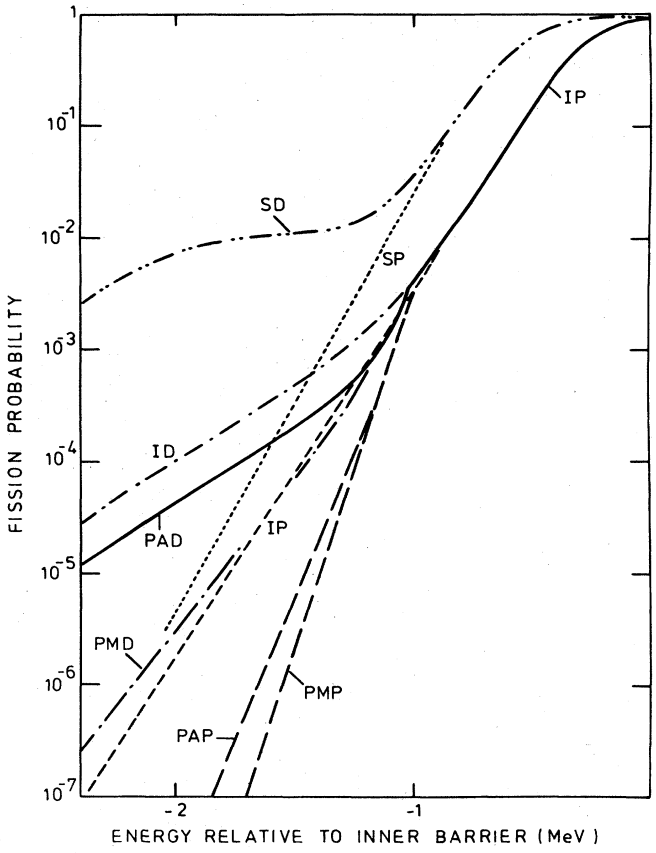

FIG. 125. Probability of fission decay of an even compound nucleus with equal barrier heights lying below the neutron separation energy. Barrier penetrability parameters are $\hbar\omega_A = 1.0$ MeV, $\hbar\omega_B = 0.6$ MeV. The radiation transmission coefficients used in the calculations are $T_{\mathrm{I}(\gamma)} = 6.4\times10^{-3} e^{(E-U_A)/0.5575}$, $T_{\mathrm{II}(\gamma)} = 7.2\times10^{-6} e^{(E-U_A)/0.5575}$. The statistical model with prompt fission only is indicated by SP, including delayed fission by SD, the intermediate structure calculation with at least moderately weak coupling by IP, ID, the very weak coupling perturbation treatment for median position of class-II and class-I lines by PMP, PMD, and the averaged perturbation treatment by PAP, PAD. The continuous curve represents the optimum choice of model.

TABLE XXX. Relevant formulas for calculating average fission cross-sections under various conditions of fission and coupling strength. The equation numbers in the text are quoted.

Regime	Conditions on coupling and fission strength	Expression for average cross section	Class-I fluctuation factor	Class-II fluctuation factor
Statistical	$T_A + T_B \gg 1$	7.1, 7.25	6.47 (or generalization for many fission channels)	
Moderately strong coupling or fission	$T_A + T_B \sim 1$	6.42	6.47	6.44, 6.45 (1 channel) 6.44, 6.46 (2 channels)
Moderately weak coupling or fission	$T_A + T_B \ll 1$ $\Gamma_{\lambda_{II}(f)} + \Gamma_{\lambda_{II}(c)} > D_I$	6.53, 6.54	6.22b	6.56 (see also 6.26)
Very weak coupling and fission	$T_A + T_B \ll 1$, $\Gamma_{\lambda_{II}(f)} + \Gamma_{\lambda_{II}(c)} < D_I$	6.59 (with $x=2$ for median) 6.60 (for long-range average)	Not given because importance of delayed fission in these regimes will usually cause these factors to be close to unity.	
Very weak coupling with effective degeneracy	$\Gamma_{\lambda_{II}(c)} + \Gamma_{\lambda_{II}(f)} < D_I$ $\Gamma_{\lambda_{II}(f)}$ or $\Gamma_{\lambda_I} > \lvert H_c \rvert$ $xD_I < \lvert H_c \rvert$	6.61	*Note*: when delayed fission is predominant, the branching ratio of the isomer state must be multiplied into the class-II fission width.	

taneous fission dominates the decay of the shape isomeric state, as has been assumed in preparing Fig. 125.

The relevant equations to be used in different energy regimes are summarized in Table XXX.

D. Barrier heights and penetrabilities

1. General remarks on analysis of data

Having established the expressions for fission cross sections averaged over suitable energy intervals, and the level densities to be used in conjunction with them, we can now survey the fission cross-section data and the extraction of barrier parameters therefrom.

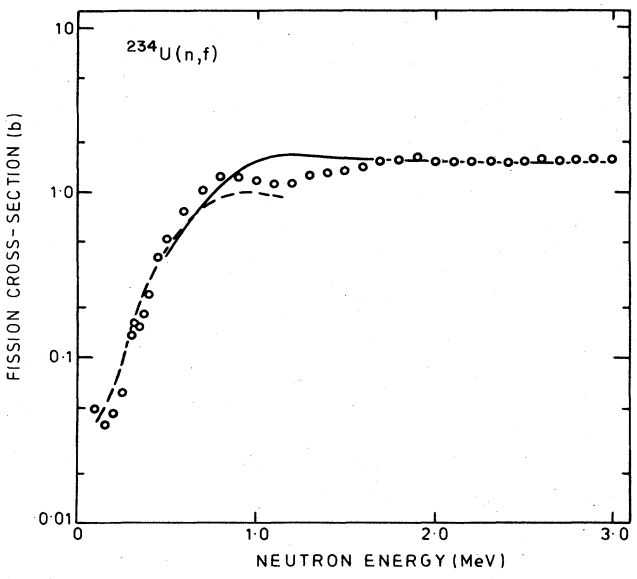

FIG. 126. Neutron fission cross section of ^{234}U (- - - - detailed Hauser-Feshbach calculation with barrier states $K^\pi = \frac{1}{2}^+$ band at 5.96 MeV (barrier *A*), 5.71 MeV (*B*), $K^\pi = \frac{3}{2}^-$ band at 6.36 MeV (*A*), 6.11 MeV (*B*) plus continuum, —statistical Hauser–Feshbach calculation.

Many of these data are neutron-induced fission cross sections. These cross sections of even and odd Z, even-N actinide targets normally have a fission barrier appreciably above the neutron separation energy. The barrier heights in these cases can usually be found fairly adequately by detailed Hauser–Feshbach or more general statistical model fitting of the cross section; because the neutron competition factor is usually strong the modifications due to intermediate structure effects are not usually very important. A typical example of such a fit is shown in Fig. 126.

The other classes of nuclides, which have barriers inaccessible to probing by neutrons, have been explored by a great variety of particle transfer reactions, the excitation energy of the fissioning nucleus being deduced from the energy of the particle emerging from the transfer. Normally, the fission probability as a function of excitation energy is extracted from these data

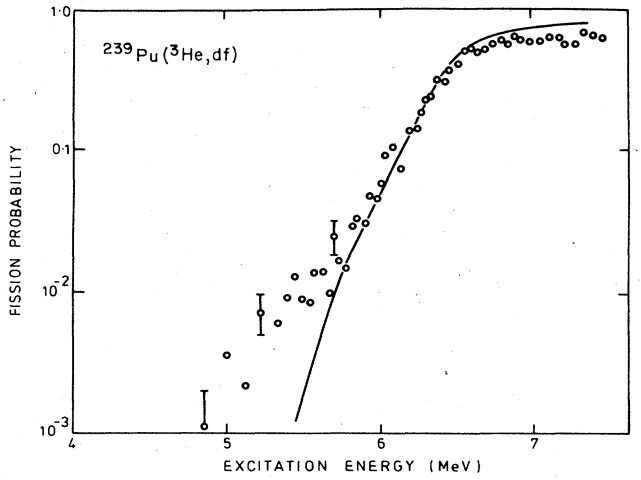

FIG. 127. The fission probability of ^{240}Am. Data and calculation on ^{239}Pu(^{3}He, *df*) reaction. The data are from Back *et al.* (1974c).

and presented, thus simplifying the analysis. The earliest reaction to be used in this way was the (d,pf) reaction. This was quickly followed by the (t,pf) reaction, and later by $(^3\mathrm{He},df)$, $(^3\mathrm{He},tf)$, and $(t,\alpha f)$. These are invaluable for determining the barriers of even and odd Z, even-N compound nuclides, which normally lie below the neutron separation energy for the actinides, and also for determining the barriers of many other nuclides that cannot be formed by neutron reactions. To carry out the analysis it is necessary to know the relative cross sections within the compound nucleus formation cross section for the different values of total angular momentum and parity J^π. These are given by Back *et al.* (1971) for the (d,pf) reaction on a few of the commoner fissile nuclides and by Back *et al.* (1974a) for the distribution of orbital angular momentum transfer in other (d,pf) and (t,pf) reactions; these latter values can be combined vectorially with the target nucleus spin to obtain the J^π relative cross sections. For extracting the barrier parameters of those nuclides with barriers below the neutron separation energy the treatments that fully include the effects of narrow intermediate structure are essential. Normally the excitation range covered by the data is limited to moderately weak coupling, as exemplified in Fig. 127. Occasionally, however, the very weak coupling formulas must be invoked, as in the case of deep sub-barrier photofission of ^{238}U. This is illustrated in Fig. 128. At the lower energy range in this diagram we see that a completely satisfactory fit is not achieved with barrier parameters that fit the higher-energy data. This can be accounted for, partially, by the strong statistical fluctuation effect mentioned in Sec. VII.C.3 (note that the data fall between the "average" and "median" curves) and partially by the occurrence of an apparent vibrational resonance at 3.5 MeV; the actual location of a nearly pure vibrational state relative to the nearest class-I state will be crucial for the magnitude of the cross section around this energy.

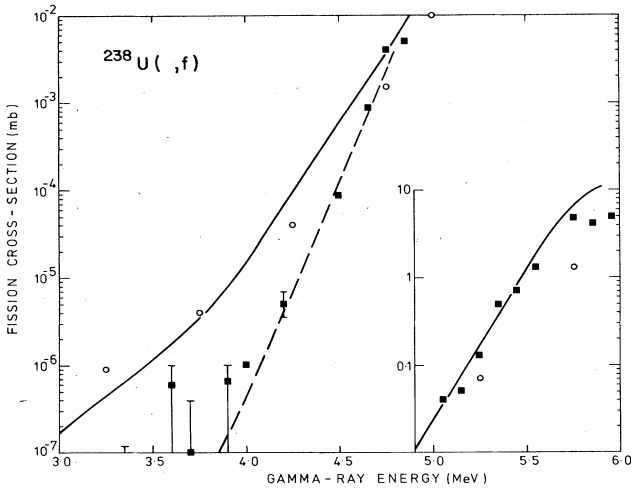

FIG. 128. Calculated sub-barrier photofission cross section of ^{238}U. The branching ratio for delayed fission of the isomeric state is assumed to be 0.1. Barrier parameters have been assumed as $U_A = 6.4$ MeV, $\hbar\omega_A = 1.0$ MeV, $U_B = 5.8$ MeV, $\hbar\omega_B = 0.6$ MeV for the $J^\pi = 1^-$ transition states. Data are from Bowman *et al.* (1975) (circles) and Zhuchko *et al.* (1978b) (squares; see also Fig. 161). The broken curve is the "median" value of the cross section calculated from perturbation theory.

When we come to the detailed fitting, it is immediately obvious, as already pointed out in Sec. VII.C, that the number of available parameters is excessive. Approximate values for some of the parameters are guided by considerations other than the cross-section data alone. For example, the penetrability parameters $\hbar\omega_A, \hbar\omega_B$ are suggested by the values required to fit the half-lives for spontaneous fission of ground states and shape isomers. There is no physical reason why the spontaneous fission penetrability parameters should be identical to those governing reaction rates at higher excitation energies, because the barriers may not be exactly parabolic in shape, inertial parameters may vary with deformation through the barrier, and other effects of interaction between the deformation mode and other degrees of freedom can occur, but it is still reasonable to expect some similarity in magnitude. Because of the lack of uniqueness we find it is possible to move the barrier heights by possibly 200–300 keV in compensating directions and to change the penetrability parameters by ~10% with ~200 keV compensatory changes in barrier heights without seriously affecting the quality of fit. For the final analysis of barrier heights a consensus of values of the penetrabilities has been used; this consensus consists of three pairs of values of $\hbar\omega_A$ and $\hbar\omega_B$, each pair being common to the even, the odd-mass, and the odd actinide nuclides, respectively. Only in exceptional circumstances in order to obtain a reasonable fit to the cross-section data has it been found necessary to depart from these common values. These values are:

$$\begin{aligned} &\text{Even: } \hbar\omega_A = 1.04 \text{ MeV}, \ \hbar\omega_B = 0.6 \text{ MeV} \\ &\text{Odd-}A\text{: } \hbar\omega_A = 0.8 \text{ MeV}, \ \hbar\omega_B = 0.52 \text{ MeV} \\ &\text{Odd: } \hbar\omega_A = 0.65 \text{ MeV}, \ \hbar\omega_B = 0.45 \text{ MeV}. \end{aligned} \tag{7.33}$$

These values are fully consistent with the $\hbar\omega_B$ values of Table III, case I and II.

The greatest problems in fitting are presented by the cross sections that exhibit apparent giant resonance effects. Not only do we have the two barrier heights and two barrier penetrabilities to consider, but also the positions and widths of the vibrational resonances. We consider here in some detail the fitting of a few such cross sections.

The first case is that of the ^{238}Pu(t,pf) reaction for the fission of ^{240}Pu. The fission probability curve of this nuclide shows the well-known vibrational resonance at 5.0 MeV (described in Sec. V.C.4.*a*) and a lower resonance at 4.5 MeV, which has been interpreted by Goldstone *et al.* (1976) (see Sec. IX.B.4) as the beta vibration with one phonon less than that of the 5.0 MeV vibration. Accepting this interpretation we can attempt to fit the fission probability curve with a phonon energy of 0.5 MeV, placing $I^\pi = 0^+$ vibrational states at ~4.4 and 4.9 MeV. In Fig. 129 three calculations of the fission probability are shown in comparison with the data [measured by Back *et al.* (1974)]. In all of them the barrier parameters are chosen to be:

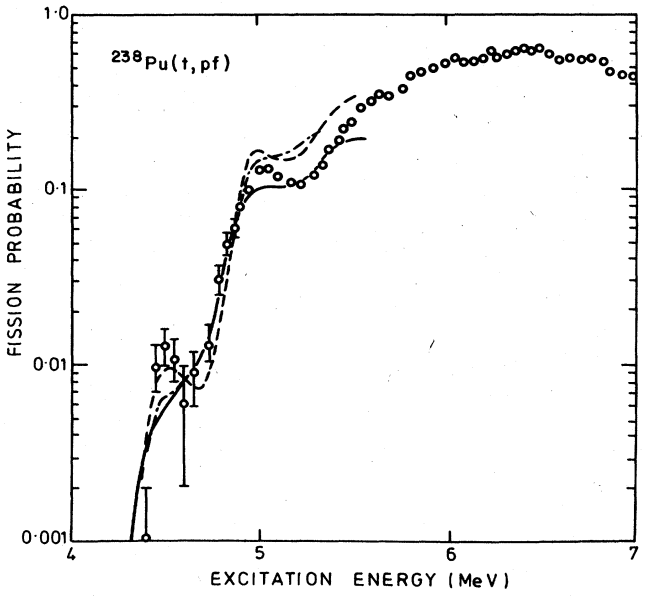

FIG. 129. The fission probability of ^{240}Pu as measured in the (t,pf) reaction (Back *et al.*, 1974a). The full curve assumes the parameters $\upsilon_A = 5.55$ MeV, $\upsilon_B = 5.05$ MeV, $\Gamma_{\nu(D)} = 0.2$ MeV, and a simple $K^\pi = 0^+$ rotational band of transition states at the inner barrier. The short dashed and dot-dashed curves assume a more complex spectrum of transition states, appropriate to axial asymmetry, at the inner barrier. Their parameters are otherwise the same with $\Gamma_{\nu II(D)} = 0.2$ MeV for the dot-dashed curve, $\Gamma_{\nu II(D)} = 0.1$ MeV for the short dashed curve.

$$\upsilon_A = 5.55 \text{ MeV}, \quad \hbar\omega_A = 1.04 \text{ MeV},$$

$$\upsilon_B = 5.05 \text{ MeV}, \quad \hbar\omega_B = 0.6 \text{ MeV}.$$

For one of the curves the barrier transition states are assumed to have the same simple rotational band structure, based on a $K^\pi = 0^+$ bandhead, as in the secondary well. For the other two curves a more complex set of barrier transition states has been assumed. The inner barrier has been assumed to have maximum axial asymmetry, and therefore a full set of gamma-rotational states is interlaced with the simple rotational band. The outer barrier, having parity and π-rotational asymmetry, has a low-lying band of $K^\pi = 0^-$ transition states, but the odd-parity class-II states make only a marginal contribution to the cross section, even with this assumption. The class-II vibrational states are assumed to have full projection onto these barrier deformation channel states. All curves contain the full effects of moderately weak damping of the class-II compound states into the fine structure states, and they also contain the effects of Porter–Thomas fluctuations in the widths of the class-II states.

Apart from the effect of the damping width the calculated curves are rather similar at lower excitation energies. But there is considerable deviation above the 5.0 MeV resonance, the calculations with the fuller transition state spectra rising considerably above the experimental data. This fault cannot be rectified readily by changing the barrier heights without worsening the fit at lower energies (see Fig. 130). The weak point in the assumptions behind these two fits is almost certainly that the vibrational states project fully onto all the transition states. In the pure form of the vibrational model this will certainly not happen, and the two simpler fits are therefore more appropriate. If fragmentation of the vibrational states (as described schematically in Sec. V.C) occurs, any strength gained for passing through the more complex channels will be lost to the channels with simpler configuration. Thus we expect the simpler calculations to give a more realistic estimate, and the other calculations to serve rather as an upper bound.

The second case is that of the ^{240}Pu(t,pf) reaction. The fission probability curve of ^{242}Pu, Fig. 131, shows evidence for only one vibrational resonance, at ~4.65 MeV. The vibrational state with one extra phonon is evidently so near the top of the secondary well that its broadness does not allow it to appear as a distinctive peak in the cross section. This introduces extra complication into the fitting by allowing the phonon energy to be a free parameter. In Fig. 131 four calculations with inner barrier transition states appropriate to an axially asymmetric deformation are shown. In the first two the phonon energy is chosen to be 0.7 MeV, the lower vibrational energy for $I^\pi = 0^+$ as 4.53 MeV, and the barrier parameters are $\upsilon_A = 5.55$ MeV, $\upsilon_B = 5.05$ MeV; they fit the experimental data (Back *et al.*, 1974) at lower excitation energies but override the data in the region of 5 MeV. Adjustment of the barrier heights alone is unlikely to improve the fit (see Fig. 130). However, a choice of phonon energy of 0.8 MeV and inner barrier height raised to 5.65 MeV gives an excellent fit from 4.4 to 5.5 MeV. For the reasons concerned with configuration mixing that were discussed in the ^{240}Pu case, these calculations are probably overestimates at the higher excitation energies. Hence a fifth calculation is shown in which the transition state spectrum of the inner barrier is reduced to the simple rotational form based on a $K^\pi = 0^+$ bandhead. The assumptions of $\upsilon_A = 5.55$ MeV, $\upsilon_B = 5.05$ MeV, and a phonon energy of 0.5 MeV yield a good fit up to 5.2 MeV; beyond this it can be assumed that more complex class-II states contribute. This is shown more clearly in Fig. 104.

Even with these complications in the fitting it is seen that we are not moving the barrier heights (once the penetrabilities are fixed) by more than about 0.1 MeV. Hence our earlier estimate of an uncertainty of ~0.2–0.3 MeV in fitted barrier heights still appears reasonable.

The detailed results of the analysis of barrier parameters is presented in Table XXXI.

2. Systematic trends in barrier parameters

The interesting evidence on the density of intrinsic states at the barrier deformations and its interpretation in terms of rotational enhancement due to a lowering of the nuclear shape symmetry has already been discussed in Sec. VII.C.2. It is noteworthy that this evidence, crude as it is, is consistent with the expectations on nuclear shape that are given by the theory of nuclear deformation energy. Some additional aspects of this topic are taken up in Sec. VII.D.3.

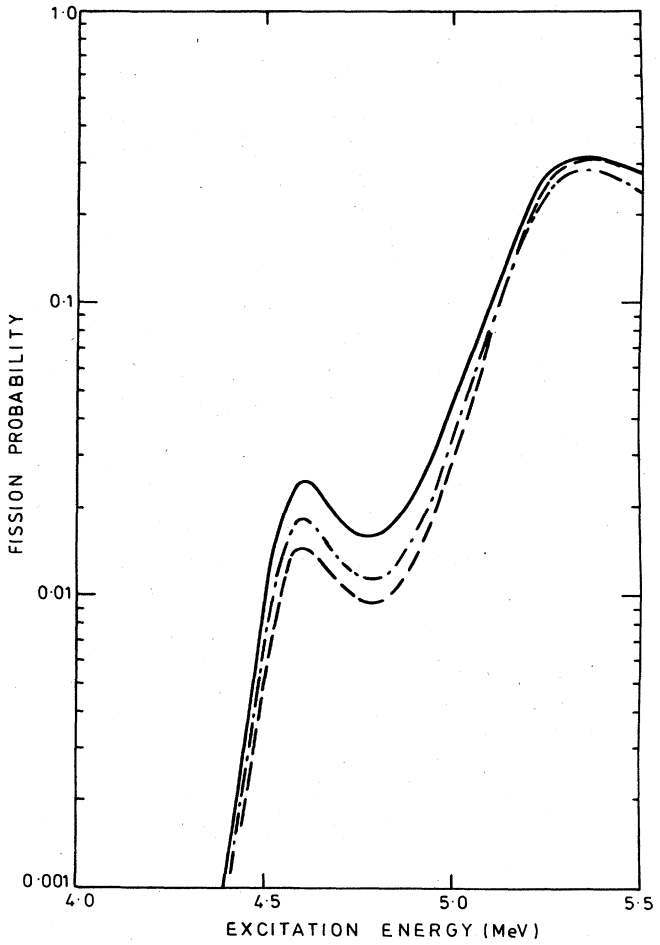

FIG. 130. Effect of changing barrier heights in a damped vibrational model calculation with an axially asymmetric inner barrier. Full curve: $\mathcal{U}_A = 5.55$ MeV, $\mathcal{U}_B = 5.05$ MeV; dashed curve: $\mathcal{U}_A = 5.55$ MeV, $\mathcal{U}_B = 5.15$ MeV; dot-dashed curve; $\mathcal{U}_A = 5.65$ MeV, $\mathcal{U}_B = 5.05$ MeV. In all cases $E_{\nu_{II}}(I) = 3.475 + 0.7 \times (\nu_{II} + \frac{1}{2}) + 0.0025\, I(I+1)$ MeV, $\Gamma_{\nu II(D)} = 0.1$ MeV.

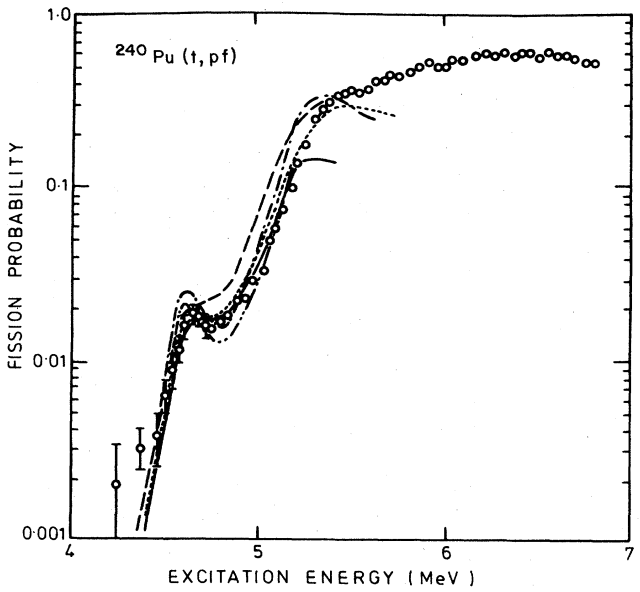

FIG. 131. The fission probability of ^{242}Pu as measured in the (t, pf) reaction (Back *et al.*, 1974a). $\mathcal{U}_A = 5.55$ MeV, $\mathcal{U}_B = 5.05$ MeV, $\Gamma_{\mu_{II}(D)} = 0.1$ MeV, $\hbar\omega_{II} = 0.7$ MeV; $\Gamma_{\nu_{II}(D)} = 0.2$ MeV; $\mathcal{U}_A = 5.65$ MeV, $\mathcal{U}_B = 5.05$ MeV, $\Gamma_{\nu_{II}(D)} = 0.2$ MeV, $\hbar\omega_{II} = 0.8$ MeV; $\Gamma_{\nu_{II}(D)} = 0.1$ MeV; $\mathcal{U}_A = 5.55$ MeV, $\mathcal{U}_B = 5.05$ MeV, $\hbar\omega_{II} = 0.5$ MeV. In all cases a simple rotational spectrum of transition states at the barriers is assumed.

The penetrability parameters $\hbar\omega_{A,B}$ require comment. They definitely exhibit an odd-even effect, the evidence being additional to that of the well-known effect in spontaneous fission half-lives discussed in Sec. IV.C. The penetrabilities have been fixed to obtain agreement with the attenuation of the fission cross section below the barrier in some of the better-known nuclides of different odd-even character. The penetrability parameters obtained for even nuclides are much more sensitive to the choice of barrier heights than are those of odd-N nuclides, but the even barrier heights would have to be lowered by almost 0.5 MeV to compensate for a reduction of $\hbar\omega_{A,B}$ to the values used for the decay of odd-A nuclides. Whereas in the case of spontaneous fission half-lives the physical reason for the odd-even effect might eventually be attributed entirely to structure effects in the special low-lying state that is decaying (i.e., specialization energy due to a mismatch of the decaying state with the lowest channel state at the outer barrier, case III of Table III), in the more highly excited states nearer the barrier energy it is possible that the difference may be due to the barrier actually being less transparent for specific J^π in the odd-A case than for the 0^+ barrier of even nuclides; in other words the 0^+ barrier of the even core provides the optimum path, energetically and inertially, for the deforming system to pass along, and the addition of single-particle or other effects with a constraint on angular momentum can only raise the potential energy of deformation on either side of the barrier turning point. The inertial parameter is also likely to increase through the addition of an unpaired particle. Part of this explanation can only apply to the lowest-lying barrier states, but these are the ones that affect the rapid energy variation of the sub-barrier fission widths. See also the discussion in Sec. IV.C.

Next, we turn to the barrier height systematics as revealed by the analysis of all the data summarized in Table XXXI. This problem will be more fully discussed in Sec. VIII in connection with an analysis of all the information available on barrier energies as well as on ground states and isomer energies. In the present preliminary analysis we shall focus attention on general trends and on odd-even effects in the light of the models used for describing the barrier parameters, especially the various level density "laws" for even, odd, and odd-A species, which we have adopted. A plot of the inner barrier height against neutron number is shown in Fig. 132, and against the fissility parameter x of Myers and Swiatecki (1967) [see Eqs. (2.4) and (2.5)] in Fig. 133. The last figure shows most clearly that for each proton number and specific odd-even character the barriers appear to cluster in a qualitatively parabolic

TABLE XXXI. Recommended values of barrier parameters from analysis of fission cross-section data on the actinide nuclides. It is not claimed that these parameters are unique in the sense of being the only sets that will fit the data. They are designed to be used with the other nuclear parameters given in this section for the purpose of establishing the systematics of actinide fission barrier parameters on a common basis.

Compound nucleus	Neutron separation energy S_n (MeV)	Reactions	Footnote	V_A (MeV)	$\hbar\omega_A$ (MeV)	V_B (MeV)	$\hbar\omega_B$ (MeV)	Comments
^{229}Th	5.23	^{228}Th(n,f)	1			~6.7		From value of σ_{nf} above 2 MeV
^{230}Th	6.79	^{231}Pa$(t,\alpha f)$	2	6.1	1.0	6.5	0.75	See Note 1
		^{229}Th(n,f)	3,4					
^{231}Th	5.13	^{230}Th(n,f)	5,6	6.02	0.9	6.27	0.57	Analysis of vibrational resonance structure reported by Yuen *et al.* (1921). Statistical Hauser–Feshbach analysis gives barriers ~0.3 MeV higher. See also Sec. V.
^{232}Th	6.43	^{230}Th(t,pf)	2	5.82	1.0	6.22	0.75	Barrier parameters from pure vibrational model analysis; statistical Hauser–Feshbach calculation with same parameters is about factor 2 too large at high energies.
^{233}Th	4.79	^{232}Th(n,f)	7,8	6.55	0.8	6.65	0.56	From statistical Hauser–Feshbach calculation. For relation to vibrational structure see Sec. V.
^{234}Th	6.18	^{232}Th(t,pf)	2	6.1	1.0	6.5	0.75	Pure vibrational resonance fit to data. See Fig. 91.
^{230}Pa	5.85	^{230}Th$(^3$He$,tf)$	9	6.1	0.65	6.1	0.45	From statistical Hauser–Feshbach calculation.
^{231}Pa	6.86	^{230}Th$(^3$He$,df)$	10,9	5.9	0.8	5.9	0.52	From statistical Hauser–Feshbach calculation.
^{232}Pa	5.57	^{231}Pa(n,f)	11	6.3	0.65	6.25	0.45	Barrier estimates (from Hauser–Feshbach statistical analysis) agree with crude analysis of vibrational resonance structure; see Sec. V.
		^{231}Pa(d,pf)	10					
		^{231}Pa$(^3$He$,tf)$	9					
^{233}Pa	6.51	^{232}Th$(^3$He$,df)$	10,9	6.2	0.8	6.2	0.52	From statistical Hauser–Feshbach analysis.
^{231}U	5.96	^{231}Pa$(^3$He$,tf)$	9	5.8	0.8	5.2	0.52	From statistical Hauser–Feshbach analysis.
^{232}U	7.28	^{231}Pa$(^3$He$,df)$	2	5.2	1.04	5.1	0.6	See Note 2.
^{233}U	5.79	^{232}U(n,f)	12,13	≈5.8		≈5.8		References cover resonance region, and cross section to 1 keV neutron energy suggests that nuclide is fissile.
^{234}U	6.84	^{233}U(d,pf)	14	5.6	1.04	5.5	0.6	See Note 2.
		^{233}U(n,f)						
^{235}U	5.31	^{233}U(t,pf)	15					
		^{234}U(n,f)	16	6.15	0.8	5.9	0.52	Detailed Hauser–Feshbach calculation with $K^\pi = \frac{1}{2}^+$ band at barriers 0.2 MeV lower than quoted barrier heights gives better fit than statistical analysis (see Sec. D.2 and Fig. 126). For relation to intermediate structure see Sec. V. C.4 and Sec. VI. D.
^{236}U	6.54	^{234}U(t,pf)	2					See Note 2.
		^{235}U(d,pf)	14					See Note 2.
		^{235}U(n,f)	17	5.63	1.04	5.53	0.6	See Note 3.
^{237}U	5.13	^{236}U(n,f)	18	6.28	0.8	6.08	0.52	From statistical analysis. Detailed Hauser–Feshbach calculation with $K^\pi = \frac{1}{2}^+$ band 0.1 MeV below these barriers and $\frac{3}{2}^-$ band 0.1 MeV above gives improved fit (see Sec. VII. D.2).
^{238}U	6.14	^{236}U(t,pf)	2	5.7	1.0	5.7	0.6	See Note 2. Also see Fig. 128 for which calculated photofission cross section has lowest $J^\pi = 1^-$ barrier states 0.7 MeV, 0.1 MeV above V_A, V_B, respectively.
		^{237}U(n,f)	19					Resonance data suggest that $K^\pi = 1^+$ barrier A state could be ~1.1 MeV above VA.
^{239}U	4.86	^{238}U(n,f)	17	6.46	0.8	6.16	0.52	Reference cross section for barrier level density parameters of odd-A nuclides (see Sec. VII. C.2). For relation to intermediate structure see Sec. VI.

TABLE XXXI. (*Continued.*)

Compound nucleus	Neutron separation energy S_n (MeV)	Reactions	Footnote	υ_A (MeV)	$\hbar\omega_A$ (MeV)	υ_B (MeV)	$\hbar\omega_B$ (MeV)	Comments
^{240}U	5.92	^{238}U(t,pf)	2	5.75	1.04	5.5	0.6	See Note 2.
^{233}Np	7.35	^{233}U$(^3$He$,tf)$	9	5.4	0.8	4.7	0.52	From statistical Hauser–Feshbach analysis.
^{234}Np	6.12	^{233}U$(^3$He$,df)$	10	5.7	0.65	5.2	0.45	From statistical Hauser–Feshbach analysis.
		^{234}U$(^3$He$,tf)$	9					
^{235}Np	6.99	^{234}U$(^3$He$,df)$	10	6.0	0.8	5.2	0.52	From statistical Hauser–Feshbach analysis.
		^{235}U$(^3$He$,tf)$	9					
^{236}Np	5.69	^{235}U$(^3$He$,df)$	10,9	5.9	0.65	5.7	0.45	From statistical Hauser–Feshbach analysis.
		^{236}U$(^3$He$,tf)$	9					
^{237}Np	6.59	^{236}U$(^3$He$,df)$	10,9	5.9	0.8	5.6	0.52	From statistical Hauser–Feshbach analysis.
^{238}Np	5.49	^{237}Np(d,pf)	10	6.2	0.65	5.9	0.45	From statistical and detailed Hauser–Feshbach analysis.
		^{238}U$(^3$He$,tf)$	9					
		^{237}Np(n,f)	20,21,17					For relation to intermediate structure see Sec. VI.
^{239}Np	6.23	^{238}U$(^3$He$,df)$	10,9	6.1	0.8	5.6	0.52	From statistical Hauser–Feshbach analysis.
^{237}Pu	5.9	^{237}Np$(^3$He$,tf)$	9	5.9	0.8	5.2	0.52	From statistical Hauser–Feshbach analysis.
^{238}Pu	7.0	^{237}Np$(^3$He$,df)$	2	5.5	1.04	5.0	0.6	See Note 2.
^{239}Pu	5.66	^{238}Pu(n,f)	22	6.3	0.8	5.7	0.52	From statistical Hauser–Feshbach analysis. Detailed Hauser–Feshbach calculations give good fit with $K^\pi=\frac{1}{2}^+$, $\frac{3}{2}^+$, $\frac{3}{2}^-$ bands of barrier states ~0.15 MeV below quoted barriers. For relation to intermediate structure see Sec. VI.
^{240}Pu	6.52	^{238}Pu(t,pf)	2	5.57	1.04	5.07	0.6	See Notes 2 and 3 and Fig. 129. Relation to intermediate structure described in Secs. V and VI.
		^{239}Pu(n,f)	17					
^{241}Pu	5.24	^{240}Pu(n,f)	23,24,25	6.1	0.8	5.5	0.52	See comment under ^{239}Pu.
		^{239}Pu(t,pf)	10					
^{242}Pu	6.30	^{240}Pu(t,pf)	2	5.6	1.04	5.1	0.6	See Note 2 and Fig. 131.
		^{241}Pu(n,f)	26,27,28					Detailed Hauser–Feshbach analysis.
^{243}Pu	5.04	^{242}Pu(n,f)	29,30	6.0	0.8	5.4	0.52	From statistical Hauser–Feshbach analysis. For relation to intermediate structure see Sec. VI.
^{244}Pu	6.02	^{242}Pu(t,pf)	2	5.4	1.04	5.0	0.6	See Note 2.
^{245}Pu	4.76	^{244}Pu(n,f)	30	5.8	0.8	5.3	0.52	From statistical Hauser–Feshbach analysis. Detailed Hauser–Feshbach calculation suggests lowest barrier states (perhaps $K^\pi=\frac{3}{2}^+-$) are ~0.1 MeV lower than this.
^{239}Am	7.25	^{239}Pu$(^3$He$,tf)$	9	6.4	0.8	5.6	0.52	From statistical Hauser–Feshbach analysis.
^{240}Am	5.94	^{239}Pu$(^3$He$,df)$	10	6.5	0.65	5.4	0.45	From statistical Hauser–Feshbach analysis
		^{240}Pu$(^3$He$,tf)$	9					
^{241}Am	6.66	^{240}Pu$(^3$He$,df)$	10	6.2	0.8	5.7	0.52	From statistical Hauser–Feshbach analysis
^{242}Am	5.54	^{241}Am(d,pf)	10	6.5	0.65	5.7	0.45	From statistical and detailed (on n,f) Hauser–Feshbach analysis.
		^{241}Pu(t,pf)	9					
		^{241}Am(n,f)	31,32					See Note 4.
^{243}Am	6.43	^{242}Pu$(^3$He$,df)$	10,9	6.2	0.8	5.6	0.52	From statistical Hauser–Feshbach analysis.
^{244}Am	5.37	^{243}Am(d,pf)	14	6.4	0.65	5.6	0.45	From statistical and detailed (on n,f) Hauser–Feshbach analysis.

TABLE XXXI. (*Continued.*)

Compound nucleus	Neutron separation energy S_n (MeV)	Reactions	Footnote	V_A (MeV)	$\hbar\omega_A$ (MeV)	V_B (MeV)	$\hbar\omega_B$ (MeV)	Comments
		^{243}Am(n,f)	33,27					
^{245}Am	6.05	^{243}Am(t,pf)	10	6.2	0.8	5.3	0.52	From statistical Hauser–Feshbach analysis.
^{247}Am	5.86	^{248}Cm$(t,\alpha f)$	10	5.8	0.8	5.0	0.52	From statistical Hauser–Feshbach analysis.
^{241}Cm	6.1	^{241}Am$(^3$He$,tf)$	9	6.6	0.8	4.3	0.52	From statistical Hauser–Feshbach analysis.
^{242}Cm	6.9	^{241}Am$(^3$He$,df)$	9	5.8	1.04	4.0	0.6	From statistical Hauser–Feshbach analysis.
^{243}Cm	5.6	^{243}Am$(^3$He$,tf)$	9	6.7	0.8	4.3	0.52	From statistical Hauser–Feshbach analysis.
^{244}Cm	6.8	^{243}Am$(^3$He$,df)$	2,9	5.8	1.04	4.3	0.6	From statistical Hauser–Feshbach analysis.
^{245}Cm	5.52	^{244}Cm(n,f)	33	6.3	0.8	5.0	0.52	From statistical Hauser–Feshbach analysis.
^{246}Cm	6.45	^{245}Cm(n,f)	33	5.7	1.04	4.3	0.6	From statistical Hauser–Feshbach analysis.
^{247}Cm	5.16	^{246}Cm(n,f)	33	6.2	0.8	4.8	0.52	From statistical Hauser–Feshbach analysis (and see Note 5).
^{248}Cm	6.21	^{248}Cm$(p,p'f)$	2	5.7	1.04	4.6	0.6	From statistical Hauser–Feshbach analysis.
^{249}Cm	4.71	^{248}Cm(n,f)	33	5.7	0.8	4.3	0.52	From statistical Hauser–Feshbach analysis (and see Note 6).
^{250}Cm		^{248}Cm(t,pf)	2	5.3	1.04	3.9	0.6	From statistical Hauser–Feshbach analysis.
^{249}Bk	6.21	^{248}Cm$(^3$He$,df)$	10	~6.2	0.8			From statistical Hauser–Feshbach analysis.
^{250}Bk	4.97	^{249}Bk(n,f)	34	6.1	0.65	4.1	0.45	From statistical Hauser–Feshbach analysis.
^{250}Cf	6.62	^{249}Cf(n,f)	35,36	5.6	1.04	3.6	0.6	From statistical Hauser–Feshbach analysis.
^{253}Cf	4.83	^{252}Cf(n,f)	37	5.4	0.8	3.6	0.52	See Note 7.

[1] Vorotnikov *et al.* (1973)
[2] Back *et al.* (1974a)
[3] Gokhberg *et al.* (1959a)
[4] Coté *et al.* (1965)
[5] James *et al.* (1972)
[6] Yuen *et al.* (1971)
[7] Henkel and Smith (1956)
[8] Lamphere (1965)
[9] Gavron *et al.* (1976)
[10] Back *et al.* (1974c)
[11] Muir and Veeser (1971)
[12] James (1964)
[13] Farrell (1970)
[14] Back *et al.* (1971)
[15] Britt and Cramer (1970)
[16] Lamphere (1962)
[17] Sowerby *et al.* (1974)
[18] Rosler *et al.* (1972)
[19] McNally *et al.* (1974)
[20] Brown *et al.* (1970)
[21] Stein *et al.* (1968)
[22] Silbert *et al.* (1973)
[23] Nesterov and Smirenkin (1960)
[24] Henkel *et al.* (1957)
[25] Byers *et al.* (1966)
[26] Kappeler and Pfletschinger (1970)
[27] Butler and Sjoblom (1961)
[28] Blons (1973)
[29] Butler (1960)
[30] Auchampaugh *et al.* (1971)
[31] Seeger *et al.* (1967)
[32] Bowman *et al.* (1965)
[33] Baybarz *et al.* (1971)
[34] Vorotnikov *et al.* (1970)
[35] Silbert (1973)
[36] Vorotnikov *et al.* (1972)
[37] Moore *et al.* (1971)

Note 1. The $(t,\alpha f)$ data can be fitted by these parameters using a pure vibrational model built on a $K^\pi = 0^+$ rotational band over the barriers and making some allowance for the presence of a $K^\pi = 0^-$ band. The data cannot be fitted by a strong damping model with the same barrier heights and $\hbar\omega_B$ reduced to 0.6 MeV. The fission cross-section data are adequately fitted by specific calculations using these barrier heights with rotational bands at the following positions (energy units in MeV)

	Barrier A	Barrier B
K^π	$E_A - S_n$	$E_B - S_n$
0^-	~0.0	~−0.25
2^+	~−0.33	~0.5
1^-	~0.22	~0.75
2^-	~1.0	~0.8 ,

statistical calculations in the region of 1 MeV are almost a factor of 2 too high; this tends to be a common feature of the statistical calculations on *Th* nuclei suggesting that barrier B densities might be overestimated (but see Sec. VII.D.3). Resonance region data give fission widths ranging from 4 meV to >160 meV and resonance spacing of 0.41 eV; this is consistent with position of $J^\pi = 3^+$ barrier state implied above (giving $\overline{\Gamma}_f(3^+) \approx 10$ meV).

TABLE XXXI. (*Continued.*)

Note 2. Barrier parameters fit a calculation of fission probability through the $K^\pi = 0^+$ rotational band across the barrier. A damped vibrational model has been assumed and the calculation includes the effect of Porter–Thomas fluctuations in the class-II levels. Porter–Thomas fluctuations in the class-I levels have not been included but neither has experimental resolution and these two effects tend to be compensatory.

Note 3. The statistical model calculations of fission cross-sections of ^{235}U and ^{239}Pu have been adjusted simultaneously to give the barrier densities that have been used for statistical calculations on other even compound nuclei (see Sec. VII.C.2).

Note 4. Analysis of spontaneous fission isomerism suggests $\nu_B \sim 5.6$ MeV. Resonance data at low neutron energies give $\Gamma_{(f)} \sim 0.18$ meV. This agrees with barrier parameters given.

Note 5. Parameters are from statistical model fit. Specific calculation employs $J^\pi = 3/2^{+-}$ barrier states 0.06 MeV below the statistical parameters, $J^\pi = 1/2^+$ 0.05 MeV above, $1/2^-$ 0.08 MeV above.

Note 6. Parameters are from statistical model fit. Specific calculation employs $J^\pi = 7/2^+, 9/2^{+-}$ barrier states 0.2 Mev below the statistical parameters, $J^\pi = 1/2^{+-}$ 0.05 MeV above.

Note 7. Parameters are from statistical model fit. Specific calculation has $J^\pi = 3/2^+, 5/2^+$ barrier states 0.25 MeV below statistical values, $3/2^-$, 0.18 MeV below. Resonance data indicate fission widths are of the order of magnitude to be explained by barrier parameters.

form about a centroid abscissa value, and that the maximum barrier height for each proton number is virtually unchanging with increasing Z. This value is

$$\upsilon_{A,\max}\,(\text{even}) \approx 5.7 \text{ MeV}$$
$$\upsilon_{A,\max}\,(\text{odd-}A) \approx 6.3 \text{ MeV}$$
$$\upsilon_{A,\max}\,(\text{odd}) \approx 6.5 \text{ MeV}. \qquad (7.34)$$

This is in contrast to the general trend of the outer barrier heights, which, insofar as they can be quantitatively assessed from shape isomer formation yields and intermediate structure data, decrease strongly and in a roughly linear fashion with A (by perhaps 3 MeV in passing from Th to Cf; see Fig. 134). Figure 132 shows that the centroid position for these inverted parabolas of intermediate barrier height is virtually the same neutron number, viz., $N = 147$, for all charges. A rough empirical equation for the inner barrier heights appears to be

$$\upsilon_A \approx \upsilon_{A,\max} - 0.01067(N-147)^2. \qquad (7.35)$$

Interestingly, this neutron number is very close to that ($N = 148$) calculated by Strutinsky from his combined liquid drop and shell correction model as being that for optimum development of the secondary well in the fission barrier; see, however, Sec. VIII.E.

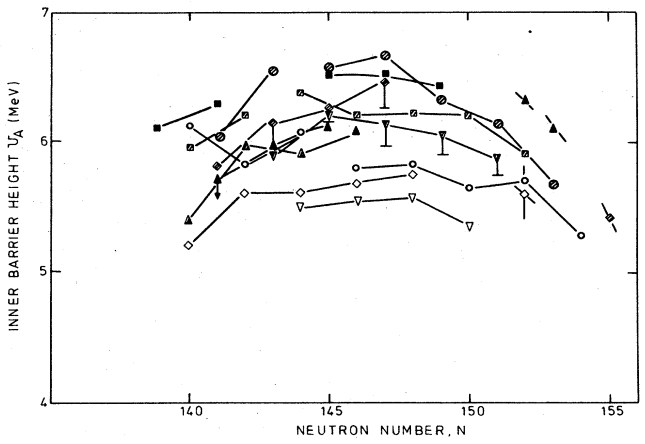

FIG. 132. Inner barrier heights as a function of neutron number. Open symbols denote doubly even nuclides, hatched denote odd-mass, black denote doubly odd, ○-Th, Cm; □-Pa, Am; ◇-U, Cf; △-Np, Bk; ▽-Pu.

Both the relevant figures, but particularly Fig. 132, immediately show a considerable odd-even effect in the height of barrier A [as also expressed in Eq. (7.34)]. The biggest difference is seen between the odd-mass and even barriers, but some reservations must be expressed about a too literal acceptance of this result. Firstly, the determination of the barriers of even nuclei is difficult, as already pointed out, because the strong fission decay in the barrier region is only in competition with weak electromagnetic radiation and hence the barrier parameters are strongly dependent on the choice of penetrability frequency. However, a raising of the even barriers can only be done at the expense of raising $\hbar\omega_A$ and hence accentuating the odd-even difference in this parameter. On the other hand, in the odd-N nuclei formed from even targets the fission decay in the barrier region is undergoing strong competition from neutron evaporation and in a statistical sense the barrier should be easily determined. However, in these nuclei there is also a strong neutron centrifugal barrier to consider; the effect of the interplay between the fission and centrifugal barriers is shown in Fig. 135, which shows that for a given change in fission barrier there is a much bigger shift in the fission cross section of low orbital angular momentum states than for those of high angular momentum. It is now apparent that the choice of barrier density for odd-A nuclei has been affected by the neutron centrifugal barrier; it seems very likely that in ^{239}U most of the lowest barrier A states carry high angular momentum, but the fission cross section is hardly affected by them at lower energies. Consequently, the fission cross section only starts to rise rapidly as many barrier states are coming in simultaneously, some way above the proper barrier energy. Thus for this reference cross section the barrier has almost certainly been deduced to be too high in energy and the density of states chosen at this barrier starts at too high a value at an already rapidly increasing rate. This is borne out by the analysis of the fission cross sections of ^{234}U (see Fig. 126) and ^{236}U for which the statistical calculation gives too high a cross section just above the barrier height, whereas

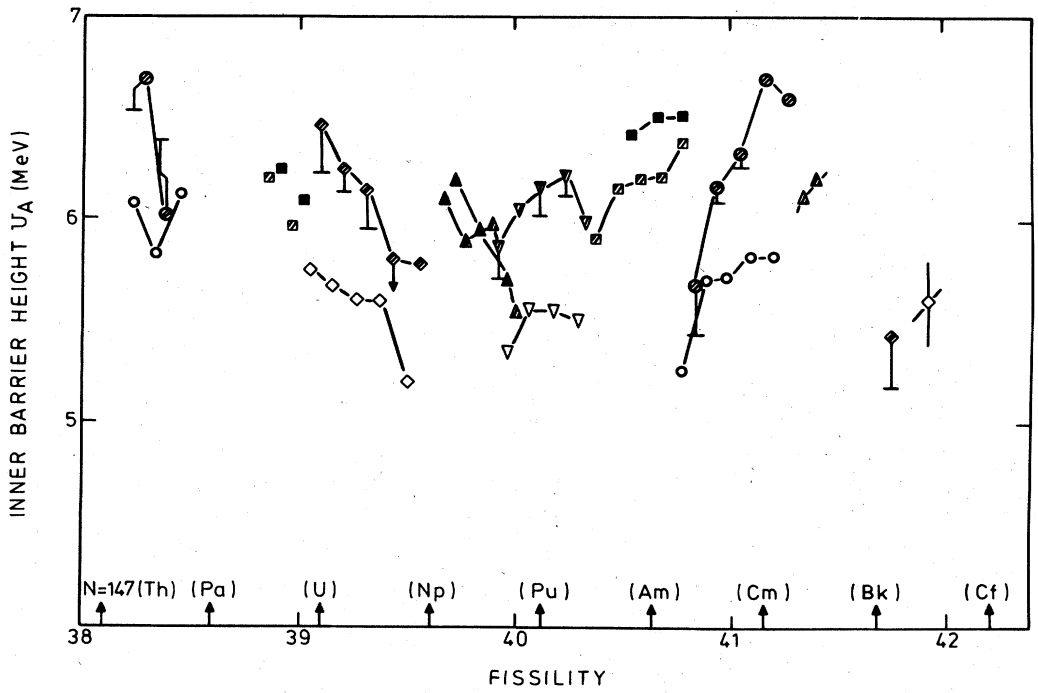

FIG. 133. Inner barrier heights as a function of fissility $Z^2/[A(1-1.78(N-Z/A)^2]$. Vertical arrows on abscissa indicate $N=147$ for various Z. Symbols in Fig. 132.

more detailed study suggests barrier states for a few low angular momentum values below the statistical barrier and some of the higher angular momentum states at some distance above. The general consensus of the analysis suggests that in these nuclides the true barrier is some 2–300 keV below the value fixed by the statistical model calculation, and this is borne out by the nature of the barrier level density, which will now lie almost midway between those of odd and even nuclides, reflecting the situation that is found for level density at normal deformation.

This downward shift of the odd-mass barrier heights still leaves a considerable difference against even barrier heights and at the same time opens up a definite gap between odd-mass and odd barrier heights. An odd-even effect in intermediate barrier heights is thus substantiated. Physically, it seems to reflect the differences in single-particle level density at different nuclear deformations that are cited by Strutinsky (1967) as the cause of maxima and minima in the shell corrections that have to be added to the liquid drop energy surface. The single-particle level density also affects the pairing energy gap, depressing the fully pair-correlated ground state of even nuclei below the lowest two-quasi-particle state (which is the character of the ground state of odd nuclei) by an amount that is therefore expected to have a maximum at the shell correction maxima (i.e., the barriers) and minima at the shell correction minima. See also Sec. VIII.D.2.

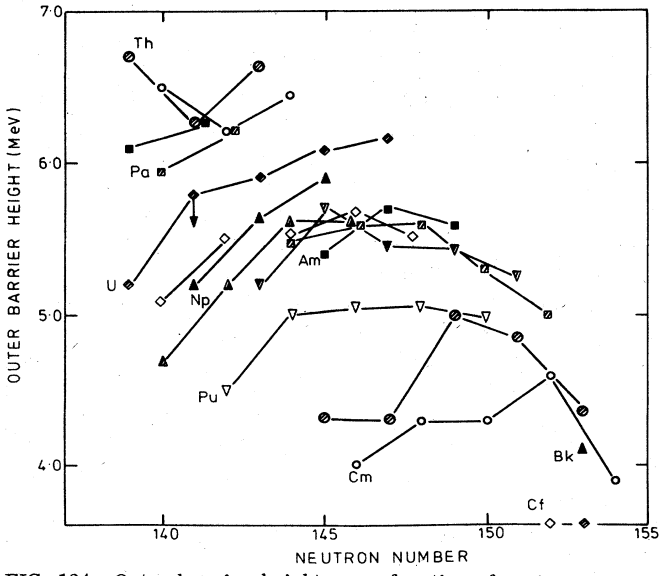

FIG. 134. Outer barrier heights as a function of neutron number. Symbols as in Fig. 132.

3. The thorium anomaly

a. Comparison with theory

It is generally found that the heights of barriers and secondary well depths determined from experimental data, and presented in Table XXXI, are in reasonable agreement with the results of theoretical calculations (as summarized in Secs. II and VIII) to within about 0.5 MeV. Nevertheless there appear to be some considerably greater discrepancies associated particularly with the thorium nuclides. The occurrence of undamped or weakly damped vibrational resonances in the fission cross sections of ^{230}Th and ^{232}Th (see Sec. V.B.5) suggests that there is comparatively little energy available

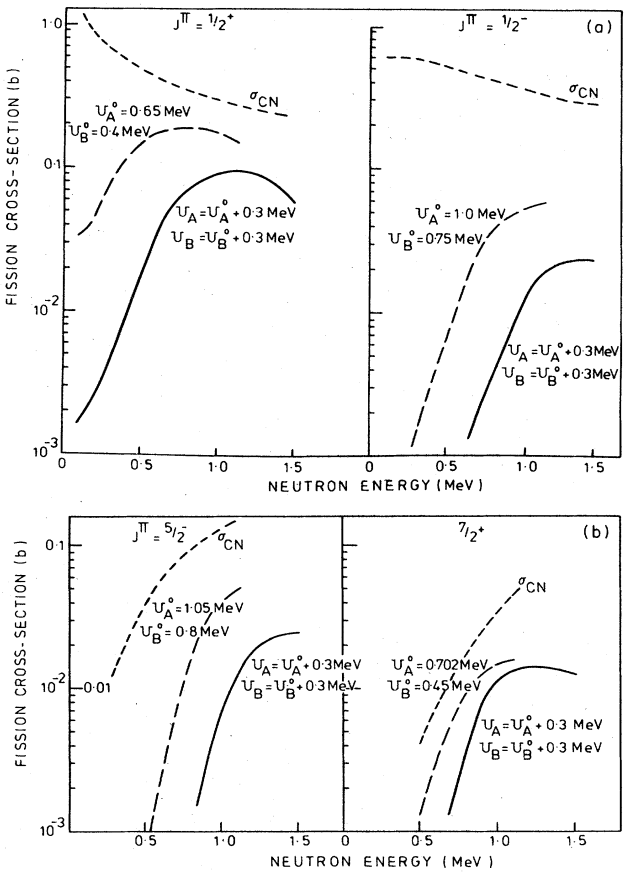

FIG. 135. Calculated neutron fission cross sections of an even nucleus for states of specified angular momentum and parity J^π illustrating interplay of fission and neutron centrifugal barriers. The short dashed curve is the compound nucleus formation cross section.

for intrinsic excitation in the secondary well; estimates from this evidence that the secondary well lies at least 4.5 MeV above the primary well contrast with theoretical estimates of the order of 2.5 MeV (see Fig. 15). A discrepancy is also found in the inner barrier height. The experimental data suggest ~6 MeV (above ground) in ^{231}Th and ^{233}Th, while calculations yield ~4.5 MeV (see Fig. 14).

b. Above-barrier cross sections and barrier transparencies of Th and Pa nuclides

Using barrier parameters derived from the analysis of near-barrier experimental data on Th and Pa nuclides, we find that the calculated values of the cross sections tend to be too high by a factor approaching two (see Fig. 136). This suggests that the barrier level densities (as given in Table XXX) are too high for these nuclides.

The cross sections of these same nuclides also appear to rise too quickly in the barrier region when they are calculated with the "universal" set of barrier penetrability parameters given in Eq. (7.33). Exact comparison is made difficult by the presence of vibrational structure, which obscures the monotonic rise in the barrier transmission coefficients of the separate barriers. However, a clear qualitative example is provided by the fission probability of ^{234}Th, as measured in the (t,pf) reaction (Back *et al.*, 1974b) and compared with calculation in Fig. 91. It is obvious that the penetrability parameters $\hbar\omega_A, \hbar\omega_B$ need to be increased considerably to get good detailed agreement with the data.

c. Interpretation with a triple-humped barrier

The first suggestion to resolve the thorium anomaly was made by Möller and Nix (1974). In their detailed calculations of the deformation surfaces of a range of actinide nuclides they found a shallow dip in the outer barrier peak (see Fig. 17). If this is a real effect it could explain the problems outlined in Subsections *a* and *b* above. The hypothesis of a shallow tertiary well at the deformation corresponding to the outer barrier in the conventional two-humped barrier model would allow the existence of undamped or weakly damped vibrational resonances, a high apparent inner barrier, and a reduced barrier state density at this new apparent inner barrier (corresponding to the expectation that this barrier will have axial symmetry). It would also suggest higher values of the penetrability parameters, of both the intermediate and outer barriers enclosing the tertiary well. Indeed, with a low enough peak for the true inner barrier A, which will allow rather thorough mixing of the class-I and class-II compound states at excitation energies approaching the value of barrier B,

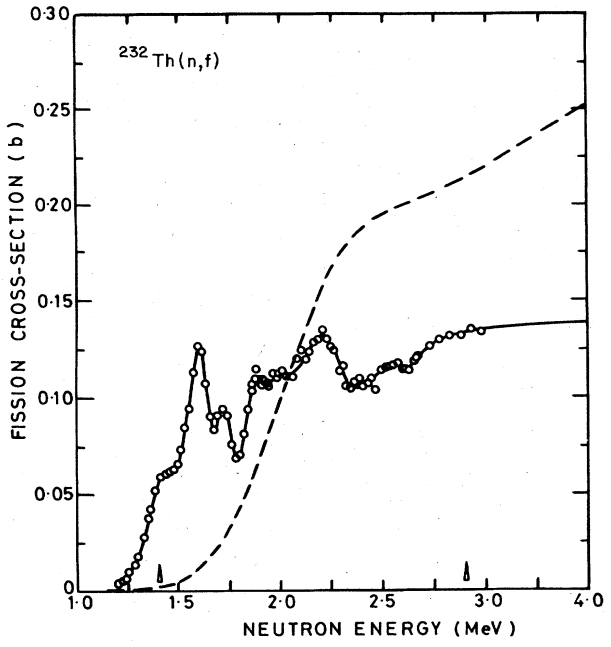

FIG. 136. The calculated neutron fission cross section of ^{232}Th up to 4 MeV, as based on the double-humped barrier parameters of Table XXXI, compared with data (circles and full curve).

the reaction theory of fission processes, as it has been described in Secs. III, V, and VI of this article, will be unchanged except that the role of the class-II states will now be taken by a new set of class-III states (which may be pure vibrational states) centered in the tertiary well, and the transmission coefficients T_A, T_B governing the coupling and fission widths will be replaced by coefficients T_B, T_C for the subsidiary peaks of the split outer barrier, their heights being υ_B/υ_C and with penetrability parameters $\hbar\omega_{BC}, \hbar\omega_C$ that are considerably larger than the original $\hbar\omega_B$.

Direct evidence to support this hypothesis is not yet conclusive. Blons *et al.* (1975a) have observed substructure in the fission cross section of ^{232}Th (see Sec. V.A.5.*b*) and have interpreted this as rotational band structure, but have not made a quantitative fit to substantiate this. The moment of inertia of the rotational band appears large enough to be associated with the high deformation of the outer barrier, but it must be borne in mind that the effective moment of inertia of a rotational band, especially in an odd-A nucleus, can be affected by Coriolis coupling with higher bands differing by one unit in the spin projection quantum number. The model of vibrational state damping described in Sec. V.C.1 and applied to the case of ^{231}Th in Sec. V.C.4.*e* lends qualitative, but not yet unambiguous, support also to the hypothesis. These questions are further discussed in Sec. IX.D.

VIII. SUMMARY AND ANALYSIS OF BARRIER INFORMATION

A. Introduction

The experiments which define fission barrier heights or the energy of the second minimum are based on a considerable variety of different methods. Most of these allow the barrier parameters of a particular isotope to be determined without requiring any knowledge of the barrier parameters in neighboring species. Sometimes a given parameter may even be measured by two or more independent methods.

The question of internal consistency between several measurements pertaining to the same isotope has been treated in the foregoing Secs. IV, V, and VII. Here we shall present "best" values for each isotope; one for each of the three extrema, first barrier, isomeric minimum, and second barrier. Summarizing the data in this way will allow for a broader test of consistency. At the same time, systematic trends in the barrier parameters can be examined.

There are three kinds of trends. First, a smooth one to be associated with average properties of nuclear matter as described by the liquid drop or droplet models; secondly the odd-even staggering due to pairing; and finally the broader oscillations for which shell effects are responsible. In this section we shall analyze the experimental data with a view to separating the three effects from each other and then compare with the theoretical models outlined in Sec. II. As we shall see, theory accounts quite well for the major trends, in particular it invariably confirms the existence of a two-humped barrier, if not a three-humped one. The isomeric minimum seems most pronounced when the neutron number equals $N = 144$. Accordingly this is the magic number for neutrons moving in the strongly deformed potential of the isomeric shape. Evidence for departures from axial and reflection symmetry at the barriers is also brought out quite strongly. As for pairing, the data appear to favor the hypothesis of a pairing strength which increases as the surface of the nucleus increases.

When it comes to details, however, especially to the variation of shell effects with proton number, there remain serious discrepancies. It is not even clear whether these are due to a misinterpretation of the experimental results or to shortcomings of the theory.

B. "Best" values of barrier heights and isomer engeries

Table XXXII summarizes the best values of the energy of the three extrema υ_A, $(E_{II} - E_I)$, and υ_B. They should be understood in analogy to the ground states as the energy of the lowest state of the relevant deformation, whatever the spin and parity of that state is. The last two columns in Table XXXII present the ground-state energy, relative to the energy of a spherical liquid drop or to a spherical droplet, respectively (see Sec. VIII.C.3).

The barrier energies are primarily based on the results summarized in Tables V–VII and XXXI. The errors quoted reflect both an eventual spread between independent determinations and the experimental uncertainties in a narrower sense. In contrast to ground-state energies it is only in exceptional cases that barrier heights can be defined with better than 0.2 MeV accuracy.

In a number of cases, slow neutron fine-structure resonances provide an additional measure of the barrier heights, Sec. VI. In these cases the barriers are defined in terms of a reaction channel of definite spin and parity (usually $I^\pi = \frac{1}{2}^+$), which may or may not represent the lowest barrier state. The energies derived in this fashion are therefore to be regarded as upper limits only.

The level density expression used in Sec. VII to analyze fission excitation functions of odd-A nuclei assumes an exponentially rising density of states beginning directly at the energy of the lowest channel. Considering the effect of pairing that pushes the onset of an exponentially rising level density towards higher energies, this assumption may represent a true situation where the barrier lies somewhat lower than assumed in the analysis. In the level density models used for even and doubly odd nuclei, there is no such ambiguity. The barrier heights of odd-A nuclei from Table XXXI have therefore been lowered by about 0.25 MeV in the process of establishing the final values of Table XXXII; compare Sec. VII.D.2 for a more detailed discussion of this crucial point.

Isomer excitation energies are mainly based on excitation function thresholds, Sec. IV, and on extrapolation of class-II level densities down to zero energy, Sec. VI. Again, the errors quoted in Table XXXII include both the spread between independent determinations and the usual experimental uncertainty. In the case of isomer energies, systematic errors are especially hard to rule out. In essence, this is because the available experimental methods are rather indirect. The results therefore tend to be model dependent.

TABLE XXXII. Summary of barrier and ground-state energies. All energies are in MeV. Most of the numbers are taken from Tables V–VII and XXXI, subtracting a small correction for odd-A nuclei; see text. The ^{228}Ra barriers are from Weber *et al.* (1976), and the ^{226}Ac, ^{227}Th, ^{228}Th, ^{232}Pu, and ^{234}Pu barrier values are due to Habs (1977). The energy E_I relative to the spherical shape of the liquid drop is based on Myers and Swiatecki (1967) with experimental masses from Wapstra and Gove (1971). Those relative to the droplet are from Myers (1977) with experimental masses from Wapstra and Bos (1977).

Isotope	v_A	E_{II} (Relative to ground state)	v_B	E_I Rel. to spherical: liq. drop	droplet
^{228}Ra	8.0 ± 0.5		8.5 ± 0.5	0.92	0.16
^{226}Ac	6.0 ± 0.6		7.7 ± 0.3	0.23	−0.95
^{227}Th	5.9 ± 0.3		6.6 ± 0.3	0.32	−0.94
^{228}Th	6.2 ± 0.3		6.5 ± 0.3	0.20	−0.95
^{229}Th			6.5 ± 0.3	0.37	−0.83
^{230}Th	6.1 ± 0.2		6.5 ± 0.3	0.33	−0.75
^{231}Th	6.0 ± 0.1	<5.8	6.1 ± 0.3	0.39	−0.73
^{232}Th	5.8 ± 0.2	≪4.5	6.2 ± 0.2	0.44	−0.54
^{233}Th	6.3 ± 0.2	<6.2	6.3 ± 0.2	0.57	−0.40
^{234}Th	6.1 ± 0.2		6.5 ± 0.2	0.63	−0.19
^{231}Pa	5.9 ± 0.2		5.9 ± 0.3	0.26	−1.03
^{232}Pa	6.1 ± 0.3	<5.7	6.2 ± 0.2	0.09	−1.16
^{233}Pa	6.1 ± 0.3		6.1 ± 0.3	0.26	−0.95
^{232}U	5.2 ± 0.2		5.1 ± 0.3	−0.19	−1.52
^{234}U	5.6 ± 0.2		5.5 ± 0.2	−0.28	−1.58
^{235}U	5.9 ± 0.2	2.5 ± 0.3	5.6 ± 0.2	−0.26	−1.59
^{236}U	5.6 ± 0.2	2.3 ± 0.2	5.5 ± 0.2	−0.15	−1.38
^{237}U	6.1 ± 0.2	2.5 ± 0.4	5.9 ± 0.2	−0.20	−1.43
^{238}U	5.7 ± 0.2	2.6 ± 0.01	5.7 ± 0.2	0.05	−1.04
^{239}U	6.3 ± 0.2	1.9 ± 0.3	6.1 ± 0.2	0.10	−1.00
^{240}U	5.7 ± 0.2		5.5 ± 0.2	0.31	−0.63
^{234}Np	5.5 ± 0.2		5.1 ± 0.2	−0.63	−2.06
^{235}Np	5.5 ± 0.2		5.2 ± 0.2	−0.51	−1.96
^{236}Np	5.8 ± 0.2		5.6 ± 0.2	−0.65	−2.08
^{237}Np	5.7 ± 0.2	2.8 ± 0.3	5.4 ± 0.2	−0.43	−1.85
^{238}Np	6.1 ± 0.2	2.3 ± 0.3	6.0 ± 0.2	−0.61	−1.98
^{239}Np	5.9 ± 0.2		5.4 ± 0.2	−0.25	−1.58
^{232}Pu	5.3 ± 0.4			−0.16	−1.50
^{234}Pu	5.8 ± 0.7			−0.50	−1.89
^{235}Pu		2.6 ± 0.4	5.1 ± 0.4	−0.71	−2.22
^{236}Pu			4.5 ± 0.4	−0.76	−2.23
^{237}Pu		2.8 ± 0.2		−0.86	−2.41
^{238}Pu	5.5 ± 0.2	2.7 ± 0.2	5.0 ± 0.2	−0.81	−2.29
^{239}Pu	6.2 ± 0.2	2.6 ± 0.2	5.5 ± 0.2	−0.98	−2.50
^{240}Pu	5.6 ± 0.2	2.4 ± 0.3	5.1 ± 0.2	−0.71	−2.15
^{241}Pu	6.1 ± 0.2	1.9 ± 0.3	5.4 ± 0.2	−0.70	−2.17
^{242}Pu	5.6 ± 0.2		5.1 ± 0.2	−0.46	−1.81
^{243}Pu	5.9 ± 0.2	1.7 ± 0.3	5.2 ± 0.2	−0.48	−1.84
^{244}Pu	5.4 ± 0.2		5.0 ± 0.2	−0.21	−1.43
^{245}Pu	5.6 ± 0.2		5.0 ± 0.2	−0.18	−1.37
^{237}Am		2.4 ± 0.2		(−1.0)	−2.54
^{238}Am		2.6 ± 0.2		−1.32	−2.83
^{239}Am	6.2 ± 0.3	2.4 ± 0.2		−1.15	−2.76
^{240}Am	6.5 ± 0.2	3.0 ± 0.2	5.2 ± 0.3	(−1.40)	−2.99
^{241}Am	6.0 ± 0.2	2.2 ± 0.2	5.1 ± 0.3	−1.05	−2.67
^{242}Am	6.5 ± 0.2	2.9 ± 0.2	5.4 ± 0.3	−1.14	−2.71
^{243}Am	5.9 ± 0.2	2.3 ± 0.2	5.4 ± 0.3	−0.76	−2.33
^{244}Am	6.3 ± 0.2	2.8 ± 0.4	5.4 ± 0.3	−0.91	−2.42
^{245}Am	5.9 ± 0.2		5.2 ± 0.3	−0.48	−1.95
^{247}Am	5.5 ± 0.2			(−0.13)	−1.49
^{241}Cm	6.3 ± 0.3	2.1 ± 0.3	4.3 ± 0.5	−1.57	−3.25
^{242}Cm	5.8 ± 0.4		4.0 ± 0.5	−1.35	−2.96
^{243}Cm	6.4 ± 0.3	1.9 ± 0.3		−1.41	−3.08
^{244}Cm	5.8 ± 0.2		4.3 ± 0.3	−1.26	−2.87
^{245}Cm	6.2 ± 0.2	2.1 ± 0.3		−1.37	−3.03
^{246}Cm	5.7 ± 0.2		4.2 ± 0.3	−1.13	−2.69
^{247}Cm	6.0 ± 0.2			−1.10	−2.70
^{248}Cm	5.7 ± 0.2			−0.86	−2.35
^{249}Cm	5.6 ± 0.2			−0.63	−2.13

TABLE XXXII. (*Continued.*)

Isotope	υ_A	E_{II} (Relative to ground state)	υ_B	E_I Rel. to spherical: liq. drop	droplet
^{250}Cm	5.3 ± 0.2			−0.28	−1.57
^{249}Bk	6.1 ± 0.2			−1.23	−2.94
^{250}Bk	6.1 ± 0.2		4.1 ± 0.3	−1.07	−2.72
^{250}Cf	5.6 ± 0.3			−1.80	−3.52
^{253}Cf	5.4 ± 0.3			−0.83	−2.55

C. The smooth reference frame: liquid drop, or droplet

1. Expressing barrier energies and minima relative to a spherical liquid drop

For a single nuclide it is natural to characterize the double barrier in terms of the heights of the two maxima and of the second minimum, relative to the ground state. When many nuclides are to be compared, the ground state becomes a poor reference point because the ground-state energy, like the other extrema, incorporates shell and pairing effects. It is better to exhibit the general liquid drop trends, the pairing, and the shell effects separately for each of the four extrema. This can be done by expressing the energy of each of these relative to the energy of the spherical liquid drop, as shown in Fig. 137. The ground-state energy (or mass) relative to that of a liquid drop sphere is accurately known from mass measurements, provided the parameters of the liquid drop model have been fixed; the energies or masses of the three other extrema are then easily obtained from the relative energies υ_A, $(E_{II} - E_I)$, and υ_B; Table XXXII. These energies, measured from the base line of Fig. 137, will be denoted by E_I, E_A, E_{II}, and E_B, respectively. They represent a sum of shell correction energies and liquid drop deformation energies. Also the deviations from a smoothly varying odd-even staggering, as assumed in the liquid drop treatments of pairing, will be reflected in these energy values.

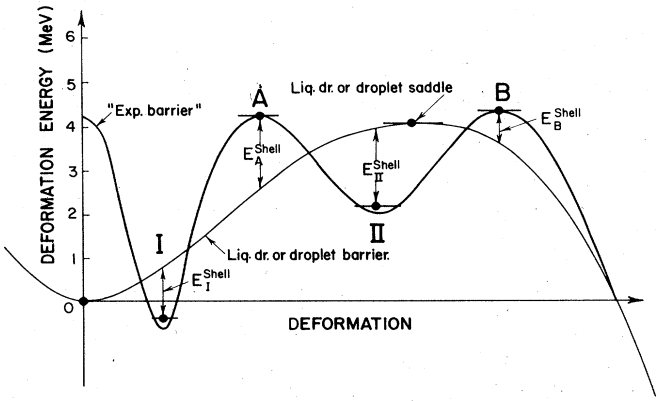

FIG. 137. Schematic diagram of the total nuclear deformation energy along the fission path. Shell effects are built on the underlying liquid drop (or droplet) reference energy. One may imagine plots of the type shown on the figure—one for each isotope—stacked according to X value and projected onto a plane perpendicular to the X direction. This will lead to plots like those shown in Figs. 139–142.

Thus, for ν denoting either I, A, II, or B,

$$E_\nu = \tilde{E}_\nu + E_\nu^{shell} \pm \delta\Delta_\nu . \tag{8.1}$$

The shell energies are generally thought to be sums of independent contributions from protons and neutrons,

$$E_\nu^{shell} = E_\nu^{shell}(Z) + E_\nu^{shell}(N) , \tag{8.2}$$

and the pairing deviation is

$$\delta\Delta_\nu = \Delta_\nu(Z,N) - \tilde{\Delta} , \tag{8.3}$$

where the liquid drop odd-even pairing correction $\tilde{\Delta}$ has the value $11A^{-1/2}$, the same for protons and neutrons and for all shapes.

To isolate the shell correction energy requires knowledge of the liquid drop deformation energy as indicated on Fig. 137 and hence of the shape in question. This knowledge is generally not available—especially for the two barriers—and therefore one cannot determine the shell correction energy unambiguously. Nevertheless, the magnitude of the deformation energy can be crudely estimated from the liquid drop model by making plausible assumptions about the shape, and the change in this energy with proton and neutron number can then be estimated rather accurately, allowing interesting trends in the remaining effective shell energy to be isolated and studied as a function of neutron and proton number. This is especially true, if it is permissible to assume that the barriers and the minima have fixed, or at least slowly varying shapes, as indeed most theoretical models predict.

2. Ground-state shell effects, a test case

For ground-state shapes the liquid drop deformation energy is small, if not zero. Therefore the shell correction energy E_I^{shell} is relatively well defined. At the same time there is a large body of accurate experimental data for the ground states, both mass measurements and spectroscopic data. The latter are essential for making a realistic choice of the shell model potential used in calculating shell energy corrections. The description of nuclear binding energies in terms of Strutinsky's shell correction method (Sec. II) can therefore be gauged by its success in fitting the ground state binding energies.

Figure 138 illustrates one such test over an extended region of the isotope chart. One sees that the main trends are well reproduced, for example, the large dip at doubly magic ^{208}Pb and the secondary depression

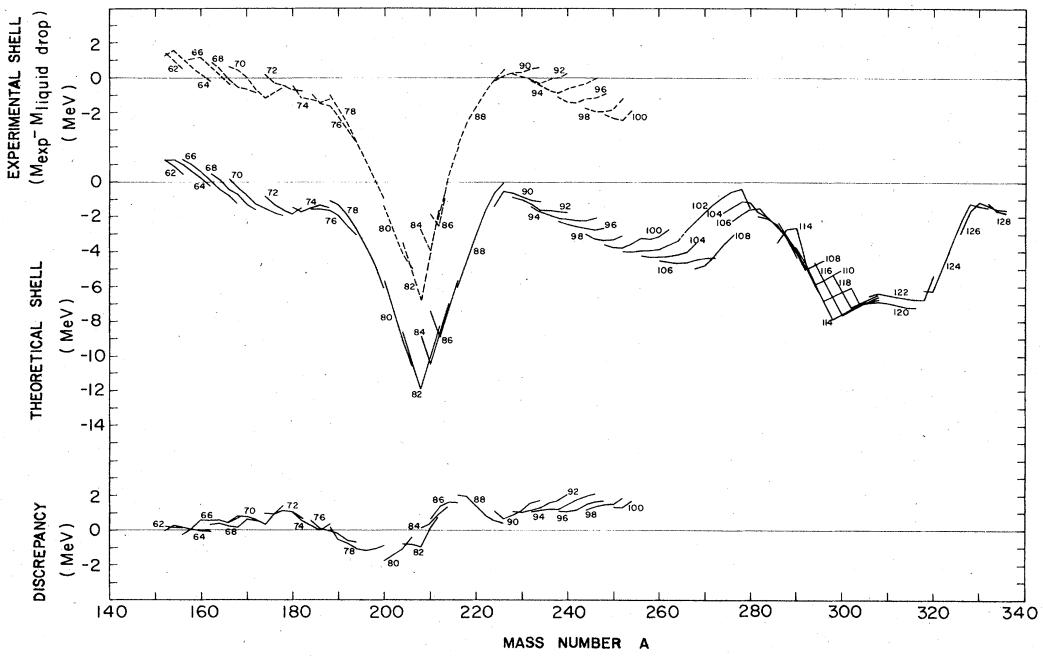

FIG. 138. Experimental mass values for $150 < A < 254$ plotted relative to the spherical liquid drop values of Myers and Swiatecki (1967)—top figure. Theoretical shell corrections plus liquid drop deformation energies—center. Difference between the two—lower figure. From Nilsson *et al.* (1969).

associated with the onset of deformation around mass number 228 and extending towards ^{252}Fm with nucleon numbers $N = 152$ and $Z = 100$. From the plot of differences between theory and experiment (in Fig. 138) one also sees that discrepancies of the order of 1–1.5 MeV remain. There seem to be two difficulties. One is to estimate the magnitude of the shell energy correctly over an extended region. This gives rise to the largest discrepancies, of order ± 1 MeV. The other and smaller difficulty is in describing the slopes for a given element and hence the variation with neutron number correctly.

Deviations of this nature are not specific to the example shown here. There have been many attempts to calculate ground-state masses using a range of liquid drop or droplet model parameters combined with different choices of single-particle potentials. Several such attempts are reviewed by Myers (1977). Although the deviations change in nature from one calculation to another, the overall discrepancies invariably remain of the order of ± 1 MeV.

3. Choice of liquid drop and droplet parameters

The introduction of the shell correction method for describing the fission barrier coincided with the appearance of the Lysekil version of Myers and Swiatecki's (1967) mass formula, including a new set of carefully fitted liquid drop parameters [see Eq. (2.5)]. A large number of early barrier calculations are therefore based on this parameter choice. Since then, the liquid drop concept has been refined in the form of the droplet model of Myers and Swiatecki (1969). In 1977 Myers presented complete tables calculated on the basis of a best fit of the droplet parameter to the most recent mass measurements (Wapstra and Bos, 1977) and barrier heights, see Myers (1977).

With this development in mind we present the four experimental energies E_{I}, υ_A, $(E_{\mathrm{II}} - E_{\mathrm{I}})$, and υ_B in two ways:

(i) relative to the 1967 Lysekil spherical liquid drop (Figs. 139 and 141), and

(ii) relative to the 1977 spherical droplet (Figs. 140 and 142).

In both cases the energies relative to the sphere are denoted E_{I}, E_A, E_{II}, and E_B, respectively.

In the decade between these two years there have been several studies of how to improve the liquid drop model parameters. Contributions have been made by groups in Lund-Berkeley-Warsaw, at Los Alamos, in Copenhagen-Basel-Moscow, and in Dubna.

Möller (1972) studied a modification of the Myers-Swiatecki liquid drop formula, namely of the isospin dependent *volume* term

$$E_V^{(0)} = a_1\left[1 - \gamma\left(\frac{N-Z}{A}\right)^2\right]A. \tag{8.4}$$

The calculated fit to the ground-state masses shows a systematically wrong isospin dependence for the actinides reflected in the upwards sloping lines in Fig. 138, lower part. Möller shows that this can be remedied by very small adjustments of the constants a_1 and γ of less than 1%. The price paid is a poorer agreement for the rare-earth nuclei. What is worse, it tends to transfer the wrong isospin dependence from the ground-state fits to the fits at the other points: barriers A and B and the second minimum. This modification is therefore not very appealing.

The Lund group combines the Lysekil liquid drop formula in unaltered form with a calculation of the shell correction in which the pairing strength increases in proportion to the surface area, $G \sim S$. One effect of

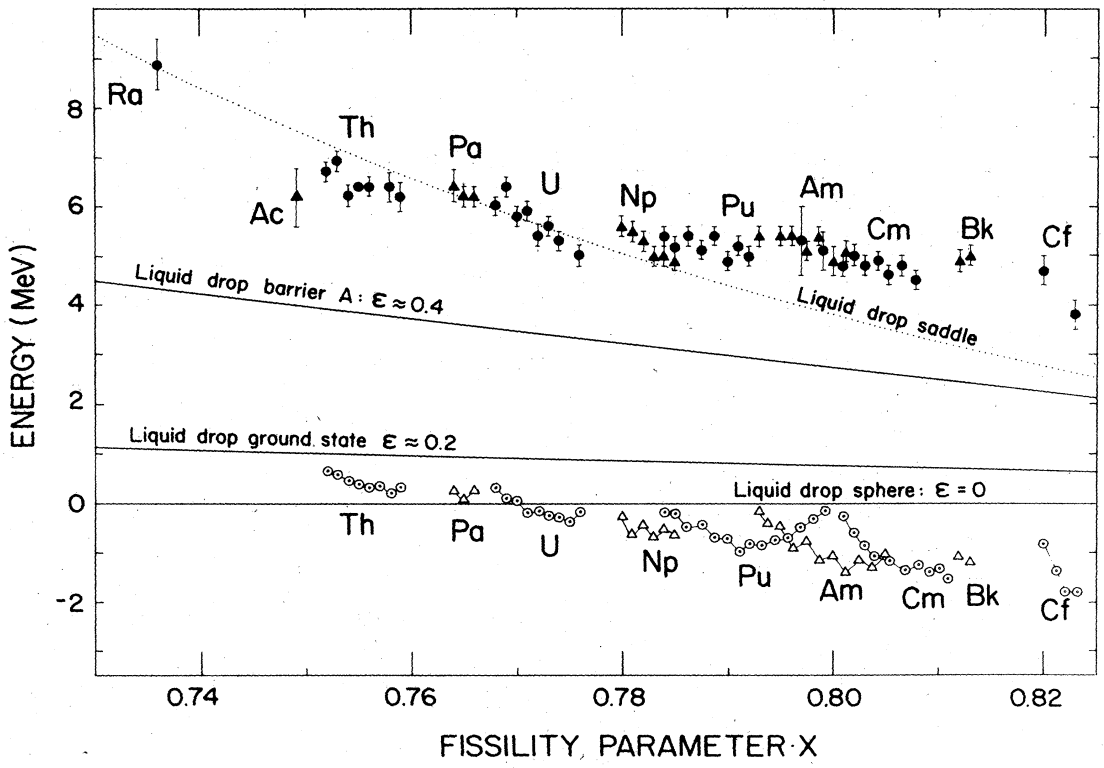

FIG. 139. Experimental binding energies for the ground states, open symbols, and for the first barrier (A), filled symbols, plotted relative to the (1967) spherical liquid drop energy as a function of the fissility parameter (Myers and Swiatecki, 1967). Even-Z elements are represented by circles, odd-Z elements by triangles. The liquid drop deformation energies for two fixed deformations corresponding to the ground-state shapes and first barrier shapes, and the energy of the (variable) saddle point shape are also indicated.

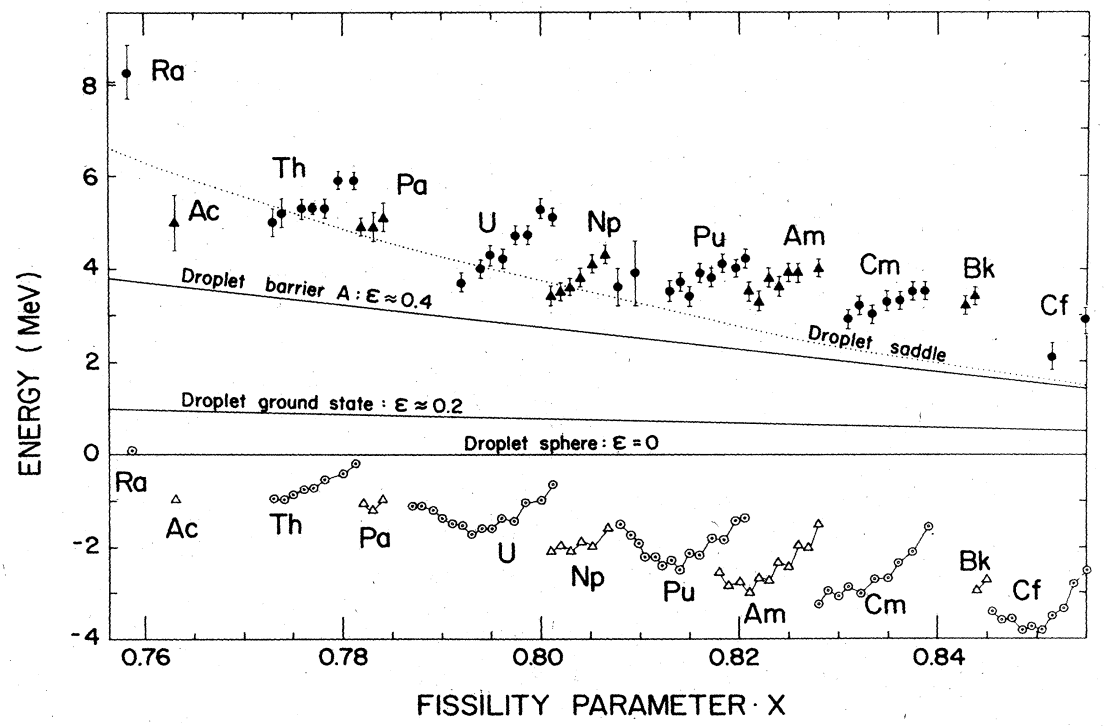

FIG. 140. Energy of ground states and barriers A as in Fig. 139 but here plotted relative to the energy of a spherical droplet of Myers (1977).

this is to damp the shell oscillations at large deformations. At the position of the outer barrier, the damping factor is of the order of 0.8 compared to a shell correction calculation with a constant pairing strength, G = const. Another effect of surface dependent pairing appears as a smooth average increase in the pair condensation energy with increasing surface area, i.e., an effective decrease of surface energy and hence of the barrier height. At the outer barrier this amounts to a 2 MeV decrease.

Apart from the moderate damping effect inherent in the assumption of $G \sim S$, the Lund group obtains nearly identical results with another version of the calculation, where G is constant. It is done by increasing the liquid drop parameter κ describing the $(N-Z)$ dependence of the *surface* energy, which for a sphere is

$$E_S^{(0)} = a_2\left[1 - \kappa\left(\frac{N-Z}{A}\right)^2\right]A^{2/3}. \tag{8.5}$$

The Lysekil version has $\kappa = \gamma = 1.78$ which is equivalent to the assumption that the volume and surface energies have the same $(N-Z)$ dependence. The Lund group increases κ from 1.78 to $\kappa = 2.53$, keeping a_2 constant. Thereby the surface energy and hence the fissility is increased by about 0.03 units on the average for the actinides. Comparison with experiments in the actinide region alone cannot decide which of the two versions is the most adequate; but the second version implies a general increase in fissility for nuclei near beta stability, which for lighter species lowers the liquid drop barrier by a larger amount. For ^{173}Lu or ^{191}Ir the Lund group will calculate fission barriers with the G = const, $\kappa = 2.53$ version that lies 4 MeV lower than the measured fission barriers, as summarized by Moretto, Thompson, Routti, and Gatti (1972). At first glance this may be seen as an argument in favor of the $G \sim S$ version with $\kappa = 1.73$. The same inconsistency with the Lu-Ir barriers as mentioned above is, however, likely to appear also with this version, because the lighter nuclei have strongly drawn-out saddle shapes, i.e., a large surface and hence a large pair condensation energy, which also lowers the barrier.

A surface dependent pairing would tend to increase the energy gap for large distortions, therefore measurements of the energy gap (odd-even staggering) can test this assumption, see Sec. VIII.D.2. On the other hand, the general increase in pair condensation energy with increasing deformation will not be visible in the comparisons, because this effect is bound to be absorbed into the general liquid drop or droplet trends in the process of fitting the parameters of these models.

Pauli and Ledergerber (1971) introduce another modification of the surface energy, Eq. (8.5). They estimate the liquid drop energy at the outer barrier for a number of isotopes with different values of $(N-Z)$ by subtrating calculated shell corrections from the experimental barrier energies using a constant pairing strength. The best fit to the remaining liquid drop part of the energy at the outer barrier is obtained for $\kappa = 2.84$. The same fit determines the quantity $2a_2/c_3$, where c_3 is related to the Coulomb energy of the spherical liquid drop

$$E_C^{(0)} = c_3 Z^2/A^{1/3}. \tag{8.6}$$

According to Myers and Swiatecki (1967) $2a_2/c_3 = 50.9$, whereas Pauli and Ledergerber (1971) obtain the value 52.8 from their best fit to the outer barrier. In the total binding energy a_2 and c_3 contribute to the sum with equal sign. There is in fact a sufficient margin to adjust the ratio $2a_2/c_3$, which influences the deformation energy, by 4% without affecting the ground-state fits. [as an example, Seeger (1967) obtains $2a_2/c_3 = 51.9$ with $\kappa = 2.38$ in his fit to the ground-state masses.] Pauli and Ledergerber's modification (1971) changes the $(N-Z)$ dependence of the fissility X in such a way that the β-stable isotope of a given element has practically unchanged X value. The barriers predicted for ^{173}Lu and ^{191}Ir agree with experiment within 1–1.5 MeV, as they agree with the Myers-Switatecki version (1967).

In the analysis of experimental barriers, the Los Alamos group (Britt, Bolsterli, Nix, and Norton, 1973) reaches a conclusion which supports the readjustments of κ and $2a_2/c_3$ proposed by Pauli and Ledergerber (1971), so does the analysis made by Ignatyuk *et al.* (1975).

For the purpose of this study two differences between the droplet model of 1977 and the liquid drop model of 1967 should be emphasized. On the one hand, the fissility of a typical beta stable actinide is increased in the droplet picture by about 0.025 units, as can be seen from a comparison of Figs. 139 and 140. This means that the droplet saddle energy is lowered by 1–2 MeV relative to the liquid drop (for Cf and Th, respectively). Secondly, the variation of fissility with neutron number is opposite in the two models. In the droplet picture the decrease in surface tension associated with an increase in the neutron excess weighs heavier than the increase in Coulomb radius with the addition of neutrons. Therefore the fissility increases with increasing neutron number (Figs. 140 and 142). In the liquid drop picture the opposite is true (Figs. 139 and 141). This is reflected in the κ values, Eq. (8.5); the liquid drop model uses $\kappa = 1.78$ whereas the effective κ value is ≈ 3.4 in the 1977 droplet model. These two κ values clearly bracket the results of the more limited searches for an optimum κ value mentioned above.

The experimental energies of maxima and minima will be analyzed in the following with reference to both models. Each of the two will give rise to a different splitting of the total energy into a smooth part and a shell correction, displaying in this way the range of uncertainty inherent in this procedure.

4. The variation of experimental barrier energies with fissility

Table XXXII and Figs. 139 and 140 show once again the striking fact that the barriers from thorium to californium have essentially constant heights. They lie in the narrow interval from 6.5 to 5.5 MeV, whereas liquid drop values decrease from 7.5 to 2.8 MeV (and droplet values from 5.0 to 1.5 MeV). The figures also show that the main cause of this effect is a steady lowering of the ground-state energies with increasing Z value due to shell effects at the ground-state deformation (most pronounced when the droplet serves as reference frame). A secondary cause is the positive shell effect at barrier A. It contributes to an increase of the barriers beyond plutonium, where the saddle shape begins to approach deformation A.

Figures 141 and 142 illustrate the large negative shell effect at the isomer deformation. The downward arrows marked Th and Pa refer to the strong undamped resonances observed in these nuclei. If associated with deformation II the arrows illustrate the possible range

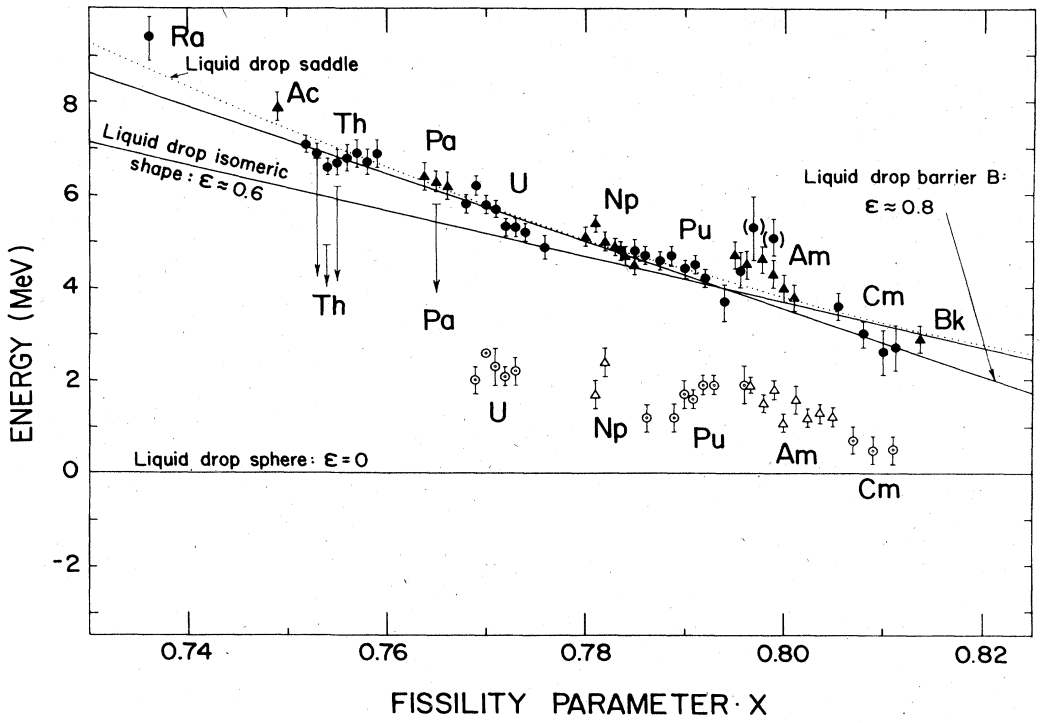

FIG. 141. Energy of second minimum (open symbols) and barrier B (filled symbols) relative to the spherical liquid drop.

(about 2Δ) for the position of the isomeric minimum at deformation II.

The measured outer barriers follow the liquid drop saddle energy rather closely. It is nevertheless incorrect to conclude that shell effects are unimportant here. The apparent weakness of shell effects at the outer barrier is rather due to balancing influences of shell effects—favoring pear-shaped distortions by several MeV—and the liquid drop tendency opposing such distortions. See Fig. 9.

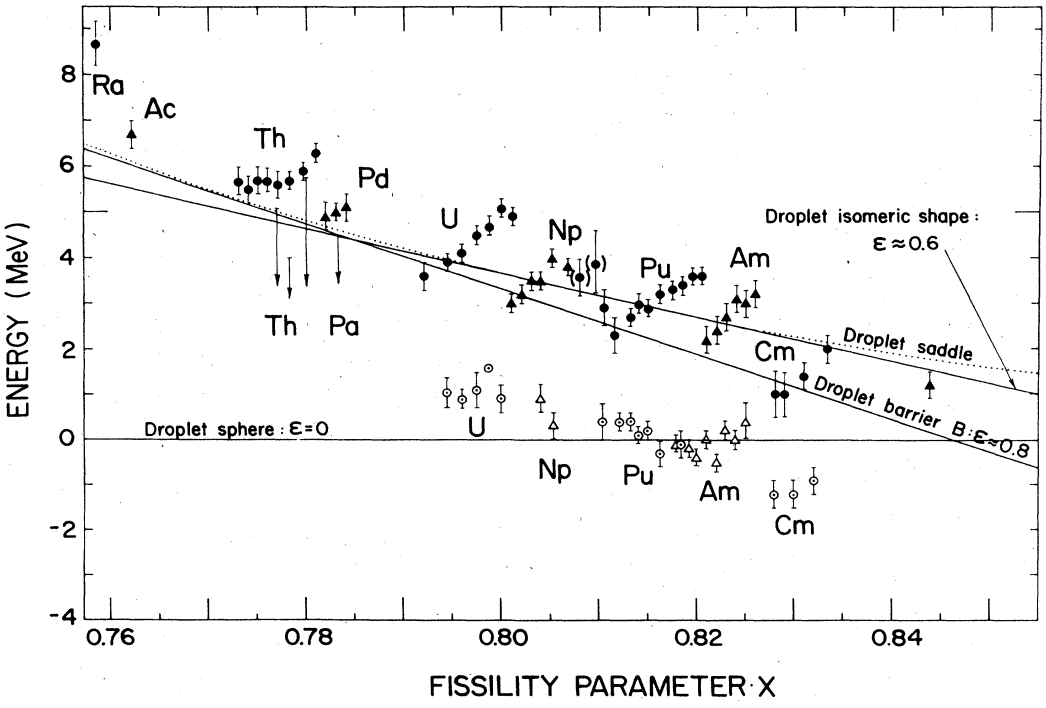

FIG. 142. Same as Fig. 141, only plotted relative to the energy of the spherical droplet.

Among the barrier points for plutonium there are two given in parenthesis. These are the values measured in a rather indirect way by Habs (1977) for ^{232}Pu and ^{234}Pu. Ambiguity exists whether these barriers should be associated with deformations A or with B, respectively. It appears from the plots that assignment to barrier A falls best in line with the remaining Pu barriers. In the following they will therefore be assigned barrier A as also proposed by Habs (1977).

D. Empirical shell corrections and pairing gaps

1. Defining the shell plus pairing correction

As previously mentioned, it is not possible to determine the smooth liquid drop (or droplet) contribution to the total barrier energies unambiguously, because the true shapes are not known. There is, however, considerable theoretical and, as far as the two minima are concerned, also experimental evidence of approximately constant and well defined shapes at each of the four extrema. We will therefore subtract the liquid drop or droplet deformation energy of an axially and reflection symmetric shape corresponding to each of the four extrema, cf. Fig. 137 and Eq. (8.1). In choosing the four shapes, we have been guided by the results obtained by Nilsson *et al.* (1969) in a full calculation of liquid drop plus shell energies.

The liquid drop (and droplet) deformation energy depends to a good approximation linearly on the fissility parameter X when the shape is fixed. Our choice of reference shapes is represented by the straight lines drawn on Figs. 139–142 and marked with the appropriate deformation ϵ. Note that they are tangent to the dotted curves, labeled saddle, at the X values where the fixed shape coincides with the changing saddle shape. The vertical distance of the experimental point from the relevant straight line is then per definition the empirical shell plus pairing correction, $E_\nu^{\text{shell}} \pm \delta\Delta_\nu$, Eq. (8.1).

The most obvious weakness with this definition is the assumption of fixed and axially and reflexion symmetric shapes. There is clear evidence from measurements of quadrupole and hexadecapole moments of a considerable variation of ground state shapes in the acinide region (Bemis *et al.* 1973). These variations are of sufficient magnitude to change the calculated shell energy by 1–2 MeV; see Brack *et al.* (1972). Similarly, deviations from reflection symmetry at the outer barrier, and from from axial symmetry of the inner barrier, are suggested by virtually all theoretical studies of these shape degrees of freedom; see Sec. II.A.1.*d*. Furthermore, the well-known mass asymmetry seen in low-energy fission is suggestive of a pear-shaped outer barrier. The empirical shell energies defined here are therefore likely to combine true shell effects with modifications of the underlying liquid drop energies, arising from distortions away from the assumed axially and reflection symmetric reference shapes. However, these distortion energies are likely to remain small compared to the main liquid drop deformation energy; see, for example, Fig. 9.

In Sec. VIII.F the empirical shell energies will be compared to theoretically calculated values. The fact that the empirical shell correction, as defined here, contains a (small) contribution of liquid drop distortion energy is not so disturbing as it may appear because the theoretical "shell" energies will also be presented in a way that includes such a correction.

2. Odd-even effects at different deformations, pairing gaps

The empirical shell energies are shown as functions of the neutron number in Figs. 143–146 for the four

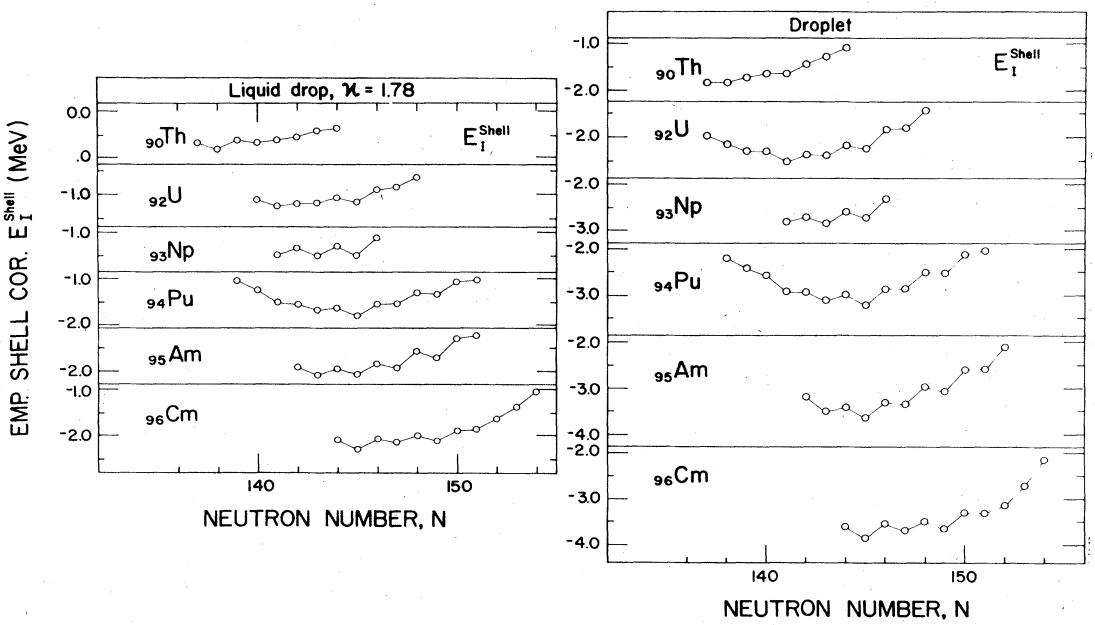

FIG. 143. The empirical shell corrections E_I^{shell} for the ground state, i.e., the distance from the experimental points to the appropriate thin lines in Figs. 139 and 140, plotted as a function of neutron number of different values of Z. Left, liquid drop reference surface; right, droplet reference surface.

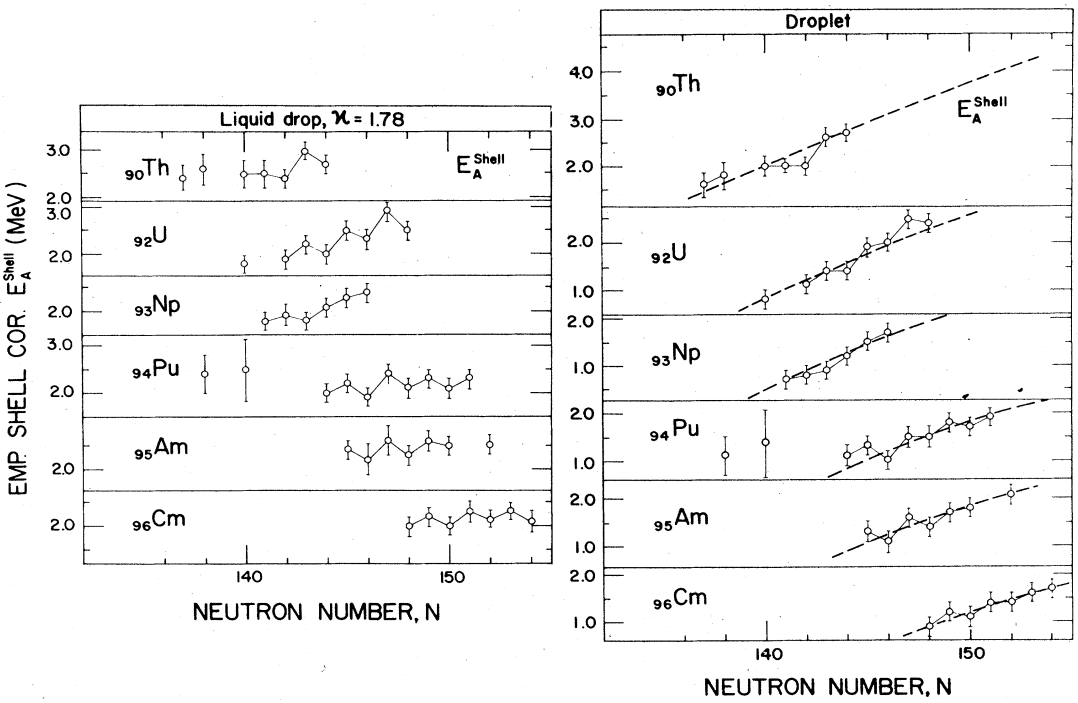

FIG. 144. The empirical shell corrections E_A^{shell} for the first barrier, shown as a function of neutron number in analogy to Fig. 143. The heavy dashed line indicates the general trend of the empirical shell correction. It appears to be approximately independent of proton number.

barrier points, respectively. In each figure the results of using the 1967 liquid drop reference surface or the 1977 droplet surface can be compared. Similarly, Figs. 147 and 148 show the shell energies as a function of proton number. In this section we will focus on the odd-even effects.

The standard odd-even mass difference $\bar{\Delta}$ of Eq. (8.3) used in the (1967) liquid drop model varies from 0.73 MeV for $A = 226$ (Ra) to 0.69 MeV for $A = 254$ (Cf). (The droplet model has a slightly more complicated way of describing the odd-even effects.) Deviations from the mean appear as a staggering of the lines connecting neighboring isotopes in Figs. 143–146, or isotones in Figs. 147 and 148.

a. Ground-state shapes

For the ground states there clearly are systematic deviations, with odd-N energies always lying lower than the even-N neighbors. This indicates that the pairing gap is lower than average, as one should expect in a region where the shell corrections are strongly negative. The odd-even proton staggering is less pronounced. From the magnitude of the deviations the true odd-even difference can be found. It is denoted by $P(Z)$ and $P(N)$ for protons and neutrons, respectively, and is equivalent to the gap parameter Δ. The results are presented in Table XXXIII. They agree with those of Table XXVI as they should, since they are based on the same experimental masses.

TABLE XXXIII. Pairing gap $P(Z)$ and $P(N)$ from odd-even mass differences (MeV).

	Ground state (I)		
Z	N	$P(Z)$	$P(N)$
92–98	140–152	0.75 ± 0.05	—
90	137–144	—	0.70 ± 0.05
92	142–148	—	0.50 ± 0.05
93	141–146	—	0.45 ± 0.05
94	142–150	—	0.50 ± 0.05
95	146–150	—	0.45 ± 0.05
96	146–150	—	0.50 ± 0.05

b. Barrier A

The shell energies at the inner barrier are shown in Figs. 144 and 147. Although the odd-even staggering hardly exceeds experimental errors, the systematically repeated and regular pattern seen on Fig. 144 as one goes from one element to the next is to be taken as evidence of a real effect. In this case it is opposite to the ground-state trend. The odd-N energies lie consistently high, i.e., the gap is larger than the average, as indeed is to be expected where the shell correction energy is positive. The resulting gap values are shown in Table XXXIV. (They would have been even higher if

TABLE XXXIV. Pairing gap $P(Z)$ or $P(N)$ from odd-even mass differences (MeV).

	Barrier A		
Z	N	$P(Z)$	$P(N)$
90–98	140–155	0.9 ± 1	—
92	142–148	—	1.1 ± 0.1
94	144–150	—	1.0 ± 0.1
95	145–150	—	1.0 ± 0.1
96	148–154	—	0.9 ± 0.1

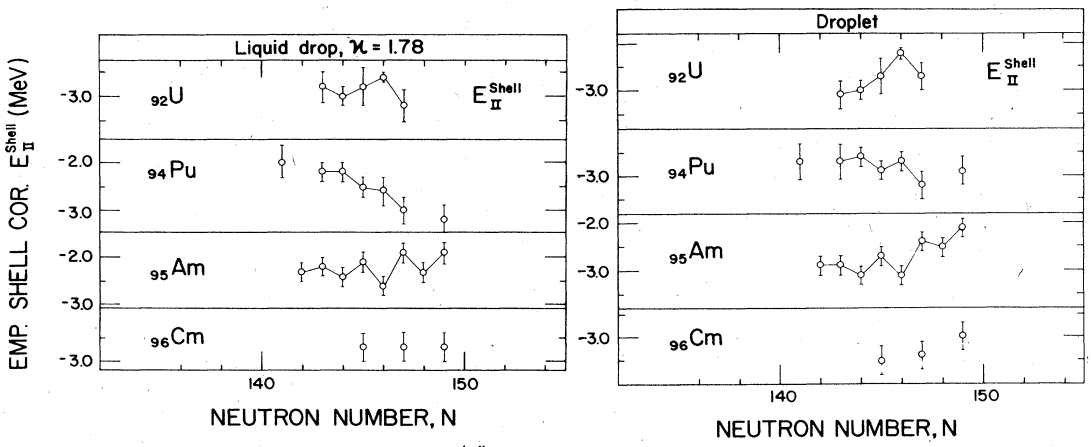

FIG. 145. The empirical shell correction E_{II}^{shell} for the isomeric minimum, as a function of neutron number.

the odd-A barriers had not been corrected downward by ≈ 0.25 MeV as mentioned in Sec. VIII.B.)

c. *The isomeric shape*

The odd-even staggering seen on Fig. 145 is to be considered inconclusive, because it goes in different direction between U-Pu on one side, and Am on the other. Systematic errors in the isomer energies may be responsible for this; cf. Sec. VIII.B.

From the excitation energy of two-quasiparticle isomers in the second well it is nevertheless possible to obtain an estimate of the neutron gap. From Sec. IX.B. 3 we obtain

$$\Delta_n \simeq P(N) = (0.65 \pm 0.15)\ \text{MeV}.$$

d. *Barrier B*

The relevant neutron data are shown on Fig. 146. The evidence for systematic odd-even deviations are marginal in this case. There seem however to be enough regularity and repetition to imply that the neutron gaps are slightly larger than average.

The proton systematics is seen in Fig. 148. Here the evidence seems to be somewhat clearer, indicating a high value for the proton gap.

Table XXXV summarizes the results.

e. *Does the pairing strength increase with surface area?*

If the pairing strength G were to vary with deformation in a manner proportional to the surface area of the nucleus, as qualitatively suggested by Kennedy, Wilets, and Henley (1964) and assumed by Nilsson *et al.* (1969), we should expect a systematic and increasing tendency of the odd-even staggering in going from the ground state towards barrier B. On this tendency would be superposed an oscillatory tendency due to changes in shell level density with changing deformation. For the general trend to stand out, gap values should be compared for a constant value of the shell energy correction. This condition must even be fulfilled for the neutrons separately when neutron pairing is studied, and similarly for the proton pairing. The empirical shell energies at the two minima are roughly equal, and on theoretical grounds it may be permissible to assume the neutron contributions to be so separately. At barrier A, on the other hand, the shell energy is not at all comparable, being of opposite sign. The situation at barrier B is more complex. The empirical shell energy is nearly zero, but as discussed in Sec. VIII.D.1 and as illustrated in Fig. 9 this is likely to be the result of compensatory effects from a large negative shell correction and an equally large liquid drop correction stemming from a pear-shaped distortion. The true shell energy at deformation B may therefore well be of the same magnitude as for shapes I and II. From the calculations of Brack *et al.* (1972) it even appears plausible that the neutron shell energy fulfils the condition separately. With all possible caution one may therefore attempt a comparison of the neutron gap values at deformations I, II, and B for $Z = 94-96$, $N = 144-150$ (Tables XXXIII and XXXV and Sec. VIII.D.2.c),

Deformation I: $P(N) = 0.50 \pm 0.05$

Deformation II: $P(N) = 0.65 \pm 0.15$

Deformation B: $P(N) = 0.90 \pm 0.15$.

Disregarding experimental errors this appears to be the correct trend if the pairing strength G is proportional to the surface area $S(G \sim S)$, whereas $G = \text{const.}$ should give a constant value in all three cases. The trend is even quantitatively the correct one if $G \sim S$; see, for example, Sobiczewski *et al.* (1973) and Flocard *et al.* (1974).

When experimental errors are taken into account together with all the assumptions that have had to be invoked it cannot be said that the evidence for G being proportional to S is conclusive. It seems nevertheless

TABLE XXXV. Pairing gap $P(Z)$ and (PN) from odd-even mass differences (MeV).

	Barrier B		
Z	N	$P(Z)$	$P(N)$
90–96	140–150	1.1 ± 0.1	—
92	142–148	—	0.9 ± 0.15
94	144–150	—	0.9 ± 0.15

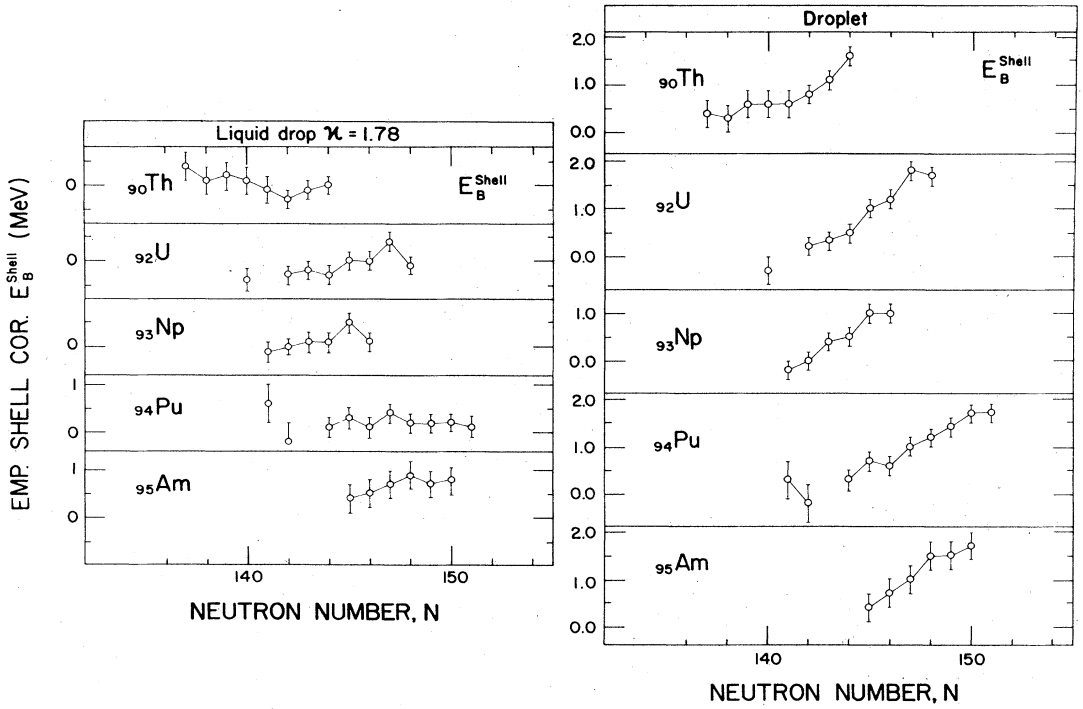

FIG. 146. The empirical shell correction E_B^{shell} for the outer barrier, as a function of neutron number.

more likely to be correct than the alternative assumption of a pairing strength that stays constant.

3. The shell corrections

Leaving now the question of pairing we may focus attention on the sign and the larger scale variation of the empirical shell correction with neutron and proton number. The extend of the ambiguity arising from the choice of liquid drop or droplet reference frame, respectively, will also be examined.

a. Systematic trends

The change in sign of the shell effects is the most conspicuous feature. The ground state and isomeric minima have large negative shell energy, whereas at barrier A it is clearly positive. At the outer barrier B the empirical correction is slightly positive, but as previously observed the true shell effect may well be negative here.

The three assumptions of, (i) independent neutron and proton contributions to the shell energy, Eq. (8.2), (ii) fixed shapes and (iii) fixed energy level diagrams, appear to be approximately fulfilled as far as barrier A and B are concerned. The trend with neutron number in Figs. 144 and 146 is roughly the same irrespective of proton number. As a consequence the variation of shell correction with proton number will repeat itself whatever the neutron number. This is why the empirical shell energies are shown as a function of Z for one neutron number only in Figs. 147 and 148.

The independence of proton and neutron contributions is not borne out by the data for the isomeric minimum, Fig. 145. This may, however, be due to practical difficulties in eliminating systematic errors. Such difficulties are not present when it comes to the ground state, Fig. 143. In spite of this, E_I^{shell} exhibits a minimum as a function of neutron number, that is not independent of proton number. As discussed in Sec. VIII.D.1 this lack of independence is understood as the result of a breakdown of the assumption of fixed shapes at the ground-state deformation.

b. Influence of the choice of smooth reference frame

For a given element the droplet model predicts a lower fission barrier than the liquid drop model. Conse-

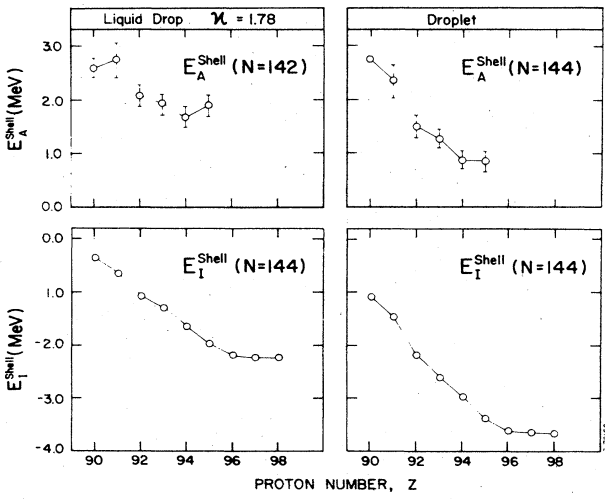

FIG. 147. The empirical shell corrections E_I^{shell} and E_A^{shell} for the ground states and barrier A, respectively, plotted as a function of proton number in analogy to Fig. 143.

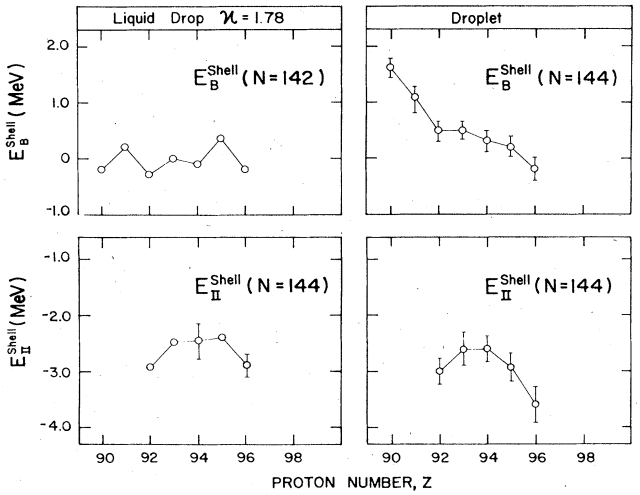

FIG. 148. The empirical shell corrections E_{II}^{shell} and E_B^{shell} for the isomeric minimum and the outer barrier, respectively, plotted as a function of proton number.

quently, shell effects are to a greater extent seen to be responsible for the actual barrier heights, when the droplet model is used as reference frame. This is reflected in Figs. 139–148 and perhaps best seen from the heavy lines on Figs. 150 and 151 which summarize the data. The empirical ground-state shell correction is typically 1.5 MeV more negative when referred to the droplet, whereas the outer barrier correction E_B^{shell} is somewhat more positive, resulting all in all in a larger amplitude for the shell effect in the droplet case. At deformation II the two reference frames give almost identical results, and at barrier A the droplet is still low compared to the liquid drop in analogy to the ground states, though less pronounced.

The other major difference between the two models lies in the different assumptions about the reduction in surface tension with increasing neutron excess. The droplet model abandons the clear but arbitrary assumption of equal influences of neutron excess on the volume energy and on the surface energy that is made in the liquid drop model by setting $\gamma = \kappa = 1.78$ in Eqs. (8.4) and (8.5).

As a consequence, the trend in fissility of the isotopes of a given element go in opposite directions in the two models. This is the reason for the very different slopes in E_A^{shell} and E_B^{shell} seen in Figs. 144, 146, and 150.

The 1977 droplet model incorporates ten years' advance in the development of the description of average nuclear properties. In the subsequent analysis preference will therefore be given to the numbers derived with reference to this model.

E. The magic neutron number for isomeric shapes

As discussed in Sec. IV.C.3, fission isomers with $N = 146$ have the longest half-lives. The effective fission barrier seen by the isomer must therefore have its maximum at this neutron number. In this section we will analyze the trends in americium isomer and outer barrier energies, to see if it is possible to learn more about the precise value of the magic neutron number characterizing the shell that is responsible for the occurrence of the second minimum.

Figure 149 shows the isomer and outer barrier energies relative to the spherical liquid drop or droplet, respectively, plotted against neutron number. The heavy, curved lines are drawn in a crude fashion to illustrate the trend of the experimental points. The thin straight lines show the slope to be expected if the shell corrections were constant, irrespective of neutron number. Both plots illustrate how the distance between two parabolas with displaced axes may have a maximum that is intermediate between the individual extrema of the two curves. This maximum lies near $N = 146$, as expected from the half-life systematics.

The isomeric minimum, on the other hand, appears to occur at a somewhat lower neutron number; which number depends among other factors on the choice of reference frame. Weighing the droplet frame heavier leads one to focus on $N = 144$ as the right magic neutron number for the isomeric shape. It agrees with the Woods-Saxon calculation, Fig. 13.

This result must be seen in the light of the very appreciable errors associated with the experimental energies, allowing in fact different curved lines to be drawn through the same points. For one thing, the difference between the thick lines on Fig. 149 which describes the variation in the effective barrier heights as a function of neutron number has a curvature three times larger than required in order to agree with Metag's (1974) analysis, Sec. IV.C.3. In a more consistent analysis the lines through the points would therefore have to be less curved, adding ambiguity to the conclusion arrived at above. There remain, nevertheless, clear indications of a displacement of the isomeric minimum somewhat below the value $N = 146$ derived from half-life systematics.

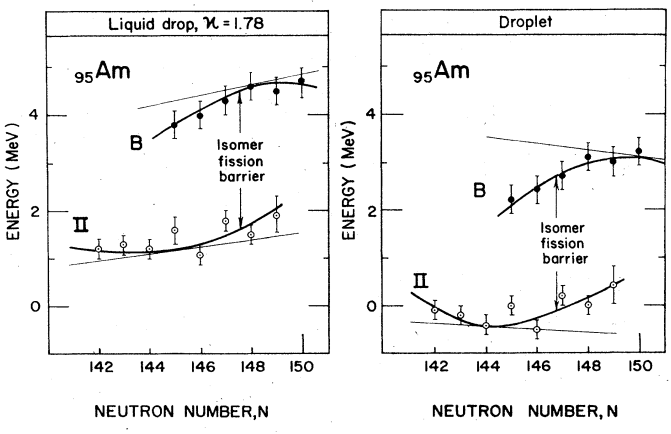

FIG. 149. The energies of the isomeric minimum II and of the outer (fission) barrier B relative to the *spherical* liquid drop (left) and to the droplet (right), plotted as a function of neutron number. Thin lines show the pure liquid drop or droplet trends. Thick lines are drawn to illustrate the experimental trends.

F. Comparison of empirical and theoretical shell corrections

It is customary to compare measured barrier heights and isomer energies with calculated values using the ground-state energy as a reference point in both cases (and adding 0.5 MeV to account for the zero-point energy at the minimum). This may conceal compensating errors at the two energies involved; cf. Sec. VIII.C.2. In this review we shall instead compare the empirical and theoretical shell energies at the four barrier points separately, keeping in mind that in both cases "shell energy" includes the true Strutinsky shell correction plus a (smaller) correction for the liquid drop energy of distortion away from the assumed axial and reflection symmetric reference shapes; cf. Sec. VIII.D.1. The comparisons are made in Figs. 150 and 151.

The most simple shell correction was introduced by Myers and Swiatecki (1967) and is still used in the droplet mass formula of Myers (1977). It assumes a spherical shell correction that varies smoothly between magic numbers, being large and negative at the closed shells and becoming positive between shells. This spherical shell energy damps out with deformation. It goes through zero at a deformation slightly smaller than the deformed ground-state shapes, runs through an over- or undershoot, and reaches zero at larger distortions.

The remaining shell corrections shown in Figs. 150 and 151 are derived from shell level densities by the Strutinsky method. The single-particle potential models used are the modified harmonic oscillator model of the Lund-Berkeley-Warsaw group (Nilsson *et al.*, 1969), the Woods-Saxon model of the Copenhagen-Basel-Moscow group (Strutinsky, 1967; Back *et al.*, 1972), and the Dubna group (Pashkevich, 1969) and the potential obtained by folding a Yukawa two-nucleon interaction function with a sharp-surface pseudodensity of given shape used by the Los Alamos group (Bolsterli, Fiset, and Nix, 1969). See Sec. II.A.1.*c*.

More important than the choice of radial dependence of the potential is the parametrization of the shape, in particular the inclusion of deviations from axial and reflection symmetry.

Möller and Nilsson (1970) were the first to show that pear shapes were important at the outer barrier. For plutonium there is an energy gain of 2.5–3 MeV in allowing the nucleus to pass the barrier with asymmetric shape. Also Pauli, Ledergerber, and Brack (1971) and Bolsterli *et al.*, (1972) obtain this result with their version of the potentials; see Figs. 9 and 150. While all calculations show the ground and isomeric minima to be stable towards asymmetric distortions, it was found by Pashkevich (1969) that the inner barrier could be unstable towards nonaxial, i.e., gamma, distortions. Subsequent calculations by Larsson, Ragnarson, and Nilsson (1972) and by Götz, Pauli, and Junker (1972) substantiate and extend this result. For ^{252}Fm the barrier is lowered by almost 2 MeV, whereas for ^{234}U the barrier is unaffected; see Fig. 15. Thus, for a meaningful comparison with experiment, the calculated barrier shapes must include the gamma degree of freedom for barrier A, and the octupole degree of freedom for barrier B.

Theoretical shell energies are compared to the empirical ones in Figs. 150 and 151. The quasi-independence found for the neutron and proton contributions (Sec. VIII.D.3) allows the experimental energies to be summarized in forms of two plots; one for $Z = 94$ with varying neutron number, the other for $N = 144$ with varying proton number. In each case the empirical energies (heavy lines) are shown both with reference to the 1967 liquid drop model and to the 1977 droplet model.

1. The dependence on neutron number

In the bottom left part of Fig. 150 ground-state energies are compared. Calculations based on the Nilsson (Nilsson *et al.*, 1969) and Woods–Saxon (Pauli and Ledergerber, 1971) levels include optimization with respect to quadrupole and hexadecapole distortions. These two calculations come closest to the droplet-based empirical energies. None of the four theoretical models reproduce the minimum for $N = 144$ characteristics of the plutonium ground state; they all predict the minimum to be near $N = 152$, which does appear as a shell minimum in the experimental energies, but not until Z reaches the value $Z = 98$ (Cf). To avoid confusion only the Woods–Saxon results are shown in the three other plots of Fig. 150.

The axially symmetric barrier A seems slightly high in comparison with the droplet based data; and the inclusion of γ asymmetry (taken from the calculation shown in Fig. 15) does lower it. The resulting change in the trend is unsatisfactory, however, and may raise doubts about the quantitative validity of the γ-asymmetry correction. It appears to depend too strongly on neutron number, and too weakly on proton number; cf. Fig. 151.

For the isomers the magnitude as well as the trend in the calculated shell energy—with a minimum showing up at $N = 144$—shows very satisfactory agreement.

At the outer barrier the neglect of a reflection-asymmetry correction clearly leads to overestimated barrier heights. The improvement resulting from the inclusion of this correction (Möller, 1972) is strong evidence for pear shapes at the outer barrier.

On the whole, the comparison of empirical and theoretical shell effects as a function of neutron number gives satisfactory agreement for the large deformations associated with the fission barrier. The quality of the fits compares favorably to the fits to ground-state masses in Sec. VIII.C.2. The agreement in sign and in the approximate trends should be especially emphasized as a measure of the quality of the fit. This has to be underlined, because the agreement with respect to the actual magnitude of the shell effect is partly coincidental, being dependent on the choice of plutonium ($Z = 94$) as the point of comparison (see below).

2. The dependence on proton number

The bottom left graph on Fig. 151 compares the experimental and theoretical ground-state shell corrections. As in the neutron case the Nilsson and Woods–Saxon potentials give the most satisfactory fit to data based on the droplet reference frame. One notices that the theoretical calculations cannot entirely reproduce

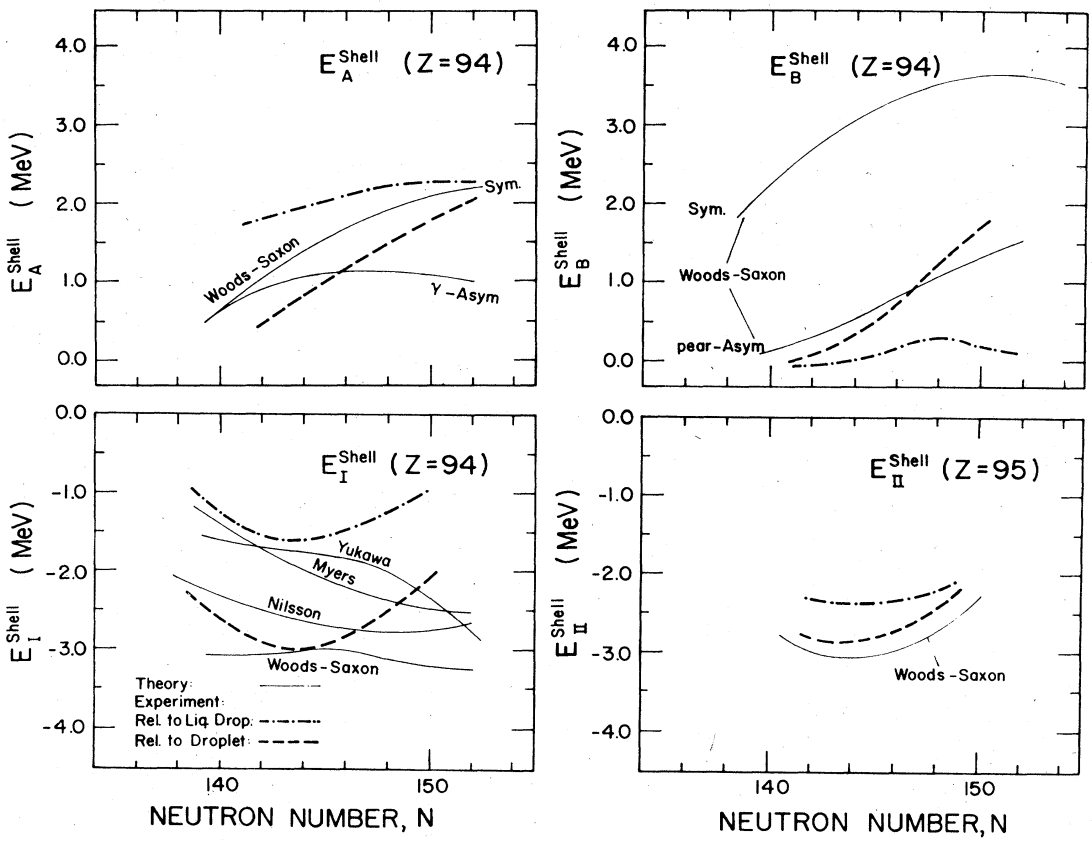

FIG. 150. Comparison of experimental (heavy lines) and theoretical (thin lines) shell correction energies versus neutron number. The theoretical models are explained in the text.

the very steep decrease of the empirical shell correction as the proton number increases.

The experimental points for the second minimum (bottom right) exhibit a downwards curving trend, which probably reflects shortcomings in the analysis of the data. This trend should therefore be neglected when comparing with the calculation. With this reservation the agreement with the Woods–Saxon calculation is satisfactory within the limited range of Z values available for the comparison. Here the evidence, in the form of undamped resonances, for a high-lying minimum in thorium ($Z = 90$) and protactinium ($Z = 91$) has been omitted. Taking it into account would reveal a large discrepancy with the theoretical estimate, a fact that is taken as evidence for the existence of a third minimum in these nuclei (see Fig. 18).

The same problem appears when barrier A is considered (top left). In drawing the experimental trend (thick lines) a discontinuity has been inserted between $Z = 91$ and $Z = 92$ (uranium) in order to illustrate a possible ambiguity in the assignment of experimental barrier heights of thorium and protactinium to deformation A. If the third minimum exists the barriers assigned in Table XXXII as belonging to deformation A may actually lie closer to the outer barrier B, and what is assigned barrier B may correspondingly represent a still more deformed barrier, C. The data is shown in more detail on Fig. 147; regrettably, the evidence for a break in the trend between $Z = 91$ and $Z = 92$ is not clearcut.

There is presumably no ambiguity above $Z = 91$ in Fig. 151 top left. Here, the comparison with the Woods–Saxon calculations with or without the inclusion of γ asymmetry shows very poor agreement. The experimental and theoretical trends are in opposite directions. The experimental data are indicative of a shell maximum at deformation A that is situated at a Z value well below $Z = 90$, whereas the Woods–Saxon shell energy landscape (Fig. 13) predicts the maximum to occur for a proton number considerably above $Z = 100$.

The situation with respect to barrier B (top right on Fig. 151) is not very satisfactory either. Clearly, the reflection asymmetry is required to obtain barrier heights of approximately the right order of magnitude, but after the inclusion of this there still remains a severe disagreement between experimental, droplet-based trends and the theoretical trend—as in the case of barrier A.

The clue to an improvement in the situation may lie in improving the proton potentials. It could perhaps also lie in the shape parametrization or in the underlying droplet model. Finally there may be flaws in the interpretation of the experimental data in terms of barriers A and B of more or less fixed shapes. After all, there are no direct measurements of the shapes of the barrier states.

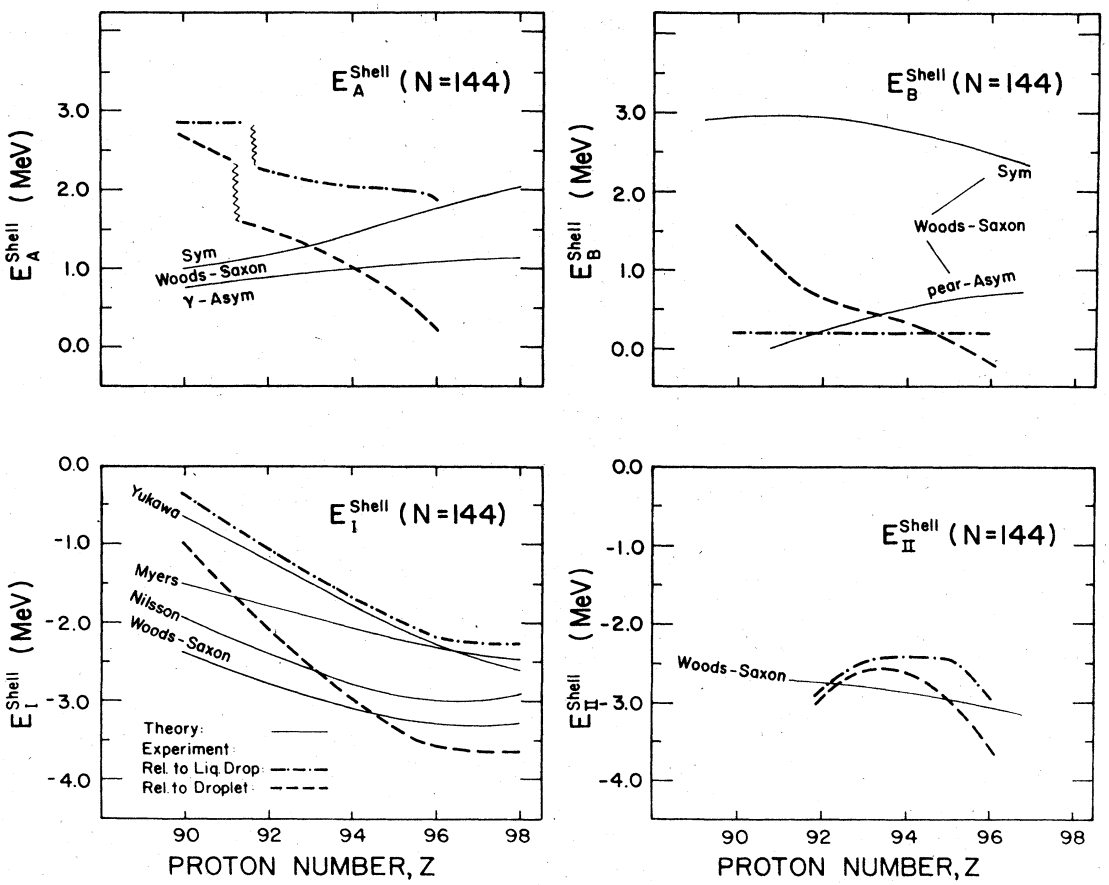

FIG. 151. Comparison of experimental (heavy lines) and theoretical (thin lines) shell correction energies versus proton number; also see text.

IX. SPECTROSCOPY OF SHAPE ISOMERS

A. Shapes of higher and lower symmetry

In the preceding sections, the role of the two-humped barrier in influencing the fission process has been particularly emphasized. Intermediate states in the second well have been regarded as interesting because they speed up fission in a striking way; and the isomers because they give rise to delayed fission and at the same time teach us something about the barrier penetration process.

In this section, the isomeric states and the intermediate resonances are viewed as spectroscopic levels in a nuclear system of an unusual shape. From this viewpoint the extraordinary instability of these states towards fission is considered to be of secondary importance. The interest will be focused on the spectroscopic properties of the ground state and the excited levels in this special sample of nuclear species, which possess a unique shape.

In this regard the interest coincides with previous attempts to study the individual transition states at the saddle point, which was believed at that time to have approximately the shape now attributed to the isomer. These attempts led actually to a number of riddles (Vandenbosch, 1967) that were not resolved until the existence of the double barrier was fully realized. Figure 152 illustrates how the interpretation of fission excitation functions and angular distributions depends on the picture of the barrier. With a single barrier, careful measurements may give information about the actual spectrum of transition states at the saddle, although there are difficulties stemming from the fact that the signature of these states is broadened by the transparency of the Hill–Wheeler barrier. It is expressed through the quantity $\hbar\omega$ that was then thought to be of the order of 3–400 keV on the average. By contrast, a double barrier is characterized by narrow resonances to be viewed as excited states of the isomeric configuration.

The relative stability of these states, as reflected by the much smaller widths, opens greatly improved possibilities for spectroscopic studies. At the same time, the increased complexity of the barrier diminishes the chances for a detailed study of the transition states at the two barriers.

In the following, the discussion will therefore be centered on the spectroscopy of the states of the second well.

These states are expected to be characteristic of a system with a large, axially symmetric, prolate deformation where the individual nucleons are subject to a pairing force. The resulting quasiparticles move relatively independently apart from long-range interactions

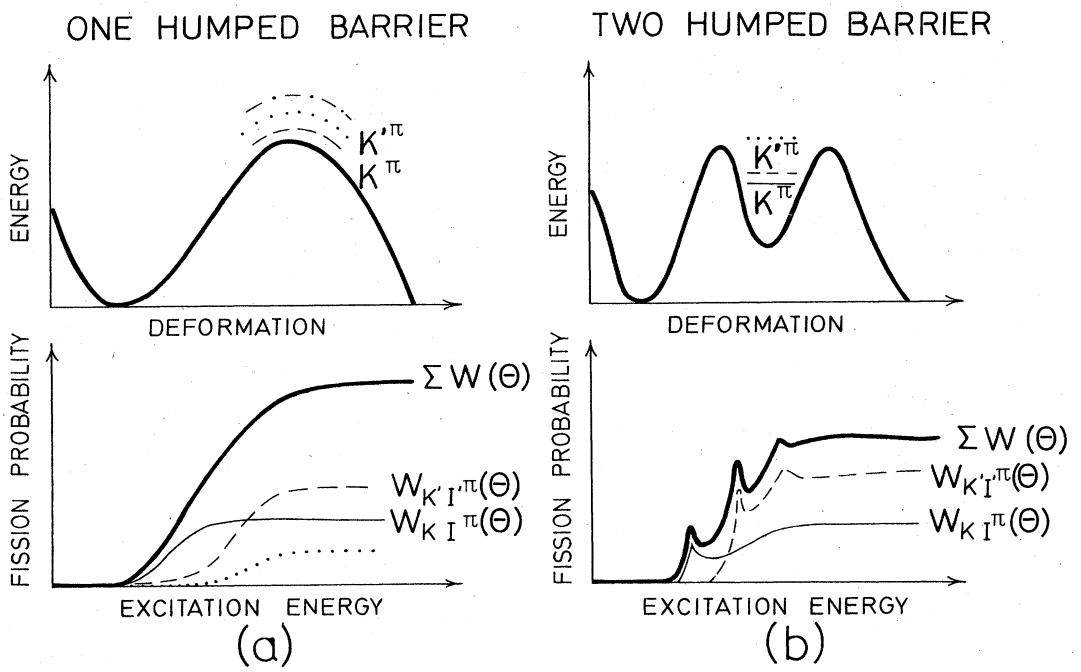

FIG. 152. Near-barrier fission excitation functions. A one-humped barrier gives smoothly rising fission probabilities. Each transition state K^{π} with its associated rotational band will give a characteristic angular distribution, and the total fission fragment angular distribution can in principle be decomposed into a sum of contributions from each channel K^{π}. With a two-humped barrier there will be much more structure in the excitation function, which will be dominated by the transition states in the second well and their associated angular distributions.

which give rise to collective vibrational excitations. Each intrinsic state will be the bandhead of a rotational band, characterized by parity and spin projection quantum number K^{π}.

In this respect, there is a close parallel to the motion in the ordinary deformed nuclei, which have been so extensively studied already. It is therefore natural to ask what specific new features one may expect to find. Figure 153 answers this in a general way: a high degree of symmetry—which one may associate with perfection or beauty—profoundly influences the excitation spectrum. The nucleus ^{208}Pb serves as example. The shell effects associated with spherical symmetry lead to the unique excitation spectrum of ^{208}Pb, because this nucleus contains the right number of protons and neutrons to exploit the shell effect fully. Conversely, large groups of nuclei have a nucleon composition that is unfavorable for a spherical shape, because of the shell degeneracies. These are driven away from the spherical symmetry by the Jahn–Teller effect until they find a less unfavorable shape. The ordinary deformed nuclei are such systems, and they do not possess special symmetry in this sense. It is true that there are what is loosely referred to as shells in these nuclei; neutron number 152 and proton number 100 are often quoted as being magic. However, the gap in the spectrum of single particle energies at these nucleon numbers is accidental in the sense that it is not connected with a special symmetry. [See, however, Strutinsky *et al.* (1977).] The shape isomers are different. These are nuclear systems with nucleon numbers being right, or approximately right, for a field of special symmetry having a ratio of axes 2 : 1. In this sense they are more perfect—or beautiful—than the ordinary deformed nuclei. The excitation spectra of the shape isomers may accordingly show special features associated with the higher symmetry.

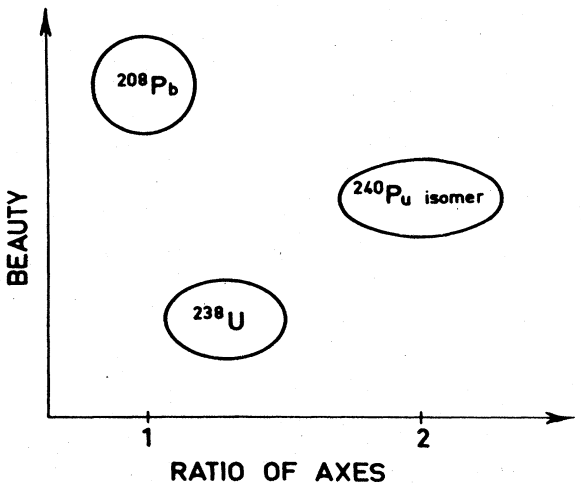

FIG. 153. The spontaneously fissioning isomers have shapes of higher symmetry than ordinary deformed nuclei. This should be reflected in their excitation spectra.

In addition there are several aspects specifically connected with the highly elongated shape. One is the question of the increase in pairing strength with surface area; the $G \sim S$ case that is discussed in Sec. VIII.D.2. The excitation spectrum of the isomeric configuration will be sensitive to the pairing strength through the rotational energy spacings (moment of inertia) and the energy

gap 2Δ separating the ground state from the lowest two-quasiparticle excitations in an even nucleus. The strength of the spin-orbit force is another quantity which is believed to depend on deformation. Such a dependency is reflected in the predicted ordering of the single-particle states and can be elucidated through spectroscopic studies of levels in the odd-A isomers. Finally, a possible pear asymmetry of the isomeric shape will give rise to a degeneracy of single-particle states with opposite parity.

B. Doubly even shape isomers

1. Rotational bands

In the process of producing shape isomers, the deexcitation process is terminated by an $E2$ cascade through the rotational band built on the isomeric level, in complete analogy to the population of the ground-state rotational bands in the first well. The fraction of the total cross section leading through the rotational band is measured by the isomer-to-prompt-fission ratio and is thus of the order of 10^{-4}–10^{-6} (see Fig. 154). It has been possible to observe the weak rotational transitions in a few cases. The first of these is ^{240}Pu (Specht *et al.*, 1972) where the rotational levels up to spin 8 have been established (see Fig. 155). For this rotational band the constant A of the expansion

$$E_{\rm rot}(I) = AI(I+1) + B[I(I+1)]^2 \qquad (9.1)$$

is less than half the value found in the first well; the constant B, which measures the deviation from strict adiabatic rotation, is an order of magnitude smaller than encountered for nuclei in the first well. The shape isomer is, in other words, the most perfect rotor ever found in connection with nuclear rotational motion. This is partly to be ascribed to the large deformation and large mass of this system as reflected in the small A value ($A = \hbar^2/2\mathcal{I}$, where $\mathcal{I}$ is the moment of inertia). At the same time the stiffness toward centrifugal distortion of the system appears to be equal to or larger than typically encountered with ordinary deformed systems (Vandenbosch, 1974, 1977).

Borggreen *et al.* (1977) have measured the rotational constant for ^{236}U, and Metag, Habs and Specht (1980) for ^{238}U. In odd-A systems, there is a very accurate measurement for the $\Omega = \frac{5}{2}^{(+)}$ band in ^{239}Pu made by Backe *et al.* (1979), and cruder estimates exist for ^{231}Th and ^{233}Th (James *et al.*, 1972; Blons *et al.*, 1978 and 1980).

A comparison with theoretical calculations of the moment of inertia follows at the end of this section.

2. Quadrupole moments

The establishment of rotational bands built on the fission isomeric ground states has opened a way for the determination of their quadrupole moments, because the lifetimes of the $E2$ rotational transitions are proportional to the square of the static electric quadrupole moment. A measurement of the rotational $E2$ lifetimes will determine the quadrupole moment and thereby the shape.

Rotational lifetimes have been determined in three different experiments.

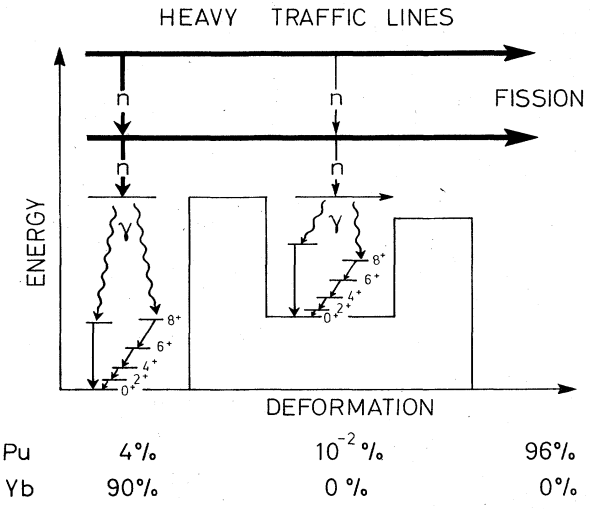

FIG. 154. Flow diagram for the deexcitation of a fissile compound nucleus with two competing wells. The last part of the deexcitation cascades will consist of γ rays and conversion electrons. The low level-density near the ground state ensures relatively heavy population of the low-lying states.

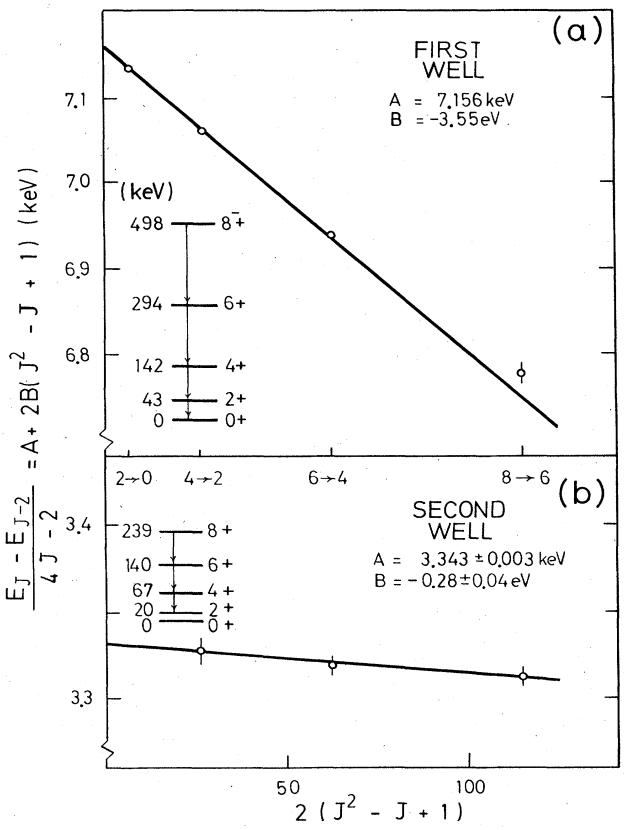

FIG. 155. Rotational bands in the two wells of ^{240}Pu. The intercept of the plots with the ordinate axis measures the rotational constant A of Eq. (9.1) and the slope gives the nonadiabaticity parameter B. [After Specht *et al.* (1972) including a slight revision of the constants A and B due to Metag, Habs and Specht (1980).

Metag and Sletten (1977) have measured these relative to the lifetimes for spontaneous fission of the ^{236m}Pu isomer. This isomer was chosen because it has a spontaneous fission half-life of 37 ± 4 psec, comparable to the expected $E2$ transition rate. The experiment is based on the fact that fragments from the spontaneous fission of a given rotational state with spin I are emitted with a characteristic angular distribution relative to the axis of the particle beam that is used to produce the isomer and aligns the reaction products with the spin perpendicular to the beam axis. The reaction products are allowed to recoil into vacuum, where the alignment is preserved (Metag *et al.*, 1976), and then to decay in flight. The lowest 0^+ state decays isotropically, but the higher spin states contribute increasingly, to the extent that they undergo fission, to an anisotropic decay pattern. The net anisotropy to be observed depends on the magnitude of the quadrupole moment through the branching ratios between $E2$ transitions and spontaneous fission. Figure 156 shows the results of the measurements. A quadrupole moment, $Q = 37 \pm^{14}_{8}$ b gives the best agreement with observation.

In the second experiment, by Habs *et al.* (1976), the feeding time of the 8-μsec isomer of ^{239}Pu, produced in the $(\alpha, 3n)$ reaction on a ^{238}U target, has been measured by an elegant adaptation of the plunger method. Recoils leaving the target will normally have an ionic charge of one to two units. If, however, an internal conversion process takes place during the flight, Auger cascades will give rise to the shakeoff of electrons, resulting in an ionic charge of 14 to 25 units. These high charge states can be reset to their original charge by passage through a thin carbon foil. By measuring the relative yields of high (N_H) and low (N_L) charge states as a function of the distance between the target and a carbon foil, Habs *et al.* have measured the feeding time for the population of the ^{239}Pu isomer in its ground state. Under the very plausible assumption that this feeding time is determined by the last electromagnetic deexcitation cascade through the lowest-lying rotational band and assuming this to have an Ω value of $\frac{5}{2}$, a quadrupole moment of 36 ± 4 b is deduced (see Fig. 157). In a later experiment, Backe *et al.* (1979a) confirm the spin assignment and show that the uncertainty introduced by a possible competition from $M1$ transitions is negligible. By an extension of this method Ulfert *et al.* (1979) have determined the quadrupole moment in ^{238m}U to be 29 ± 3 B, and Metag, Habs and Specht (1980) have measured a value of 32 ± 5 b for ^{236m}U.

Finally, Bemis *et al.* (1979) have succeeded in measuring the ^{240m}Am quadrupole moment by a completely different technique. They study the optical isomer shift of the $^8S_{7/2} \rightarrow {}^{10}P_{7/2}$ atomic transition by directing a tunable, polarized laser beam onto a sample of 1 msec metastable americium atoms produced by stopping reaction recoils in helium gas. Resonance absorption of polarized photons leads in turn to an alignment of the nucleus that will reveal itself as a measurable change in fragment angular distribution from the isomer decay. The observed hyperfine shift implies a change in nuclear root mean square radius of 5.1 ± 0.2 fm^2, corresponding to a charge quadrupole moment of 33 ± 2 b.

The measurements are thus in agreement. As discussed later they also agree fairly well with the calculated quadrupole moment of a prolate ellipsoid with a

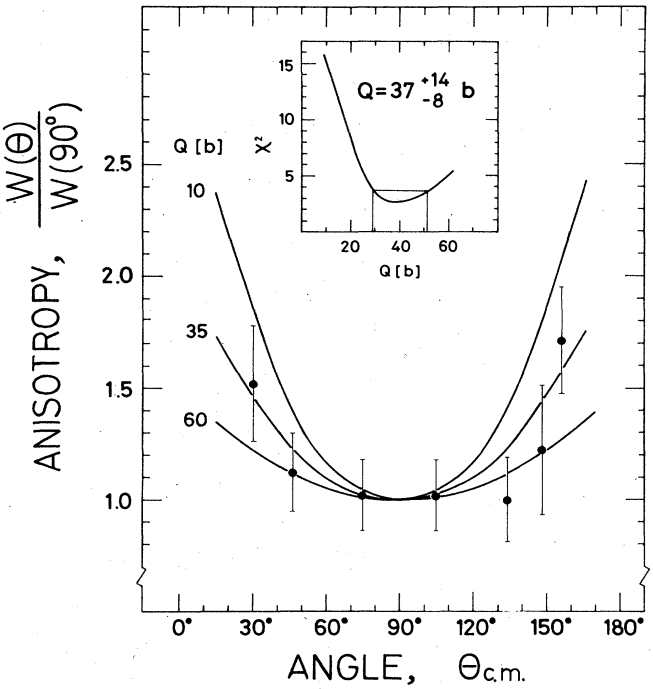

FIG. 156. Angular distribution of delayed fission fragments emitted in flight from the 37 psec isomer of ^{236}Pu. The non-isotropic distribution shows that spontaneous fission takes place from excited rotational states with nonzero spin in competition with rotational $E2$ transitions: A static quadrupole moment of 37b gives best agreement with the data; see insert. (Metag and Sletten, 1977).

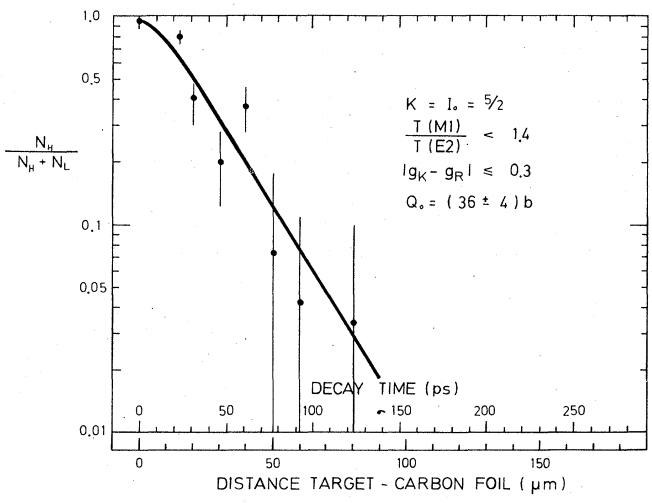

FIG. 157. Probability distribution for the arrival of excited ^{239}Pu nuclei in the isomeric ground state as a function of flight time for the reaction recoils, i.e., feeding time (Habs *et al.*, 1977). The theoretical curve represents a cascade calculation for the $\frac{5}{2}^{(+)}$ rotational band with a quadrupole moment of 36b . The $(M1/E2)$ branching ratio and the $|g_K - g_R|$ value are deduced from the conversion electron spectra of Backe *et al.* (1979).

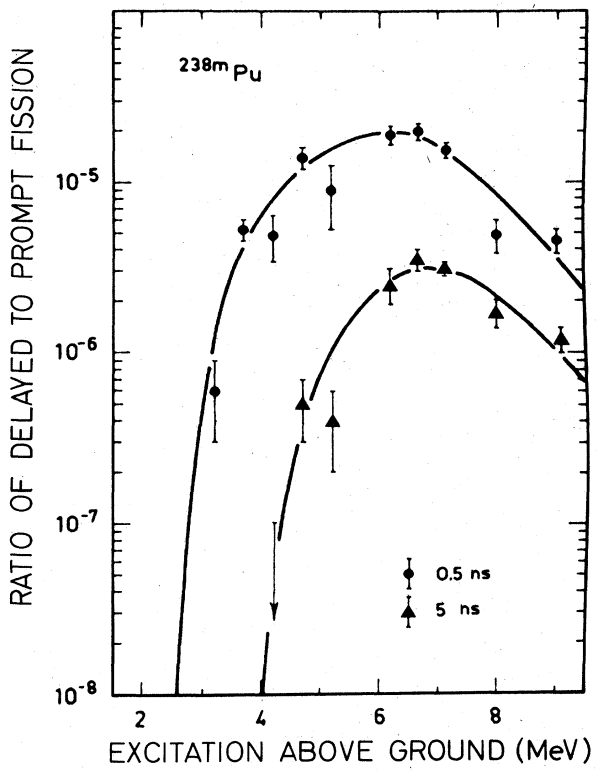

FIG. 158. Yields of two different fission isomers of ^{238}Pu relative to the prompt fission yields in the ^{236}U(α, $2n$) reaction plotted as a function of the maximum energy available to the reaction product ^{238}Pu. From Limkilde and Sletten (1973).

ratio of axes of two to one (see Table XXXVII).

The measurement of the quadrupole moments show in the most direct and independent way that the fission isomers are indeed prolate shape isomers.

3. K isomers, energy gap

In the doubly even ^{238}Pu there are two shape isomers with different half-lives and different excitation energies as measured by Limkilde and Sletten (1973) in reaction threshold measurements (see Fig. 158).

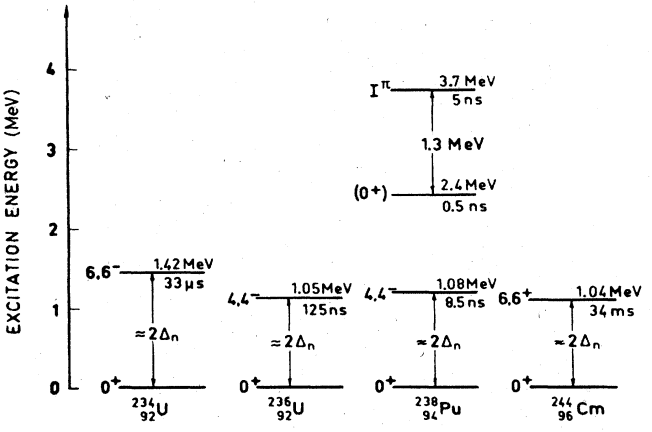

FIG. 159. Two-quasi-particle isomeric states in the first and second well. From Limkilde and Sletten (1973).

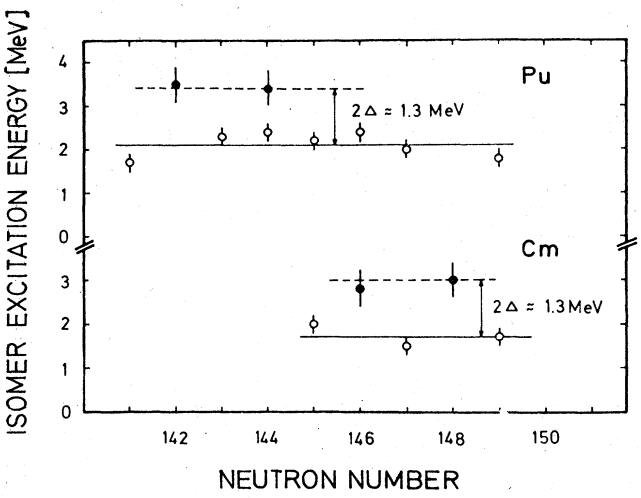

FIG. 160. Comparison of the excitation energies of "normal," short-lived fission isomers (open circle) to "abnormal," longer-lived isomers. From Metag (1974).

In the first well of ^{238}Pu, as in many other doubly even nuclei, there exists an isomeric state which is generated by breaking a neutron pair and coupling the two spin projections to a large K value which hinders the gamma decay to the ground-state levels. The excitation energy measures the magnitude of the neutron energy gap $2\Delta_n$ with a determinacy of about 0.2 MeV. The existence of two spontaneously fissioning isomers in ^{238}Pu appears to parallel this situation and is interpreted accordingly as illustrated on Fig. 159. In a number of other nuclei there are isomers with unexpectedly long half lives and high reaction thresholds as compared to general systematics. Figure 160 summarizes the situation, and it is seen that an excitation energy for the two-quasiparticle isomers and hence an energy gap $2\Delta_n$ of 1.3 ± 0.3 MeV is found on the average for all cases. The gap value is specifically ascribed to the breaking of a neutron pair by analogy to the first well.

4. Vibrational states

The class-II eigenstates of the fission degree of freedom are identical to the beta-vibrational states with

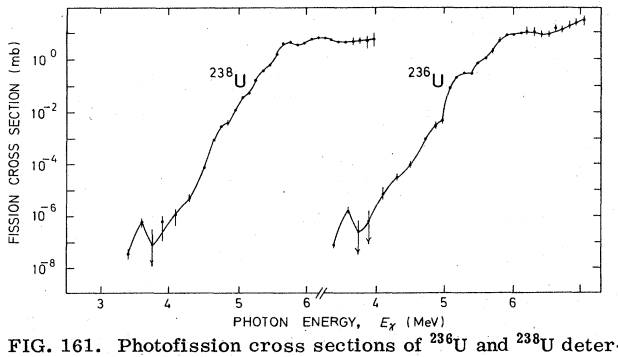

FIG. 161. Photofission cross sections of ^{236}U and ^{238}U determined by deconvoluting the bremsstrahlung photofission yield curves and descending to very low photon energies. Vibrational resonance structures at about 3.5 MeV photon energy are indicated by the data; see also Fig. 128. From Zhuchko *et al.* (1978b).

$K^\pi = 0^+$ built on the isomeric ground state. Their special role in giving rise to broadly spaced resonances in the fission cross section is discussed in Sec. V. A comprehensive experimental review of such resonances in doubly even nuclei is due to Back *et al.* (1974), and an especially penetrating study of ^{240}Pu is described by Glässel *et al.* (1976); see Fig. 102a. Similarly, in-depth studies of ^{236}U and ^{240}Pu have been performed by Goldstone *et al.* (1975, 1976) and by Goerlach *et al.* (1978). The photofission reaction has been exploited by Zuchko *et al.* (1978a, b) locating extremely low-lying resonances in ^{236}U and ^{238}U, previously described as a "shelf" in the photofission cross section (Bowman *et al.*, 1975); see Figs. 161 and 128.

As a rule, strong resonances are found in the energy region just below the lower of the two barriers. This is 2–3 MeV above the lowest state of the second well. The maximum possible energy of a beta-vibrational quantum is thus about 3 MeV, to be compared to values ranging from 0.6 to 1.2 MeV in the first well. There is inconclusive evidence of two successive vibrational resonances with $K^\pi = 0^+$ in ^{238}U and in ^{240}Pu, where the spacings are 0.7 and 0.5 MeV, respectively. This constitutes a lower limit for the vibrational quantum. Fragmentation and anharmonicity effects near the top of the barriers are likely to lower the spacing compared to the first vibrational excitation, so perhaps 1 MeV is the order of magnitude indicated by this type of evidence.

There is unambiguous evidence of mixing of the beta vibration with the underlying spectrum of $I^\pi = 2^+$ compound states (Glässel *et al.*, 1976) (see Sec. V.C.4.a) and it is usual to describe this in terms of a strength function with a width of the order of 100 keV or more. The location of the originally pure beta-vibrational state is identified as the center of the resonance. A "new" resonance with $K^\pi = 0^+$, appearing some 0.5–0.7 MeV higher or lower, is accordingly interpreted as the next state in the vibrational spectrum [see Goldstone *et al.* (1976) and Fig. 162]. Such an interpretation is in fact quite dubious. As shown in Sec. V.C, one cannot generally exclude the possibility of an irregular fragmentation of the beta-vibrational strength over an energy interval of 1 MeV giving the appearance of separate vibrational states, each with a mixing width of the order of 100 keV.

Only at very low excitation energy is the vibrational state likely to remain pure (Secs. V.B.3 and V.C.1.*c*). The resonancelike structures seen by Zhuchko *et al.* (1978b), Fig. 161, do lie very low, just 1.0–1.3 MeV above the isomeric ground state. They may indeed by the pure vibrational states; and if they can be regarded as the first phonon state, a phonon energy of about 1 MeV will result (Table XXXVI and Fig. 162). An assignment as the two-phonon state seems unlikely. It would correspond to a phonon energy near ground of 0.5–0.6 MeV. At higher energies, near the top of the barriers, the 0^+-0^+ resonance spacing would then be expected to be considerably smaller than 0.5 MeV both because of anharmonicities and as a result of fragmentation. This in conflict with the available experimental results.

Superposition of intrinsic excitations with the beta-vibrational states can give rise to new resonances with quantum numbers differing from $K^\pi = 0^+$. These must be rather low-energy modes, because the fission strength will be determined by the beta-vibrational component of the combined motion. In the region of steeply rising fission probability characteristic of the resonance region, a satellite resonance is likely to be obscured unless it lies relatively close in energy to the pure beta-vibrational state; cf. Fig. 81. Nevertheless Goldstone *et al.* (1975) have performed an analysis that leads them to identify a series of no less than four different intrinsic excitations, built on the beta-vibrational resonance at 5.1 MeV in ^{236}U. They all have the same absolute strength (and width) and energies 0.25, 0.35, 0.55, and 0.72 MeV, respectively, above the beta-vibrational state.

Table XXXVI summarizes the properties of vibrational states in the second well. Tentative assignments are bracketed. For a more detailed discussion, see Secs. V.B.5 and V.C.4.

5. Compound levels

The intermediate structure in the neutron-induced fission cross sections with low-energy neutrons is interpreted in terms of class-II compound states of definite spin and parity, as discussed in Sec. VI. The same interpretation applies to the fine-structure states observed with the vibrational resonances using charged particle transfer reactions of high energy resolution and with simultaneous measurements of the fission fragment angular distributions; Sec. VI.E.4.*c*.

As a result, the specific class-II compound nucleus level density in one or more energy intervals lying from 3 to 4.5 MeV above the lowest state can be measured.

TABLE XXXVI. Vibrational states in the second well.

Nucleus	K^π	Energy above: Ground state (MeV)	Isomeric state (MeV)
^{232}Th	(0^+)	5.50 ± 0.05	—
^{234}Th	0^+	5.50 ± 0.05	—
	(0^-)	5.80 ± 0.05	—
^{234}U	0^+	5.00 ± 0.05	≃2.5
	?	(5.50)	≃3.0
^{236}U	0^+	3.60 ± 0.10	≃1.3
	0^+	5.12 ± 0.05	≃2.8
	?	5.37 ± 0.05	≃3.1
	?	5.47 ± 0.05	≃3.2
	?	5.67 ± 0.05	≃3.4
	?	5.84 ± 0.05	≃3.5
^{238}U	0^+	3.60 ± 0.10	1.0
	0^+	5.15 ± 0.05	2.60
	0^+	5.80 ± 0.05	3.25
^{240}U	0^+	5.40 ± 0.05	≃2.8
^{238}Pu	0^+	(5.1)	≃2.4
^{240}Pu	?	4.0 ± 0.10	1.60
	(0^+)	(4.5)	2.10
	(0^-)	4.65 ± 0.05	2.25
	0^+	5.05 ± 0.02	2.65
^{242}Pu	0^+	4.65 ± 0.05	≃2.4
^{244}Pu	0^+	(4.6)	≃2.4
^{250}Cm	?	(3.4)	≃1.8
	0^+	4.0	≃2.4

At present unambiguous results for doubly even nuclei are available for ^{240}Pu only. Here, the correlation analysis of James and Patrick (1969) indicates a spacing of 460 eV for the 1^+ class-II states at the neutron binding energy, i.e., 6.534 MeV above the ground state and 4.1 MeV above the isomeric state. In addition the class-II fine structure of the 5.05-MeV resonance has been resolved in the (d,pf) measurement of Glässel *et al.* (1976) and ascribed to $I^\pi = 2^+$ states on the basis of fragment angular correlation measurements. The spacing, $D_{II}(2^+)$, is found to be 11 keV at this energy, which is estimated to be about 2.65 MeV above the isomer.

6. Summary of experiments

A review of the available information on the level structure in the best studied even isotopies of uranium and plutonium is shown in Fig. 162.

The excitation energy of the different states is given relative to the isomeric ground state. This representation is accurate as far as the rotational bands are concerned. The K isomer of ^{238}Pu is also measured relative to the position of the spontaneously fissioning ground state, albeit with lower accuracy; see Fig. 158.

The remaining excitation energies are determined relative to the ground state of the first well, typically with an accuracy of 50 keV or better. The main uncertainty in the excitation energy is due to a poor knowledge of the position of the isomer itself. The only exception is ^{238}U, where the energy is derived from the observation of gamma rays feeding well known states in the first well (see Fig. 48). This evidence is in conflict with some features of the threshold measurement in the (n,n') reaction populating the isomer [Wolf and Meadows (1974); see Sec. IV.D.3.*d*. It will nevertheless be used in the following.

The isomer energies E_{II} used for the determination of excitation energies in the second well are indicated in Fig. 162. The symbol ≃ means that the number is based on threshold measurements; cf. Table VI. For ^{240}Pu the value 2.4 MeV is based on class-II level densities. The symbol ≈ means that the number is found by extrapolation.

Fission fragment angular distribution measurements have contributed to the determination of K values. This is indicated by writing the K value above the level (or band) in question.

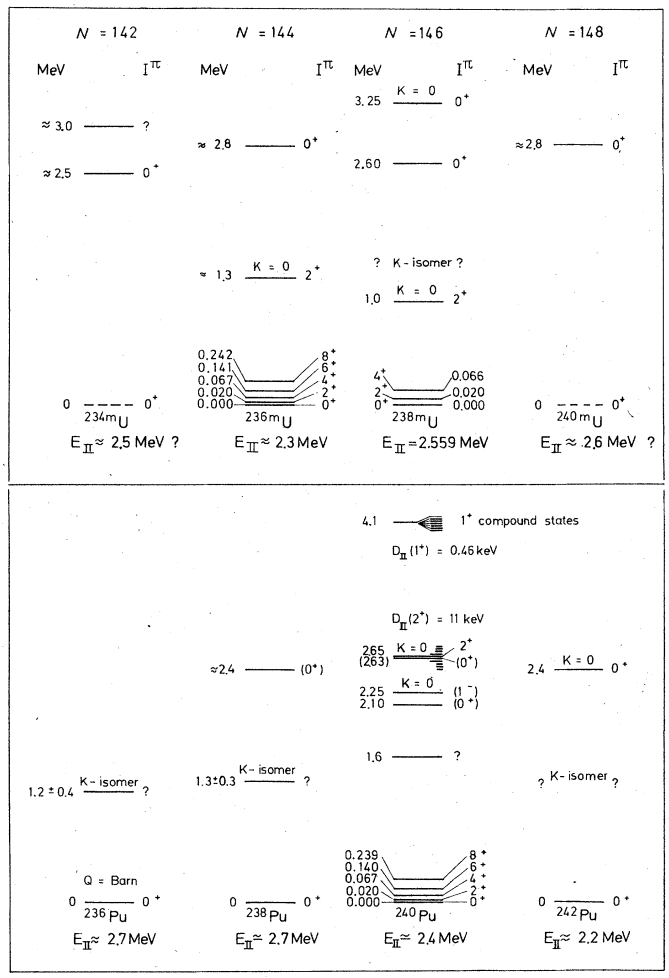

FIG. 162. Nuclear data sheet for shape isomers of doubly even uranium and plutonium isotopes. The excitation energies are given relative to the position of the isomeric state. The energy of this state is generally known with poor precision ($\Delta E = \pm 0.3$ MeV, except for ^{238}U). As a consequence the excitation energies of the higher-lying states are equally uncertain in many cases, although their energy relative to the normal ground state is well known.

7. Comparison with theory

a. The quadrupole moment

With the isomeric shape given as the local minimum in a shell-plus-liquid-drop energy landscape the electric quadrupole moment can be calculated. Brack *et al.* (1974) and Pomorski and Sobiczewski (1978) have done this, arriving at nearly the same values. It should be noted that in the theoretical calculations the shape of the isomeric minimum is invariably found to be axially and reflection symmetric. See, e.g., Larsson and Leander (1974).

The theoretical values shown in Table XXXVII are from Brack *et al.* (1974). One notices a satisfactory agreement between theory and experiment. As stated before, this is the most direct proof of the validity of the interpretation of fission isomers as prolate shape isomers.

The experiments are not sensitive to the sign of the quadrupole moment. From this point of view the isomers might as well be oblate shape isomers with the same quadrupole moment, but of opposite sign. Such a

TABLE XXXVII. Experimental and theoretical quadrupole moments.

Nucleus	Electric quadrupole moment Experiment $e^2 \times 10^{-24}$ cm	Theory $e^2 \times 10^{-24}$ cm
^{236}U isomer	32 ± 5	+33.1
^{238}U isomer	29 ± 3	+36.7
^{236}Pu isomer	37 $\pm \frac{14}{8}$	+36.7
^{239}Pu isomer	36 ± 4	—
^{240}Am isomer	33 ± 2	—
^{240}Pu ground state	11.3 ± 0.5	+11.9

situation is actually completely unrealistic. An oblate nucleus would have to have an axis ratio of 3 : 3 : 1 to possess the same quadrupole moment, and the liquid drop deformation energy required to produce such a shape is over 50 MeV.

b. Moments of inertia

The rotational constant A in Eq. (9.1) is related to the moment of inertia $\mathcal{I}$ through

$$\frac{2\mathcal{I}}{\hbar^2}=\frac{1}{A}\ (\mathrm{MeV}^{-1}) \tag{9.2}$$

The measured moments of inertia for deformed even nuclei in their ordinary ground states are systematically found to be two to three times smaller than expected for a rigid rotor.

Theoretical calculations of the moment of inertia are based on the Inglis (1954) cranking formula with inclusion of pairing effects. In an extensive study by Nilsson and Prior (1961) it is shown how superfluidity as described by the pairing formalism is responsible for the large reduction of the moment of inertia. Quantitatively the formalism gives persistently a somewhat too large reduction with calculated moments of inertia about 20% smaller than the measured values.

Similar calculations for shape isomers are due to Sobiczewski *et al.* (1973) and to Pomorski and Sobiczewski (1978) who also use the Nilsson harmonic oscillator base. In the more strongly deformed shape isomers the reduction of the moment of inertia due to superfluidity is less drastic, and the agreement between calculated and measured moments of inertia is better for the large deformations, with the calculated values being slightly low with $G\sim S$ and slightly high for $G=\mathrm{const}$.

In a parallel study by Brack *et al.* (1974) the Nilsson oscillator base is replaced by Woods–Saxon wave functions and again good agreement with experiment is obtained for the isomers ^{236m}U, ^{238m}U, and ^{240m}Pu. For ground states the agreement is generally less satisfactory.

There have been serious doubts whether the BCS pairing formulation should actually be expected to lead to quantitative agreement, because of its lack of rotational invariance (Migdal, 1959a, b). Using again Nilsson oscillator wave functions Hamamoto (1974, 1975) has extended the theoretical treatment by adding to the standard monopole term of the pairing interaction a quadrupole, or Migdal, term, which corrects for this failure. The correction (Hamamoto, 1974) reduces the discrepancies otherwise occurring between the calculated energy gap and moment of inertia for ordinary deformed nuclei to about 2%.

The results of Hamamoto's (1975) calculations of isomeric shapes are compared to experimental values in Table XXXVIII. The new theoretical calculations overestimate the moment of inertia of the isomers by 18% in case of $G=\mathrm{const}$ and 9% when $G\sim S$. Thus the inclusion of quadrupole pairing terms, which successfully corrected a long standing discrepancy with respect to the ground-state moments of inertia, is less successful for the description of the isomer moments of inertia.

Part of the trouble may have to do with the $\mu(l^2-\langle l^2\rangle)$ term in the Nilsson Hamiltonian, which tends to give unrealistically large moments of inertia for strongly deformed nuclei. At any rate, there still seem to be unsolved problems in understanding the dynamics of nuclear rotational motion for strongly distorted systems.

c. The energy gap

The experimental evidence on the magnitude of the neutron gap is summarized in Sec. IX.B.3. The uncertainties are large, resulting in an estimated magnitude of 1.3 ±0.3 MeV as an average for the four shape-isomeric nuclides ^{236,238}Pu and ^{242,244}Cm.

Pomorski and Sobiczewski (1978) have calculated the gap, $2\Delta_n$, and find it to be 1.16 MeV on the average for the four nuclides in the case where $G=\mathrm{const}$, and 1.52 MeV in the case of $G\sim S$. The evidence with respect to these two alternatives is therefore inconclusive when seen in isolation; see, however, Sec. VIII.D.2.

d. Vibrational excitations

Zielinska-Pfabe and Gabrakov (1973) have attempted to calculate the energies and $B(E2)$ values of beta and gamma vibrations in the second minimum. They estimate values of 0.75–1.25 MeV for the gamma-vibrational phonon in ^{236,238}U and ^{240}Pu. There is no experimental evidence to test this result. The attempt to calculate energies of beta vibrations that might more readily be compared with experiments (cf. Table XXXVI and Fig. 162) is not believed by the authors to yield meaningful results.

The theoretical exploration of collective vibrations in the second well thus remains open.

C. Odd-A shape isomers

An odd-A nucleus can be thought of as a doubly even core to which an extra particle is coupled. With the core in its paired ground state, the odd particle determines the spin, spin projection Ω, and parity of the

TABLE XXXVIII. Experimental and theoretical moments of inertia. The theoretical values are from Hamamoto (1975). The numbers quoted assume a pairing strength $G\sim S$ for both neutron and proton contributions. The neutron contribution for the ^{236m}U isomer has been corrected to a value found for adjacent nuclei, since there is a strong singularity in the calculation due to a shell gap at $N=144$ that is believed to be unrealistically large. With $G=\mathrm{const}$ the calculated moments of inertia are 8% bigger. The values of the rigid moment of inertia refer to the the isomeric shape with deformation $\epsilon=0.6$.

Nucleus	Moment of inertia, $2\mathcal{I}/\hbar^2$ Experiment (MeV^{-1})	Theory (MeV^{-1})	Rigid (MeV^{-1})
^{231}Th isomer	520 ±30	—	365
^{233}Th isomer	450 ±50	—	370
^{236}U isomer	297 ± 1	324	378
^{238}U isomer	306 ± 3	—	384
^{239}Pu isomer	297 ±10	—	387
^{240}Pu isomer	299.1 ± 0.3	332	390
^{236}U ground state	132 ± 0.5	131	274
^{240}Pu ground state	140 ± 0.5	150	283

systems as a whole. Different single-particle configurations with given Ω^π values have different energies, which may vary considerably with deformation. This is the origin of the specialization energy, Fig. 53. It means that the double-humped barrier may look different for different single-particle configurations. In particular the location and width of the fission resonances will vary with the value of Ω^π. With a given spin distribution and alignment, produced in a particular nuclear reaction, there will be a specific pattern of fragment angular distributions associated with each band of given Ω^π value, Fig. 152. In principle, all that is required is to find the fission resonance peaks, measure the angular distribution, and deduce Ω, I^π. Then one has to judge whether the resonance corresponds to the zero-order beta-vibrational motion of the core or to a higher-order phonon coupled to the single particle. If it is the zero-order phonon, the resonance represents the single-particle state in the second well with its associated rotational band.

When the secondary well is deep as evidenced by the existence of fission isomers, measurements of rotational and interband transitions following a reaction are possible just as in the case of even isomers discussed in Sec. IX.B.1. but the experimental difficulties are greater. In recent years there have, nevertheless, been major advances in this area. The work of Backe *et al.* (1979) on ^{239m}Pu seem to open new avenues for spectroscopic studies of shape isomeric odd-A nuclei Metag, (1980) and Metag, Habs and Specht (1980).

The spin of the isomer may be aligned as a result of the reaction, and the alignment may under favorable conditions be preserved during a period which is longer than the decay time. The fission fragments will then be emitted according to an anisotropic pattern that can be brought to rotate under the influence of an externally applied magnetic field, thanks to the nonzero magnetic moment of the isomeric nucleus. As a result, spins and magnetic moments of odd-A isomers can in principle be determined. So far, however, it has scarcely been possible to overcome the experimental difficulties associated with this type of measurement.

There is a fundamental interest in measurements of the properties of the individual single-particle states. It allows the most detailed test of the theoretical calculations of the single-particle motion in potentials of varying shapes that form the basis for the whole picture of the double-humped barrier.

An example of four different calculations of single-particle levels, which all lead to a second minimum of comparable magnitude, is given in Fig. 23.

1. The ^{231}Th and ^{233}Th resonances

The only odd-A nuclei where very pronounced and sharp resonances of the vibrational type have been observed are ^{231}Th and ^{233}Th. They are found in neutron induced fission at energies almost 6 MeV above the ground state (Sec. V.B.5.)

From the present knowledge of damping, or of vibrational strength functions, this implies that the resonances must be located in a shallow intermediate well with a minimum lying at least 4 MeV above the ground state. For all we know the lowest-lying resonance may even represent the ground state of the intermediate minimum. As discussed in Secs. IV, V, VIII and X, the theoretical calculations have consistently failed to predict such high-lying secondary minima in the thorium isotopes. This is the "thorium anomaly." As one solution, Möller and Nix (1974) have pointed to the possible existence of a third, shallow minimum at still larger deformations. Such a minimum appears in their theoretical barrier calculations for the lighter actinides. See Figs. 18 and 165.

The most conspicuous resonance is found in the ^{230}Th(n,f) reaction at 700 keV neutron bombarding energy, as is seen in Fig. 84. James *et al.* (1972) have measured the fission excitation function and fragment angular distribution with a neutron energy resolution of 5 keV. The fragment angular distribution in the region of the peak shows uniquely that the Ω value is one-half. The various rotational states of this $\Omega = \frac{1}{2}$ band are hidden in the peak. By extremely careful high-resolution measurements of the angular distributions at the flanks and across the top of the peak [see also Yuen *et al.* (1971)], the outline of a strongly decoupled rotational band of negative parity emerges. Nature has been unkind in this case. The angular distributions are not as rich in structure as one might have expected with a different value of the decoupling parameter a.

As a result of these measurements, a $\Omega^\pi = \frac{1}{2}^-$ band with a rotational constant $A = 2.3 \pm 0.5$ keV and a decoupling parameter $a = -2.1 \pm 0.2$ is known to lie 5.85 MeV above the ground state. There is evidence of an $\Omega = \frac{3}{2}$ band slightly higher, at 6.12 MeV (see Sec. V.B.5.a).

The predicted single-particle spectra for the second minimum (Fig. 23) contain states which could explain the measurements, but this is no proof and does not exclude the possibility that the resonances are due to levels in a possible third minimum at larger deformations. In Sec. V.C, the case of ^{231}Th is discussed from this point of view; indeed it is shown there that schematic models for fragmentation of the vibrational states seem better able to explain the observations on ^{231}Th if the Nilsson states in the region of the outer barrier deformation (third minimum) are considered.

Recently, Blons *et al.* (1978 and 1980) have reported additional structure in the region of the decoupled $\frac{1}{2}$ band. Their analysis (1978) suggests the presence of an additional, almost degenerate $\frac{1}{2}$ band of opposite parity; and they regard this as evidence of a permanent reflection asymmetry of the field in which the odd spin $\frac{1}{2}$ particle moves. Qualitatively, this explanation cannot be excluded. In such a case, however, the two $\frac{1}{2}$ bands of opposite parity should have numerically equal decoupling parameters but of opposite sign (Bohr and Mottelson, 1975). The interpretation suggested by Blons *et al.* (1978) is not in quantitative agreement with this. A renewed examination of the problem shows that the data are consistent with decoupling parameters of equal and opposite sign, (Blons *et al.* 1980). See Sec. X.B.2.a.

The ^{232}Th(n,f) reaction has been known for a long time to show broad structures at neutron energies 1.3–1.8 MeV (see Sec. V.B.5.6). These structures are accompanied by pronounced variations in the fission fragment angular distribution patterns (Andosenko *et al.*, 1969).

More recently, Blons, Mazur, and Paya (1975a,b) have observed what might perhaps be rotational fine structure in the excitation function. Caruana *et al.* (1977) in a renewed analysis of the ^{232}Th(n,f) data conclude that only a shallow minimum behind relatively thin barriers (large $\hbar\omega$ values) can explain the measurements, thus supporting the third minimum hypothesis.

Attempts have been made by Androsenko *et al.* (1969) as well as by Blons, Mazur, and Paya (1975b) to interpret the date in terms of resonance structures with characteristic values of Ω^{π} (cf. Fig. 152), and in the latter case with characteristic moments of inertia. The two groups do not focus the attention on quite the same neutron energy regions, but the measurements are consistent where they can be compared.

As a result, a more or less tentative scheme of single particle states, possibly coupled to vibrations, in the second or perhaps the third minimum can be presented as in Table XXXIX. It should be emphasized again that there are major ambiguities in connection with the interpretation of these experimental results, especially as regards ^{233}Th.

2. Single-particle properties of shape isomeric states

a. ^{237}Pu

In ^{237}Pu there are two fission isomers, one with a 1.1 μsec half-life, the other decaying with a 0.11 μsec period. Russo *et al.* (1971) have studied the relative population of these two isomers in compound nucleus reactions with different amounts of angular momentum brought into the compound system. They find that increased angular momentum favors the population of the 1.1 μsec isomer. Using a traditional, statistical, isomer-ratio analysis of the results they conclude that the spin of the short-lived isomer is likely to lie between $\frac{3}{2}$ and $\frac{7}{2}$, whereas the longer-lived isomer would have a spin value several units higher. Günther *et al.* (1979) reach the same conclusion based on photon excitation of the isomers.

In a subsequent study, Vandenbosch *et al.* (1973) measured the thresholds for producing the two isomers by the $(\alpha,2n)$ reaction separately, and found that the longer-lived, higher-spin isomer is lying (0.30 ± 0.15) MeV above the other isomer, which then presumably is the ground state in the second well.

The nuclide ^{237}Pu has 143 neutrons. It is not difficult to identify levels which can explain these results in the diagrams of Fig. 23, and similar diagrams. For the high-spin isomer, the $[615]\frac{11}{2}^{+}$ or the $[505]\frac{11}{2}^{-}$ states at that time seemed likely candidates that would explain the highly hindered gamma decay to the lower-lying ground-state band, for which the assignment $[512]\frac{3}{2}^{-}$ appeared to be a likely possibility.

Experimental data of the nature just described are in effect insufficient to allow definite assignments and to test the theoretical predictions in a crucial way. It therefore appeared to be a major step forward when it was realized by Specht *et al.* (1974) that fission fragments from the spontaneous decay of isomers that had recoiled into a lead backing were emitted nonisotropically. Of the two isomers of ^{237}Pu the long-lived one was found to emit the fragments preferentially sideways with respect to the beam, thus indicating a high Ω value, whereas fragments from the short-lived isomer were mainly emitted along the beam direction (low Ω value). This result immediately showed that the two isomers decay by spontaneous fission independently of each other, and that a possible gamma transition between them is absent or at least weak. At the same time these findings opened the way for spin- and Ω-value determinations and for the measurements of magnetic moments and g factors. Anisotropy measurements

TABLE XXXIX. Single-particle resonances in ^{231}Th and ^{233}Th (tentative).

Nucleus	Ω^{π}	Neutron bombarding energy (MeV)	Energy above first minimum (MeV)	Moment of inertia $2\vartheta/\hbar^2$ (MeV^{-1})	Footnote
^{231}Th	$\frac{1}{2}^{-}$	0.71	5.84	520 ± 30	a
	$\frac{3}{2}$	0.99	6.12	—	b
^{233}Th	$\frac{5}{2}^{+}$	1.0	5.80	—	c
	$\frac{1}{2}$	1.1	5.90	—	c
	$\frac{5}{2}^{-}$	1.2	6.00	—	c
	$\frac{3}{2}^{+}$	1.2	6.00	—	c
	$\frac{3}{2}^{-}$	1.35	6.15	—	c
	$\frac{1}{2}$	1.415	6.20	—	d
	$\frac{3}{2}$	1.504	6.30	410 ± 15	d
	$\frac{3}{2}$	1.579	6.37	365 ± 15	d
	$\frac{1}{2}$	1.711	6.50	—	d

[a] The more recent measurements of Blons *et al.* (1980) have a higher value of the moment of inertia, cf. Table XXXVIII.
[b] James, Lynn, and Earwaker (1972).
[c] Androsenko *et al.* (1969).
[d] Blons, Mazur, and Paya (1975).

from isomers recoiling into vacuum are also reported to yield positive results, particularly in the case of the 34 nsec isomer of ^{236}Pu (Galeriu *et al.*, 1974).

An attempt to exploit these new possibilities was made by Kalish *et al.* (1974) who employed perturbed angular correlation techniques to the study of the ^{237}Pu isomers. Their measurements resulted in a g factor for the 1.1 μsec isomer of 0.18 ± 0.02 with positive sign. Similarly the other isomer was tentatively found to have a g factor of 0.54 ± 0.06, again positive. Subsequent work by the Copenhagen group and at Heidelberg (Habs *et al.*, 1975, 1976, 1977) failed to arrive at reproducible results. The original measurements must therefore be considered highly uncertain until the experimental situation becomes more clear.

The collective motion of the nucleus gives a negative contribution to the g factor. To obtain a positive g factor with an odd neutron nucleus requires a positive contribution from the neutron spin magnetic moment, and this means in turn that the neutron spin σ must be antiparallel to the neutron orbital angular momentum projection Λ ($\Omega = \Lambda - \frac{1}{2}$). The significance of eventually finding a positive g factor becomes clear, when it is realized that none of the high spin levels on the three left-hand diagrams in Fig. 23 fulfils the condition $\Omega = \Lambda - \frac{1}{2}$ for neutron numbers near $N = 143$.

b. ^{239}Pu

The conversion electron measurements of the 3 nsec delayed transitions feeding the 8 μsec fission isomer in ^{239}Pu, Fig. 163, can be interpreted unambiguously in terms of a single-particle state of spin $\frac{9}{2}^{(-)}$ at 203 keV excitation energy, decaying into the rotational ground band with spins $\frac{9}{2}^{(+)}$, $\frac{7}{2}^{(+)}$, $\frac{5}{2}^{(+)}$, and Ω^{π} value $\frac{5}{2}^{(+)}$ (Fig. 164). Moreover, a careful analysis of the $M1 - E2$ competition within the band leads to the conclusion that $|g_K - g_R|$ for this band is ≤ 0.30. This means that the predominant component of the isomeric state has to be an orbit with antiparallel coupling of spin and orbital angular momentum, and that a possible admixture of a component with **l** and **s** parallel amounts to less than 40%. As already noticed in the previous subsection, none of the $\frac{5}{2}$ levels on the three left-hand diagrams of Fig. 23 fulfils the condition of $\Omega = \Lambda - \frac{1}{2}$ for neutron numbers near $N = 145$ [see Metag (1980) and Metag, Habs and Specht (1980)].

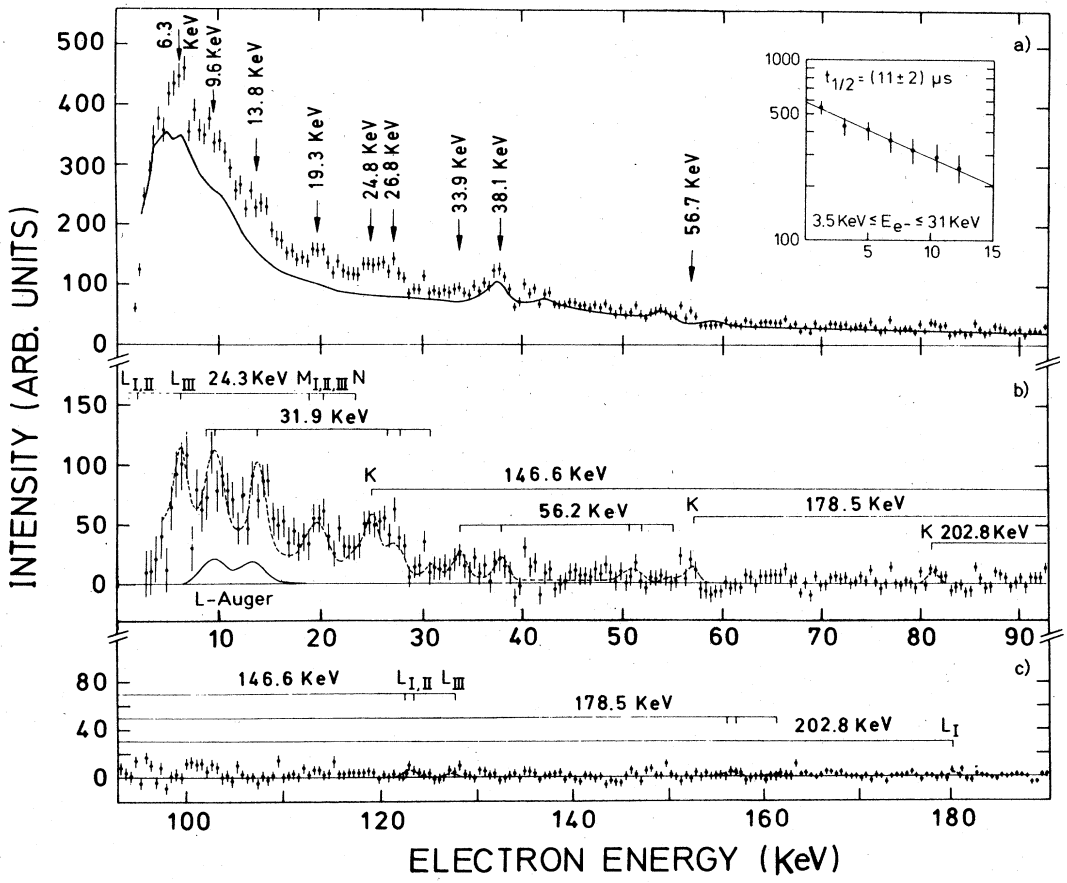

FIG. 163. Spectrum of electrons measured in delayed coincidence with fission of the 8 μs ^{239}Pu fission isomer. (a) Raw data in the range from 3 to 190 keV. Peaks in the background arise from the ^{241}Am source. (b), (c) the electron spectrum corrected for random coincidences in the range from 3 to 190 keV. The dashed curve represents the fit to the data. The position of the K, L, M, and N components of the different transitions are indicated. From Backe *et al.* (1979).

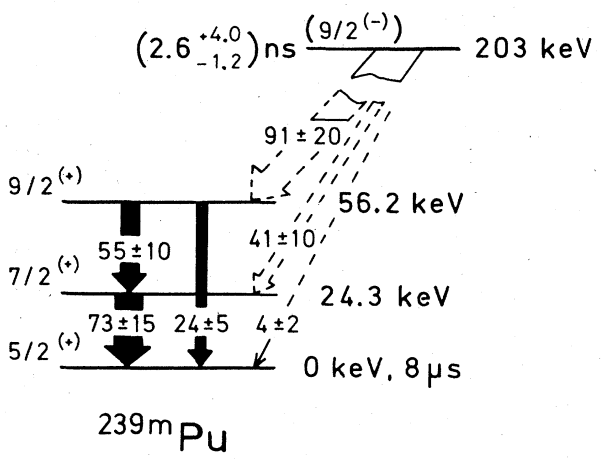

FIG. 164. Decay scheme of the 2.6 ns isomer decaying to the lower lying 8 μs fission isomeric state in ^{239}Pu. The intensities of the feeding transitions are total intensities, being corrected for internal conversion by assuming multipolarities $E1$ (147, 179 keV) and $M2$ (203 keV). The positive parity of the $\frac{5}{2}$ state is suggested by comparison with theory, since no $\frac{5}{2}^-$ state is expected close to the Fermi surface. Compare Fig. 23.

3. Comparison with theory

a. Magnetic properties of neutron states in plutonium

Hamamoto and Ogle (1975) have addressed themselves to a study of single-particle level properties in terms of the parameters of the Woods–Saxon potential at large distortions. They argue, partly on the basis of optical model fits to nuclear scattering experiments in the entire region from ^{40}Ca to ^{208}Pb, and partly on the basis of Hartree–Fock and Thomas–Fermi calculations, that the spin-orbit force is defined by the nuclear matter density gradient rather than by the gradient of the potential. In consequence thereof the spin-orbit strength λ is increased in their calculation from its "standard" value $\lambda = 33$–37 to the value $\lambda = 38$. More importantly, in the same spirit the spin-orbit radius is taken to be $r_{ou} = 1.10$ fm, to be compared with the Woods–Saxon radius parameter $r_{on} = 1.25$ fm for the (central) potential. Both these shifts increase the spin-orbit strength. The effect of this modification is illustrated in Fig. 23.

Examination of the three, more conventional, level diagrams on the left-hand side of the figure shows that in neither of these three cases is there a level near $N = 145$ with antiparallel orbital and spin projection quantum numbers, and an Ω value of $\frac{5}{2}$. So there is no candidate for the $\frac{5}{2}^{(+)}$ band in ^{239}Pu found by Backe *et al.* (1979). In the diagram by Hamamoto and Ogle, on the other hand, the orbital $[633]\ \frac{5}{2}^+$, which has indeed an $\Omega = \Lambda - \frac{1}{2}$, has moved up from below and now lies in the immediate vicinity of the Fermi surface for $N = 145$ (^{239}Pu). There is also a candidate for the other single-particle state, found to have $\Omega^\pi = \frac{9}{2}^{(-)}$, namely, the $[734]\ \frac{9}{2}^-$ state.

The comparison of theory and experiment thus appears to support the idea of an increased spin-orbit strength in highly deformed nuclei suggested by Hamamoto and Ogle (1975). It will be interesting to see generally how renewed shell energy corrections based on this type of potential will influence the potential energy landscape in the barrier region; in particular whether the discrepancies between empirical and theoretical proton shell energy corrections discussed in Sec. VIII.F will disappear. Such calculations are under way (Leander, 1980).

b. The resonances in thorium

The spectroscopic properties of the resonances in ^{231}Th and ^{233}Th (Tables XXXVIII and XXXIX) may throw some light on the question of the thorium anomaly. It must be remembered, however, that the assignments of these tables in terms of rotational bands and Ω values are highly tentative, except for the $\frac{1}{2}$ bands in ^{231}Th.

The moments of inertia ($\approx$500 MeV^{-1}) are 60% larger than the corresponding moments for the doubly even isomeric nuclei as well as for the odd-A ^{239}Pu (Table XXXVIII). For shapes near the outer barrier B Sobiczewski *et al.* (1973) calculate values of 420–490 MeV^{-1} for a doubly even $A = 232$ nucleus depending on the pairing strength, $G \sim S$ or $G = \text{const}$. The rigid moment is about 530 MeV^{-1}. These pairing calculations of Sobiczewski *et al.* are unrealistically low because they are performed for reflection-symmetric shapes B for which the shell correction and the single-particle level density is especially high. A calculation that includes the negative shell effects associated with reflection asymmetry at deformation B (Fig. 9) would be more realistic and would result in a moment of inertia much closer to the rigid value 530 MeV^{-1}. As a consequence an experimental value of about 500 MeV^{-1} is evidence for a highly distorted shape lying at deformation corresponding to the position of barrier B.

The sequence of close lying bands in ^{233}Th of equal Ω value and opposite parity—if substantiated—is also suggestive of a spectrum of intrinsic states in a pear-shaped potential, as implied by the third minimum hy-

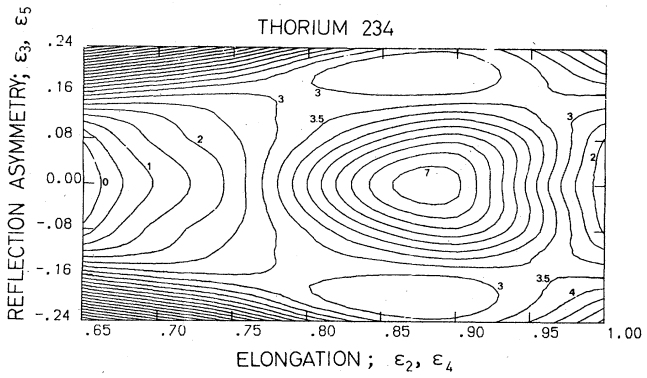

FIG. 165. The reflection asymmetric second fission barrier for ^{234}Th calculated in the modified oscillator (Nilsson) model. The potential energy surface is shown as a function of ε_2 with ε_4 implicitly included and ε_3 with ε_5 implicitly included. The droplet model (Myers, 1977) is used for the macroscopic energy. The second minimum is at the extreme left-hand side. The third minimum at $\varepsilon_2 = 0.86$, is split into two symmetric parts separated by a 4–5 MeV barrier. It is possible to circumvent this "mountain" in a motion where both ε_2 and ε_3 are varied at the same time. From Åberg *et al.* (1980).

pothesis. For a perfectly stable pear shape, levels of opposite parity will be degenerate. But if an inversion mode, as in the ammonia molecule, is possible due to tunneling through a (symmetric) barrier which separates two pear-shaped minima, then the degeneracies are split by an amount $\hbar\omega$, where ω is the frequency of the inversion oscillations. The energies in Table XXXIX and the more recent results of Blons *et al.* (1980) suggest values of $\hbar\omega$ between 3 and 200 keV, depending on the Ω value, see Sec. X.A.2.*a*. Examination of Fig. 165 and similar energy landscapes that include the reflection asymmetry (Möller and Nix, 1974) suggests that an inversion mode, which at the same time includes considerable changes in elongation, is possible. Whether or not such a mode will turn out to have frequencies $\hbar\omega$ of the order 3–200 keV remains a matter of speculation.

D. The third minimum hypothesis

The experimental evidence which has been accumulated for ^{231}Th and ^{233}Th is weighing more and more heavily towards the picture of a shallow intermediate well with very little damping of the intermediate states. In addition some of the evidence points to a highly elongated intermediate shape that is pear shaped. All this supports the third minimum hypothesis of Möller and Nix (1974), but does not unequivocally prove it. See Sec.X.A. and B.

If it were possible to find evidence of the remains of the second minimum, presumably lying low in energy and separated by a relatively low barrier from the ground-state minimum, then the situation would be more definite. The photofission measurements on ^{232}Th by Zhuchko *et al.* (1975, 1978a,b) may contain the clue in this connection, since these measurements suggest the presence of a shelf in the excitation function below 4.5 MeV photon energy.

As discussed in Sec. VII.C.3, such a shelf is expected to occur at an energy where a delayed fission branch from an isomer populated through gamma decay of the intermediate states in the second minimum begins to dominate over prompt fission. The shelf is thus indicative of the existence of a minimum lying appreciably below 4.5 MeV. This may be the second minimum missed so far.

If this interpretation is correct it should be possible to find a shape isomer in ^{232}Th and presumably also in the neighboring isotopes. Such isomers are likely to decay by a strong gamma branch and relatively weak fission.

X. TRIPLE-HUMPED AND OTHER MULTIPLY COMPLEX BARRIERS

A. Introduction

Although the title of this review proclaims that it is about the double-humped fission barrier, scattered references have been made throughout the text to the triple-humped barrier. Indeed, it is axiomatic to the Strutinsky theory, on which all the development of the double-humped fission barrier has been based, that structure in the fission barrier can be of a general and variable nature, depending on the shape-dependent shell structure of the nucleus concerned. In this sense, the double-humped fission barrier is merely the first and most dramatic detailed form discovered for the fission barrier and is common to a wide range of nuclides in the transactinium group. It is our purpose in this section to survey the evidence for more complicated forms of the fission barrier.

B. The possibility of a triple-humped barrier for the light actinides

1. Theoretical indications

All theoretical calculations that have been done to survey the fission barriers of the actinides indicate that the lower charge nuclides around thorium should have a secondary minimum at a potential energy (relative to the primary well minimum) 2.5 to 3.0 MeV. The inner barrier peak should also be considerably depressed relative to the outer peak. That the experimental data, analyzed within the context of a double-humped barrier, agree with neither of these features has been discussed in Sec. VII.D.3.*a*. and Sec. VIII.F.2. Some of the more detailed calculations, especially those of Möller and Nix (1974), indicate a feature that could reconcile data and theory. This feature appears in Fig. 18 as a shallow splitting of the outer barrier peak of the barriers of low Z, moderate N nuclides such as ^{232}Th and ^{236}Th. The source of this splitting is a minor shell effect for pear shapes only, occurring at an elongation greater than that of the major shell closure responsible for the second well. In the U–Pu region the elongation of the major shell closure nearly coincides with that of the liquid drop saddle. In the Th region the liquid drop saddle occurs at larger elongation, causing a depressed inner barrier and a broader (pear shaped) outer barrier, now split by the minor shell closure.

The tertiary minimum thus generated in the fission barrier is thus split in the direction of the mass asymmetry deformation coordinate (see Fig. 165). This has important spectroscopic consequences. For even nuclides states with one extra phonon in a mass asymmetry vibrational mode, and hence with γ and π quantum numbers of opposite sign from the basic intrinsic states, will be lowered, thus giving rise to near degeneracy of rotational bands of opposite parity. For odd-mas nuclides the ordinary Nilsson wave functions describing the particle motion will split into two states of opposite parity in the pear shaped field. The result will again be nearly degenerate rotational bands of opposite parity. For all cases the amount of splitting ΔE of the near degenerate states is related to the tunneling frequency ω_3 for inversion of the pear shape through $\Delta E = \hbar\omega_3$. Further, the spectroscopy of states associated with the tertiary minimum will be affected by the increased moment of inertia of the rotational bands at the greater elongation of the tertiary well; this will be perhaps 50% to 60% greater than that associated with the secondary well (see Fig. 24).

In the energy region in which intermediate resonance effects are important, cross sections will be affected in magnitude in two ways. Intermediate resonance size and spacing will be much greater than the values associated with the class-II compound states of the usual

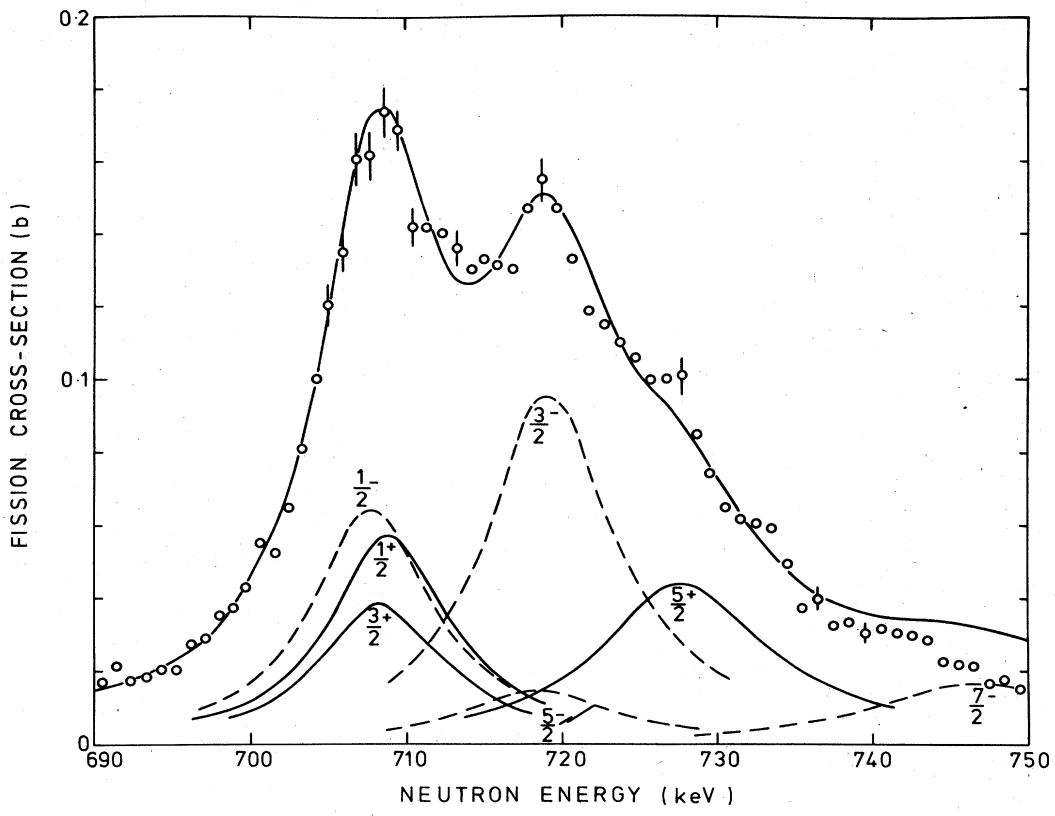

FIG. 166. High resolution data on the neutron fission cross section of ^{230}Th (Blons *et al.*, 1980) and attempted fit with the model of Boldemann *et al.* (1980) based on near-degeneracy of $K^\pi = \frac{1}{2}^+$ and $\frac{1}{2}^-$ rotational bands. Cross-section components for individual spin and parity combinations J^π are also shown.

secondary well, because of the shallowness of the tertiary well; and the overall rate of rise of cross sections with energy will be slower because of the relative thinness of the barriers encapsulating the tertiary well. Because the innermost peak of the new complex barrier is expected to be lower than the tertiary well base, new forms of intermediate structure are not likely. The formal treatment of cross-section theory can be adapted straightforwardly from the development for the two-humped barrier described in Sec.III.C.5; the class-I compound states of that formalism will now be a rather thoroughly admixed set of class-I and class-II states; and a new set of class-III states, based on vibrational wavefunctions with their principal component of amplitude in the tertiary well, takes the place of the class-II states. At lower energies (below the lowest of the class-III states, which will be an extremely short-lived fissioning isomer, only observable as a resonance in a nuclear reaction cross-section) intermediate structure should exist in principle, but should now show the standard characteristics of coupling between class-I compound states and class-II states that are substantially denser and very much narrower than the class-III states expected at higher energies. Narrowness of the class-II states will be dictated by the substantial broad outer double-barrier to be overcome by fission. At these energies the shallow dip in this barrier at higher potential energy is immaterial. It is likely indeed that the principle mode of decay of these class-II states will be radiative deexcitation to a class-II shape isomer which itself has a strong branching ratio in favor of radiation to the ground state.

2. Evidence from intermediate resonance structure

Possible candidates for the role of the class-III states within the triple-humped barrier hypothesis are to be found in the striking, large-scale intermediate resonances found in the fission cross sections of some of the thorium and protoactinium isotopes. These have been treated in Sec. V.B.5 as pure vibrational resonances in a secondary well, thus leading to the thorium anomaly described in Sec.VII.D.3. Difficult features in the analysis of these resonances have also led us to consider them as special forms of weak, incipient damping (see Sec.V.C.4.*e*). Since the submission of Secs. I through IX of this review for publication new data and analyses have become available, and these lend considerable support to the hypothesis of the triple barrier.

a. ^{231}*Th*

Most work has been concentrated on ^{231}Th, because the comparatively large and well isolated intermediate resonance at 710 keV in the neutron fission cross section of ^{230}Th is most conducive to analysis. The latest high energy resolution data on the fission cross section (Blons *et al.*, 1980) do not confirm the existence eight separate peaks within the resonance envelope that were

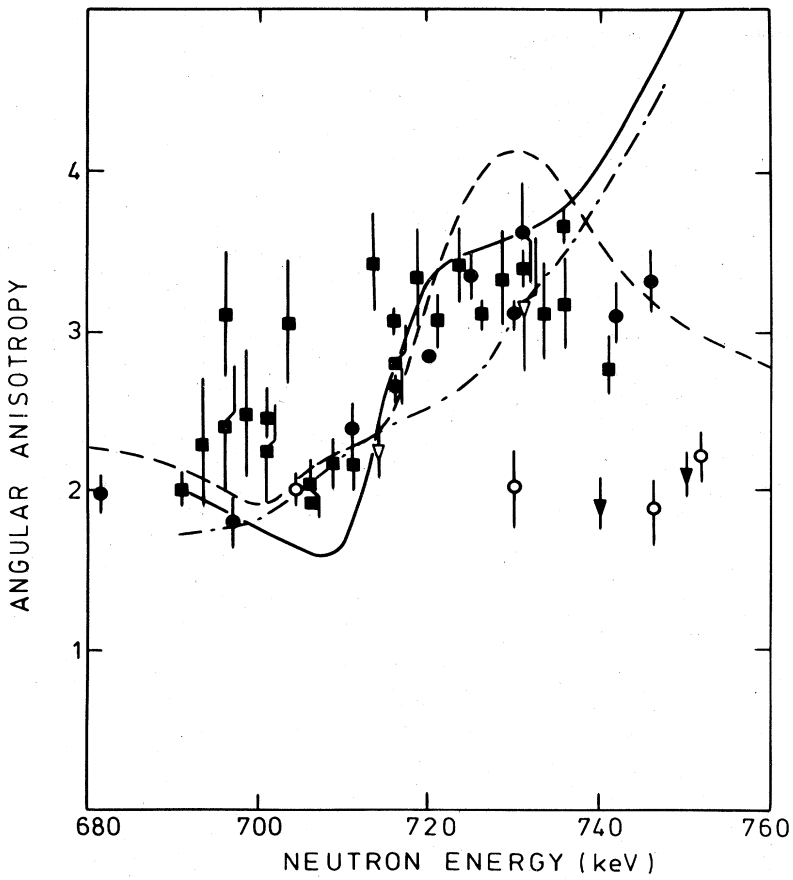

FIG. 167. Angular distribution of fission products from neutron-induced fission of ^{230}Th. Solid points were made with high energy resolution, open with power resolution; ■ Leroux *et al.* (1980), ● Boldeman *et al.* (1980), ▽, ▼ Yuen *et al.* (1971), ○ James *et al.* (1972). The continuous curve has been calculated for the model of Boldeman *et al.* (1980) with infinitely good resolution dot-dash curve with 25 keV (full width at half-maximum) resolution. The dashed curve is a calculation for the model of Bolns *et al.* (1980).

claimed earlier to exist (Blons *et al.*, 1978) but reveal a number of shoulders (up to 4) in addition to two well defined peaks (see Fig. 166). In addition to the cross-section data, more measurements (Leroux *et al.*, 1980); Boldeman *et al.*, 1980) have been made on the angular distribution of fission products, with improved resolution over those discussed in Sec. V.B.5.

Two analyses of these data have been made. Both are based on a pure vibrational model, which differs from that described in Sec.V.B.5, first, in not allowing different widths among the various rotational members of the band, and, secondly, in allowing two nearly degenerate rotational bands (instead of one) having the same intrinsic spin ($K=\frac{1}{2}$) and opposite parity. The essential feature of the new analyses that distinguishes them from earlier ones (e.g., Blons *et al.*, 1978) is that the decoupling parameter, $a_{1/2}$ (see Eq. 5.34) is of opposite sign (and similar magnitude) for the two parities. This (see Bohr and Mottelson, 1975) is an essential requirement for the degeneracy brought about by reflection asymmetry of the deformed nuclear field in which the spin-$\frac{1}{2}$ particle moves; as such it is an important element in validating the triple-humped barrier hypothesis.

Within these constraints the work of Boldeman *et al.* first of all establishes the inadequacy of a fit based on a single rotational band; this is not a consequence of the new data but, rather, of the assumption of equal coupling and fission widths of all the rotational components of the vibrational resonance. Secondly, the work establishes that a double rotational band model will give a reasonably good representation of the new data. In the analysis there are six adjustable parameters: the intrinsic plus vibrational energy, $\mathcal{E}_\nu$ of the $K^\pi=\frac{1}{2}^+$ state (with quantum number $r=+1$ for the $\mathcal{R}$ operation—see Sec.VII.B.3), the energy separation $\Delta\mathcal{E}$ from the second intrinsic vibrational state of opposite value of $r(=-1)$ and $\pi(=-1)$, the effective moment of inertia $\mathcal{I}$, the decoupling parameter for one of the rotational bands, $a_{1/2}$, and the coupling and fission widths $\Gamma_{\nu(c)}$, $\Gamma_{\nu(f)}$ for a single rotational band component. These give sufficient parameters for calculating the detailed fission transmission coefficient. The neutron and radiative transmission coefficients are calculated as in standard Hauser-Feshbach calculations (see Sec.VII.B), and, at the rather high neutron energy, should not differ significantly for different models. The parameters found for a reasonable fit to the data are $\mathcal{E}_\nu=705.3$ keV, $\Delta\mathcal{E}=3$ keV, $\hbar^2/2\mathcal{I}=1.85$ keV, and $a_{1/2}=-1.1=-a_{-1/2}$. The coupling and fission widths are not explicitly quoted by Boldeman *et al.*; instead, the triple-humped barrier

parameters are given. We have recalculated the cross section with essentially the same model as Boldeman *et al.* (using neutron transmission coefficients based on resonance region neutron strength functions rather than optical model parameters) for the purpose of calculating fission product angular distributions convoluted with experimental energy resolution functions. Our calculation is compared with the experimental data of Blons *et al.* (1980) in Fig. 166. The coupling width $\Gamma_{\nu(c)} \approx 9$ keV and $\Gamma_{\nu(f)} \approx 1$ keV.

The second analysis is due to Blons *et al.* (1980). The model is essentially the same, but with parameters $\mathcal{E}_\nu = 702.5$ keV, $\Delta\mathcal{E} = 0$, $\hbar^2/2\mathcal{I} = 2.0$ keV, $a_{1/2} = 1.3$, $a_{-1/2} = -1.5$ (*n.b.*, reversed decoupling parameters), $\Gamma_{\nu(c)} \approx 6.3$ keV, $\Gamma_{\nu(f)} \approx 0.7$ keV. The fit to the cross-section data is virtually as good as that of the Boldeman *et al.* model shown in Fig. 166, but this good agreement is somewhat artificial inasmuch as the compound nucleus formation cross sections and total neutron transmission coefficients for some of the total angular momentum components have been used as additional adjustable parameters. For example, the subsidiary peak at 720 keV only appears in the calculated curve because an unacceptably large adjustment to the neutron properties of the $J^\pi = \frac{3}{2}^+$ component of the cross section was made.

The anisotropy (defined as $\sigma(0°)/\sigma(90°)$) of the angular distribution of the fission products is shown in Fig. 167. The good energy resolution data of Leroux *et al.* (1980), Boldeman *et al.* (1980), and Yuen *et al.* (1971) are shown in black symbols. Older data with poorer energy resolution (spread ~20 keV) are shown by open symbols. The newer data tend to support the calculated curves from the new reflection–asymmetric well models, although the scheme of Blons *et al.* is uncomfortably high in the region of 730 keV and that of Boldeman *et al.* in the region of 745 keV. A calculated curve based on the latter model with the cross sections convoluted with a Gaussian resolution function of width 25 keV at half-maximum is also shown in Fig. 167. The difference between this and the perfect resolution curve is not nearly great enough to account for the spread in the data, and the discrepancy thus revealed in the data must be regarded as worrying.

Of the two models, that of Boldeman *et al.* must be preferred, mainly because of the excessive adjustment of neutron properties used in the scheme of Blons *et al.* (1980). Nevertheless, reservations must be drawn about either of these analyses as constituting proof of the third well hypothesis. Reference to Fig. 166 shows that many of the individual J^π components are nearly degenerate, indicating that a model with as many as seven separate rotational components is not, in itself, necessary. Secondly, there are large discrepancies in the angular distribution data; but even so, the model calculations lie well outside the range encompassed by the data in significant energy regions. All the evidence suggests that a pure vibrational model cannot explain all the data, whether the model is limited to a single parity rotational band or to two parities as required by the reflection-asymmetric third well. Fission through the higher spin components of the band may be weaker, either because of reduced coupling and/or fission width. Alternatively, components of higher spin-projection K may be mixed into the intrinsic state (this is incipient damping of the type described in Secs. V.C.1 and V.C.4.*e*). Yet again there could be accidental energy overlap of a $K = \frac{1}{2}$ vibrational band (of single parity) with a band of higher K. Any of these possibilities would reduce the angular anisotropy in particular energy regions as apparently required by the experimental data. But the latter themselves also require more definitive study.

The most significant conclusion to emerge from all these analyses, particularly strengthened by the new high resolution experimental data on the fission cross section, is the high value of the moment of inertia of the rotational band. At a value of $\hbar^2/2\mathcal{I} \approx 2$ keV, it is significantly higher than the value we would expect for a nucleus with the deformation of the secondary well, even after allowing for possible compression by Coriolis coupling with a higher K band at higher energy. This in itself is significant support for the validity of the triple-humped barrier hypothesis.

b. ^{233}Th

The greater number of close intermediate resonances and the higher neutron energies at which they occur make the analysis of the fission cross section of ^{232}Th much more complex than that of ^{230}Th. In addition, angular distribution data are not available with the very good energy resolution used for ^{230}Th. Consequently, no detailed comparison of these data with the quantitative calculations that may be based on a third well model have yet been made. It does appear, however, that the moment of inertia could be high [$\hbar^2/2\mathcal{I} \approx 2$ keV (Caruana *et al.*, 1977)], in accord with the model.

c. ^{232}Pa

Data on the neutron fission cross section and fission product angular distribution of ^{231}Pa were described in Sec. V.B.5.*c*. Again new data with improved neutron energy resolution have become available. These have revealed new weak substructure (James *et al.*, 1979; Plattard *et al.* 1979) in addition to the main gross structure previously observed, and fission has also been observed in the fine-structure resonances at very low energy (Plattard *et al.*, 1979).

The overall picture is reasonably consistent with a very shallow well in the main fission barrier. From Sec. VII.C.2 we would expect the density of bandhead states in a reflection symmetric system that could be excited strongly by neutron s and p waves at neutron energies up to about 400 keV to be about 20 MeV^{-1} at very low excitation. This is in agreement with the observation of groupings of strong intermediate fission resonances. This conclusion is not affected by the possibility that rotational bands of opposite parity are introduced by a reflection-asymmetric tertiary well, so long as the degeneracy splitting is smaller than about 20 keV. The overall level density would be ~90 MeV^{-1} and this is consistent with the density of narrow intermediate structures observed within the groups, thus confirming the overall impression of clustering into a set of rotational bands. The widths of the clusters will have an

upper limit of $\approx(\hbar^2/2\mathcal{I})J(J+1)$, where $J\approx 3$. The observed widths are in rough agreement with a high moment of inertia corresponding to $\hbar^2/2\mathcal{I}\approx 2$–$2.5$ keV.

A particularly sharp intermediate resonance (of width 2.9 keV) occurs at 156.7 keV. It has been established (see Sec. V.B.5.*c*) to have $K^\pi = 3^+$. Plattard *et al.* (1979) have observed non-Lorentzian behavior and evidence of substructure in its wings. Two possible explanations advance themselves. One is that the substructure could be due to the existence of complex class-II levels, the non-Lorentzian behavior being due to Porter–Thomas fluctuations. The second possibility is the existence of a nearly degenerate $K^\pi = 3^-$ band. If this is slightly lower than the $K^\pi = 3^+$ states, weak peaks with total angular momentum $J^\pi = 3^-$, 4^- due to excitation by neutron d waves could appear below, or straddle, the main resonance. This explanation would certainly favor the third well hypothesis. To support it high energy resolution measurements of the angular distribution of fission products would be required.

Fission widths of fine-structure resonances have been measured up to 60 eV by Plattard *et al.* (1979). They do not show the pattern of narrow intermediate structure described in Sec.VI (e.g., as in the ^{237}Np cross section). Therefore they may well be coupled directly to the gross structures observed at higher energies without any more complex class-II level structure intervening. If they were outliers from a $K^\pi = 2^-$ vibrational resonance at about 200 keV [this would be consistent with the angular distributions observed by Sicre (1976)], their fission widths could be expected to be $\approx 3\times 10^{-7}$ eV, which would be one to two orders of magnitude smaller than the widths observed. This suggests an even closer vibrational state of $K^\pi = 0^-$, 1^- or 2^-.

Again, no *conclusive* evidence for a triple-humped barrier emerges from the present data on this reaction. But in view of the narrowness, and hence the possibility of discrete observation of many of the structures, further detailed studies with the aim of establishing near degeneracy with states of opposite parity in a few of the rotational bands could be productive.

3. Other evidence

Other evidence that points in favor of the triple-barrier hypothesis for Th and Pa nuclides has been mentioned briefly in Sec.VII.D.3. Cross sections calculated with the standard barrier level densities of Sec.VII.C.2 tend to be too high in the region above the barrier by a factor approaching 2; (See e.g. Fig. 136). To correct this it would appear to be necessary to reduce the rotational enhancement of one or both of the barrier level densities implying higher shape symmetry than assumed in the standard calculation. The new picture would suggest that the two outer barriers B and C usurp the roles of barrier A and B, thus replacing axially asymmetric barrier A with an axially symmetric, but reflection-asymmetric barrier C. This indeed reduces the transition state density for this barrier approximately by the required factor of two. But this fact could also be explained by a low degree of axial symmetry of the thorium nuclides as actually predicted by calculations (see Sec. II.A.1.*d*.(i)). But in support of the triple-humped barrier hypothesis, the rate of rise of the cross section is much less than expected, suggesting thin barriers with large values of $\hbar\omega$.

There is some evidence that subbarrier photofission cross section behavior may be different for Th nuclides than for higher charge actinides [see, e.g., Zhuchko *et al.* (1978ab)]. The behavior expected for the photofission cross section of a nucleus with triple-humped barrier of the character described in Sec. X.B.1 will be as follows. At energies in the region of barriers B and C typical vibrational resonance phenomena will be apparent. At lower energies, below the tertiary well, the photofission cross section will decrease at a rate proportional to the transmission coefficient $T_{(B+C)}$ of the outer barrier. Below inner barrier peak A the rate of decrease will become even faster, becoming proportional to $T_A^{1/2}T_{(B+C)}$, but will also begin to show new irregularities owing, first, to fluctuations due to accidental degeneracy of class-II and class-I levels, and, secondly, to class-II vibrational levels. At very low energies the cross section is unlikely to show the "shelf" expected for delayed fission following radiative decay of class-II states, because delayed fission will be strongly suppressed in favor of gamma decay back to the first well. It is this last feature (the "shelf") that is dubious in the photofission measurements made on ^{232}Th to date.

C. Complex barriers for Ac and Ra nuclides

It is well known that fission of Ac and Ra nuclides at relatively high excitation energies exhibits a triple-humped mass-yield curve, the two outer peaks in the fission product yields being similar to the normal asymmetric yield curve of most of the transactinium nuclides at low excitation energy, and the center peak being symmetric fission similar to that characteristic of lower-charge nuclides like the isotopes of Po. Measurements (Konecny *et al.*, 1974; Weber *et al.*, 1976) of fission induced at low excitation energies of Ac and Ra nuclides by charged particle transfer reactions such as (t,pf) reveal considerable differences in the cross-section behavior as a function of energy for asymmetric and symmetric fission in the region of the barrier.

In the work of Konecny *et al.* measurements were made on a number of Ac isotopes (odd-Z)- and odd-N Ra isotopes. In all cases it appears that asymmetric fission proceeds through a well defined barrier, with typical Gamow penetration apparent at sub-barrier energies. Symmetric fission appears to pass through a barrier some 1.5 MeV higher. In one case (^{227}Ac) a resonance effect appears near the barrier in the cross section for asymmetric fission but not in that for symmetric division.

This latter phenomenon is found more strongly in the fission of ^{228}Ra (Weber *et al.*, 1976). It is taken as an indication that symmetric division does not follow the same route through the potential energy surface in the barrier region as that of normal asymmetric fission. Weber *et al.* attempt to reproduce the cross-section for symmetric division at higher energy by calculation from statistical theory. They find it necessary to assume an axially asymmetric outer barrier (giving rotational enhancement of barrier transition states) to re-

produce the correct magnitude of the cross section. They speculate that asymmetric division of this nuclide and of related ones proceeds across a barrier with an axially asymmetric innermost barrier and a reflection asymmetric outer barrier while symmetric division is governed by a quite different route through two axially asymmetric barriers. There is some suggestion (Gavron *et al.*, 1977) that a similar double route through a two-humped barrier may exist for ^{238}U, enhancement of the density of barrier states being required to explain the photofission cross section in the photon energy region of 7–11 MeV. Gavron *et al.* present calculations of potential energy surfaces as a function of three deformation parameters (elongation, mass asymmetry, and axial asymmetry) that show such dual barrier routes to be possible.

D. Complex barriers for heavy actinides

There is evidence that giant intermediate resonances are found again at the upper end of the transactinium range. Britt *et al.* (1978) have measured the fission probability as a function of excitation energy for a number of high charge actinides with neutron numbers in the range $N=150$–154, using (t,pf), (d,pf), and $(p,p'f)$ reactions. A distinct change is apparent in the properties of the fission barrier at $N=154$. For both Cm and Cf there is a fall of 0.5–1 MeV in barrier height at this neutron number, and for ^{252}Cf strong resonance effects appear. In this resonance the anisotropy that appears in the angular distribution of fission fragments indicates that $K\neq 0$, which is surprising for the first vibrational resonance of an even nuclide. Britt *et al.* interpret this as possible evidence that the axially asymmetric inner barrier is split at $N=154$, in analogy with the subshell splitting of the reflection asymmetric outer barrier of the lighter actinides. Axial asymmetry of this new barrier well would imply that K is not a good quantum number for its vibrational state and hence account for the anomalous behavior of the angular distribution. There are, as yet, no theoretical calculations of the potential energy surface that support this speculation.

XI. SUMMARY AND CONCLUSIONS

It has been our purpose in this article to make a critical survey of the vast amount of experiments relating to the fission barriers of the actinide group of nuclides. In numerous ways observations are reflecting the existence of a complex structure of the barrier with at least two barrier peaks and an intermediate minimum between these. In essence it has emerged that the fission of actinide nuclei proceeds as a two-step process. As a consequence, reaction theories, both purely quantal and quantum-statistical, have had to be reformulated and developed further to meet this new situation. This is the second major purpose of this review. Based on the extended theoretical framework, the data have now been subjected to a detailed analysis in order to determine the extent to which they can be understood within a coherent, quantitative picture of the barrier and its associated spectra of excited states.

To do this we have had to be guided, at least qualitatively, by the modern structure theory of the fission barrier. This explicitly underlines the importance of shell effects in deformed nuclei and draws out the fact that in the actinides, the strong deformation at which a major shell closure occurs more or less coincides with the saddle in the liquid drop potential energy surface of the nucleus; the consequence is the double-humped barrier. In Sec. II we have summarized these theoretical developments and indicated the main conclusions that can be drawn from them. Inner barriers are more or less constant at 5 to 6 MeV (above ground) for the main range of the actinides, but begin to fall rather rapidly at the thorium end of the range and more slowly at the fermium end. The depth of the secondary well between the two barrier peaks is also calculated to be fairly constant at about 2 to 3 MeV. By contrast, outer barriers fall quite strongly from the lighter to the heavier actinides, being calculated to be about 6 to 7 MeV in the thorium isotopes and only 2–3 MeV in the fermiums. These general trends in the heights of the peaks and depth of the secondary well can be explained quite simply by the changing deformation of the liquid drop saddle in relation to the shell closure responsible for the secondary well.

A secondary, but important, conclusion that emerges from theory is that the route of minimum potential energy for a fissioning nucleus does not necessarily preserve maximum symmetry of shape. Axial asymmetry is indicated for the inner barrier, and reflection asymmetry (with respect to a plane perpendicular to the cylindrical symmetry axis) at the outer barrier. The secondary well appears to retain axial and reflection symmetry. Axial asymmetry at the inner barrier increases in going to the higher charge nuclides. These results not only have large implications for the barrier heights that must be traversed in going to fission, but also for the density of transition states that govern fission cross sections at higher energies and for many detailed spectroscopic effects.

We have seen that the double-humped barrier, with its strongly developed secondary well nestling between the barrier peaks, is responsible for a range of remarkable phenomena in nuclear spectroscopy and nuclear reaction physics. To analyze these data quantitatively we have had to review critically and to contribute to the theory of nuclear reaction processes that involve fission. Many fission yields measured as a function of nuclear excitation energy are so spectacular in their structure as to invite treatment by a relatively simple one-dimensional picture of transmission through a two-humped barrier; and quantitive models, both analytic and numerical, of this kind were developed relatively early in the last decade. But suspicion, and later on evidence, of substructure within these giant resonances in the fission probability curve led to modified one-dimensional theories that include damping (by means of an imaginary term) in the secondary potential well, and, in order to deal with the detail of the substructure, to more formal theories that explicitly allow reference to other degrees of freedom of the nuclear system (states of "intrinsic" excitation) than the fission deformation coordinate.

Such a formal development, with strong emphasis on

the basis for the concept of deformation channels, is described fully in Sec. III ; and many of the specific and structurally very rich consequences in terms of intermediate structure in fission cross-section curves are derived there. In Sec. III.C intermediate structure was developed in terms of two sets of basis states; the class-I states are largely localized, by the nature of the vibrational wavefunctions entering their structure, to the region of normal, quite moderate deformation, about which the primary well in the deformation energy curve is centered; and the class-II states are localized at the more extended shape of the secondary well. The class-I states approximate to the relatively dense fine-structure resonances that appear in neutron cross sections at moderate excitation energies, while the properties of the class-II states govern the scale of the intermediate structure in the fission channel. One of these properties is the coupling interaction with class-I states, and this is dominated by the height of the inner barrier between the two wells. A second is the fission width, governed by the outer barrier, and a third is the spacing of class-II states, governed by the depth of the secondary well. But quite detailed properties of the intermediate states can be accommodated in principle within the formal theory, through the detailed spectroscopy of the class-II states. These aspects have been exploited considerably in later parts of the review, particularly for analyzing fission at deep sub-barrier energies.

At near- and above-barrier energies structure phenomena become less conspicuous in the fission cross sections. Simpler theories encompassing the gross statistical properties of the class-I and class-II states then become appropriate (Sec. III.B). The statistical theory is particularly appropriate for analyzing data on yield of spontaneously fissioning isomers resulting from high energy reactions followed by neutron evaporation and for estimating the magnitudes of fission cross sections above the barrier. Various formal aspects of these topics are further developed in Secs. IV, VI, and VII.

In Secs. IV–VII we have used these reaction theories as tools to analyze most of the experimental data relating to the fission barrier that have been assembled over the past decade. Section IV has been devoted to shape isomers. In Sec. IV.A we reviewed the evidence and arguments that established the remarkable spontaneously fissioning isomers as the lowest of the set of states with the greatly extended deformation characteristic of the secondary well of the theoretical double-humped barrier. In Sec. IV.B we outlined the known extent of shape isomerism (the uranium–berkelium island) and drew attention to the fact that these shape isomers have so far been identified entirely through their fission decay. It has been observed, mainly deductively through reduction in the observed yields of delayed fission, but also directly by observation of gamma rays, that the preferential mode of decay of shape isomers of low Z and N is by electromagnetic radiation. This is consistent qualitatively with theoretical expectations, in which the outer barrier against fission strengthens and the inner barrier against radiation weakens as Z and N are lowered within the actinide group. It is highly desirable to extend the known limits of shape isomerism by developing methods that will detect the gamma branch in the isomer decay, independently of the fission branch.

In Sec. IV.C we reviewed the systematics of decay properties of the shape isomers. Systematic dependence of the spontaneous half-life on neutron number, showing maximum stability at $N=146$, and proton number, showing strongly decreasing half-life with increasing Z, and also a strong odd-even effect, are readily apparent in the data. The dependence on N is direct evidence for a combination of shell effects, at extended deformation, that results in maximum half life for $N=146$, in agreement with theoretical expectations. In contrast, the odd-even effect calls for new demands on theory; currently there are three possible explanations, increase in inertial parameter, increase in pairing gap, and increase in specialization energy, in all of which the theoretical argument is qualitative rather than quantitative. Further experimental work could also contribute greatly to resolving these questions, particularly extended work on the spectroscopy of states associated with the secondary well and on the transition states at the outer barrier. The gains in understanding the physics of deformed many-body systems, in particular the dependence of pairing energy on deformation, could be great here.

In Sec. IV.D we analyzed the excitation functions for yields of the shape isomers. These gave us two important classes of information. One is the excitation energy of the shape isomer, relative to the ground state, and the second is the outer barrier height, normally of the nucleus with one neutron more than that of the isomer. The excitation energy is of course a direct measure of the depth of the secondary well and can be compared directly with theoretical estimates of this quantity. Agreement for the main body of isomers from Pu to Cm is quite good. But more comprehensive and more precise information on the excitation energies of these isomers is badly needed for other purposes. One is to help pin down the cause of the odd–even effect in half-life, and a second is for the study of level density of class-II states as deduced from intermediate structure in fission cross sections. Two methods have been shown to be possible for increased precision. One is the observation of the excitation curve by the (n,n') reaction, and the other is the measurement of energies of gamma rays emitted in the gamma branch decay of the isomer. Both methods have been applied to ^{238}U but at present a certain measure of disagreement remains.

Outer barrier heights as deduced from shape isomer excitation functions are in qualitative agreement with theory in showing the expected fall with increasing Z. But, in view particularly of the rather indirect nature of the deduction of barrier heights from such data, major improvements in the experimental data, both in energy precision and in absolute yield measurement, would be highly desirable.

Turning now to the phenomena of structure in fission cross sections, we came across the first major apparent discrepancy with nuclear structure theory in Section V. It is demonstrable that the very large scale resonances ob-

served in the cross sections of some light actinides are explicable in terms of pure vibrational resonances in the secondary well of a double-humped fission barrier (although some detailed quantitative discrepancies appeared in the analysis of the best-studied cases). But our considerations of the mechanisms that can lead to damping of the vibrational resonances of odd-A nuclides indicate that this can be quite strong above the very lowest excitation energies in the secondary well. From this we inferred that the secondary well in Th and Pa actinides is shallow and some 4 to 5 MeV higher than the primary well, while the inner barrier must be, at least, almost as high as the outer barrier. These conclusions are in direct conflict with the trends that the theory of the potential energy surface has established. These studies of the experimental situation have led to the serious consideration of a feature observed in some theoretical work, namely, that the outer barrier may be split to give a shallow tertiary well that houses the vibrational resonances; we took this matter up again in Sec. X (with passing references in other sections). New precise data on vibrational resonances are badly needed for even nuclides. The difficulty here is that the barriers of such nuclides normally lie below the neutron separation energy, which makes the vibrational resonances inaccessible to the high energy resolution of neutron measurements. The requirement is for increased energy resolution in fission induced by charged-particle transfer reactions.

By contrast, the study of damped vibrational resonances leads to no great discrepancies with structure theory. The best examples occur in even nuclides, so the comparatively modest damping widths observed seem quite consistent with the excitation energy based on the expected (or known) depth of the secondary well. But the possibility that the vibrational resonance belongs to a tertiary well and that the damping is a consequence of coupling of this class-III state to denser class-II states within a secondary well has not been ruled out. More complete information on the sequence of vibrational states through the full excitation range of the secondary well is required, and intensive theoretical work on damping of vibrational levels would be very desirable. Damping can be a quite complex phenomenon and such simple models as we have studied in this review indicate that the patterns of coupling and fission width associated with a vibrational resonance could differ considerably from each other, with significant consequences for the cross-section patterns. For this reason the resolution of the narrower intermediate structure due to the complex class-II states into which the vibrational level is fragmented, could give important checks on theories of damping mechanisms. In two cases at least the class-II sub-structure has been observed, but not to the precision that yields this kind of information.

We took up the study of the narrow intermediate structure due to complex class-II levels in Sec. VI. The available data exhibit a range of spacing width, and strength properties that are mostly consistent with barrier heights that have been deduced from other kinds of data (excitation energies and yield curves of shape isomers, Sec. IV, near-and above-barrier cross-section curves, Sec. VII). Some phenomena of specialized but intriguing interest have been reviewed here, e.g., accidental degeneracy of a class-I and a class-II level; this plays an important role in the energy dependence of very deep sub-barrier average cross sections. In one case (^{240}Pu) the density of class-II states in the neutron cross section can be related to that observed at a much lower excitation energy in the (d,pf) reaction, thus providing a useful check on the level density behavior of complex states at the secondary well deformation. But the total volume of data on class-II resonances is still very sparse. Only about 4 or 5 such intermediate groups have been studied with the amount of detail that can be regarded as definitive. So tests on their expected statistical properties (especially correlations between coupling and fission widths) are very crude, and our knowledge of their trends with energy and angular momentum are virtually nonexistent.

In spite of many searches there is no direct evidence of radiative cascades from class-II resonance states to lower class-II states, a process that should culminate in delayed fission from the shape isomer. This process has particular relevance to the one case so far that is not fully consistent with other data on barrier heights, namely, the neutron fission cross section of ^{238}U. Here the intermediate structure indicates barriers (for the $J^\pi = \frac{1}{2}^+$ states) that are much lower than those indicated by the fast neutron fission cross section. Delayed fission following radiative "capture" in the class-II state could explain the discrepancy, but so far no spontaneously fissioning shape isomer has been observed for ^{239}U, and systematics suggest that such an isomer could have too long a half-life and too small a branching ratio for fission to fulfill the required role. In addition to searches for the isomer and class-II radiation (extremely difficult in view of the weakness of the intermediate resonances) high energy resolution measurements of the angular distribution of fission products from the intermediate resonances observed at high neutron energies (100–200 keV) in the ^{238}U cross section could help to resolve this problem.

The largest body of evidence on the heights of the barrier peaks, particularly that of the inner barrier, has come from analysis of fission cross sections at energies near and above the barrier. Such cross section data are generally without structure (because of insufficient resolution in the measurements below the barrier, and because it is broadened to disappearance above); the evidence for analyzing them systematically in terms of a double-humped barrier comes from the structure phenomena at lower energies and the analysis of shape isomer data as well as the indirect knowledge gained from the systematic trends of the cross sections as functions of Z and A. With this insight we have analyzed most available cross-section data, much of it on fission induced by charged-particle transfer reactions, to obtain a fairly comprehensive set of barrier parameters for the actinide nuclides. In doing this we have reviewed also the evidence from the magnitude of the cross sections that gives strong indirect support for the asymmetries in nuclear shape at the inner and outer saddle points strongly suggested by the theoretical calculations. This evidence manifests itself in the form

of enhancement of the cross section due to the increased density of transition states at inner and outer barriers brought about by the extra rotational bands required by the broken symmetries. The agreement with theory is at least semiquantitative. More careful comparison between experiment and theory will await more precise measurements of the fission cross sections, particularly those of the charged-particle transfer reactions. The elucidation of the energy gap in the spectra of transition states at the two barriers of odd-A nuclides could follow from careful analysis of such data, particularly if angular distribution data become available also.

We have presented a detailed analysis of the full set of barrier parameters and their systematic trends in Sec. VIII. Here we have attempted to separate the effects of the smooth liquid drop (or droplet), the pairing, and the shell contributions to the energy. The ground-state energies (at normal deformation) have been included in the analysis, all points on the barrier energy curve being referred to the spherical liquid drop energy. Although there is some ambiguity in the choice of liquid drop or droplet model in extracting the smooth "background" contribution to ascertain the shell plus pairing corrections, the procedure does make certain major trends apparent in the experimental data and allows more incisive comparison with the theory (compensating errors between ground state and barrier energies are at least partly eliminated).

The magnitude at different deformations of odd-even staggering in the data thus reduced shows that the energy gap has an increasing trend with deformation. Observation in even nuclides of excited shape isomers with a two-quasiparticle configuration gives another assessment of the energy gap and confirms this trend. Taken together, these observations, though not conclusive, do tend to convince us that the pairing correlation force is proportional to the surface area of the nucleus.

The shell energies are not completely reproduced by theory. For $Z=92-96$, the shell energy at ground-state deformation appears with a minimum at $N=144$ in the data, but not in theory. At barrier A the experimental shell energies plotted against neutron number have a quite different trend from the theoretical calculations with axial asymmetry included, suggesting that the latter effect has not been quite correctly treated. At the secondary minimum, on the other hand, there is good indication of agreement (at moderate Z numbers ≈ 95) with theory, the observed minimum lying near $N=144$. At the outer barrier agreement between experiment and theory in the N-dependence is not unsatisfactory, provided the all-important mass-asymmetry degree of freedom is allowed. Dependences on proton number also show deviations with theory. The comparison at the two minima is not bad, provided that data for the second minimum of thorium and protoactinium are omitted. Similarly the magnitudes of the shell corrections at the barrier deformation are reasonable overall, but trends are unsatisfactory, and again, at barrier A, the low charge data effect a discontinuity (the thorium anomaly) with the main trend of experimental data; this discontinuity is simply not explained by the two-humped barrier theory.

Although there could be flaws in the interpretation of the experimental data, further investigation on the theoretical plane is certainly called for.

The theoretical spectroscopy of the class-II states associated with the secondary well is closely allied with the theory of the potential energy surface. Furthermore, the experimental spectroscopy of these states can give us information on both static and dynamic aspects of the deformation of the nucleus in the secondary well. We have reviewed these aspects of the subject in Sec. IX and have mostly found agreement with the concepts of the double-humped barrier. Particularly striking are the observations of rotational bands built on the shape isomers of even nuclides and the deduction from these of moments of inertia fully consistent with the standard deformation expected for the nuclear potential of the isomeric state. The lifetimes of the transitions within these bands have allowed determination of the quadrupole moments, thus confirming the extended shape as being that of a prolate nucleus with a major to minor axis ratio of 2:1. The agreement of these results with quantitative theory is satisfactory for the quadrupole moment, and for the moment of inertia the cranking model with superfluidity in its most elaborate formulation reproduces the results within 10%–20% accuracy.

The spectra of highly deformed odd-A nuclides are particularly important in yet a different way. Comparison with the spectra calculated in Nilsson-type models allows an indirect assessment of the deformation as well as a check upon the basic theory of shell corrections. In two cases of plutonium isotopes precise or approximate values of the spin projection of two bandhead states have been measured and also their gyromagnetic factors. Although the spins can be fitted loosely into a Nilsson scheme at reasonable deformation, there is disagreement with the standard theory on the g factors. This disagreement may indicate that the spin-orbit force is stronger than generally assumed at large deformations. There is great incentive here for continued efforts in the spectroscopic field.

Finally, we have devoted a special section to summarizing the possibilities for even more complex forms of the fission barrier than the double-humped one. The main thrust to considerations of this kind arises from the thorium anomaly and leads to the consideration of the spectroscopy of "quasi-isomers"—the vibrational states—observed in the cross sections of thorium and protoactinium nuclides. We have shown that the present data, although now existing in considerable detail, on the cross section of ^{230}Th in particular, are neither consistent enough among themselves, nor yielding to a sufficiently unambiguous analysis, to confirm in a definite way the hypothesis of a triple-humped barrier with shallow tertiary minimum that is suggested by theory. Nevertheless, the third minimum hypothesis seems the most reasonable explanation of the data. Even more careful measurements with high energy resolution are required on the vibrational resonances, and additional information on their counterparts in even nuclides would be valuable. In addition, careful exploration of the deeper sub-barrier

region—below the hypothesized innermost barrier, by means of charged-particle transfer or photofission—might confirm the picture by picking up the true class-II states. Once again, however, we must mention that we have no illusions about the difficulties of performing such experiments.

As a broad overall conclusion we can say that this review has revealed that a vast amount of data is in broad agreement with the concept of a two-peaked fission barrier; and it has been shown how the properties of the intermediate states resulting from a structured barrier, as well as the barrier parameters themselves, can give new information on the forces operating in many-body systems with large deformations. Many detailed problems remain, however. These are now mainly concerned with the spectroscopic properties of the intermediate states that so dramatically affect the rate of fission. But in turn the elucidation of the spectroscopy of the intermediate states is intimately connected with a more quantitative theoretical understanding of the deformation surface, affecting the calculation of the shell correction and the pairing energy correction through such matters as the dependence of spin-orbit force and pairing force on the nuclear deformation. It is on spectroscopic evidence, too, that the question of the existence of more complex structure, such as the third minimum, in the deformation surface will ultimately be resolved.

ACKNOWLEDGMENTS

In the preparation of this review we have been assisted greatly by discussions and correspondence with very many colleagues in the international nuclear physics community. We deeply appreciate their help. Of special value to us have been the penetrating and constructive comments and suggestions, some of them far reaching, from our referees and from Dr. P. E. Hodgson, who have done a very careful work in going through the entire manuscript. We also wish to thank our respective Institutes (J.E.L.'s gratitude to Niels Bohr Institute, and S.B.'s thanks to Harwell) for their periodic hospitality over many years, and special thanks are due to Los Alamos Scientific Laboratory which has provided us (J.E.L. in particular) with extended hospitality and facilities for carrying out a great deal of the development and analysis described in the foregoing pages. Clearly we have depended very greatly on our secretaries for the preparation of the manuscript, and we wish to extend our deep thanks in particular to Miss Irene Blundell who has carried out, to a very high standard, the bulk of this work, including the very exacting aspect of multitudinous corrections and alterations to the final text.

APPENDIX: PARAMETRIZATION OF DEFORMED NUCLEAR SHAPES

The development of quantitative theories of nuclear fission is dependent upon an adequate parametrization of the shape of a deformed body. Many different parametrizations are to be found in the literature and this can give rise to inconvenience when attempting to compare the results of one paper with those of another. In this Appendix we list definitions of shape parametrizations that commonly occur, and give relationships, analytical or numerical, among them.

The requirements of a shape parametrization can have different sources. In nuclear fission theory a prime requirement is to define in detail the sharp surface configuration of the electrically charged liquid drop, which appears as a prime concept in the development of the theory. The later theoretical developments that led to the subject matter of the present review demand the definition of the shape of a single-particle potential well. This can be done either by defining the shape of the potential at a certain contour (generally the midpoint between maximum depth and zero) and prescribing the radial dependence of the potential about that contour, or by defining the directional dependence of the force constants that give the potential (as in the deformed harmonic oscillator potential).

Often, however, it is the shape of the nuclear density distribution that is required (usually as an end product of the theoretical calculation). Again this shape can be defined for a specific contour in the density. In some work the density is used as a basis upon which the potential for the single-particle levels is constructed.

In such requirements a detailed surface parametrization is called for, demanding, normally, several independent parameters. In many studies (of cross sections and fission reaction rates, for examples) only a single parameter, a measure of the overall elongation of the system, is required. This can usually be constructed from the detailed description of the shape that is provided by the many-parameter description.

Among the many-parameter descriptions of the nuclear shape there are a number that are very familiar from their use in the studies of nuclear ground-state properties. Such parametrizations are commonly used in theories of fission up to the barrier region but become increasingly inadequate for studies of extreme elongations.

One of the most familiar and general is the spherical harmonic expansion. The radius of the body (at sharp surface or chosen contour, as appropriate) is defined as a function of spherical polar angles θ, ϕ, in the frame of reference

$$R(\theta,\phi)=R_0\left[\alpha_0+\sum_{lm}\alpha_{lm}Y_{lm}(\theta,\phi)\right]. \tag{A1}$$

Often the frame of reference is body-fixed, and in this case the expansion is written with specialized coefficients, $a_{\lambda\mu}$:

$$R(\theta',\phi')=R_0\left[a_0+\sum_{lm}a_{lm}Y_{lm}(\theta',\phi')\right]. \tag{A2}$$

The transformation from the a_{lm} to the α_{lm} is effected by the rotation matrices D^l_{mn}:

$$\alpha_{lm}=\sum_{n=-l}^{l}D^l_{mn}(\theta_i)a_{ln}, \tag{A3}$$

where the θ_i are the Euler angles specifying the transformation from the laboratory to the body-fixed frame of reference. The reality of the nuclear surface imposes the conditions

$$a_{\lambda-\mu}=(-1)^{\mu}a^{*}_{\lambda\mu}\,, \tag{A4a}$$

$$\alpha_{\lambda-\mu}=(-1)^{\mu}\alpha^{*}_{\lambda\mu}\,. \tag{A4b}$$

The condition to fix the center of mass at the origin of the body-fixed frame gives $a_{10}=a_{1-1}=a_{11}=0$, and the incompressibility of the body demands the constancy of the volume

$$V=\frac{R_0^3}{3}\left\{4\pi\alpha_0^3+3\alpha_0\sum_{lm}|\alpha_{lm}|^2+C\right\}, \tag{A5a}$$

where

$$C=\sum_{lm}\sum_{l'm'}\sum_{l''m''}C(ll'l''mm'm'') \tag{A5b}$$

with

$$C(ll'l''mm'm'')=\alpha_{lm}\alpha_{l'm'}\alpha_{l''m''}\left[\frac{(2l+1)(2l'+1)(2l''+1)}{4\pi}\right]^{1/2}\left[\frac{(l-|m|)!\,(l'-|m'|)!\,(l''-|m''|)!}{(l+|m|)!\,(l'+|m'|)!\,(l''+|m''|)!}\right]^{1/2}$$
$$\times(-)^{\Lambda-l'-m''}\frac{(l'+|m'|)!\,(l''+|m''|)!\,(l+l'-l'')!\,\Lambda!}{(l'-|m'|)!\,(\Lambda-l)!\,(\Lambda-l')!\,(\Lambda-l'')!\,(l+l'+l''+1)!}$$
$$\times\sum_{k}(-)^{k}\frac{(l+|m|+k)!\,(l'+l''-|m|-k)!}{(l-|m|-k)!\,(l'-l''+|m|+k)!\,(l''-|m''|-k)!\,k!}\,. \tag{A5c}$$

The term $C(ll'l''mm'm'')$ is zero unless $m+m'+m''=0$, Λ is an integer, where $2\Lambda=l+l'+l''$, and $l+l'\geq l''$, $l+l''\geq l'\geq|l-l''|$. The ordering of coefficients in the expression for $C(ll'l''mm'm'')$ is arranged so that $|m|=|m'|+|m''|$. For the ranges of deformation for which Eqs. (A1) and (A2) are useful expressions α_0 (or a_0) does not differ greatly from unity. Within this approximation

$$\alpha_0=1-\frac{1}{12\pi}\left[3\sum_{lm}|\alpha_{lm}|^2+C\right]. \tag{A6}$$

[Equation (A6) also holds for the relation between a_0 and the a_{lm}, of course.]

For small values of the deformation the quadrupole parameters a_{2m} of Eq. (A2) are often considered adequate as a description of deformation. In the description of an ellipsoidal surface with axes of the reference frame coinciding with the major axes of the ellipsoid, $a_{21}=a_{2-1}=0$, and the two remaining independent parameters are usually written as

$$a_{20}=\beta\cos\gamma \tag{A7a}$$

$$a_{22}=a_{2-2}=(\beta\sin\gamma)/\sqrt{2}\,. \tag{A7b}$$

The next higher-order coefficients in the spherical harmonic expansion describe other important features in the incipient deformation towards fission. The coefficient a_{30} describes the tendency of the body to be pear shaped and is generally known as the "mass asymmetry" parameter. The $l=3$ coefficients with $\mu\neq0$ can be used to describe bending and/or wiggling deformations (which may not be of importance in quasistatic calculations but would be of significance in dynamic considerations). The a_{40} coefficient describes necking of the waist of the body (if a_{40} is negative) or thickening of the waist (a_{40} positive).

In the description of the early stages of fission discussion is often confined to prolate spheroids, for which an approximate description is given by $\gamma=0$ in Eqs. (A7) and $a_{20}=\beta$, $a_{2|2|}=0$. By contrast, the oblate spheroid is described by $\gamma=\frac{1}{3}\pi$, $a_{20}=\frac{1}{2}\beta$, $a_{2|2|}=(\frac{3}{8})^{1/2}\beta$. More generally, axially symmetric shapes are commonly described by an expansion in Legendre polynomials:

$$R(\theta)=R_0\left[\alpha_0+\sum_{\lambda\geq2}\alpha_\lambda P_\lambda(\cos\theta)\right]. \tag{A8a}$$

The equivalent expansion in spherical harmonics is usually written

$$R(\theta)=R_0\left[\beta_0+\sum_{\lambda\geq2}\beta_\lambda Y_{\lambda0}(\theta,\phi)\right]. \tag{A8b}$$

The expansion coefficients of Eq. (A8a) are related to those of Eqs. (A2) and (A8b) by

$$\alpha_\lambda=a_{l0}\left(\frac{4\pi}{2l+1}\right)^{1/2}=\beta_\lambda\left(\frac{4\pi}{2\lambda+1}\right)^{1/2}, \tag{A9}$$

for $\lambda\equiv l$. In Eq. (A8a) α_0 is adjusted with deformation to maintain volume conservation. [Use Eq. (A6) with Eq. (A9) substituted for the $\alpha_\lambda, \lambda\neq0$.] The quadrupole parameter in this system is closely related to another commonly used parameter δ for expressing small deformations of a prolate spheroid:

$$R(\theta)=R_0[1+\tfrac{2}{3}\delta P_2(\cos\theta)]. \tag{A10}$$

Clearly,

$$\delta=\tfrac{3}{2}\alpha_2\,. \tag{A11}$$

In first order δ is identical to the principal parameter ε of a series of parameters employed (usually) for describing the deformation of a harmonic oscillator potential well. The axially symmetric harmonic oscillator potential

$$V_{\rm osc}(x,y,z)=\tfrac{1}{2}M[\omega_\perp^2(x^2+y^2)+\omega_z^2z^2] \tag{A12}$$

can be described in first approximation by the single deformation parameter ε by introducing

$$\omega_z=\omega_0(\varepsilon)(1-\tfrac{2}{3}\varepsilon)\,, \tag{A13a}$$

$$\omega_\perp=\omega_0(\varepsilon)(1+\tfrac{1}{3}\varepsilon)\,, \tag{A13b}$$

and the stretched coordinates

$$\xi=x[M\omega_\perp/\hbar]^{1/2}\,, \tag{A14a}$$

$$\eta=y[M\omega_\perp/\hbar]^{1/2}\,, \tag{A14b}$$

$$\zeta=z[M\omega_z/\hbar]^{1/2}\,, \tag{A14c}$$

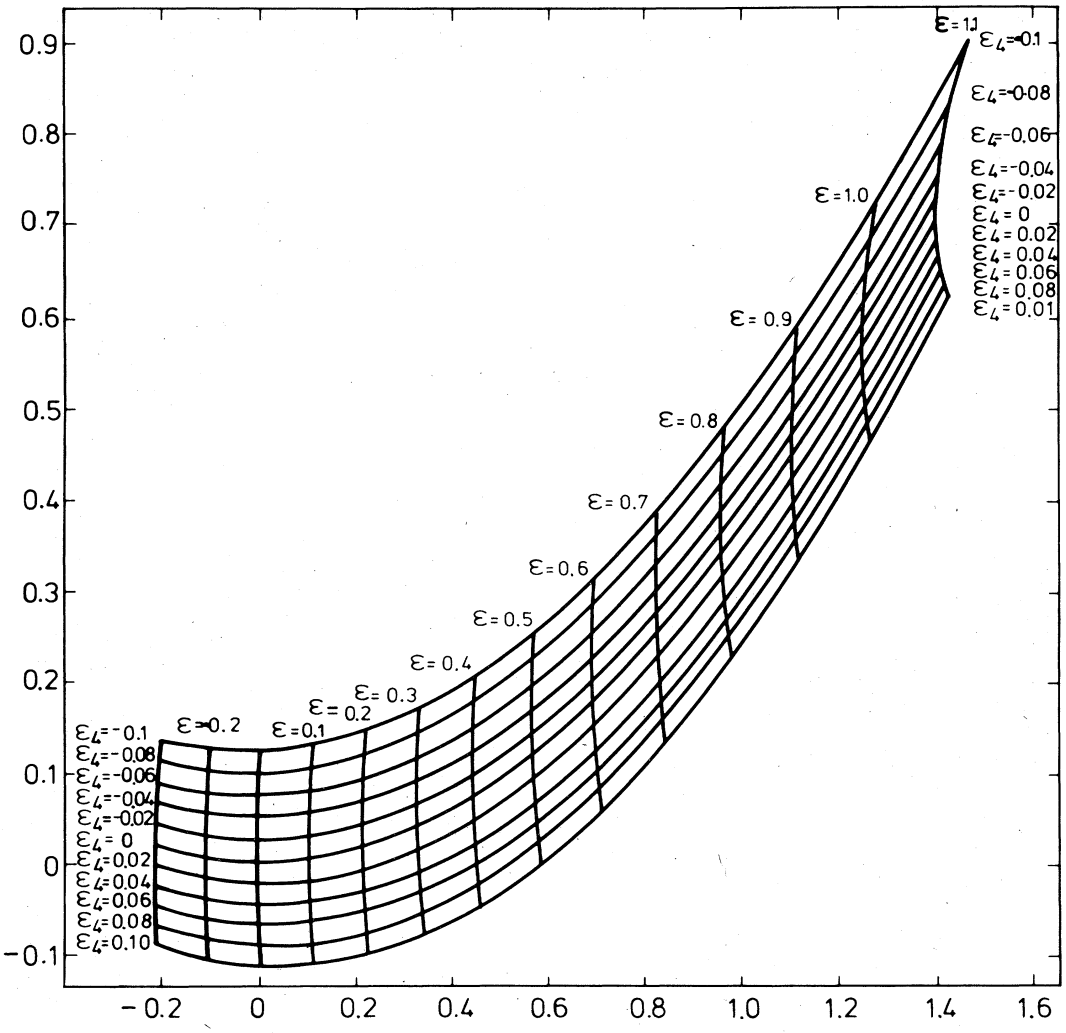

FIG. 168. Relationship between lowest-order parameters of a spherical harmonic expansion [Eq. (A8b)] and those of a stretched coordinate system [Eq. (A16)]. From Nilsson *et al.* (1969).

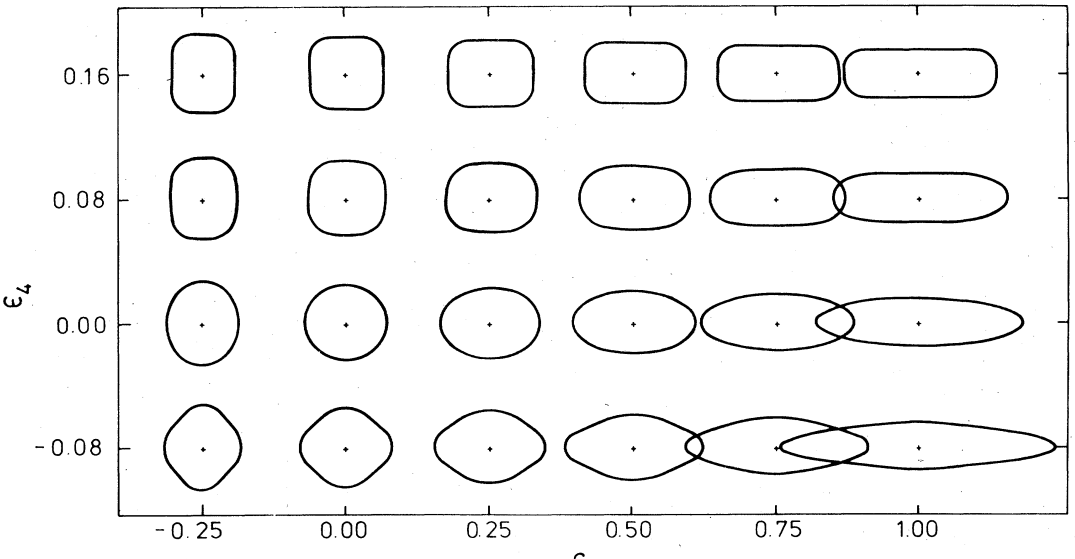

FIG. 169. Some shapes with axial symmetry that can be described in the stretched coordinate system. From Nilsson *et al.* (1969).

$$\rho^2 = \xi^2 + \eta^2 + \zeta^2 , \tag{A14d}$$

to give

$$V_{\rm osc} = \tfrac{1}{2}\hbar\omega_0\rho^2[1 - \tfrac{2}{3}\varepsilon P_2(\cos\theta_t)] , \tag{A15}$$

θ_t being the polar angle in the stretched coordinates. This form can be extended to higher multipolarities:

$$V_{\rm osc} = \tfrac{1}{2}\hbar\omega_0(\varepsilon, \varepsilon_3, \varepsilon_4 \ldots,)\rho^2\left[1 - \tfrac{2}{3}\varepsilon P_2 + 2\sum_{\lambda \geq 3}\varepsilon_\lambda P_\lambda\right] . \tag{A16}$$

Ellipsoidal forms can be described by extending the expression to include spherical harmonic terms of the type Y_{22}, Y_{2-2}, as in Eq. (2.7). "Mass-asymmetric" forms (pear shapes) are described by the inclusion of odd terms ($\lambda = 3, 5$, etc.).

The relationship between the lowest order parameters β_2, β_4 of the simple spherical harmonic expansion of Eq. (A8b) and those of the stretched coordinate description (A16) is shown in Fig. 168. Some shapes in the $\{\varepsilon, \varepsilon_4\}$ parametrization are shown in Fig. 169.

Expansions of the type (A16) are useful for the description of the shapes of fissioning actinide nuclei up to about the outer barrier peak ($\varepsilon \sim 0.85$) with terms up to $\lambda = 6$ included. But other shapes with a finite number of parameters have also been used to cover this range of the double-humped barrier. The family of surfaces used by Brack *et al.* (1972) is expressed in terms of the cylindrical coordinates z, ρ:

$$\rho^2/C^2 - (1 - z^2/C^2)(A + Bz^2/C^2 + \alpha z/C) = 0 , \quad B \geq 0 \tag{A17a}$$

$$\rho^2/C^2 - (1 - z^2/C^2)[(A + \alpha z/C)\exp(Bc^3 z^2/C^2)] = 0 , \quad B < 0 . \tag{A17b}$$

Here, C is determined by the volume conservation condition

$$\int_{z_1}^{z_2} dz\, \rho^2 = \tfrac{4}{3}R_0^3 \tag{A17c}$$

in terms of the radius R_0 of the undeformed sphere, z_1 and z_2 being the end points of the surface at which ρ becomes zero, and α describing the asymmetry of the shape in the z direction. The parameter c is a dimensionless elongation parameter

$$c = C/R_0 . \tag{A17d}$$

With the form (A17) $2c$ is the length of the surface along the symmetry axis from z_1 to z_2 in units of R_0. With the volume conservation condition applied to Eq. (A17a)

$$c = (A + \tfrac{1}{5}B)^{-1/3} , \tag{A18}$$

and this is approximately true also for Eq. (A17b). Thus the shapes described by Eqs. (A17) can also be described by use of the elongation parameter c together with a parameter h, which can be chosen to describe the variation of thickness of the waist of the surface without change in the elongation. The connection between $\{A, B\}$ and $\{c, h\}$ is

$$B = 2h + \tfrac{1}{2}(c - 1) , \tag{A19a}$$

$$A = 1/c^3 - \tfrac{1}{5}B . \tag{A19b}$$

Some shapes in the $\{c, h, \alpha\}$ parametrization are shown in Fig. 170. The relation between the $\{c, h\}$ parametrization and the two principal parameters β_2, β_4 of the mass-symmetric and axially symmetric spherical harmonic expansion is shown graphically in Fig. 171.

It is to be noted that the $\{c, h\}$ parametrization is capable of describing the bifurcation of the surface into two parts, a property that is eminently desirable for theoretical descriptions of the later stages of fission. Another family of surfaces that has this property is the Cassinian oval, defined in cylindrical coordinates by

$$(\rho^2 + z^2)^2 + 2\varepsilon(\rho^2 - z^2)R^2 + (\varepsilon^2 - 1)R^4 = 0 . \tag{A20}$$

The constant R is determined in terms of the elongation coordinate ε by volume conservation, R being the spherical radius R_0 when $\varepsilon = 0$. For small deformations ε is approximately equal to the parameter of same notation in Eq. (A16). At $\varepsilon = 1$, Eq. (A20) describes a scission configuration, and separated fragments occur

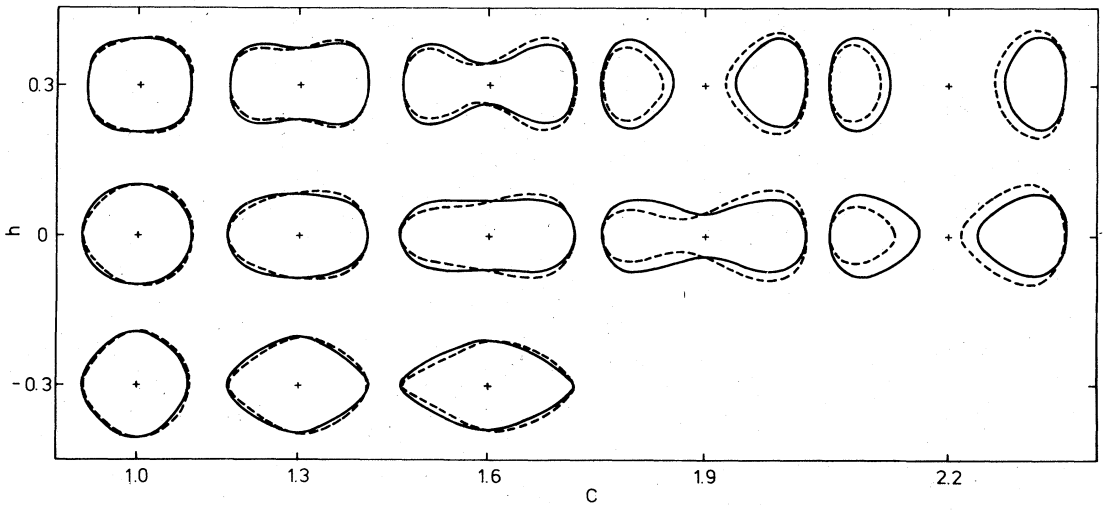

FIG. 170. Some shapes that can be described in the $\{c, h\}$ parametrization. Solid lines show shapes that are symmetric to a rotation by π about an axis perpendicular to the symmetry axis ($\alpha = 0$). The dotted lines show shapes with π-rotation asymmetry introduced ($\alpha = 0.2$). From Brack et al. (1972).

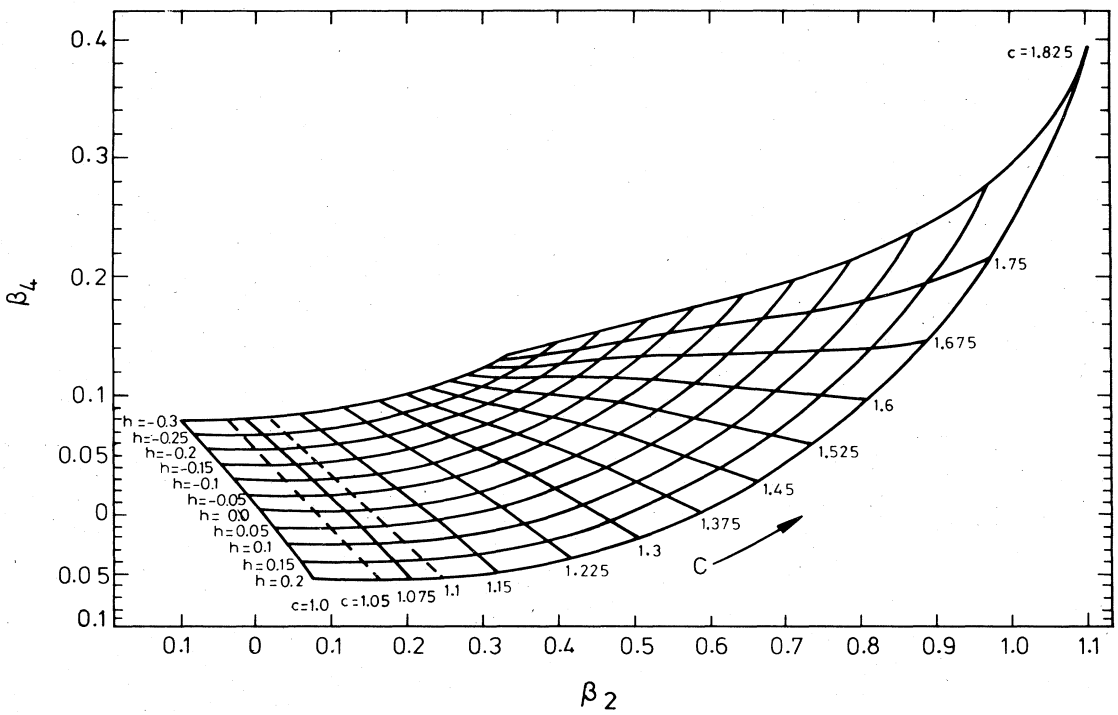

FIG. 171. Relation between the $\{c,h\}$ parametrization and the $\{\beta_2,\beta_4\}$ spherical harmonic expansion. From Brack *et al.* (1972).

for $\varepsilon > 1$; see Pashkevich (1971).

It is often more satisfactory, however, to describe a sequence of shapes in which the division into two parts is an essential component by families based on two centers. For two bodies such a description is the natural one and the single undivided body can be described by the exterior parts of the two overlapping surfaces. Usually each part is described by a shape parametrization of the kind discussed above, each part having its own separate set of deformation parameters (including volume), and an additional elongation or separation parameter is introduced, being, essentially, the distance (absolute or normalized) between the centers of the two parts. In the description of the unseparated body, the sharp cusp that appears in the surface where two center shapes intersect is an unsatisfactory feature. Various prescriptions have appeared in the literature for smoothing out this cusp. Clearly a large choice of parametrizations and elaborations of parameter sets becomes available in such schemes.

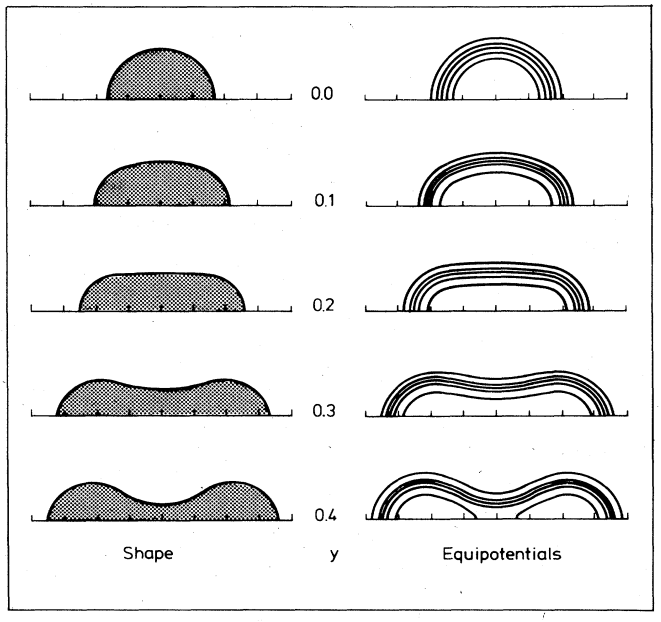

FIG. 172. Nuclear shapes and potentials described by the parameter y. From Nix (1972).

At the opposite extreme are the descriptions of an elongating system in terms of a single parameter. These are usually statistical parameters of the kind described in Sec. III.C. The commonest parameter of this kind is the quadrupole moment

$$Q=\sum_{i=1}^{A}(3z_i^2-r_i^2)$$
$$=\int d\Omega\int^{R_0(1+\beta_2 Y_{20})} dr\,\rho(\mathbf{r})r^2(3z^2-r^2)\,, \qquad \text{(A21)}$$

where ρ is the number density function of the body, the integration being taken over the volume of the body. For small deformations and sharp surfaces this parameter is simply related to the quadrupole parameter in the axially symmetric spherical harmonic expansion:

$$Q\approx\frac{3AR_0^2}{4\pi}\left(\frac{16\pi}{5}\right)^{1/2}\beta_2\,. \qquad \text{(A22)}$$

A single parameter description of elongation that is *not* of a simple statistical nature is the y parameter introduced by Hill and Wheeler (1953) and commonly used in papers by Nix and his collaborators [see, e.g., Möller and Nix (1974)]. This parameter is defined by

$$y = 1 - X \,, \tag{A23}$$

where X is the fissility parameter [see Sec. II.A.1.*c*, Eq. (2.4)] of an ideal liquid drop with the deformation described by y at its saddle point. To first order y is related to some of the simpler deformation parameters we have already introduced by

$$y = \frac{2}{7}\varepsilon = \frac{3}{7}\alpha_2 = \frac{3}{7}\left(\frac{5}{4\pi}\right)^{1/2}\beta (\approx 0.270\beta) \,. \tag{A24}$$

An illustration of deformed shapes for various values of y is shown in Fig. 172.

REFERENCES

Åberg, S., S. E. Larsson, P. Möller, S. G. Nilsson, G. Leander, and I. Ragnarsson, 1980, in *Physics and Chemistry of Fission*, Proceedings of a conference at Jülich (IAEA, Vienna), to appear.

Abramowitz, M., and I. A. Stegun, 1965, editors, *Handbook of Mathematical Functions* (National Bureau of Standards, USA), p. 686.

Alm, A., T. Kivikas, and L. J. Lindgren, 1974, in *Physics and Chemistry of Fission*, Proceedings of a conference at Rochester, (IAEA, Vienna), Vol. 1, p. 55.

Androsenko, C. C., S. B. Ermagambetov, A. V. Ignatjuk, N. S. Rabotnov, G. N. Smirenkin, A. S. Soldatov, L. N. Usachev, D. L. Spak, S. P. Kapitza, J. M. Tsipenjuk, and L. Kovach, 1969, in *Physics and Chemistry of Fission*, Proceedings of a conference at Vienna (IAEA, Vienna), p. 419.

Auchampaugh, G. F., and C. D. Bowman, 1973, Phys. Rev. C **7**, 2085.

Auchampaugh, G. F. and L. W. Weston, 1975, Phys. Rev. C **12**, 1850.

Auchampaugh, G. F., J. A. Farell, and D. W. Bergen, 1971, Nucl. Phys. A **171**, 31.

Back, B. B., 1974, Nucl. Phys. A **228**, 323.

Back, B. B., J. P. Bondorf, G. A. Otroschenko, J. Pedersen, and B. Rasmussen, 1969, in *Physics and Chemistry of Fission*, Proceedings of a conference at Vienna, (IAEA, Vienna), p. 351.

Back, B. B., J. P. Bondorf, G. A. Otroschenko, J. Pedersen, and B. Rasmussen, 1971, Nucl. Phys. A **165**, 449.

Back, B. B., O. Hansen, H. C. Britt, and J. D. Garrett, 1974a, Phys. Rev. C **9**, 1924.

Back, B. B., O. Hansen, H. C. Britt, J. D. Garrett, and P. Leroux, 1974b, *Physics and Chemistry of Fission*, Proceedings of a conference at Rochester (IAEA, Vienna), Vol. 1, p. 3.

Back, B. B., H. C. Britt, O. Hansen, B. Leroux, and J. D. Garrett, 1974c, Phys. Rev. C **10**, 1948.

Backe, H., L. Richter, D. Habs, V. Metag, J. Pedersen, P. Singer, and H. J. Specht, 1979a, Phys. Rev. Lett. **42**, 490.

Batchelor, R., W. B. Gilboy, J. H. Towle, 1965, Nucl. Phys. **65**, 236.

Baybarz, R. D., J. R. Berreth, F. B. Simpson, W. K. Brown, M. E. Ennis, R. R. Fullwood, G. A. Keyworth, J. H. McNally, M. S. Moore, and M. C. Thompson, 1971, Los Alamos Report LA-4566.

Bell, R. E., S. Bjørnholm, and J. S. Severiens, 1960, Mat. Fys. Medd. Dan. Vid. Selsk. **32**, No. 12.

Bellia, G., A. Del Zoppo, and E. Migneco, 1976, Catania University, Italy, preprint PP/512.

Belov, A. G., Yu. P. Gangrskii, B. Dahlsuren, and A. M. Kucher, 1971, Yad. Fiz. **14**, 685.

Bemis, C. E., J. R. Beene, J. P. Young, and S. D. Kramer, 1979, Phys. Rev. Lett. **43**, 1854.

Bemis, C. E., F. K. McGowan, J. C. L. Ford, W. T. Milner, P. H. Stelson, and R. L. Robinson, 1973, Phys. Rev. C **8**, 1466.

Bengtsson, R., 1974, in *Physics and Chemistry of Fission*, Proceedings of a conference at Rochester (IAEA, Vienna), Vol. 1, p. 203.

Bergen, D. W. and R. R. Fullwood, 1971, Nucl. Phys. A **163**, 577.

Bjørnholm, S., 1972, J. Phys. (Paris) **33**, C5-33.

Bjørnholm, S., A. Bohr, and B. Mottelson, 1974, in *Physics and Chemistry of Fission*, Proceedings of a conference at Rochester (IAEA, Vienna), Vol. 1, p. 367.

Bjørnholm, S., J. Borggreen, and E. K. Hyde, 1970, Nucl. Phys. A **156**, 561.

Bjørnholm, S., J. Borggreen, L. Westgaard, and V. A. Karnauchov, 1967, Nucl. Phys. A **95**, 513.

Bjørnholm, S., and V. M. Strutinsky, 1969, Nucl. Phys. A **136**, 1.

Blatt, J. M. and V. F. Weisskopff, 1952, *Theoretical Nuclear Physics* (Wiley, New York).

Block, R. C., R. W. Hockenbury, R. E. Slovacek, E. B. Bean, and D. S. Cramer, 1973, Phys. Rev. Lett. **31**, 247.

Blons, J., 1973, Nucl. Sci. Eng. **51**, 130.

Blons, J., C. Mazur, and D. Paya, 1975a, Phys. Rev. Lett. **35**, 1749.

Blons, J., C. Mazur, and D. Paya, 1975b, *Proceedings of the Conference on Nuclear Cross Sections and Technology*, Washington, D.C., 1975 (NBS, Washington, D.C., 1975), Special Publication No. 425, p. 642.

Blons, J., C. Mazur, D. Paya, M. Ribrag, and H. Weigmann, 1978, Phys. Rev. Lett. **41**, 1282.

Blons, J., C. Mazur, D. Paya, M. Ribrag, and H. Weigmann, 1980, Paper delivered at XVIII International Winter Meeting on Nuclear Physics, , Bormio, Italy.

Boca, I., N. Martolugu, M. Sezon, I. Vilcov, N. Vilcov, G. N. Flerov, A. A. Pleve, S. M. Polikanov, and S. P. Tretyakova, 1969, Nucl. Phys. A **134**, 541.

Bohr, A., 1956, in *Peaceful Uses of Atomic Energy*, Proceedings of a conference at Geneva, 1955 (United Nations, New York), Vol. 2, p. 220.

Bohr, A. and B. Mottelson, 1969, *Nuclear Structure*, Vol. 1 (Benjamin, New York).

Bohr, A. and B. Mottelson, 1975, *Nuclear Structure*, Vol. 2 (Benjamin, New York).

Bohr, N., and J. A. Wheeler, 1939, Phys. Rev. **56**, 426.

Boldeman, J. W., D. Goguy, A. R. D. Musgrove, and R. L. Walsh, 1980, private communication.

Bolsterli, M., E. O. Fiset, and J. R. Nix, 1969, in *Physics and Chemistry of Fission*, Proceedings of a conference at Vienna (IAEA, Vienna), p. 183.

Bolsterli, M., E. O. Fiset, J. R. Nix, and J. L. Norton, 1972, Phys. Rev. C **5**, 1050.

Bondorf, J. P., 1970, Phys. Lett. B **31**, 1.

Borggreen, J., E. Kashy, J. Hattula, and V. Maarbjerg, 1973, Nucl. Phys. A **218**, 621.

Borggreen, J., J. Pedersen, G. Sletten, R. Heffner, and E. Swanson, 1977, Nucl. Phys. A **279**, 189.

Bowman, C. D., M. S. Corps, G. F. Auchampaugh, and S. C. Fultz, 1965, Phys. Rev. **137**, B326.

Bowman, C. D., I. G. Schröder, C. E. Dick, and H. E. Jackson, 1975, Phys. Rev. C **12**, 863.

Brack, M., 1980, in *Physics and Chemistry of Fission*, Proceedings of a conference at Jülich (IAEA, Vienna), to appear.

Brack, M., J. Damgaard, A. S. Jensen, H. C. Pauli, V. M. Strutinsky, and C. Y. Wong, 1972, Rev. Mod. Phys. **44**, 320.

Brack, M., T. Ledergerber, H. C. Pauli, and A. S. Jensen, 1974, Nucl. Phys. A **234**, 185.

Britt, H. C., 1973, At. Data Nucl. Data Tables **12**, 407.

Britt, H. C., M. Bolsterli, J. R. Nix, and J. L. Norton, 1973, Phys. Rev. C **7**, 801.

Britt, H. C., S. C. Burnett, and J. D. Cramer, 1969, in *Physics and Chemistry of Fission*, Proceedings of a conference at Vienna (IAEA, Vienna), p. 375.
Britt, H. C., S. C. Burnett, B. H. Erkkila, J. E. Lynn, and W. E. Stein, 1971, Phys. Rev. C **4**, 1444.
Britt, H. C. and J. D. Cramer, 1970, Nucl. Sci. Eng. **41**, 177.
Britt, H. C., and B. H. Erkkila, 1971, Phys. Rev. C **4**, 1441.
Britt, H. C., B. H. Erkkila, and B. B. Back, 1972, Phys. Rev. C **6**, 1090.
Britt, H. C., A. Gavron, P. D. Goldstone, R. Schoenmackers, J. Weber, and J. B. Wilhelmy, 1978, Phys. Rev. Lett. **40**, 1010.
Britt, H. C., W. R. Gibbs, J. J. Griffin, and R. H. Stokes, 1965, Phys. Rev. **139**B, 354.
Britt, H. C., R. A. Rickey, and W. S. Hall, 1968, Phys. Rev. **175**, 1525.
Brown, W. K., D. R. Dixon, and D. M. Drake, 1970, Nucl. Phys. A **156**, 609.
Butler, D. K., 1960, Phys. Rev. **117**, 1305.
Butler, D. K., and R. K. Sjoblom, 1961, Phys. Rev. **124**, 1129.
Byers, D. H., B. C. Diven, and M. G. Silbert, 1966, *Proceedings of the Conference on Neutron Cross-Sections and Technology*, USAEC Report CONF-660303, Vol. 2, p. 903.
Caruana, J., J. W. Boldeman, and R. L. Walsh, 1977, Nucl. Phys. A **285**, 205.
Christiansen, J., G. Hempel, H. Ingwersen, W. Klinger, G. Schatz, and W. Witthuhn, 1975, Nucl. Phys. A **239**, 253.
Coté, R. E., H. Diamond, and J. E. Gindler, 1965, in Brookhaven National Laboratory compilation BNL 325, 2nd edition, supplement No. 2, Vol. III, p. 3.
Cramer, J. D., and J. R. Nix, 1970, Phys. Rev. C **2**, 1048.
Dahlsuren, B., G. N. Flerov, Yu. P. Gangrsky, Yu. A. Lasarev, B. N. Markov, Nguyen Cong Khan, 1969, Dubna Report E15-4744.
Damgaard, J., H. C. Pauli, W. M. Strutinsky, C. Y. Wong, M. Brack, and A. S. Jensen, 1969, in *Physics and Chemistry of Fission*, Proceedings of a conference at Vienna (IAEA, Vienna), p. 213.
De Saussure, G., D. K. Olsen, R. B. Perez, and F. C. Difilippo, 1978, Oak Ridge Report ORNL/TM-6152.
Dietrich, K., 1972, in *Structure of Nuclei*, a lecture course at International Centre for Theoretical Physics in Trieste, 1971 (IAEA, Vienna), p. 373.
Difilippo, F. C., R. B. Perez, G. de Saussure, D. K. Olsen, and R. W. Ingle, 1977, Nucl. Sci. Eng. **63**, 153.
Dlouhy, Z., J. Kristiak, and Ts. Panteleev, 1976, Czech. J. Phys. B **26**, 1334.
Dresner, L., 1957, in *Neutron Interactions with the Nucleus*, Proceedings of a conference at New York, U.S. AEC Report No. TID 7547, p. 71.
Dyson, F. J., and M. L. Mehta, 1963, J. Math. Phys. **4**, 701.
Egelstaff, P. A., 1958, J. Nucl. Energy **7**, 35.
Evans, J. E., and G. A. Jones, 1965 (private communication).
Farrell, J. A., 1970 (private communication).
Flerov, G. N., and V. A. Druin, 1966, Dubna report, JINR P-2539.
Flerov, G. N., J. P. Gangrsky, B. N. Markov, S. M. Polikanov, and H. Jungclaussen, 1968, Sov. Nucl. Phys. **6**, 12.
Flerov, G. N., A. A. Pleve, S. M. Polikanov, S. P. Tretyakova, N. Martalogu, D. Pcenaru, M. Sezon, I. Vilcov, and N. Vilcov, 1967, Nucl. Phys. A **97**, 444.
Flerov, G. N., and S. M. Polikanov, 1964, Compt. Rend. Cong. Int. Phys. Nucl. (Paris), **1**, 407.
Fleury, A., F. H. Ruddy, M. N. Namboodiri, and J. M. Alexander, 1973, Phys. Rev. C **7**, 1231.
Flocard, H., P. Quentin, D. Vautherin, and A. K. Kerman, 1974, in *Physics and Chemistry of Fission*, Proceedings of a conference at Rochester (IAEA, Vienna), Vol. 1, p. 221.
Ford, K. W., D. L. Hill, M. Wakano, and J. A. Wheeler, 1959, Ann. Phys. (NY) **7**, 239.
Fröman, N., and Ö. Dammert, 1970, Nucl. Phys. A **147**, 627.
Fröman, N., and P. O. Fröman, 1965, *JWKB Approximation, Contributions to the theory* (North-Holland, Amsterdam).
Fröman, N., and P. O. Fröman, 1970, Nucl. Phys. A **147**, 606.
Fromm, W. D., H. G. Ortlepp, S. M. Polikanov, U. Schmidt, G. N. Zorin, R. Arlt, and G. Musiol, 1977, Nucl. Phys. A **278**, 387.
Fubini, A., J. Blons, A. Michaudon, and D. Paya, 1968, Phys. Rev. Lett. **20**, 1373.
Galeriu, D., M. Marinescu, D. Poenaru, I. Vilcov, and N. Vilcov, 1974, in *Physics and Chemistry of Fission*, Proceedings of a conference at Rochester (IAEA, Vienna), Vol. 1, p. 297.
Gangrskii, Yu. P., V. N. Markov, I. F. Kharisov, and Yu. M. Tsipenyuk, 1973, Sov. J. Nucl. Phys. **16**, 151.
Gangrskii, Yu. P., B. N. Markov, and Yu. M. Tsipenyuk, 1970, Phys. Lett. B **32**, 182.
Gangrskii, Yu. P., T. Nad', I. Vinnai, and I. Kovach, 1971, At. Energ. **31**, 156.
Gangrskii, Yu. P. Nguen Kong Khan, and D. D. Prelatov, 1972, At. Energ. **33**, 829.
Gavron, A., H. C. Britt, E. Konecny, J. Weber, and J. B. Wilhelmy, 1976, Phys. Rev. C **13**, 2374.
Gavron, A., H. C. Britt, P. D. Goldstone, J. B. Wilhelmy, and S. E. Larsson, 1977, Phys. Rev. Lett. **38**, 1457.
Gilbert, A., and A. G. W. Cameron, 1965, Can. J. Phys. **43**, 1446.
Glässel, P., H. Rosler, and H. J. Specht, 1976, Nucl. Phys. A **256**, 220.
Goerlach, U., D. Habs, M. Just, V. Metag, P. Paul, and H. J. Specht, 1978, Z. Phys. A **287**, 171.
Gokhberg, B. M., G. A. Ostroschenko, and V. A. Shigin, 1959a, Dokl. Akad. Nauk. USSR **128**, 911.
Gokhberg, B. M., G. A. Ostroschenko, and V. A. Shigin, 1959b, Dokl, Akad. Nauk. USSR **128**, 1157.
Goldhaber, M., and E. Teller, 1948, Phys. Rev. **74**, 1046.
Goldstone, P. D., F. Hopkins, R. E. Malmin, P. von Brentano, and P. Paul, 1976, Phys. Lett. B **62**, 280.
Goldstone, P. D., F. Hopkins, R. E. Malmin, and P. Paul, 1975, Phys. Rev. Lett. **35**, 1141.
Götz, U., H. C. Pauli, and K. Junker, 1972, Phys. Lett. B **39**, 436.
Grant, I. S., 1976, Rep. Prog. Phys. **39**, 955.
Griffin, J. J., 1971, Nucl. Phys. A **170**, 395.
Griffin, J. J., and J. A. Wheeler, 1957, Phys. Rev. **108**, 311.
Groshev, L. V., A. M. Demidov, V. N. Lysenko, and V. I. Pelekov, 1958, *Atlas of Capture Gamma-Ray Spectra*, Akad. Nauk, Moscow.
Grütter, A., H. R. von Günten, V. Herrnberger, B. Hahn, U. Moser, H. W. Reist, and G. Sletten, 1974, in *Physics and Chemistry of Fission*, Proceedings of a conference at Rochester (IAEA, Vienna), Vol. 1, p. 305.
Gustafson, C., I. L. Lamm, B. Nilsson, and S. G. Nilsson, 1967, Ark. Fys. **36**, 613.
Günther, W., K. Huber, U. Kneissl, H. Krieger, and H. J. Maier, 1979, Phys. Rev. C **19**, 433.
Habs, D., 1977, *Habilitationsschrift*, Max Planck Institut, Heidelberg.
Habs, D., S. Hanna, B. Herskind, V. Metag, P. Paul, J. Pedersen, G. Schultz, G. Sletten, and H. J. Specht, 1975, 1976, 1977, Max-Planck-Institut für Kernphysik, annual reports.
Habs, D., M. Just, V. Metag, E. Mosler, B. Neumann, P. Paul, P. Singer, H. J. Specht, and G. Ulfert, 1975, Max Planck Institute, Heidelberg, Annual Report, 56.
Habs, D., V. Metag, H. J. Specht, and G. Ulfert, 1977, Phys. Rev. Lett. **38**, 387

Hamamoto, I., 1974, Nucl. Phys. A **232**, 445.
Hamamoto, I., 1975, Phys. Lett. B **56**, 431.
Hamamoto, I., and W. Ogle, 1975, Nucl. Phys. A **240**, 54.
Hauser, W., and H. Feshbach, 1952, Phys. Rev. **87**, 366.
Henkel, R. L., and J. E. Brolley, 1956, Phys. Rev. **103**, 1292.
Henkel, R. L., R. A. Nobles, and R. K. Smith, 1957, Los Alamos Report AECD-4256.
Henkel, R. L., and R. K. Smith, 1956, in BNL 325, edited by D. J. Hughes and J. A. Harvey.
Hill, D. L., and J. A. Wheeler, 1953, Phys. Rev. **89**, 1102.
Hofmann, H., 1972a, Phys. Lett. B **42**, 177.
Hofmann, H., 1972b, Z. Phys. **250**, 14.
Holmberg, M., L. G. Strömberg, and L. Wallin, 1969, Nucl. Phys. A **129**, 149.
Howard, W. M. and J. R. Nix, 1974, in *Physics and Chemistry of Fission*, Proceedings of a conference at Rochester (IAEA, Vienna), Vol. 1, p. 145.
Huizenga, J. R., 1965, in *Proceedings of the Scottish Universities Summer School in Physics*, (Glasgow University).
Huizenga, J. R., and R. Vandenbosch, 1962, *Nuclear Fission in Nuclear Reactions* (North-Holland, Amsterdam), Vol. 2, p. 42.
Hurwitz, M., and H. A. Bethe, 1951, Phys. Rev. **81**, 898.
Ignatyuk, A. V., M. G. Itkis, V. N. Okolovich, G. N. Smirenkin, and A. S. Tishin, 1975, Yad. Fiz. **21**, 1185.
Ignatyuk, A. V., N. S. Rabotnov, and G. N. Smirenkin, 1969, Phys. Lett. B **29**, 209.
Inglis, D., 1954, Phys. Rev. **96**, 1059.
Jackson, J. D., 1956, Can. J. Phys. **34**, 767.
Jägare, S., 1970, Phys. Lett. B **32**, 571.
James, G. D., 1964, Nucl. Phys. **55**, 517.
James, G. D., 1969, Nucl. Phys. A **23**, 24.
James, G. D., J. W. T. Dabbs, J. A. Harvey, N. W. Hill, and R. H. Schindler, 1977, Phys. Rev. C **15**, 2083.
James, G. D., J. E. Lynn, and L. Earwaker, 1972, Nucl. Phys. A **189**, 225.
James, G. D. and B. H. Patrick, 1969, in *Physics and Chemistry of Fission*, Proceedings of a conference at Vienna (IAEA, Vienna), p. 391.
James, G. D., and E. R. Rae, 1968, Nucl. Phys. A **118**, 313.
James, G. D., and G. G. Slaughter, 1969, Nucl. Phys. A **139**, 471.
James, G. D., D. B. Syme, and M. C. Cooke, 1979, Harwell Nuclear Physics Progress Report, AERE PR/NP.26.
Jensen, H., and H. Koppe, 1971, Ann. Phys. (N.Y.) **63**, 586.
John, J., and V. J. Orphan, 1970, General Atomic Report GA-10186.
Kalish, R., B. Herskind, J. Pedersen, D. Shackleton, and L. Strabo, 1974, Phys. Rev. Lett. **32**, 1009.
Käppeler, F., and E. Pfletschinger, 1970, in *Proceedings of the Conference on Nuclear Data for Reactors* (IAEA, Vienna), Vol. 2, p. 77.
Kemble, E. C., 1958, *Fundamental Principles of Quantum Mechanics with Elementary Applications* (Dover, New York), p. 100.
Kennedy, R. C., L. Wilets, and E. M. Henley, 1964, Phys. Rev. Lett. **12**, 36.
Keyworth, G. A., J. R. Lemley, C. E. Olsen, F. T. Seibel, J. W. T. Dabbs, and N. W. Hill, 1973, Phys. Rev. C **8**, 2352.
Kolar, W., and K. H. Böckhoff, 1968, J. Nucl. Energy **22**, 299.
Kolar, W., J. P. Theobald, and E. Lanzana, 1971, Z. Phys. **248**, 355.
Konecny, E., H. J. Specht, and J. Weber, 1974, in *Physics and Chemistry of Fission*, Conf. Proc., Rochester, 1973 (Vienna: IAEA), Vol. 2, p. 3.
Kuiken, R., N. J. Pattenden, and H. Postma, 1972, Nucl. Phys. A **196**, 389.
Lamphere, R. W., 1962, Nucl. Phys. **38**, 561.
Lamphere, R. W., 1965, in *Physics and Chemistry of Fission*, Proceedings of a conference at Salzburg (IAEA, Vienna), Vol. 1, p. 63.
Landau, L. D., and E. M. Lifshitz, 1958, *Quantum Mechanics* (Pergamon, London).
Lane, A. M., and J. E. Lynn, 1957, Proc. Phys. Soc. (London) A **70**, 557.
Lane, A. M., J. E. Lynn, and J. D. Moses, 1974, Nucl. Phys. A **232**, 189.
Lane, A. M., and R. G. Thomas, 1958, Rev. Mod. Phys. **30**, 257.
Lark, N. L., G. Sletten, J. Pedersen, and S. Bjørnholm, 1969, Nucl. Phys. A **139**, 481.
Larsson, S. E., and G. Leander, 1974, in *Physics and Chemistry of Fission*, Proceedings of a conference at Rochester (IAEA, Vienna), Vol. 1, p. 177.
Larsson, S. E., G. Leander, I. Ragnarsson, and J. Randrup, 1974, Phys. Scr. A **10**, 65.
Larsson, S. E., I. Ragnarsson, and S. G. Nilsson, 1972, Phys. Lett. B **38**, 263.
Leander, G., 1980, in *Physics and Chemistry of Fission*, Proceedings of a conference at Jülich, (IAEA, Vienna), to appear.
Leboeuf, J. N., and R. C. Sharma, 1973a, Can. J. Phys. **51**, 446.
Leboeuf, J. N., and R. C. Sharma, 1973b, Nucl. Phys. A **208**, 514.
Lederer, M., J. M. Hollander, and I. Perlman, 1967, *Table of Isotopes* (Wiley, New York), p. 577.
Levinger, J. S., and H. A. Bethe, 1950, Phys. Rev. **78**, 115.
Leroux, B., G. T. Barreau, A. Sicre, T. Benfoughal, F. Caitucoli, J. P. Doan, and G. D. James, 1980, in *Physics and Chemistry of Fission*, Conf. Proc., Jülich, 1979 (IAEA, Vienna), to appear.
Levinger, J. S., and H. A. Bethe, 1950, Phys. Rev. **78**, 115
Limkilde, P., and G. Sletten, 1973, Nucl. Phys. A **199**, 504.
Lynn, J. E., 1964, Phys. Rev. Lett. **13**, 412.
Lynn, J. E., 1965, Phys. Lett. **18**, 31.
Lynn, J. E., 1966a, *Nuclear Data for Reactors* (IAEA, Vienna), Vol. 2, p. 89.
Lynn, J. E., 1966b, in *Nuclear Structure Study with Neutrons*, Proceedings of a conference at Antwerp (North-Holland, Amsterdam), p. 125.
Lynn, J. E., 1968a, *The Theory of Neutron Resonance Reactions* (Clarendon, Oxford).
Lynn, J. E., 1968b, Harwell Report AERE-R 5891.
Lynn, J. E., 1968c, in *Nuclear Structure*, Proceedings of a conference at Dubna (IAEA, Vienna), p. 463.
Lynn, J. E., 1969, in *Physics and Chemistry of Fission*, Proceedings of a conference at Vienna (IAEA, Vienna), p. 249.
Lynn, J. E., 1970, *Nuclear Data for Reactors* (IAEA, Vienna), Vol. I, p. 106.
Lynn, J. E., 1971, Harwell Report AERE-M 2505.
Lynn, J. E., 1972, Harwell Report AERE-R 7279.
Lynn, J. E., 1973, J. Phys. A **6**, 542.
Lynn, J. E., 1974a, Harwell Report AERE-R 7373.
Lynn, J. E., 1974b, Harwell Report AERE-R, 7468.
Lynn, J. E., 1980, in *Fission Cross Sections*, edited by A. Michaudon (Pergamon, Oxford) Chapter V, to appear.
Lynn, J. E., and B. B. Back, 1974, J. Phys. A **7**, 395.
Lynn, J. E., and J. D. Moses, 1980, J. Phys. G (in press).
Mahaux, C., and H. A. Weidenmüller, 1967, Nucl. Phys. A **91**, 241.
McNally, J. H., J. W. Barnes, B. J. Dropesky, P. A. Seeger, and K. Wolfsberg, 1974, Phys. Rev. C **8**, 717.
Meitner, L., and O. R. Frisch, 1939, Nature **143**, 239.
Metag, V., 1974, *Habilitationschrift*, Max-Planck-Institute für Kernphysik, Heidelberg.
Metag, V., 1980, in *Physics and Chemistry of Fission*, Proceedings of a conference at Jülich (IAEA, Vienna) to appear.

Metag, V., S. M. Lee, E. Liukkonen, G. Sletten, and S. Bjørnholm, 1973, Nucl. Phys. A **213**, 397.
Metag, V., R. R. Repnow, and P. von Brentano, 1971, Nucl. Phys. A **165**, 289.
Metag, V., D. Habs, H. J. Specht, G. Ulfert, and C. Kozhuharur, 1976, Hyperfine Interactions **1**, 405.
Metag, V., and G. Sletten, 1977, Nucl. Phys. A **282**, 77.
Michaudon, A., 1973, Adv. Nucl. Phys. **6**, p. 1.
Michaudon A., 1976, in Proceedings of the International Conference on Interactions of Neutrons with Nuclei, ERDA Report CONE-760715-P1, 641.
Migdal, A. B., 1959a, Sov. Phys.-JETP **37**, 249.
Migdal, A. B., 1959b, Nucl. Phys. **13**, 655.
Migneco, E., G. Russo, R. De Leo, and A. Pantaleo, 1977, Phys. Rev. C **16**, 1919.
Migneco, E., and J. P. Theobald, 1968, Nucl. Phys. A **112**, 603.
Moldauer, P. A., 1967, Phys. Rev. **157**, 907.
Moore, M. S., J. H. McNally, R. D. Baybarz, 1971, Phys. Rev. C **4**, 273.
Moretto, L. G., S. G. Thompson, J. Routti, and R. C. Gatti, 1972, Phys. Lett. B **38**, 471.
Moses, J. D., 1976 (private communication).
Muir, D. W., and L. R. Veeser, 1971, Proceedings of the Conference on Nuclear Cross Sections and Technology, (USAEC Report CONF 71031, Vol. 2, p. 292.
Myers, W. D., 1977, *Droplet Model of Atomic Nuclei* (IFF/Plenum, New York).
Myers, W. D., and W. J. Swiatecki, 1966, Nucl. Phys. **81**, 1.
Myers, W. D., and W. J. Swiatecki, 1967, Ark. Fys. **36**, 343.
Myers, W. D., and W. J. Swiatecki, 1969, Ann. Phys. (NY) **55**, 395.
Möller, P., 1972, Nucl. Phys. A **192**, 529.
Möller, P. and S. G. Nilsson, 1970, Phys. Lett. B **31**, 283.
Möller, P. and J. R. Nix, 1974, in *Physics and Chemistry of Fission*, Proceedings of a conference at Rochester (IAEA, Vienna), Vol. 1, p. 103.
Nagy, T., A. G. Belov, Yu. P. Gangrsky, B. N. Markov, I. V. Sizar and I. F. Kharisov, 1970, Dubna Report P7-5162.
Namboodiri, M. N., F. H. Ruddy, and J. M. Alexander, 1973, Phys. Rev. C **7**, 1222.
Nesterov, V. G., and G. N. Smirenkin, 1960, At. Energ. **4**, 185.
Nilsson, S.G., 1969, *Proceedings of the Robert A. Welch Foundation Conference* XIII *on Transuranic Elements*, Houston, Texas (Robert A. Welch Foundation, Houston), p. 471.
Nilsson, S. G., and O. Prior, 1961, Mat. Fys. Medd. Dan. Vid. Selsk. **32**, No. 16.
Nilsson, S. G., C. F. Tsang, A. Sobiczewski, Z. Szymanski, S. Wycech, C. Gustafson, I. Lamm, P. Möller, and B. Nilsson, 1969, Nucl. Phys. A **131**, 1.
Nix, J. R., 1967, Ann. Phys. (NY) **41**, 52.
Nix, J. R., 1969, Nucl. Phys. A **130**, 241.
Nix, J. R., 1972, Annu. Rev. Nucl. Sci. **22**, 65.
Nörenberg, W., 1970, *Habilitationsschrift*, University of Heidelberg.
Nörenberg, W., 1973, Z. Phys. **260**, 165.
Northrop, J. A., R. H. Stokes, and K. Boyer, 1959, Phys. Rev. **115**, 1277.
Pashkevich, V. V., 1969, Nucl. Phys. A **133**, 40.
Pashkevich, V. V., 1971, Nucl. Phys. A **169**, 275.
Patrick, B. H., and G. D. James, 1968, Phys. Lett. B **28**, 258.
Pauli, H. C., 1974, Phys. Scr. A **10**, 127.
Pauli, H. C., and T. Ledergerber, 1971, Nucl. Phys. A **175**, 545.
Pauli, H. C., and T. Ledergerber, 1974, in *Physics and Chemistry of Fission*, Proceedings of a conference at Rochester (IAEA, Vienna), Vol. 1, p. 463.
Pauli, H. C., T. Ledergerber, and M. Brack, 1971, Phys. Lett. B **34**, 264.
Paya, D., J. Blons, H. Derrien, A. Fubini, A. Michaudon, and P. Ribon, 1968, J. Phys. (Paris) **29**, 159.
Paya, D., J. Blons, H. Derrien, and A. Michaudon, 1969, in *Physics and Chemistry of Fission*, Proceedings of a conference at Vienna (IAEA, Vienna), p. 307.
Pedersen, J., and B. D. Kuzminov, 1969, Phys. Lett. B **29**, 176
Pedersen, J., and B. Rasmussen, 1972, Nucl. Phys. A **178**, 449.
Pedersen, J. and G. Sletten, 1976 (private communication).
Perez, P. B., G. de Saussure, and M. N. Moore, 1969, in *Physics and Chemistry of Fission*, Proceedings of a conference at Vienna (IAEA, Vienna), p. 283.
Plattard, S., 1973, Thesis, Orsay.
Plattard, S., G. F. Auchampaugh, N. W. Hill, G. de Saussure, R. B. Perez, and I. A. Harvey, 1979, *Proceedings of the Conference on Neutron Cross-Sections and Technology*, (DOE, Washington D.C., 1980), to appear.
Plattard, S., J. Blons, and D. Paya, 1976, Nucl. Sci. Eng. **61**, 477.
Polikanov, S. M., and G. Sletten, 1970, Nucl. Phys. A **151**, 656.
Polikanov, S. M., V. A. Druin, V. A. Karnauchov, V. L. Mikheev, A. A. Pleve, N. K. Skobelev, V. G. Subotin, G. M. Ter-Akapian, and V. A. Fomichev, 1962, Zh. Eksp. Teor. Fiz. **42**, 1016.
Pomorski, K., and A. Sobiczewski, 1978, Acta Phys. Pol. B **9**, 61.
Porter, C. F., and R. G. Thomas, 1956, Phys. Rev. **104**, 483.
Rabotnov, N. S., G. N. Smirenkin, A. S. Soldatov, L. N. Usachev, S. P. Kapitza, and Yu. M. Tsipenyuk, 1970, Sov. J. Nucl. Phys. **11**, 285.
Rahn, F., H. S. Camarda, G. Hacken, W. W. Havens, H. I. Lion, J. Rainwater, M. Slagavitz, and S. Wynchank, 1972, Phys. Rev. C **6**, 1854.
Randrup, J., S. E. Larsson, P. Möller, S. G. Nilsson, K. Pomorski, and A. Sobiczewski, 1976, Phys. Rev. **13**, 229.
Randrup, J., C. F. Tsang, P. Möller, S. G. Nilsson, and S. E. Larsson, 1973, Nucl. Phys. A **217**, 221.
Reich, C.W., and M. S. Moore, 1958, Phys. Rev. 111, 929.
Rosler, H., F. Plasil, and H. W. Schmitt, 1972, Phys. Lett. B **38**, 501.
Ruddy, F. H., and J. M. Alexander, 1969, Phys. Rev. **187**, 1672.
Russo, P. A., J. Pedersen, and R. Vandenbosch, 1974, *Physics and Chemistry of Fission*, Proceedings of a conference at Rochester (IAEA, Vienna), Vol. 1, p. 271.
Russo, P. A., J. Pedersen, and R. Vandenbosch, 1975, Nucl. Phys. A **240**, 13.
Russo, P. A., R. Vandenbosch, M. Metha, J. R. Tesmer, and K. L. Wolf, 1971, Phys. Rev. C **3**, 1595.
Ryabov, Y., J. Trochon, D. Shackleton, and J. Frehaut, 1973, Nucl. Phys. A **216**, 395.
Schultheiss, H., and R. Schultheiss, 1971, Phys. Lett. B **34**, 245.
Seeger, P. A., 1967, *Proceedings of the Third International Conference on Atomic Masses*, Winnipeg, (University of Manitoba Press), p. 85.
Seeger, P. A., A. Hemmendinger, and B. C. Diven, 1967, Nucl. Phys. A **96**, 605.
Shackleton, D., 1974, Thesis, University of Paris.
Sicre, A., 1976, Thesis, University of Bordeaux.
Sicre, A., F. Caitucoli, G. Barreau, T. P. Doan, T. Benfoughal, and B. Leroux, 1980, in *Physics and Chemistry of Fission*, Proceedings of a conference at Jülich (IAEA, Vienna), to be published.
Silbert, M. G., 1969, Los Alamos Report LA-4108-MS.
Silbert, M. G., 1973, Nucl. Sci. Eng. **51**, 376.
Silbert, M. G., and J. R. Berreth, 1973, Nucl. Sci. Eng. **52**,

187.
Silbert, M. G., A. Moat, and T. E. Young, 1973, Nucl. Sci. Eng. **52**, 176.
Skyrme, T. H., 1956, Philos. Mag. **1**, 1043.
Sobiczewski, A., S. Bjørnholm, and K. Pomorski, 1973, Nucl. Phys. A **202**, 274.
Sobiczewski, A., Z. Szymanski, and S. Wycech, 1969a, in *Physics and Chemistry of Fission*, Proceedings of a conference at Vienna (IAEA, Vienna), p. 905.
Sobiczewski, A., Z. Szymanski, S. Wychech, S. G. Nilsson, J. R. Nix, C. F. Tsang, C. F. Gustafson, P. Möller, and B. Nilsson, 1969b, Nucl. Phys. A **131**, 69.
Sowerby, M. G., B. H. Patrick, and D. Mather, 1974, Ann. Nucl. Sci. Eng. **1**, 409.
Specht, H. J., J. S. Fraser, and J. C. D. Milton, 1966, Phys. Rev. Lett. **17**, 1187.
Specht, H. J., J. S. Fraser, J. C. D. Milton, and W. G. Davies, 1969, in *Physics and Chemistry of Fission*, Proceedings of a conference at Vienna (IAEA, Vienna), p. 363.
Specht, H. J., E. Konecny, J. Weber, and C. Kozhuharov, 1974, *Physics and Chemistry of Fission*, Proceedings of a conference at Rochester (IAEA, Vienna), Vol. 1, p. 285.
Specht, H. J., J. Phys. G. (to be published).
Sperber, D. and A. Aframe, 1972, Phys. Lett. B **41**, 574.
Stein, W. E., R. K. Smith, and H. L. Smith, 1968, *Neutron Cross-Sections and Technology*, NBS Special Publication 299, Vol. 1, p. 627.
Strutinsky, V. M., 1967a, Ark. Fys. **36**, 629.
Strutinsky, V. M., 1967b, Nucl. Phys. A **95**, 420.
Strutinsky, V. M., and H. C. Pauli, in *Physics and Chemistry of Fission*, Proceedings of a conference at Vienna (IAEA, Vienna), p. 155.
Strutinsky, V. M., A. G. Magnev, S. R. Ofengenden and T. Døssing, 1977, Z. Phys. A **283**, 269.
Swiatecki, W. J., 1955, Phys. Rev. **100**, 937.
Szymanski, Z., 1974, Phys. Scr. A **10**, 122.
Teichmann, T., and E. P. Wigner, 1952, Phys. Rev. **87**, 123.
Thomas, R. G., 1955, Phys. Rev. **97**, 224.
Tsäng, C. F., and S. G. Nilsson, 1970, Nucl. Phys. A **140**, 275.
Ulfert, G., D. Habs, V. Metag, and H. J. Specht, 1978, Nucl. Instrum. Methods, **148**, 369.
Ulfert, G. V. Metag, D. Habs, and H. J. Specht, 1979, Phys. Rev. Lett. **42**, 1596.
Urin, M. G., and D. F. Zaretsky, 1966, Nucl. Phys. **75**, 101.
Vandenbosch, R., 1967, Nucl. Phys. A **101**, 460.
Vandenbosch, R., 1972, Phys. Rev. C **5**, 1428.
Vandenbosch, R., 1974, in *Physics and Chemistry of Fission*, Proceedings of a conference at Rochester (IAEA, Vienna), Vol. 1, p. 257.
Vandenbosch, R., 1977, Annu. Rev. Nucl. Sci. **27**, 1.
Vandenbosch, R. and J. R. Huizenga, 1973, *Nuclear Fission* (Academic, New York).
Vandenbosch, R., P. A. Russo, G. Sletten, and M. Metha, 1973, Phys. Rev. C **8**, 1080.
Vautherin, D., and D. M. Brink, 1972, Phys. Rev. C **5**, 626.
Veeser, L., 1976 (private communication).
Veysière, A., H. Bail, R. Bergère, P. Carlos, and A. Lepretre, 1973, Nucl. Phys. A **199**, 45.
Vogt, E., 1958, Phys. Rev. **112**, 203.
Vogt, E., 1960, Phys. Rev. **118**, 724.
Vorotnikov, P. E., S. M. Dubrovina, V. N. Kosyakov, L. V. Chistyakov, V. A. Shigin, and V. M. Shubko, 1970, Nucl. Phys. A **150**, 56.
Vorotnikov, P. E., Z. S. Gladhik, A. V. Davydov, S. M. Dubrovina, G. A. Otroschenko, E. S. Pal'shin, V. A. Shigin, and V. M. Shubko, 1973, Sov. J. Nucl. Phys. **16**, 505.
Vorotnikov, P. E., B. H. Gokhberg, S. M. Dubrovina, V. N. Kosyakov, G. A. Otroschenko, L. V. Chistyakov, V. A. Shigin, and V. M. Shubko, 1972, Sov. J. Nucl. Phys. **15**, 20.
Wapstra, A. H., and K. Bos, 1977, Nucl. Data Tables **19**, 175.
Wapstra, A. H., and N. B. Gove, 1971, Nucl. Data Tables **9**, 265.
Weber, J., H. C. Britt, A. Gavron, E. Konecny, and J. B. Wilhelmy, 1976, Phys. Rev. C **13**, 2413.
Weidenmüller, H. A., and K. Dietrich, 1966, Nucl. Phys. **83**, 332.
Weigmann, H., 1968, Z. Phys. **214**, 7.
Weigmann, H., and J. D. Theobald, 1972, Nucl. Phys. A **187**, 305.
Weisskopf, V. F., 1937, Phys. Rev. **52**, 295.
Werz, R., Rohr, G., J. P. Theobald, and H. Weigmann, 1973, Proceedings of the Symposium on Nuclear Physics with thermal and resonance energy neutrons, Petten Report RCN-203, p. 172.
Wheeler, J. A., 1956, *Peaceful Uses of Atomic Energy*, Proceedings of a conference at Geneva (United Nations, New York), Vol. 2, p. 155.
Wheeler, J. A., 1963, in *Fast Neutron Physics*, edited by J. B. Marion and J. L. Fowler (Interscience, New York), Vol. 2, p. 2051.
Wigner, E. P., 1938, Trans. Faraday Soc. **34**, 29.
Wigner, E. P., 1956, *Proceedings of the Conference on Neutron Physics by Time-of-Flight*, Gatlinburg (Oak Ridge National Laboratory, Oak Ridge, Tennessee) ORNL-2309, p. 59.
Wigner, E. P., 1959, *Group Theory*, English translation by J. J. Griffin (Academic Press, New York).
Wigner, E. P., and L. Eisenbud, 1947, Phys. Rev. **71**, 29.
Wilets, L., and D. M. Chase, 1956, Phys. Rev. **103**, 1296.
Winhold, E. J., C. Demos, and O. Halpern, 1952, Phys. Rev. **87**, 1139.
Wolf, K. L., and J. W. Meadows, 1974, Bull. Am. Phys. Soc. **19**, 595.
Wolf, K. L., and J. P. Unik, 1972, Phys. Lett. B **38**, 405.
Wolf, K. L., and J. P. Unik, 1973, Phys. Lett. B **43**, 25.
Wolf, K. L., R. Vandenbosch, and W. D. Loveland, 1968, Phys. Rev. **170**, 1059.
Wolf, K. L., R. Vandenbosch, P. A. Russo, M. K. Mehta, and C. R. Rudy, 1970, Phys. Rev. C **1**, 2096.
Wong, C. Y., and J. Bang, 1969, Phys. Lett. B **29**, 143.
Yuen, G., G. T. Rizzo, A. N. Behkami, and J. R. Huizenga, 1971, Nucl. Phys. A **171**, 614.
Zhuchko, V. E., A. V. Ignatyuk, Yu. B. Ostapenko, G. N. Smirenkin, A. S. Soldatov, and Yu. M. Tsipenyuk, 1975, JETP Lett. **22**, 255.
Zhuchko, V. E., Yu. B. Ostapenko, G. N. Smirenkin, A. S. Soldatov, and Yu. M. Tsipenyuk, 1978a, Yadern. Fiz. **28**, 1170.
Zhuchko, V. E., Yu. B. Ostapenko, G. N. Smirenkin, A. S. Soldatov, and Yu. M. Tsipenyuk, 1978b, Yad. Fiz. **28**, 1185.
Zielinska-Pfabe, M., and S. Gabrakov, 1973, Phys. Lett. B **44**, 405.